MISSILE AND SPACE DIVISION C04

FINAL REPORT

VOYAGER SPACECRAFT

PHASE B, TASK D

VOLUME II (BOOK 4 OF 5)

SYSTEM DESCRIPTION

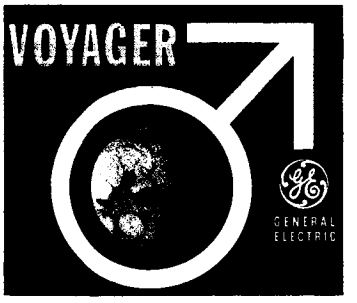

GENERAL ELECTRIC

DIN 67SD4379
16 OCTOBER 1967

FINAL REPORT

VOYAGER SPACECRAFT

PHASE B, TASK D

VOLUME II (BOOK 4 OF 5)

SYSTEM DESCRIPTION

PREPARED FOR

GEORGE C. MARSHALL SPACE FLIGHT CENTER

UNDER MSFC CONTRACT No. NAS8-22603

GENERAL ELECTRIC

MISSILE AND SPACE DIVISION
Valley Forge Space Technology Center
P.O. Box 8555 • Philadelphia 1, Penna.

VOLUME SUMMARY

The Voyager Phase B, Task D Final Report is contained in four volumes. The volume numbers and titles are as follows:

Volume I	Summary
Volume II	System Description
Book 1	Guidelines and Study Approach, System Functional Description
Book 2	Telecommunication
Book 3	Guidance and Control Computer and Sequencer Power Subsystem Electrical System
Book 4	Engineering Mechanics Propulsion Planet Scan Platform
Book 5	Design Standards Operational Support Equipment Mission Dependent Equipment
Volume III	Implementation Plan
Volume IV	Engineering Tasks
Book 1	Effect of Capsule RTG's on Spacecraft
Book 2	Applicability of Apollo Checkout Equipment
Book 3	Central Computer
Book 4	Mars Atmosphere Definition
Book 5	Photo-Imaging

VOYAGER TASK D
VOLUME II
SYSTEM DESCRIPTION

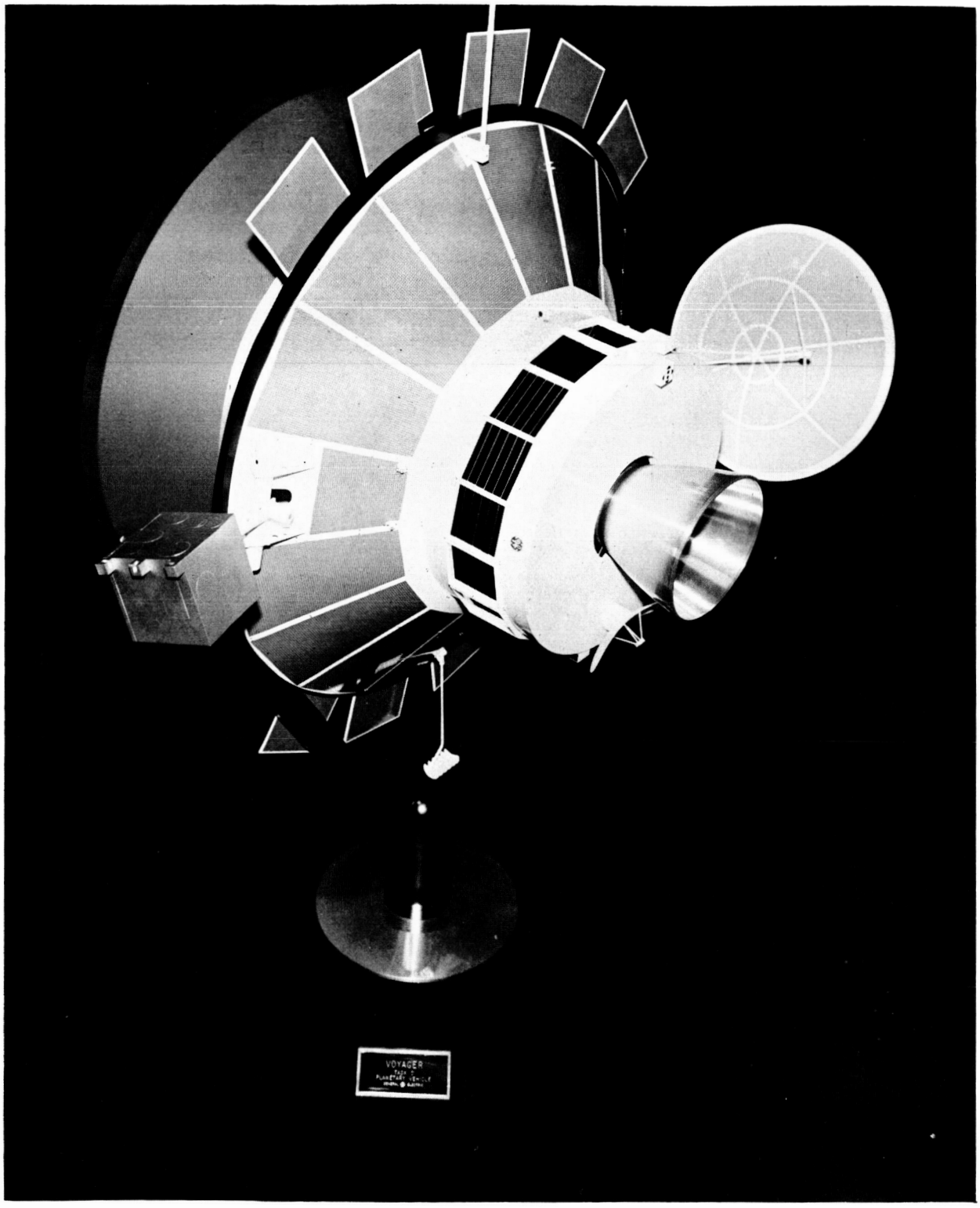

Voyager Planetary Vehicle (Task D)

VOYAGER TASK D
Volume II
PREFACE

This volume describes the design of the Voyager Spacecraft System, the Operational Support Equipment requirements, and the Mission Dependent Equipment requirements resulting from the system update study.

The mission concept for Voyager has not changed substantially since the previous Phase B, Task B study in late 1965. The Saturn V Launch Vehicle is used to inject two identical planetary vehicles on a Mars trajectory. Each planetary vehicle consists of a flight spacecraft and a flight capsule and, after separation from the Saturn V, the two vehicles provide complete mission redundancy. The flight spacecraft serves as a bus to deliver the flight capsule into Mars orbit from which it subsequently descends and soft lands to carry out surface experiments. The flight spacecraft then carries out an orbiting science mission for periods ranging from six months for early missions to two years for subsequent missions.

The flight spacecraft developed in this system update is shown in the illustration on the page opposite. This design is described in detail in this volume which is organized in the following major sections:

Section	Subject	Identification No.
I	Guidelines and Study Approach	VOY-D-100
II	System Functional Description and Analysis	VOY-D-200
III	Subsystem Functional Description and Analysis	VOY-D-300
IV	Design Standards	VOY-D-400
V	Operational Support Equipment	VOY-D-500
VI	Mission Dependent Equipment	VOY-D-600

Section I describes the study approach and discusses major constraints and guidelines that were imposed, with emphasis on requirements or guidelines which have changed since the last Voyager System design study.

Section II is a system level description of the resulting spacecraft design and its interfaces with other systems. Major system analyses and trade studies, such as trajectory and orbit selection, are covered.

Section III describes the baseline design of each subsystem, with discussion of alternates that were considered in arriving at the selected design.

Section IV covers some limited areas of design standards to be applied to the Voyager spacecraft.

Section V is an analysis of Operational Support Equipment (OSE) requirements and an evaluation of a number of OSE concepts with selection of a preferred approach.

Section VI analyzes the space flight operation together with the current and planned capabilities of the deep space network to define probable requirements for mission dependent hardware and software to support the mission.

VOY-D-361
STRUCTURE

1. INTRODUCTION

The purpose of this section is to present the salient features of the preliminary structural design of the baseline spacecraft. The evolution of the structural design is an inseparable part of the Configuration Development Section (VOY-D-220). That section included consideration of operational details, manufacturing, quality control and test. In this section some of the structural trade-offs as well as the shaping and sizing of the structural elements to carry the imposed loads efficiently are described. The Space Division of Chrysler Corporation provided assistance in the preparation of this section of the report.

2. FUNCTIONAL DESCRIPTION

The planetary vehicle basic geometry is presented in Figure 1. An isometric sketch of the orbit configuration is shown in Figure 2. A more detailed structural arrangement drawing of the spacecraft is presented in Figure 3 and of the propulsion support in Figure 4. An exploded view showing the structural subassemblies for manufacturing and test purposes is presented in Figure 5. In Figure 5, the spacecraft consists of a propulsion module, a support module, and an electronic module. Two sets of jury struts are used temporarily to stiffen the support module and are removed after the support and propulsion modules are mated.

The assembled support module and the conical section of the propulsion module (including skin, longerons, upper and lower ring) form the primary structural elements of the Spacecraft (Figure 6).

The propulsion support structure consists of the rest of the propulsion module support elements including the midring of the conical section (Figure 7). The Electronic Equipment module is shown in Figure 8.

2.1 PRIMARY LOAD PATHS

The primary load paths of the selected configuration efficiently transmit the loads induced by the three major mass items (flight capsule, propulsion system, and electronics module) to the shroud. The predominant axial loads of these mass items are carried by direct stresses in the eight primary truss segments formed through the juncture of the support struts, the array radials, and the inner shell longerons. Capsule loads are applied at eight hard points at the forward end of the inner periphery of the truss segment envelope, with the major portion of the axial propulsion system axial loads and all of the electronic equipment loads being delivered to a similar number of hard points at the aft end of the truss segment envelope. Relatively stiff kick rings at the forward and aft ends of the truss segment envelope provide the necessary reaction points for truss equilibrium considerations and also limit the "toroidal" twisting of the truss segments. The predominantly aft axial loading for the critical maximum boost acceleration condition produces compressive loads in the support struts and tensile loading in the array radials. As such, this tends to prohibit the development of significant kick loads in the shroud interface ring, and allows for a relatively lightweight structural element to be employed. Increasing the stiffness of the shroud interface ring will reduce somewhat the maximum axial loads in the truss segment members, but investigations clearly indicate that the weight penalty involved in such a design would exceed the benefits derived from the corresponding reduction in truss member sizes.

Capsule lateral shears are delivered to the spacecraft at the capsule interface ring and are transmitted to the shroud through direct loading of the inclined upper struts. The lateral loading attendant to the propulsion system are delivered to the primary structure at the inner shell mid-ring and at the equipment module interface ring. With regard to the loading at the mid-ring, a portion is carried forward in shear and bending to the capsule interface ring and thence to the shroud. The remainder is transmitted in a similar manner aft to the equipment module interface ring and thence to the shroud through axial loading of the array

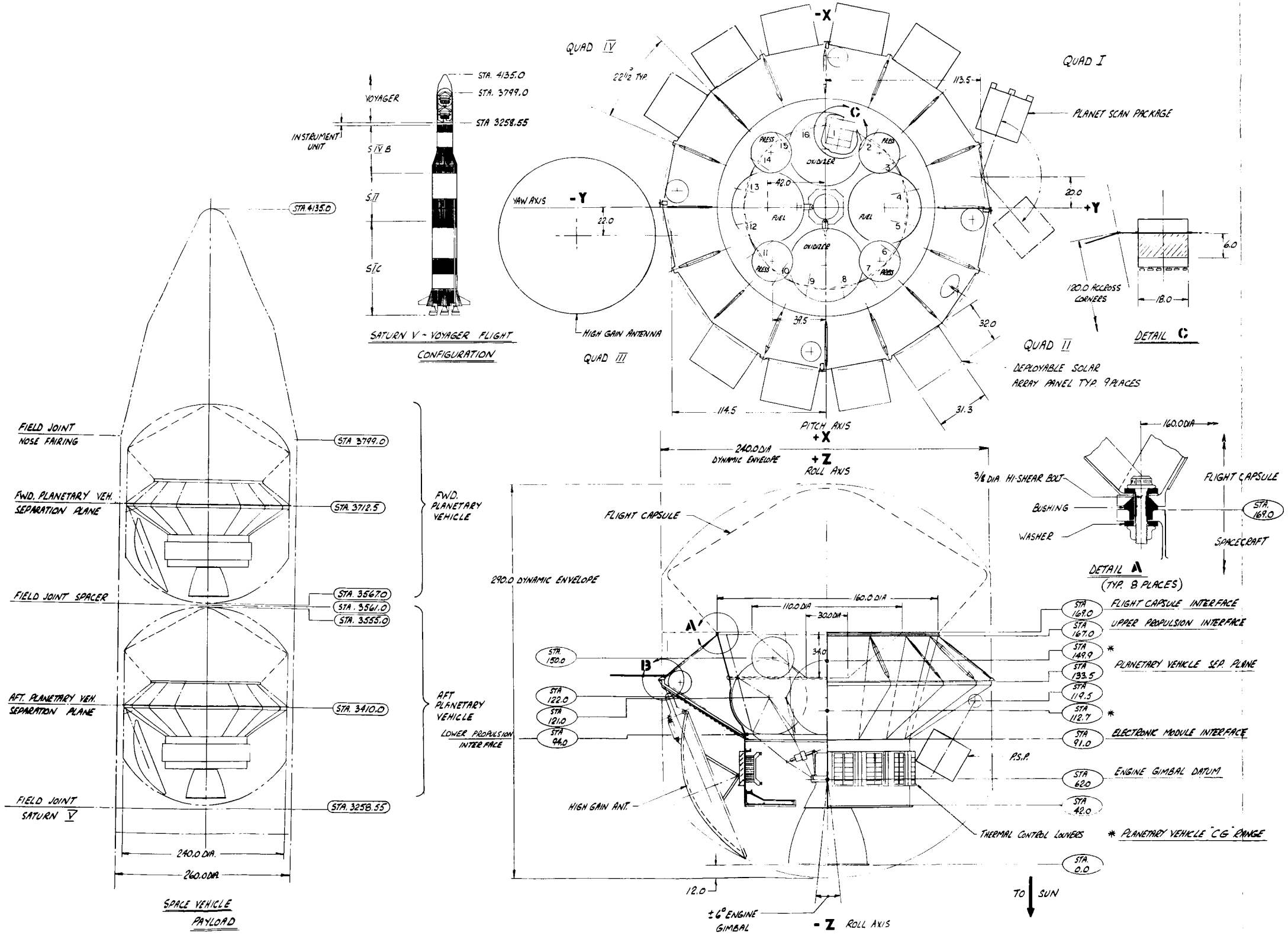

Figure 1. Planetary Vehicle Geometry

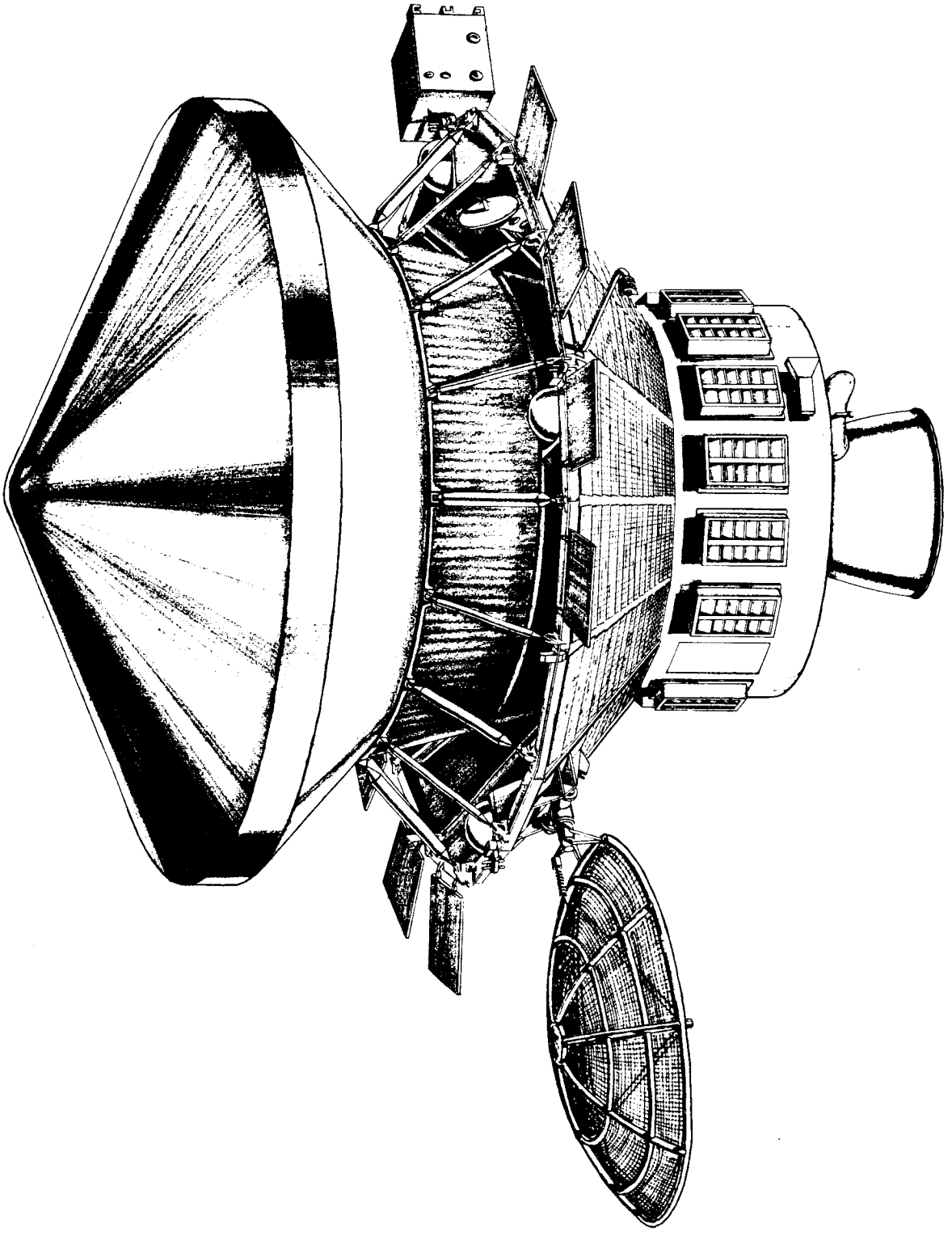

Figure 2. Orbit Configuration

radials and shear in the solar array panels. Equipment module lateral loads are also transmitted to the shroud through direct stresses in the array radials and shear in the solar array panels.

2.2 PLANETARY VEHICLE SUPPORT CONSIDERATIONS

Structural efficiency was an important factor in determining the number of primary truss segments to be used in the selected configuration. With regard to the support struts, it may be concluded that a fewer number of relatively large members can more effectively carry a given overall load because higher allowable buckling stresses are achieved with the more massive sections than otherwise possible. Kick frames, on the other hand, are generally lighter when the radial loads are applied in a more distributed fashion.

The basic field of choice as to the number of truss segments was narrowed to two, namely:

a. A 16-truss segment configuration consistent with the 16 bay areas of the electronic module.

b. An eight segment configuration consistent with the anticipated number of capsule pick up points and also with the propulsion system support structure.

The selected eight-segment configuration is more advantageous structurally because of the magnitude of the capsule and propulsion loads in comparison with those of the electronic equipment module. Since these predominant loads are largely applied to only eight of the segments, it would be structurally inefficient to attempt to shear these loads through the skin of the inner cone in an attempt to develop significant loading in intermediate truss sections. Also the load path continuity is interrupted at four places where the propellant tanks bulge through. A major consideration in the decision to carry the planetary vehicle loads to the shroud at eight points is the desire to minimize the number of pyrotechnic separation bolts.

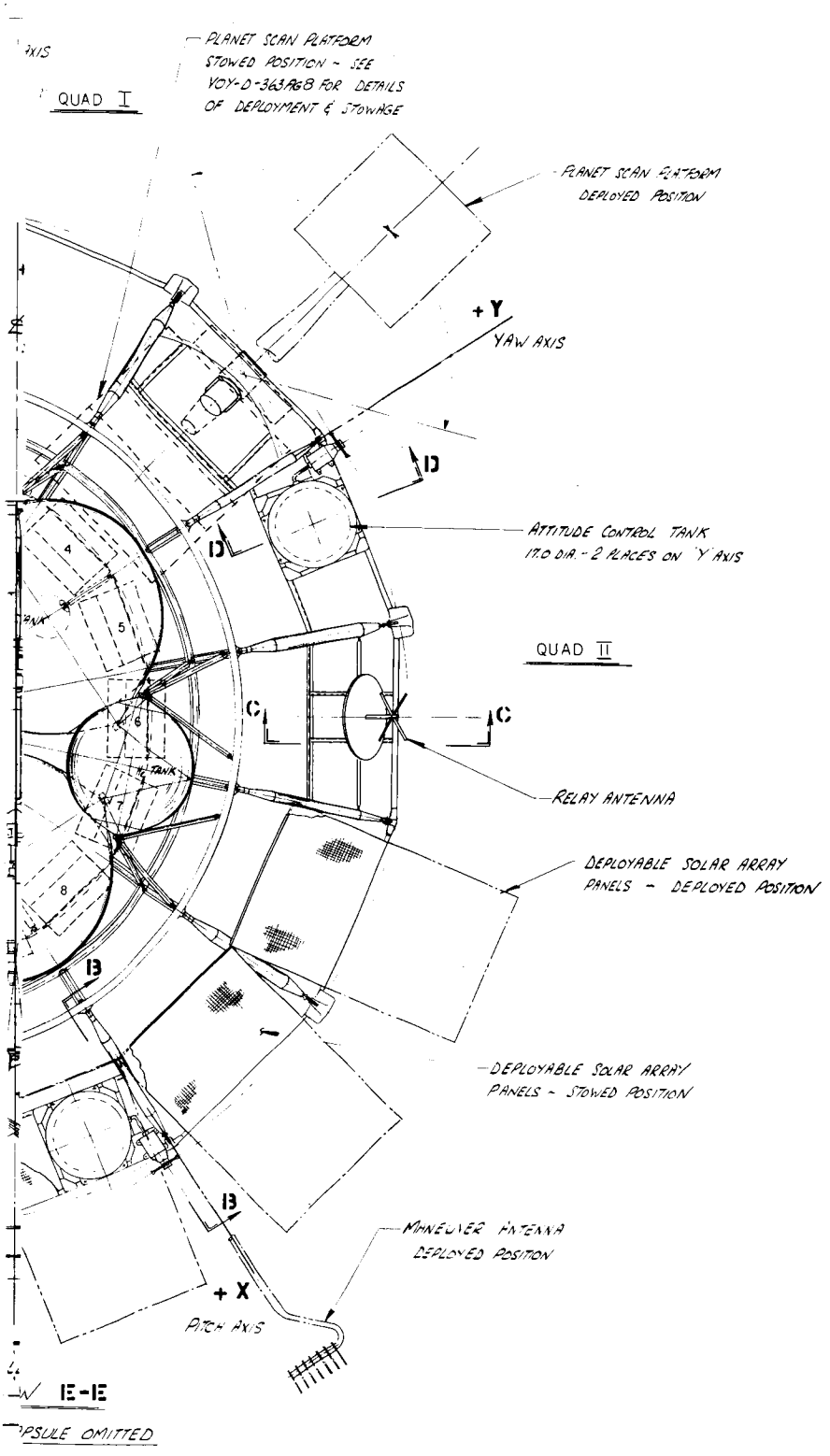

Figure 3. Spacecraft General Arrangement
(Sheet 1 of 2)

FOLDOUT FRAME 3

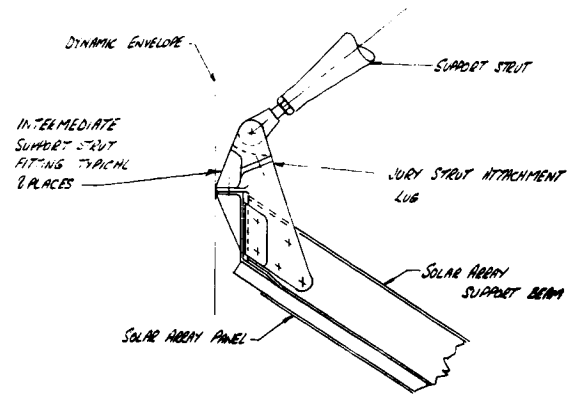

SECTION P-P

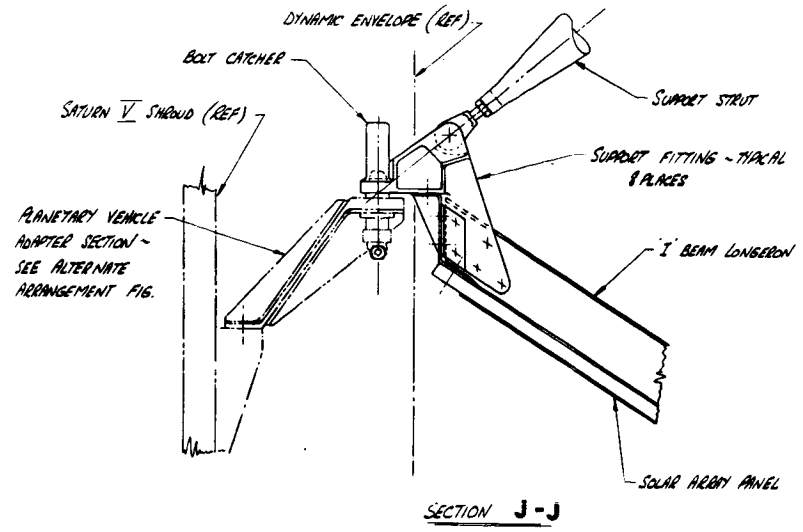

SECTION J-J

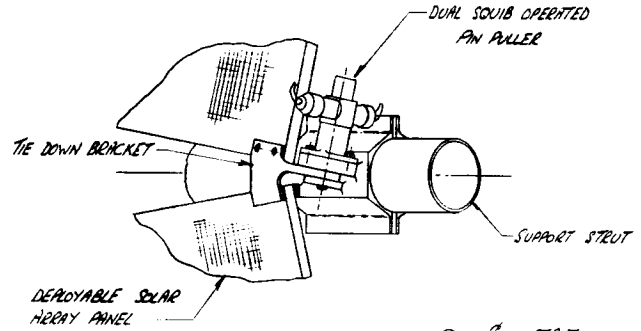

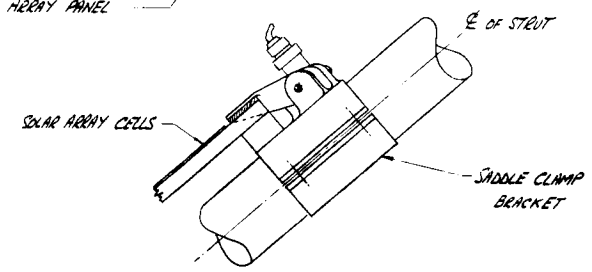

DETAIL N

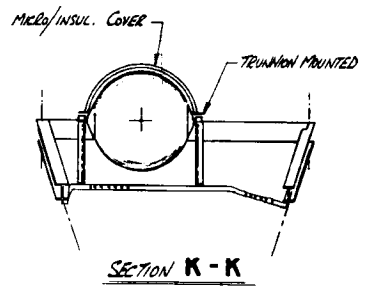

SECTION K-K

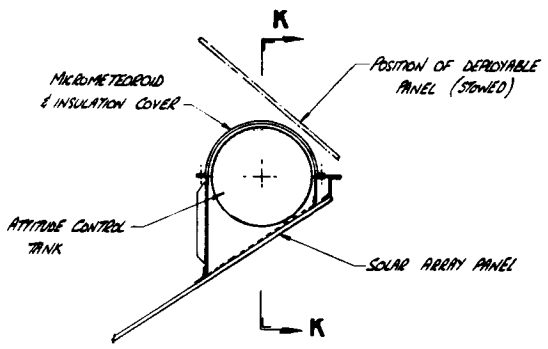

SECTION D-D

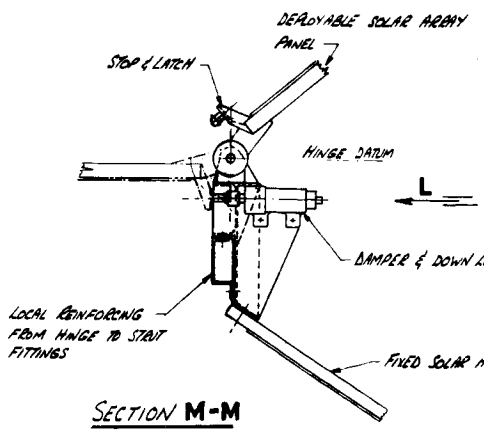

SECTION M-M

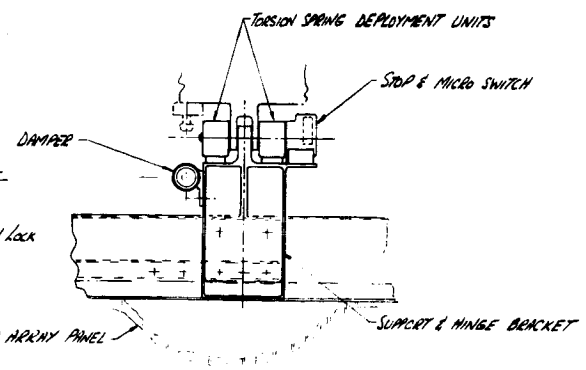

VIEW L

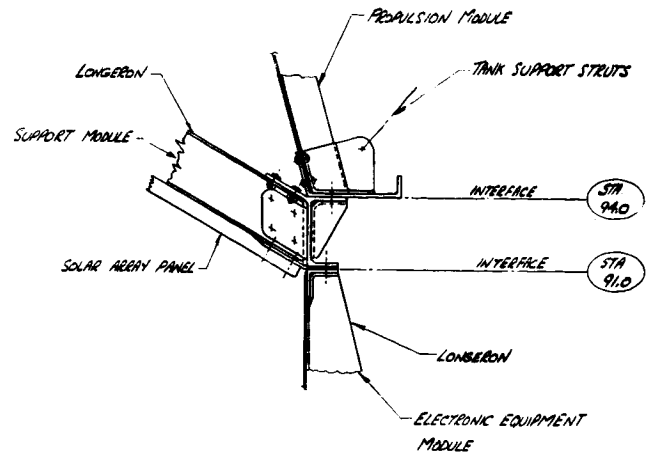

DETAIL G

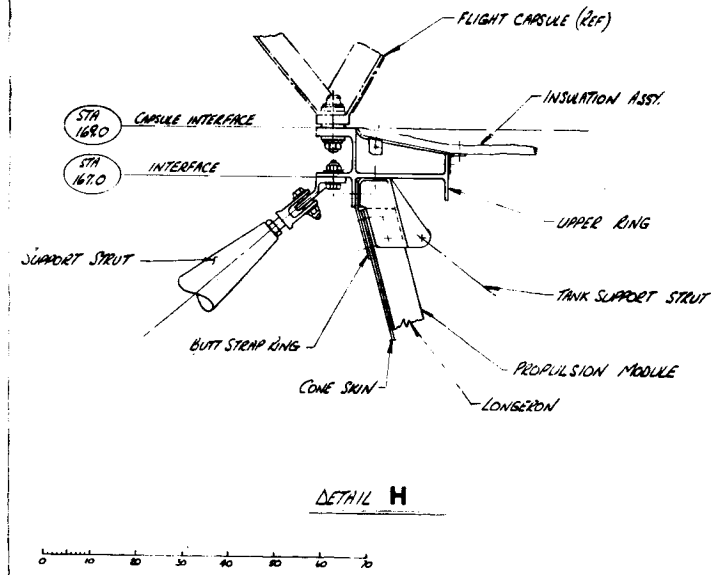

DETAIL H

Figure 3. Spacecraft General Arrangement (Sheet 2 of 2)

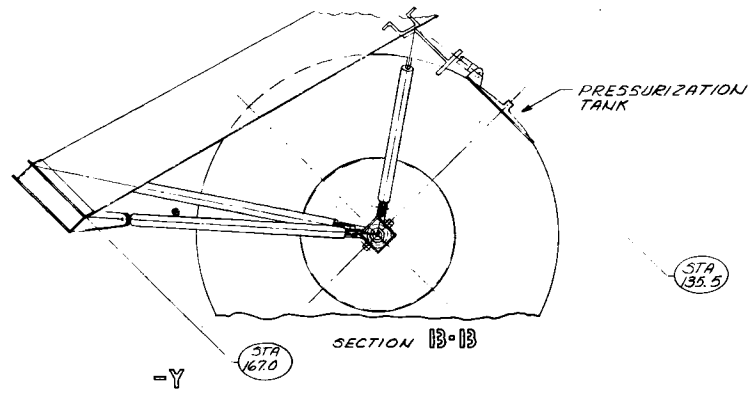

SECTION 13-13

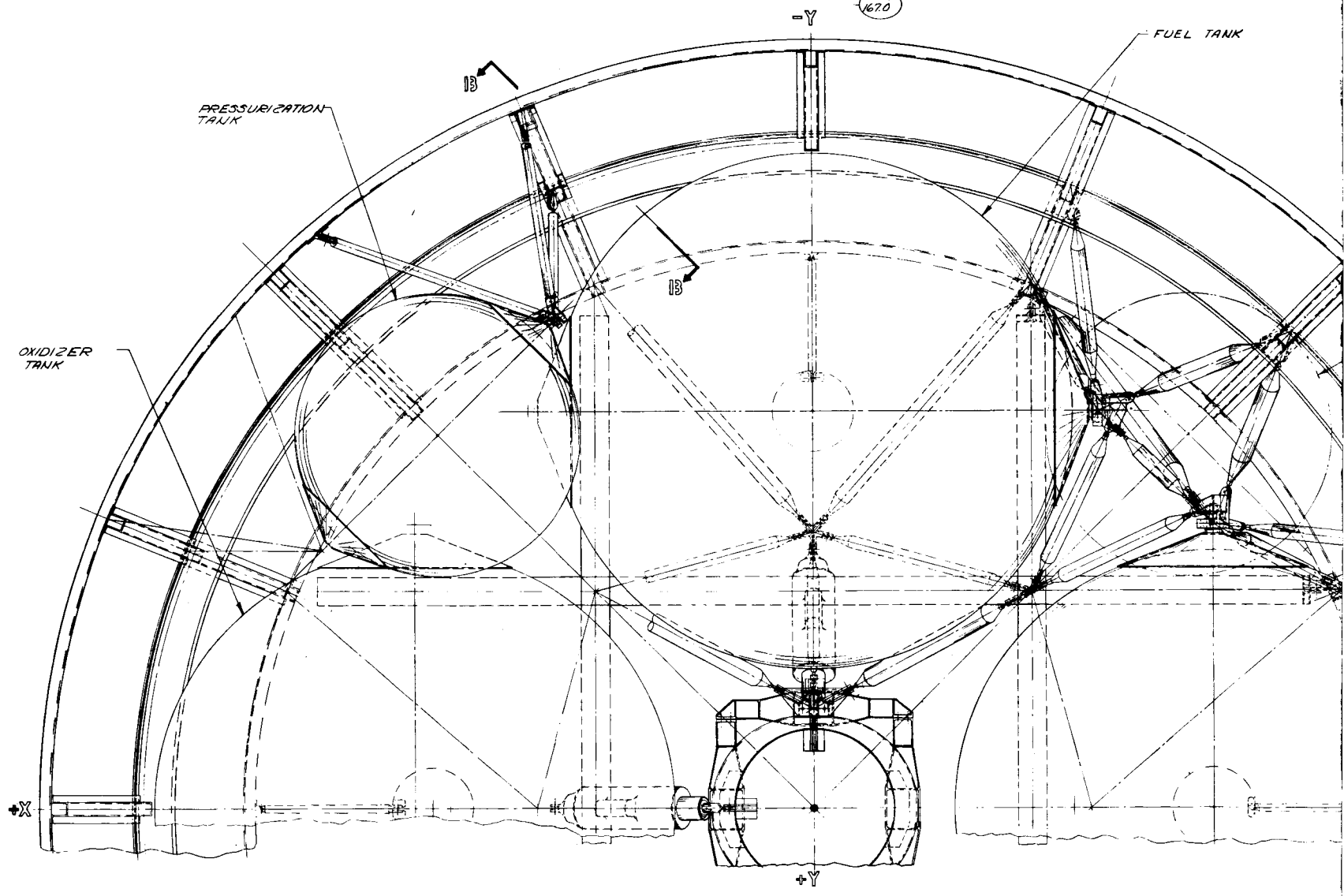

DETAIL A
ROTATED 90° CW

FOLDOUT FRAME 1

11

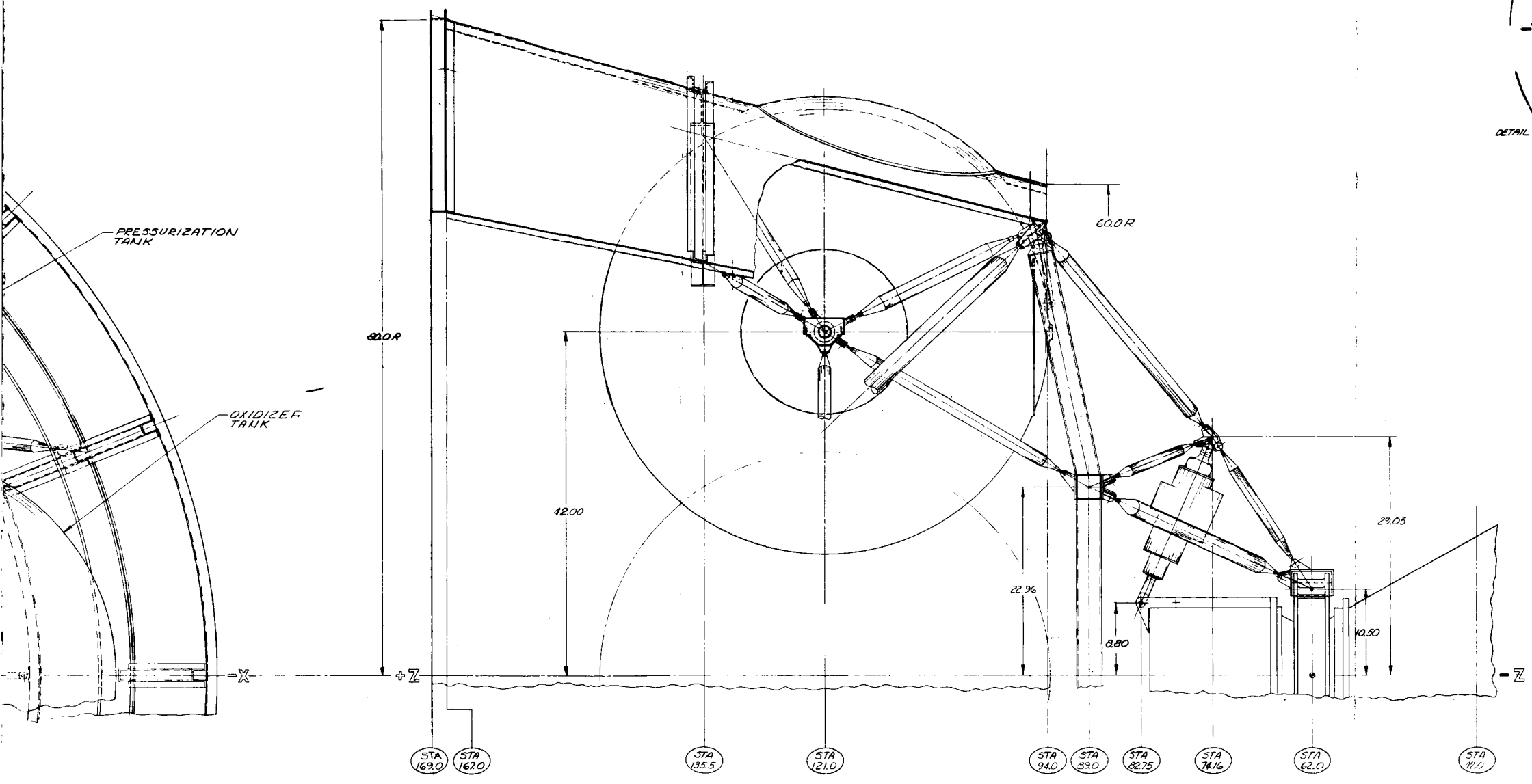

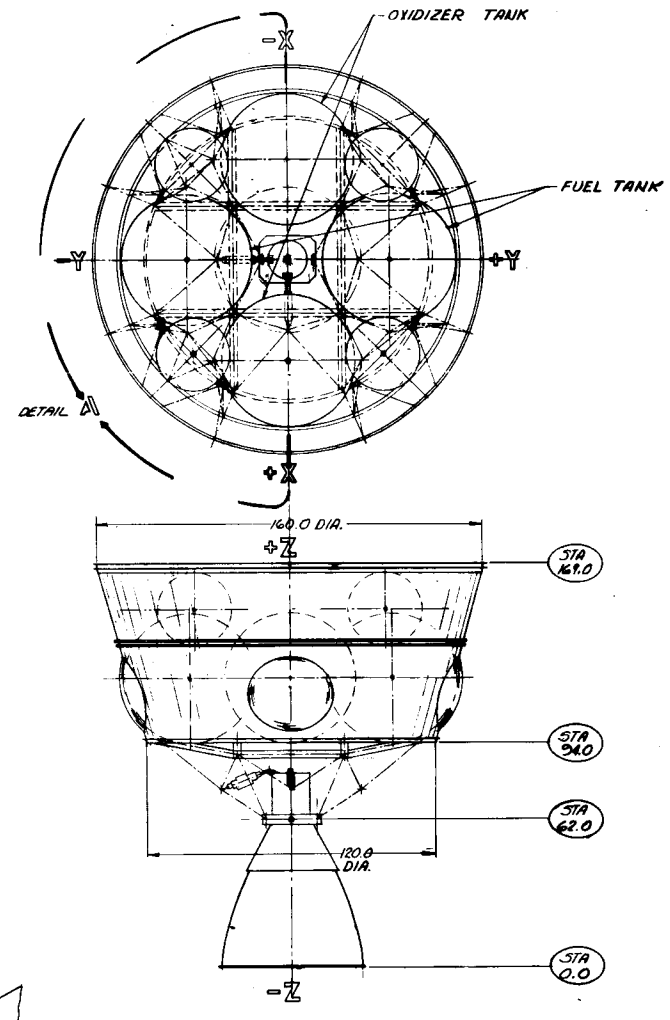

Figure 4. Propulsion Module Structure

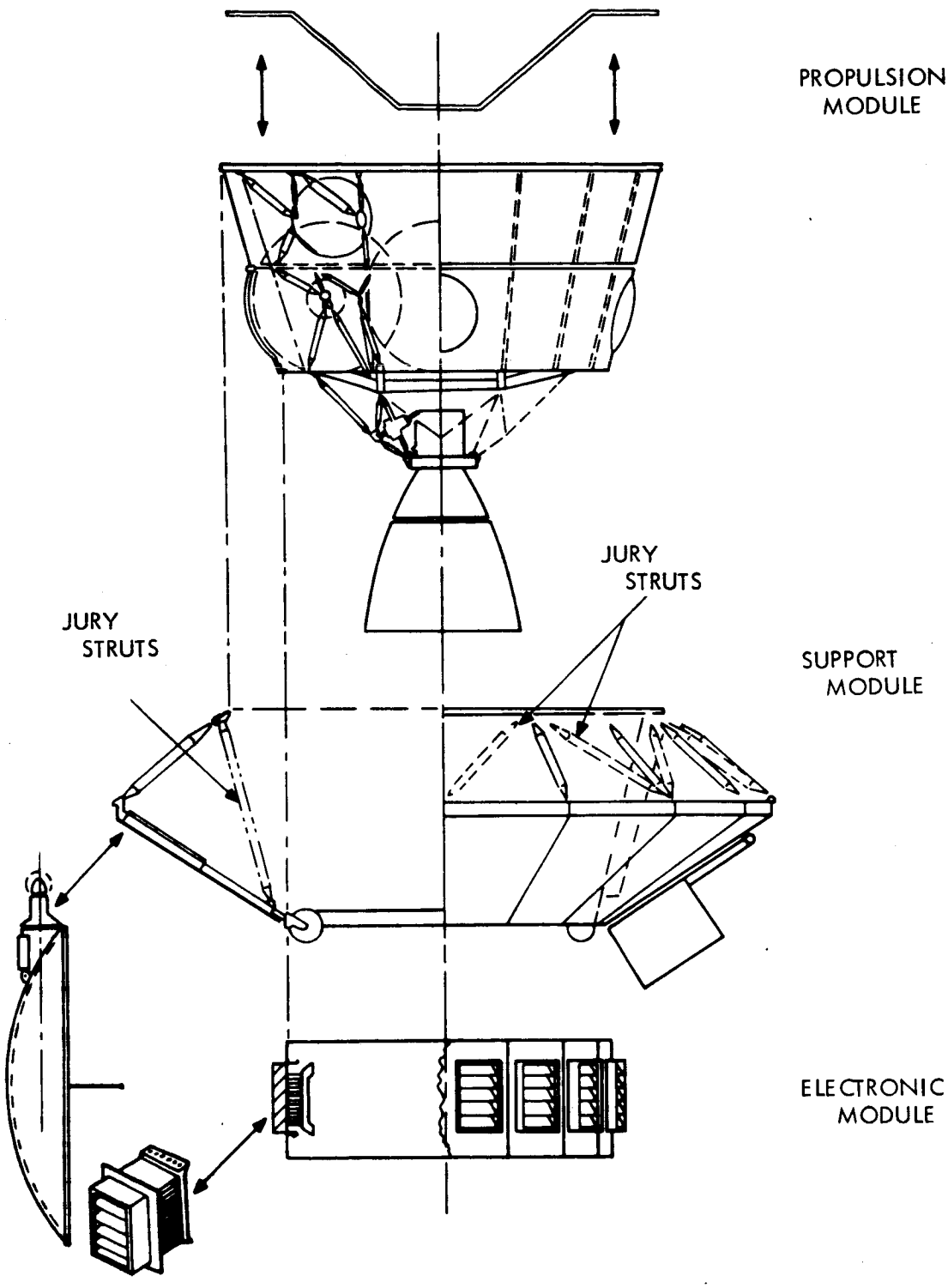

Figure 5. Spacecraft Modules

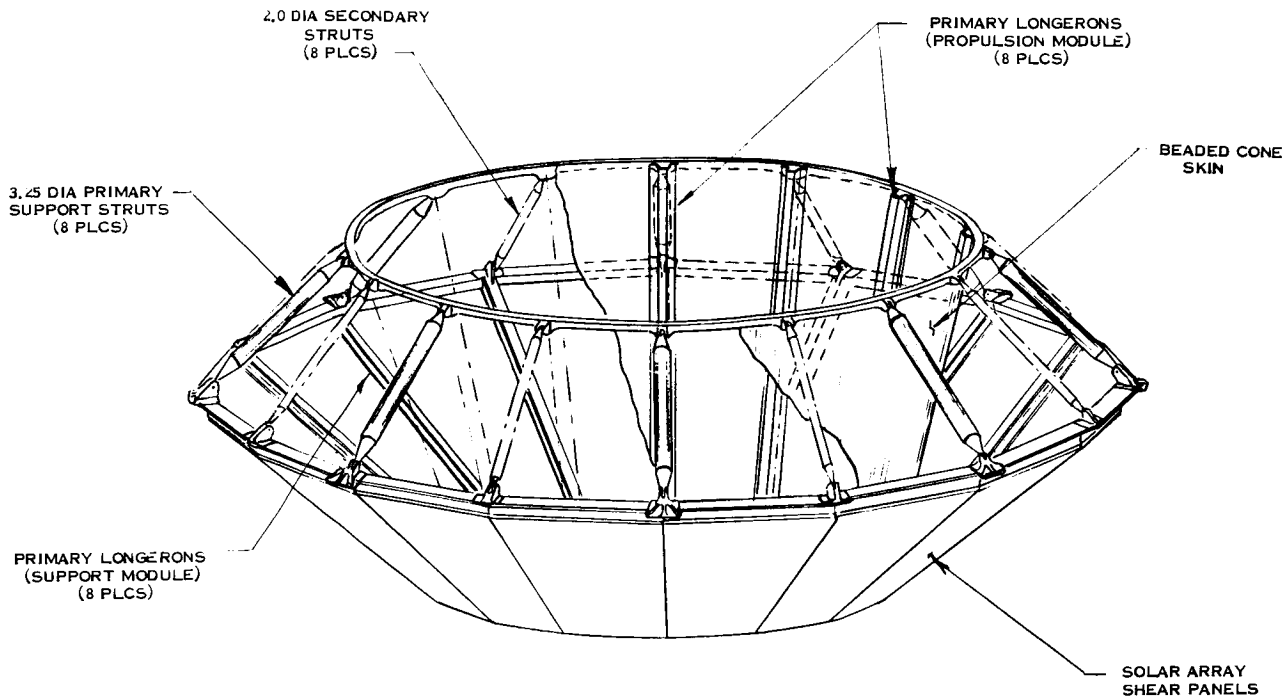

Figure 6. Primary Structural Elements

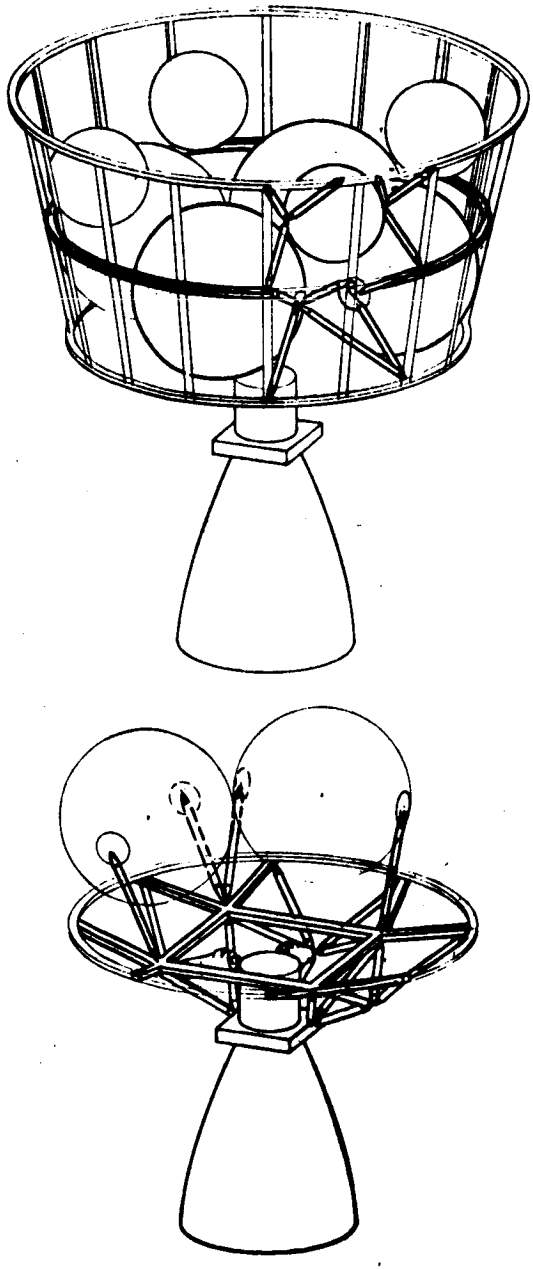

Figure 7. Propulsion Support Structural Elements

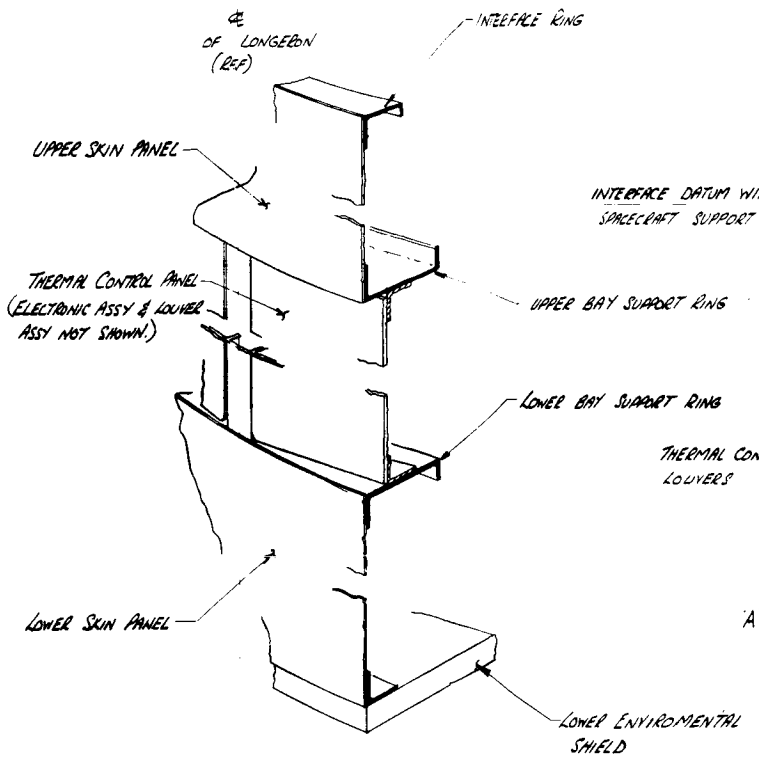

ISOMETRIC SECTION THRU MODULE

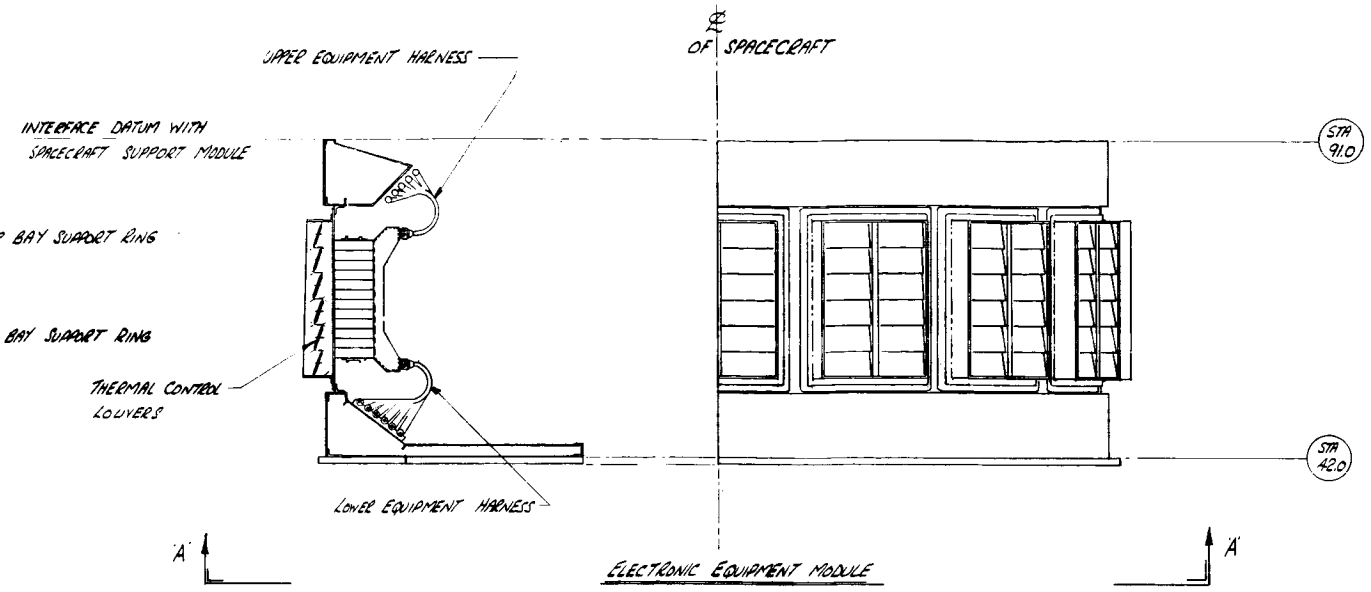

ELECTRONIC EQUIPMENT MODULE

SHOWING OUTSIDE VIEW & SECTION THRU EQUIPMENT BAY

DETAIL 'D'

SHOWING TYPICAL CORNER ARRANGEMENT

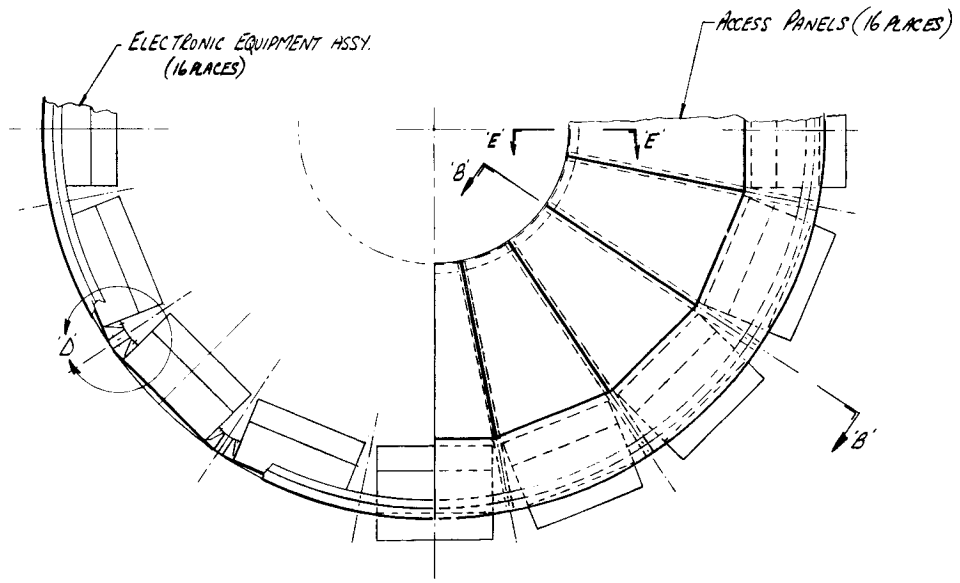

VIEW A-A

SHOWING UNDERSIDE VIEW OF ELECTRONIC MODULE & PART SECTION WITH BOTTOM COVER REMOVED

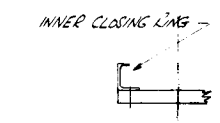

SECTION E-E

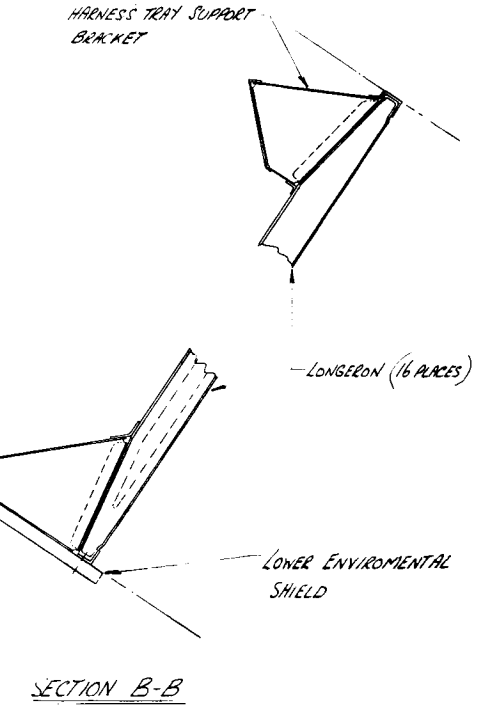

SECTION B-B

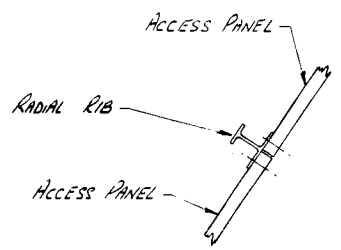

SECTION C-C

Figure 8. Electronic Equipment Module

Comparative evaluation of structural analyses performed on several candidate configurations indicated several favorable features of the selected configuration from a stress standpoint.

2.2.1 Short Load Paths

The major loads of the capsule and propulsion system are delivered directly through the support module to the shroud. Thus, no high loads are transmitted through the electronics module.

2.2.2 Reduced Bending Moment Loads

By virtue of the close proximity of the combined C.G. of the planetary vehicle to the vehicle/shroud attachment plane, the bending moments induced by lateral loads are significantly less than those attendant to the low support concepts in which the planetary vehicle is "cantilevered" from the attachment plane.

2.2.3 Utilization of Solar Array Panels as Primary Structure

The selected concept utilizes the solar array panels to carry lateral shear and to provide torsional stability in a manner similar to that in which the skin of a semi-monocoque conical support shell would perform these functions. This concept requires that the panels be affixed to the supporting framework with structural attachments, and that provisions be made to distribute high localized shear flows. The penalties associated with these requirements are small, however, when compared to the weight of additional structure that would be required if the array panels functioned only as a mounting surface for the solar cells.

2.3 PROPULSION SYSTEM SUPPORT STRUCTURE

The function of the propulsion system support structure is to provide support points for the trunnions of the spherical tanks and the required hard points for the actuators and gimbal ring of the LEMDE engine. Consequently, a system of trusses was chosen as the most

efficient structure to establish these discrete points in space. A sketch of this baseline configuration is shown in Figure 9.

The location of the four pressurization tanks are such that the simplest support is a tripod at each trunnion which is reacted by the forward and the intermediate ring. The structure is designed by loads imposed on the system during flight which are in general relatively low.

The propellent tanks,which comprise a significant portion of the mass of the Planetary Vehicle during boost, are located between the intermediate and aft ring of the conical shell structure. Growth of a typical tank under load is permitted by providing a sliding joint at one trunnion. This trunnion is supported by a tripod and the other is attached in such a manner as to provide a pinned joint by a quad-pod. The quad-pod was selected to reduce the severity of local loading on the supporting rings resulting from a lateral acceleration of the vehicle.

The aforementioned tripod and quad-pod are made integral by an additional strut spanning the trunnion points between adjacent tanks. This strut also helps to alleviate the high local loading induced into the supporting rings. The intermediate ring, for example, is designed primarily by the stiffness requirements necessary to provide an adequate support for the propellant tanks under a lateral mode of vibration.

The LEMDE Engine, located aft of the aft ring, is supported by the engine support subassembly which transmits longitudinal loads to the eight trunnion points of the propellant tank support subassembly.

2.4 ALTERNATE PROPULSION SUPPORT STRUCTURES

Several alternate propulsion support concepts were examined. Briefly, these concepts included a stabilized cruciform structure which provides support for both propellant tanks and the LEMDE (Figure 10), a modified baseline configuration which utilizes radial tension

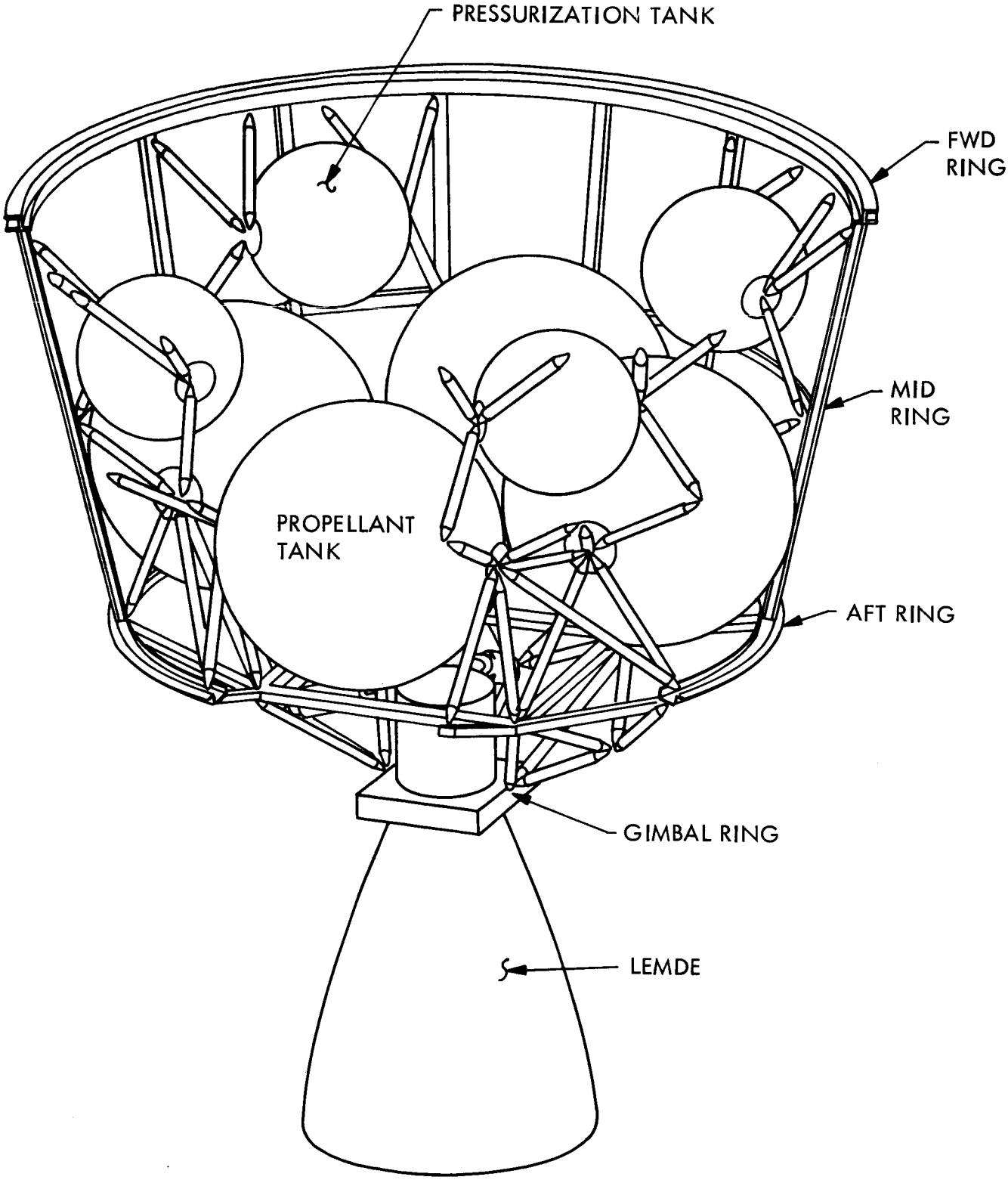

Figure 9. Baseline Configuration - Propulsion Structure

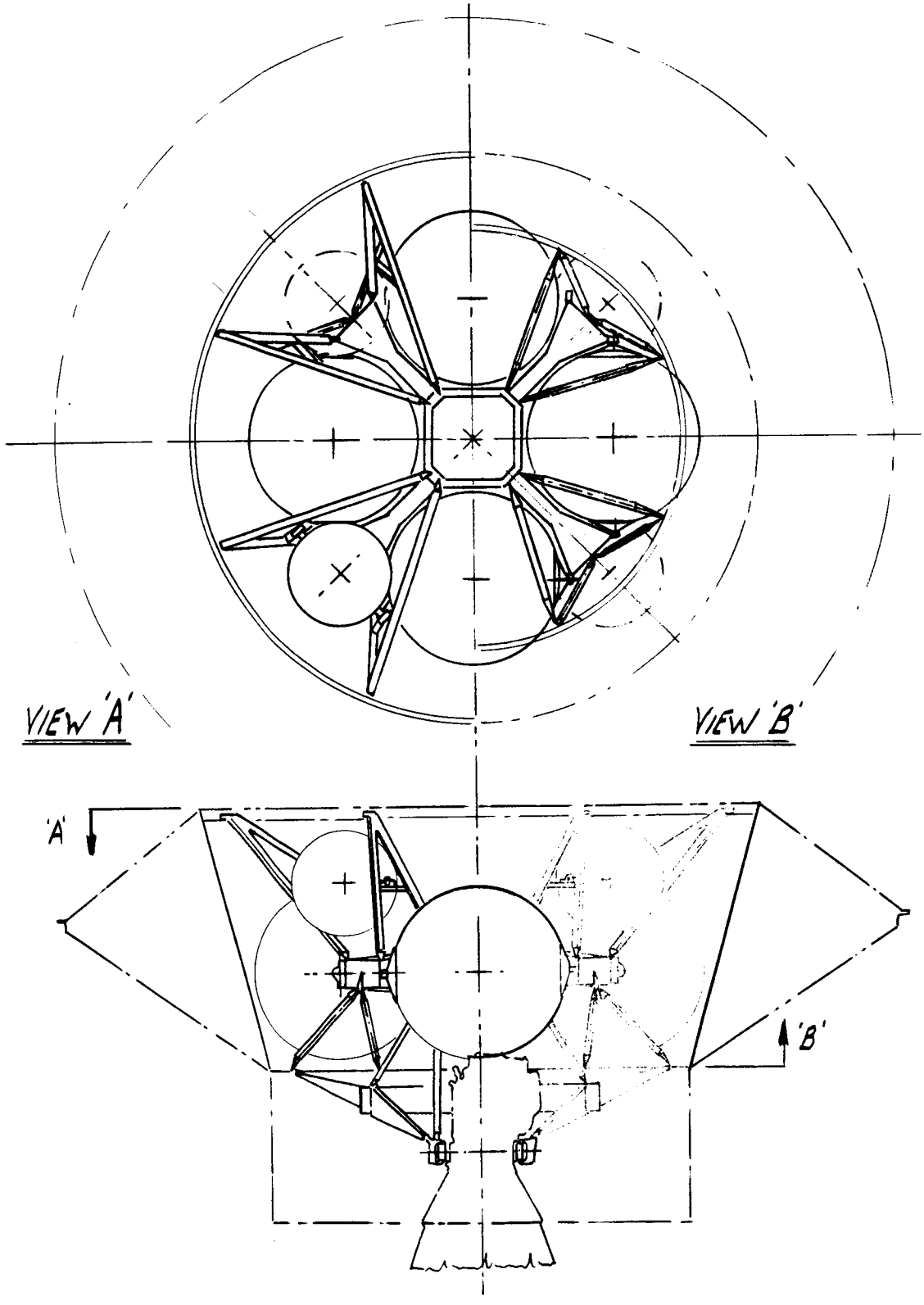

Figure 10. Stabilized Cruciform Support Structure

struts (Figure 11), and a support structure which involves both beams and struts (Figure 12). The stabilized cruciform structure of Figure 10 is soft in the lateral direction. The radial tension struts of Figure 11 were added in an attempt to reduce the weight of the mid ring of the baseline design. Its effectiveness depends on the stiffness of the outer ring which in turn depends on the final disposition of the Planetary Vehicle - shroud interface. In general it is more efficient to add ring weight at the smaller diameter to obtain increased stiffness.

Inclusion of the radial struts would add complexity to the assembly procedures. The platform design of Figure 12 shows promise of weight reduction over the baseline design. However it presented a difficult problem in design of the joint between the propulsion and support module.

In summary, all of the alternate designs hold some promise. The problems they contain may be overcome with more design and analysis effort. The baseline design was selected because it presented the least number of design problems.

3. DESIGN ENVIRONMENTS, LOADS AND CRITERIA

3.1 STRUCTURAL DESIGN LOADS

Critical loading conditions for each significant phase of the mission are presented in Table 1 for spacecraft primary structure. These flight limit lateral and longitudinal loads are derived from information received from NASA/MSFC, Saturn V - Planetary Vehicle flight loads analyses and the environmental predictions of Reference 3.1.

The flight loads analyses illustrate that the magnitude of the longitudinal flight loadings experienced by the Planetary Vehicle, are not appreciably affected by planetary vehicle frequency. The variation of maximum vehicle dynamic load factors with vehicle frequency is illustrated in Figure 13 for the S-IC shut-down condition.

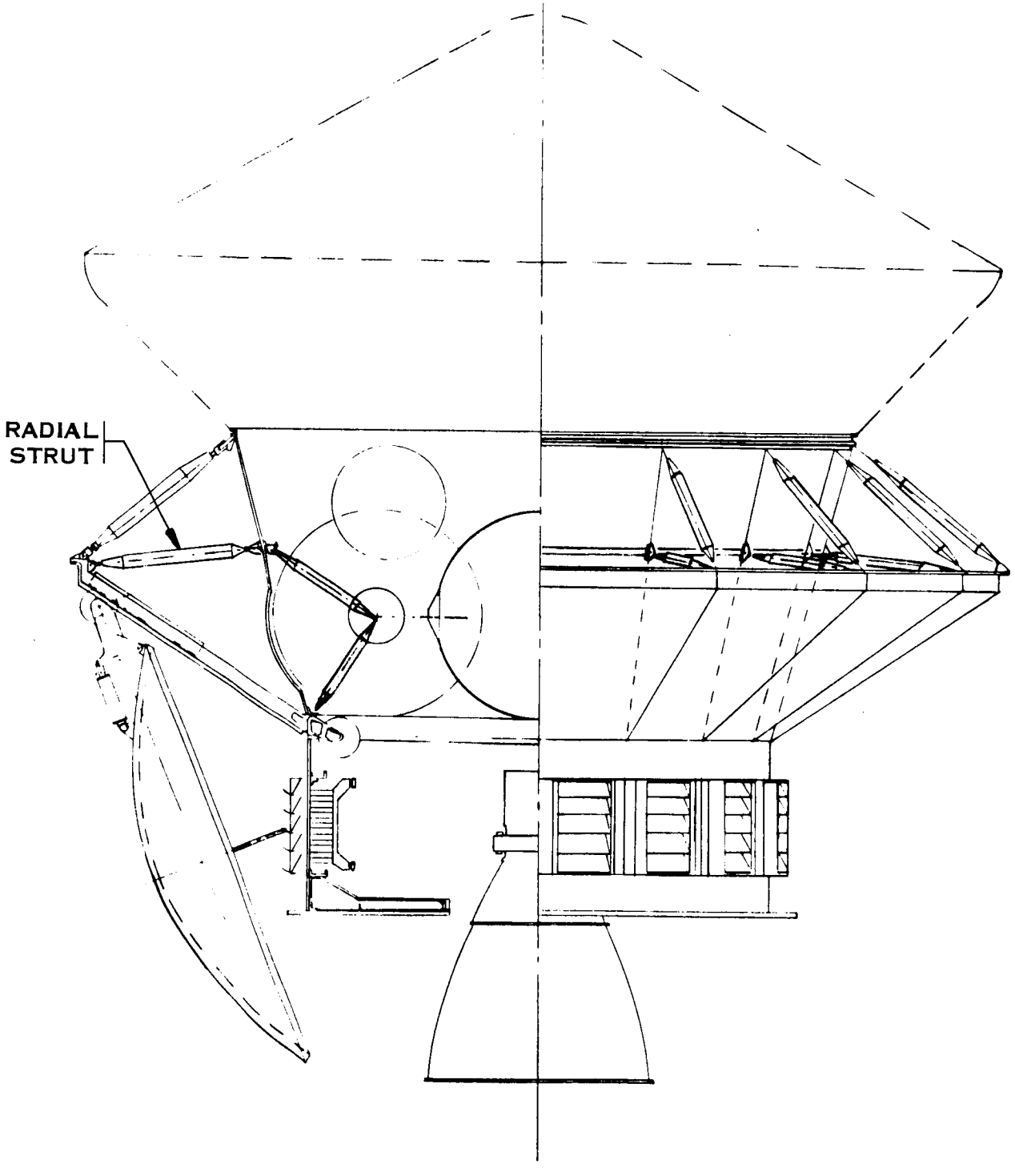

Figure 11. Radial Strut Design

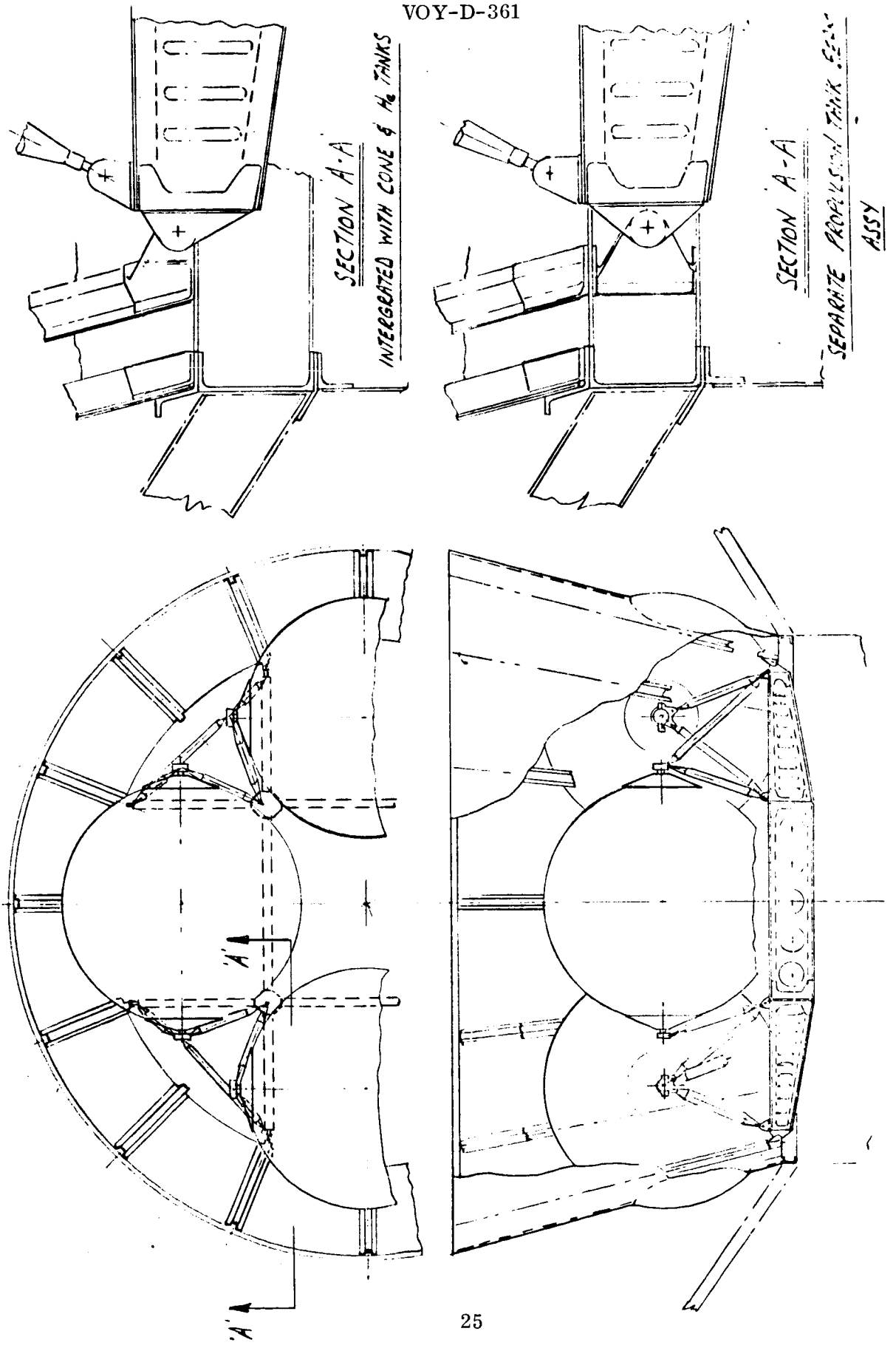

Figure 12. Platform Design

Table 1. Limit Load Factors Employed for Primary Vehicle Structure

Mission Phase (Condition)	Lateral Load Factor (g)			Longitudinal Load Factor (g)		
	Static	Dynamic	Total	Static	Dynamic	Total
Launch Release	-	1.5	1.5	-1.3	0.7	-2.0
Max q	-	0.3	0.3	-2.0	-	+0.6
Max Boost Accel	0.4	-	0.4	-4.75	-	-4.75
S-IC Shut-down	-	0.5	0.5	-	1.0	±1.0
S-IC Separation	-	-	-	-	1.5	±1.5

NOTE:

1. Torsional Accelerations are not listed in this table because they are very low.
2. Engine Thrust Load (Limit) = 10,500 lbs. with a maximum gimbal angle of 6^{o} off the roll axis.
3. Lateral and longitudinal load factors are simultaneously applied for each condition.

The preliminary limit load factors in Table 2 were employed for secondary structure.

3.2 STIFFNESS REQUIREMENTS

The Planetary Vehicle stiffness is considered adequate if the fundamental longitudinal and lateral fixed base frequencies of the primary structure are not less than 7 cps (with a design objective of 10 cps). Planetary Vehicle frequency requirements have been established from the Launch Vehicle control system requirements.

For components other than the high gain antenna, the minimum criteria is 35 cps in any direction in their boost phase (undeployed) attitudes. The antenna stowed (boost phase) configuration criteria is 20 cps.

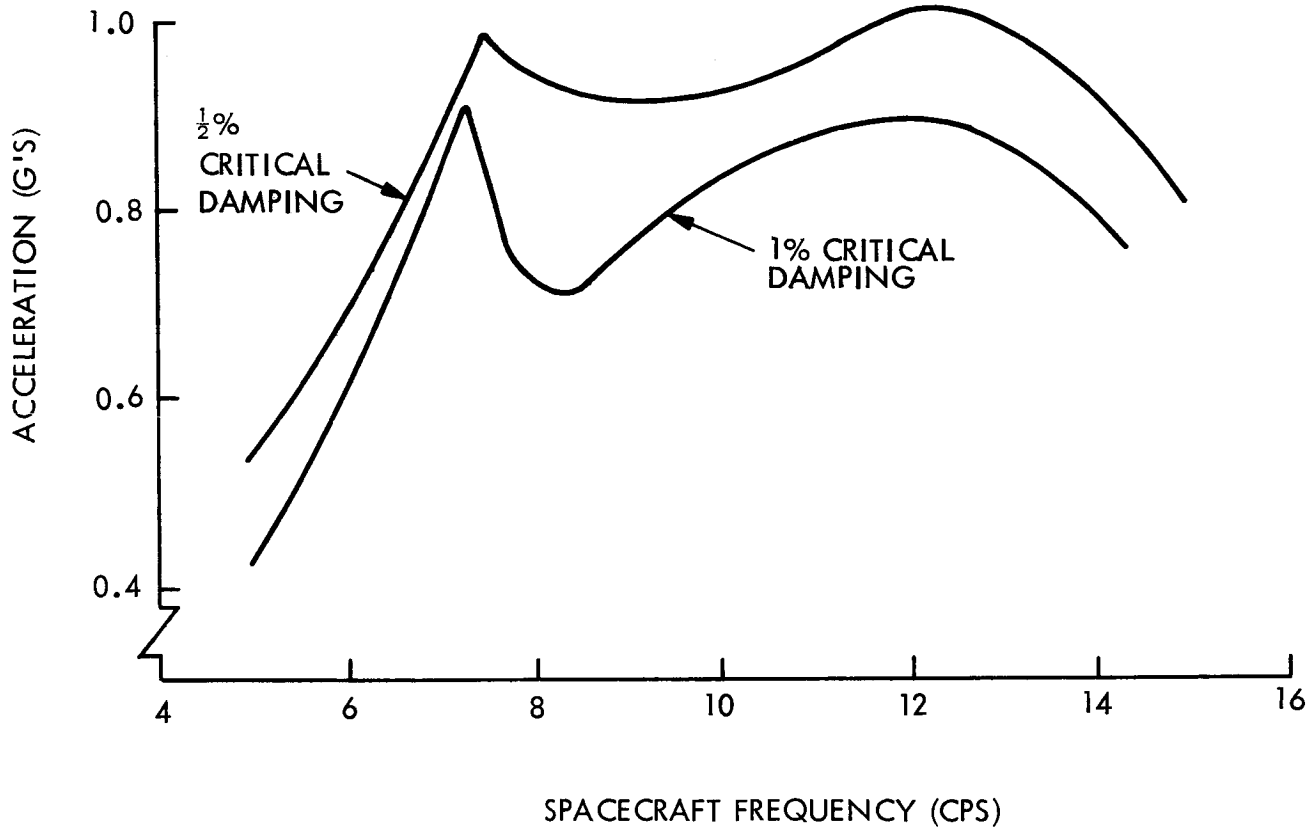

Figure 13. Variation of Planetary Vehicle Maximum Dynamic Load Factor with Spacecraft Frequency - S-IC Shutdown

Table 2. Secondary Structure Load Factors (Limit)

Phase	Longitudinal Load Factor (g)	Lateral Load Factor (g)
Boost	±20.	+10.
Orbit Insertion	±6.5	±3.0
Orbit Trim	±0.41	±0.10

NOTE: These lateral and longitudinal load factors are not simultaneously applied.

The fundamental cantilever frequency of deployed appendages (e.g., Medium Gain Antenna) is to be no less than 6 cps, with 10 cps a design objective. The high-gain antenna and PSP are excepted from this criteria; a 4 cps requirement is imposed on these appendage.

Separate frequency criteria have been imposed on the antenna and PSP by virtue of their size, and the weight penalties associated with imposing higher stiffness requirements. The 4 cps deployed, criteria has been established by auto-pilot requirements during interplanetary flight.

3.3 OTHER DESIGN ENVIRONMENTS

Additional design environments considered include acoustic fields, both internal and external to the shroud and equipment vibration spectra, induced by the vibro-acoustic field within the shroud. Acoustic environmental predictions were formulated utilizing an unsteady pressure definition on the shroud during hold-down, lift-off and the subsequent atmospheric flight, and the anticipated shroud configuration noise reduction. In each case a mean surface acoustic level was developed by averaging the local mean-square fluctuating pressures over the surface of the shroud. The individual planetary vehicle experiencing the more severe environment for the engine-generated and aerodynamically-induced sound pressure levels, was considered in order to determine realistic design environments consistent with the principal of spacecraft interchangeability. The predicted Voyager environmental overall acoustic time history is presented in Figure 14. The third-octave band acoustic levels at lift-off are shown in Figure 15.

The dynamic response of equipment support structure to this acoustic field inside the shroud, was also established. This provided: (1) estimates of equipment (random) vibro-acoustic design environments; (2) stiffener (panel breaker) positioning requirements and weights estimates for equipment support structure; and (3) secondary structure design loads data.

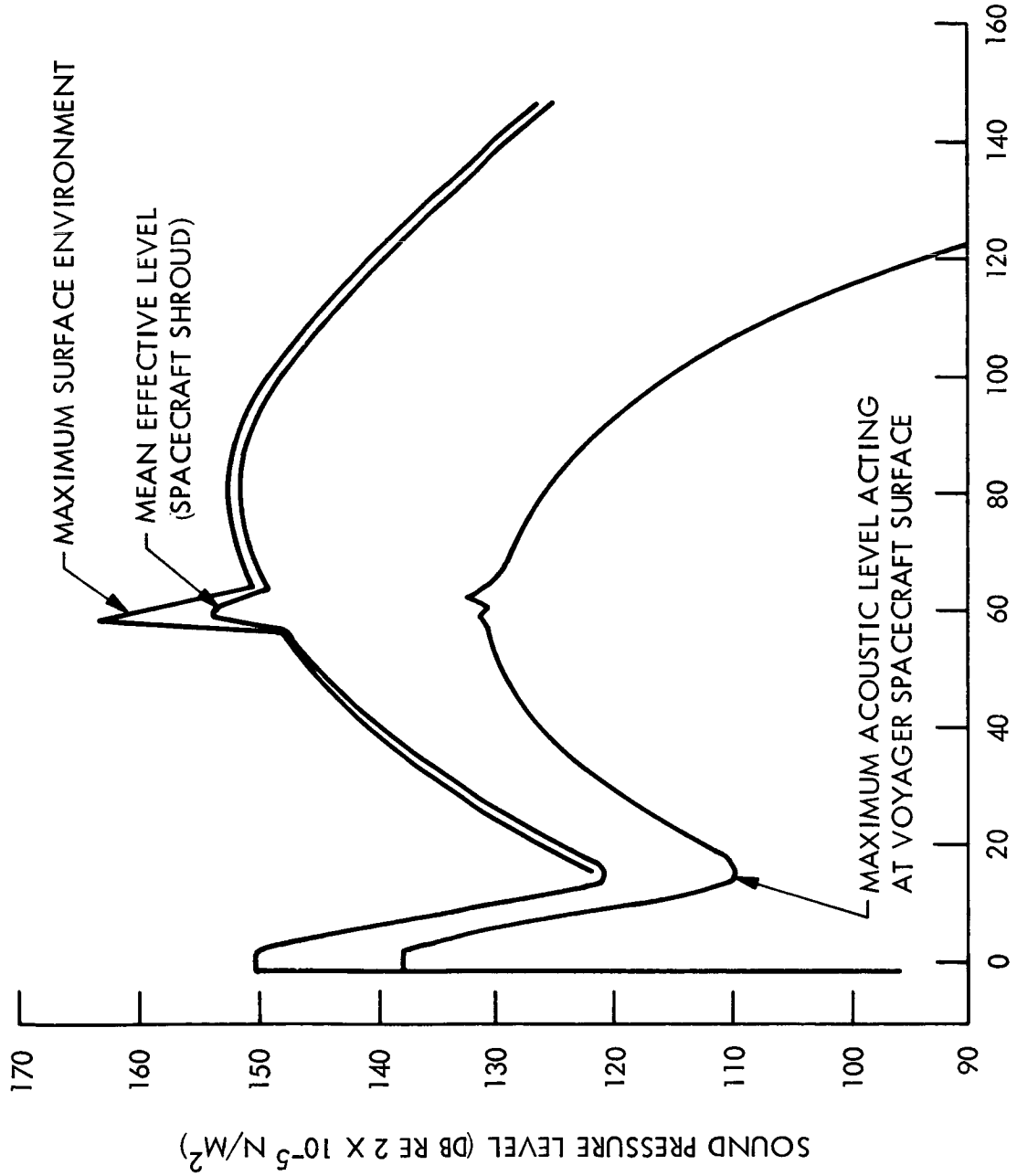

Figure 14. Voyager Environmental Overall Acoustic Time History

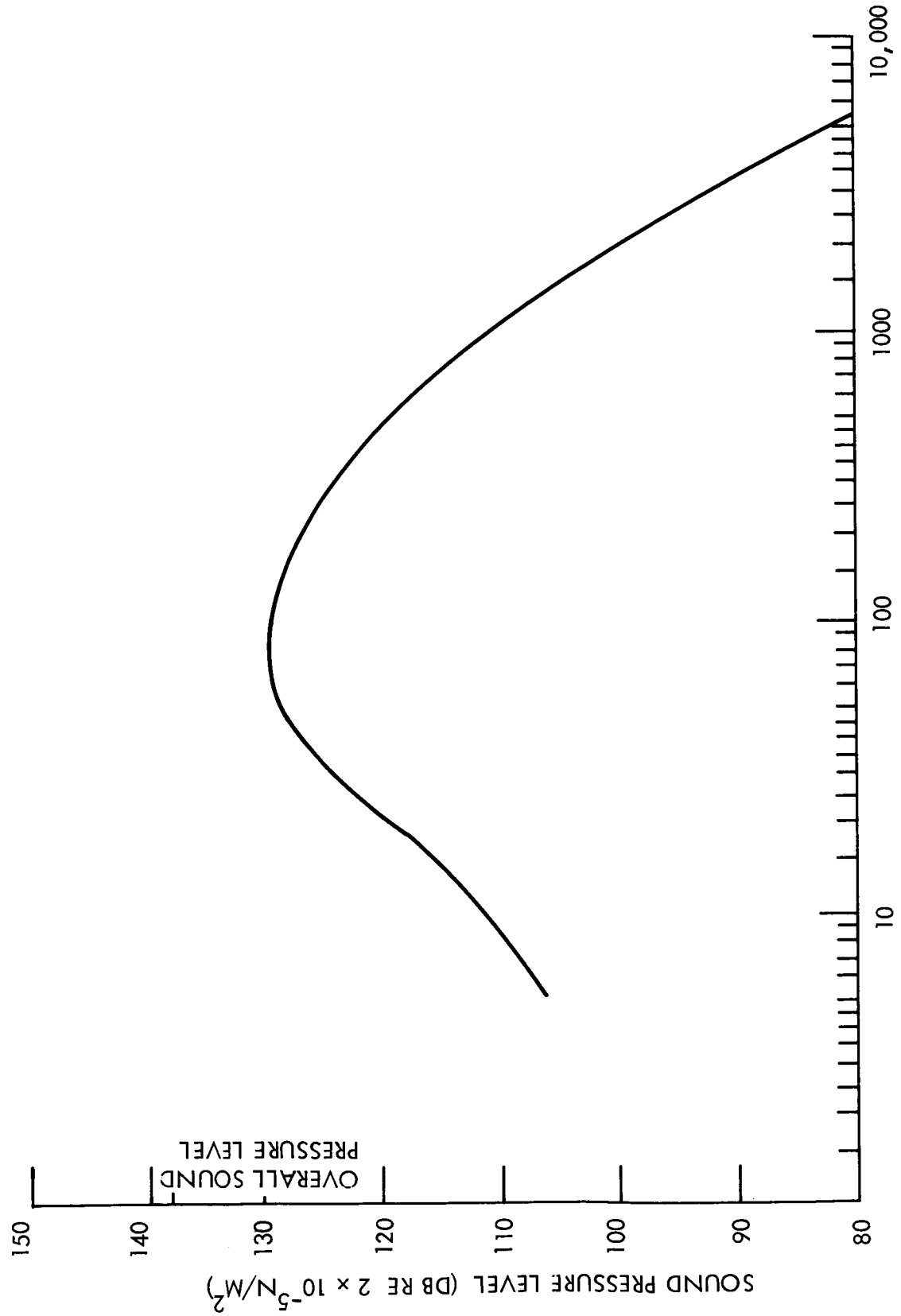

Figure 15. Anticipated One-third Octave Band Acoustic Levels at Voyager Spacecraft

3.4 DESIGN CRITERIA

The structural design criteria, can be briefly summarized by the following:

a. **The Planetary Vehicle shall possess sufficient strength and rigidity to survive design environments at a minimum expenditure of structural weight.**

b. **The structure shall neither yield under limit loads nor fail under ultimate loads.**

c. The spacecraft shall not deflect excessively.

d. The spacecraft shall not present a hazard to personnel.

e. The factors of safety of Table 3 shall apply:

Table 3. Factors of Safety

Structure			
Yield	1.10		
Ultimate	1.25		
Pressure Vessels	**Proof**	**Yield**	**Burst**
Propellant Tanks	1.50	1.65	2.0
Reservoirs, accumulators and pressurant tanks	1.50	1.65	2.0
Hydraulic and pneumatic equipment			
a) Flexible lines less than 1.5 inch diameter	2.0		4.0
b) Flexible line equal or greater than 1.5 inch diameter	1.5		2.5
c) Valves, switches, filters actuating cylinders	1.5		2.5

4. STRUCTURAL INTEGRITY

4.1 PRIMARY STRUCTURE

The structural integrity of all major items have been verified analytically. Primary structural elements are generally critical for the maximum boost acceleration condition with the exception of the inner shell longerons, the inner shell beaded panels, and the array panels which receive critical loading at launch release.

The structure associated with the electronic equipment module is sized from equipment mounting and thermal considerations. The overall stress levels relating to any of the loading conditions are low with high safety margins, even though sections are generally composed of minimum manufacturing gage elements.

Analytical models of the primary structure and electronic module are shown on Figures 16 and 17. Details of the structural sections, materials of construction, and margins of safety for the primary structure and the equipment module structure are presented in Table 4 and 5 respectively.

4.2 PROPULSION STRUCTURE

A structural schematic of the propulsion module is shown in Figure 18. In this figure, the tank support struts are represented by solid lines and the engine support struts are indicated by the dashed lines. In general, all tank support struts are designed by the maximum boost acceleration and all engine support struts are designed by retro motor burn loads.

Internal loads were obtained by use of a computer program and were verified by statics wherevere applicable. In statically indeterminate members, compatibility was assured.

The size of the mid-ring was dictated by stiffness requirements resulting from the 7 cps lateral planetary vehicle frequency criterion. This leads to relatively high margins of safety under load.

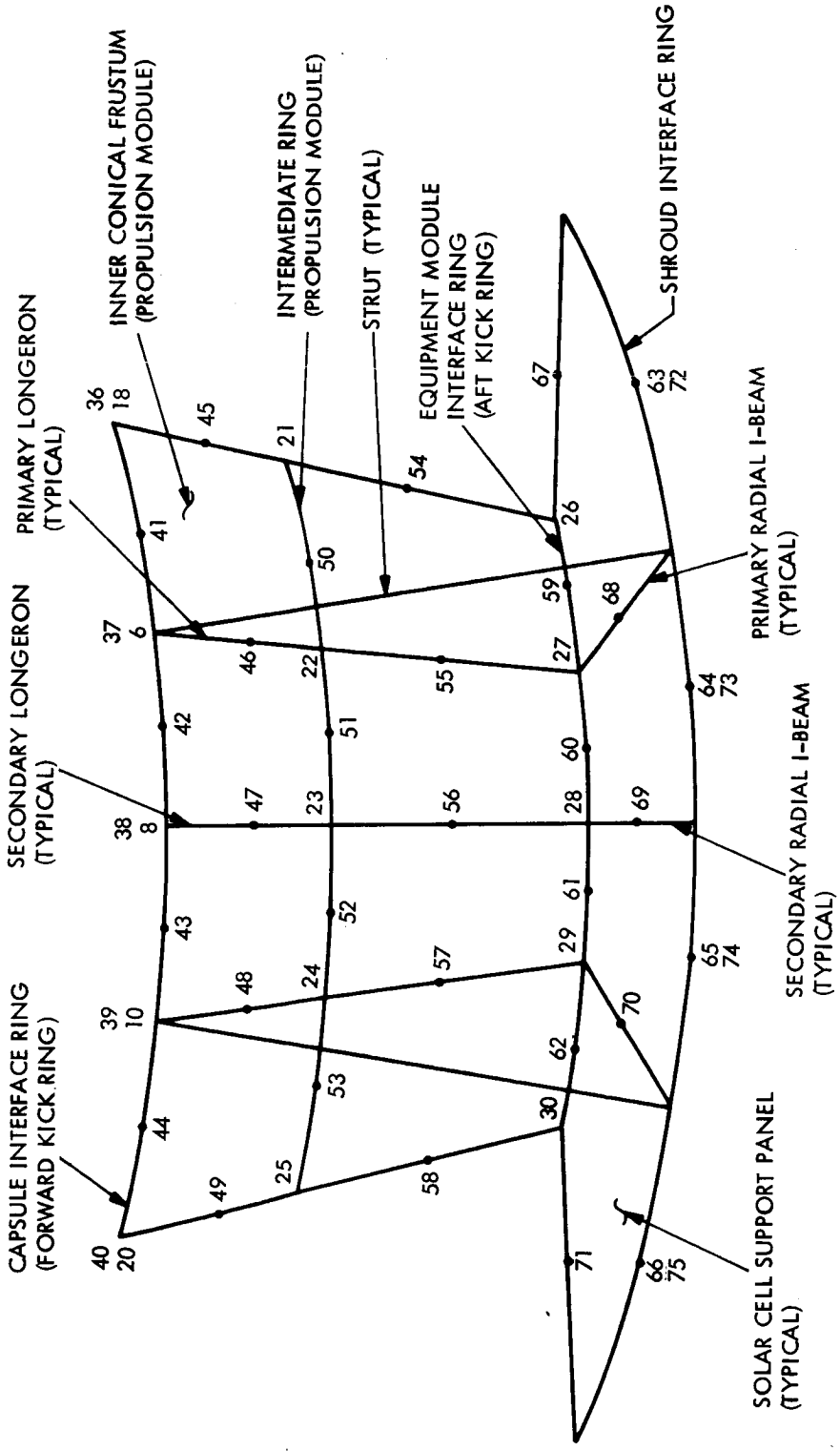

Figure 16. Analytical Model of Support Module

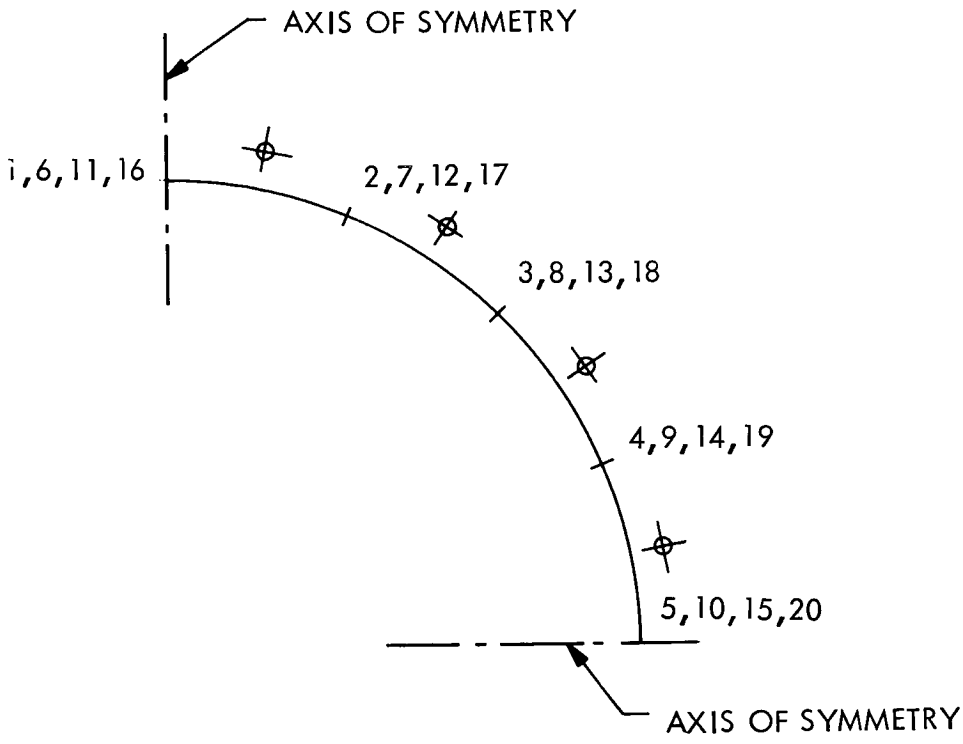

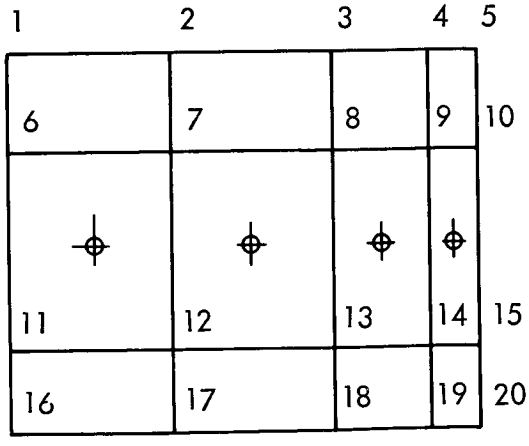

Figure 17. Analytical Model of Electronics Module

Table 4. Primary Structural Elements

Member	Material	Physical Geometry	Mode of Failure	Margin of Safety
Capsule Interface Ring	7075T6 Alum. Roll Forging	Modified I	Flange Crippling	+.09
Equipment Module Interface Ring	7075T6 Alum. Roll Forging	Modified [	Flange Crippling	+.07
Shroud Interface Ring	7075T6 Alum. Extruded Sections	Modified Z	Flange Crippling	High
Support Struts	2024T3 Alum.	3 1/4" O.D. X 0.058" W.T. Tubing	Buckling	+.04
Inner Cone Longerons	2024T4 Alum.	1.5" x 1.5" X .049" Hat Sections	Buckling	+.27
Inner Cone Skin Panels	2024T4 Alum.	0.032" thick Beaded @ Min. Spacing	Shear Buckling	+.04
Solar Array Radials	2024T4 Alum.	2" X 2" X .064" I Section	Tension	+.31
Solar Array Panels	Fiberglass Face Sheets - Alum. Core	Honeycomb Panel .017" thick face sheets .625" thick core	Shear Buckling	High

Table 5. Structural Elements of Electronic Module

Member	Material	Physical Geometry	Mode of Failure	Margin of Safety
Upper equip bay ring segment (16)	Aluminum 7075-T6	Channel t = 0.040 in.	Flange crippling	High
Lower equip bay ring segment (16)	Aluminum 7075-T6	Channel t = 0.040 in.	Flange crippling	High
Lower ring segment (16)	Aluminum 7075-T6	Angle t = 0.040 in.	Flange crippling	High
Longeron (16)	ZK60A-T5 magnesium	Box beam t = 0.040 in.	Flange crippling	High
Shear panel (16)	HM 21A-T8 magnesium	0.025 in. sheet	Shear buckling	High
Thermal panel (16)	HM 21A-T8 magnesium	0.065 in. sheet	Shear buckling	High
Shear panel (16)	HM 21A-T8 magnesium	0.025 in. sheet	Shear buckling	High

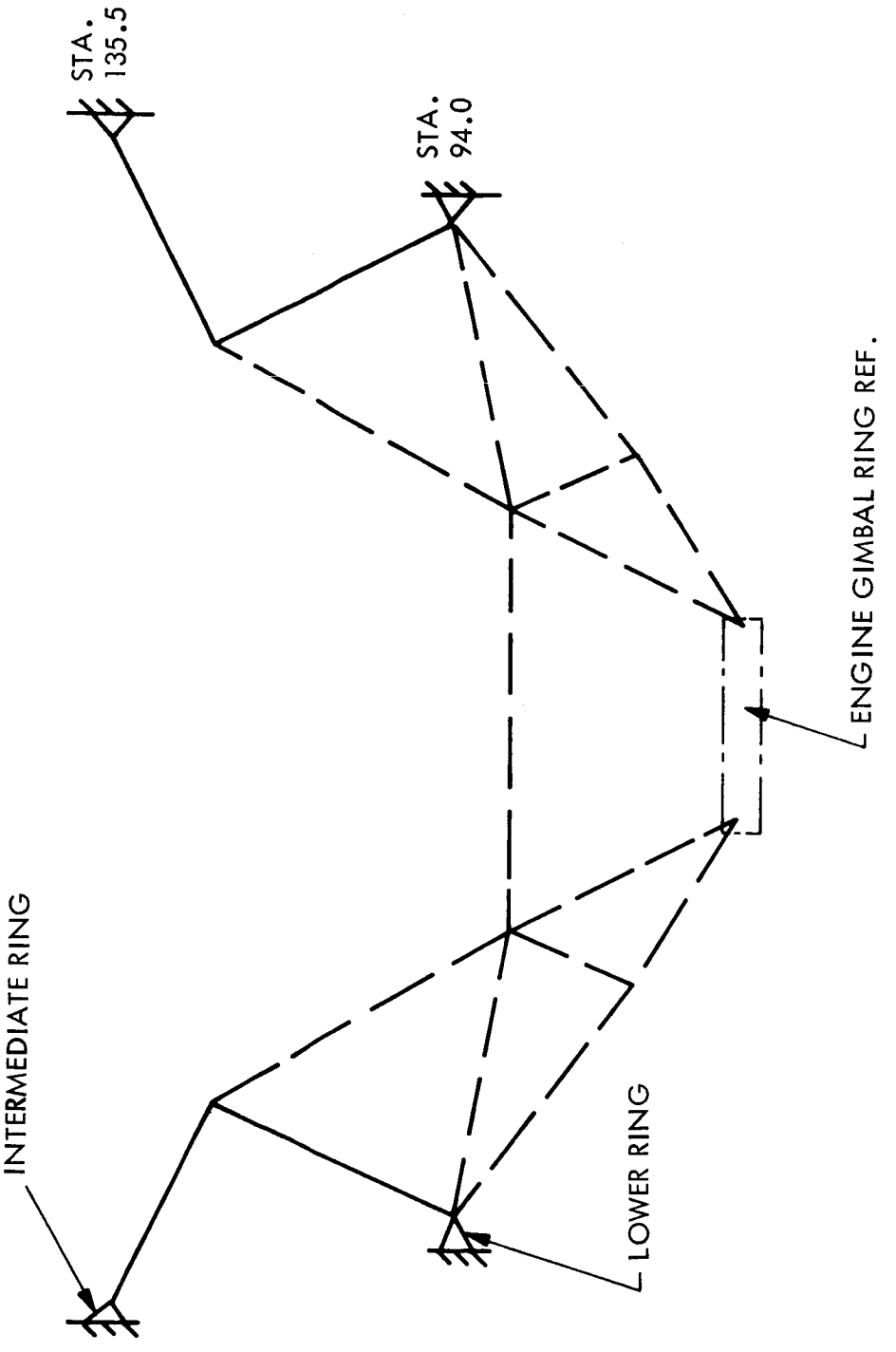

Figure 18. Structural Schematic of the Propulsion Module

All struts were analyzed for tension, crippling, and column buckling. While some margins of safety seem high, it is noted that only tubes of standard sizes were considered and a slight decrease in stiffness and/or area of any strut results only in a small decrease in weight, while indicating a highly efficient member. Thus, from an optimization viewpoint, the margins of safety are considered satisfactory although they may appear high.

Figures 19 and 20 show the geometry of the propulsion module support structure. The results of the structural analysis are displayed in Table 6.

4.3 APPENDAGES

Strength and stiffness analyses were also performed on the planet scan platform, deployable solar panels and high gain antenna.

A 10-foot antenna was subjected to detailed analyses to evolve an arrangement capable of meeting its frequency criterion (4.5 cps). This parabolic dish (Figure 21) is constructed of three rings, 6 meridional members, a feed tripod, and a mesh (covering the ribs and webs). An arrangement utilizing 2" O.D. aluminum tubing was synthesized. This array weighs 38.7 pounds, of which 7.6 pounds is allocated to the mesh. Structural elements of the antenna illustrated in Figure 24, are described in Table 7. (Note: A 9.5 ft Dia antenna was used in the final design.)

Thermal distortion and thermal stress analyses were also performed on the antenna and solar cell support structure to verify that mission temperature gradients did not produce adverse effects. Margins under the anticipated thermal profile are high.

5. MICROMETEOROID PROTECTION

5.1 INTRODUCTION

This section discusses the philosophy and application of micrometeoroid protection to the Voyager Mars missions. Work done during this system update study has been concentrated

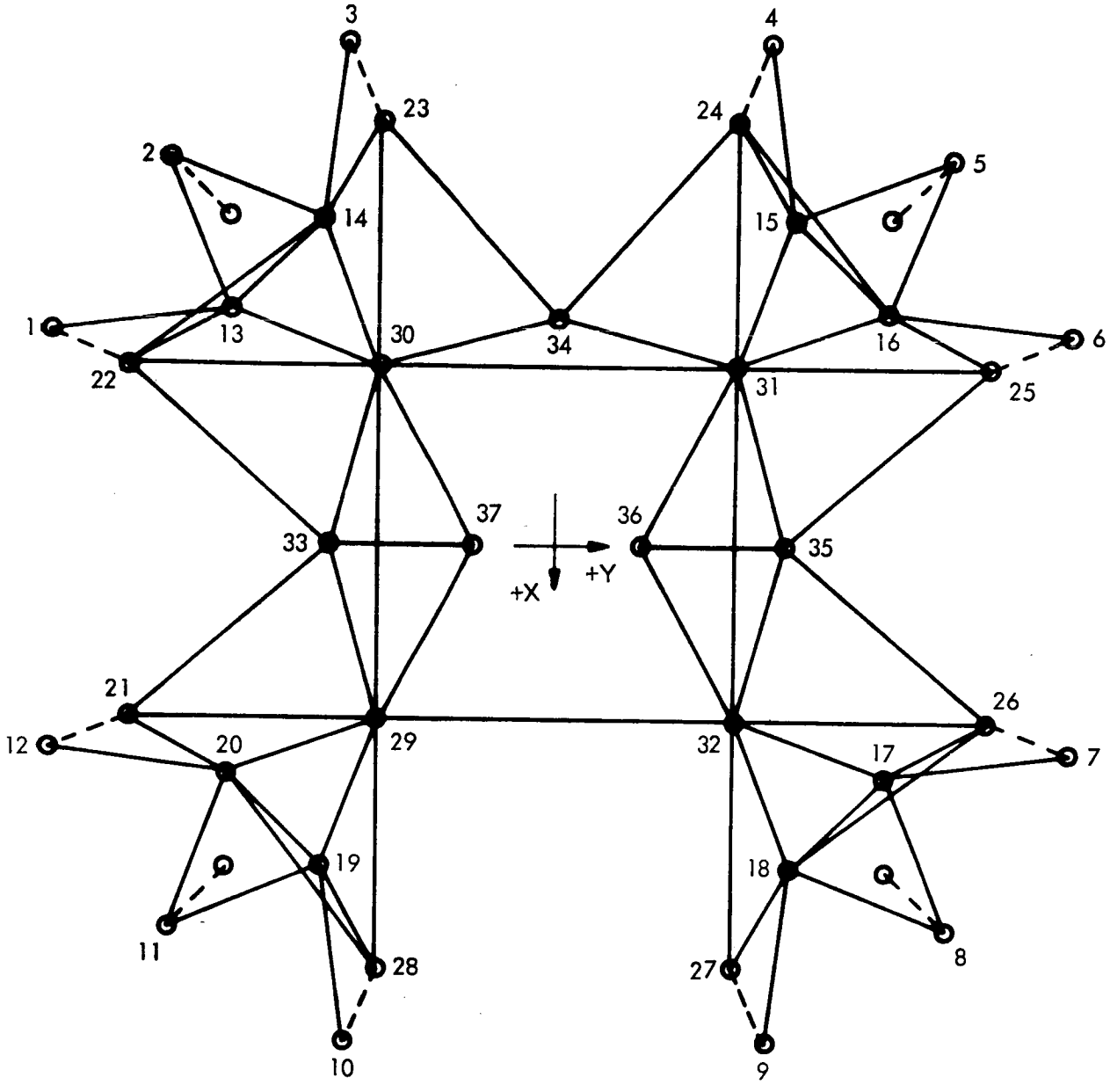

NODES 1-12 LOCATED ON INTERMEDIATE RING STA. 135.5
NODES 13-20 FUEL & OXYGEN TANK TRUNNION POINTS STA. 121
NODES 21-28 LOCATED ON LOWER RING STA. 94
NODES 29-32 INTERSECTION OF CROSS STRUTS STA. 89
NODES 33-35 ACTUATOR REACTION POINTS STA. 74
NODES 36-37 ENGINE GIMBAL POINTS STA. 62

Figure 19. Propulsion Tank and Engine Support Structure

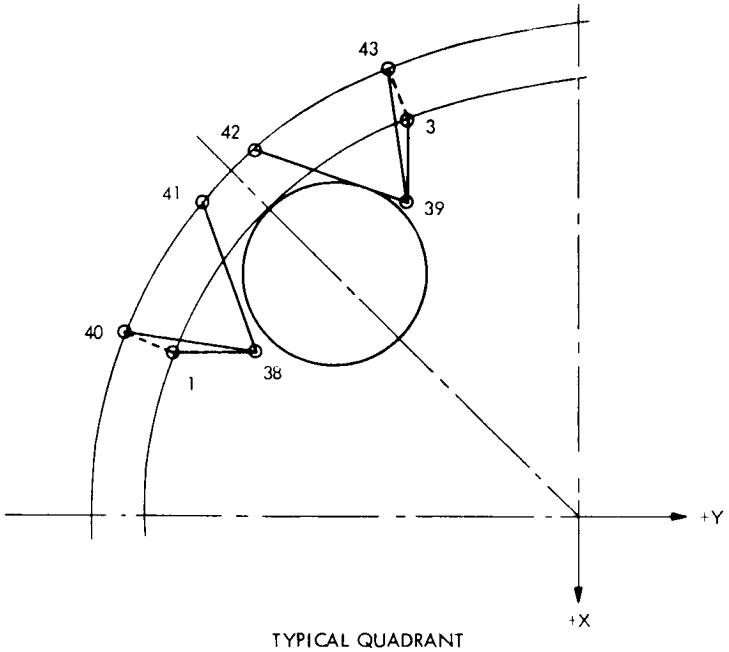

Figure 20. Pressure Tank Support Structure

on development of protection criteria and a review of penetration mechanics. The major conclusion of this study is that large, and possibly unwarranted weight penalties may be incurred for micrometeoroid protection, unless careful consideration is given to the following:

a. Selection of a "Probability of Zero Penetrations." The weight required to achieve higher than optimum values could be more effectively applied to improve the probability of mission success, or "mission worth" through added redundancy, improved capability, etc.

b. Penetration Mechanics. Further studies are required to reduce the wide differences between alternate micrometeoroid penetration criteria in current use. A first effort in this direction based on analytical studies of hypervelocity particle impact into a double bumper system, is presented. Unfortunately, currently available experimental data is insufficient to validate this analysis, or to resolve the differences discussed above. More experiments are highly desirable. Such

Table 6. Propulsion Module Support Structure

Members (See Figures)	Weight (lbs.)	Material	Physical Geometry	Structural Description	Mode of Failure	Margin of Safety
14-23, 20-21, 18-27, 16-25	5.6	↑	2 1/4" O.D. x 1/16" wall	↑	Cripp-ling	+ .19
14-3, 20-12, 18-9, 16-6	1.7		1 1/2" O.D. x 1/32" wall		Tension	+ .28
14-2, 20-11, 18-8, 16-5	3.1		1 1/2" O.D. x 1/16" wall		Cripp-ling	+ .33
14-22, 20-28, 18-26, 16-24	7.5		2 1/4" O.D. x 1/16" wall		Buck-ling	+ .45
13-1, 19-10, 17-7, 15-4	3.9		1 3/4" O.D. x 1/16" wall	Propulsion Tank Support	Tension	+ .26
13-2, 19-11, 17-8, 15-5	1.6		1 1/2" O.D. x 1/32" wall		Cripp-ling	+ .55
13-22, 19-28, 17-26, 15-24	8.3		1 3/4" O.D. x 1/8" wall		Cripp-ling	+ .52
14-13, 20-19, 18-17, 16-15	2.0		1 1/2" O.D. x 1/16" wall		Cripp-ling	+ .53
14-30, 13-30, 20-29, 19-29, 18-32, 17-32, 15-31	10.4	6061-T6 Alum.	1 3/4" O.D. x 1/16" wall	↓	Buck-ling	+ .33
38-41, 39-42 (4 places)	2.5		1" O.D. x 1/32" wall	↑	Buck-ling	+ .98
38-40, 39-43 (4 places)	2.3		1" O.D. x 1/32" wall	Helium Tank Support	Buck-ling	+ .52
38-1, 39-3 (4 places)	1.6		1" O.D. x 1/32" wall	↓	Buck-ling	+1.35
37-33, 36-35	1.2		1 1/4" O.D. x 1/16" wall	Engine Support	Buck-ling	+ .33
37-30, 37-29, 36-31, 36-32	5.8		2" O.D. x 1/16" wall	Engine Support	Tension	+ .79
33-29, 33-30, 34-30, 34-31, 35-31, 35-32	2.1		1 1/4" O.D. x 1/32" wall	Actuator Reaction	Buck-ling	+ .82
33-21, 33-22, 34-23, 34-24, 35-25, 35-26	4.4		1 3/4" O.D. x 1/32" wall	Actuator Reaction	Tension	+ .44
30-22, 30-23, 31-24, 31-25, 32-26, 32-27, 29-28, 29-21, 30-31 31-32, 32-29, 29-30	20.0	↓	2" Sq. Tube .049" wall	Engine Support	Cripp-ling	+1.54
Fittings	61.0	——	——	Strut, Trunnion, and Ring Fittings	——	——

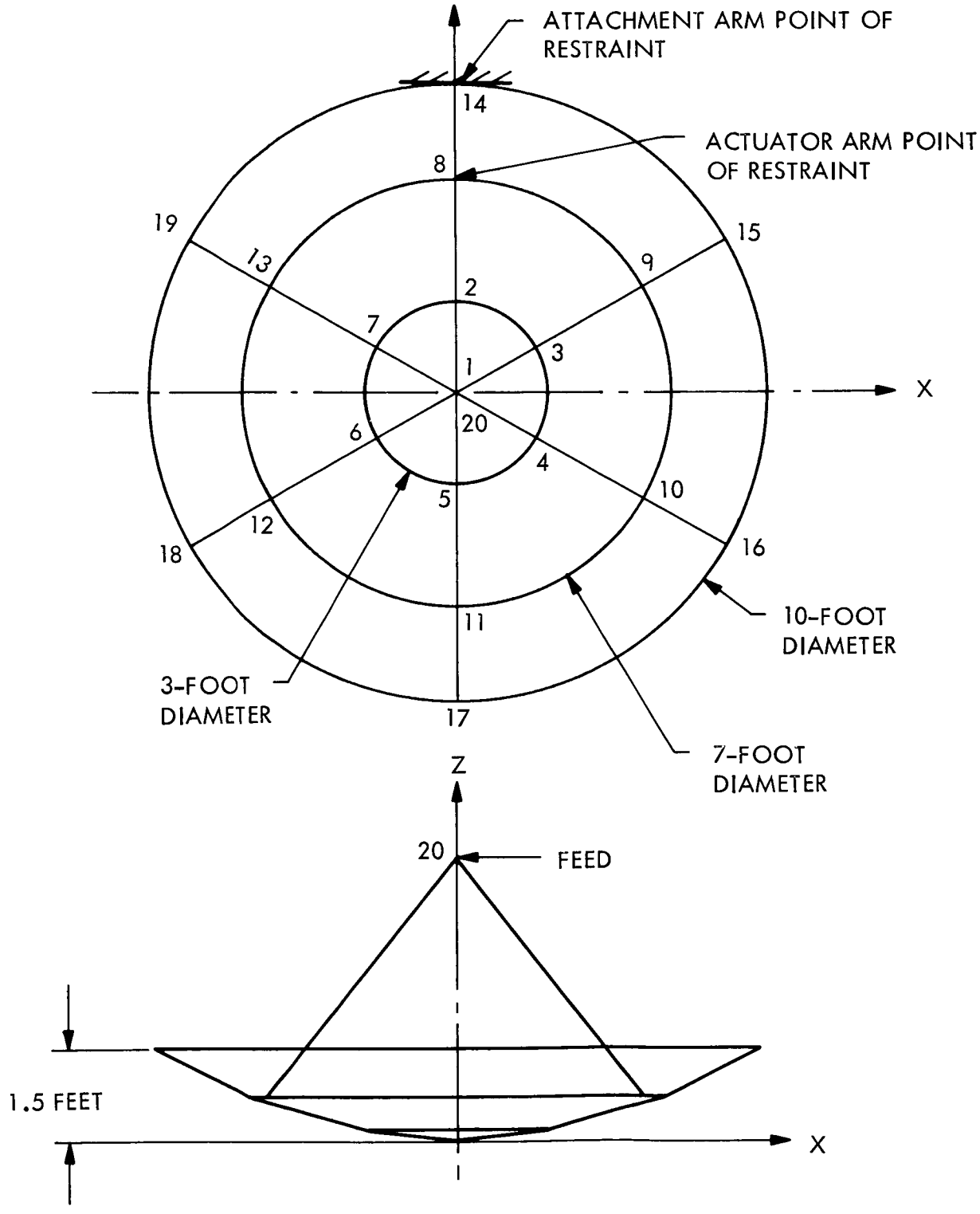

Figure 21. High Gain Antenna Analytical Model

Table 7. Structural Elements of High-Gain Antenna

Member	Material	Weight (lb)	Physical Geometry	Mode of Failure	Margin of Safety*
Radial Ribs (6) 1-2, 1-3, 1-4, 1-5, 1-6, 1-7	Aluminum 6061-T6	2.34	Tubing 2 in. Diameter 0.035 in. wall	Bending	High
Radial Rib (1) 2-8	Aluminum 6061-T6	0.99	Tubing 2 in. Dia. x 0.035 in. wall	Bending	High
Radial Ribs (5) 3-9, 4-10, 5-11, 6-12, 7-13	Aluminum 6061-T6	2.70	Tubing 2 in. Dia. x 0.035 in. wall	Bending	High
Radial Rib (1) 8-14	Aluminum 6061-T6	1.01	Tubing 2 in. Dia. x 0.083 in. wall	Bending	High
Radial Ribs (5) 9-15, 10-16, 11-17, 12-18, 13-17	Aluminum 6061-T6	2.20	Tubing 2 in. Dia. x 0.035 in. wall	Bending	High
Inner Ring Segments (6) 2-3, 3-4, 4-5, 5-6, 6-7, 7-2	Aluminum 6061-T6	2.46	Tubing 2 in. Dia. x 0.035 in. wall	Bending	High
Middle Ring Segments (6) 8-9, 9-10, 10-11, 11-12, 12-13, 13-8	Aluminum 6061-T6	5.70	Tubing 2 in. Dia. x 0.035 in. wall	Bending	High
Outer Ring Segments (2) 14-15, 19-14	Aluminum 6061-T6	1.44	Tubing 2 in. Dia. x 0.058 in. wall	Bending	High
Outer Ring Segments (4) 15-16, 16-17, 17-18, 18-19	Aluminum 6061-T6	5.44	Tubing 2 in. Dia. x 0.035 in. wall	Bending	High
Speed Tripod Struts (8) 12-20, 10-20, 8-20	Aluminum 6061-T6	3.81	Tubing 2 in. Dia. x 0.035 in. wall	Bending	High
Mesh	Aluminum 6061-T6	7.59	Wire 1/32 in. Dia. x 1/4 in. spacing	Distortion (Deflection Exceeding One Wave Length)	High

*Sizing of structural members was dictated by frequency rather than stress consideration.

experiments simulate the mechanism of particle impact through a double wall target, including the change of state caused by the energy of penetration. This requires higher velocities than currently achieved in light gas gun facilities or the use of low melting point materials.

c. Effect of Configuration. In the baseline configuration a large portion of the vulnerable spacecraft surface is partially protected by the solar array and the capsule. Direct impacts on the propulsion module skin are restricted to an angular zone of 70^{o} to 120^{o} from the longitudinal axis.

In addition to the considerations of mission success, micrometeoroid penetration must be considered in terms of the quarantine requirement. Contamination of the planet due to an explosion caused by micrometeoroid penetration of a pressurized tank must be prevented.

5.2 PROTECTION CRITERIA

The amount of micrometeoroid protection required for Voyager depends on two major factors:

a. Mission success

b. Quarantine: Preventing contamination of the planet due to an explosion caused by micrometeoroid penetration of a pressurized tank.

5.2.1 Mission Worth Considerations

Achieving valuable mission outcomes, i.e., a high mission expected worth (Ref. 5.1) required that the entire spacecraft have high dependability (reliability), capability and availability. One method of improving the dependability of the spacecraft is by preventing a micrometeoroid from "hitting" the fuel or oxidizer tanks of the propulsion module. Other methods of improving the spacecraft include:

a. Improved reliability through functional and block redundancy, (Ref. 5.1).

b. Improved capability through increased system performance. (Reduced maneuver errors, improved engine transients, reduced receiver noise levels, etc.).

c. Improved availability of the spacecraft on the launch pad (good operational procedures, easy access to the fuel lines, etc.).

Improvement of the mission expected worth through higher dependability (reliability), capability and availability generally requires some expenditure of important spacecraft commodities (weight, power, etc.).

Micrometeoroid protection involves the expenditure of weight. This increase in weight can be expended in

a. Increasing the thickness of the main structural skin.

b. The introduction of a whipple bumper which generally is more effective.

c. The addition of aluminum foil as outer layers of a thermal blanket mounted outside the structural skin.

This last method minimizes the bumper support weight and simplifies assembly.

Other means of improving the mission expected worth should be compared with the micrometeoroid protection on a weight basis. The Task C redundancy model provides a means to the selection of the proper amount of micrometeoroid protection required to improve the expected mission worth. Providing alternate designs with respective weights and improvements in spacecraft reliability to the Task C Redundancy Model (Ref. 5.1), the model's optimization procedures will select the optimum amount of micrometeoroid protection.

Figure 22 illustrates a typical plot of mission expected worth versus system weight obtained during the Task C Redundancy Study. The dashed curve indicates the mission expected worth versus the weight of the system if all weight is applied to micrometeoroid protection above what is normally provided by the suggested design. Notice that available weight should not be expended in micrometeoroid protection until a substantial amount of redundancy has been applied elsewhere.

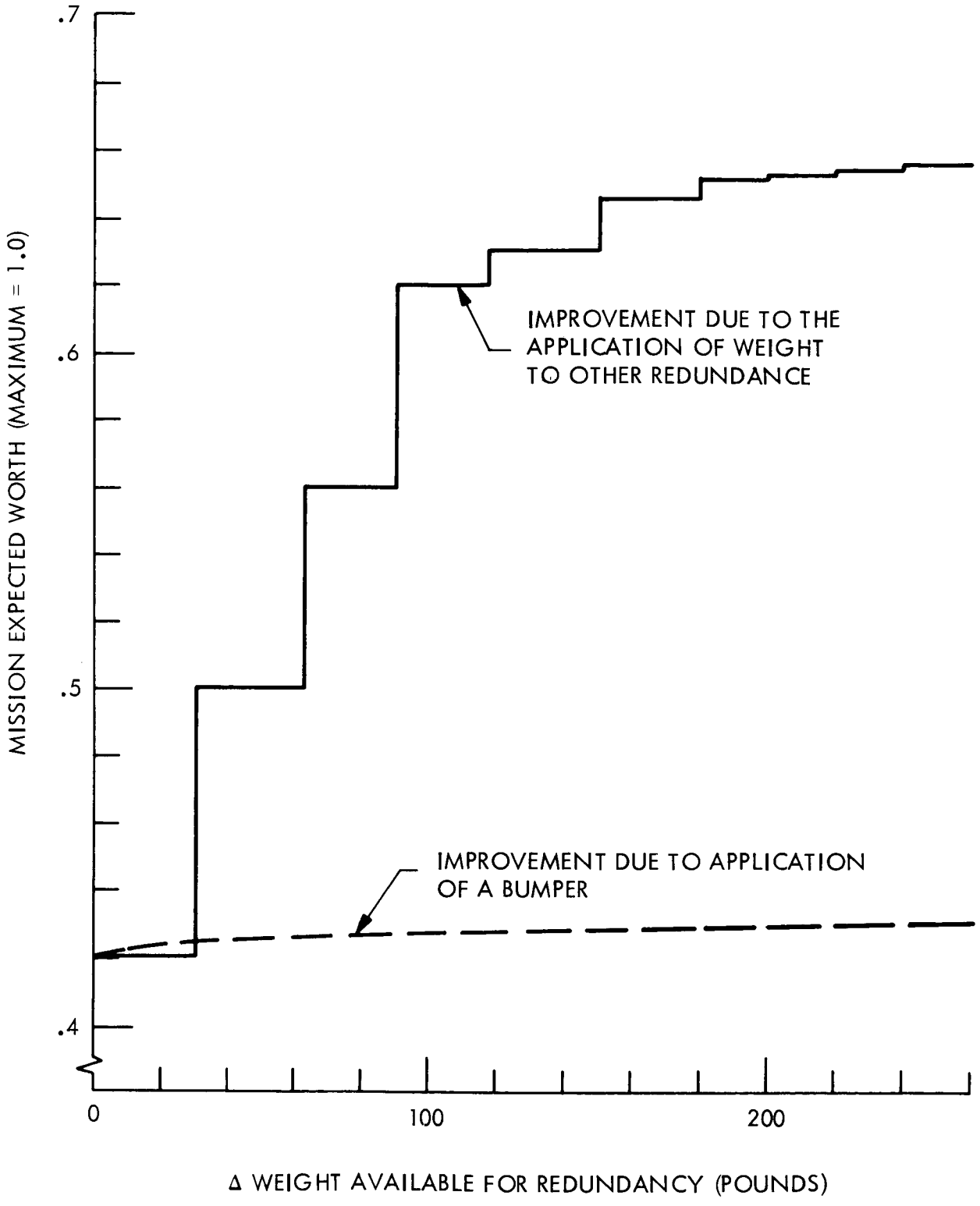

Figure 22. Mission Expected Worth vs. Δ Weight as Applied to Redundancy

5.2.2 Quarantine Considerations

Preventing the contamination of the planet requires that the micrometeoroid protection keep the probability of contamination due to an explosion within safe limits. The basic requirement in the planetary quarantine plan for the Voyager Project (Ref. 5.2) is that the probability of contamination of Mars from a single spacecraft, its ejecta, or its portion of the launch vehicle shall not exceed 3×10^{-5}. This allocation has been apportioned in the Quarantine Study (Ref. 5.3) with a probability of 5×10^{-6} to special spacecraft hardware cases, such as explosions, spin up, debris from separation hardware, instrument covers, and nozzle inserts and ablative liners. The largest potential design problems are in the area of reducing the probability of contamination due to an explosion, therefore, an assignment of 4×10^{-6} to this source is desirable.

The parameters associated with determining the probability of contamination due to an explosion is dependent upon the following factors:

a. Mission Phase - The orbiting phase is the most critical to the problem of quarantine, an explosion in orbit would most certainly contaminate the planet. However, the release of some of the pressuring gas in the propulsion system after orbit insertion will reduce the probability of an explosion. This procedure effectively eliminates the problem in orbit (Ref. 5.4). The heliocentric phase of the mission is also critical to the problem of quarantine and an explosion when near to encounter, will provide a means to contaminate the planet. In this phase of the mission, the remaining factors are important in determining the required amount of micrometeoroid protection.

b. Orbit Mechanics - Orbit mechanics to determine if pieces get to Mars is of prime importance. The problem of orbit mechanics is characterized by the M/C_dA and velocity distributions of the ejected pieces. Another important parameter is the angle of ejection. An explosion before orbit insertion implies that the capsule will be on the spacecraft, and depending upon whether the capsule also explodes or not, the ejecta will be constrained in the direction it can take.

c. Entry heating will become an important factor since the ejected pieces will be traveling at hyperbolic orbit velocities. This speed will tend to decrease the chance that viable organisms will survive.

d. Since the ejecta from the explosion will be given a complex motion, high energy radiations will directly affect the survival of the viable organisms on the ejecta.

e. The initial bioburden at the time of the explosion and the probability of the viable organisms surviving the explosion will also affect the probability of contaminating the planet.

A preliminary investigation of the probability of contamination from an explosion during the time period 11 days before encounter was conducted by analogy with the attitude control gas source presented in the Quarantine Study (Ref. 5.3). Although the ejection velocity and M/C_dA distributions were not correct, the investigation indicated that a low (0.001 to 0.1) probability of contamination given an explosion is possible.

The probability of one or more penetrations of the outer skin during the 11 days before encounter is approximately 0.003 (Table 11). Additional tank protection is afforded by the spacing between outer skin and the tanks themselves, the increased size and velocity of particles necessary to produce a tank "flaw" sufficient to induce a brittle rupture, and the fact that near Mars the tank temperature and therefore internal pressures are at reduced values. Also in the event that a tank rupture occurs in such a manner to cause other tanks to rupture and produce conditions favorable for an explosion, very high temperatures will result. Such high temperatures will have a sterilizing effect. A probability factor of 0.1 associated with these factors has been assumed, so that the probability of contamination lies between 3×10^{-7} and 3×10^{-5}. Careful study is required to remove the uncertainty and establish the amount of micrometeoroid protection required.

The final amount of micrometeoroid protection required will therefore depend upon the complete understanding of the probability of contamination and the expected mission worth.

5.3 PENETRATION MECHANICS

During Task D, a review of penetration mechanics was conducted and preliminary estimates of the probability of zero penetrations were made. These analyses were dependent upon the following parameters:

a. The penetration criteria was found to be a very sensitive parameter.

b. The spacecraft configuration is also a very important parameter since the critical areas will be limited due to the placement of solar arrays and the location of the propulsion tanks.

c. The micrometeoroid flux and velocity distribution are the parameters which describe the environment to be encountered and are important in obtaining an accurate estimate of the probability of zero penetrations.

d. In addition to penetration of the spacecraft wall the capability of the tanks themselves to withstand impact is dependent on the material properties, stress conditions and proximity to the spacecraft wall.

5.3.1 Comparison Between Penetration Criteria

A detailed comparison between four penetration criteria has been made in Reference 5.8. In order of optimism, they are listed in Table 8.

Table 8. Penetration Criteria

Criterion	Type	Remarks
NASA Langley (Ref. 5.9)	Double-bumper system	Theoretical. Probably too optimistic.
NASA Houston (Ref. 5.10)	Can be used for double-bumper systems	A variant of Charters and Summers' Equation derived semi-empirically from relatively low-velocity tests into semi-infinite targets.
Herrmann and Jones	Single Sheet	Developed for semi-infinite targets. Extended to single sheets.
Brown Engineering (Ref. 5.11)	Single Sheet	Developed from single-sheet impact experiments conducted at NASA Ames.

A detailed numerical study of the impact of a hyper-velocity particle into a double bumper system has been made by Woodall and Riney at General Electric Company. The study used the hydrodynamic computer code known as VISTA for the front sheet impact, and a structural computer code (DEPROSS) to calculate the response of the rear sheet to the impulsive

loads transmitted by the debris from the front sheet. A preliminary numerical calculation produced a curve of maximum strain in the rear plate versus its thickness for a given target and impacting particle. The curve is shown in Figure 23. In addition, results of an experimental study on thin plate fracture under impulsive concentrated loads conducted by Lockheed (Ref. 5.13) are shown. The type of loading is very similar to that experienced by the rear plate. The curves denote the strain-to-failure of plates of various thicknesses. The intersection of the theoretical and experimental curves give a rough idea of the thickness of the rear plate that would have withstood the impact of the particle used in the theoretical study. The criteria of NASA Langley and NASA Houston fall to either side of this prediction. Thus, on the basis of these preliminary results, it can be said that a micrometeoroid shield should be chosen that falls between the predictions of NASA Langley and NASA Houston.

5.3.2 Spacecraft Configuration

Table 9 gives the areas of spacecraft which are important to protect. The angles given in the table are the available impact angles of micrometeoroids upon the area of the spacecraft. These restrictions in angles effectively reduce the area of the spacecraft which is subject to micrometeoroid hits, because the normal component of the micrometeoroid velocity relative to the surface determines the depth of penetration.

5.3.3 The Micrometeoroid Environment

Meteoroids may be divided into three broad categories: those which have unknown orbits and origin, those associated with meteoroid streams of known orbit, and those of asteroidal origin. The three types are known as sporadic meteoroids, stream meteoroids, and asteroidal debris. Observations indicate that the flux of sporadic meteoroids is fairly constant in time, but that of the stream meteoroids may vary greatly according to which meteoroid stream is being crossed. Some estimates of the velocity and density of micrometeoroids have been made. Figure 24 shows the distribution of geocentric velocity and of micrometeoroid density (from References 5.5 and 5.6).

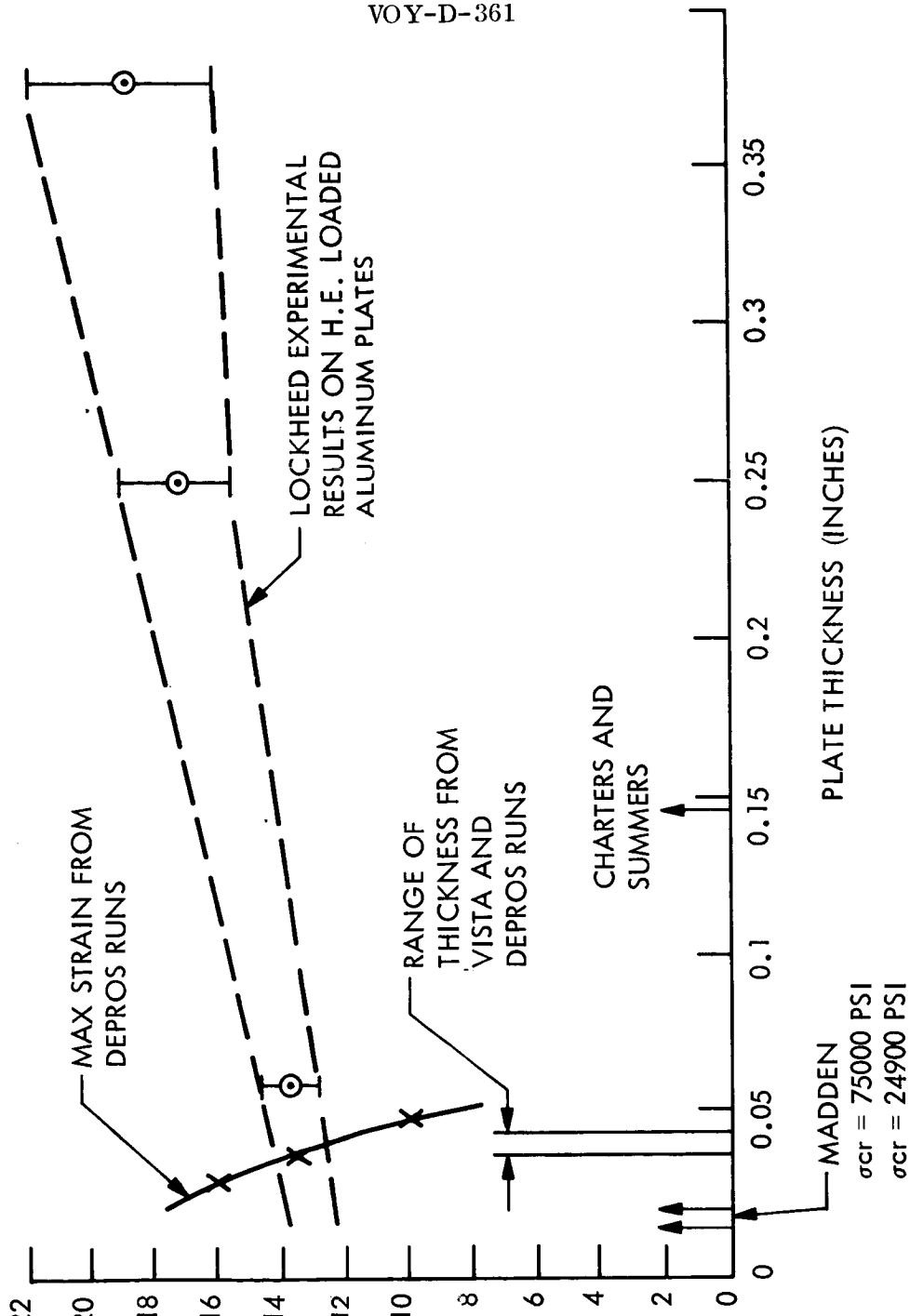

Figure 23. Comparison of Penetration Criteria

Table 9. Area of Spacecraft to be Analyzed

Description	Area (in.^{2})	α (Deg) Min $\leq \alpha \leq$ Max
Skin of the Propulsion Module (A_1)	34,100	$70^o \leq \alpha \leq 120^o$
Skin of the portion of the Electronics Module above the Thermal Control Shutters (A_2)	3,862.5	$0^o \leq \alpha \leq 70^o$
Aft end of the electronics module excluding the thrust nozzle opening (A_3)	6,780	$25^o \leq \alpha \leq 125^o$
Aft biobarrier either on or off (A_4)	24,000	$2^o \leq \alpha \leq 178^o$

The environment is described by a flux equation which gives N, the number of particles per square meter per second of mass M grams or greater.

$$N = 10^{C_1 M^{C_2}} \tag{1}$$

Table 10 gives the JPL micrometeoroid environment for various portions of the Mars mission. Using the table's values for minimum and maximum flux, and if we assume this as covering 95 percent of the cases, then the equation for the flux is described by guassian distribution of the variables C_1 and C_2.

$$C_1 = G(-14.14, .114) \tag{2}$$

$$C_2 = G(-1.17, .0574) \tag{3}$$

Where the notation $G(M, \sigma)$ describes a gaussian distribution with mean, M, and a standard deviation σ.

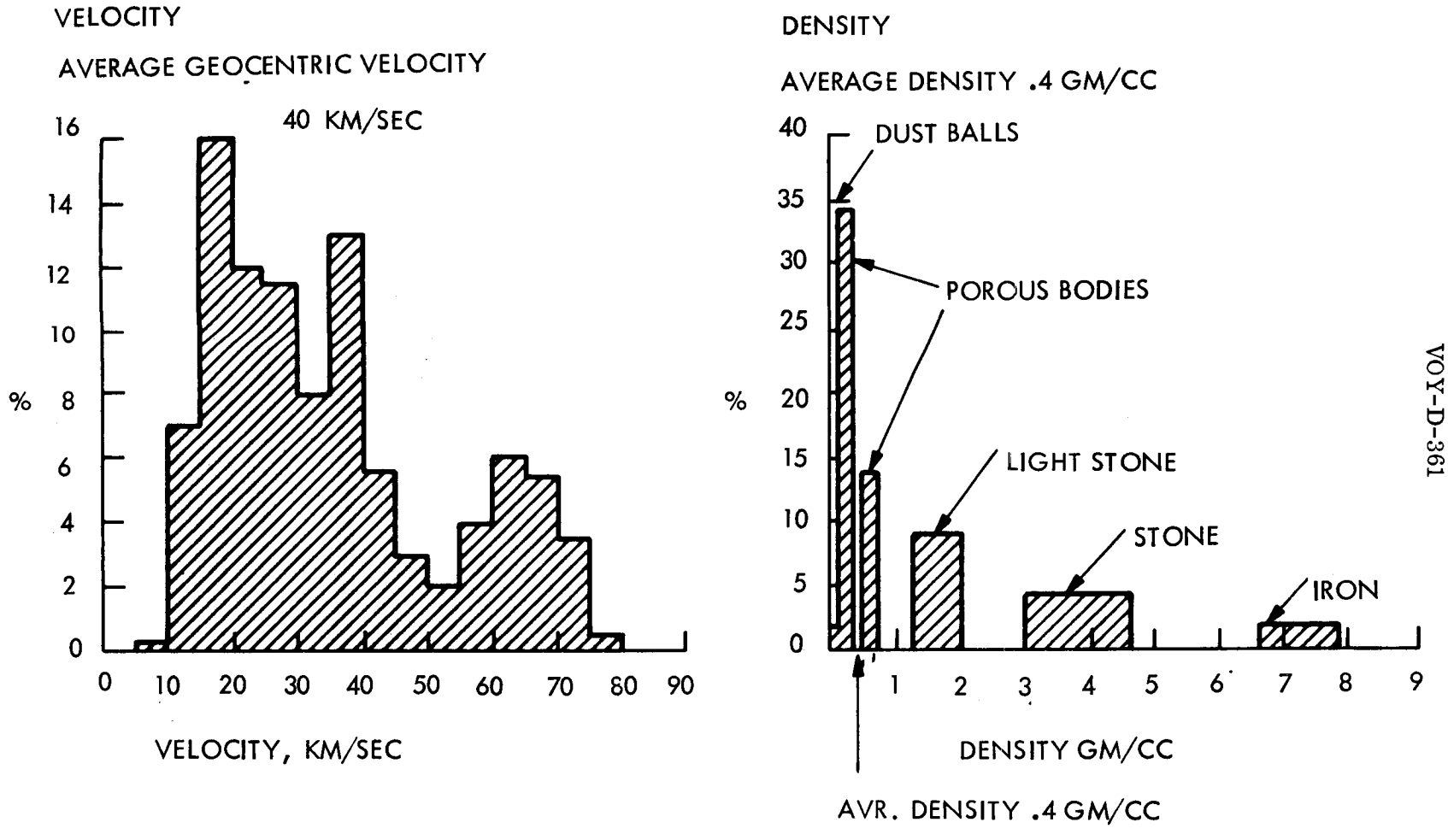

Figure 24. Some Meteoroid Properties

Table 10. Meteoroid Environment

Position	Particle Flux	Velocity		Density gms/cm^3
		Range Km/sec	Average Km/sec	
Near Earth	log N = -17.0-1.70 log M from -13.80	0-10 (rel. to Earth)	-	0.4
Cruise	log N = -log M+log F to -14.48-1.34 log M + log F	10-70	40	0.4
Stoney Particles	log N = -16.20-0.77X log M + 3.4(R-1)	10-70	40	3.5
Iron Particles	log N = -16.9-0.76X log M + 3.4(R-1)	10-70	40	7.7
Mass Flyby	log N = from -13.40 - log M to -14.08-1.34 log M	10-70	40	0.4
Within one Mars radius	log N = -17.60-1.70X log M	0-5 (rel. to Mars)	-	0.4
Stoney Particles	log N = -14.5-0.77X log M	0-5 (rel. to Mars)		3.5
Iron Particles	log N = -15.2-0.76X log M	0-5 (rel. to Mars)		7.7

Notes: N is the number of particles/m^2 sec of mass M and greater.
F is a correction factor for the region between Earth and Mars.

Solar distance in Astronomical Units	F Value
1.0 -1.25	1.0
1.25 -1.36	3.0
1.36 -1.43	5.0
1.43 -1.49	3.0
1.49 -1.56	2.5

R is one astronomical unit.

For the orbiting phase we combined the flux outside and inside one Mars radius equally and the following distributions of the variables of C_1 and C_2 are obtained:

$$C_1 \quad G\ (-15.58,\ .125) \tag{4}$$

$$C_2 \quad G\ (-1.37,\ .0675) \tag{5}$$

The variability associated with these equations is assumed to be associated with very long independent time samples. That is one mission will see a low environment over its life time while another two years later may see a relatively high environment. Due to this assumption the distributions in orbit and cruise were not considered independent. A low flux in cruise implies a low flux in orbit and conversely a high cruise flux implies a high flux in orbit.

MSFC has also specified the number N to the micrometeoroid mass M as follows:

a) Asteroidal Debris

$$N = R^{13.15}\ 10^{-15.93}\ M^{-1} \tag{6}$$

b) Cometary Flux

$$\mathrm{Log}_{10}\ N = 14.20 - 1.386\ (\mathrm{Log}_{10} M) - .0331\ (\mathrm{Log}_{10} M)^2 + .00051\ (\mathrm{Log}_{10} M)^3 - 1.5\ \mathrm{Log}_{10}\ R \tag{7}$$

which when linearized becomes

$$N = R^{-1.5}\ 10^{-14.20}\ M^{-1.386} \tag{8}$$

The differences in the JPL environment and the MSFC environment are slight. The MSFC environment is near to the mean environment flux predicted from the JPL environment flux spread. However, the JPL environment predicts an increase and then a decrease in the flux as a function of the distance from the sun, while MSFC cometary flux equation has the flux decreasing as the distance from the sun increases.

5.3.4 Probability of Zero Penetrations

The probability of zero penetrations P_o is given by the Poisson distribution of penetrations.

$$P_o = \text{EXP}\left\{-NAT\right\} \tag{9}$$

where

T is the number of seconds spent in the flux for various ranges of R (in AU)

A is the area exposed to given angles of impacts, and

N is the number of particles of critical mass and velocity per unit area per unit time which result in a penetration.

The analysis of penetration probability considered the statistical distributions of velocity, angle of impact, and the variation of micrometeoroid flux versus time. This was done with a Monte Carlo computer program, using the distributions illustrated on Figure 24 and Table 10.

Table 11. Probability of Zero Penetration

	Bumper			Main Wall					
Area[1]	Thickness (inches)	Separation (inches)	Material	Thickness (inches)	Material	Exposure Time (Days)	$\bar{P}_o$	σ_{P_o} [2]	Total Weight (pounds)
$A_1+A_2+A_3$	0.006	0.516	AL	0.032	AL	271	0.982	0.12×10^{-2}	165
$A_1+A_2+A_3$	0.002	0.516	AL	0.032	Mg	271	0.955	0.70×10^{-2}	100.0
$A_1+A_2+A_3$	0.006	0.516	AL	0.025	AL	271	0.978	0.133×10^{-2}	136.6
$A_1+A_2+A_3$	0.027	0.516	AL	0.025	AL	271	0.9969	0.28×10^{-4}	229.2
$A_1+A_2+A_3$	0.027	0.516	AL	0.025	AL	106	0.99923	0.23×10^{-5}	229.2
$A_1+A_2+A_3$	0.006	0.516	AL	0.032	AL	11	0.997	0.49×10^{-4}	165

[1] See Table 9

[2] Time = 106 is the time in orbit or near encounter in which an explosion leads to contamination of the planet.

Time = 271 is the time to be required before depressurization of tanks.

Time = 80 is the time in orbit after capsule separation.

Time = 11 is the time critical to quarantine before encounter.

A number of protection configurations were analyzed as indicated on Table 11. This analysis indicated that an outer bumper 0.006 inches thick placed outside the thermal insulation blanket would provide a probability of zero penetrations of approximately 0.98 over the life of the mission. While this may not be an optimum design, there is insufficient evidence at this point to determine whether the weight required to increase this probability above 0.98 could not be more effectivelv utilized otherwise.

During the time period before encounter when an explosion due to meteoroid penetration could cause contamination of the planet, this amount of protection results in a probability of no skin penetrations of 0.997. An estimate of the resulting probability of planet contamination, using the techniques developed in the quarantine study (Reference 5.3) is between 3×10^{-7} and 3×10^{-5}. Careful study is required to reduce the many uncertainties associated with this estimate.

5.3.5. Conclusions

The limited analysis performed for Task D indicates that a very light micrometeoroid protection system may afford a level of protection consistent with the optimization of mission success through proper allocation of weight. More important than this very tentative definition of micrometeoroid protection, is the general approach developed for evaluation of protection requirements. An important conclusion was that proper selection of micrometeoroid protection should be done in conjunction with an overall system optimization (VOY-D-275), and consideration of planetary quarantine requirements.

A simplified flow chart describing the sequence of steps and some of the major considerations for selection of a micrometeoroid protection system is illustrated on Figure 25.

6. STRUCTURAL DYNAMICS OF SELECTED CONFIGURATION

6.1 VIBRATION CHARACTERISTICS AND CRITERIA

Structural dynamic analyses were performed to demonstrate compliance with the stiffness criteria, derived supplementary frequency criteria for modules and assemblies and verify that these modules and assemblies meet such frequency criteria.

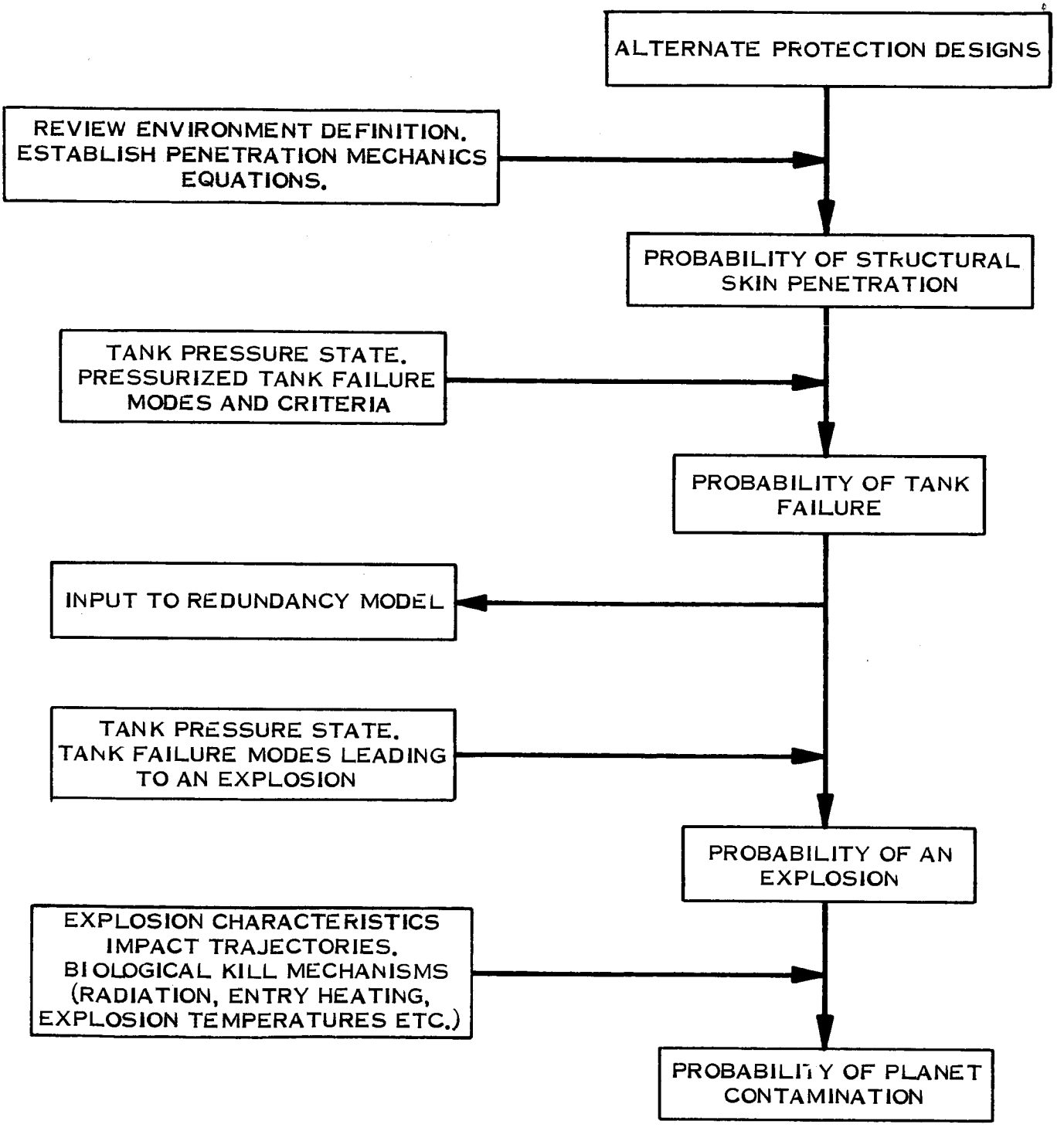

Figure 25. Micrometeoroid Protection System Selection

The Planetary Vehicle (selected configuration) has been idealized by the 17 lumped mass model illustrated in Figure 26. Of these mass stations, eight represent structural stations and three represent the LEMDE engine. The other six stations represent the lander tank assembly, bay electronics, high-gain antenna, planet scan platform and aft bulkhead.

This analysis assumed that there was no lateral-longitudinal-torsional vibration coupling; consequently, separate analytical models were established for the lateral and longitudinal vibration cases.

Thirty-three lateral coordinates of motion (degrees of freedom) were selected; these include both translational and rotational motions, and incorporate the effects of rotational discontinuities across the structural joints (reference 6.1).

Employing this analytical model, the planetary vehicle dynamic analysis was performed. The fundamental lateral and longitudinal frequencies are 7 cps and 10.8, respectively. These values satisfy the criteria.

Dynamic analyses were also performed on the following assemblies and appendages: (1) tank support structure; (2) engine support structure; (3) electronic bays; (4) solar cell array support structure (both fixed and deployable segments); (5) high-gain antenna and (6) planet scan platform. The results of these investigations are summarized in Table 12.

The analytical model shown in Figure 26 was also used to determine the displacements of the various mass stations relative to each other for the boost longitudinal limit load, and the launch release lateral limit loads.

6.2 TANK AND ENGINE SUPPORT STRUCTURE

The mathematical model of the Tank-Engine Support Structure includes the tank support struts, the engine support struts and cross beams, and the ring at station 135.5. The mass of the tanks, plumbing, engine and structure is concentrated at 37 nodal points. Due to the

manner in which the tanks are connected to the support structure, (sliding joint at one end) the lateral mass distribution differs from the longitudinal mass distribution. In the longitudinal case half of the mass of a tank is concentrated at each of its two connection points. In the lateral case all the mass of a tank is concentrated at one connection point (the fixed end).

The computer program ASSET (Reference 6.2) was used for this analysis.

The first two longitudinal natural frequencies are 9.91 and 10.19 cps. The first two lateral - pitch natural frequencies are 13.57 and 13.68 cps. The first two lateral - Yaw natural frequencies are 15.16 and 16.19.

7. SEPARATION AND CLEARANCE ANALYSES

7.1 INTRODUCTION

Dynamic analyses have been performed to verify that no interference exists between Planetary Vehicles and shrouds during forward ejection ("over the nose") separation and clearance phases. Separation velocities have also been established for the two Planetary Vehicles and the (aft) shroud segment between them; these velocities will preclude one body from catching up with a previously separated object during interplanetary flight.

The entire separation and clearance sequence is illustrated in Figure 27. The forward shroud will be separated in an (earth) parking orbit, in a direction selected to avoid collision when the S-IVB is reignited for insertion into interplanetary trajectory. While in this trajectory, the forward planetary vehicle, intermediate (aft) shroud, and aft planetary vehicle will be separated sequentially.

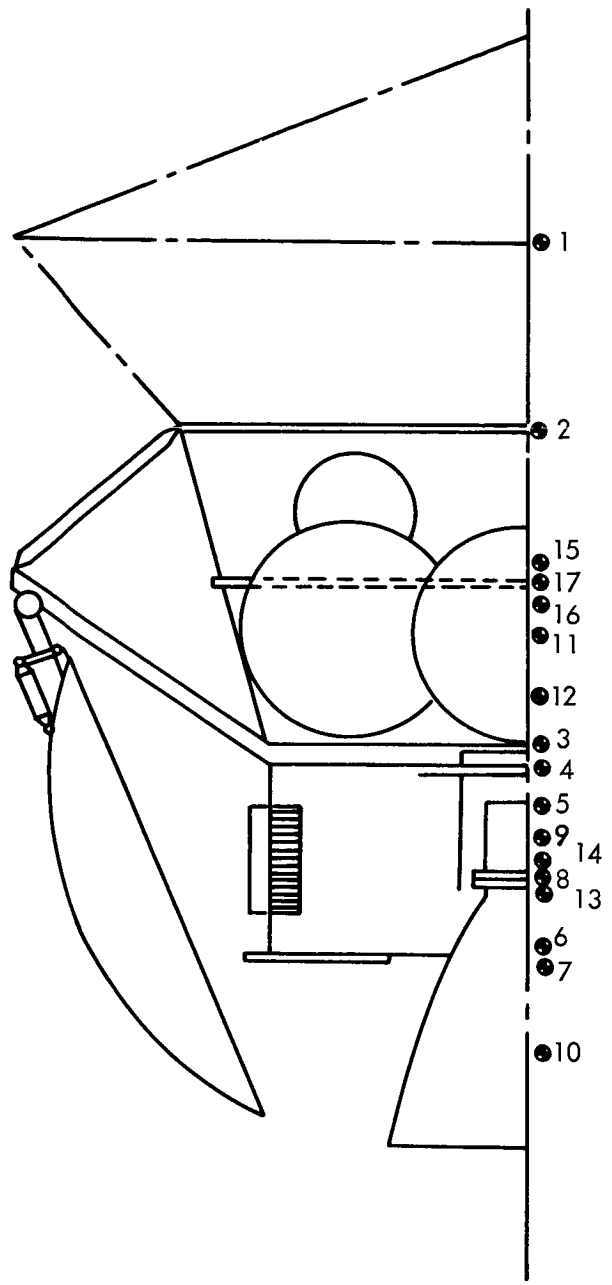

MASS STATION LOCATION

FOLDOUT FRAME 1

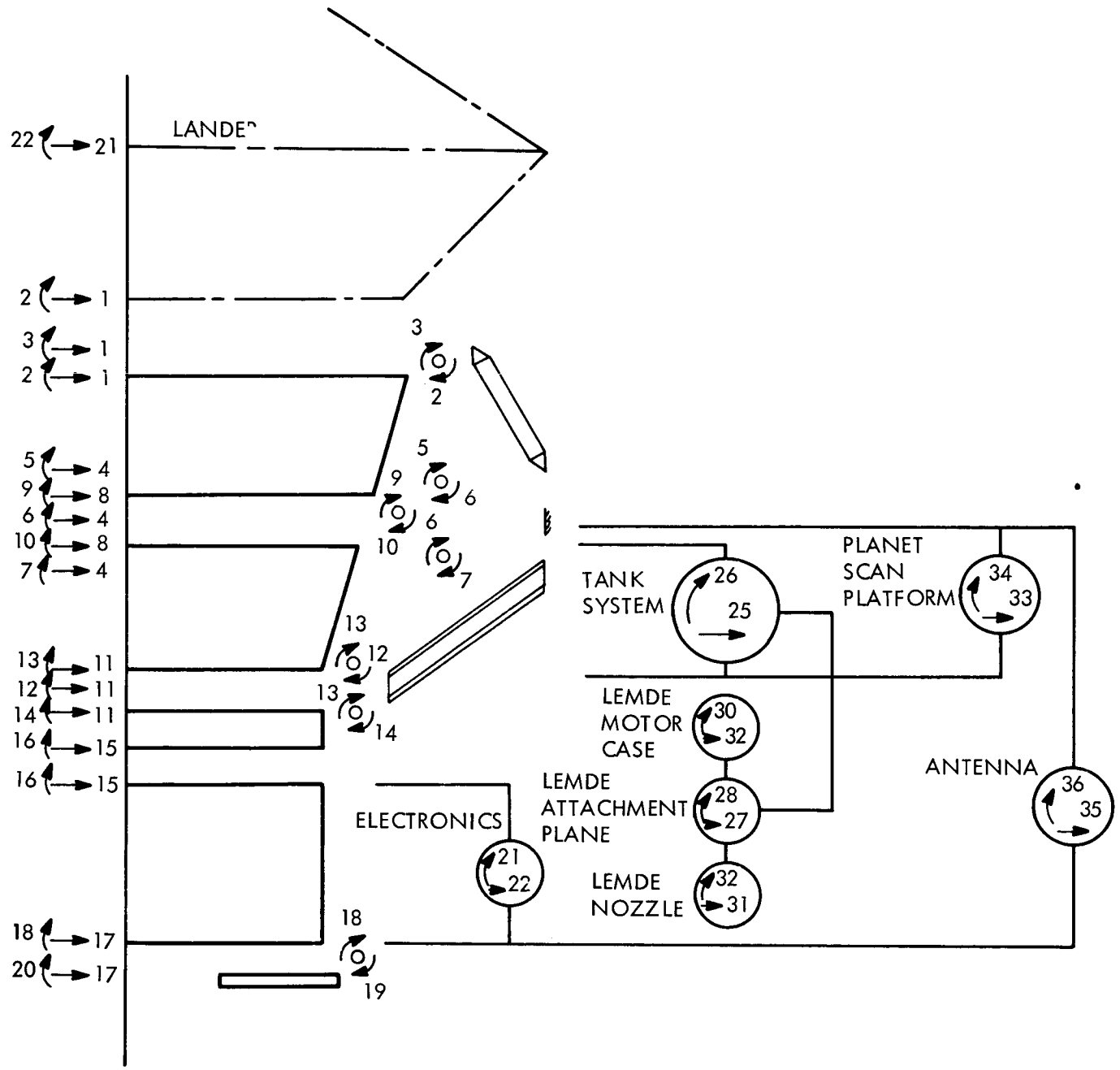

LATERAL MODEL

FOLDOUT FRAME 2

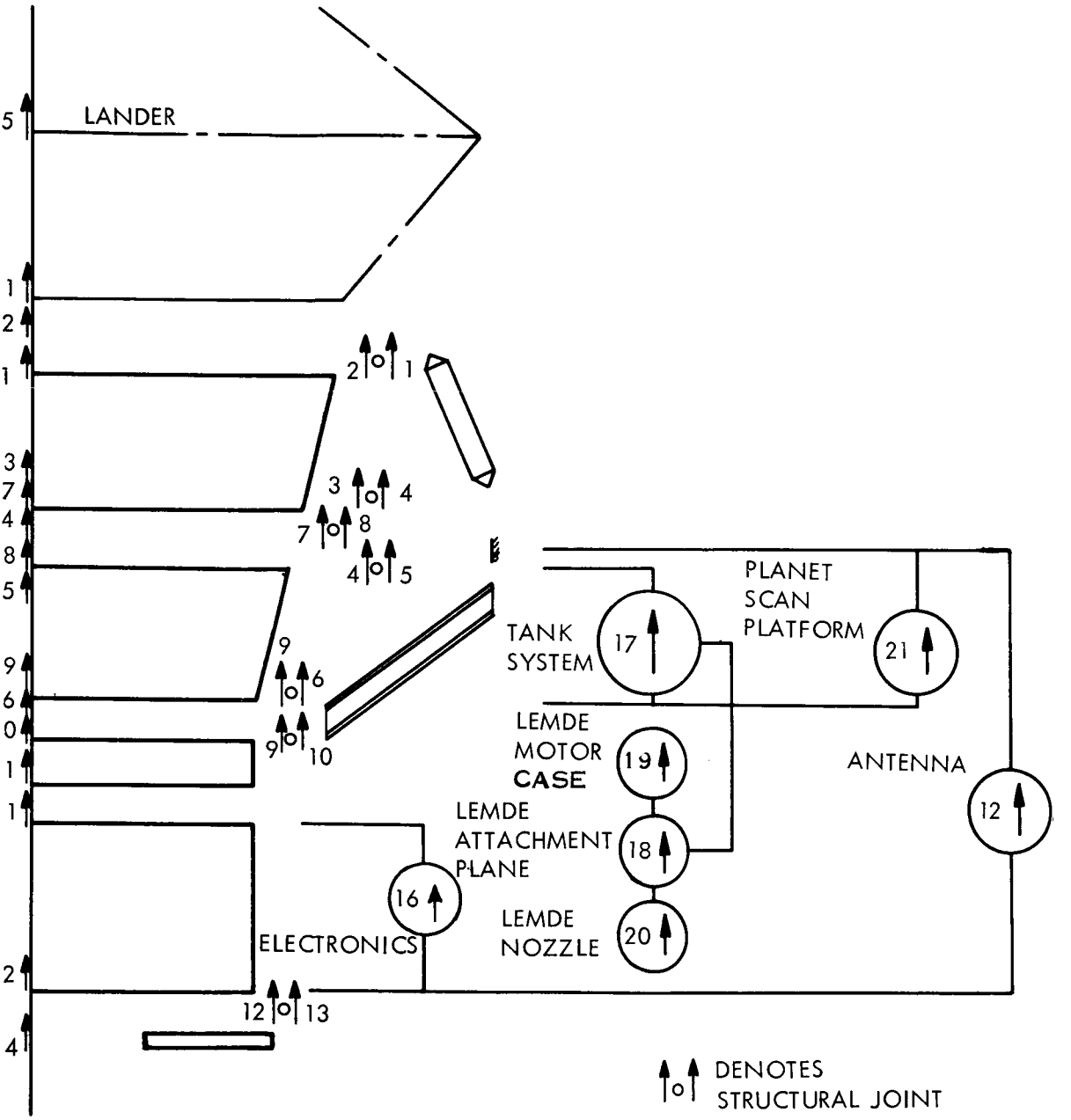

LONGITUDINAL MODEL

Figure 26. Selected Configuration General Array and Structural Dynamic Analytical Model

FOLDOUT FRAME 3

Table 12. Calculated Natural Frequencies (cps)

A. Planetary Vehicle

Boost Phase Configuration Vehicle Supported on Shroud

Minimum Criteria	Achieved
7 cps (min. Allow)	7.0

B. Modules and Assemblies

Item	Minimum Criteria	Achieved	
Propulsion Module	10	9.9	
Capsule/Lander	30		
Electronic Bays	35	35	(Bay-Longeron Assembly)
		472	(Bay Alone)
Micrometeoroid Bumper Panels	20	32	
Fixed Solar Cell Array Support Structure	35	60	

C. Deployable Appendages

Item	Stowed Attitude		Deployed Attitude	
	Criteria	Achieved	Criteria	Achieved
High-Gain Antenna	20	25	4	4.8
Planet Scan Platform	35	35	4	4.0
Deployable Solar Cell Array ("Flipper")	35	35	10	32

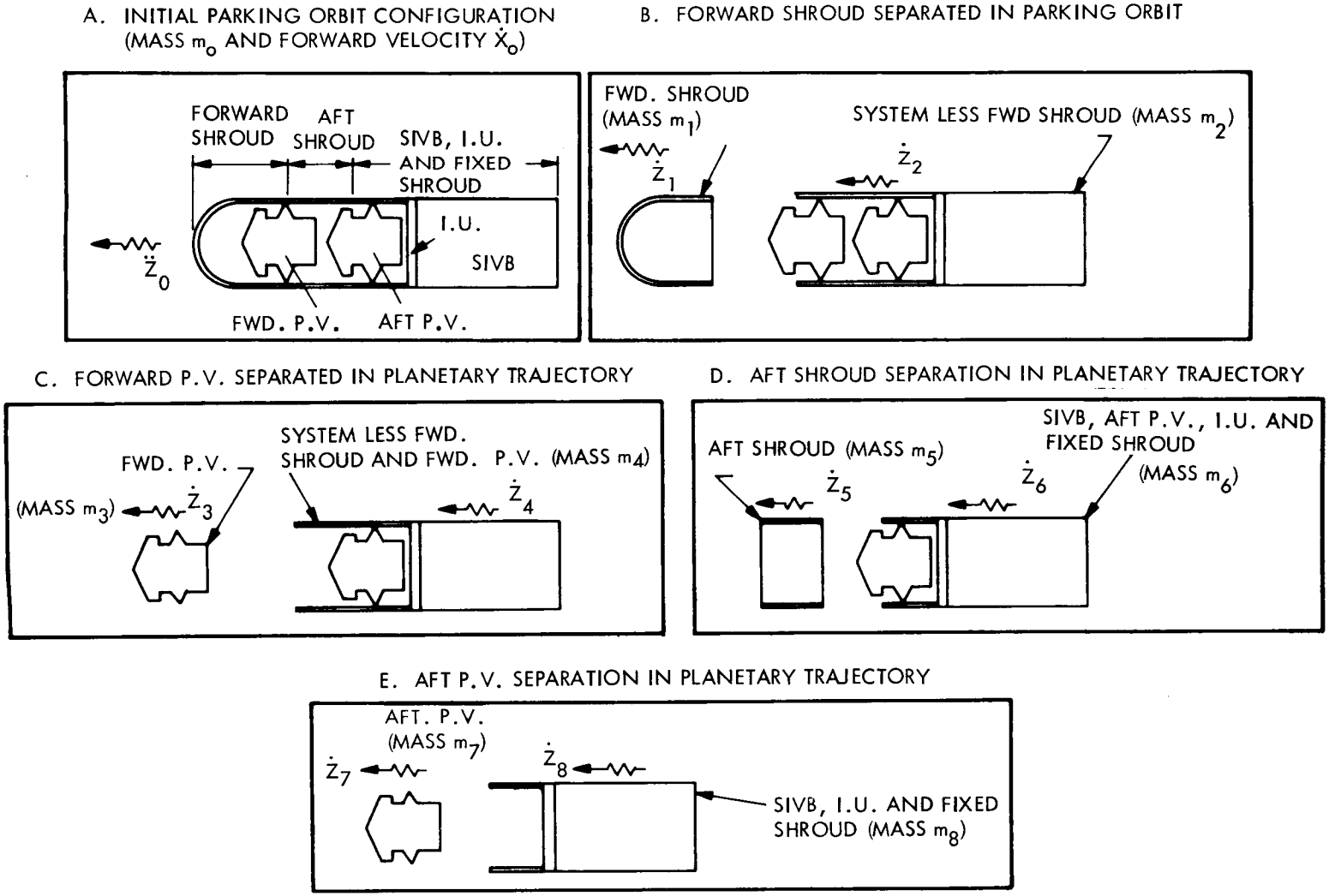

Figure 27. Separation Sequence of Nomenclature

In addition to the forward velocities ($\dot{Z}$), transverse velocities ($\dot{x}$) and pitching rates will be present. These rsult from the S-IVB rates at the time of separation. The transverse velocities are equal to the product of the pitching velocity and the distances between new and old centers of mass (C.M.), as illustrated in Figure 28.

Following an ideal separation, the pitching velocities of the separated body ($\overset{o}{P}_1$) and the remainder of the system ($\overset{o}{P}_2$) would be identical.

7.2 MOMENTS INDUCED BY SEPARATION

Radial C.M. off-sets in both the separated body and in the remaining system, and deviations inherent in the separation system induce pitching moments. The deviations include: (1) spring rate deviations (k*); (2) spring pre-load errors (δ*); (3) spring radial (r_s*) and tangential (θ*) positioning errors; and (4) release time lags (t*). (Table 13.)

Numerical values have been based on 3σ values established by analysis of experimental results on the Nimbus separation system. The maximum planetary vehicle C.M. off-set (e_1) was taken as 3.0 inches. The comparable value for the shroud sections was estimated at 1.0 inch.

7.3 CLEARANCE ANALYSES

The clearance phase is initiated as soon as the separation springs reach the end of their stroke. This phase ends when body 1 has traveled a distance from body 2 sufficient to insure that there will be no impact between them. Kinematic relationships were employed to describe the longitudinal (Z_A) and transverse (X_A) absolute motions of a critical point A on body 1, over the time interval (t) elapsed following the end of the separation phase. Similar procedures were utilized to define the longitudinal (Z_B) and transverse (X_B) absolute motions of a critical point B on the remaining system, into which point A would strike if

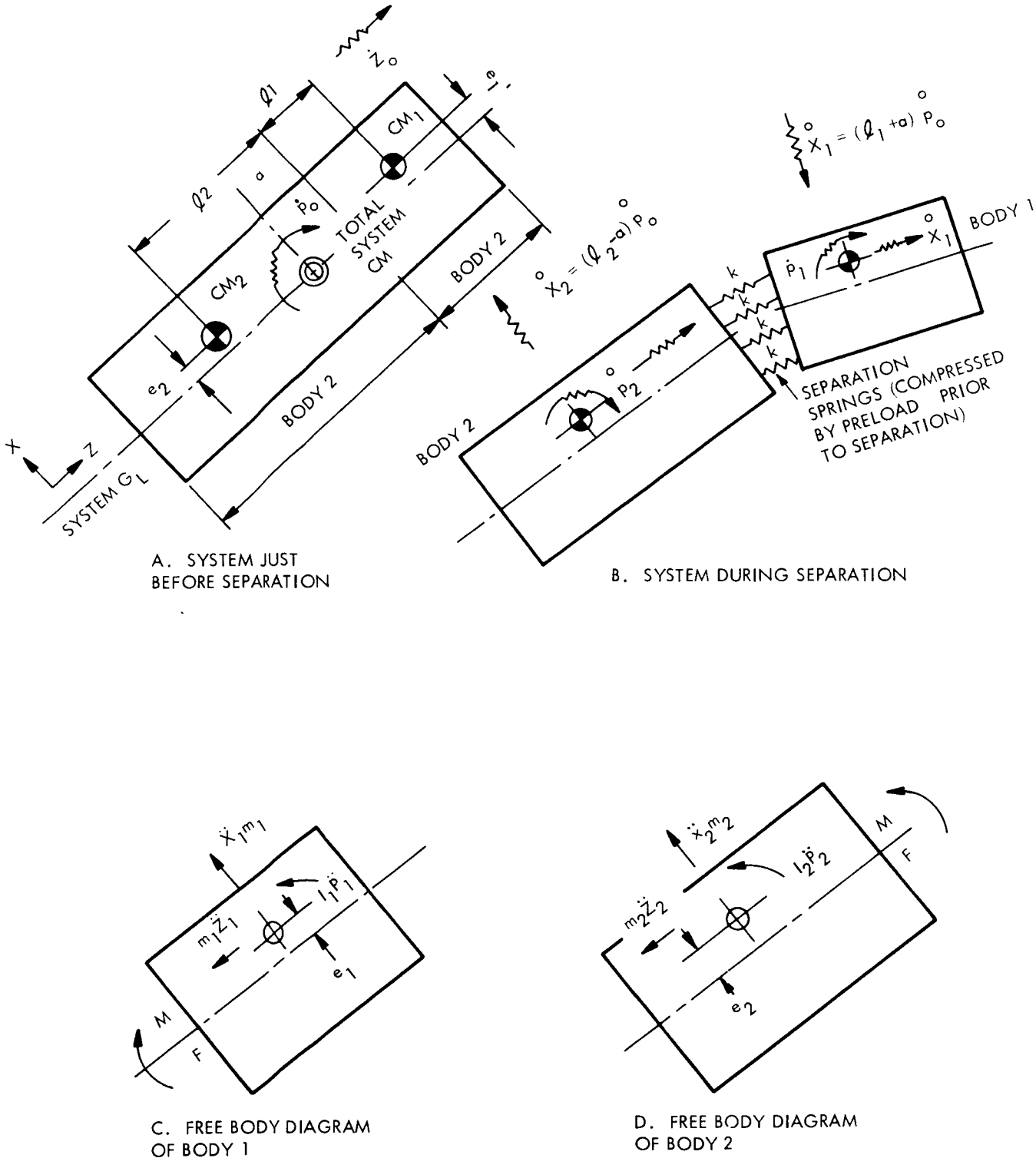

Figure 28. Separation Sequence

Table 13. Clearance-Dictated Separation Velocity Criteria

Separated Element	Clearance Criteria	Allotted Separation Velocity (In/Sec)	Separation Velocity Required for Clearance (in/sec)			
			Attitude Control System Inactive		Attitude Control System Active	
			Practical Pitch Rate	Max. Pitch Rate	Practical Pitch Rate	Max. Pitch Rate
Forward Shroud	Aft End Clears Fwd. Capsule	20.6	0.3	3.0	5.4	53.9
Aft Shroud	Aft End Clears Aft Capsule	16.0	0.3	3.0	4.2	41.8
Forward Planetary Vehicle	Adapter Clears Shroud	16.9	0.03	0.3	1.4	14.0
	Aft End Clears P.V. Support Ring On Shroud		0.3	2.9	2.2	22.2
Aft Planetary Vehicle	Adapter Clears Shroud	18.2	0.03	0.3	1.2	11.9
	Aft End Clears P.V. Support Ring On Shroud		0.3	3.1	1.9	18.9

NOTES: (1) C.M. Offsets (e_1 and e_2) are taken as zero
(2) The practical pitch rate is 0.02 degrees/second
(3) The maximum pitch rate is 0.20 degrees/second

clearance margins were inadequate. The relative transverse and longitudinal clearance margins are established from the differences between the absolute forward and transverse motions of points A and B.

Clearance analyses are separated into two categories: (1) clearance with the S-IVB attitude control system inactive; and (2) clearance with this control system activated. In the former case, body 2 pitching motion (p_2) is that produced by separation. The activated control system imparts an opposing pitch rate ($p_2 = -p_o$) to the booster. The maximum possible S-IVB pitch rate is ± 0.20 degrees per second. Based on data furnished by Douglas, a "practical maximum" rate of ± 0.02 degrees per second has been used as a lower bound for numerical studies.

Clearance criteria were derived for the following critical clearance conditions: (1) shroud clears planetary vehicle; (2) planetary vehicle adapter/truss clears shroud; (3) aft end of Planetary Vehicle clears shroud's vehicle support ring; and (4) aft end of the Planetary Vehicle space envelope clears shroud separation plane.

For "high truss" Planetary Vehicle configurations (Figure 29), it is desirable to define the trace of the separation clearance envelope aft of the vehicle separation plane. Such an envelope describes the actual space available for the system general arrangement. From Figure 29, this envelope aft of the separation plane can be described as a conical frustrum from which the clearance-dictated space requirement can be expressed in terms of a maximum allowable cone semi-vertex angle (α), as a function of: (1) the weights, C.M. off-sets and locations, and inertias of bodies 1 and 2; (2) the separation velocity; (3) booster pitch rate prior to separation; and (4) the geometry of these bodies. These equations were derived by expressing the radius (r_c) of the aft end of the clearance envelope in terms of (α), the truss/adapter radius (r_v) and the effective height ($\ell + d_c$) of this frustrum.

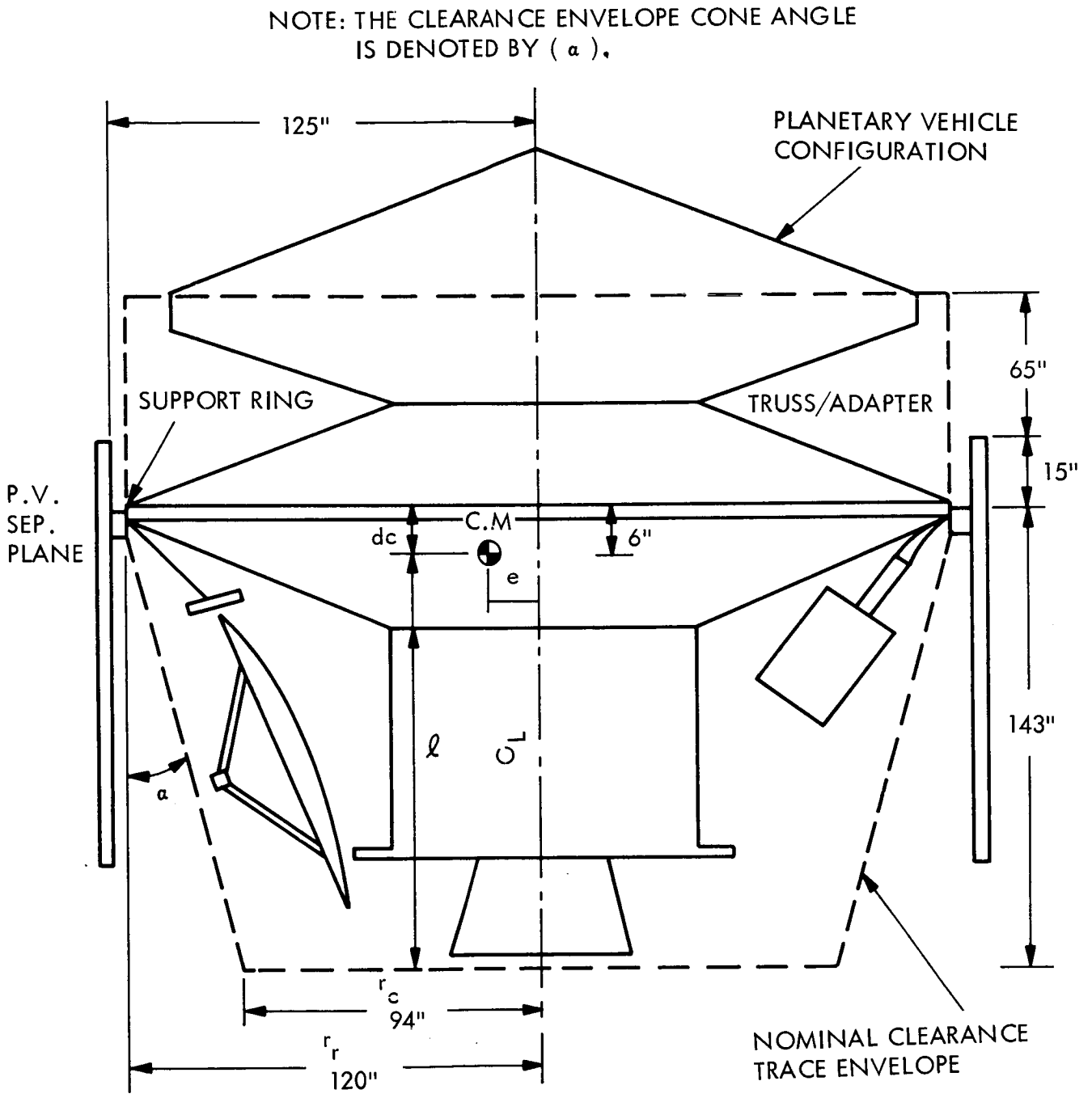

Figure 29. Planetary Vehicle Clearance Trace

Clearance analyses of both Planetary Vehicles and shroud segments indicated that the forward shroud and planetary vehicle clearance margins were somewhat less than those for their aft counterparts. As evidenced by Figure 30, there is nevertheless ample clearance space for the forward shroud, even with the S-IVB control system activated during separation (assuming a shroud C.M. radial off-set of 1.0 inch). Constraining the S-IVB control system into inactivity during forward shroud separation, would allow a fairing with a 5.3 inch C.M. radial off-set to clear the planetary vehicle.

The planetary vehicle space envelope cone angle (α) is given as a function of booster pitch rate in Figure 31. These curves, predicated on a 3.0 inch C.M. off-set, show that a cone angle of 5.1 degrees is required for the maximum possible booster pitch rate, with the S-IVB control system inactive. The 10-degree cone angle of the selected configuration precludes collision with the shroud even if the S-IVB control system is activated during the clearance phase with a rate up to 0.1 degree per second. This margin is felt to be more than ample. The selected configuration provides an ample margin of safety with respect to collision between planetary vehicles and shrouds during an over-the-nose separation sequence.

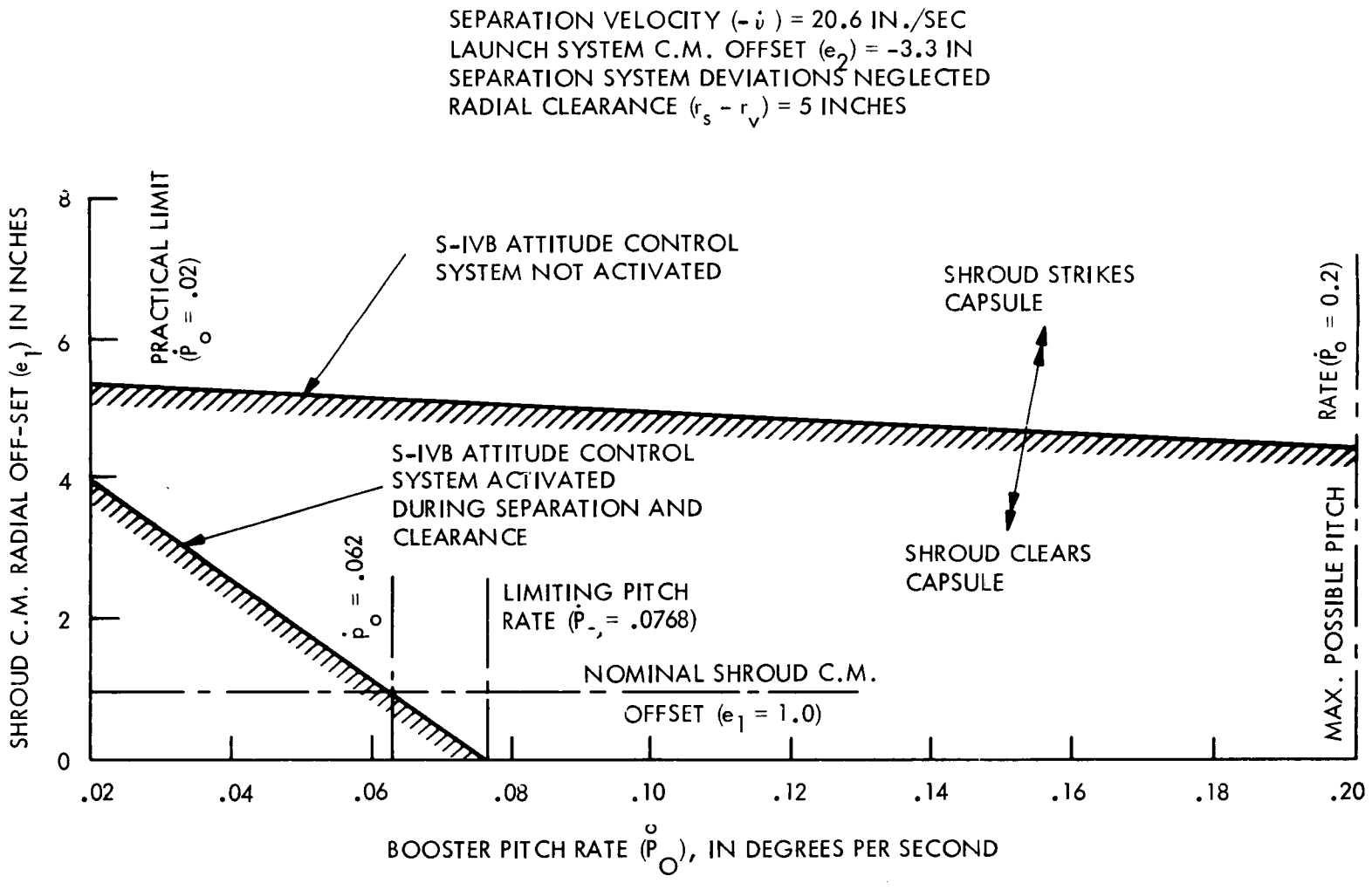

Figure 30. Forward Shroud Center of Mass Radial Offset as a Function of Booster Pitch Rate

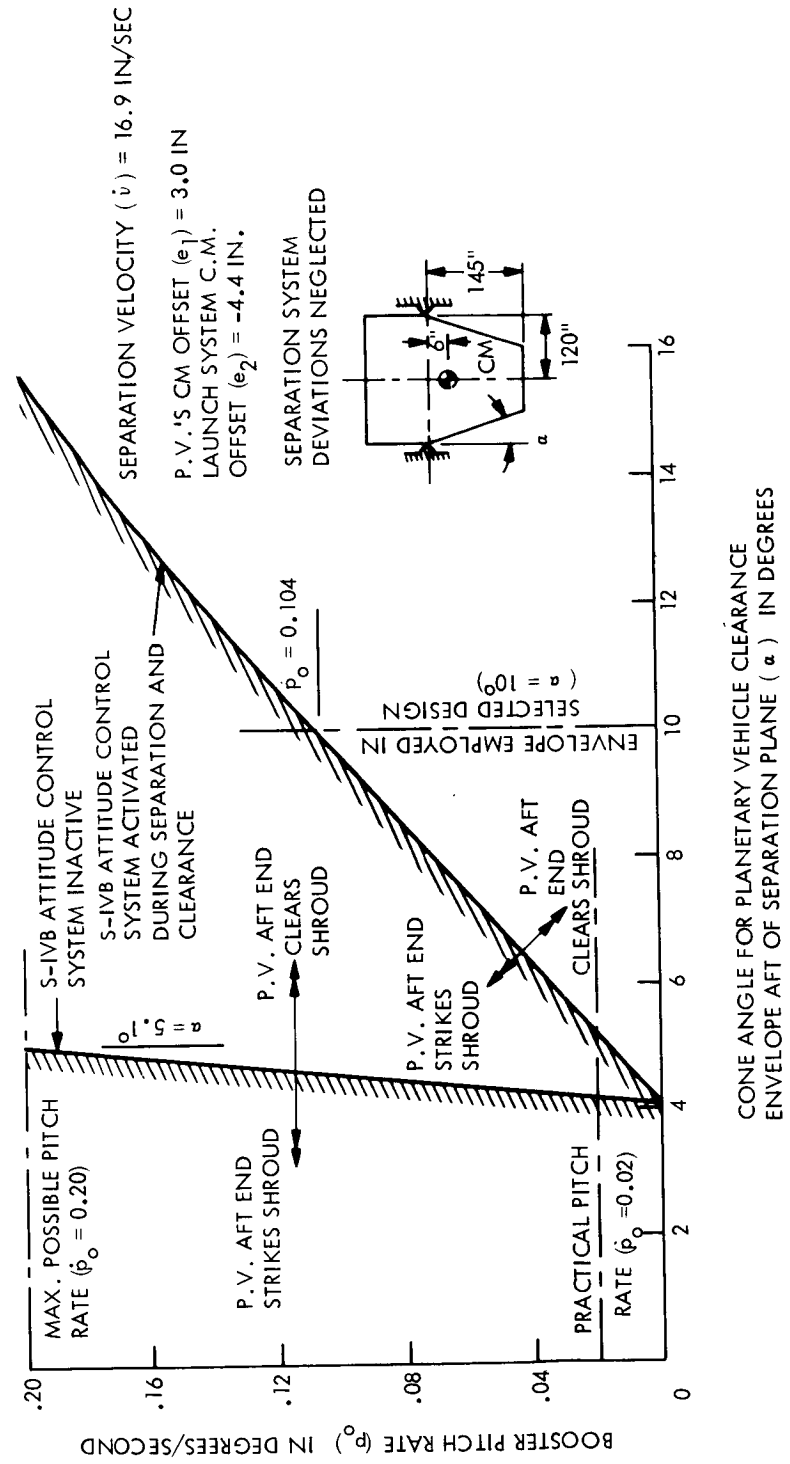

Figure 31. Planetary Vehicle Space Envelope Cone Angle as a Function of Booster Pitch Rate

8. REFERENCES

3.1 "Voyager Environmental Predictions Document," E. Pounder, Jet Propulsion Laboratory Document #SE 003 BB 001-1B28

5.1 VOY-CO-FR, "Application of Redundancy Study" Volume 4, Lee Hargrave, Jr. July 1963

5.2 818-11-PQ001, "Planetary Quarantine Plan, Voyager Project, 15 March 1966, 3rd Revision, 1 June 1967," NASA - OSSA, Voyager Project Office

5.3 VOY-CO-FR, "Planetary Quarantine Study" Volume 3, R. Wolfson, July 1963

5.4 04480-6004-R00, "Voyager Support Study - LM Descent Stage Applications," Final Report Volume 1, Propulsion Studies, February 1967, JPL Contract No. 951113

5.5 D.W.R. McKinley, Meteoroid Science and Engineering, McGraw Hill Book Co., 1961, pp. 135-137

5.6 J.J. Volkoff, "Protection Requirements for the Resistance of Meteoroid Penetration Damage of Interplanetary Spacecraft Systems," JPL TR 32-410, 1 July 1964

5.7 "Natural Environment Design Guidelines for MSFC Voyager Spacecraft for Mars 1973 Mission," Editors: D.K. Wieder and C.L. Hasseltine, NASA TM X-53616

5.8 J.P.D. Wilkinson, "A Study of Micrometeoroid Protection," GE-MSD DIN 67 SD 4371, 8 Sept 1967

5.9 R. Madden, "Ballistic Limit of Double-walled Meteoroid Bumper Systems," NASA TN D-3916

5.10 "Penetration Mechanics for Metallic Structures," NASA Engineering Criteria Bulletin EC-1, NASA Houston, Texas

5.11 J.R. Powers, "Structural Design for Micrometeoroid Protection," Brown Engineering Company, Huntsville, Alabama, T.C. CI-SAA-054, 23 March 1967

5.12 S. Woodall, "A Numerical Method for Analysing Meteoroid/Two-Sheet Structural Configuration Problems," GE-MSD Mechanics Section Tech. Memo No. 067-04, July 1967

5.13 Hardening Technology Studies, Volume 5, Part I, "Hypervelocity Countermeasures Tasks," by R. P. Robertson and P. E. Sandorff, Lockheed Missiles and Space Co., Sunnyvale, California, September 1965

5.14 "Micrometeoroid Shielding Requirements for the Voyager Mars Mission Based on the Langley Criterion," GE-MSO PIR U-6230-DHF-106, August 1967

6.1 Alley, V. L., and Ledbetter, S. A., "Prediction of Natural Frequencies of multi-stage Launch Vehicles," AIAA Journal, Vol. 1, No. 2, February 1963.

6.2 Asset - An Engineer's Programming Tool for Structural Analysis, 1967 National Symposium of American Astronautical Society, Huntsville, Alabama, June 1967.

VOY-D-362
THERMAL CONTROL SUBSYSTEM

1. SCOPE

This section describes the thermal control subsystem, consisting of insulation, thermal coatings, louvers, heaters, and control of structural features to provide desired heat transfer paths. It also presents a discussion of alternatives and an analysis of spacecraft temperatures during all mission phases.

2. FUNCTIONAL DESCRIPTION AND REQUIREMENTS

The prime function of the thermal control subsystem is to maintain all equipments within specified temperature limits for the purpose of enhancing and maintaining operational reliability.

The operating temperature limits of critical components are listed in Section 5, Table 5.

The definition and performance of the thermal control subsystem are different in several respects from Task B. Some of the changes are caused by differences in the spacecraft configuration. The most significant, from a thermal standpoint, are:

a. Change from solid to liquid propulsion system.

b. Change in relative locations of electronic bays, propulsion system, and solar array.

Other changes have been introduced for improvements in performance or reliability as a result of flight experience, test programs and design studies conducted since Task B. The most significant are:

a. Change from louvers actuated by fluid-filled bellows to bi-metallic louvers.

b. Selection of gold-coated mylar as an alternate to aluminized mylar, to provide for possible future ETO decontamination requirement.

3. SUBSYSTEM ALTERNATIVES

3.1. LOUVERS

The fluid-filled bellows actuation system was chosen for Task B because of its excellent performance and flight-proven long life reliability aboard the Nimbus Spacecraft. This system is still operating very successfully after more than one year in earth orbit.

Since Task B, Mariner and Pegasus Spacecraft have provided additional flight demonstration of bi-metallic actuated louvers. Since both systems fulfill the functional and reliability requirements, the selection of bi-metallic actuation for the baseline configuration was based on simplicity of installation and lower weight.

3.2. INSULATION

An extensive test program has been conducted by General Electric under JPL Planetary Vehicle Insulation System (PVTIS) Contract No. 95137 with the objective of determining insulation requirements and establishing techniques for application of super insulation to planetary vehicles such as Voyager. Materials examined included aluminum and gold-coated mylar, teflon and kapton, dimplar, and dacron mesh. Thermal performance measurements were made on samples with different number of layers to assess effects of coating the plastics film on both sides with metal, embossing or wrinkling the layers, separating the layers with dacron mesh. Candidate outer cover materials were evaluated with respect to temperature resistance capability and thermal optical properties. A summary of pertinent thermal results of the program is given in Tables 1 and 2.

Criteria for selection of the Voyager blankets are:

a. Weight

b. Thermal performance

Table 1. Thermal Conductance Test Data

Configuration	Material Source	Temperature (°F)	No. of Layers	Thickness (inches)	Layers (inch)	Pressure (Torr)	Density (lb/ft^3)	Heat-Flow (BTU/hr-ft^2)	Effective k (BTU/hr-ft-°F)	Effective Emittance	ρ k $\frac{BTU-lb}{(hr-ft^4-°F)}$	Heat flow with 1 foot of joint and 1 attachment post per square foot of insulation (BTU/hr-ft^2)	Remarks
(1) 1/4 mil Mylar aluminized 1 side and crinkled	NRC	T_H = 73 T_C = -322	35 (wrinkled)	0.5	70	0.9×10^{-5}	1.52	0.304	3.2×10^{-5}	0.0022	4.86×10^{-5}		
(1A) Same design as (1), samples independently constructed	NRC	T_H = 71 T_C = -322	35 (wrinkled)	0.5	70	2.5×10^{-5}	1.45	0.472	5.0×10^{-5}	0.0035	7.25×10^{-5}		Sample seemed tight in apparatus
(2) 1/4 mil preshrunk Mylar aluminized 1 side and double crinkled	NRC	T_H = 71 T_C = -323	35	0.5	70	1.8×10^{-5}	1.46	0.369	3.9×10^{-5}	0.0027	5.69×10^{-5}		Did not entirely fill 0.5 inch test gap
(3) Same sample as (2)		T_H = 72 T_C = -323	35 (wrinkled)	0.85	41	2.6×10^{-5}	0.86	0.317	5.7×10^{-5}	0.0023	4.89×10^{-5}		
(4) 1/2 mil Mylar tin coated 1 side	NRC	T_H = 68 T_C = -322	35 (wrinkled)	0.5	70	1.3×10^{-5}	3.22	0.686	7.3×10^{-5}	0.0052	23.5×10^{-5}		Would have half the density with 1/4 mil Mylar
(5) 1/4 mil Mylar aluminized 2 sides - embossed	Hastings	T_H = 68 T_C = -322	51	0.4	128	1.4×10^{-5}	2.79	0.391	3.3×10^{-5}	0.0030	9.21×10^{-5}		
(6) 33 layers 1/4 mil Mylar aluminized 1 side and crinkled plus 2 layers 1/2 mil Kapton aluminized 1 side, crinkled, and installed next to cold plates	NRC	T_H = 72 T_C = -323	35	0.5	70	2.5×10^{-5}	1.54	0.382	4.0×10^{-5}	0.0028	6.16×10^{-5}		
(7) 23 layers 1/4 mil Mylar aluminized 2 sides; 24 layers Dacron net spacers	Hastings Fablok	T_H = 73 T_C = -322	23 reflectors	0.5	46 reflectors per inch	1.6×10^{-5}	5.52	0.303	3.2×10^{-5}	0.0022	17.7×10^{-5}		
(8) Same sample as (7)		T_H = -3 T_C = -322		0.5	46 reflectors per inch	1.2×10^{-5}	5.52	0.128	1.68×10^{-5}	0.0017	9.27×10^{-5}		Data questionable, all heat to insulation from guard to main conductance
(9) 23 layers 1/4 mil Mylar aluminized 2 sides 24 nylon tulle spacers, 1 layer 1/2 mil. Kapton aluminized one side, and installed next to cold plates	NRC Sears	T_H = 68 T_C = -323	24 reflectors	0.5	48 reflectors per inch	2.4×10^{-5}	2.44	0.476	5.1×10^{-5}	0.0036	12.4×10^{-5}		
(10) 1/2 mil aluminized mylar Dimplar	Super-Temp	T_H = 70 T_C = -321	8 layer pairs	0.75	21	0.7×10^{-5}	1.03	0.819	13.1×10^{-5}	0.0061	13.5×10^{-5}		
(11) Same sample as (10)		T_H = 72 T_C = -323		0.85	19	2.3×10^{-5}	0.905	0.586	10.5×10^{-5}	0.0043	9.5×10^{-5}		
(12) 1/4 mil Mylar - uncoated	NRC	T_H = 72 T_C = -322	35 (wrinkled)	0.5	70	2.8×10^{-5}	1.50	8.31	88×10^{-5}	0.0609	132.4×10^{-5}		
(13) Rabbeted joint and support post per Figure 2.1; insulation same as (1)	NRC Nylatch	T_H = 73 T_C = -322	35 (wrinkled)	0.5	70	1.3×10^{-5}		0.380 per 0.695 ft^2		0.00399			Effective emittance shown to compare (13) and (14)
(13A) Same design as (13), samples independently constructed	NRC Nylatch	T_H = 73 T_C = -321	35 (wrinkled)	0.5	70	2.0×10^{-5}		0.412 per 0.695 ft^2					
(14) Same sample as (13)		T_H = -4 T_C = -322	35 (wrinkled)	0.5	70	0.65×10^{-5}		0.216 per 0.695 ft^2		0.00421			
(15) Configuration (1) with support post in center	NRC Nylatch	T_H = 69 T_C = -322	35 (wrinkled)	0.5	70	1.2×10^{-5}		0.308 per 0.695 ft^2					
(16) Configuration (1) with rabbeted joint only per Figure 3	NRC	T_H = 70 T_C = -322	35 (wrinkled)	0.5	70	2.3×10^{-5}		0.353 per 0.695 ft^2					
(16A) Retest of sample (16)	NRC	T_H = 71 T_C = 318		0.5	70	1.5×10^{-5}		0.330 per 0.695 ft^2					
Configuration (1) with joint and support post (calculated)		T_H = 72 T_C = -320	35 (wrinkled)	0.5	70	$< 5 \times 10^{-5}$	1.50		4.9×10^{-5}	0.0034	7.35×10^{-5}	0.47	From tests 1, 1A, 2, 6, 13, 13A, 15, 16, 16A
(17) Configuration (10) with support post at center	Super-Temp	T_H = 69 T_C = -323	8 layer pairs	0.85	19	2.6×10^{-5}		0.520 per 0.695 ft^2					0.3 inch hole for 0.225 inch diameter nylon post 0.835 inch long
(18) Configuration (10) with post, joint and stitching like Figure 3	Super-Temp	T_H = 73 T_C = -323	8 layer pairs	0.85	19	3.2×10^{-5}		1.073 per 0.695 ft^2		0.012			0.3 inch hold in insulation
(18A) Same design as (18), samples independently constructed	Super-Temp	T_H = 72 T_C = -323	8 layer pairs	0.85	19	2.5×10^{-5}		0.610 per 0.695 ft^2					0.25 inch hole for 0.225 inch diameter nylon post 0.835 inch long
(19) Same sample as (18)		T_H = -24 T_C = -323		0.85	19	1.8×10^{-5}		0.628 per 0.695 ft^2		0.0147			
(20 Same sample as (18)		T_H = -43 T_C = -323		0.85	19	2.4×10^{-5}		0.513 per 0.695 ft^2		0.0144			
Configuration (10) with joint and support post (calculated)		T_H = 72 T_C = -320	8 layer pairs	0.85	19	$< 5 \times 10^{-5}$	0.91		12.8×10^{-5}	0.0052	11.6×10^{-5}	0.71	From tests 11, 17, 18A. Sample 18 performance not used in calculation
(21) Two layers 1 mil Kapton Dimplar separating 3 layers 1/2 mil crinkled Kapton. All aluminized 1 side	Super-Temp NRC	T_H = 150 T_C = 73	5	0.312	16	2.0×10^{-5}	1.16	1.70	57.4×10	0.0170	65.9×10^{-5}		
(22) Same samples as (21)		T_H = 251 T_C = 72	5	0.312	16	2.4×10^{-5}	1.16	4.37	66.0×10^{-5}	0.0152	76.8×10^{-5}		
(23) 1/4 mil Mylar gold-coated one side	Hastings	T_H = 71 T_C = -324	34 (wrinkled)	0.5	68	2.9×10^{-5}	1.84	0.349	3.7×10^{-5}	0.0026	6.77×10^{-5}		

Table 2. Combined Space Environments Effects on Cover Materials

Sample Material	Air Convection Before Irradiation			In-Situ					Air Convection After Irradiation			After Exposure To Simulated Plume Heating		
				Air/ Vac	116 UVESH	116 UVESH 10^{15} p/cm^2	1000 UVESH 10^{15} p/cm^2	1000 UVESH 10^{16} p/cm^2						
	α_S	ϵ_N	α_S/ϵ_N	α_S	α_S	α_S	α_S	α_S	α_S	ϵ_N	α_S/ϵ_N	α_S	ϵ_N	α_S/ϵ_N
2-mil aluminized Kapton (2 in. x 3 in.)				0.460	0.472	0.447	0.477	0.507 (Vac) 0.447 (Air)				0.443	0.768	0.58
2-mil aluminized Kapton (2 in. x 3 in.)				0.443	0.449	0.425	0.460	0.491 (Vac) 0.449 (Air)				0.433	0.768	0.56
2-mil aluminized Kapton (Disc)	0.391	0.674	0.58	0.472	0.444	0.510	0.489	0.457 (Air) 0.450 (Vac)	0.415	0.751	0.56			
2-mil aluminized Kapton (2 in. x 3 in.)				0.480		0.450	0.483	0.429 (Vac) 0.438 (Air)				0.435	0.766	0.56
2-mil aluminized Kapton (2 in. x 3 in.)				0.488	0.441	0.463	0.429	0.433						
NRC-2 (Al Up) (Disc)	0.150	0.030	5.0	0.209	0.237	0.221	0.198		0.134	0.024	5.6			
3-mil Gold Kapton (Disc)	0.412	0.811	0.52	0.450	0.447		0.419	0.410	0.414	0.795	0.52			
3-mil Gold Kapton (2 in. x 3 in.)				0.430	0.426	0.396	0.415	0.409				0.422	0.797	0.53
5-mil Al Teflon (2 in. x 3 in.)				0.240	0.264	0.258	0.293	0.315				0.450	0.795	0.56
D.S. aluminized Mylar (Disc)	0.220	0.04	5.0	0.216	0.230	0.175	0.220		0.218	0.036	6.1			
5-mil aluminized Teflon (2 in. x 3 in.)				0.251	0.234	0.266	0.297	0.251						
5-mil aluminized Teflon (2 in. x 3 in.)				0.225	0.292	0.244	0.312	0.260 (Air)						
5-mil aluminized Teflon (2 in. x 3 in.)				0.241	0.247	0.243	Sample out of position							
5-mil aluminized Teflon (Disc)	0.195	0.822	0.24	0.256	0.292	0.225	0.321 0.369		0.189	0.809	0.23			
$\alpha_S \pm .02$ Beckman $\alpha_S \pm .06$ in-situ														
$\epsilon_N \pm .02$														

Note: UVESH Ultra violet equivalent sun hours;
P/cm^2 Proton/cm^2

c. Adhesive characteristics

d. Ability of outer cover to withstand a wide range in temperatures.

Aluminized mylar is selected for insulation blankets, because of its history of successful flight applications. The outer layer is aluminized kapton.

The PVTIS tests indicated that aluminized mylar has a pronounced tendency to discolor or have the vapor-deposited aluminum coating completely removed from the substrate when exposed to ETO cycles with high values of relative humidity. Gold-coated mylar, on the other hand, was found to be unaffected by ETO and high humidity. Gold-coated mylar and kapton, therefore, provide an effective alternate insulation system if ETO decontamination or high humidity are anticipated.

Considerable efforts have been devoted to obtaining gold depositions on mylar and kapton that exhibit good adherence properties. Data to date indicates that proper process control yields good results. The weight of gold coated insulation will not be significantly different from aluminized blankets which exhibit minimum weight for given effective conductivity. The thermal performance of gold coated mylar is at least as good, if not superior to, its aluminum-coated counterpart, which as Table 1 indicates, gives the best performance on the basis of weight.

The selection of kapton as the outer cover sheets provides the ability to withstand steady state temperatures up to 400°C (752°F). The thermo-optical properties are stable and result in reasonably low α/ϵ characteristics which is particularly desirable in regions of solar incidence.

3.3. COATINGS

The criteria for selecting thermal control coatings involve the following considerations:

a. The appropriate combination of thermo-optical properties for achieving requisite temperatures.

b. Satisfactory handling characteristics in a ground environment. This includes durability and the ability to be cleaned or repaired.

c. Adhesion characteristics.

d. Durability in the space environment, i.e., resistance to degradation due to UV and particulate radiation. (UV stability is not as significant for a Mars mission as for a Venus mission.) Table 3 lists coatings which have been used on the Mariner and other spacecraft which have potential application to Voyager.

4. BASELINE DESIGN

4.1. INSULATION BLANKETS

The insulation design for the three principal regions indicated in the sketch below is given in Table 4. Except as otherwise noted, the material is 1/4 mil wrinkled aluminized mylar.

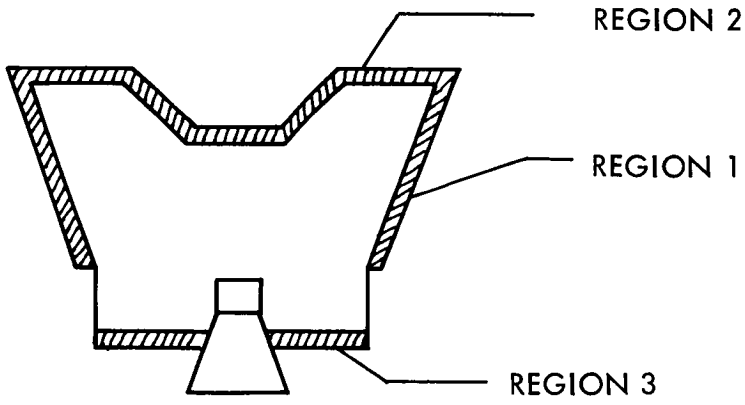

The blanket configuration selection was based on a thermal balance of the spacecraft at near Earth and near Mars conditions. The latter (with lander ejected) results in the maximum heat leak from the spacecraft and was taken as the criterion for selection. The average spacecraft temperatures used to derive the heat leak were taken from preliminary thermal analyses and are as follows:

Table 3. Thermal Coatings

Coatings	Solar Absorptivity	Emissivity	α/ϵ	Application to Voyager
Metals				
Aluminum (Polished)	< 0.2	$< .05$		Attitude control nozzles
Gold	0.24	$< .05$	$\sim 5.$	Internal surfaces where high reflectivity is desired,
Rhodium		$< .05$		eg, interface between lander and spacecraft
Conversion Coatings				
Dow 7		0.7		Utilized on magnesium for high emittance applications, eg, electronic chassis
Alzak	0.18	0.73	0.25	Equipment bay radiator plates
Black Paints				
Cat-a-lac (Epoxy)		> 0.9		Internal surfaces of spacecraft, back of solar array
3M Optical Velvet				
Parsons Black (Lacquer)				
White Paints				
Vitavar PV 100 (TiO_2 pigment in silicone alkyd binder)	0.21	0.83	0.24	Equipment bay radiator panels
Z-93 (ZnO in Potassium)	0.17	0.92	0.19	Equipment bay radiator panels
S-13 IIT (Zn in methyl silicone)	0.2	0.9	0.22	Equipment bay radiator panels
Rutile (TiO_2 in methyl silicone)	0.23	0.85	0.27	Equipment bay radiator panels
Metal Filled Paints				
Chrome Oxide Pigmented Polyurethane	~ 0.7	~ 0.7	~ 1.0	High gain antenna
D4D-Aluminum leaf pigment in silicone-alkyd	0.26	0.27	0.96	External Equipment (To minimize Mars orbit transients

Near Earth $T = 80°F$

Near Mars $T = 50°F$

These temperatures are very nearly equal to the temperature experienced by the propellant tanks which are located near regions 1 and 2. These regions represent over 80 percent of the heat leak area considered.

Table 4. Voyager Insulation System

Region	Area, FT^2	Total No. Layers	Effective* Emissivity	Blanket** Outer Cover
No. 1 (Upper bus model)	277	30	0.006	2 mil Kapton - aluminized one side - outer surface Kapton
No. 2 (Interface between spacecraft and lander)	139	30	0.006	
No. 3 (Aft surface of spacecraft)	123	20 + 9 layers 1/2 mil aluminized Kapton + cover	0.006	2 mil Kapton - aluminized on one side - outer surface Kapton

* Effective emissivity based on PVTIS results for 35 layers of insulation with an added margin of 50 percent.

** The thermo-optical properties of the Kapton surface of the cover material is $\alpha = 0.41$; $\epsilon = 0.8$ and was determined from PVTIS tests (after UV exposure).

The total weight of the insulation system is 45 pounds.

Figure 1 shows the heat leak from the spacecraft for the various regions; Figure 2 gives the total spacecraft heat leak including shorts in the blankets due to struts, appendage structural ties, and conduction to the biobarrier as a function of insulation weight. Rationale for selecting the number of layers (weight) was based on the following considerations for the near Mars condition without the lander, since this represents a condition for which the largest heat leak from the blankets will occur.

a. Total internal power generation is 500 watts under normal operating conditions. The sum of the heat loss through blankets and thermal shorts and the power radiated from equipment bays must therefore equal 500 watts.

b. With all louvers on equipment bays closed ($\epsilon_{eff} = 0.1$), the minimum power radiated from the bays will be 255 watts at the low limit ($40^{o}F$) of the required operating range. (The radio bay does not have louvers and alone will dissipate 91 watts.)

c. The insulation design must limit the heat leak to the difference of (a) and (b), i.e. 500-255 = 245 watts if requisite temperatures are to be maintained.

d. From Figure 2, it is evident that approximately 20 pounds ($\sim$10 layers) is required to limit the heat leak to 245 watts.

An adequate design must of course allow for margins. As a ground rule, the blanket design was selected to allow for a 25 percent decrease in spacecraft generated thermal power and still maintain requisite temperatures. Determination of the required insulation weight to provide for this contingency of a 125-watt reduction in power (which can be considered the thermal margin) is as follows:

a. Total spacecraft thermal dissipation = 375 watts.

b. Power radiated from bays at minimum average temperature of $40^{o}F$ is as before, 255 watts.

c. Insulation heat leak = 375 - 255 = 120 watts.

d. From Figure 2 approximately 45 lbs (30 layers) is required.

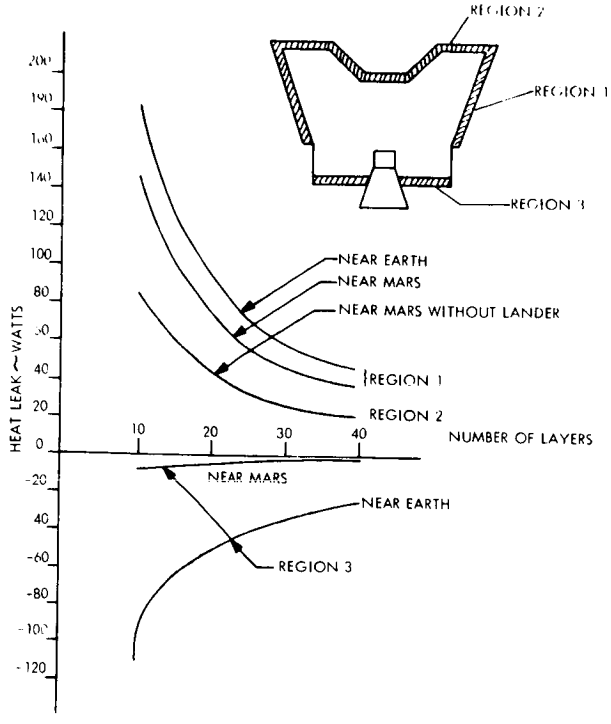

Figure 1. Heat Leak From Spacecraft Through Insulation Blankets

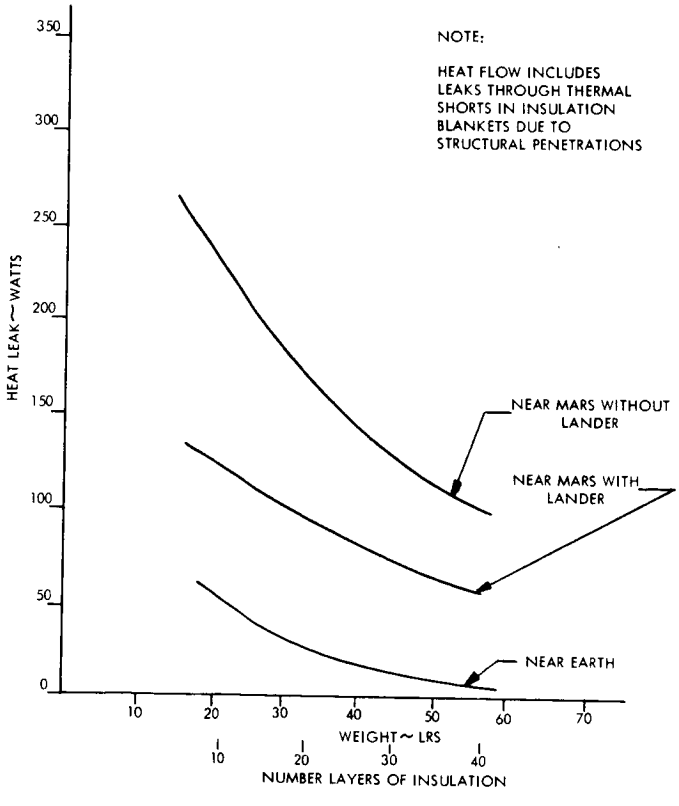

Figure 2. Heat Leak From Spacecraft Versus Insulation Weight

It should be recognized that severe thermal stresses may result at the attachment points of the spacecraft to the biobarrier when the capsule is ejected. If the biobarrier structural surface is exposed to space it will attain very low temperatures and temperature differences between it and the spacecraft structure can well exceed 250°F. This problem may require insulation blankets on the capsule side of the biobarrier to preclude excessive temperature differentials.

4.1.1. Insulation Attachment Technique

Blanket insulation joints designs and fasteners have been developed during the course of the PVTIS program which will be utilized on Voyager. A rabbeted joint and support post configuration used in PVTIS tests is shown in Figure 3. The new fastener for attaching insulation to the spacecraft is shown in Figure 4 and has the following advantages:

a. The fastener posts are inserted into holes drilled through a multi-layer material lay-up during insulation blanket manufacture. The retaining washers are snapped on, so the blanket layers are constrained within the assembly without any stitching or other restraints.

b. The Velcro pile pad bonded to the spacecraft skin is larger than the Velcro hook disc bonded to the base of the fastener. Therefore, there is no problem with close tolerance at assembly as the Velcro hook will attach to the pile anywhere on its surface. Position adjustment is easily performed by pulling the fastener loose from the pile and re-positioning.

c. This fastener system has been demonstrated to withstand satisfactorily 200 g shock, 148 decibal acoustic exitation, and 15 g rms random vibration.

4.1.2 Insulation Venting

Venting is required to avoid "ballooning" during ascent depressurization. Figure 5 summarizes the results from a series of depressurization tests performed as part of the PVTIS program on 4-foot by 10-foot multilayer insulation assemblies with different numbers of random vent holes in each material layer. Assemblies G5, G6, and G8 had fasteners only around the insulation periphery, while G7 included a center row of fasteners that effectively divided the assembly into two 2 x 10 foot blankets. Based on these tests, four 1/8-inch

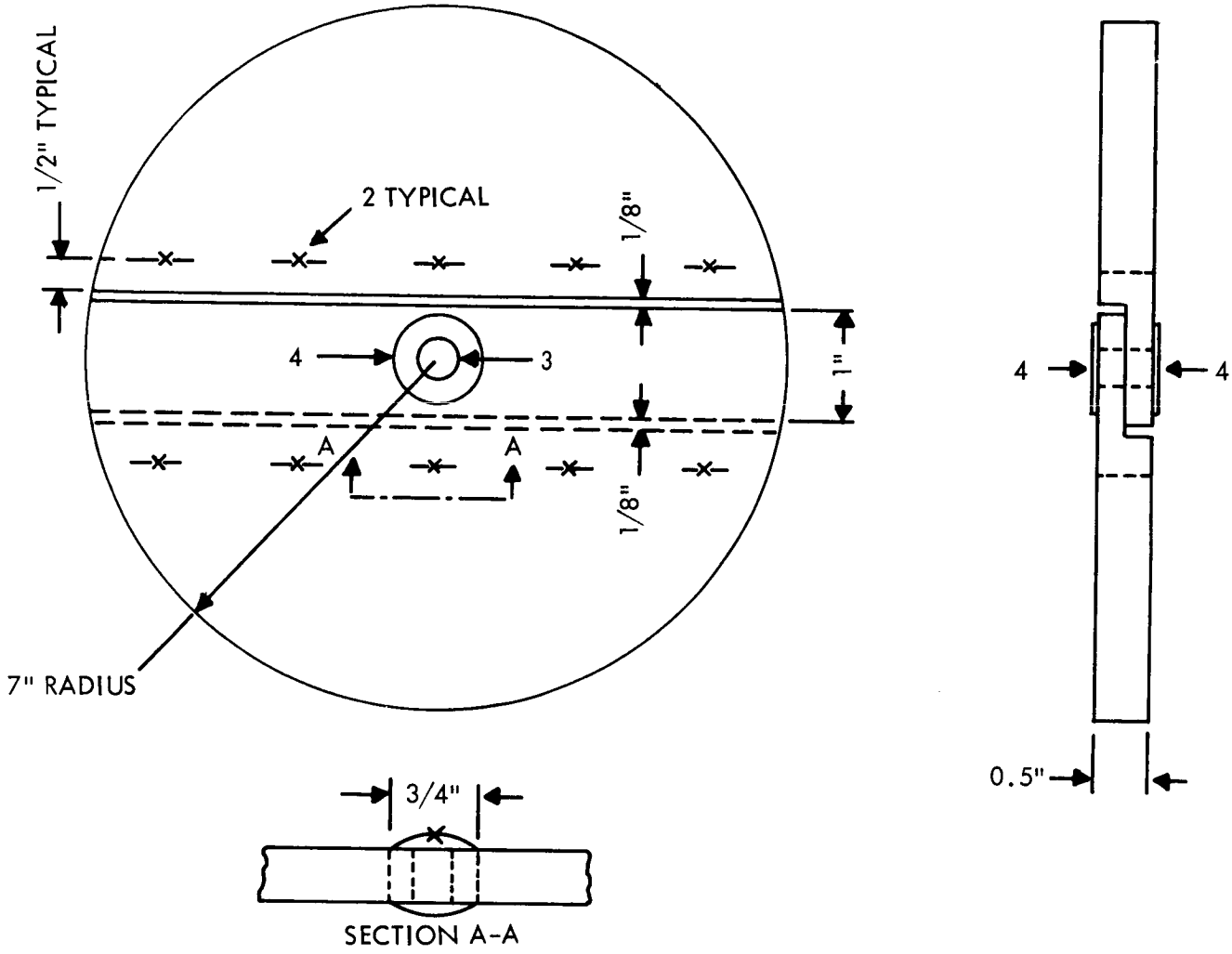

NOTES:

1. 36 layers NRC-2 crinkled aluminized Mylar insulation 18 layers each group at joint
2. Single fiberglass thread stitch, begin stitch 1/2 inch from circumferential edge; evenly spaced
3. 1/4-inch-diameter nylon (Nylatch) post, cut 0.485± 0.005 inch
4. 1/2-inch-diameter piece of adhesive aluminized Mylar tape (Permacel) to retain post in sample

Figure 3. PVTIS Rabbeted Joint and Support Post Configuration

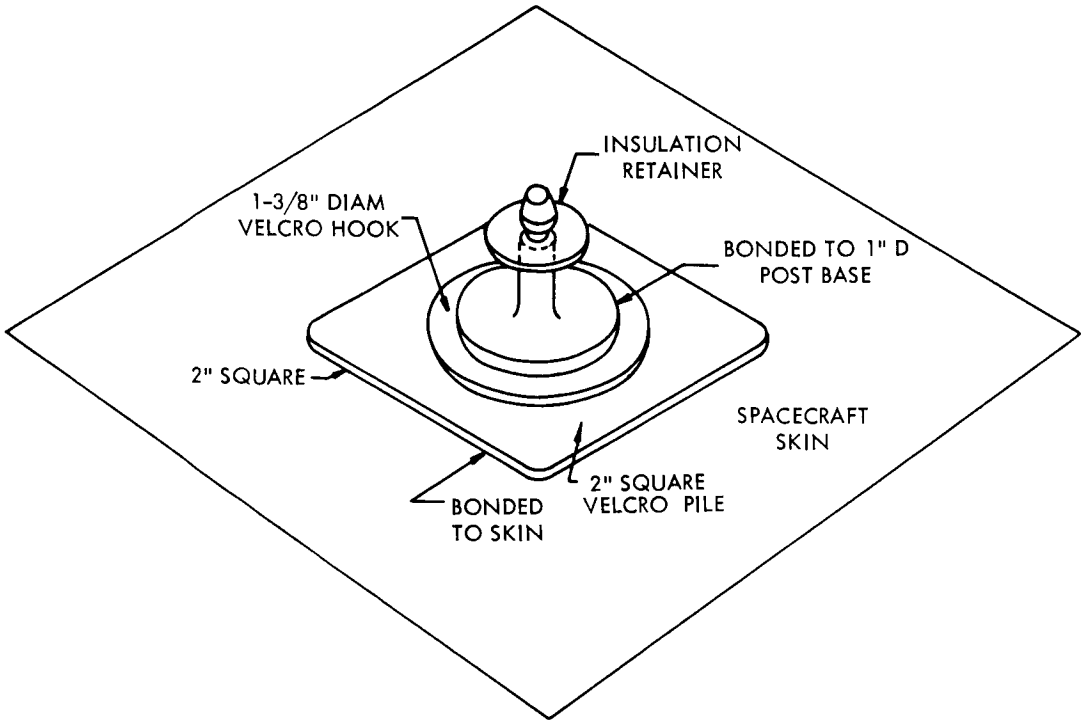

Figure 4. Insulation Fastener

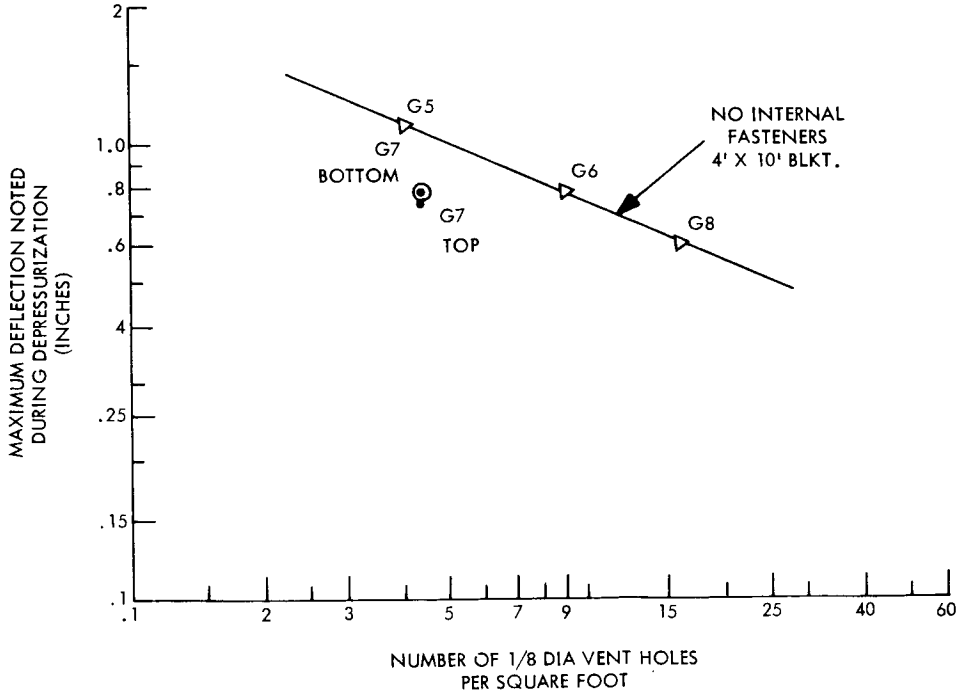

Figure 5. Maximum Deflection Versus Number Vent Holes Per Square Foot

diameter holes per square foot have been slected for insulation design and manufacture. The vent holes in each layer are misaligned with respect to adjacent layers, avoiding a direct heat leak path.

The vent holes are not expected to affect the insulation thermal performance by a measurable amount. Conductivity tests have been performed on gold-coated mylar insulation samples which were similar except that one had nine 1/8-inch diameter vent holes per square foot. These two assemblies yielded the same performance values, confirming that four holes per square foot will have no effect.

4.2. PRELIMINARY COATING SELECTION FOR VOYAGER

The following preliminary coating selections have been made for the spacecraft:

a. Equipment bay radiator plates
Outboard surface
Vitavar - PV100 white paint
$\epsilon = 0.83$
$\alpha_s = 0.21$

This paint has good adhesion characteristics, is reasonably easy to apply, can be cleaned, is insensitive to ETO decontamination and is reasonably stable to UV.

The choice of a white paint with a higher emissivity than alzak (selected in Task B) results in a larger thermal design margin in bay radiator power dissipation capability.

Inboard Surface

Catalac Black - $\epsilon \approx 0.9$

b. Back of solar array
Black paint, selected for avoiding stray reflections to sensors.

c. Interior of spacecraft - structure, tanks, and components
Catalac black - $\epsilon \approx 0.9$

d. External surfaces of insulation blankets
Uncoated - Plastic (Kapton) side of cover sheets will face out board.
$\epsilon = 0.8$
$\alpha = 0.41$

4.3. LOUVERS AND RADIATOR PLATES

The radiating plate of each equipment bay has an area of 3.5 ft^2 and is painted with a white paint (VITAVAR PV100) having an emissivity of 0.83 and solar absorbivity of 0.21. The plates are 0.063 inches HM21A-T8 magnesium alloy. All bays except the high power radio bay (No. 12) will be equipped with a louver assembly that attaches to supporting structure at the periphery of the radiator plates. Each louver assembly consists of six louver blades, 4 inches by 21 inches, and will have the capability of opening a full 90 degrees. Louvers will be fully closed at 40 °F and fully open at 70 °F. Each louver will be activated by a bi-metallic coil. If tests determine inadequate design margin in actuator control, the blade dimensions will be reduced to 2 inches x 24 inches (similar in size to the Mariner '64 blades.) Figure 6 is a schematic diagram of the basic design features which will be applied to the Voyager spacecraft. (Ref. JPL Technical Report 32-955.) The louver blades will be a thin wall aluminum tube with cover sheets approximately 0.005 inches formed into a box section. The blades will have highly polished specular surfaces (either highly polished aluminum or gold-coated aluminum). A schematic of the louver blades is given in Figure 7.

4.3.1. Louver System Thermal Performance

Louver system performance is based on heat dissipation capability as a function of blade angle opening, which is influenced by the presence of the solar array. In the presence of such external factors the effective emissivity of the louvers is given by:

$$\epsilon_{eff}(\varphi) = \frac{2\epsilon_K \,\mathrm{SIN}\,\varphi}{\epsilon_K + \rho_K \,\mathrm{SIN}\,\varphi}\left\{.5 - S_{F_{K4}}\epsilon_4\left\{\frac{T_4}{T_K}\right\}^4\right\}$$

where:

$S_{F_{K4}}$ = Specular view factor between equivalent backplate surface and external panel.

ϵ_4 = Emissivity of the solar panel

T_4 = Solar panel temperature

T_K = Backplate temperature

ϵ_K = Backplate emissivity

φ = Louver blade opening angle

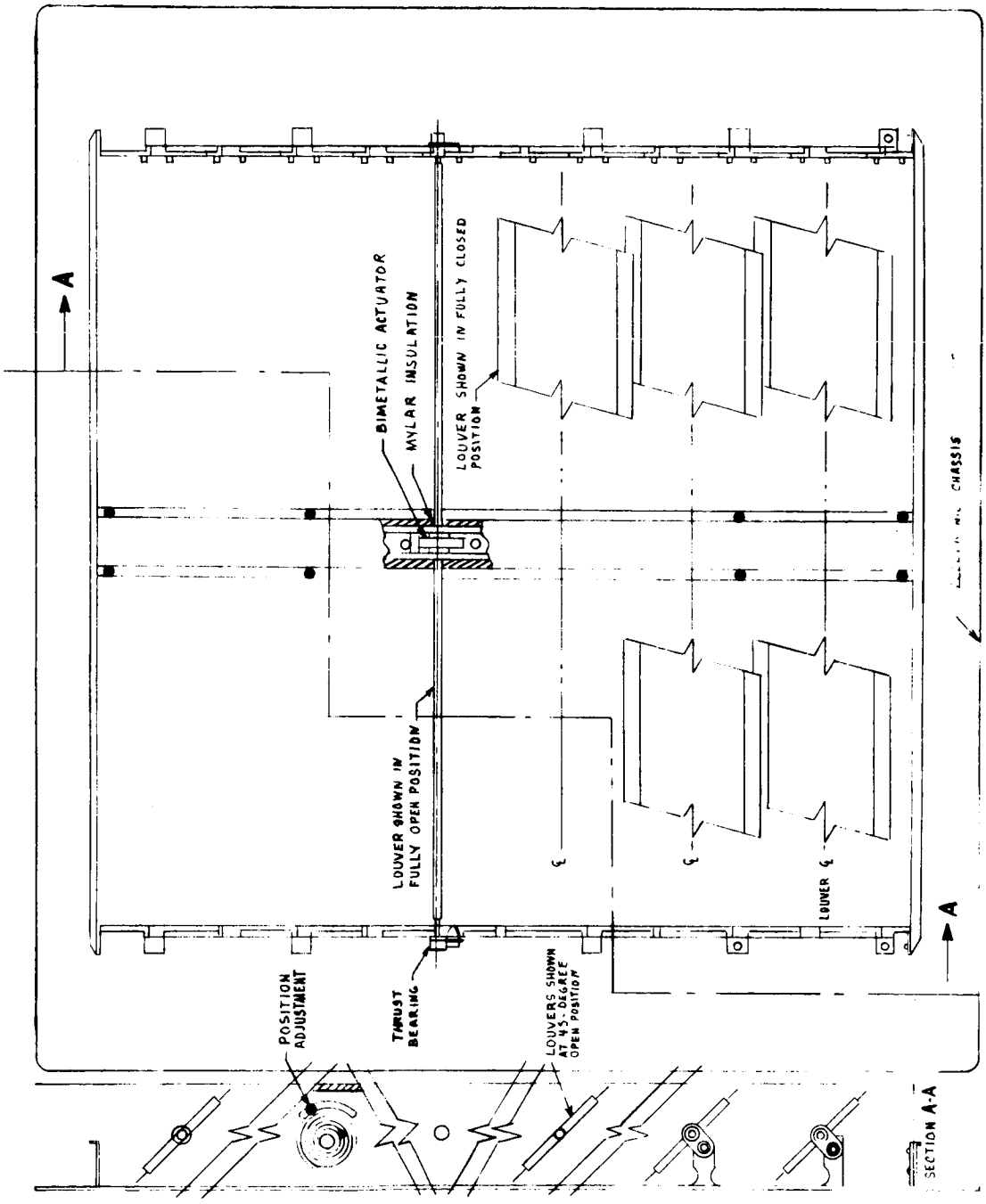

Figure 6. Louver Installation

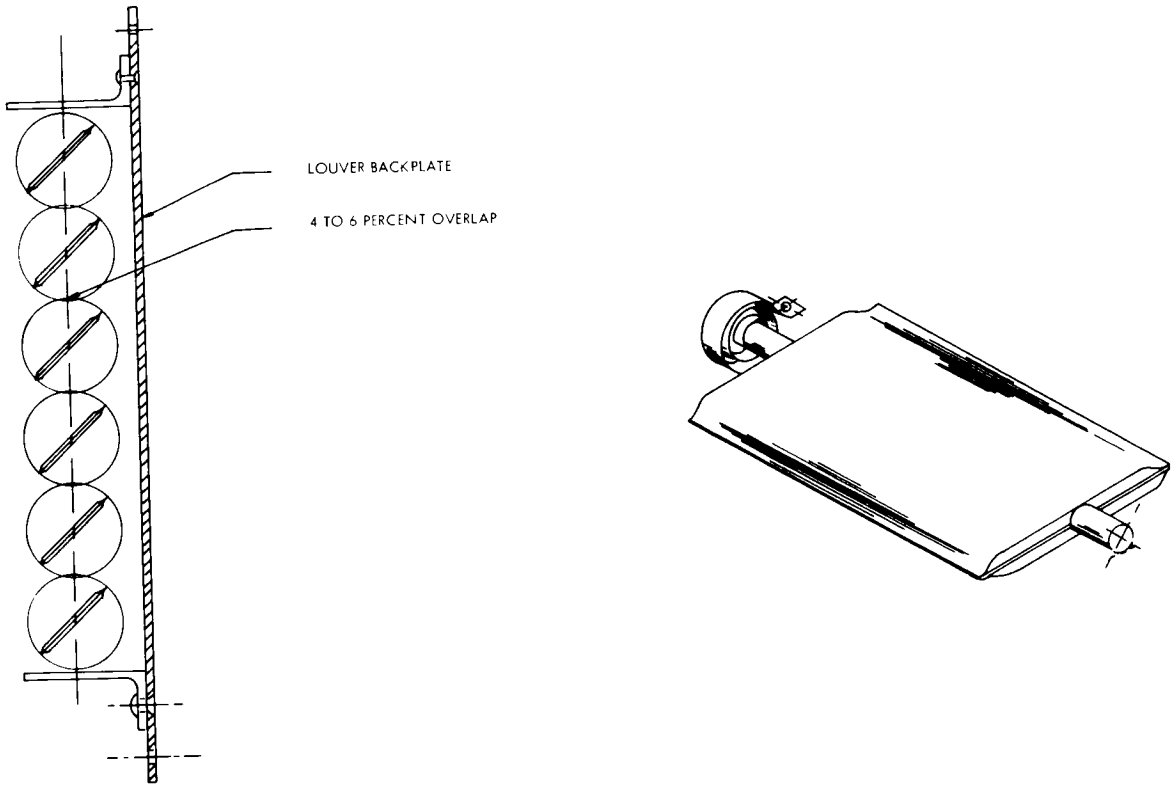

Figure 7. Schematic Diagram of Louver Actuation System

The heat dissipation is then given by:

$$Q(\phi) = \sigma A \epsilon_{EFF}(\phi) T_K^4$$

where:

$Q(\phi)$ = Heat dissipation capability at a specific louver blade angle opening.

σ = Stefan - Boltzmann constant.

T_K = Backplate temperature.

A = Surface area of radiation

This set of equations along with solution of the specular view factors were programmed on a digital computer. The results for the baseline configuration are given in Figure 8 for both clockwise and counter-clockwise rotation. Counter-clockwise rotation is selected for Voyager applications to provide for maximum heat dissipation at smaller louver angle openings. As indicated on the figure the maximum heat dissipation for the louver system is 94 watts and which occurs for a maximum effective emissivity of 0.72 at angles openings close to 70 degrees.

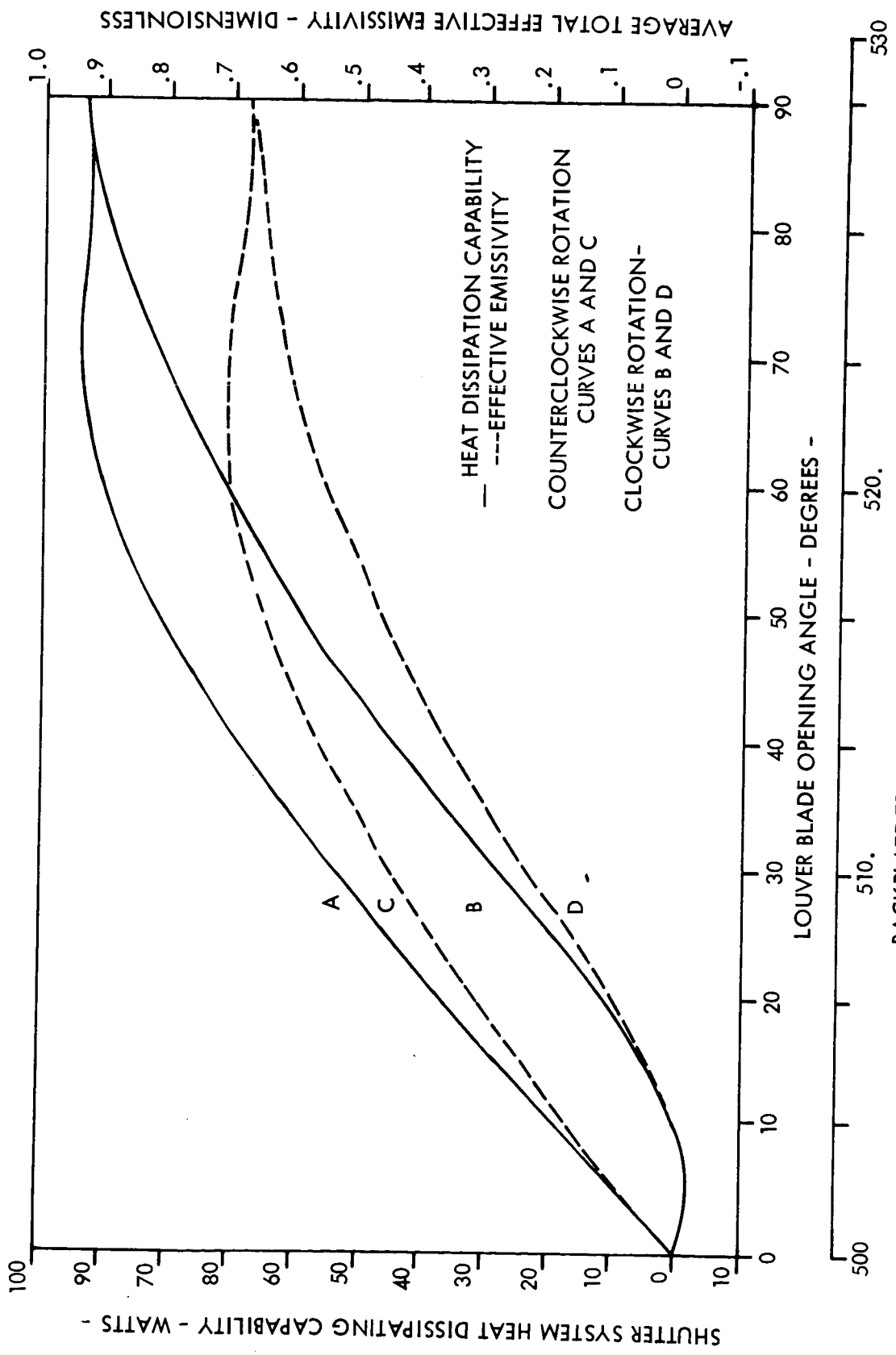

Figure 8. Heat Dissipation Capability Louver Blade Angle Opening

4.4. EQUIPMENT BAY THERMAL COUPLING

Electronic sub assemblies within each bay will be bolted to the radiator cover plates with approximately 40 to 50 bolts. This thermal coupling along with other heat paths, will limit temperature differences between the module surfaces and the radiator plate to less than 7°F for the highest equipment power anticipated. No thermal grease will therefore be required. Bolts will be torqued to at least 20-in-lb. to assure adequate conductance.

Over-all conductive and radiative coupling of the electronics module is sufficient to damp out large temperature differences if the sun is directly incident on any bay. For example, if the sun is incident on the highest power equipment bay (-112 watts), during sun acquisition or mid-course correction, only a 12°F temperature rise is experienced. The effects of louvers failing open or closed will also be minimized by the good thermal coupling within the electronics module.

4.5. HEATERS

Five watt strip heaters will be provided on propellant tanks to provide redundancy in the thermal control system and preclude freezing of the propellants in the event of catastrophic failure of the thermal control system. Heaters will also be provided on external nitrogen gas lines. These heaters will generally be sized between 2 and 5 watts. Heaters will be controlled by bi-metallic thermoswitches (e.g. Klixson type M25 - Texas Instruments).

4.6. LEMDE ENGINE

4.6.1. Nozzle Extension

A comparison was made of the effects of a radiation cooled nozzle extension and an insulated nozzle extension. It was found for the radiation cooled nozzle that at orbit insertion, the outer surface of the insulation blankets at the aft end of the spacecraft would reach temperatures of the order of 1100°F. This exceeds the property capabilities of Kapton and would require material such as steel foil. Heat leakage through possible thermal shorts in the blankets, could be a problem at this elevated temperature. Use of Fibrefrax (6 lb/ft^3)

insulation on the outside surface of the nozzle extension will reduce this temperature to 500 °F even if the insulation has a high emissivity on its outer surface. Calculations indicate that if a low emissivity ($\epsilon = 0.15$) is obtained on the insulation, one eighth of an inch (1/8) of the fibrefrax weighing less than 5 pounds can reduce the blanket temperatures to approximately 350°F. The use of an insulated nozzle extension is consequently part of the baseline thermal design.

4.6.2. Plume Heating

Radiation effects on the spacecraft were calculated for the LEMDE plume and were found to cause a steady-state increase in temperature on the aft surface of the insulation blankets of less than 30°F. The calculations were based on a MSFC program using a statistical band model with modified Curtis-Godson approximation which accounts for both doppler and collision broadening. Only emission from the water, carbon dioxide and carbon monoxide constituents were considered. At a radial distance of 60 inches from the nozzle throat, the radiant heat flux at the spacecraft aft surface is 33.84 BTU/HR-FT^2.

The engine plume characteristics generated by TRW indicate that no convective heating will occur on the spacecraft.

5. SPACECRAFT THERMAL ANALYSES

5.1. THERMAL MODEL

The spacecraft configuration was modeled by 43 lumped mass nodes for analyses on the 7094 digital computer. A detailed nodal breakdown is given in Figure 9. The major assumptions in the development of the model were as follows:

a. Equipment bays (nodes 1-16)
   1. Bay radiator plate
      (a) External area - 3.5 ft^{2}bay
      (b) Plate painted with PV100 white paint ($\epsilon = 0.825$)

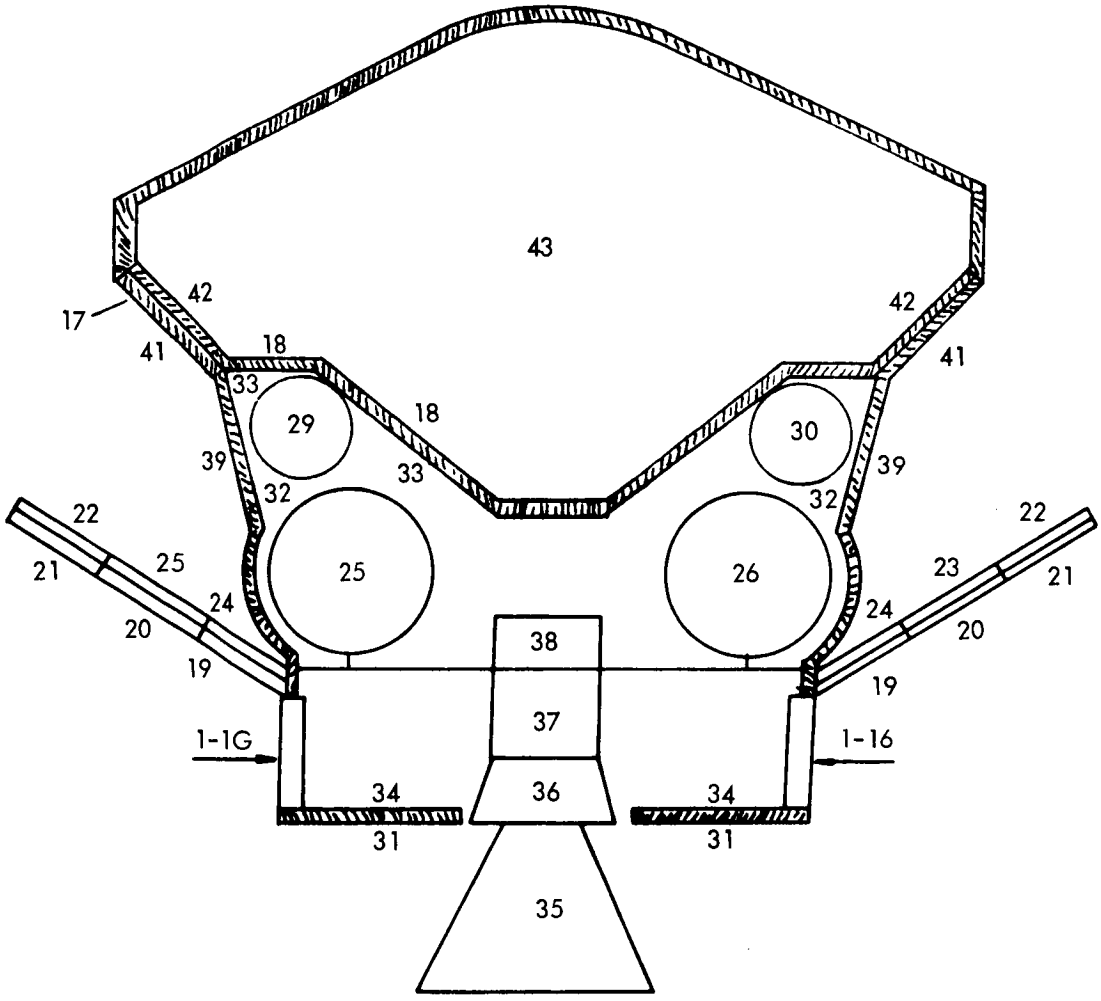

NODE NO.

1. Power
2. Power
3. Science Electronics
4. Spare
5. Science Electronics
6. Science Data Automation System
7. Data Storage
8. Data Storage
9. Telemetry
10. Command
11. Radio
12. Radio
13. Relay Radio
14. Computer & Sequence

NODE NO.

15. Guidance & Control
16. Power
17. BioBarrier
18. Sup.-Ins. on Top of S/C
19. Solar Array
20. Solar Array
21. Solar Array
22. Rear of Solar Array
23. Rear of Solar Array
24. Rear of Solar Array
25. Fuel & Oxidizer Tanks
26. Fuel & Oxidizer Tanks
27. Fuel & Oxidizer Tanks
28. Fuel & Oxidizer Tanks

NODE NO.

29. Pressure Tanks
30. Pressure Tanks
31. Super Ins. on Bottom
32. Inside Structure
33. Top Super Insulation
34. Bottom Structure
35. Nozzle
36. Nozzle
37. Engine
38. Engine
39. Outside Super Insulation
40. Space
41. Sup,-Ins. on Bottom of Bio.
42. Sup.,-Ins.on Top of Biobar.
43. Lander

Figure 9. Spacecraft Nodal Breakdown

(c) Shutters in fully opened position at 70°F will reduce effective emissivity of plate to 0.68 and in fully closed position at 40°F to $\epsilon_{eff} = 0.1$.

2. Internal surface

(a) Area = 3.14 Ft^2bay

(b) Emissivity = 0.90

3. Conductance between bays = 1.0 Btu/hr-°F

4. Weight and thermal dissipation as given in table.

b. LEMDE engine and insulated extension nozzle (nodes 35-38)

1. External emissivity

Engine = 0.15

Nozzle extension = 0.80 (from personal communication with TRW)

2. Temperature histories on exterior surface during midcourse correction and orbit insertion. (from reference 1)

c. Fuel, oxidizer, and pressure tanks (nodes 25-30)

1. Fuel and oxidizer tanks

(a) Area = 54.5 ft^2/tank

(b) Emissivity = 0.90

2. Presure tanks

(a) Area = 19.6 ft^2/tank

(b) Emissivity = 0.90

d. Solar array (nodes 19-21)

1. Cell packing factor = 0.90

2. $\alpha_s = 0.75$, $\epsilon = 0.80$

3. Conductance from front to back of array = 7.0 Btu/hr-°F-FT^2

4. Back of array, emissivity = 0.90

e. Superinsulation

1. Top of spacecraft (node 33)

(a) Thickness = 30 layers

(b) Effective emissivity from innermost to outermost layer = 0.006

2. Side of spacecraft (node 39)

(a) Thickness = 30 layers

(b) Effective emissivity from innermost to outermost layer = 0.006

3. Bottom of spacecraft (node 34)

(a) Thickness = 30 layers

(b) Effective emissivity from outermost to innermost layer = 0.006.

(c) Emissivity of innermost layer = 0.05.

4. Bio-barrier - 15 layers on each side of bio-barrier structure (nodes 41 and 42) 0.012.

f. Structure (node 32)

1. Internally painted with low emissivity coating ϵ = 0.05.

5.2. DESIGN CONDITIONS

The thermal analysis was performed for the complete Voyager mission profile.

a. On-pad operation

b. Ascent Through Parking Orbit

c. Near Earth - Steady-state hot soak condition with a solar flux of 442 Btu/ft^2-hr

d. Midcourse correction - Transient temperature response of the spacecraft after low thrust firing of LEMDE engine with high initial spacecraft temperature.

e. Near Mars - Steady-state cold soak condition with solar flux of 175 Btu/ft^2-hr (at furthest distance from Sun -1.6 AU)

f. Orbit insertion - Transient temperature response of spacecraft after high thrust firing of LEMDE engine.

g. Near Mars after lander ejection--Steady-state cold soak condition with solar flux of 175 Btu/ft^2-HR and additional heat leak from top of spacecraft. This represents the coldest condition for the spacecraft.

h. Transient condition during non-illuminated portion of Mars orbit.

To provide adequate thermal design margin, the temperature constraint that governed the thermal design was to maintain propellant tanks and all electronic equipment within the range of 40 to 70 °F. The spacecraft thermal response for the mission phases are discussed in the following paragraphs.

5.3. RESULTS - THERMAL RESPONSE OF SPACECRAFT

A summary of all temperature and equipment thermal dissipation for the mission phases is given in table 5.

5.3.1. On-the-Pad Operation

Steady state analysis for an on the pad condition with spacecraft electronics operating at the power levels given in Table 5 (for a near earth condition) indicate an average equipment bay temperature of approximately 110 °F. This was calculated in the absence of any forced cooling, with ambient air temperature of 90 °F and a solar load on the shroud at an angle of incidence of 45 °. In order to maintain electronic equipment temperatures below 70 °F for long life reliability, on-pad cooling is required. It is proposed that this be accomplished by providing filtered dry air-conditioned air or a combination of air and gaseous nitrogen at temperatures between 40 to 55 °F, and directing this flow over the electronic bays. A flow rate of approximately 10 pounds per minute would maintain electronics below 70 °F. Since ground conditioning equipment typically can supply of the order of 300 pounds per minute at temperatures between 20 °F and 70 °F, a large cooling margin is anticipated.

Table 5. Thermal Balance

Spacecraft Components	Bay No.	On Pad	Temperature (°F)											Thermal Dissipation (Watts)		Operating Temperature Limits (°F)	
			Parking Orbit		Near Earth	Mid-Course Maneuver		Near Mars	Orbit Insertion		Near Mars W/O Lander	Mars Eclipse		Near Mars	Near Earth		
			Minimum	Maximum		Minimum	Maximum		Minimum	Maximum		Minimum	Maximum			Minimum	Maximum
Power Compartment	1	< 70	85	89	55	55	62	54	54	63	53	51	53	48.3	39.7	40	90
Power Compartment	2	< 70	80	84	53	53	60	54	54	63	52	49	52	43.5	35.2	40	90
Science Electronics	3	< 70	65	67	49	49	56	52	52	61	50	48	50	37.0	0.0	15	122
Spare	4	< 70	59	63	48	48	55	48	48	57	47	44	47	0.0	0.0	-	-
Science Electronics	5	< 70	59	63	48	48	55	51	51	60	50	48	50	37.0	0.0	15	122
Science DAE	6	< 70	61	65	48	48	55	50	50	59	49	46	49	30.0	0.0	15	167
Data Storage Subsystem	7	< 70	69	73	50	50	57	48	50	59	47	44	47	12.51	18.01	0	158
Data Storage Subsystem	8	< 70	70	74	51	51	58	48	48	57	46	43	46	12.51	18.01	0	158
Telemetry	9	< 70	67	71	50	50	57	47	47	56	46	43	46	8.26	8.26	0	176
Command Subsystem	10	< 70	72	75	51	51	58	49	49	58	47	44	47	20.4	20.4	0	185
Radio Subsystem	11	< 70	70	74	49	49	56	49	49	58	48	45	48	15.4	7.1	0	194
Radio Subsystem	12	< 70	87	91	17	47	54	52	52	61	50	48	50	112.4	61.4	15	167
Relay Radio Subsystem	13	< 70	73	79	49	49	56	50	50	59	48	45	48	13.0	0.0	15	167
Computer & Sequencer	14	< 70	89	92	56	56	63	53	53	62	52	50	52	50.0	50.0	0	114
Power Subsystem	15	< 70	82	86	54	54	61	52	52	61	51	49	51	32.7	28.0	40	90
Guidance & Control	16	< 70	85	89	55	55	62	52	52	61	51	49	51	27.7	36.4	15	90
Bio-Barrier	-										-70	-75	-70			-	-
Avg. Solar Panel (Solar Cell Face)		-	-63	51	143	143	143	17	17	17	17	-204	17			-250	250
Avg. Solar Panel (Back Surface)		-	-65	51	126	126	126	10	10	10	9	-204	9			-250	250
Avg. Fuel & Oxidizer Tanks		-	72	72	76	76	76	49	49	52	43	38	43			30	100
Avg. Pressure Tanks		-	72	72	76	76	76	49	49	52	43	38	43			30	100
Inside S/C Structure Cone		-	68	71	75	75	86	43	43	75	39	36	39			-	-
Side Structure on Top of S/C		-	70	73	76	76	99	49	49	91	30	26	30			-	-
Outside Superinsulation on Bottom Annulus		-	-30	51	202	202	245	58	58	151	58	-247	58			-	-
Inside S/C Structure Bottom Annulus		-	67	70	94	94	99	52	52	74	47	22	49			-	-
Nozzle Exterior Section		-	26	55	195	122	760	66	50	940	66	12	66			-	-
Nozzle Interior Section			64	64	135	100	355	62	100	485	58	27	58			-	-
Lower Section of Engine		-	72	74	70	100	355	50	100	485	44	14	44			-	-
Upper Section of Engine		-	72	74	70	100	355	50	100	485	44	14	44			-	-

5.3.2. Ascent and Parking Orbit

During the ascent stage, the shroud will reach temperatures as high as 300 °F. However, this elevated temperature level is shortlived since the ascent heating peaks at approximately 2 minutes and decays to negligible value 4 minutes after lift-off. The combination of this short heating pulse plus the high thermal mass of the spacecraft result in equipment bay temperature rises of less than 1 °F during ascent.

At the beginning of earth parking orbit, the shroud cover for the forward spacecraft is ejected and the equipment bays can reject heat directly to space. However, the shroud encapsulating the aft spacecraft is not ejected until the end of parking orbit which can be up to 90 minutes. Calculations indicate that during the Sun illuminated portion of parking orbit, maximum electronics temperatures will not rise higher than the peak values experienced during ascent heating. During the eclipse portion of earth parking orbit, the inside shroud temperature will decay to a minimum of minus 86 ° F resulting in a minimum average electronics temperature 4 °F below the maximum.

5.3.3. Near Earth Hot Soak Condition

The temperature distribution for the near earth condition is summarized in Figure 10 with detailed equipment bay temperatures given in Table 5. The average equipment bay temperature is 51 F with bays ranging between 47 °F and 55 °F. The propellant tanks at 76 °F are 25 degrees higher than the average of the electronics. This is primarily due to the influence of the solar array which causes elevated temperatures on structure adjacent to the tanks.

5.3.4. Midcourse Correction

The analyses to determine transient effects during midcourse correction and orbit insertion was performed for the LEMDE engine with an insulated nozzle extension. The potential thermal problem for this phase of the mission is overheating of the propellant tanks and electronics bays due to radiative interchange with the hot engine surface and overheating of the Kapton insulation cover at the bottom of the spacecraft due to radiative exchange with the nozzle extension. Because of the location of the solar array, it experiences no temperature rise during midcourse firing. The surface temperatures of the engine and nozzle extension are shown in Figure 11; Figure 12 summarizes the results. Inspection of this figure reveals

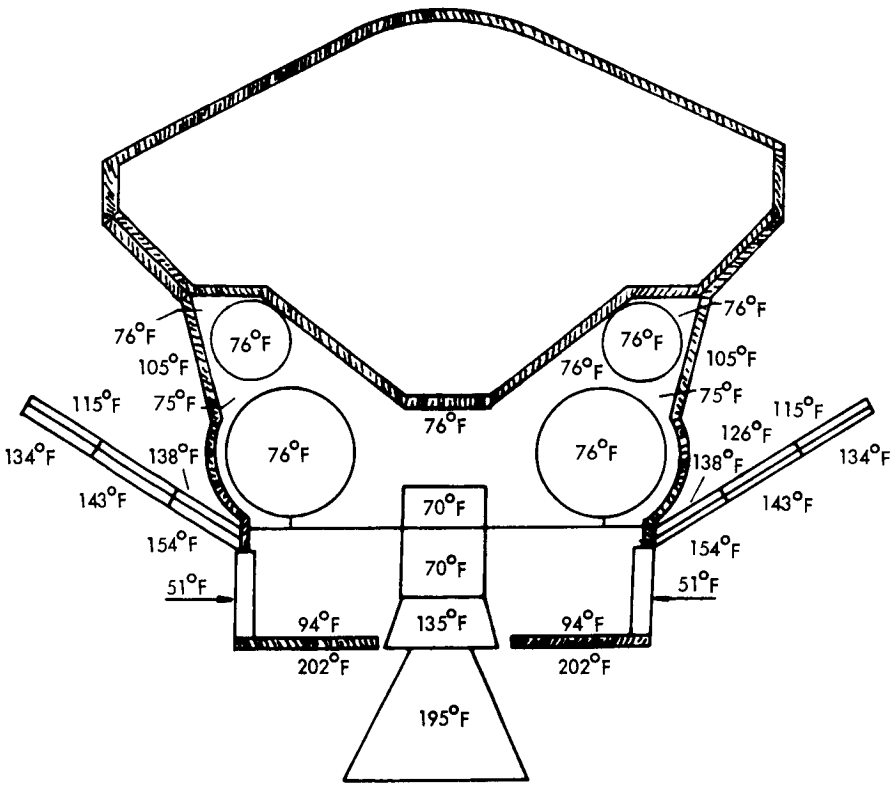

Figure 10. Temperature Distribution Near Earth (1.0 A.U.)

that the insulation blanket rises by approximately 43°F to a peak temperature of 245°F six minutes after firing and decays to approximately its initial temperature 0.5 hours later. The blanket can withstand this temperature rise with no significant degradation of performance. The temperature rise of both the electronics and propellant tanks are less than 7°F throughout firing and soakback. The soakback and heating during midcourse firing are consequently quite small, and no thermal problems are anticipated.

5.3.5 Near Mars

The near Mars condition is summarized in Figure 13. The equipment bay average temperature is 51°F. Because of the lower solar panel temperatures (8°F to 26°F) the propellant

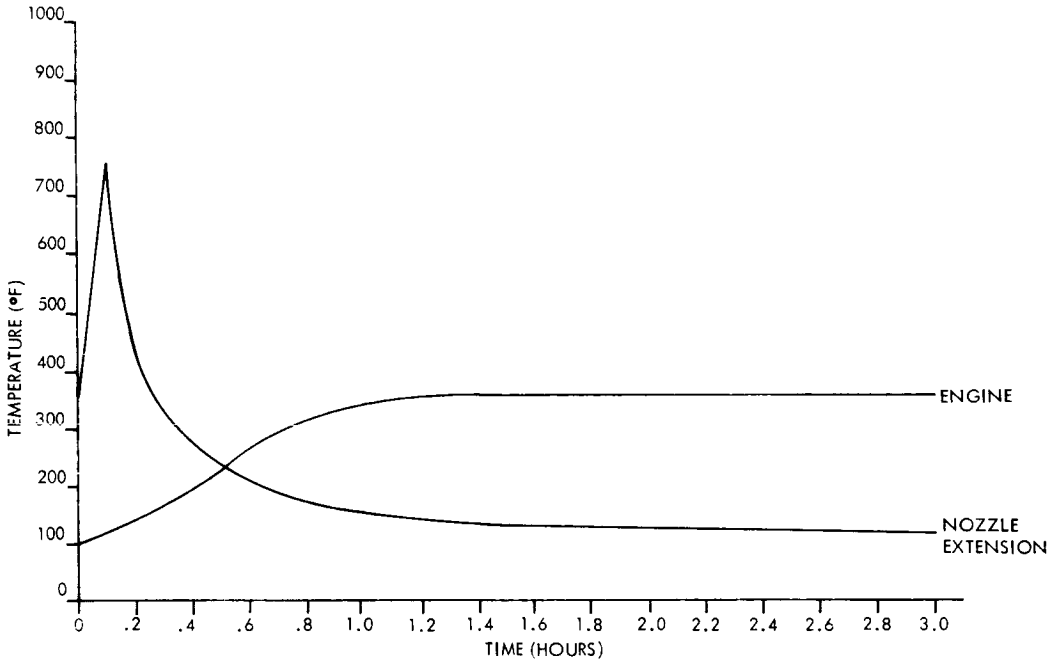

Figure 11. Engine and Nozzle Temperatures during Midcourse Maneuver Firing

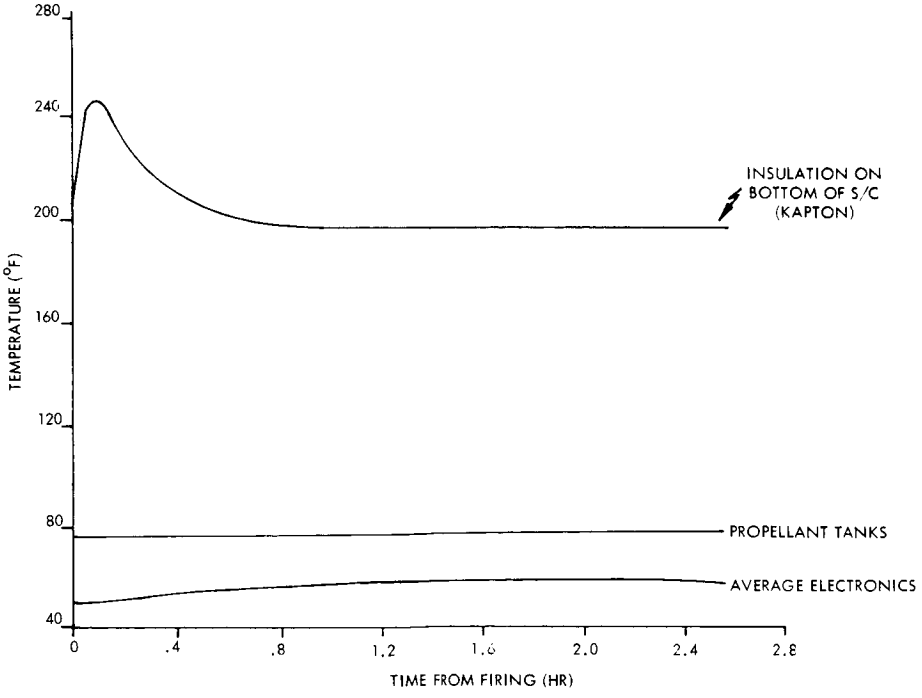

Figure 12. Effect of Midcourse Firing on Spacecraft Temperatures

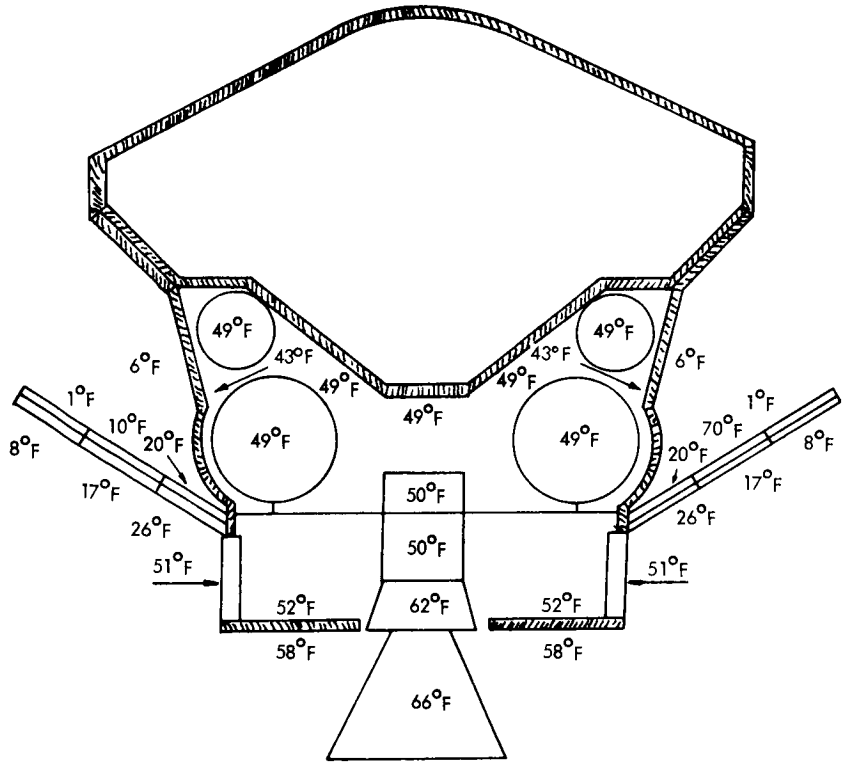

Figure 13. Temperature Distribution Near Mars

tank temperatures are reduced to 49°F. During the major time spent in transit, the spacecraft temperatures will fall between the near Earth and near Mars values.

5.3.6 Orbit Insertion

The orbit insertion analysis parallels the midcourse correction analysis with the main exceptions being primarily:

a. Initial temperatures are typical of a near Mars condition.

b. Engine and nozzle extension exterior temperatures are as given in Figure 14.

c. Electronics bay dissipations are typical of near Mars.

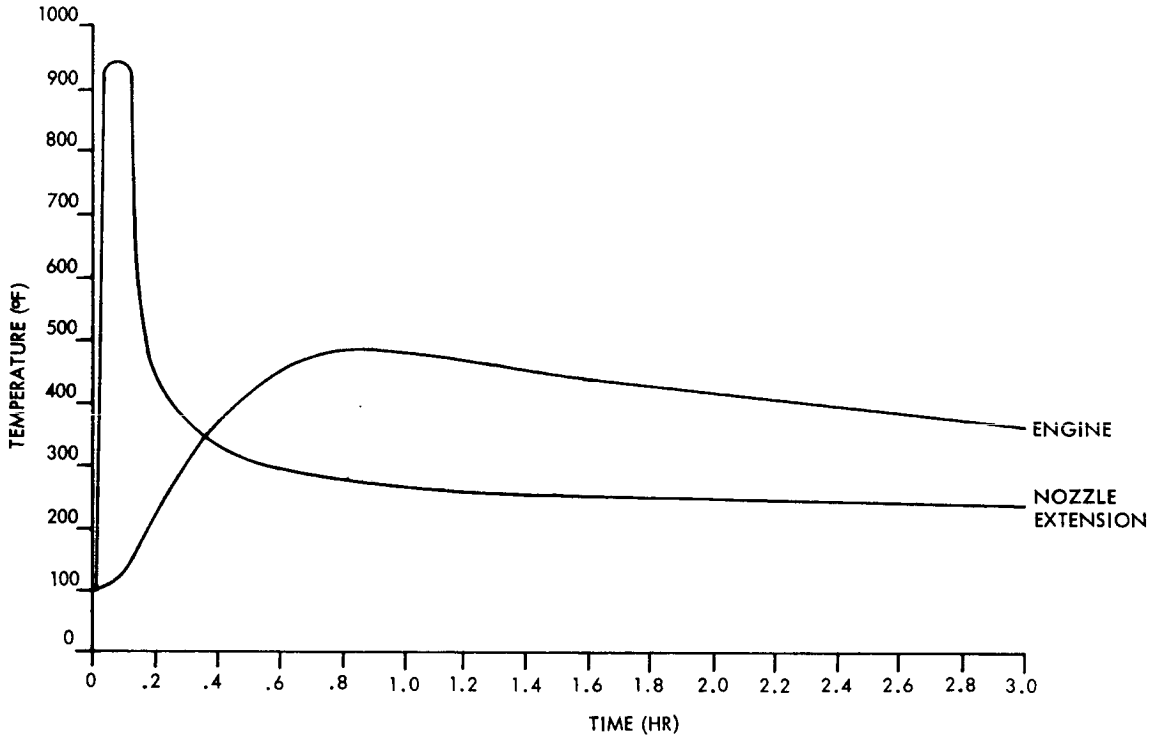

Figure 14. Engine and Nozzle Temperatures During Orbit Insertion Firing

Although the temperature rise caused by orbit insertion firing is more significant than midcourse firing, the initial temperature before orbit insertion is low enough so that the maximum temperatures of spacecraft components are lower than the peaks encountered during midcourse firing. Figure 15 shows the bottom insulation cover, electronics, and propellant tanks temperatures as a function of time after firing. Inspection of this figure reveals that there are no significant thermal problems during orbit insertion firing since the maximum temperature of the insulation blanket, electronics bays, and propellant tanks are 151°F, 58°F, and 52°F, respectively.

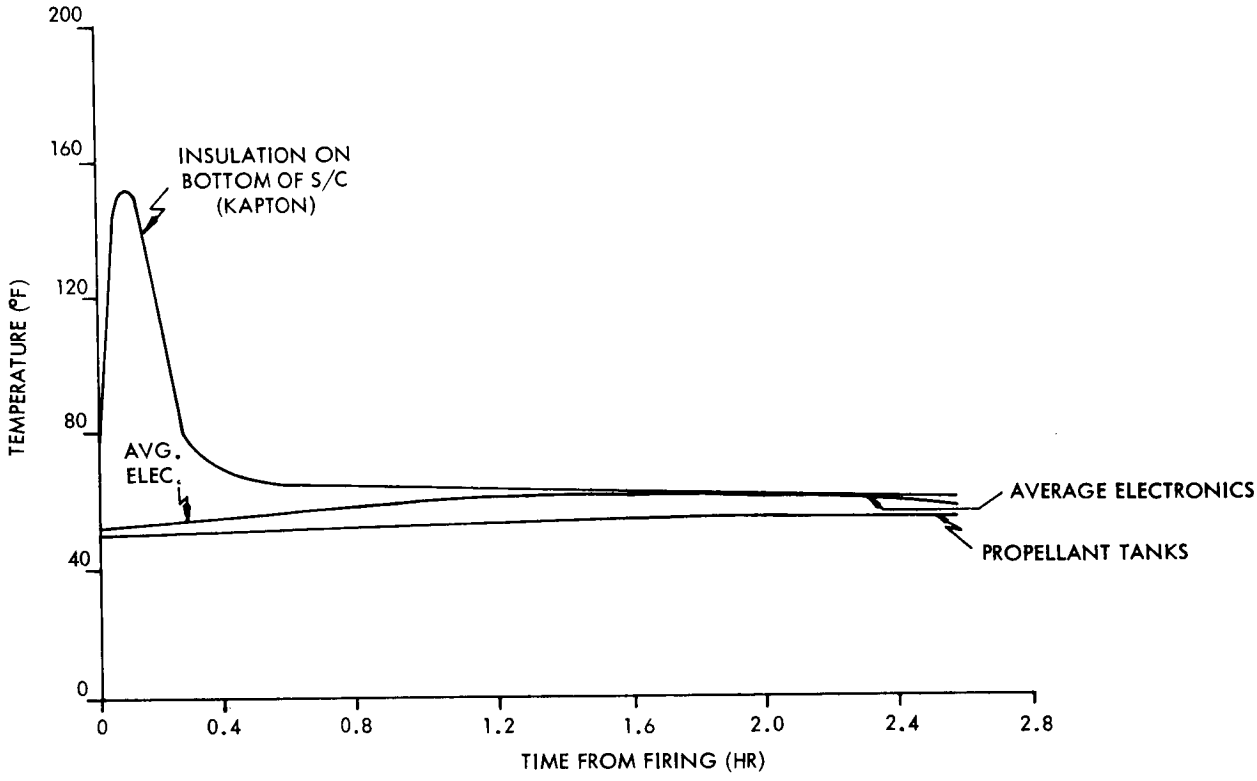

Figure 15. Effect of Orbit Insertion on Spacecraft Temperatures

5.3.7 Near Mars Without Lander

Figure 16 gives the temperatures for this coldest steady-state condition of the spacecraft. The average bay temperature is 49°F with individual bays ranging between 46°F and 53°F (see Table 5). The propellant tank temperature is 43°F.

5.3.8 Mars Orbit Solar Occultation

The transient effects on the spacecraft were examined for the portion of a Mars orbit during which the sun is occulted. The temperature variation is shown in Table 5. It can be seen that the electronic bays decrease to 47°F and the propellant tanks to 38°F after 1.5 hours. The strip heaters on the propellant tanks will preclude temperatures from falling below the propellant and oxidizer freezing points.

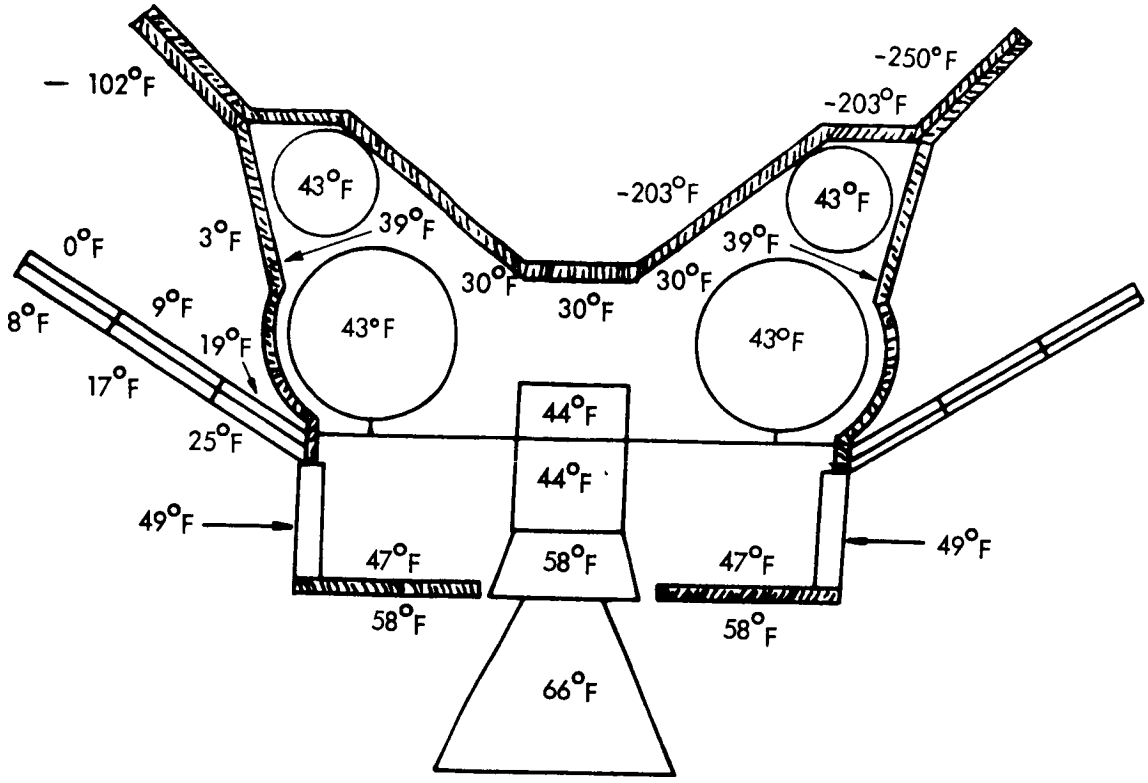

Figure 16. Temperature Distribution Near Mars (1.6 A.U.) W/O Lander

5.3.9 Solar Array

As a part of the over-all spacecraft thermal balance, solar array temperatures were calculated for the entire mission profile. The following information was used in modeling the solar array:

a. Solar array at an angle of 57 degrees from the spacecraft centerline.

b. Thermal properties of array

   a. $\alpha_s = 0.75$, $\epsilon = 0.80$

c. Back of array, $\epsilon = 0.90$

d. Conductance through the array equal to 7.0 Btu/hr-ft^2-°F

e. Conductance along the array.

The temperature of the solar array on the pad and during parking orbit will remain relatively close to the inside shroud temperature. After shroud ejection and sun acquisition, the solar array temperature will be a strong function of the spacecraft's distance from the Sun. Figure 17 shows solar array temperature variation as a function of array distance from the spacecraft for three selected points among those studied, which shows the array gradient during a Martian mission (1.0 to 1.6 A.U.). The average solar array temperature will vary during the cruise phase from 144°F to 17°F. Analysis has shown that during midcourse maneuver and orbit insertion, firing of the LEMDE engine has a negligible effect on the solar array because of the large distance separating the array and nozzle extension. During Mars

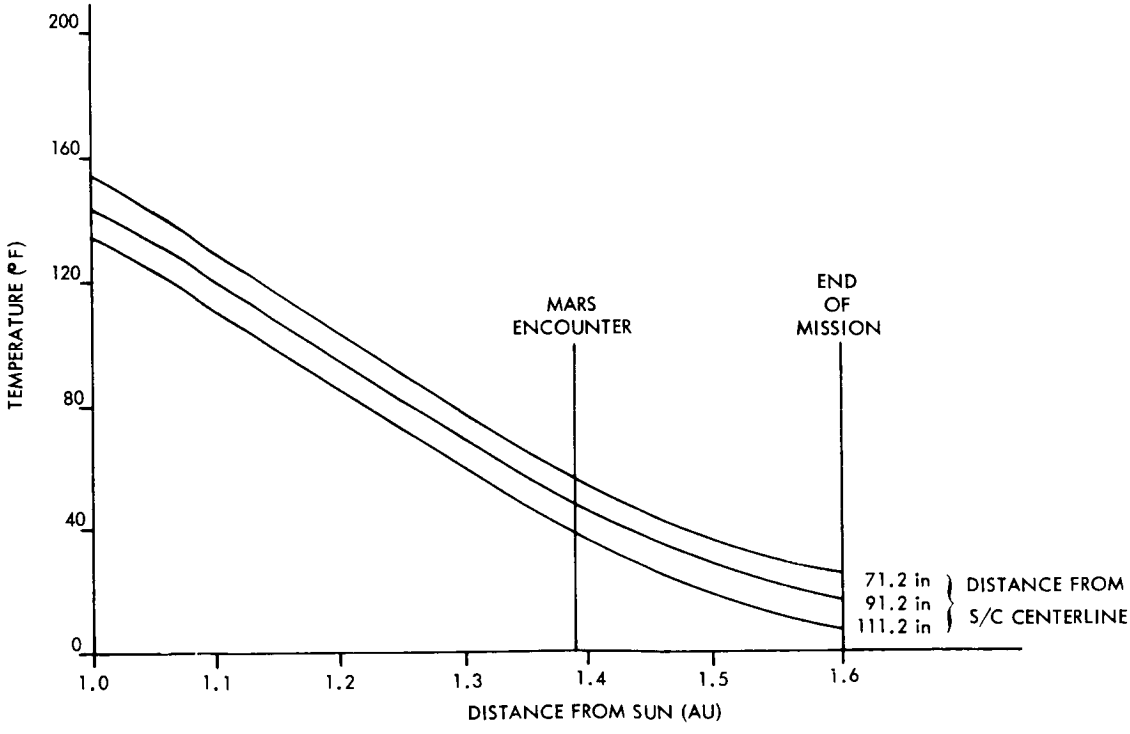

Figure 17. Solar Array Temperatures versus Distance from Sun

orbit, the spacecraft will be subjected to a 90-minute eclipse. The temperature decay of the solar array during this 90-minute period is shown in Figure 18. During this time period, the average solar array temperature will decrease from 17°F to minus 206°F. Throughout the entire Martian mission, the solar array temperature levels are within the array temperature capability.

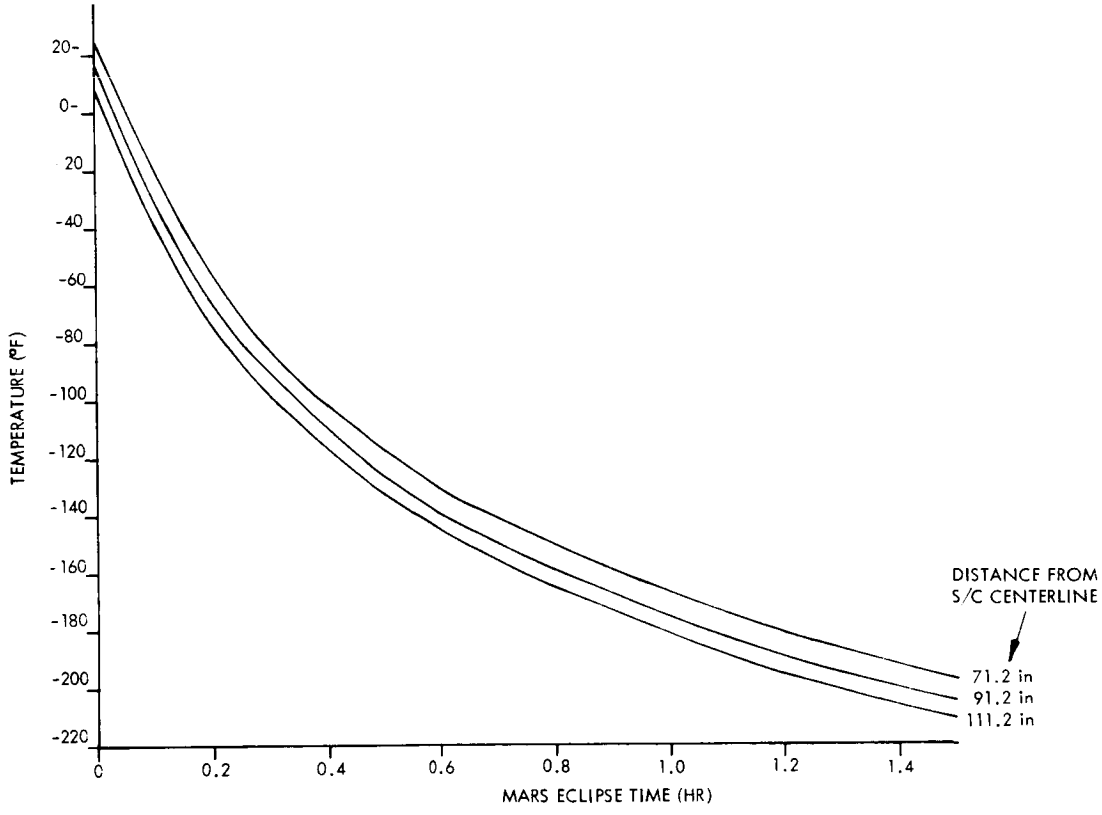

Figure 18. Solar Array Temperatures During Mars Eclipse

VOY-D-363
MECHANISM SUBSYSTEM

1. SCOPE

The Mechanism Subsystem performs the functions of deployment, articulation and actuation of the high gain antenna (HGA) and the planetary scan platform (PSP). The gimbal actuators for thrust vector control, the deployment mechanisms for the auxiliary solar panels, and the maneuver and broad coverage antennas are also included in this subsystem.

2. HIGH GAIN ANTENNA DEPLOYMENT AND GIMBAL ACTUATION MECHANISMS

These mechanisms rotate the HGA from the stowed to the deployed position and point the antenna toward Earth during the Cruise and Mars Orbital phases of the Voyager mission.

2.1 FUNCTIONAL DESCRIPTION

Upon command, the antenna is released from the stowed position. The deployment mechanism rotates the HGA and the gimbal drive mechanism through 110 degrees (measured in a plane parallel to the spacecraft Y-Z plane) into the X-Y plane (see Figure 1). The nominal deployment rate is 3 degrees/second. In the fully-deployed position, a positive stop and latch prevent subsequent rotation in either direction of the deployment shaft holding the final rotational position of the HGA deployment axis within $\pm$ 0.05 degree of the desired position.

The HGA is linked to the spacecraft by two orthogonal axes, A and B. The inboard or A axis is parallel to the spacecraft Y axis when deployed. At A and B rotation of 0 degrees, the outboard or B axis is parallel to the spacecraft X axis, and the antenna principal axis is pointed parallel to the -Z axis. The A and B gimbal angles as a function of time after launch for the A, B (rotate, then nod) gimbal order noted above, are presented in Figure 2.

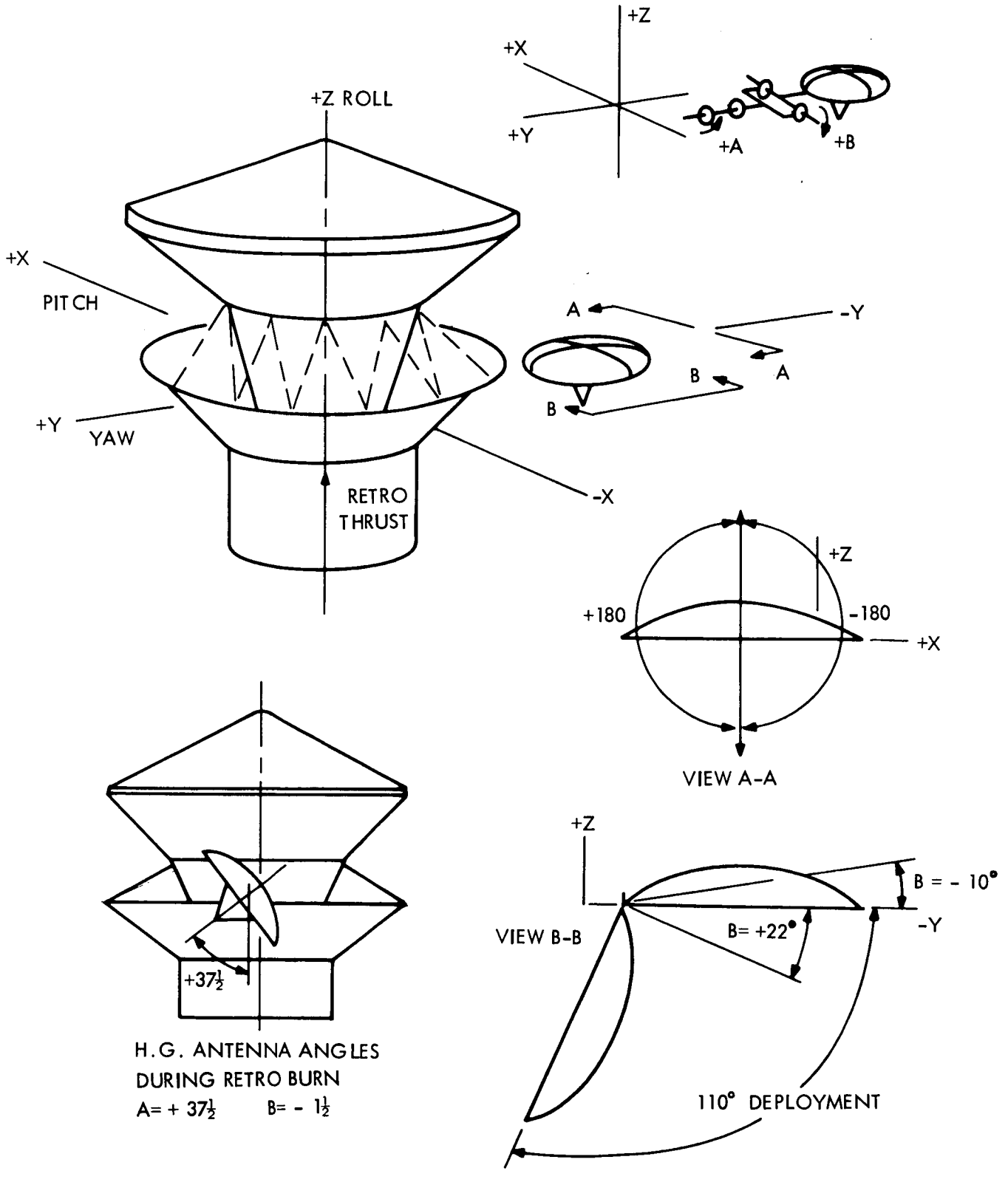

Figure 1. High Gain Antenna Articulation and Deployment Geometry

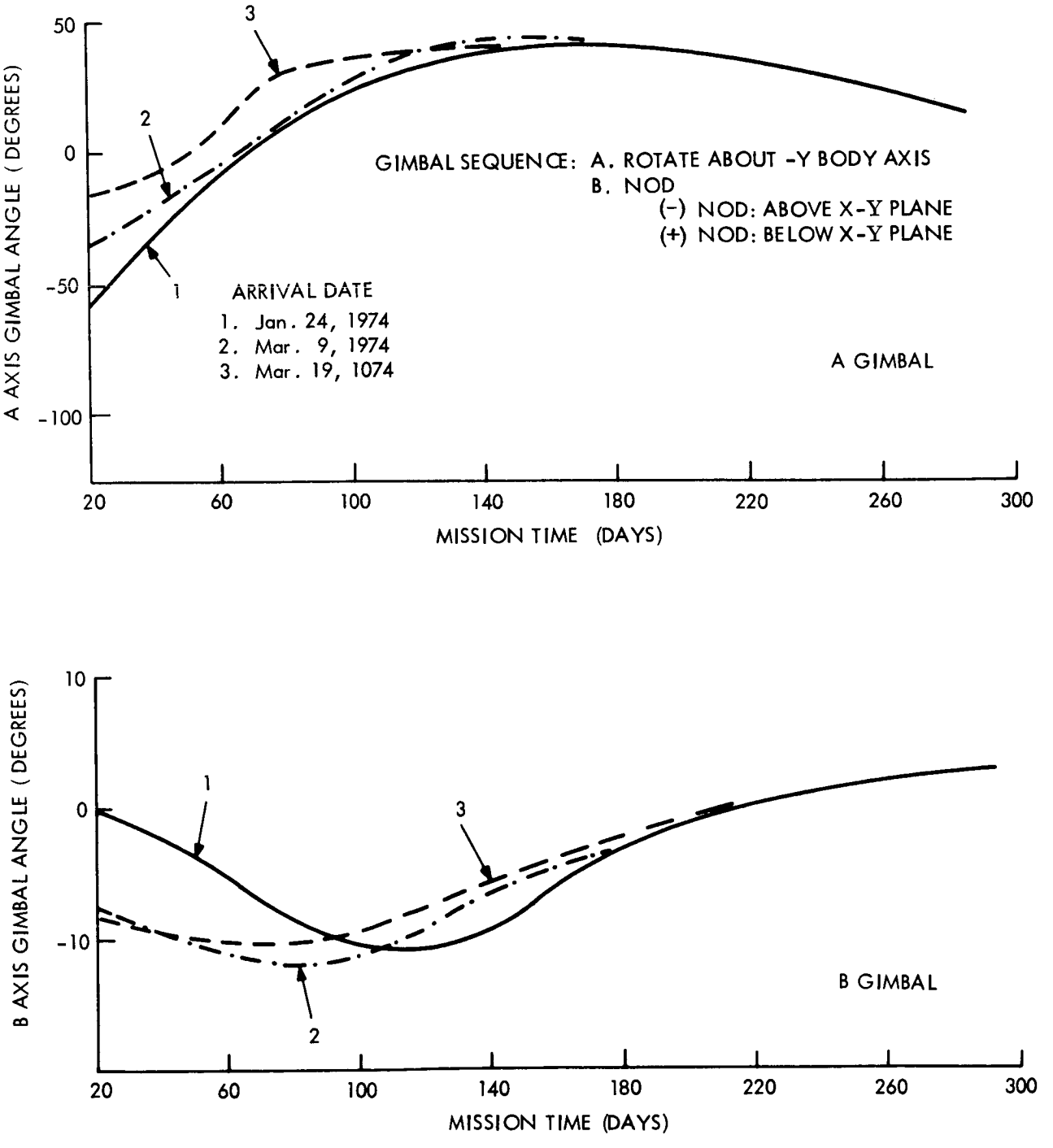

Figure 2. Antenna Gimbal Angles

This figure shows the inter-relationship of the motions of the two antenna axes for three spacecraft arrival dates at Mars: 24 January, 9 March, and 19 March 1974. To provide the capability to meet future mission requirements, additional gimbal range is provided:

a. The A gimbal has ± 180-degree rotational freedom and control about its axis.

b. The B gimbal has -10, + 22-degree rotational freedom and control about its axis.

For the 1973 missions considered, the maximum A axis drive rate required for cruise phase tracking is about 1 degree per day. In the Mars orbital phase, the maximum rate is much lower: 1 degree of motion is necessary in 3+ days. B axis rates are even lower: 1 degree in 10 days during cruise, and 1 degree in 25 days during Mars orbit.

The A and B gimbal actuators are capable of rotating their respective axes in 3/16 degree increments to within ± 0.1 degree within their range of rotation. Each 3/16 degree step is completed within 10 seconds after initiation. Gimbal angles are monitored by counting actuator steps on each axis, to within ± 0.1 degree (non-cumulative) relative to the gimbal null.

Each gimbal actuator can hold the angular position of its respective axis against any external disturbance ≤ 0.5 g without power input to the actuator, and ≤ 6.5 g with power input to the actuator. Each actuator will operate at the nominal flight rates in a 1 g environment if the operating axis is aligned near the local vertical. In other orientations, suitable counterbalancing or levitation will be required for nominal operation. The HGA mechanisms and their inter-relationships are shown in the block diagram, Figure 3.

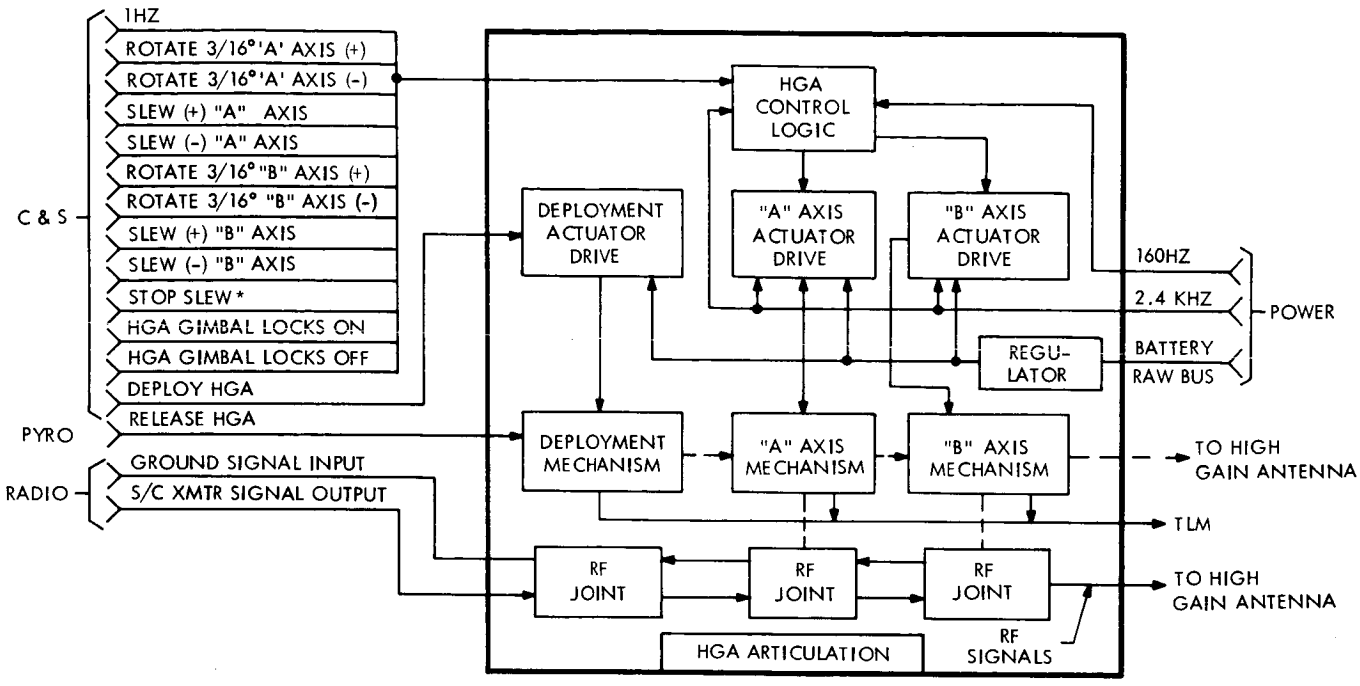

Figure 3. HGA Mechanisms and Inter-relationships

2.2 PHYSICAL DESCRIPTION

The selected design for the HGA deployment and actuation mechanisms embodies a number of significant improvements over the Task B design on which it is based.

2.2.1 Retention

Prior to deployment, a latch supports the A axis actuator near the B axis bearing attachment points (see Figure 4). This support point will protect the actuator mechanisms during launch by reacting vibration-induced torques and forces in the Y-Z plane. The retention latch is a clevis with a dual EED pin-puller provided to perform the release function prior to deployment.

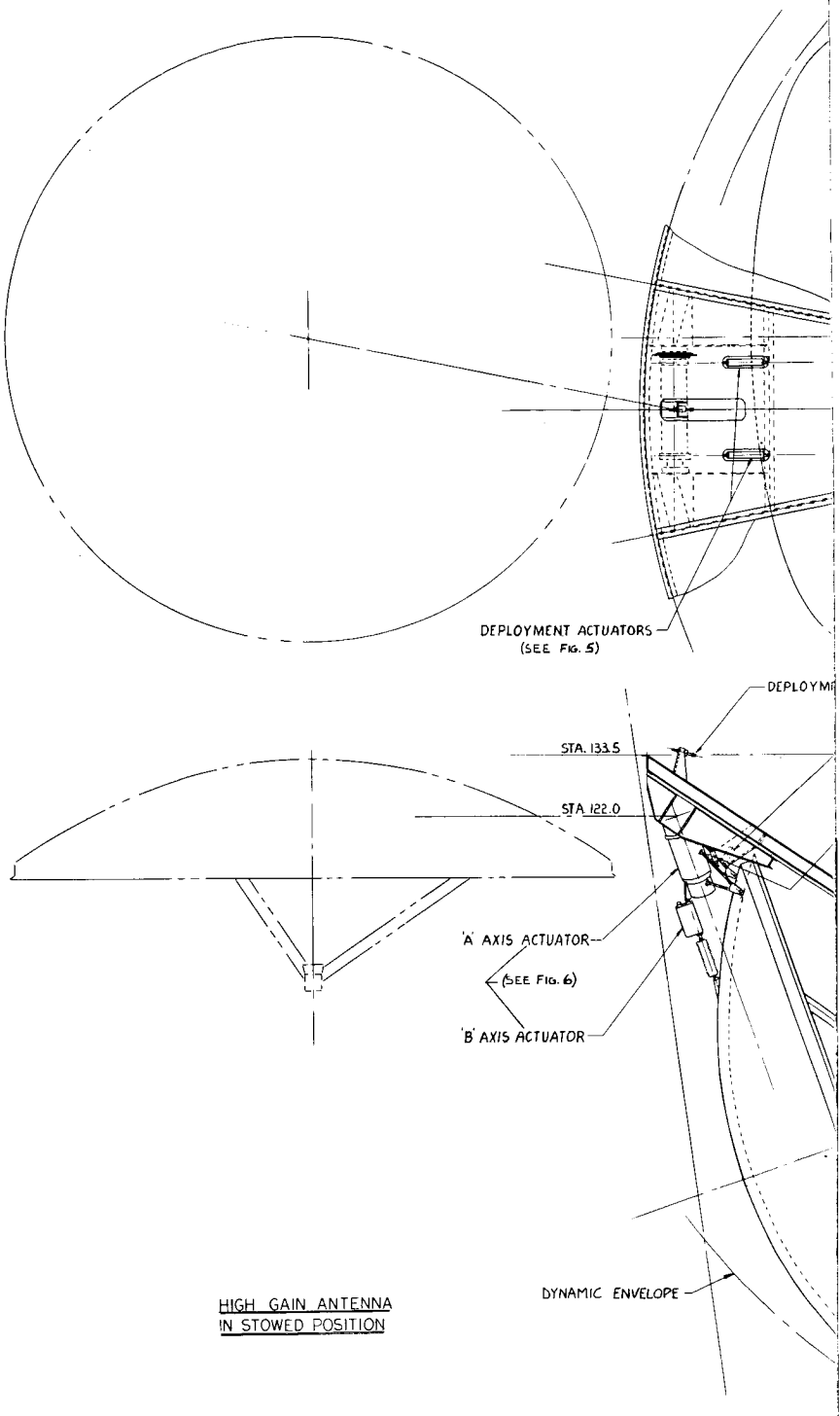

HIGH GAIN ANTENNA
IN STOWED POSITION

FOLDOUT FRAME 1

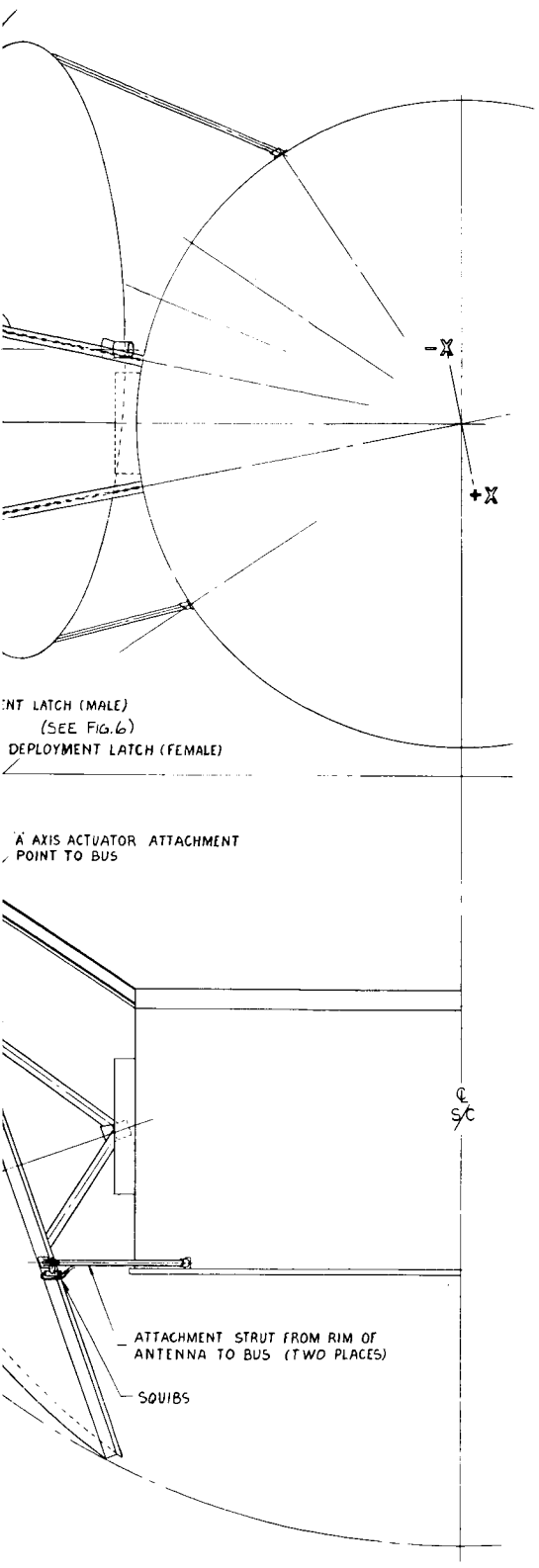

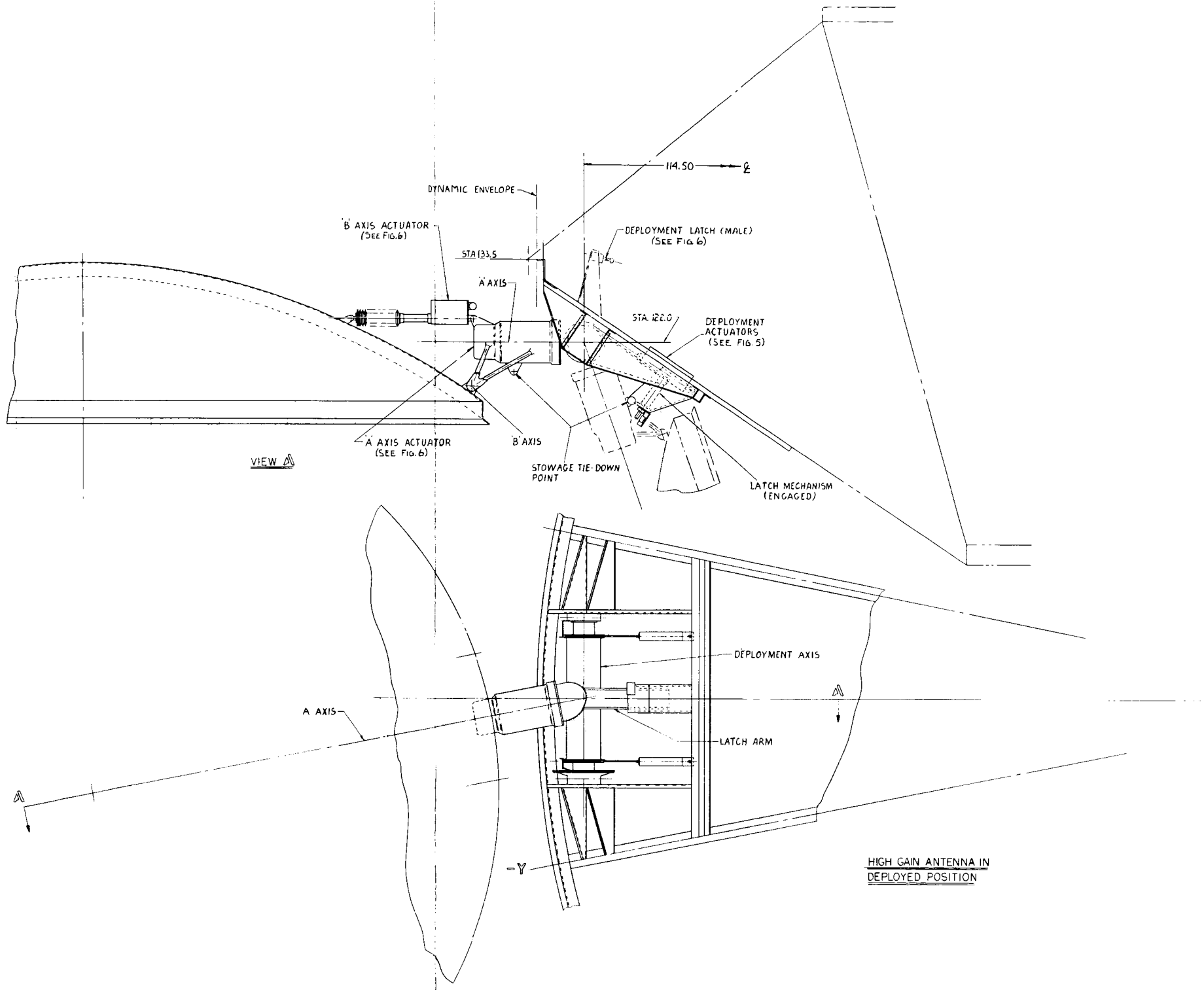

Figure 4. High Gain Antenna Installation

FOLDOUT FRAME 2

FOLDOUT FRAME 3

2.2.2 Deployment and Latching

A pair of motor-driven linear actuators deploy the HGA and its gimbal actuators (see Figure 5). These actuators are used to rotate the tubular deployment shaft about a non-rotating inner shaft on the deployment axis. The antenna positioning mechanism is mounted at the middle of the outer (deployment) shaft. Deployment rotation occurs as each linear actuator retracts, pulling a woven, flexible-steel cable which is partially wrapped around a sheave attached to the deployment shaft. Two pre-load torsion springs, located between the non-rotating and outer shafts provide countertorque to maintain tension in the flexible cables in zero g.

The deployment actuation system is fully redundant to ensure reliable performance of this critical function. Each linear actuator retracts a separate cable; no single failure, of either actuator or its associated cable, can interfere with completion of HGA deployment.

An integral latch and stop mechanism is provided to ensure accurate positioning of the deployed HGA relative to the spacecraft (see Figures 4 and 6). This device is located on a 10-inch radius arm attached to the outer (rotating) deployment shaft. The adjustable stop sleeve and the multi-fingered collet latch are concentric to minimize misalignments due to differential thermal gradients on latching members, and spacecraft structural deformations. A tapered, spring-loaded plunger holds the collet members in the expanded, locked position, after engagement.

2.2.3 Gimbal and A Axis Actuator

A rotary actuator mounted on the deployment axis provides A axis (rotation) drive for the HGA. The actuator, shown in Figure 6 consists basically of a step servo motor, spur gear reduction stages and incremental step sensor, and a high-reduction ratio, low-backlash nutator output gear. The overall gear reduction from the stepper motor to the antenna gimbal is 30,000:1. The actuator mechanism also incorporates temperature

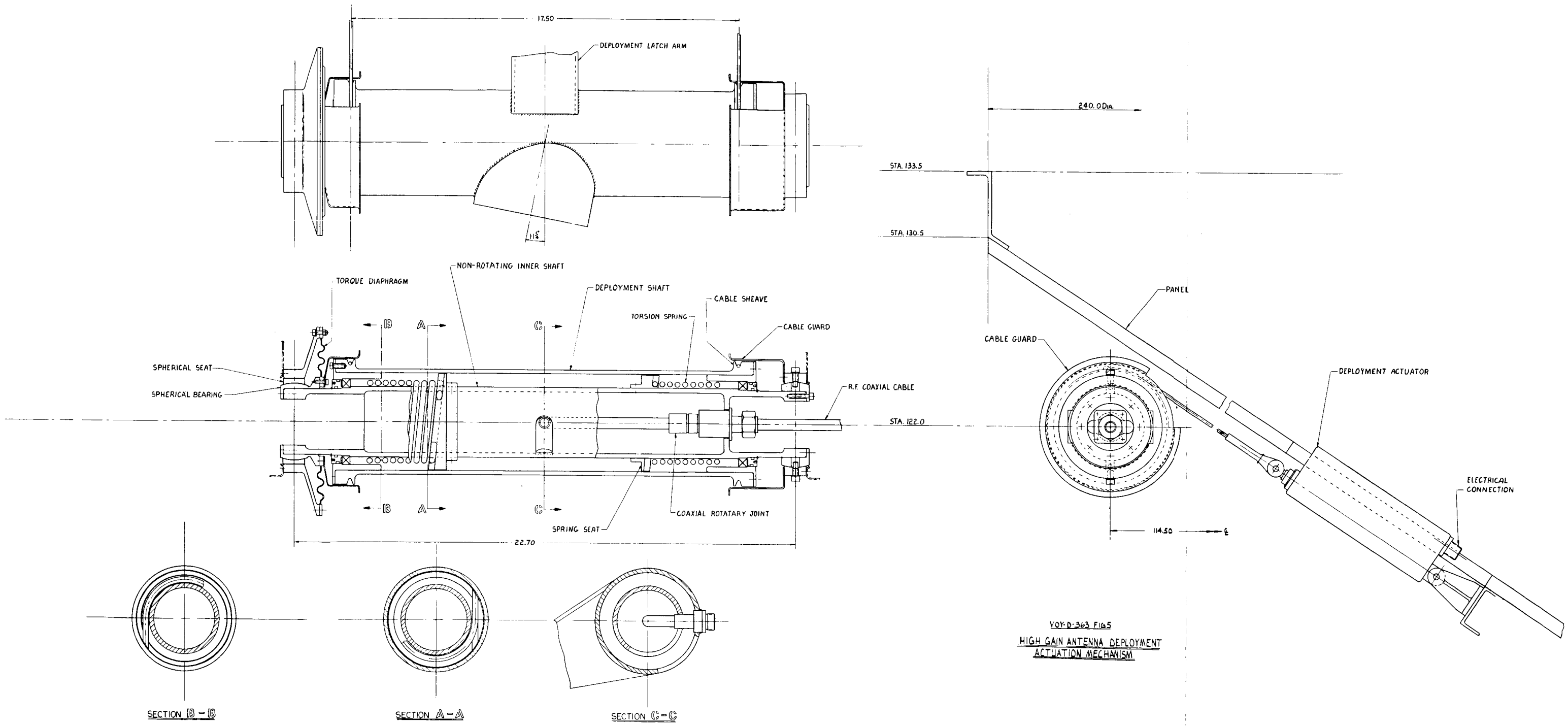

VOY-D-363 FIG 5

HIGH GAIN ANTENNA DEPLOYMENT ACTUATION MECHANISM

Figure 5. High Gain Antenna Deployment Axis and Drive Layout

FOLDOUT FRAME 1

11

FOLDOUT FRAME 2

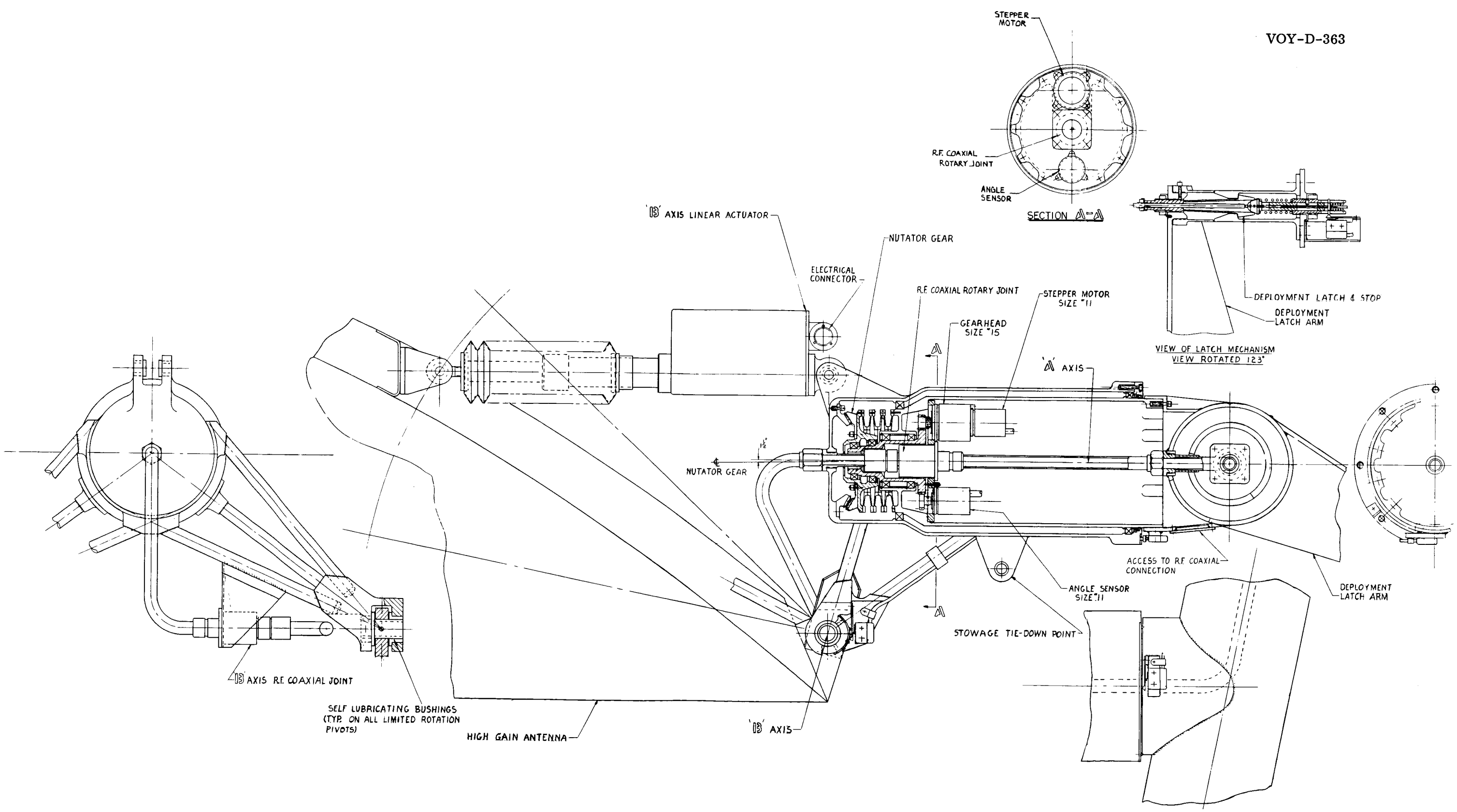

Figure 6. High Gain Antenna A and B Axes Gimbal and Actuator

FOLDOUT FRAME 1

13

FOLDOUT FRAME 2

14

sensors and redundant position limit switches. This actuator design provides the ability to maintain antenna position without loss of preselected gimbal shaft position during engine firing, and the ability to operate in a 1 g field for ground testing.

The A axis actuator has undergone extensive redesign since the Task B report was issued. The most significant feature is the concentric arrangement of the antenna RF rotary joint with the final gear reduction, without restricting rotation of the HGA about the A axis. In addition, the higher speed spur gear meshes have been placed in a gearhead assembly integral with the motor, to simplify assembly and test of this drive component.

Ball bearings are used for uniform and low operating torque, particularly under ground test conditions, and to permit tight control on radial play without danger of binding. Dry lubricants selected through extensive vacuum testing at GE-MSD for Voyager application suitability are used throughout the mechanism, eliminating the need for hermetic sealing.

The step sensing switch has been packaged with its drive gearing into a size 11 housing for ease of test and alignment.

2.2.4 B Axis Gimbal Actuator

The B axis drive motor is a size 11, 45-degree PM step servo motor with a spur gearhead integral with the motor. The ratio between the motor and the ball screw will be 600:1.

The ratio sizing was based on:

a. Motor drive rate of 160 pulses per second.

b. 45-degree motor rotation per drive pulse.

c. 0.2 inch-lead ball screw.

d. Predicted $\pm$ 6.5 g vibratory disturbance during LEMDE firing (maximum load seen by B axis actuator).

e. HGA weight of 44 pounds.

The actuator and HGA geometry at gimbal null also entered into the analysis. The 600:1 ratio will permit completion of a 3/16 degree step in 10 seconds and requires a maximum holding torque of 1.2 oz-in. at the motor, neglecting gear friction which will further reduce the reflected torque. A typical size 11 PM stepper, the Clifton Precision Products MSA-11A2, has a minimum energized holding torque of 1.5 oz-in., which gives adequate margin. HGA holding and drive torques under reduced g-levels will require proportionately lower motor torque.

The peak loading on the 0.625 pitch diameter actuator ball screw (1400 pounds) is less than 25 percent of its rated load capacity. The ball screw is used because of its high efficiency and its suitability for use with dry film lubrication.

2.3 PERFORMANCE PARAMETERS

The three HGA axes, deployment, A (rotation), and B (nod), are provided with suitable articulation to permit movement of the antenna through the angles shown in Table 1. The deployment angle is fixed by the relationship between the stowed and deployed positions. The angles about the A and B axes are those which permit the pointing of the antenna toward Earth for all spacecraft - Earth relationships required during the 1973 and later missions. The pointing accuracies are dictated by the telecommunications system requirements; the rates are a function of both the type of mechanization and of the 160 Hz synch pulse frequency.

Table 1. Axis Angles, Rates, and Pointing Accuracy

Axis	Angle (deg)	Nominal Rate (deg/sec)	Pointing Accuracy* (deg)
Deployment	110	3	$\pm$ 0.05 (Down-lock)
A	$\pm$180	0.24	$\pm$ 0.05
B	+22, -10	0.04	$\pm$ 0.05

*Relative to nominal position

2.4 PHYSICAL PARAMETERS

The outline and approximate sizes of the HGA mechanisms are shown on Figures, 4, 5, and 6. The weights are summarized in Table 2.

Table 2. HGA Mechanisms Weight Summary

Item	Weight (lb)
Actuator, A axis	6.0
Actuator, B axis	3.0
Actuator, Deployment	1.4
Actuator, Deployment	1.4
Axis, Deployment	9.0
Release Mechanisms	1.2
Latch Mechanisms	2.0
Electronics, Control and Regulator	3.6
Cabling, Control	1.2
	28.8
(Reference) Telecommunications Hardware	
Antenna, High Gain	38.7
Rotary Joints, RF (3 required)	1.1
Cable, RF	1.5
Feed, RF	3.5
HGA Structural Reinforcements	2.8
	47.6
Total weight (excluding related spacecraft structure)	
Mechanisms	28.8
Telecommunications	47.6
	76.4

2.5 DESCRIPTION OF INTERFACES

The HGA actuation mechanism shares interfaces with the following systems or subsystems: C&S, Command, Telecommunications, Power, Vehicle Structure, and Pyrotechnics. The HGA functional block diagram (Figure 3) shows the electrical and mechanical interconnections. In addition, these interfaces are discussed in more detail in the sections following.

2.5.1 C&S and Command Interface

The HGA A&B control electronics receive operational commands from the C&S listed below, and has provision to receive identical backup commands from the Command Subsystem. All commands are received as 60-ms switch closures and are fed into the input command signal processing units in the HGA control, which serve both to "or" C&S and Command inputs and to examine command switch closures for proper duration. Provision for execution of the following commands is included:

a. A axis: step 3/16 degree plus, step 3/16 degree minus, slew plus, slew minus.

b. B axis: step 3/16 degree plus, step 3/16 degree minus, slew plus, slew minus.

c. A and B axis: stop slew, gimbal locks on, gimbal locks off.

2.5.2 Telemetry Interface

The sensor signals provided to the Telecommunications Subsystem are listed in Table 3. The A and B axis limit sensor and overtravel sensor outputs are also gated to the "slew stop" input of the actuator control circuitry.

2.5.3 RF Interface

The telecommunications signals are conducted through the ADM axes with a combination of low-loss coaxial cable and a non-contact rotary joint (similar to those used on the Ranger Spacecraft, JPL Report No. 32-241, pp. 189-191) on each of the three HGA motion axes.

Table 3. Telemetry Output Signals

Signal Output	Source
Stowed Latch	3 switch pairs
Deployed Latch	1 switch pair
A Axis ± Limit Sensors	2 redundant switch pairs/axis
A Axis ± Overtravel Sensors	2 redundant switch pairs/axis
B Axis ± Limit Sensors	2 redundant switch pairs/axis
B Axis ± Overtravel Sensors	2 redundant switch pairs/axis
A Axis + $3^{o}/16$ step	Pulse on line from control electronics
A Axis - $3^{o}/16$ step	Pulse on line from control electronics
B Axis + $3^{o}/16$ step	Pulse on line from control electronics
B Axis - $3^{o}/16$ step	Pulse on line from control electronics
A Axis Motor Temperature	Thermal (resistance) sensor
B Axis Motor Temperature	Thermal (resistance) sensor
Coaxial Cable Temperature	Thermal (resistance) sensor
A Axis motor current	Threshold detector (2 level)
B Axis motor current	Threshold detector (2 level)

2.5.4 Power Interface

The HGA mechanisms receive raw DC, 160 Hz signal, and 2400 Hz power from the Power Subsystem.

The raw DC is internally regulated to provide 28 VDC (± 5 percent) for all actuator motor drives. The 160 Hz signal is used only to synchronize the step servo motor drive oscillators. The 2400 Hz is rectified internally to provide power and logic levels for the HGA control electronics. Table 4 shows the average and peak requirements on each input.

Table 4. HGA Mechanisms Power Requirements

Type	Average	Peak
Unregulated DC	0*	13 watts
160 Hz	Signal	Signal
2400 Hz	5.3 watts	5.3 watts

*NOTE: The deployment, A and B axis drives operate so infrequently that input power to the regulator will be turned on only when actuation commands occur. This will result in a significant power saving throughout the mission.

2.5.5 Structural Interface

The HGA structural interfaces are shown in Figure 4. The deployment axis is supported by box beams and trusses between two solar array support longerons. The deployment latches are also attached to the inboard cross-beam. The stowed HGA also is held by two supports near the sun shield (below the electronic modules).

2.5.6 Pyrotechnics Interface

The HGA deployment is initiated by three dual-squib, redundant bridge wire pin-pullers. These devices are provided and actuated by the Pyrotechnic Subsystem. Each pin puller releases one of the three HGA stowage latches.

2.6 DISCUSSION OF ALTERNATIVES CONSIDERED

2.6.1 Lubricant Selection

Selection of lubricant systems for spacecraft mechanisms applications is affected by many factors. Life, weight, power, space, speed, cleanliness, and reliability considerations preclude the use of hydrodynamic or hydrostatic lubrication, in most cases. Sprayed

mist and blown powder systems must be eliminated for most of the same reasons. Boundary lubrication is the only method suitable for use in Voyager mechanisms. Boundary lubrication properties are possessed in varying degrees by all oils, greases and dry lubricants. Dry and liquid lubricants have particular advantages that affect their proper application. These advantages are compared in Table 5.

Table 5. Advantageous Properties of Dry and Liquid Lubricants for Spacecraft Applications

Dry Lubricants	Liquid Lubricants
a. Does not require hermetic sealing or thermal control	a. More experience and history
b. Lower volatility (by several decades)	b. Lower friction at optimum temperature
c. High thermal and oxidative stability	c. Simplicity of application to gears, bearings
d. Predictable life	d. Ease of inspection
e. Sterilization and radiation resistance	
f. Long shelf-life	

Typically, linear actuators such as the B axis drive on the HGA can be readily sealed, since the change in length of the sealed volume can be accommodated with a welded metal bellows. This permits use of liquid lubricants within the sealed volume, but in turn requires tighter thermal control than dry lubricants would.

On rotary actuators with large angular motions, some elements must be outside the sealed volume. In the existing design this would include the nutator gear mesh and the gimbal support bearings. It becomes obvious that some dry lubricant must be used on Voyager; liquid lubricant cannot be guaranteed to perform reliably in the areas where hermetic sealing is not possible.

GE-MSD has extensive experience in the application of low vapor pressure grease and oil lubricants such as the G-300 and F-50 Versilubes in less severe long-life applications. A comparable basis for the selection of suitable dry lubricants was felt to be needed for Voyager. Therefore, a program to evaluate the suitability of a group of commercially available dry (solid) lubricants for use in Voyager was begun at GE in 1966. Conventional sliding friction tests in air were supplemented with X-ray, spectroscopic, and electron probe techniques for quantitative and qualitative evaluation of selected lubricant coatings. These lubricants were also applied to groups of rolling-element bearings, and spur gears, which were then run-in and subjected to extensive visual, dimensional, and performance tests in air. Pairs of bearings selected from each lubricant group were then evaluated in ion-pumped vacuum systems (at 10^{-9} TORR) to determine starting and running torque as a function of load and accumulated operating cycles (revolutions). Provision was made in each vacuum test fixture to continuously monitor the torque, temperature, and revolutions of each pair of bearings, and the partial pressure of outgassed materials through mass spectroscopy. Vacuum tests of dry lubricated gears are scheduled for early 196ε.

Tests include intermittent and continuous rotation with reversals at varied intervals. Tests have also been performed to determine the effect of static dwell (of one- to-eighty hour duration) on starting and running torque. Although testing is still in progress, significant data has already been obtained. Definite trends in starting torques as a function of dwell time have been identified.

Two lubricants are operating satisfactorily after 56 million revolutions. These are Hi-T Lube, a multi-layered, plated, low-shear metallic film with MoS_2 diffused onto the outer layer, and Duroid 5813, a glass-filled, sintered MoS_2-PTFE resin mixture. Hi-T Lube is plated directly onto races and retainers protecting all sliding surfaces in contact in the bearing. A softer lubricating film is created with the second type of lubricant; the ball retainer machined from solid Duroid 5813 rod or tubing serves as a self-sacrificing lubricant source. A thin layer of PTFE and MoS_2 is transferred by the balls from the retainer to the raceways. This film is self-replenishing throughout the life of the retainer.

In the static dwell tests, the bearings lubricated with the softer PTFE-based lubricant films have shown a general trend of increasing starting torque with increases in dwell time; the harder films have not demonstrated this characteristic.

2.6.2 Gimbal Order

The order of gimbals for HGA articulation received considerable attention in the Task A and B studies. The order selected - inboard (A) gimbal axis parallel to spacecraft Y axis, and outboard (B), parallel to X, permits maximum antenna utilization during cruise and Mars orbital phases with essentially no minimum communication distance. In the current mechanism update task, evaluation of a possible reversal of gimbal axis order has been conducted. These potential advantages were anticipated:

a. Possible elimination of separate deployment actuators with attendant savings in weight

b. Flexibility of a greater range of antenna positions for maneuver verification and future growth

c. Use of identical actuators on both the A and B axes, which offers potentially greater reliability by reducing the number and complexity of development, manufacture and test operations.

The potential advantages were reviewed, with these conclusions:

a. The weight saving in the deployment mechanism would largely be offset by the increased weight of the actuator for the B axis (parallel to spacecraft X axis) since this actuator would now be rotary and would have to hold the HGA during engine firing against a thrust-induced torque. The magnitude of this torque is:

$$\text{Torque} = \text{acceleration} \times \text{HGA mass} \times \text{moment arm}$$

$$T = 6.5\ g \times \frac{50\ \text{lb}}{g} \times 6\ \text{ft}$$

$$T = 1950\ \text{lb} - \text{ft}$$

This would probably increase B axis actuator weight to about 30 pounds versus 3 pounds for the linear B axis actuator in the present arrangement. The increased weight would more than offset the saving from elimination of the new HGA deployment mechanism.

b. The only gain in flexibility proved to be about the B axis, where it is least needed. All anticipated Mars missions can be accommodated with the configuration mechanization of Task B. For some launch dates, changing the order results in a loss in flexibility of HGA utilization since pointing parallel to the X axis is required and B axis pointing (nod) becomes impossible since the inboard B axis is parallel to the X axis. Although the broad coverage antenna could be used in the primary link when this occurs, mode switching would be required, and this would reduce overall system reliability.

c. If identical actuators were used, the A axis actuator would be extremely oversized (hence overweight) for the minimal torque it would be required to produce.

2.6.3 Drive Motor Selection

The use of a stepping drive is clearly preferable to a continuous drive. Stepping power is on the order of 6 watts for 1 to 5 sec per 0.187^{o} step, with no holding power between steps in the absence of major disturbances. A stepping drive can produce a fixed incremental motion reliably, with open loop control. The antenna gain reduction caused by the use of finite steps is negligible.

The choice of the type of drive motors to use for positioning the HGA depended upon the following factors:

a. Type and power level of the control signals available

b. Endurance life

c. Reliability

d. Positioning accuracy

e. Response

f. Holding or braking effect.

The motor types considered were the DC commutator-type motor, ratchet and pawl steppers, variable reluctance step-servos, and permanent magnet rotor step-servos. The only type that satisfies all of the above requirements is the permanent magnet rotor step-servo motor. It is readily operated from digital input pulse trains by a simple logic controller and its output will be in discrete angular increments. Because there are no brushes or other forms of mechanical contact between the rotor and the stator, good endurance life, reliability, and response are readily obtained. The noncontact magnetic detenting inherent in these motors provides sufficient holding torque without the need for a separate brake, which all the non-stepping motors would require. Additional holding torque (as required during engine firing periods) may easily be obtained by continuously energizing one winding, or both windings simultaneously.

Alternatively, incremental stepping motors such as the Hughes roller detent/axial solenoid motor, the Abrams cam-latched motor, or the Ledex spring detent motor could be used. These provide much higher holding torques than PM steppers of comparable size. However, because of their contact type of operation, e. g., rolling elements, and cams, latches, springs, pawls, etc., as internal locking members, these motors are less desirable from an overall reliability viewpoint.

2.6.4 Gear Reduction Mechanization

The Task B actuator design employed several stages of open spur gearing between the motor pinion (integral with the shaft) and the final reduction (nutator gear or ball screw). While this approach represents good recognized practice, the use of smaller motors, (hence, smaller gears and bearings in the high speed end of the drive) favors the use of a gearhead integral with the motor.

In the servo gearhead, which has been developed to a high degree of reliability for space applications by GE and Kearfott-General Precision, all the small gears, bearings, and shafts can be accurately assembled and aligned within a small housing integral with the motor frame. The motor gearhead assembly provides ease of test, assembly and replacement. This approach was proven on Nimbus (over one year of continuous - and continuing - operation in space with a size 11 motor on a size 15 gearhead) and on vehicles such as Mariner (Mars and Venus), OGO, and OSO.

In addition to the nutator gear shown in the Phase IA Task B design, other types of reductions have been considered. The harmonic drive has been examined, as has a differential high reduction capability drive using plane-gyrating eccentric spur gears and internal gears with a tooth difference of one tooth in each mesh. The latter offers the advantage over the nutator gear and the harmonic drive of not requiring a flexing torque reaction member. The nutator gear has proven to be superior in packaging form factor for this particular gimbal drive configuration, and is relatively easy to assemble and align accurately.

2.6.5 Gimbal Position Holding

In the Task B study, the use of brakes, latches, and self-locking (low efficiency) mechanisms for gimbal actuator holding against engine thrust-induced disturbances were excluded from consideration, primarily due to reliability considerations. The remaining gimbal position holding methods to be considered are reflected motor torque with and without energization of the motor.

In the unenergized case, the PM rotor of the stepper motor is attracted to the permeable pole structure of the stator and gives rise to a detent torque (also referred to as parasitic or cogging torque) when the rotor is subjected to an angular displacement of its rest position. This torque can be used to hold the HGA against external disturbances if the drive gear ratio selected suitably multiplies this torque to exceed the torque induced by the disturbance.

This approach requires that a higher gear ratio be used by at least a factor of 10:1 (the normal ratio between energized and unenergized detent holding torque). Since high reliability of gimbal holding is desired, margin is attainable more simply by energizing the motor windings than by making a significant increase in gear ratio. An added advantage of using the lowest possible ratio is that back driving of the actuator during ground handling places lower stress on the gear trains than if it were geared up to employ the detent torque for gimbal locking.

2.6.6 Gimbal Position Monitoring

The application of magnetic encoders to monitor and store HGA gimbal angles via a direct shaft coupling to the gimbal actuator was examined. These devices offer non-contact, non-volatile storage of the gimbal position to the nearest 3/16 degree step. The complexity and power consumption of the electronics, however, made this device unattractive.

Potentiometers of the multi-revolution type could be used, but they involve rubbing mechanical contact and should be sealed for long-life operation in space. Difficulty in obtaining one part in 2000 resolution for telemetry is also a problem. The selected design, a refinement of the Task B angle sensor and counter, uses a pair of non-contact parallel redundant sealed reed switches which are actuated by magnet (s) on a shaft in the gimbal drive, which rotates once or at an integral submultiple of a revolution for each 3/16 degree of gimbal rotation. The switch closures are counted by a non-volatile magnetic core storage bidirectional counter. Parallel interrogation of all stages of the counter gives the current gimbal angle encoded directly in binary for telemetry input.

2.6.7 Deployment Actuator Types

The use of electric motor-driven actuation offers several potential advantages over stored energy actuation for deployment of large appendages. Briefly, these are:

a. Simplicity of drive rate control

b. No separate kinetic energy absorption device required

c. Uses power source (batteries) already on vehicle for other purposes during low utilization period

d. Readily reversible for repeated ground testing

e. No stored high energy safety problem

f. Simplicity of redundant application.

Review of the deployment function has shown that complete functional redundancy can be provided at a considerably reduced weight. The updated deployment mechanism design weighs approximately 12 pounds including 3 pounds for inclusion of all mechanisms required to provide fully redundant actuation.

Although spring-type stored energy actuation is suitable for small appendages, the weight of the spring and the rate damper (which absorbs much of the stored energy) make these systems less desirable for deployment of heavy appendages, particularly when testing in a gravity field is required.

3. PLANETARY SCAN PLATFORM DEPLOYMENT AND GIMBAL ACTUATION MECHANISMS

This section deals only with PSP stowage, deployment and gimbal actuation. Gimbal arrangement selection and intra-subsystem design considerations and interfaces are discussed in VOY-D-380.

After deployment, the PSP is articulated about three orthogonal axes. Two gimbal actuators erect and maintain scan axis perpendicular to the orbital plane about Mars. This permits tracking of the sub-satellite point through rotation of the PSP about the scan axis alone.

3.1 FUNCTIONAL REQUIREMENTS

Prior to initial deployment, the PSP is supported by the stowage cradle (below the solar array) and by the PSP boom which is identical with the scan axis as shown in Figure 7.

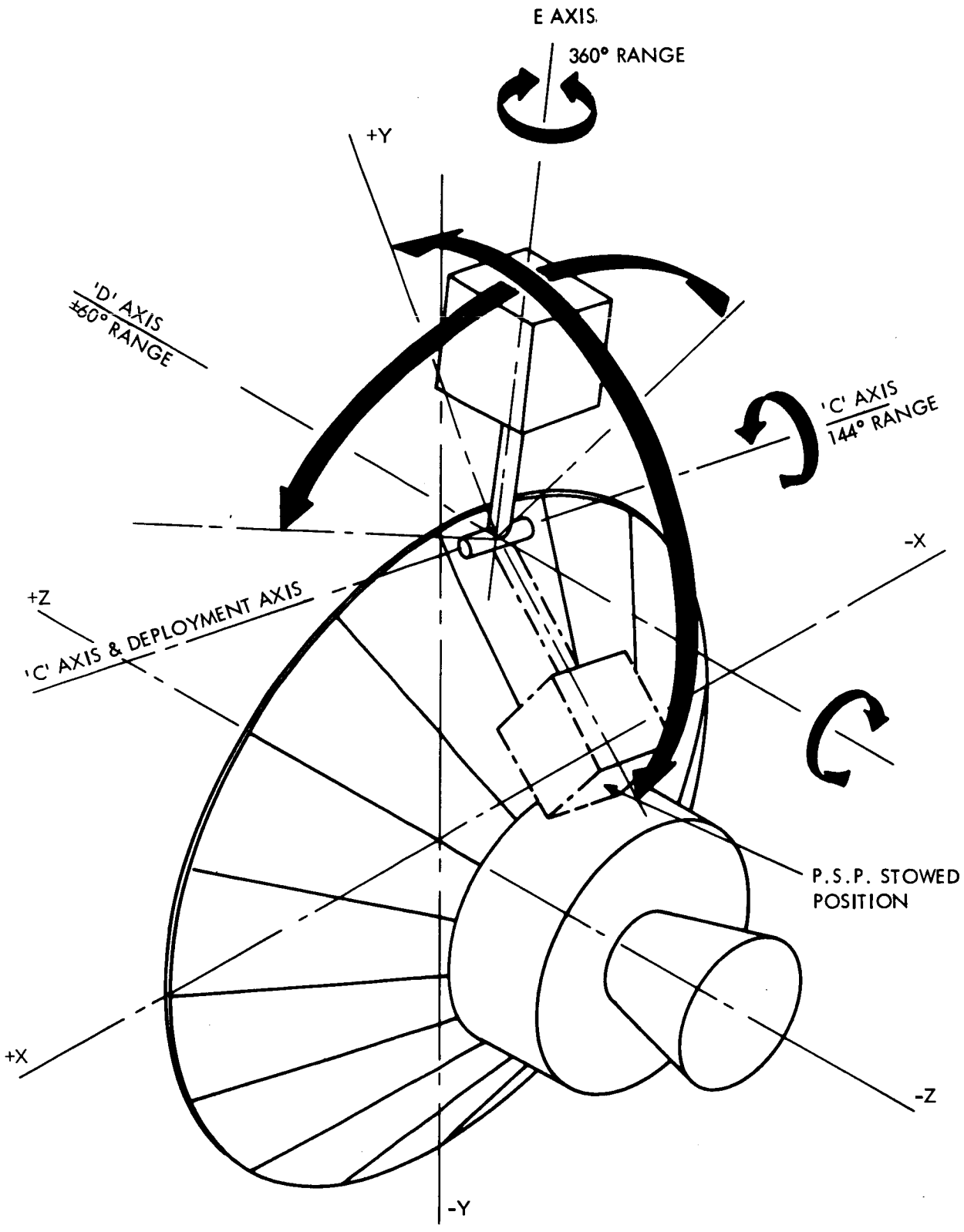

Figure 7. Gimbal Axes

The boom reacts the PSP load component along the boom axis; remaining loads are reacted by tiedown pads and latches.

When deployment of the PSP is desired, the PSP tie-down latches are released by EED-actuated separation devices. The C axis gimbal actuator (shown in Figure 8) then rotates the PSP away from the PV into the desired position for initial scanning.

As soon as the PSP has cleared the stowage latches, rotation of the boom and PSP about the D axis (normal to and intersecting C) is also begun. The combined rotations bring the boom perpendicular to the orbital plane. The C and D gimbal positions are updated periodically throughout the remainder of the mission to compensate for orbital plane precession and seasonal progression.

Rotation of the PSP about the third orthogonal axis, E, provides the scanning function.

As shown in Figure 7, the range of rotation of the C gimbal is 144 degrees, D is $\pm$ 60 degrees, and E is $\pm$ 180 degrees relative to its angular position when PSP is stowed.

The C and D gimbal actuators each drive their gimbals in 3/16-degree steps at a maximum rate of 11.4 degrees per minute. The scan drive is capable of rotating the PSP relative to the boom at all rates between 0.3 and 15.0 degrees per minute with a rate stability of one percent of desired value.

Position sensors are provided on all three PSP axes; these indicate gimbal angle to the nearest $\pm$0.1 degree, non-cumulative, throughout the range of travel of their respective gimbals. Each gimbal actuator retains the angular position of its respective axis against any external disturbances (0.05 g) without power input to the actuator. Gimbal drive energization is required to hold the PSP against disturbances of greater magnitude and to provide adequate stiffness to prevent interaction with the autopilot. The actuators retract

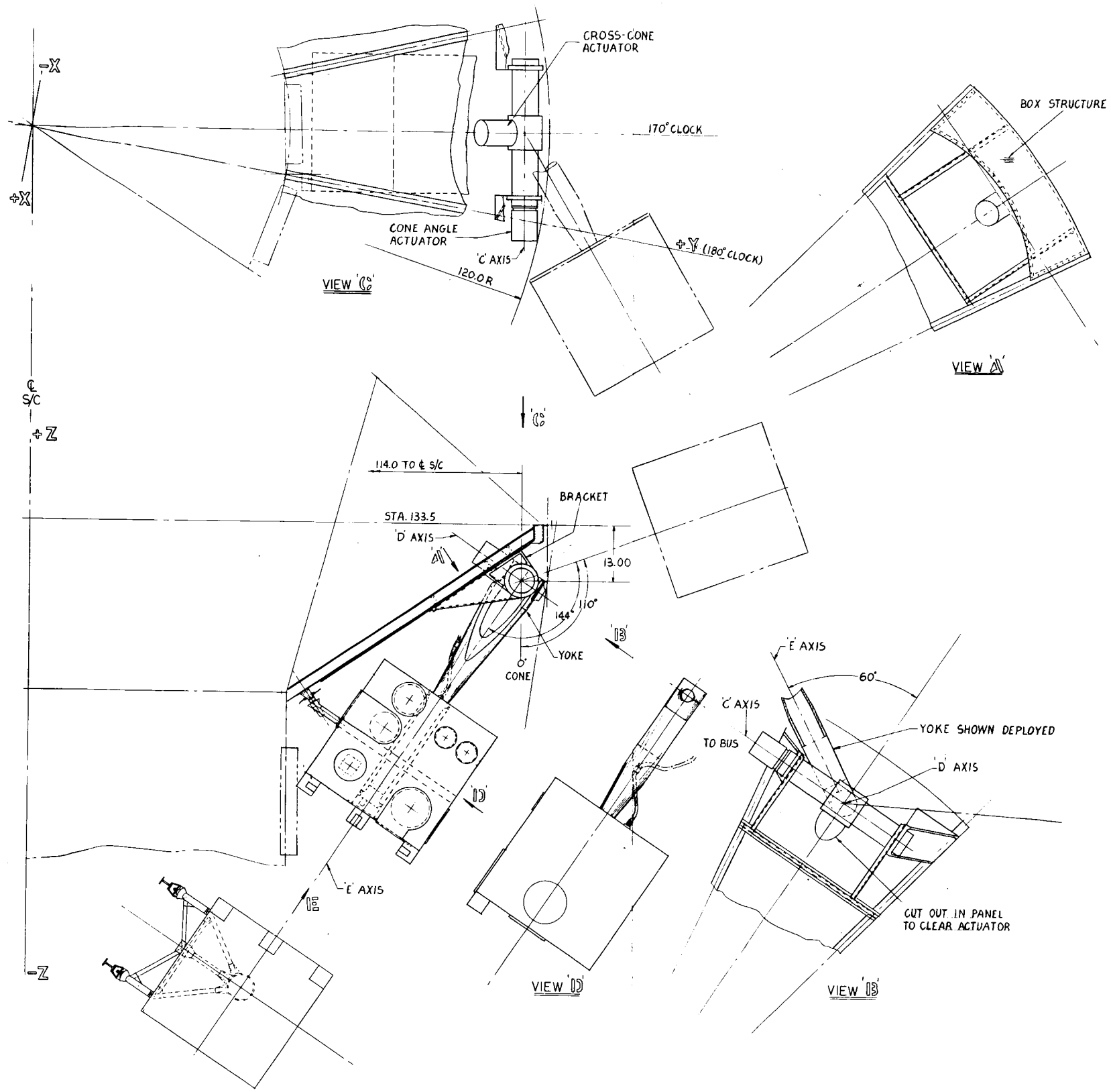

Figure 8. Planet Scan Platform Installation

FOLDOUT FRAME

FOLDOUT FRAME

the PSP to the stowed position (one or more times during orbital phase) and support it during orbit trim engine firing(s). This serves to lessen c. g. offset, to protect the PSP mechanisms from thrust induced torques, and to provide maximum shielding of PSP science instruments from engine plume radiation and combustion products.

3.2 DESCRIPTION OF BASELINE DESIGN

A simplified block diagram for the C and D axis gimbal drives is shown in Figure 9. The motor drives its respective gimbal open loop through a gear train (N_1 x N_2) in response to plus and minus step commands and holds the gimbal during orbit trim firing. The step sensor drives a reversible counter to store gimbal position information for telemetry. The output of the minus gimbal stop sensor resets the gimbal angle counter to zero. This permits counter reset if there is any uncertainty regarding indicated gimbal position.

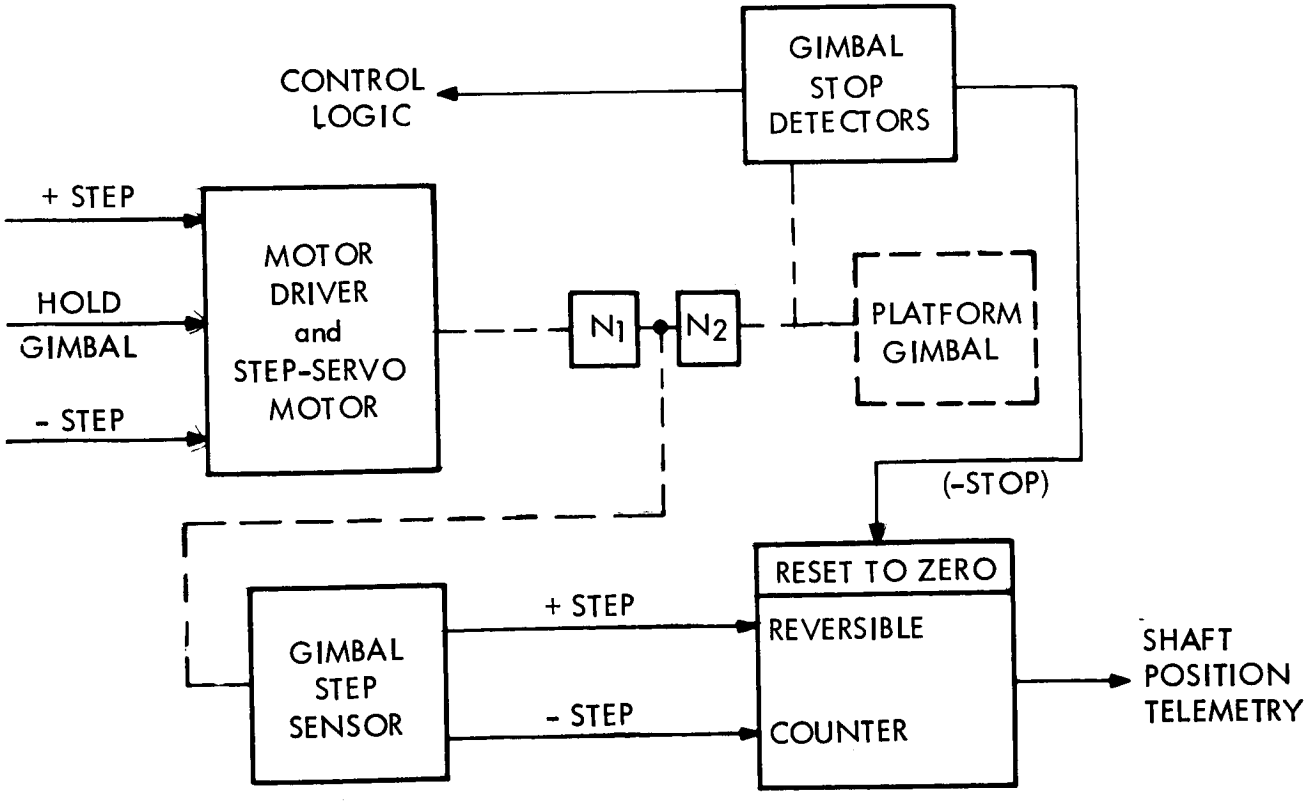

Figure 9. Gimbal Drive, Typical of C & D PSP Gimbals

The E (scan) axis drive is shown in Figure 10. The functions are similar to those in the control systems in the other axes, except that an analog error input signal and a rate feedback loop are used to control the direct drive torque motor. The gimbal angle sensor is driven through a suitable gear ratio and functions exactly the same as the C and D sensors.

Physical Description - The PSP C and D gimbal axis drives are rotary actuator mechanisms. Each drive is powered by a suitably geared reversible permanent magnet step servo motor. The C and D gimbal actuators have similar performance and are identical in design and appearance. For convenience, they will be called Rotary Incremental Actuators (RIA).

The RIA has a cylindrical housing approximately 6 inches in diameter and 9 inches in length, with a one-inch diameter output shaft at one end concentric with the housing. A mounting flange at the shaft end permits mounting of the C RIA to the PSP C axis support

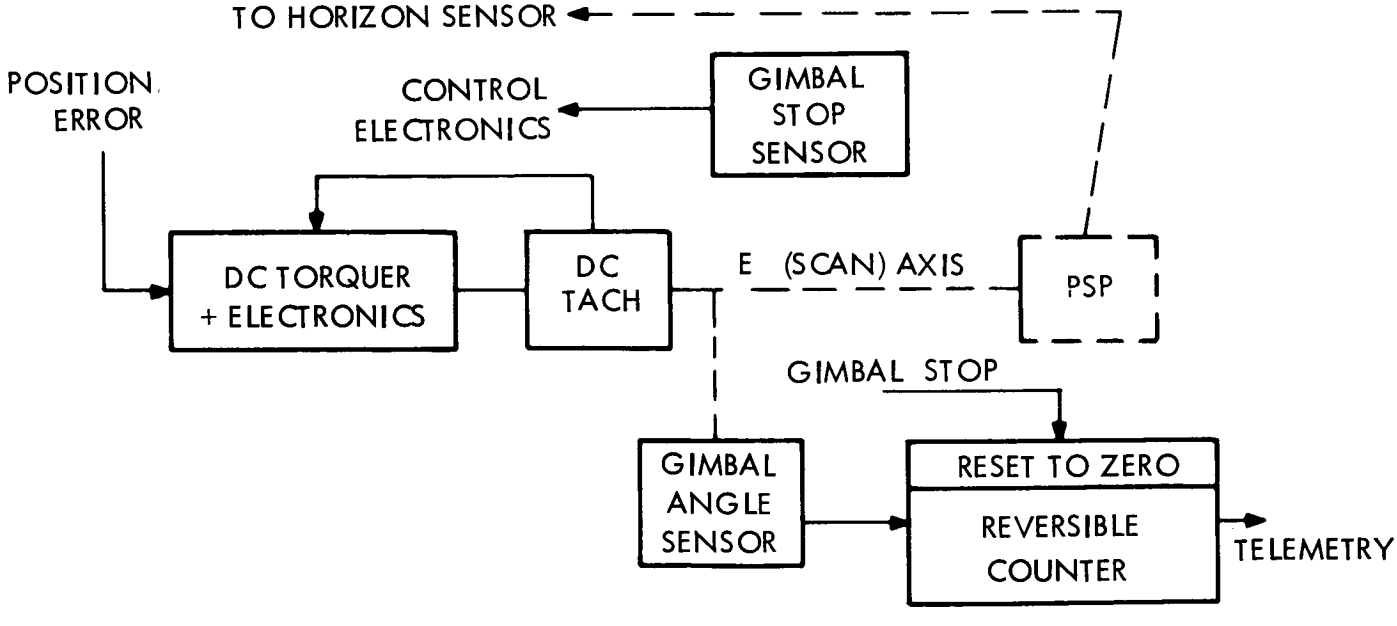

Figure 10. Scan Axis Block Diagram

structure. The C gimbal shaft is supported in preloaded bearings at each end to prevent backlash between the shaft and the structure, and to ensure that only torque is transmitted by the actuator shaft.

The D RIA is similarly mounted on the E axis boom: perpendicular to the C-E plane. The D RIA shaft engages a torque coupling into the C axis. Thus, the C RIA shaft stands still while the housing rotates with the E boom about the D axis.

Because of the similarity of the C and D axis RIAs only one will be discussed here. Functionally, the RIA is similar to the high gain antenna (HGA) A axis gimbal actuator. The physical design differs considerably however. Because of the relative masses of the PSP and the HGA ($\simeq$6:1) a higher RIA stiffness is required. For stiffness and low backlash the two output gear stages are large, (24 and 32 dia. pitch respectively) high precision spur gear meshes with ratios of 3:1 and 4:1, respectively. After a 6:1 stage of 48 pitch gearing, a torque-limiting clutch similar either to the type used on the Mariner 69 scan drive or the Nimbus solar array drive will be provided. The clutch, which slips at a back-driving torque of 400 lb-ft protects the actuator gears from damage in ground handling due to back-driving, and prevents the motor torque from damaging the gearing if the motor is operated with the output shaft stalled.

Beyond the clutch, a nutator gear drive (as in the HGA A axis actuator) provides a high-ratio, high-torque reduction that is driven by the gearhead-step-servo motor combination.

The step sensor drive is coupled to the gear train between the nutator and the gearhead. The step sensor is of the type provided in the HGA axis drive; the limit sensor is a suitably geared cam drive that operates redundant pairs of sealed snap action switches. It is driven from the gear train on the output side of the clutch to retain synchronization with the output shaft even if clutch slippage occurs.

Gear clusters are machined integrally with their shafts for maximum precision and reliability.

The actuator performance and physical parameters specifications are as listed in Table 6.

Table 6. Actuator Performance and Physical Parameters

Type: stepper motor/gear train
Motor size: size 15 permanent magnet rotor - IMC 015-815 (or equivalent)
Motor power: 39 watt per phase at 28 VDC
Step angle: 90^{o}
Holding torque: 7 oz-in, min.
Detent torque: 0.7 oz-in, min.
Working rate: 160 motor steps/sec
Gear reduction: 76000 to 1
Actuator weight: 12 lb, max.
Actuator size: 9 x 6 dia., max.
Stiffness: 250,000 ft-lbs/rad., min.
Rated holding torque: 400 ft-lbs (clutch limited)
Slewing speed: 3/16 deg/sec at 160 Hz drive frequency
Output angle sensing: 3/16 degree increments of output rotation
Output backlash: 5 arc-min., max.

The scan (E) gimbal actuator is shown in Figure 11. It consists of a direct drive 7.0 lb-ft torque motor, (Inland T-5730) and a specially designed, state-of-the-art tachometer based on an Inland tachometer currently in production. The tachometer is the same frame size and construction as the torque motor. The PSP support bearings on the E axis boom also serve as bearings for the torquer and tachometer. The rotors of each are mounted on an adapter attached directly to the PSP boom near the bearings for accurate alignment. The

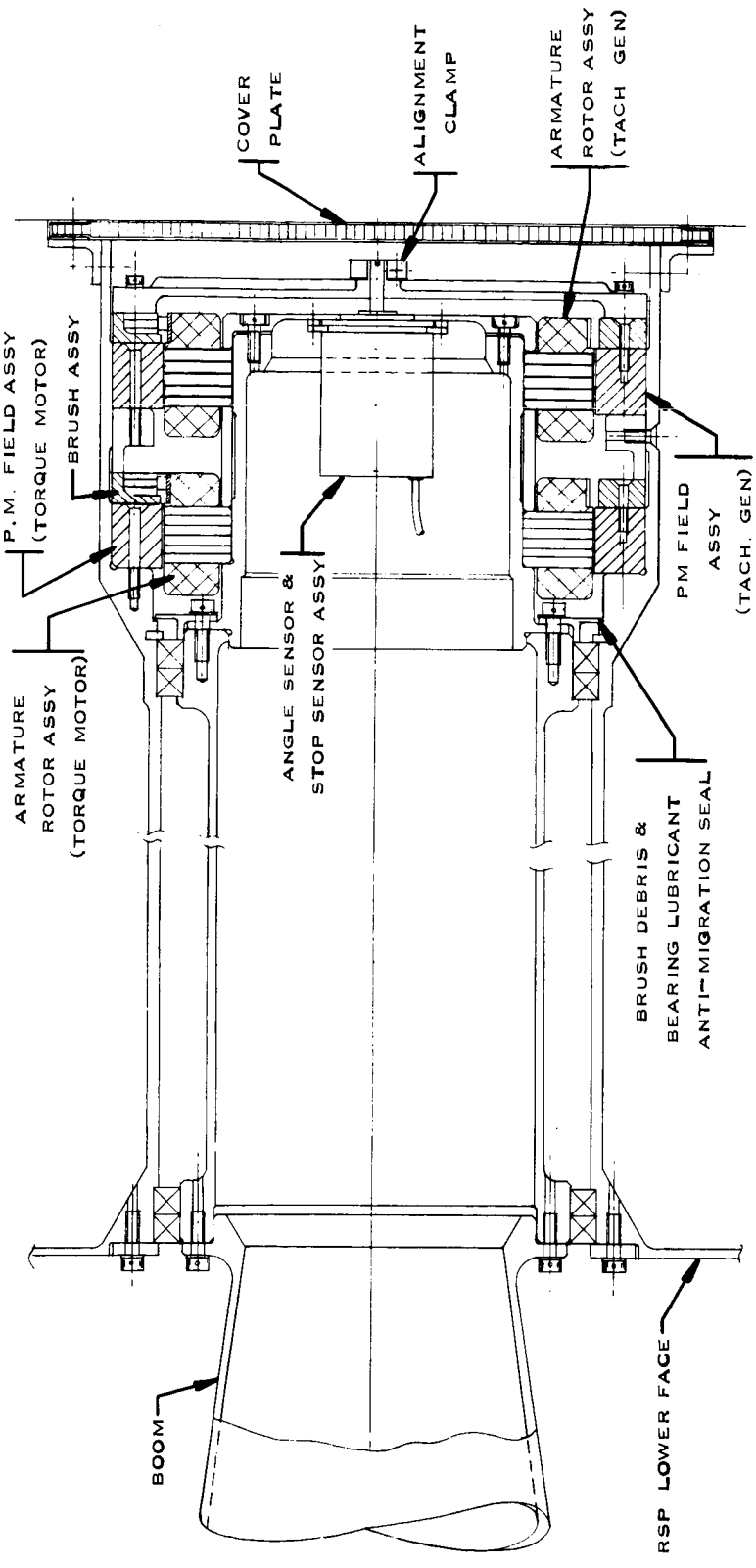

Figure 11. Scan (E) Axis Actuator

motor "stators" and brush rings are nested in the PSP bearing support tube and rotate with the platform (as in an inertial platform gimbal).

The torquer and tachometer brushes will be exposed to vacuum in the PSP gimbal drive. Vacuum tests at GE have shown that conventional Ag-MoS_2 brushes running on inlayed gold commutators will operate at considerably higher rubbing velocities for wear cycles greater than the Voyager PSP drive must meet. Newer materials such as those developed by Clauss and Van Wyck specifically for vacuum applications will afford still greater operating margin. A shield is provided to prevent brush debris from migrating into the support bearings.

The angle sensor and limit sensors are similar to those discussed in the HGA axis and will be mounted in the end of the boom, inside the motor rotor adapter. They will be attached to the rotor adapter and will be driven by a member attached to the PSP scan bearing support tube.

3.3 DISCUSSION OF ALTERNATIVES CONSIDERED

A number of the tradeoffs made here are similar to those for the HGA actuators and have been discussed in Section 2.6.

Step servo motors were selected for the PSP C & D gimbal drives for reasons already discussed in Section 2.6.3. The scan E axis gimbal drive, however, has rate smoothness requirements which are unlike those of the other gimbals.

Step servo motors could be used with variable frequency oscillator drive for velocity control, but very high gear ratios would be necessary to reduce the stepping jitter to acceptable limits. Initial analysis indicated that smooth stepping over the entire range would be virtually impossible to obtain with a finite duration drive pulse.

Several types of AC servos were considered. These also required extremely high gear ratios (e.g., 360,000:1) and the wide velocity range again presented a problem. A drive based on a hysteresis synchronous two-phase motor was designed. It had the characteristics listed in Table 7.

Table 7. Scan Actuator Characteristics

Type: synchronous hysteresis/gear train
Motor size: size 11 - Kearfott CRO D174 003 (or equivalent)
Motor power: 8 watt max. per phase 115V 400 cps at 8000 rpm 2 phases
Synchronous speed: variable, 1000 to 15000 rpm
Gear reduction: 360,000:1 (type as required)
Lubrication: as required
Actuator weight: 5 lbs, max.
Actuator size: 8 x 5 dia., max.
Stiffness: 250,000 ft-lbs/rad., min.
Output speed: variable 1^{o}/min. to 15^{o}/min.
Output backlash: 5 arc-min., max.
Output torque rating: 25 ft-lbs, min. (clutch limit)

Velocity control here was complicated by the fact that both the input frequency and voltage would have to be varied to obtain desired motor performance.

The brushless DC torque motor offers promise for the future. Dr. Manteuffel at GE-LMED is currently developing brushless DC torquers that may be adaptable to this precision drive within the next few years.

4. THRUST VECTOR CONTROL ACTUATORS

The Thrust Vector Control (TVC) actuators orient the propulsion thrust chamber assembly during mid-course corrections, orbit insertion and orbit trim, in compliance with autopilot commands. This action is implemented by two linear actuators mounted 90-degrees from each other, parallel to the pitch and yaw axes of the vehicle.

4.1 FUNCTIONAL REQUIREMENTS

The actuator must provide a total stroke of 4.8 inches, corresponding to an angular travel of ± 6 degrees for the thrust chamber assembly. The required peak force is 500 pounds. Dynamic performance requirements are discussed in conjunction with the autopilot studies (VOY-D-323).

The actuator must operate reliably during each engine firing, be unaffected by long idle periods in the space environment, and must not introduce contamination into the spacecraft.

4.2 DESCRIPTION OF BASELINE DESIGN

4.2.1 Block Diagram

A functional block diagram of the TVC actuator system is shown in Figure 12. The preamplifier accepts the command signal, mixes it with the existing negative position signal and amplifies the algebraic difference. This proportional signal is further amplified by the power amplifiers. These amplifiers include current limiting such that the maximum DC current to the drive motors does not exceed the rated level. Excessive current would cause partial demagnetization of the motors and resultant degradation of performance. The direct-drive DC torque motor has a wound armature and a permanent magnet field which, acting together, convert electrical currents directly into torque, to maintain desired accuracy in the positioning system. This torque is converted to linear motion through a high efficiency ball bearing screw, the position of which is detected by a potentiometer and transmitted back to the preamplifier, closing the control loop.

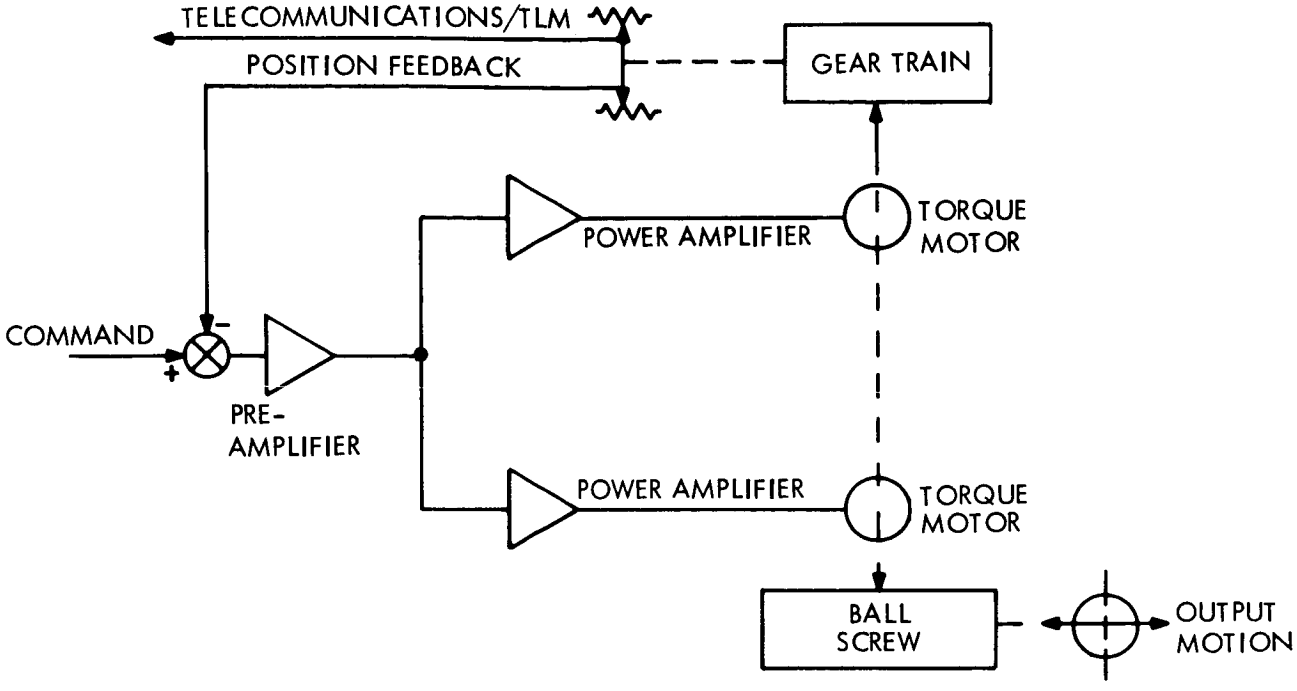

Figure 12. Single Axis TVC Control Loop

4.2.2 Actuator Design

The design considered most favorable to meet the Voyager TVC actuator requirements is a DC torque motor - ball screw combination. The design is an adaptation of the LEMDE Throttle Actuator designed and produced by Bendix Eclipse-Pioneer. The actuator consists of a pair of DC torque motors directly connected to a ball screw. The motor rotation and torque is converted to linear motion through the ball screw without intermediate gears. Stroke position information is provided by potentiometers mounted internally and driven from a planetary gear system off the motor shaft. The actuator consists of a housing and motor heat sink, permanent magnet DC torque motors, bearings, ball screw assembly, single-stage precision planetary gearing, potentiometer assembly (for control feedback and telemetry), hermetic sealing bellows, and the end fittings (ball and clevis) for structural attachment.

The torque motor characteristics selected for the control simulation are those of Type T-5730 (Inland Motor Corporation). These units have a 7.0 lb-ft stall torque, are 7.198 inches in diameter by 1.625 inches wide and weigh 7.25 pounds each. For redundancy two rotors will be mounted to a common shaft. This shaft in turn will drive the ball screw which is 1 inch in diameter with a lead of 1 inch.

Hermetic sealing permits the use of conventional lubricants and brush-commutator materials in this mechanism.

4.2.3 Description of Interfaces

Guidance and Control

The actuator receives its input control voltage from the autopilot control amplifier and returns to the autopilot an electrical signal of engine position. Dual feedback potentiometer elements will be operated in parallel to improve the reliability of the component.

Telecommunications - A potentiometer similar to the feedback transducer will provide a position signal to telemetry.

Structural - The actuator will be fastened to the structure by a double-pin gimbal (universal joint). The purpose of this attachment is to prevent actuator rotation during torque motor momentum changes. The engine end of the actuator will be provided with a self-lubricating ball type rod end joint for clevis connection.

4.3 ALTERNATE DESIGNS CONSIDERED

These three types of actuators were considered applicable to the Voyager TVC requirement:

a. Electrohydraulic

b. Reversible motor

c. Clutched motor:

Magnetic particle clutch

Spring clutch

The reversible DC torque motor and ball screw was selected as the best approach for this application due to its simplicity and reliability. The component has fewer moving parts, and has direct electromechanical power conversion without intermediate clutches or the risk of spacecraft contamination due to hydraulic leakage. Its frequency response is not as good as that of alternate systems discussed below, but was found to be adequate through a computer simulation of the control system (see VOY-D-323).

4.3.1 Self-Contained Electrohydraulic Actuator

This component is a completely self-contained unit with an integral motor, pump, reservoir, servo-valve and actuator. The pump would be driven by its electric motor from the spacecraft raw DC bus. The servo valve is energized directly from the autopilot signal amplifier. The servo valve controls the rate and direction of hydraulic flow into the cylinder. A linear transducer attached to the output shaft provides a position signal.

4.3.2 Clutched Motor

Two types of clutches were considered in this category - the magnetic particle clutch and the spring clutch. These components are similar; they differ only in the method by which they deliver motor torque to the load. The prime mover is a constantly rotating DC motor. The power from the motor is coupled into the leadscrew by the clutches in proportion to the signal from the autopilot. In the case of the spring clutch the control signal fully engages one of two spring clutches between the clockwise or counterclockwise rotating drums being driven by the motor and the lead screw. Whenever the clutch is engaged, full torque and speed is applied to the lead screw, i.e., the spring clutch actuator is a true on-off system. In the magnetic clutch actuator, a clutch for each direction is again used. A ferrous powder material will transmit a torque in proportion to the magnetic packing of the

material in the air gap, which is a function of the control signal. Torque from the energized clutch is transmitted through gear trains and converted to linear motion by a lead screw. Position feed back is provided by a linear potentiometer driven by the moving member. Locking the magnetic clutch actuator can be accomplished through the use of a non-reversible screw. Locking is provided internally in the spring clutch actuator; the springs lock the screw to the actuator body when there is no input signal to the clutch engagement coils.

4.3.3 Comparison

The three methods of implementation of the TVC actuator investigated were compared by various characteristics which are essential to the Voyager mission. These competing characteristics are summarized in Table 8.

5. DEPLOYMENT MECHANISMS

This section describes the general types of actuation to be used for the one-shot deployment operations of smaller spacecraft appendages. These include the deployable solar array panels, the maneuver antenna, and the broad coverage antenna.

5.1 FUNCTIONAL REQUIREMENTS

The deployment mechanisms must rotate their respective panel or antenna boom through a range of 120 to 150 degrees, depending on the specific application. All actuators are initiated by the pyrotechnic release of the appendage to be deployed. Suitable end-of-travel dampers and latch mechanisms are provided to ensure that the appendage is stopped without damage and reliably held in the deployed position.

5.2 DESCRIPTION OF BASELINE DESIGN

In each case, a stored energy actuator has been provided. These are comprised of a redundant pair of cylindrical torsion springs wound with the ends straight to prevent stress raisers. These are similar to the springs used in the Nimbus solar panel deployment mechanisms.

Table 8. TVC Actuator Tradeoff Summary

System	Development	Advantages	Disadvantages	Estimated Weight and Size	Estimated Power (Watts)	Remarks
Reversible Motor DC torque motor and ball screw	An actuator of this configuration has been produced for the LEMDE throttle actuator (360-pound stall load).	1. Simple and straightforward design 2. Ease of adding redundancy 3. Electrical to Mechanical power conversion without slip 4. Power input demand proportional to required output power	1. No holding force when de-energized 2. Will require power amplifier 3. Major scaling of LEMDE actuator	24.5 lb Length: 16 in. Diameter: 8 in.	No Load-0 Rated-300 Max. -600	1. High current output transistors available 2. Manufacture of LEMDE throttle actuator does not foresee any design problems
Integrated Hydraulic Actuator Actuator pump, electric motor and reservoir are one unit	Integrated actuators are in use for missile guidance (Pershing and Polaris). A modified Polaris actuator has been tested satisfactorily to the Apollo Service Module dynamic requirements.	1. Small control signal required 2. State-of-art well developed	1. Concern for space contamination 2. No holding power when de-energized 3. No known redundant integrated actuators	20 lb Length: 16 in. Diameter: 6 in.	No Load-375 Rated-525 Max. -750	1. Use hermetic sealing to protect against contamination 2. Use two actuators for redundancy 3. Requires design scaling
Clutched Motor DC motor, 2 magnetic particle clutches and screw	An actuator of this configuration is being used for the TVC system of the Apollo Service Module.	1. Fast response from high speed motor 2. Small control signal required 3. State-of-art well developed 4. Redundant or dual-actuator developed	1. Slipping clutch generates heat which changes output 2. Large clutch hysteris 3. Apollo had trouble in development 4. Recommended to stay under 3/10 hp and under 1 hp	32 lb (Dual) 20 lb. (Single) Length: 16 in. Height: 6.5 in. Width: 9 in.	No Load-100 Rated-? Max. -750	1. Apollo Service Module Actuator would require redesign in gear ratio, total length, and travel.
Clutched Motor DC motor, 2 spring clutches and screw	Method employed in military aircraft and industrial applications (Condor missile jet vane actuator).	1. Small control signal required 2. State-of-art well developed 3. No difficulty in matching TVC dynamic requirements 4. Reverse locking provided	1. No previous space development 2. Requires analog to 28 VDC 3. Major scaling of prototype	20 lbs. Length 16 in. Width 6 in. Height 7 in.	No Load-150 Rated-400 Max. -800	1. Would require major design and development effort

The energy absorber will be in contact with the appendage for the final 20 to 30 degrees of travel and will be designed to provide a gradual deceleration. The spring will have torque remaining at the fully-deployed position, to ensure appendage seating.

Energy absorbtion may be accomplished by axially crushing thin-walled aluminum or stainless steel tubes. Extensive research over the past several years at the GE Space Science Laboratories has proven this to be an efficient and reliable method of one-shot energy absorption. This method has the particular advantage that its absorption capability is independent of temperature and relatively independent of rate-of-force application.

While one-shot devices preclude flight acceptance testing, the performance variations of these energy absorbers from sample-to-sample are likely to be smaller than performance variations of a hydraulic damper under varying conditions of temperature and impact velocity. Sampling tests can be used to establish the performance parameters within satisfactory statistical tolerances.

A two-barb, one-way mechanical latch catches a hook on the appendage and prevents bounce-back. This is backed up by a one-way wrap spring clutch (only one part required) wrapped around the deployment shaft. The clutch prevents counter rotation of the load; only rotation in the direction of deployment is possible.

The springs are sized so that one can complete rotation of the load in zero g and compress the energy absorber. Deployment loads are minimized by the use of self-lubricating, self-aligning spherical rod end bushings for all hinges. A redundant switch pair senses the arrival of the member at the deployed position.

5.3 ALTERNATIVES CONSIDERED

The use of hydraulic dampers for energy absorption is undesirable because of their complexity, and their change in performance with changes in temperature.

Motorized deployment was considered to be too complex and ganged deployment, as in the case of one rotary actuator driving five solar panels through flexible shafting, was not susceptible to redundant drive and could entail the loss of several panels if one hung up, or if the actuator failed.

Geared clock springs were also judged too complex and were ruled out for that reason.

VOY-D-364
PYROTECHNICS AND PLANETARY VEHICLE SEPARATION

1. SCOPE

This section describes devices used to initiate and accomplish pyrotechnic events by explosive actuation. It also describes the Planetary Vehicle Separation System. The explosive devices include:

a. Parallel redundant separation switches which are used as a positive block to electrical power to maintain the subsystem in a "safe" condition during pad and prelaunch checkout. Arming, by applying electrical power, does not occur until the planetary vehicle is separated from the launch vehicle.

b. Electro-explosive devices (EEDs), which convert electrical energy into controlled explosive energy, are used to operate each pyromechanical device. The EEDs utilized in the subsystem conform to all safety requirements of AFETR 127-1.

c. Pyro-mechanical devices are pin pullers, separation nuts and valves (normally open and normally closed) which are activated by the explosive force genrated by the EEDs when fired. These pyro-mechanical devices are used for control of other subsystem functions and for mechanical unlatching of deployed devices.

2. PYROTECHNICS

Pyrotechnic events during the mission are listed in Table 1. Included in the list are the number and type of pyro-mechanical devices required for each event. The numbers of electro-explosive devices (EEDs) required for initiation also are shown. Both EEDs and pyro-mechanical devices include those required for redundancy.

Events 1 and 2 are controlled and fired by the booster. All other events are fired by the Pyrotechnic Controller (PC). Programmed events are initiated by signals from the Controller and Sequencer (C&S) to the PC. Backup signals from the Command Decoder Subsystem (CDS) to the PC can also be used to initiate the pyrotechnic events if required.

Table 1. Pyrotechnic Events

	Event	Type Device	No. Req'd.	EEDs
1	Operate PV IFD	PP	2	2
2	Separate PV	SN	8	16
3	Release Solar Panels	PP/DET.	18/4	4
4	Release High Gain Antenna	PP	3	6
5	Release Broad Coverage Antenna	PP	1	2
6	Release maneuver antenna	PP	1	2
7	Enable Propellant Flow-Start	NCV	2	2
8	Enable Oxidizer Flow-Start	NCV	2	2
9	Enable Propellant Flow-Main	NCV	2	2
10	Enable Oxidizer Main	NCV	2	2
11	Enable Helium Flow (1st Mid course)	NCV	1	1
12	Disable Helium Flow	NOV	1	1
13	Enable Helium Flow (2nd Mid course)	NCV	1	1
14	Disable Helium Flow	NOV	1	1
15	Enable Helium Flow (3rd Mid course, Orbit Insertion, 1st Orbit Trim)	NCV	1	1
16	Deploy Planetary Scan Platform	SN	2	4
17	Remove Instrument/Science Covers	PP		8
18	Initiate Cold Gas Jet Switch	SS	2	2
19	Disable Helium Flow	NOV	1	1
20	Enable Helium Flow (Back-up and/or 2nd Orbit Trim)	NCV	1	1
21	Disable Helium Flow	NOV	1	1
22	Emergency Helium Flow Enable	NCV	2	2
23	Final Lock-up	NOV	2	2
		EED TOTAL		66
		Fired from LV		18
		Fired from PV		48

Abbreviations			
EED	Electro-Explosive Device	SN	Separation Nut
PP	Pinpuller	PV	Planetary Vehicle
NOV	Normally Open Valve	IFD	In-Flight Disconnect
NCV	Normally Closed Valve	SS	Squib Switch

2.1. ALTERNATE DESIGNS

Two types of EEDs were considered for Voyager: (1) hot-wire and (2) exploding bridgewire (EBW). The hot wire EEDs chosen in earlier studies were the Apollo Standard Initiator (ASI) and a standard initiator developed by GE. A study to determine the feasibility of using EBWs for pyrotechnic initiation on the Voyager program was completed.

2.1.1. Exploding Bridgewire Study Results

The advantages of using EBW in any vehicle as compared with "hot-wire" initiators are safety and a rapid functioning time. The advantage of rapid functioning is not important to the pyrotechnic subsystem for Voyager as no pyrotechnic event requires the extremely rapid response times (less than one millisecond) of EBW initiators.

The other advantage (safety) is obviously important. EBW devices are safer than hot wire initiators for two reasons: (1) only secondary explosives are used and (2) a special firing pulse is required for proper operation. The use of secondary explosives eases handling and installation restrictions and the special firing pulse requirement reduces the probability of premature firing due to stray currents to practically zero.

The two disadvantages of using an EBW initiation system for Voyager are: (1) a weight penalty and (2) problems due to high operating voltage in deep space.

Systems which are using or have used EBW initiators are: Pershing, Sprint, Polaris, Poseidon, Saturn, Asset, Snap-10A and several classified programs. Table 2 is a compilation of available data on the characteristics of these systems. The weights are high because each initiator has its own firing unit.

One of the problems in applying current EBW systems to Voyager is the attendant weight penalty. As shown in Table 1, it is expected that at least 48 initiators will be required to perform the pyrotechnic event for the Voyager mission (excluding PV separation and IFD removal). The total weight of firing units is as shown in Table 3.

Table 2. Current EBW Systems

Property	Asset	Pershing	Sprint	Saturn	Snap-10A
*Weight (lb)	0.625	3.1	3.0	3.6	2.3
Size (in.) (l x w x h)	2.63 x 2 dia.	5.5 x 4.0 x 2.5	--	--	4.8 x 3.4 x 2.0
Power Type	dc	dc	ac	dc	dc
Charge Time (sec)	4	7.0	--	--	1.5
Capacitor (mf)	1.0	0.6	0.6	1.0	1.0
Voltage	2000	2350	2500	2000	2300
No. of Outputs	1	2	2	1	1
Initiating Explosive	RDX	PETN	RDX	PETN	--
Pin Gap Breakdown	700 volts (Nominal)	600 to 1200 volts	None	600 to 1200 volts	
Squib	None	$BKNO_3$	$BKNO_3$	--	--
Cable Type	Double Coax	Twisted Shielded Pair	Twisted Shielded Pair	Shielded Parallel Pair	--
Electronics Manufacturer	Aerojet-General	ITT	Martin-Orlando	GLA	Bendix
Ordnance Manufacturer	Aerojet-General	McCormick-Selph	Martin-Orlando	McCormick-Selph	

*Each system consists of an EED and a firing unit.

The weight penalty can be reduced by initiating simultaneous pyrotechnic events by an explosive train: two EBW detonators (for redundancy) initiate a confined detonating fuse (CDF) which carries the explosive stimulus to as many cartridges as required. In this way, the number of required firing units can be reduced as shown in Table 3. Even with this reduction, the weights are greater than for a hot wire controller even before considering the weight of confined detonating fuse.

Table 3. EBW Firing Unit Weights

System	Without CDF		With CDF	
	No. of Units	Weight (lb)	No. of Units	Weight (lb)
Pershing	24	74.5	11	34.1
Sprint	24	72	11	33.0
Saturn	48	173	22	78.2
Snap 10A	48	111	22	50.6
Asset	48	30	22	13.7

Notes:

1. Weight estimate for hot-wire pyrotechnic controller = 10 lb.
2. Confined detonating fuse for initiating multiple detonators simultaneously from a single firing unit.

Other methods of reducing weight were investigated and the most promising is a central firing system. The power supply and firing capacitor would be common, and each output (as many as 10) would use a gap tube to switch the firing pulse. This would reduce the volume and the number of heavy components (i.e., capacitors and power transformers) decreasing the weight considerably.

Another method of reducing weight is to fire the EBW devices in series. This method has been shown feasible by Martin-Orlando for two initiators with the possibility of firing up to four. The firing energy on the capacitor must be increased by either increasing the charge voltage or capacitor size slightly to fire all the EBWs. The increase in energy is not linear and is currently being investigated.

The packaging of the electronic firing units can also be optmized to decrease the overall weight of EBW systems. Most firing units are "potted" and the potting compound is an appreciable percentage of the firing unit weight. Therefore, a reduction in volume eliminates some of the potting compound, gaining a substantial weight decrease.

The packaging technique is also affected by the other major problem of EBW systems. This problem is the effect of a long space flight on a firing unit with a capacitor charged to high voltage (2000 volts or more). Most units are hermetically sealed to prevent arcing problems. However, for a long space flight, it is possible that the leakage of the sealed unit can be such that at some time during the flight the critical pressure-distance point can be reached and arcing can occur. Any loss of the firing energy due to arcing during the EBW firing will cause an EBW failure. The integrity of the hermetic seal becomes an important factor in design. Another solution to this problem is to open the firing unit and allow it to outgas. If the outgassing is large enough so that a vacuum exists around the high voltage terminals, no arcing will occur. This will also allow a weight reduction by eliminating the potting and sealing compounds. This problem area must be investigated more fully to determine the extent of the problem and methods of checking solutions. A combination of sealed units for earth orbit operations and open units for deep space operations may help to solve both problems of weight and high voltage arcing of EBW systems.

2.1.2. Hot Wire Initiators

Two hot wire initiators were investigated for use on the Voyager: the Apollo Standard Initiator (ASI) and a standard initiator developed by GE. Both initiators studied earlier were dual bridgewire units. The GE initiator was constructed so that the unit could be modified to produce three pressure outputs as well as a detonator output. Each initiator output would be an integrated unit as opposed to the ASI. The ASI output is amplified by welding the ASI into booster bodies to produce pressure or a detonation as required.

The GE initiator was chosen as the preferred design for both Task A and Task B for the following reasons:

a. The ignition mix was nonconductive; thereby, eliminating electrical leakage between bridgewires (which was a problem with the ASI).

b. The GE initiator had less explosive interfaces.

c. A monitor loop was provided to ensure that all initiators were connected and had the capability to check proper operation if required.

d. The Voyager mission specification required a capacitor discharge firing system and the feasibility of firing by this method had been proven, at that time, for the GE initiator but not for the ASI.

Since completion of the Voyager Task B study, development work has continued on the ASI. The major change was the removal of one of the two bridgewires, eliminating the electrical leakage problem between bridges. In addition, capacitor discharge tests have been conducted on the ASI for use on the ALSEP portion of the Apollo program. Thus, two of the advantages of the GE initiator have been neutralized. The single-bridgewire ASI has passed the qualification program for the Apollo mission and further testing is being done. The monitor loop and the simpler construction of the GE initiator are still desirable, but no further development has been accomplished.

2.1.3. Conclusions and Recommendations

Based on the above information, the single-bridgewire ASI was selected as a standard electro-explosive device for all Voyager pyrotechnic events. This initiator is preferred over the GE standard initiator because it is in a more advanced development stage and can easily be integrated into Voyager.

By proper shielding of the firing cables and following accepted wiring procedures (as specified in the range safety manual) the probability of premature firing can be minimized. In addition, arming of the pyrotechnics does not occur until after planetary vehicle separation. With EBWs the probability of premature firing would be even lower, but while a light weight EBW system applicable to Voyager is feasible it has not yet been developed and a full assessment of possible arcing resulting from the high voltage associated with EBW systems has not yet been made.

2.2. FUNCTIONAL DESCRIPTION

Three initiators are required for Voyager:

a. An electro-explosive pressure cartridge.

b. A detonator cartridge.

c. A through bulkhead initiator.

The EED chosen for initiating all pyrotechnic events on Voyager is the ASI. The ASI output is not capable of initiating confined detonating fuse (CDF) and is therefore amplified by the Apollo detonator cartridge. Through bulkhead initiators (TBI) are used to operate the pin-pullers which release the solar panels for deployment and are fired by confined detonating fuse.

2.2.1. Apollo Standard Initiator

The basic electro-explosive device which initiates all pyrotechnic events is the ASI (Figure 1). It has been qualified on the Apollo program and is manufactured by Space Ordinance Systems, Inc. as Part No. S01-10197-11. It has a single bridgewire in an Inconel alloy body and is hermetically sealed.

The Apollo program normally fires the ASI by constant current, but the ALSEP portion of the program plans to fire the ASI by capacitor discharge and has conducted firing tests for this method. Figure 2 shows a plot of the ALSEP data and estimated curves based on the data points.

The curves are plotted for three firing energy probability levels based on the results of Bruceton-type tests:

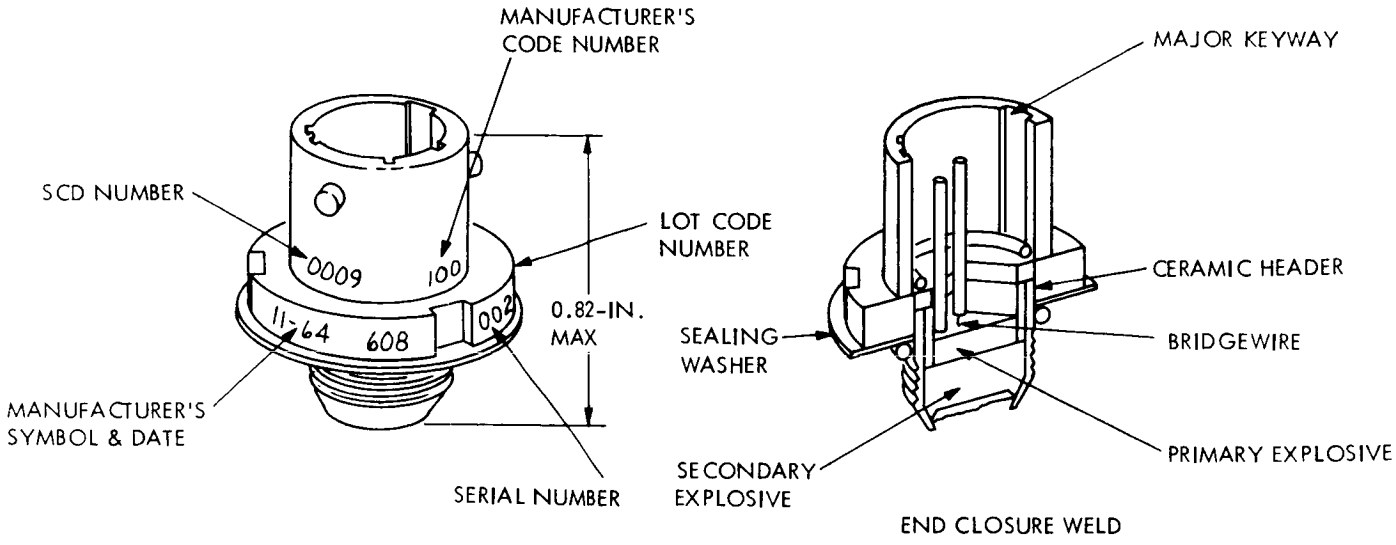

Figure 1. Apollo Standard Initiator (ASI)

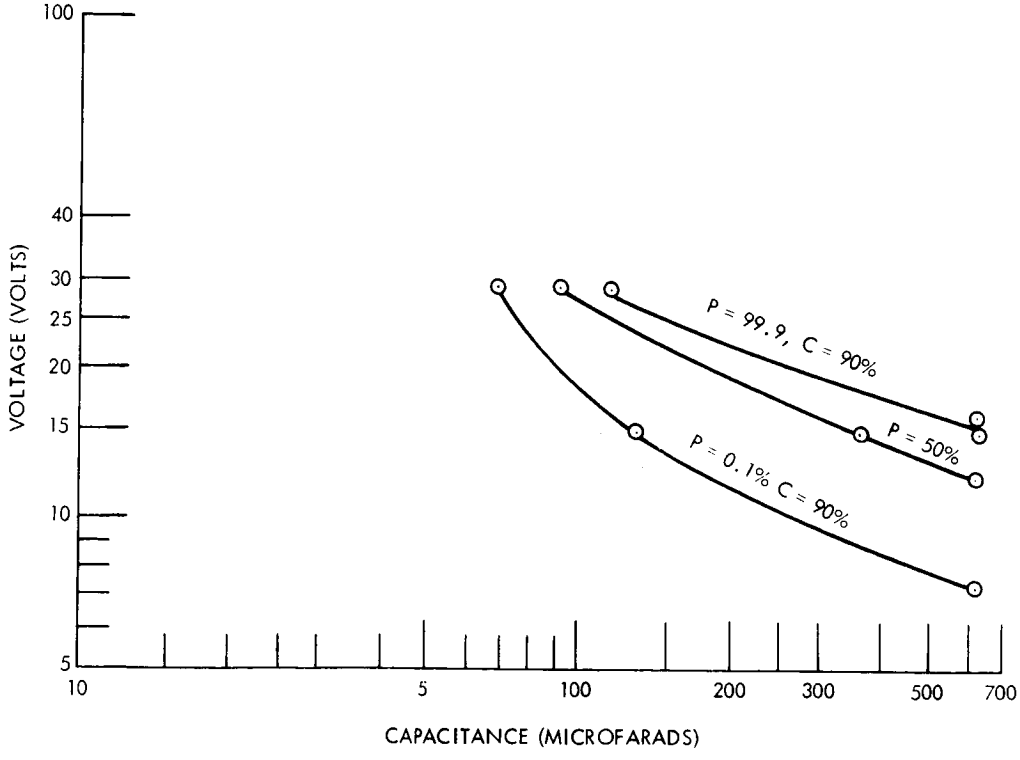

Figure 2. Capacitor Discharge Firing Characteristics of ASI

a. All-fire (99.9% probability at 90% confidence).

b. Mean (50% probability).

c. No-fire (0.1% probability of firing at 90% confidence).

Estimates of capacitor-voltage combinations can be made from these curves.

The peak pressure output of the ASI is 650 $\pm$ 125 psi in a 10cc bomb with a time peak less than 10 milliseconds. Where higher pressures are required to operate the pin-pullers, valves, etc. (depending on the size of the device), boosters are used.

2.2.2. Apollo Standard Detonator (ASD)

The ASD (Figure 3) is used to initiate the CDF which is used both to operate the separation system and fire the TBIs which operate the pin-pullers used for solar panel deployment.

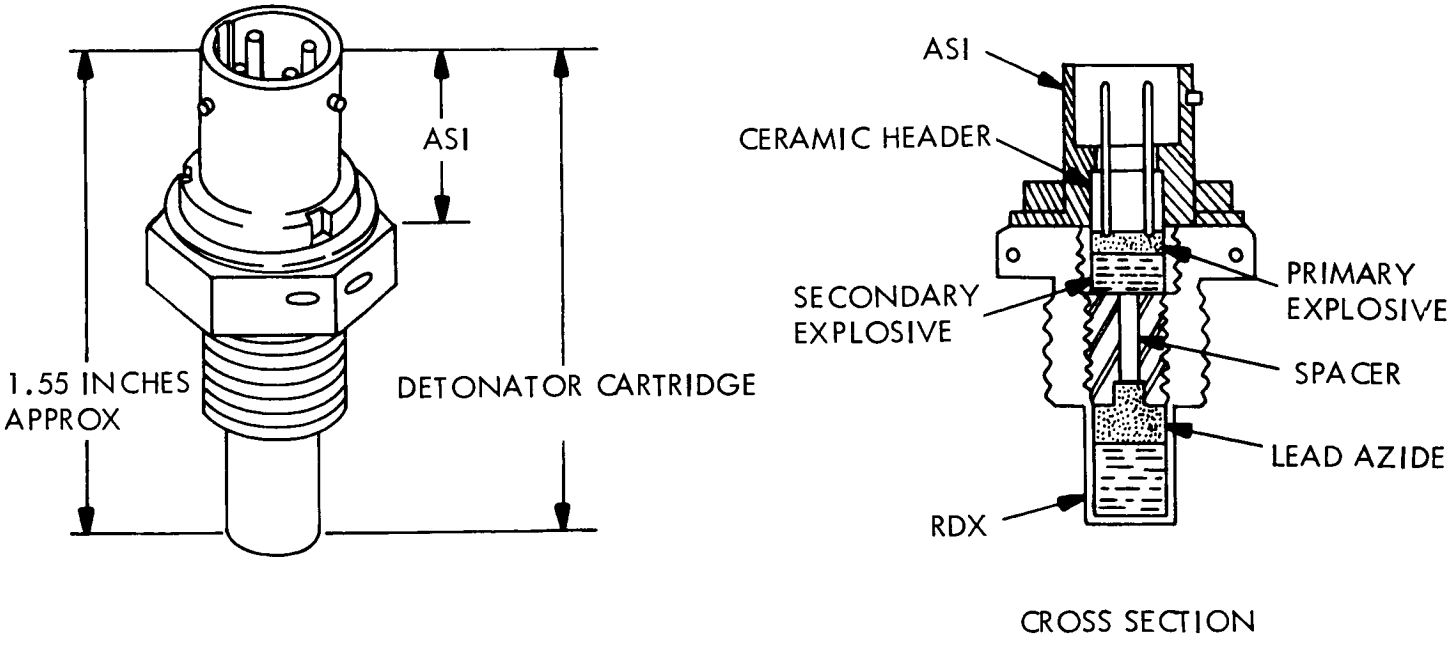

Figure 3. Apollo Standard Detonator (ASD)

The detonator uses the ASI for the initiation and has a detonation output capable of initiating explosive cords. It produces a dent in a steel witness plate of 0.051 to 0.060 inch when tested in accordance with Military Standard 316.

2.2.3. Through Bulkhead Initiator (TBI)

A cross-section of the TBI is shown in Figure 4. A detonation wave is transmitted by an explosive train (confined detonating fuse) and is amplified by the donor charge. The output of the donor charge is an intense detonation wave which passes through the metal bulkhead and initiates the acceptor charge without rupturing the bulkhead. The acceptor charge is attenuated and used to ignite the propellant which produces gas pressure operating the pin-pullers. The integrity of the bulkhead assures that no leakage will occur through the initiator.

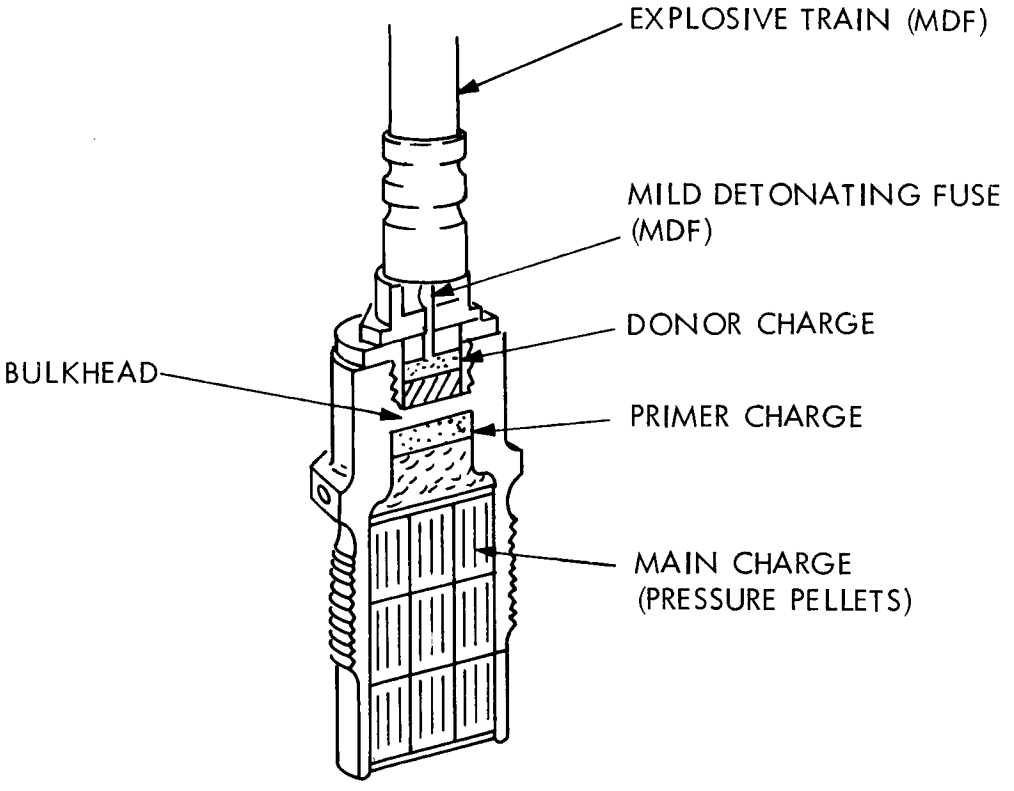

Figure 4. Through Bulkhead Initiator (TBI)

2.2.4. Pyrotechnic-Mechanical Devices

Pyrotechnic-mechanical devices used on Voyager are pin-pullers, separation nuts, and valves (both normally open and normally closed). The valves and separation nuts will be operated by the ASI (with a booster, if required) and are standard devices which have been used successfully on many programs. Two pin-pullers will be used, a dual cartridge pin-puller and a single cartridge pin-puller. Twenty dual cartridge pin-pullers are used to release the solar panels and are operated by TBIs. The single cartridge pin-pullers pull the IFD and are fired by the ASI. The weights of all pyrotechnic-mechanical devices are included with the subsystems using them.

2.3. PHYSICAL CHARACTERISTICS

2.3.1. Apollo Standard Initiator

The outline dimensions of the ASI are shown in Figure 5. The weight of the ASI is 1 ounce maximum. The electrical connector mates with various connectors depending on the keyway

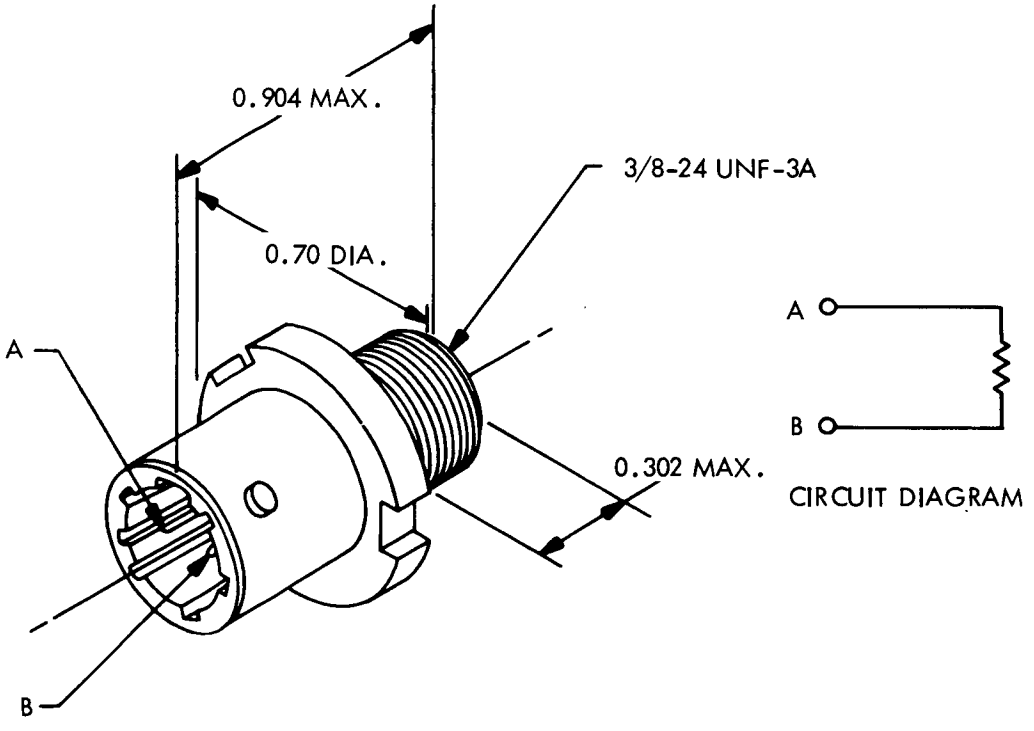

Figure 5. Outline Dimensions of ASI

orientation. These connectors are NAA/ME414-0503, MS3116E-8-2S, PT06E-8-2S and KPD6F8-25AG. The keyways can be blocked to provide special indexing as required.

2.3.2. Apollo Detonator Cartridge

The outline dimensions of the detonator are shown in Figure 6. The weight of the detonator cartridge is 2 ounces.

2.3.3. Explosive Train Initiated Cartridge

The estimated weight of this cartridge is 1.5 ounces.

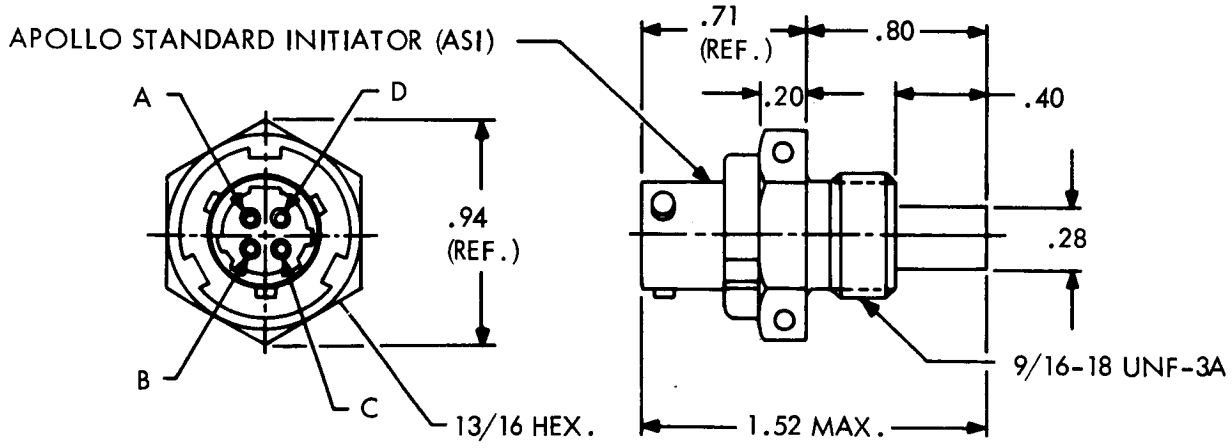

Figure 6. Outline Dimensions of ASD

2.4. INTERFACE REQUIREMENTS

2.4.1. Launch Vehicle

The mechanical interface between the launch vehicle and the planetary vehicle is described elsewhere in this report. Electrical firing power for the PV separation devices will be supplied by the launch vehicle. The in-flight disconnect (IFD) will be operated before separation by two pin-pullers (each pin-puller actuated by a single ASI). The firing current for the ASI is 5.0 amp minimum (10 amp required for the IFD).

The separation of the planetary vehicle is accomplished by the operation of eight separation nuts each initiated by two EEDs. Each EED requires a minimum firing current of 5 amp from the launch vehicle so that a total of 80 amp is required. The proper sequencing of IFD and separation firing signals are controlled by the launch vehicle.

2.4.2. Pyrotechnic Controller

All ASIs will receive their electrical firing current from the pyrotechnic controller, by discharge of a charged capacitor through each bridgewire. The timing and sequencing as well as instrumentation also will be provided by the pyrotechnic controller. The minimum energy to be delivered to each ASI must be determined by Bruceton tests. The nominal firing energy being provided by the pyrotechnic controller is a 660 microfarad capacitor charged to 25 volts. The estimated energy required for 99.9 percent probability at 90 percent confidence is a 150 microfarad capacitor charged to 25 volts based on data gathered for the ALSEP program. Therefore, a safety margin is being provided but the exact extent of this margin must be determined.

3. PLANETARY VEHICLE SEPARATION

The Planetary Vehicle Separation System consists of pyrotechnic separation nuts and springs.

3.1. BASELINE DESIGN DESCRIPTION

Separation of the planetary vehicles from the launch vehicle will be accomplished by eight separation nuts which are operated by redundant EED. The EEDs will be the ASI with a booster propellant, if required.

A cross-section of a typical separation nut is shown in Figure 7 and operates as follows: The firing signal from the launch vehicle initiates the EED whose output drives the locking piston forward. This allows the threaded nut segments to be driven outward by the separation piston as the fingers on the segments can drop into the spaces of the locking piston. The ejector piston then moves forward driving the bolt out of the cavity into the bolt catcher. The bolt catcher traps the bolt and prevents it from flying free.

As soon as the nuts are released, 16 compression springs provide the separation velocity. Two springs are located at each attachment point. The spring characteristics are listed in Table 4. Lefthand wound springs alternate with righthand springs so that the total torque applied to the PV is minimized. These springs are designed with margin against buckling, so that friction producing guide tubes are unnecessary.

Precipitation hardening 17-7 PH in the full hard CH900 condition is used. It can be obtained with a copper lubrication coating which provides dry lubricant antigalling protection in service.

The springs will be calibrated and arranged in a sequence designed to minimize tipoff rate.

The separation sequence is illustrated in Figure 8.

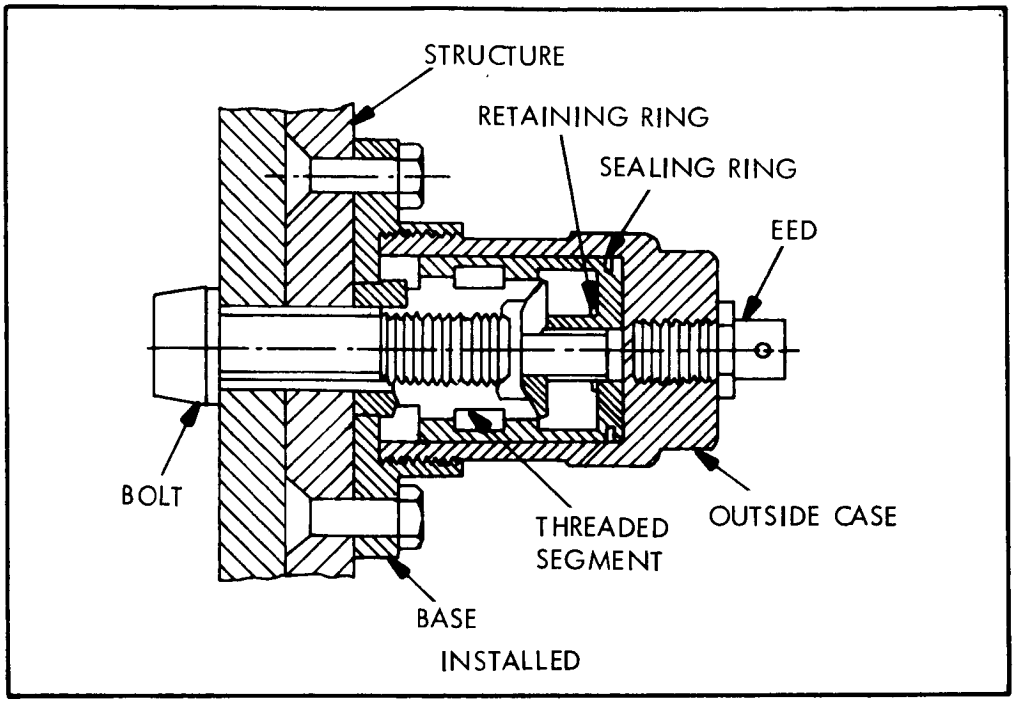

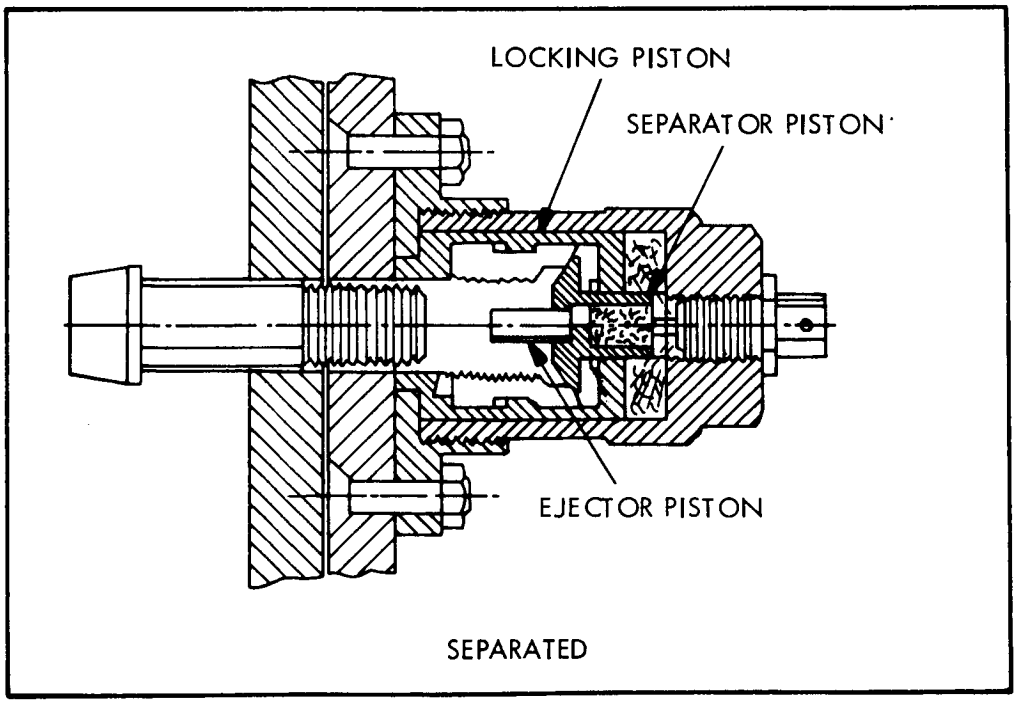

Figure 7. Typical Separation - Nut

Table 4. Separation Springs

Required Separation Energy	6850 in.-lb
Estimated Hysteresis Loss	685 in.-lb
Energy Released	7535 in.-lb
Precompression Energy	245 in.-lb
Total Energy Storage	7780 in.-lb
Number of Springs	16 in.-lb
Energy per Spring	485 in.-lb
Compressed Load	235 lb
Free Stroke	4.12 in.
Spring Gradient	57 lb/in.
Average Coil Diameter	1.88 in.
Wire Diameter	0.225 in.
Active Coils	9.5 in.
Free Length	6.75 in.
Weight per Spring	0.65 lb
Total Weight per PV	10.4 lb
Spring Length/Buckling Spring Length	0.36 in.
Material	17-7 PH aged
Shear Yield Stress	140,000 psi
Corrected Max Working Stress	115,000 psi
Weight of Associated Hardware	5.6 lb
Spring System Weight per PV	16.0 lb

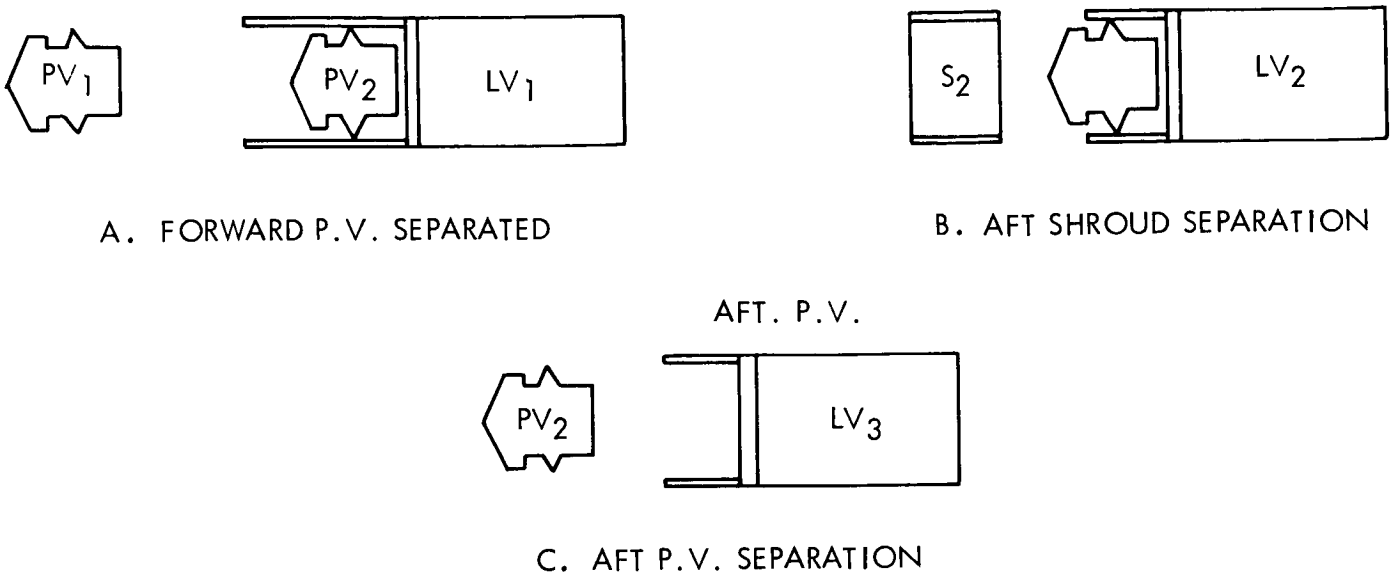

Figure 8. Separation Sequence and Nomenclature

The relative velocities will be as follows:

a. Between PV1 and LV_1 16.95 in.-sec

b. Between S2 and LV_2 13.05 in.-sec

c. Between PV_2 and LV_3 19.4 in.-sec

d. Between PVd and S_2 5.35 in.-sec

e. Between S_2 and PV_2 2.65 in.-sec

f. Between PV1 and PV_2 8.0 in.-sec

These velocities are adequate to avoid contact between planetary vehicles and shrouds during separation. With a relative velocity of 8 in./sec., the two planetary vehicles will be separated by 100 meters in about 3 minutes, allowing initiation of attitude control with little risk of occultation of celestial references by the other vehicle. In 24 hours, they will be separated by 195 km allowing midcourse corrections with little risk of mutual plume impingement.

3.2. ALTERNATE SEPARATION SYSTEMS

3.2.1. Resettable Release Nuts with Linear Gas Generator

An alternate method for operating the separation nuts is by using explosive cord (such as mild detonating fuse) as a linear gas generator to operate the separation nuts. This method of operation increases the reliability as only the cord requires initiation. The reliability of the cord, once initiated is extremely high. By use of a resettable release nut, the nut can be easily reset allowing operability testing during the assembly cycle.

The combination of the linear gas generator and the resettable release has distinct advantages. Manifold redundancy is simplified because equal line length from a pressure source is not required. The manifold can be pressurized by air, with linear cord installed, to checkout nut operation in the installed configuration and the resettable release nut can be reset without disassembly of the nut.

This system appears very promising for this application because of high reliability, testability, and light weight. It has not been selected for the baseline design because it is in the early stage of development.

The separation of the planetary vehicle is accomplished by releasing eight release nuts which attach the planetary vehicle to the launch vehicle shroud. The resettable release nut (RRN) is similar in operation to the standard separation nut. Instead of having threaded nut segments, it has locking segments to hold a notched piston which can be drilled and tapped or externally threaded as shown in Figure 9. The RRN will be functioned by a linear gas generator which is routed through a manifold at the top of the nut. Two linear gas generators will be used for redundancy. The initiation of the linear gas generator produces a gas front which drives the locking collar forward. The locking segments are thereby allowed to be driven outward by the motion of the unlocking piston and the resetting fastener. The resetting fastener is then driven out of the RRN body. Resetting is accomplished by loosening the

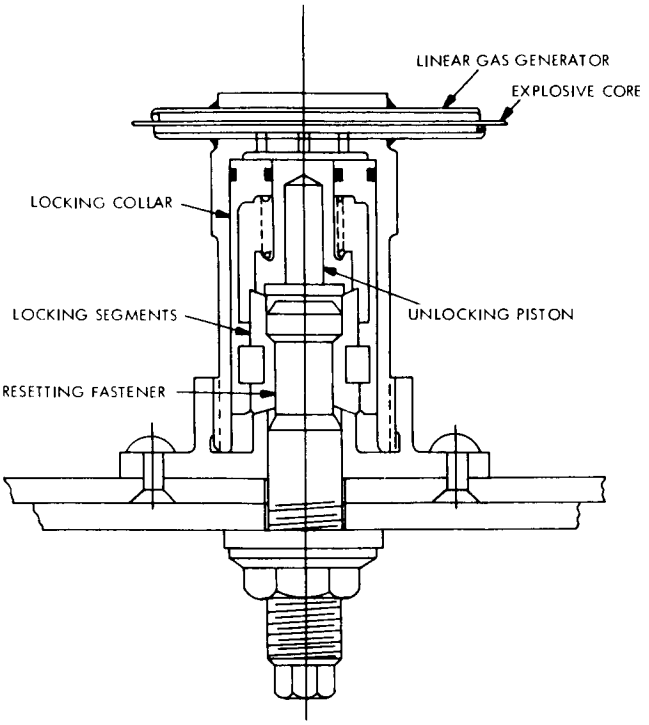

Figure 9. Resettable Separation Nut

attachment nut and pushing the resetting fastener into the cavity. As the unlocking piston is driven upward, the segments and locking collar are pushed into place. The attachment nut can then be tightened to a predetermined torque and the RRN is ready to be operated again.

Prior to installation, the system can be tested on the flight vehicles. The fastening bolts are torqued into the resettable release nuts. A pneumatic source is connected to the stainless steel tube with the linear gas generator inside. The pressure of the gas will operate the resettable release nuts to test the system. Each released piston can then be pushed into the release nut housing after the bolt has been loosened, thereby resetting the nut. The final torquing of the fastening bolts can then be accomplished.

3.2.2. Cold Gas Pneumatic Thruster

The cold gas thruster system consists of a high pressure tank filled with nitrogen gas, two explosive valves and eight pneumatic-release thrusters. The explosive valves are fired

allowing the high pressure gas to flow in the manifolds and operate the thrusters. The thruster system is shown in Figure 10 and operates as follows: The gas pressure drives the piston forward. The tip of the piston unlocks the spring fingers allowing the nut to move. The piston continues on, pushing the PV and imparting a velocity differential as required.

This system was the preferred design for the Task B study because of its dual capability of releasing and providing the required separation velocity. The system is clean (produces little or no contamination), can be tested readily during development, and has been used on a military program. While some experience has been gained on a small vehicle, adapting this system to a large vehicle may create problems in balancing line drop and assuring simultaneous actuation.

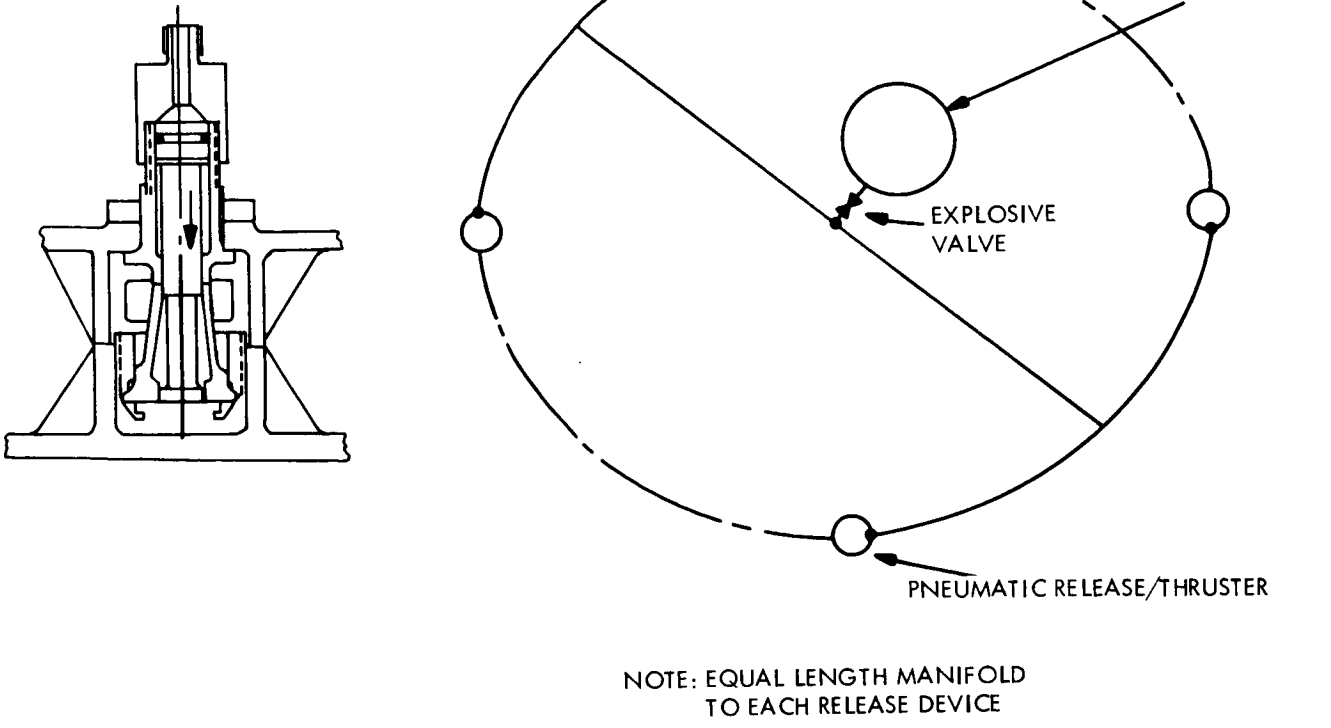

Figure 10. Pneumatic Release Thruster

3.2.3. Encapsulated Mild Detonating Fuse

Encapsulated MDF was the preferred design for the Task A study. It is more adaptable to a monocoque structure than a hard-point attachment configuration. The reliability is high, but the weight increase due to the addition of an adapter as well as the complications of the adapter installation outweigh the advantages.

3.2.4. V-Clamp

V-clamps are probably the most popular method for releasing small size space vehicle from boosters as they are extremely reliable and can be tested. In the large size required for this application, V-clamps are heavy, difficult to handle, and difficult to test.

VOY-D-370
PROPULSION SUBSYSTEM

1. SCOPE

This section of the report describes the design of the baseline spacecraft Propulsion Subsystem using the lunar module descent engine. As discussed in VOY-D-274, the baseline system uses the LEMDE engine to accomplish all required propulsion functions - trajectory corrections, orbit insertion, and orbit trim. Trade-offs that were considered in configuring the baseline system are described in this section.

In addition other liquid propulsion alternatives to the baseline system were considered and are described briefly. These include a configuration in which the LEMDE is supplemented with auxiliary thrusters, configurations which use the Agena and Transtage engines, and one which uses four Apollo subscale thrusters.

The Space Division of Chrysler Corporation provided major assistance in the preparation of this section of the report.

2. REQUIREMENTS AND CONSTRAINTS

The Propulsion Subsystem is based on the use of the LEMDE thrust chamber assembly (TCA) as specified in the statement of work. This TCA, with its unique throttling capability, offers a distinct advantage for the Voyager duty cycle. It is possible with a single thrust chamber to accommodate the wide variety of requirements for the midcourse corrections, orbit insertion maneuver, and orbit trim functions.

The basic operational requirement of the Propulsion Subsystem is to provide a total velocity change capability of 1.95 km/sec to the planetary vehicle at various phases of the mission profile. These phases include midcourse correction in which booster injection inaccuracies are removed and time of arrival adjustments are made. For 1973 missions this amounts to

approximately 10 percent of the total usable propellant or 0.13 km/sec used in three separate burns. The second phase is the orbit insertion maneuver, which requires about 70 percent of the available propellant in providing 1.33 km/sec ΔV. The orbit trim maneuvers account for the remaining 19 percent of the available propellant, or 0.49 km/sec. A summary of ΔV requirements for 1973-79 is shown in Table 2-1.

Table 2-1. Velocity Requirements for 1973-1979 Launch Periods

Description	MISSION YEAR			
	1973	1975	1977	1979
	VELOCITY (MPS)			
Time-of-Flight Adjustment	120	60	60	100+
Trajectory Correction	10	4	4	6
Orbit Insertion				
Impulsive	1277	1638	1661	1663
Losses (Est)	50	50	50	50
Orbit Trim	493	198	175	131
Total	1950	1950	1950	1950

To provide capability for missions in the four launch opportunities, the propulsion system was sized on the worst case conditions - that is, when payload and ΔV's are maximum. This results in tankage that is sized for approximately 13,000 pounds of propellant.*

Guidance requirements, trajectory analysis and operational sequences generally dictate the requirements for the minimum impulse bit (MIB), the tailoff uncertainties and tailoff impulse requirements. Data in this area is also presented in Reference (1). It is a conclusion of that report that no strong operational or mission requirement has been determined for the minimum

*GE Milestone Report VOY-P-TM-13, dated 11 August 1967.

impulse bit that must be provided by the propulsion subsystem. The minimum impulse bit given in the current mission specification ** is accepted for the present study. For both the midcourse and the orbit trim maneuvers, the tailoff uncertainty should be maintained at less than 106 pound-second.

3. SUBSYSTEM TRADEOFF STUDIES

In this section the major tradeoffs for a liquid propulsion system are presented. These include the selection of the pressurant and the pressurant method, propellant acquisition, tankage design, and subsystem weight analysis. A summary is shown in Table 3-1. Tradeoffs, which are basically hardware oriented, are presented in Paragraph 3.2

3.1. PRESSURIZATION SYSTEM

The Propellant Pressurization System was analyzed in detail from the standpoints of choice of pressurant gas and the method of pressurant containment and control. Stored gas and pressurized ullage systems using inert pressurant gases (helium and nitrogen), heated inert gas systems, and reacting products systems (main tank injection and gas generator) were considered. The system requirements, trade-off criteria, types of system evaluated, and results are discussed below.

Design data which apply to the pressurization system are given in Table 3-2.

3.1.1. Pressurant Gas Tradeoff

The trade-off was between helium and nitrogen, primarily on the basis of weight. The analysis was conducted for two extremes of thermodynamic behavior, isothermal and adiabatic, as defined below.

** "Performance and Design Requirements for the 1973 Voyager Mission, General Specification for", dated January 1, 1967.

Table 3-1. Summary of Tradeoff Studies

Item	Area of Tradeoff	Baseline Selection	Major Factors of Influence
Pressurization	1. Pressurant Gas (He, or N_2)	Helium	Weight; solubility in propellants
	2. Method	Regulated	Weight; State of Art
Propellant Acquisition	1. Type of device	Bellows, baffles screens	Positive; most ground testable
Thrust Chamber Assembly	1. Thrust level selection	1050 min 9850 max	Existing design
	2. Propellant selection	NTO and A50	Existing test data
	3. Head End Controls	LEMDE Design	Existing test data
	4. Nozzle design	Insulated	Temperature limits
Tank Design	1. Materials	6A1 4V Titanium	Weight, existing experience and usage
	2. Mounting methods	Trunnion	Weight; packaging ease
Subsystem Design Tradeoff	Component arrangement	See schematic	Reliability flexibility growth

Table 3-2. Pressurization System Design Data

Propellant Tank Dia. (in.)	54.5
Propellant Tank Volume (ft^3)	196
Number of Propellant Tanks	4
Number of Pressurant Tanks	4
Propellant Tank Pressure, (psia)	235 (stored gas system)
Pressurant Initial Pressure, (psia)	3600 (stored gas system)
Operating Temperature, ($^\circ F$)	40-100
Engine Inlet Pressure, (psia)	220 (high thrust) 235 (low thrust)

The isothermal process assumes no temperature changes during expansion. Pressurant requirements are calculated according to the equation:

$$W_{press} = \frac{N \; P_t \; V_t}{R \; T_i} \left(\frac{1}{1 - P_{f/P_i}} \right)$$

Where:

W_{press} = Pressurant weight (lb)

N = Excess factor

P_t = Propellant tank pressure (psia)

V_t = Propellant tank volume (ft^3)

R = Gas constant ($ft/^\circ R$)

T_i = Initial gas temperature ($^\circ R$)

P_f = Final pressurant tank pressure (psia)

P_i = Initial pressurant tank pressure (psia)

For the purpose of this study, N was set equal to 1.40 which included a 15 percent leakage factor and a 25 percent increase to account for actual variations from the isothermal process. This was verified by using a computer program which calculates the actual process, as reported above. The adiabatic process accounts for the temperature decrease by multiplying the isothermal pressurant requirements by the ratio of specific heats of the gas.

The solubility of both pressurants in N_2O_4 and A-50 was determined for the baseline propellant weights, using data from a NASA Reference*. Because of the chemical similarity of nitrogen to both propellants, the solubility is far greater than for helium, as shown in Table 3-3.

Table 3-3. Solubility of Gases in Propellants

Propellant	Helium	Nitrogen
N_2O_4	0.306 lb	30.55 lb
A-50	0.048 lb	3.34 lb

Table 3-4 lists the weight comparison for nitrogen and helium. The pressurant weight includes the weight of gas in solution. The data are for a stored gas system designed to the requirement previously stated for an isothermal case.

Table 3-4. Weight Comparison (Helium versus Nitrogen)

	Helium	Nitrogen
Pressurant Weight (lb)	64.5	478.0
Pressurant Tank Weight (lb)	613.0	613.0
Propellant Tank Ullage Gas (lb)	2.1	14.3
	679.6	1105.3

* NASA Technical Brief 67-10083, April 1967

Based on the above 425.7 pound weight saving for helium, and potential problems of engine operation with such a large amount of nitrogen in solution, helium was selected as the pressurant gas for the baseline design.

Several methods of pressurization were investigated during the course of the propulsion system study. Systems such as main tank propellant injection, solid propellant gas generators, and dual bipropellant gas generators can be eliminated as not being state-of-the-art.

A helium heat exchanger design was investigated, but the majority of effort was expended in investigation of the blowdown, makeup gas and regulated system. These four are discussed in the following paragraphs.

A regulated stored gas pressurization system employing a heat exchanger to reduce the pressurizing gas requirements was analyzed. This system is shown schematically in Figure 3-1.

The gas from the high pressure storage bottle reaches low temperature during the isentropic expansion process. By passing the gas through a heat exchanger through which the propellant flows, the gas can be warmed about to approximately the temperature of the liquid propellant with negligible changes to propellant temperature. Given the following data:

- Leakage: 30 percent (increased number of leak points)
- Heat Exchanger Efficiency: 80 percent
- Heat Exchanger Weight: 10 pounds (estimated)
- Temperature difference (propellant-gas): 75°F

The gas requirements and system weights may be obtained. Table 3-5 compares these with a conventional stored gas system.

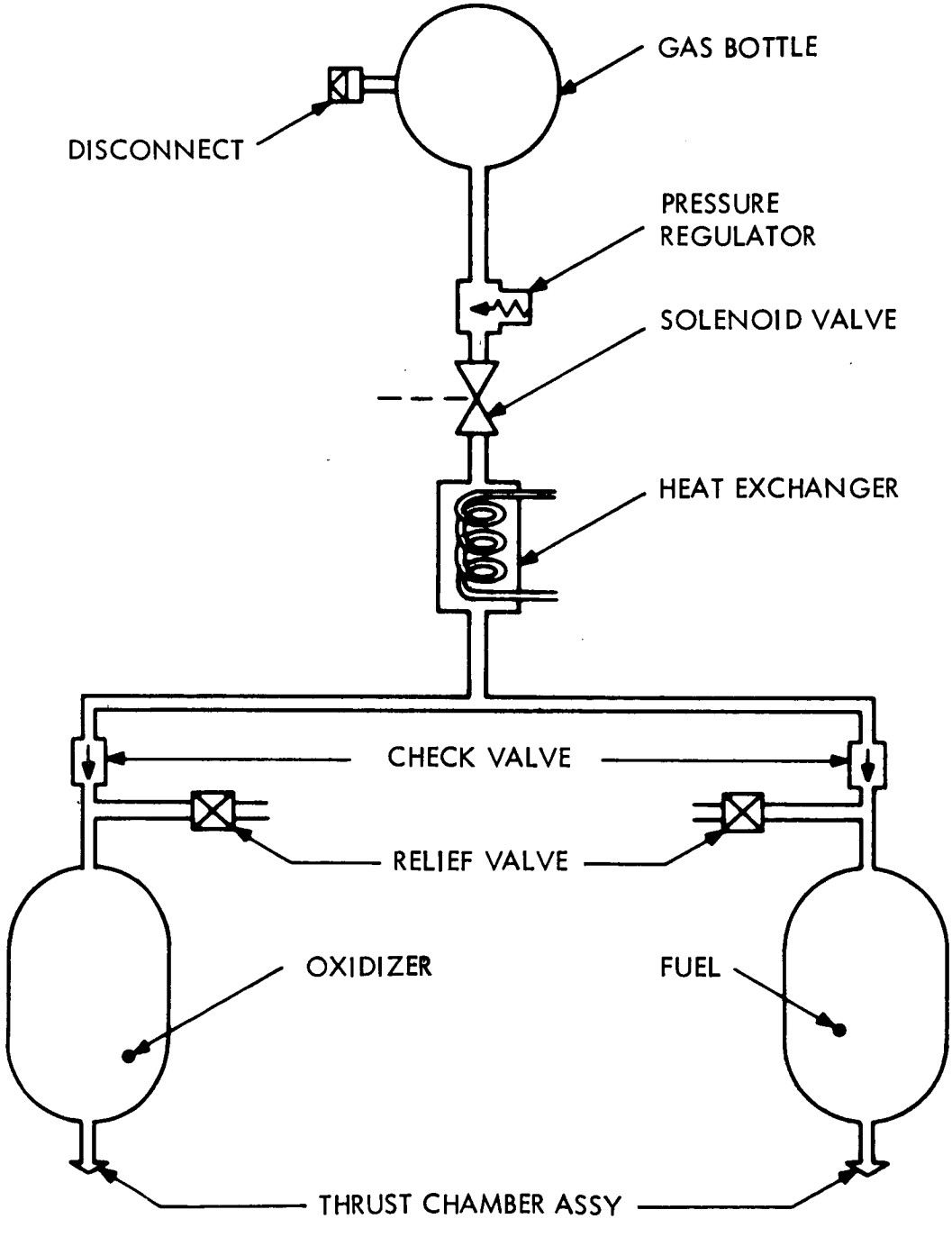

Figure 3-1. Stored Gas (Heated)

Table 3-5. Comparison of Stored and Heated Gas Systems

	Stored Gas	Heated Stored Gas
Pressurant Gas (lb)	64.5	55.1
Pressurant Tank (lb)	613.0	567.0
Heat Exchanger	--	10.0
TOTAL	677.5	632.1

The net weight savings for heated gas system is 45.4 pounds. When coupled with a small reliability degradation by introduction of the heat exchanger, a need for further study of the heated stored gas pressurization system for potential use on the Voyager spacecraft is suggested.

The three major methods studied (pressurized ullage, make-up gas and constant pressure regulated) are depicted schematically in Figure 3-2. Table 3-6 contains the operating description, advantages and disadvantages of each system.

The evaluation led to the immediate conclusion that no particular advantages occurred to the make-up gas system which would justify its further detailed analysis. Such analyses were performed, however, for the other two systems and are discussed below.

In a pressurized ullage system, formulas used to calculate the weight of the pressurant weight and tank weight follow:

3.1.1.1. Tank Weight

$$W_{pt} = \frac{3\rho}{\sigma} P_i \left[\frac{V_t}{1 - \left(T_i/T_f \right) \left(P_f/P_i \right)} \right]$$

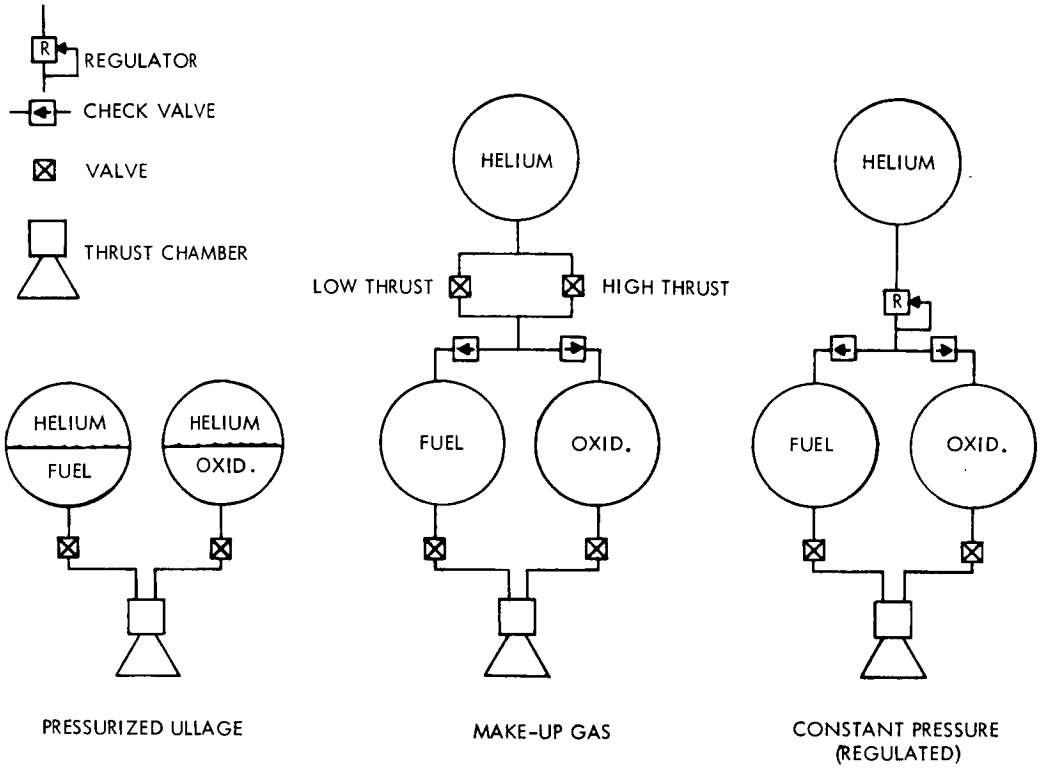

Figure 3-2. Pressurization System Schematics

3.1.1.2. Pressurant Weight

$$W_{pr} = \frac{N\ P_f}{R\ T_f} \left[\frac{Vt}{1 - \left(T_i/T_f \right) \left(P_f/P_i \right)} \right]$$

Where:

W_{pt} = Propellant tank weight, lb.

W_{pr} = Pressurant weight, lb.

ρ = Tank material density, lb./in.^{3}

σ = Tank material working stress, psi

Table 3-6. Comparison of Pressurization System Concepts

Table 3-6. Comparison of Pressurization System Concepts

System	Operating Description	Total System Weight (lb)	Advantages	Disadvantages
Pressurized Ullage	The propellant tank is sized to hold the entire supply of pressurizing gas in addition to the propellant. Initial pressure is twice the minimum allowable engine inlet pressure plus line and valve losses.	1266	Simplicity of design, assembly, testing and operation. Eliminates pressurant tanks, lines and valves associated with high pressure gas storage. Minimum leakage system compared to other studied.	Heaviest system due to necessity of pressurizing large diameter tanks. Envelope limitations restrict either the amount of propellant or the operating pressure range, unless cylindrical tanks (with a concomitant weight penalty) are resorted to. Tanks remain under high pressure for duration of flight increasing failure probability.
Make-up Gas	Helium is stored in a separate tank, flowing to the propellant tank when a solenoid valve is opened. Because of the highly different flow rates for orbit insertion and mid-course/orbit trim maneuvers, separate lines and valves are provided to reduce pressure excursions in the propellant tanks.	1080	Pressue variations in the propellant tanks are lower for the pressurized ullage, permitting more constant engine operation.	Tanks must be sized for slightly higher pressure than for a constant pressure system. Pressure excursions must remain within engine operating limits, making optimization from the weight standpoint difficult.
Constant Pressure Regulated	Helium is stored in a separate tank and metered to the propellant tank through a regulator at constant pressure. A back-up regulator is enabled if failure of the primary regulator is sensed via a pressure switch.	1050	Most extensive flight experience and usage data for reliability estimates. Constant feed pressure means constant engine operating conditions. Propellant tank can be optimized for constant pressure, leading to weight savings.	Complexity of sensing and command network for redundant regulators.

V_t = Tank volume, $in.^3$

N = Excess factor

R = Gas constant, ft./°R

T = Gas Temperature (°R)

P = Pressure, psia

Subscripts:
i = initial
f = final

The limiting processes by weight effect were isothermal and adiabatic, as has been discussed. Solubility weight effects remained unchanged from data already given. Because there is no transfer of pressurant after initial vehicle loading, the excess factor, N, was taken to be 1.05.

The pressurized ullage system was evaluated in two configurations: spherical tanks and spherical with a cylindrical center section to meet the envelope limitations.

The tank is sized to permit sufficient final pressure for propellant expulsion while minimizing initial pressure for weight savings, resulting in $P_f/P_i = 0.5$. This large initial ullage is reflected in increased propellant tankage weight, as shown in the following list, as compared to a stored gas system. Because of the large propellant tank volume required, envelope restraints limited the amount of usable propellant to 7200 pounds. As this fell short of the required amount, further study of this system was not conducted.

Parameter	Stored Gas	Pressurized Ullage
Pressurant Gas, lb.	53.9	-
Pressurant Tank, lb.	500.5	-
Propellant Tank, lb.	370.8	1199.8
Propellant Tank Ullage Gas, lb.	2.1	52.5
	927.3	1252.3

For the stored gas system the equation for the weight of the pressurant given earlier applies. Pressurant tank weight is given by:

$$W_{prt} = \frac{3\rho\ W_{pr}\ RT_i}{\sigma}$$

Comparison of the above equation with that for pressurant weight shows that W_{prt} is independent of the gas, as the only gas property is R.

Figure 3-3 shows the temperature increase in both pressurant and propellant tanks during orbit insertion firing, due to rapid expansion of the gas.

Figure 3-4 shows the decrease in propellant tank ullage pressure from the initial pressure of 260 psia. Heat input during the two-day coast period following orbit insertion results in this initial pressure. When the pressure reaches 235 psia, the regulator opens and pressure is constant thereafter. As figure 3-5 shows, pressure in the helium sphere is constant before regulator opening, and then decreases as gas is supplied to the propellant tanks.

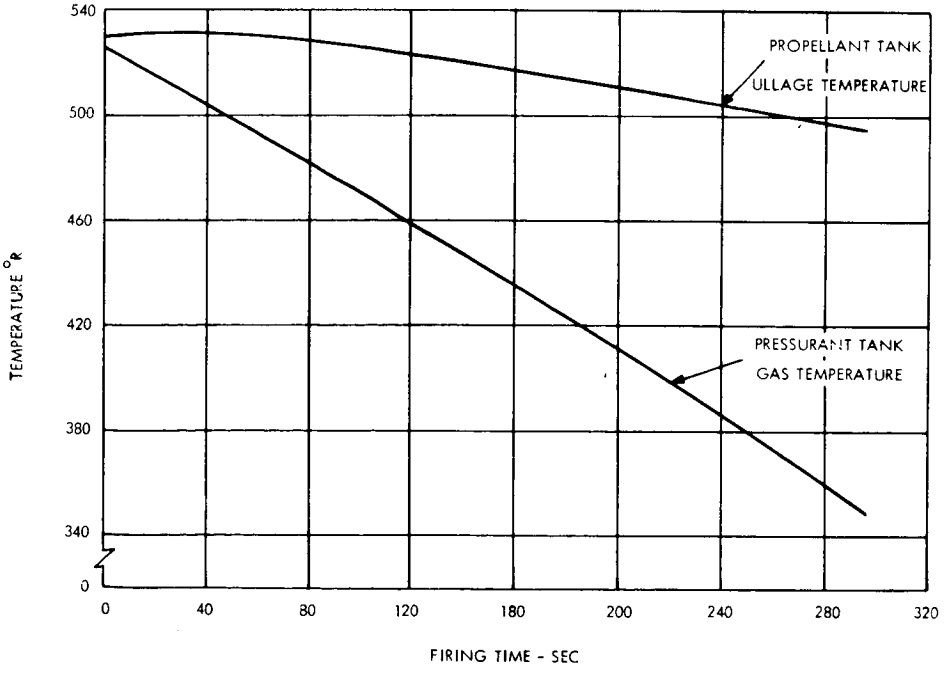

Figure 3-3. Temperature vs Time During Orbit Insertion

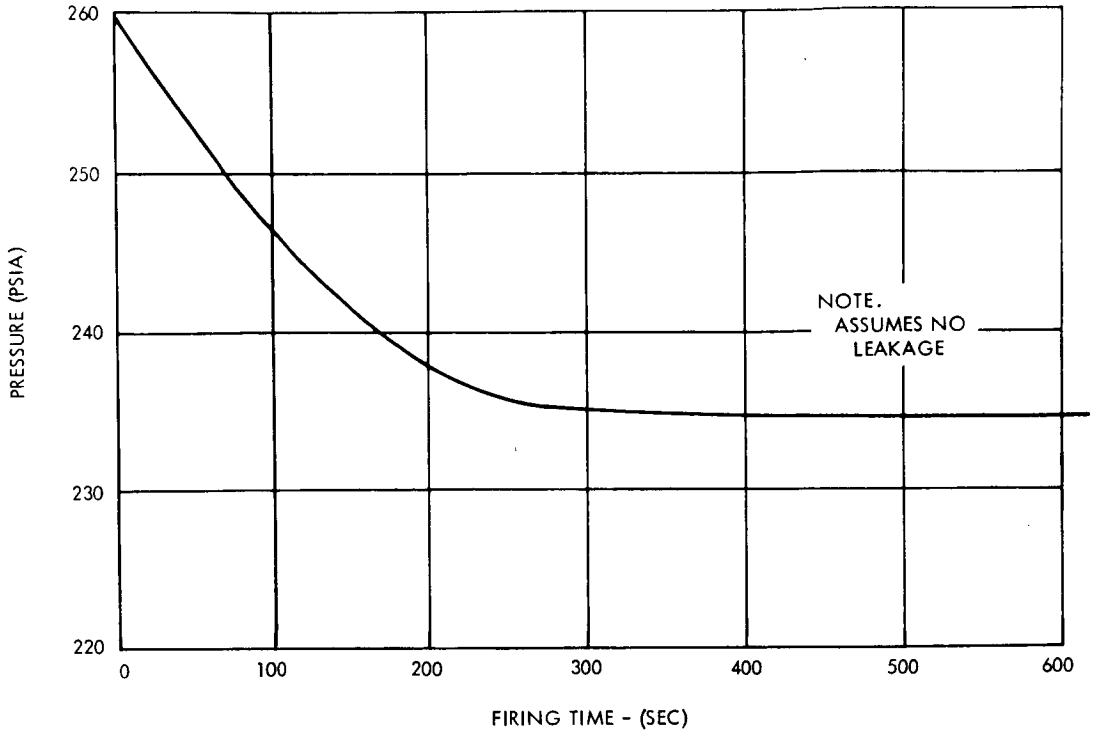

Figure 3-4. Propellant Tank Ullage Pressure During Orbit Trim Firing

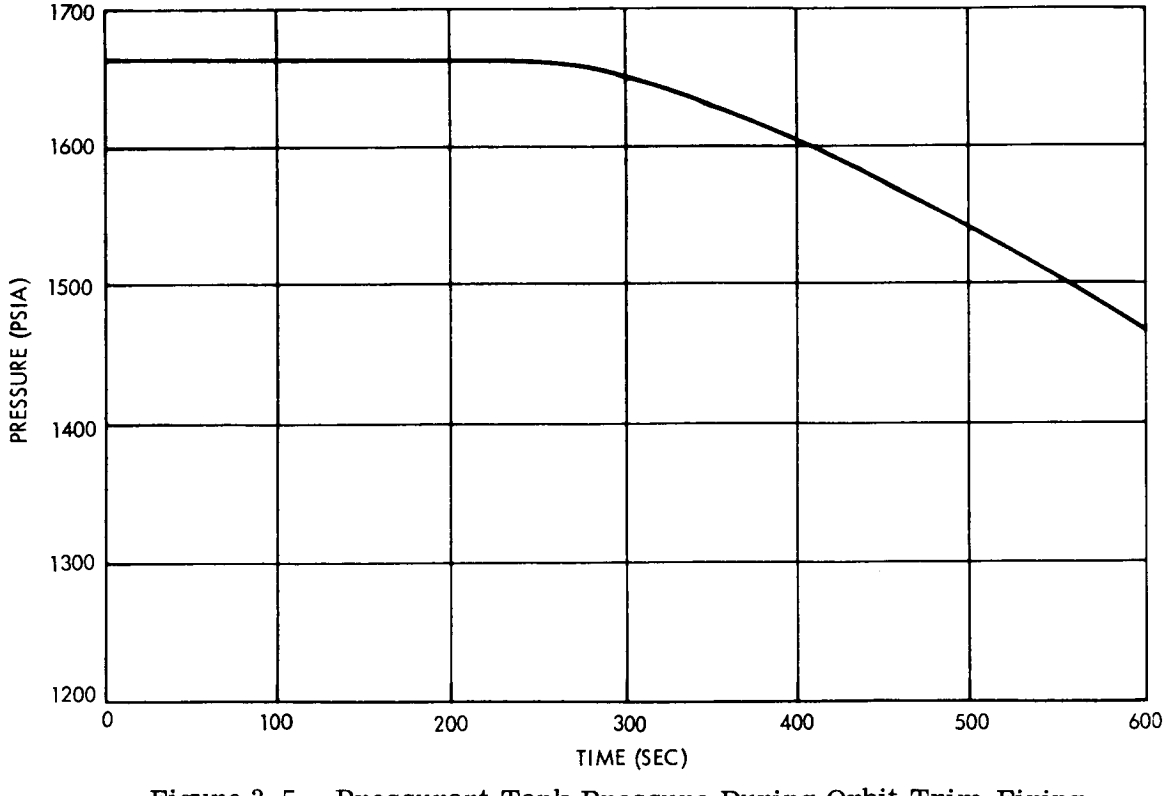

Figure 3-5. Pressurant Tank Pressure During Orbit Trim Firing

3.2. PROPELLANT ACQUISITION AND SLOSH CONTROL

A study was made of several methods of providing propellant acquisition and slosh control during engine firing and cruise portions of the flight. This study encompassed analytical and conceptual design activities.

3.2.1. Candidate Systems

The following devices and certain combinations thereof were evaluated (Figures 3-6 through 3-15):

a. Metal Bellows

   1. Internal and external

   2. Rechargeable and non-rechargeable

b. Reversing Hemispherical Diaphragms

   1. Metal

   2. Elastomeric

c. Full Spherical Elastomeric Bladder

d. Convoluted Metal Diaphragm

e. Surface Tension Screens

f. Baffles

g. Settling Rockets

Table 3-7 (Sheets 1 and 2) and referenced Figures 3-6 through 3-16 give the operating description, weights, advantages, and disadvantages of these devices and the evaluation of these characteristics indicated that three of the concepts possessed features that were complementary when used in combination. Thus, the selected design uses an internal non-rechargeable bellows to provide initial propellant settling, surface tension screens for propellant-gas

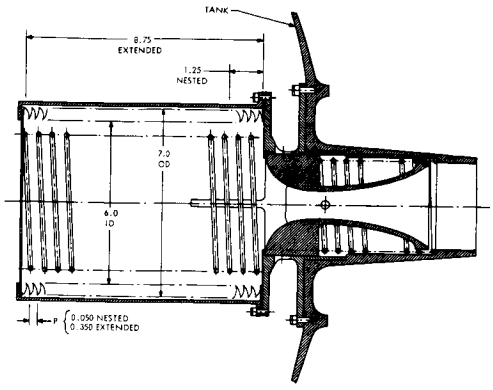

Figure 3-6. Internal Rechargeable Bellows Start Tank

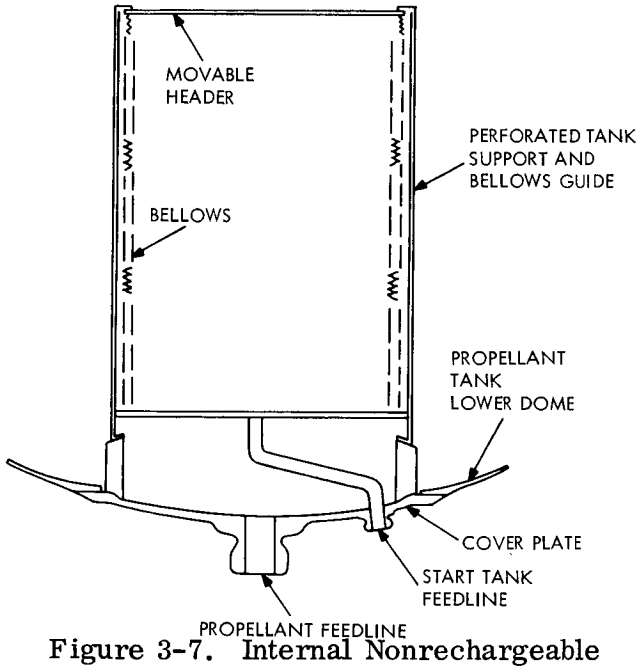

Figure 3-7. Internal Nonrechargeable Bellows

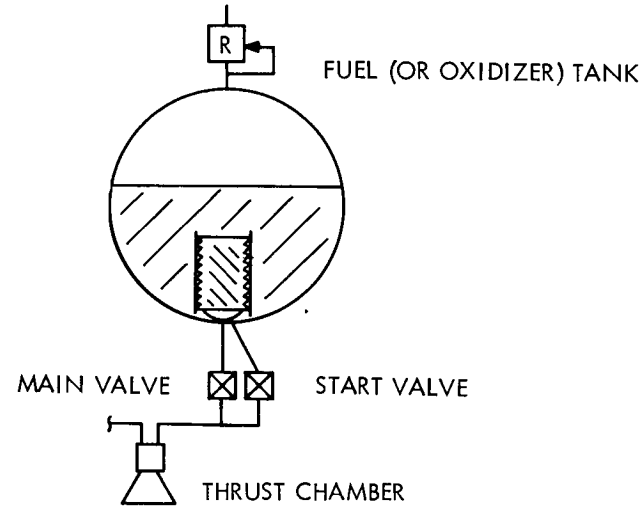

Figure 3-8. Internal Nonrechargeable Bellows Schematic

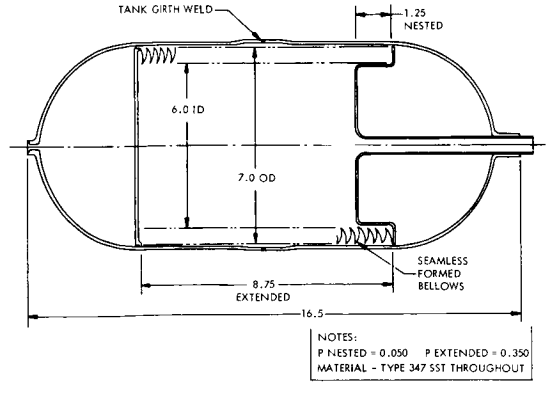

Figure 3-9. External Rechargeable Start Tank

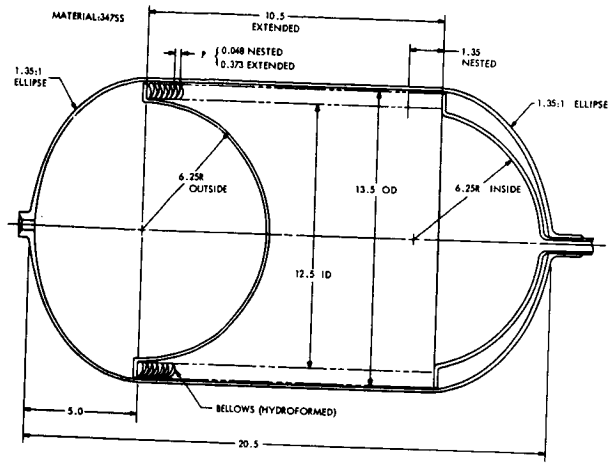

Figure 3-10. External Non-Rechargeable Start Tank

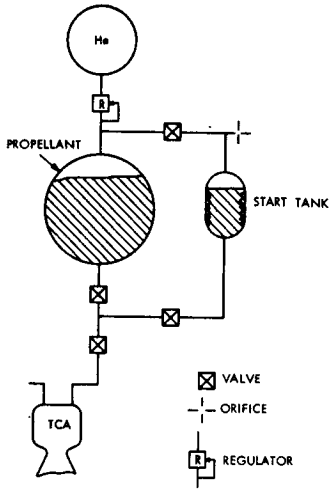

Figure 3-11. External Rechargeable Bellows Schematic

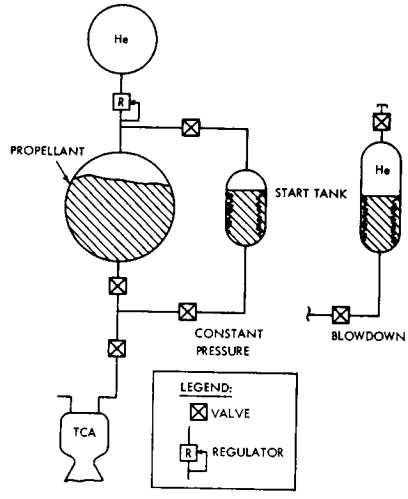

Figure 3-12. External Nonrechargeable Bellows Schematic

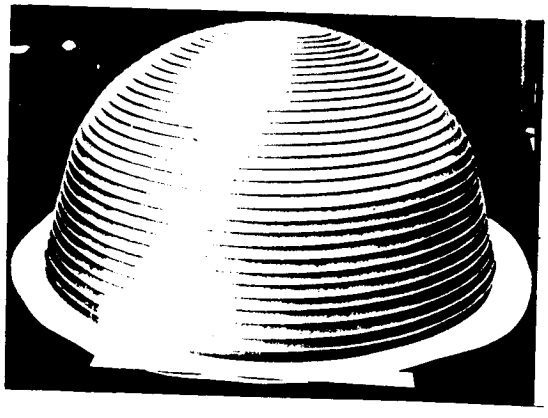

Figure 3-13. Metal Hemispherical Reversing Diaphragm

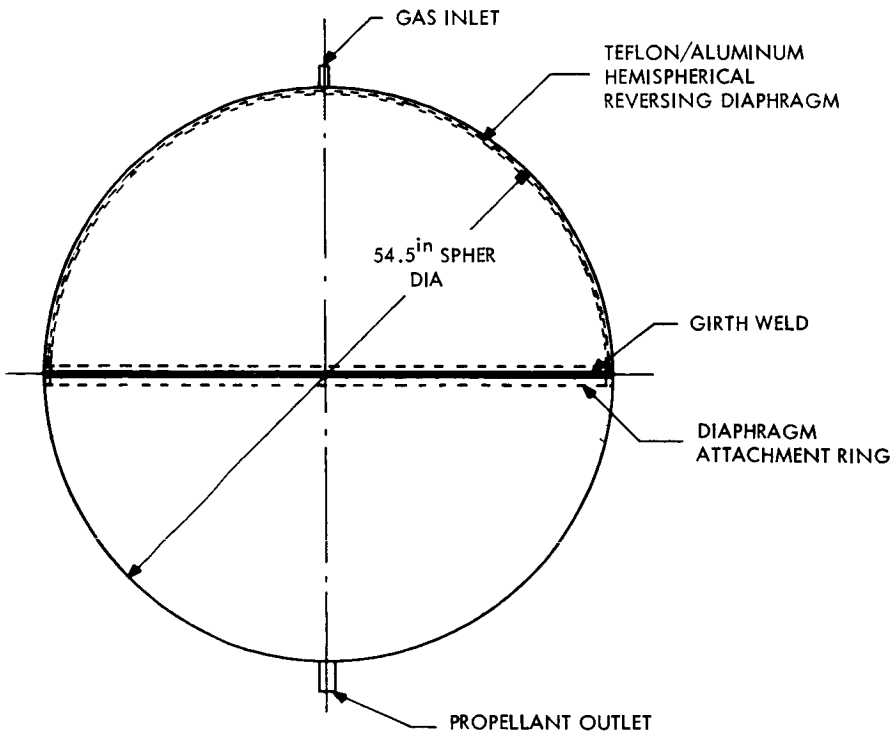

Figure 3-14. Elastomeric Reversing Hemispherical Diaphragm

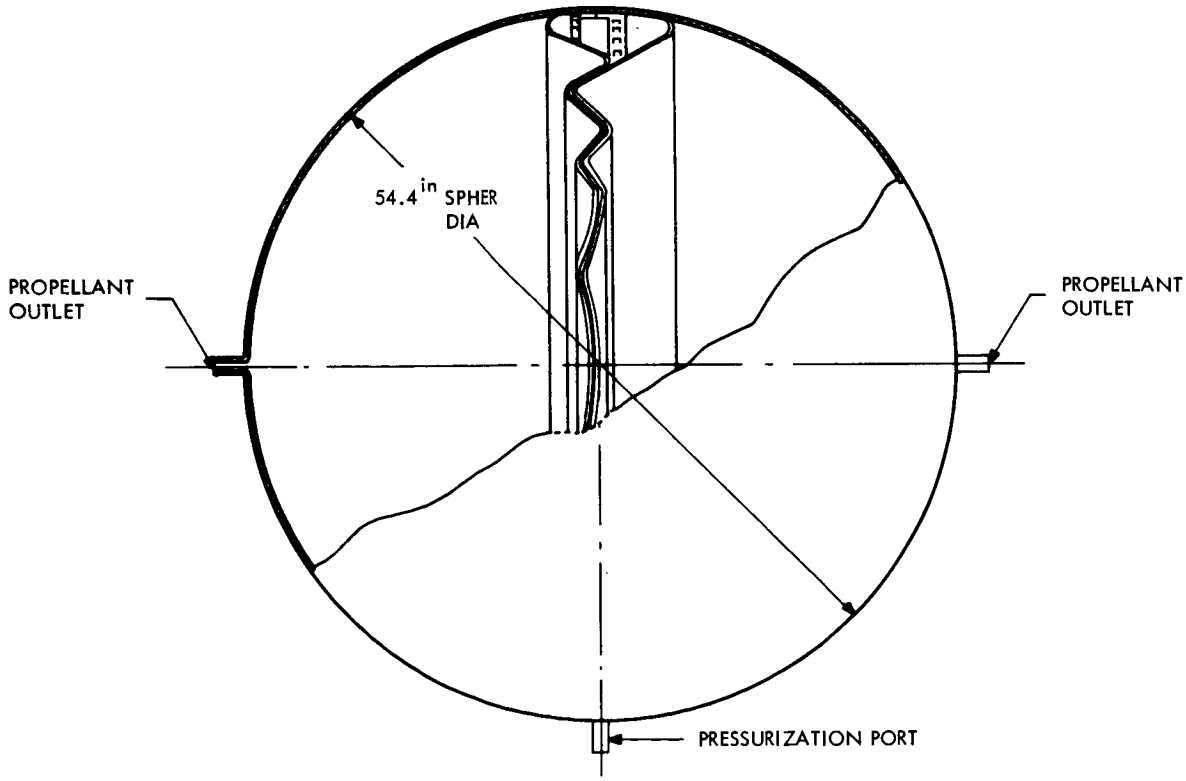

Figure 3-15. Convoluted Metal Diaphragm

separation in the main tank and also to limit fluid motion forces under zero gravity, and ring baffles to damp fluid motion during powered flight. Some redundancy is provided by having the screens and bellows, as both performed the function of assuring gas-free propellant, to the engines at the start of the burn. The design philosophy is to include the bellows until such time as experimental data from screen tests demonstrate that they can perform the propellant acquisition function by themselves.

Figure 3-16 shows the internal configuration of the tank with the devices installed.

A detailed analysis of the selected configuration is presented in Appendix A.

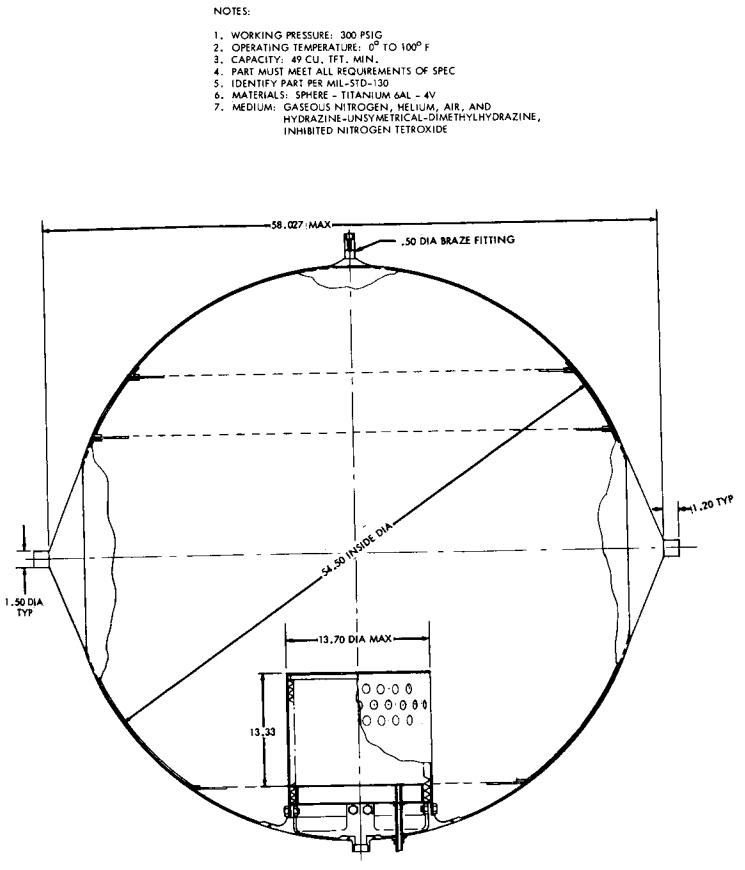

Figure 3-16. Propellant Tank Assembly

Table 3-7. Comparison of Propellant Acquisition Devices (Sheet 1 of 2)

Concept	Figure	Operating Description	Total System Weight	Advantages	Disadvantages
Internal Rechargeable Bellows	3-6	The bellows stores sufficient propellant to settle the main propellant through engine thrust for a single maneuver. Pressure in the main tank collapses the bellows, expelling the propellant through a nozzle, when the downstream propellant valve is opened. Flow through the nozzle establishes a pressure differential, moving the nozzle down and exposing the outlet ports to the main tank propellant. Upon closing the propellant valve, spring force extends the bellows, refilling it through the ports from the main tank before the nozzle returns to the closed position, also by spring force.	50 lb	The device refills itself automatically after each firing, limited only by the recycling capability of the bellows. The flow control nozzle isolates the down-stream propellant valves from main tank pressure when closed. The bellows and its support need not be designed to withstand internal pressure, nor is a separate pressure vessel required.	The design involves inherent complexities due to the sliding nozzle. A delicate balance of fluid forces and spring rates is required to ensure that the bellows refills before the ports close. There is a possibility of gas entrapment at the main tank ports, dependent on hardware configuration in this area. Failure in the nozzle in the closed position precludes flow out of the tank, while failing open would expose the downstream valves to propellant thereafter as well as defeating the gas/liquid isolation feature of the bellows. There is no current development activity on this device.
Internal non-rechargeable Bellows	3-7, 3-8	The bellows stores sufficient propellant to settle the main propellant through engine thrust for all maneuvers. Pressure in the main tank collapses the bellows, expelling propellant through a separate line when the valves in the start line network are enabled. (See Figure 3-8 schematic). After a predetermined interval, the valves of the start network are closed and the main propellant valves to the engine opened.	100 lb	The device provides positive separative separation of the gas and propellant, assuring gas-free operation for the engine during the settling transient. The bellows to be used is of a size currently under development, so that existing technology may be utilized. The system does not require a separate pressure vessel or external pressure supply to the start tank.	Must be resized for any significant change in mission requirements. Propellant valve sequencing interface is required with the vehicle command system.
External Rechargeable	3-9, 3-10	The bellows contain sufficient propellant to settle the main propellant through engine thrust for one maneuver. The pressurization valves (see schematic, Figure 3-11) and start line propellant valves are opened to fire the engine in the low thrust mode. After a given interval, the pressurization valves are closed and the main propellant valve opened. This permits refilling of the start tank as well as operation of the engine in the desired mode. The helium pressure is bled off through an orifice to control the rate of refill of the start tank.	40 lb	Positive separation of gas and propellant is assured by the metal bellows. The device may be recycled any desired number of times, thus providing flexibility for various missions. The unit may be developed, tested and qualified separately from the main propellant tank. One tank is required for each propellant.	A mounting structure must be provided for the tanks and associated components. The sequencing of the pressurization and propellant valves is the most complex of all systems studied. Helium is lost during expulsion and refilling.
External Non-rechargeable	3-11, 3-12	The operating sequence is the same as for the internal non-rechargeable, with the addition of enabling the pressurization valve (see schematic, Fig. 3-12) for each maneuver. If the start tank is operated in the blowdown mode, no external pressurization line is used.	120 lb	Advantages are the same as listed above for the external rechargeable tank, except for the flexibility and increased weight for the greater propellant load.	The blowdown version is the heaviest configuration of all the bellows devices studied. Mounting structure and sequencing for valves must be provided.
Metal Reversing Hemispherical Diaphragm	3-13	Gas pressure on the upstream side of the diaphragm forces it from one hemisphere to the other, expelling propellant from the tank outlet. Circumferential rings control the reversing of the diaphragm and prevent the formation of highly stressed folds. Stainless steel is commonly used for the diaphragm.	105 lb	The diaphragm positively separates the entire propellant supply from the pressurant gas. The gas cannot permeate the diaphragm but pinhole leaks may develop during cycling. The diaphragm has limited cycling capability for ground testing, if desired. Slosh damping is provided by the relatively rigid diaphragm.	There is no development experience with tanks this large using this type of diaphragm. The diaphragm is susceptible to localized fatigueing due to temperature cycling and asymmetric propellant motion effects, leading to angular distortion of the bellows and localized overstressing

Table 3-7. Comparison of Propellant Acquisition Devices (Sheet 2 of 2)

Concept	Figure	Operating Description	Total System Weight	Advantages	Disadvantages
Elastomeric Reversing Hemispherical Diaphragm	3-14	The operating principle is the same as for the metal diaphragm, with the exception that no circumferential rings are required. Teflon or Teflon/aluminum laminates are used to limit permeation of propellant and gas through the diaphragm.	15 lb	The diaphragm provides positive separation of the gas and propellant, and may be cycled more times than the metal diaphragm. This type of diaphragm has been used extensively in smaller size tanks.	Permeation of propellant and gas through the diaphragm trap propellant in an unusable location and presents the possibility of a gas bubble being ingested upon starting the engine. Only a limited amount of slosh damping is provided by the flexible diaphragm, and the use of internal baffles is precluded. The capability to manufacture a diaphragm this large and join it to a tank has yet to be demonstrated. Incorporation of an aluminum permeation barrier reduces flexure capability and cycle life.
Full Spherical Bladder (Elastomeric)		This type of device expels the propellant by collapsing around a central standpipe which contains propellant outlet ports.	30 lb	Same as for the hemispheric diaphragm.	Same as above with the additional problem of highly localized stresses if the bladder does not properly fold.
Convoluted Metal Diaphragms	3-15	The diaphragms nest at the equator of the tank when the tank is full expanding outwards when pressure is applied between them. The surface area of the diaphragms is equal to the internal surface area of the tank, permitting high expulsion efficiencies. Propellant is expelled from two outlets - one at each pole.	105 lb	Positive separation of gas and propellant is assured, and slosh control is provided by the relatively rigid diaphragms. Feasibility has been demonstrated in a 54 in. tank size.	No recycling capability is provided, and some center of gravity uncertainty is present due to differential expansion of the diaphragms. Experience is limited to a demonstration program and no further development is underway.
Surface Tension Screens		A liquid film is established across the pores of the screen, separating the gas and propellant. The pore size is established by the diameter of the tank, Bond number of the propellant and the magnitude of the adverse accelerations under which the screens must provide gas/liquid separation. The screens are located in accordance with liquid levels resulting from propellant usage for the various propulsive maneuvers.	5 lb	The system is completely passive and requires no external plumbing, actuating commands or structural mouting provisions. Screens are the lightest methods of providing propellant separation, and are compatible with the installation of baffles for slosh control. The effectiveness of screens has been proven analytically and demonstrated experimentally in drop tower tests. No major perturbations to the tank are presented in design manufacture and assembly.	While screens have been flown in space-restartable propulsion systems, they have never been relied upon for propellant acquisition without the use of auxilliary settling rockets, so that their effectiveness under actual zero gravity conditions has not been unequivocally demonstrated. Flexibility for changing mission requirements is limited by the need to relocate the screens for maximum effectiveness if the fluid level changes.
Baffles		The ring baffles are located at the periphery of the tank at specified distances from the fluid surface. Damping of the fluid motion is accomplished by the baffles.	20 lb	A completely passive method of slosh damping is provided. The damping effectiveness of baffles has been well characterized analytically and demonstrated in flight (booster vehicles). Manufacturing and installation in the main tank are readily accomplished.	An auxiliary method of propellant acquisition must be provided.
Settling Rockets		Small thrusters are fired for a duration dictated by the fluid level and acceleration imparted by the thrusters. This acceleration settles this propellant to the tank outlet.	100 lb	This is the method used on Transtage for restarting the engines, and will be used on Apollo as well.	No slosh control provision. This is the heaviest and most complex method studied. Growth potential and flexibility limited by propellant requirements.

3.3. THRUST CHAMBER ASSEMBLY

For the Task D System Update Studies, MSFC specified the use of the TCA used on the descent stage of the lunar excursion module (LEMDE). This TCA, shown in Figure 3-17, has an ablative cooled combustion chamber and nozzle to an expansion ratio of 16:1. From that point until the exit expansion ratio of 47.5:1, it is radiatively cooled with a columbium skirt. A titanium shell provides the structural member for the chamber. It is overwrapped with a layer of insulation which limits back wall temperatures at the end of soakout for the nominal duty cycle to approximately 750°F. For the LEM mission the propellants are Aerozine -50 (50 percent by weight mixture of hydrazine and UDMH) and nitrogen tetroxide, combined in a weight reactant ratio of 1.6:1 (oxidizer/fuel) and a volume ratio of 1:1.

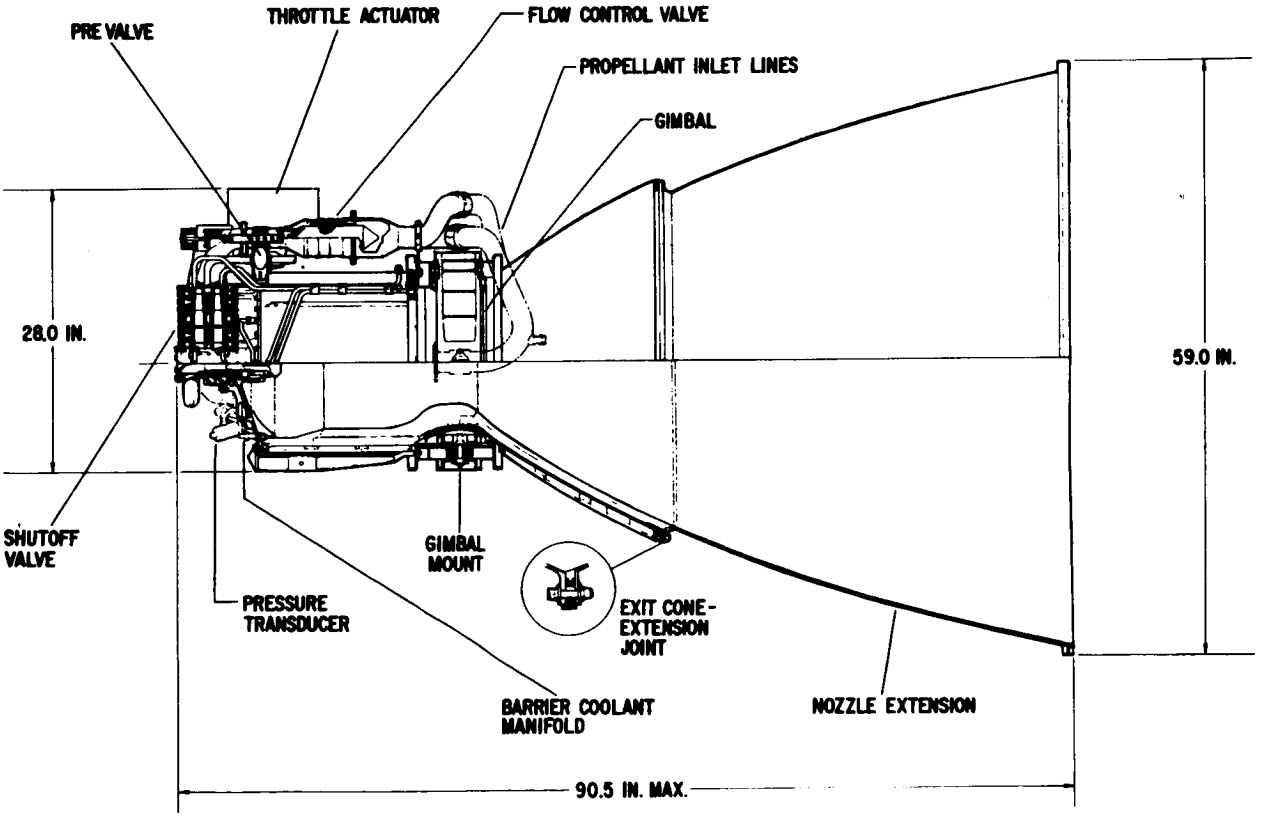

Figure 3-17. LEMDE Thrust Chamber Assembly

Figure 3-18 shows schematically the control elements used in providing the unique throttling capability available with this thrust chamber. An electric motor positions the throttler actuator in the variable area cavitating venturi assembly and the variable area injector so that thrusts in the range from 1,050 to 10,500 pounds are available. The corresponding range of chamber pressures is approximately 10 to 100 psi. A gimbal ring mounted at the throat allows ±6 degrees of motion of the thrust chamber assembly for thrust vector control. In the following paragraph tradeoffs directly affecting the TCA will be presented.

3.3.1. Thrust Level Selection

The throttling capability of the LEMDE thrust chamber from 1,050 to 10,500 pounds of thrust allows a wide selection in operating thrust levels. The minimum impulse requirements for the midcourse correction and orbit trim maneuvers dictate the use of lower thrust levels.

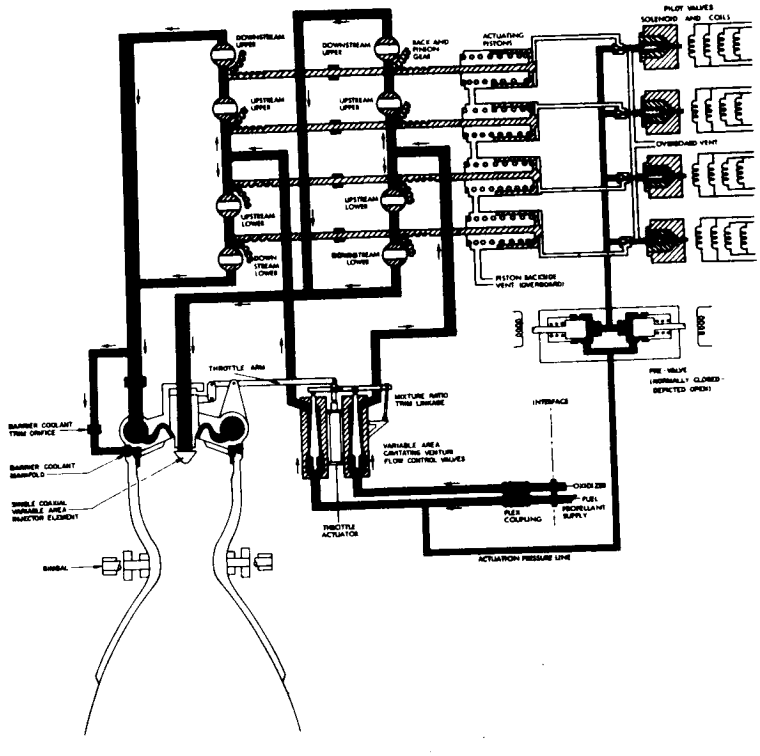

Figure 3-18. LEMDE Propellant Flow Control Schematic

Conversely, the high total impulse of the orbit insertion maneuver and desire for short burn time indicates a requirement for a high thrust level. The performance characteristic of the chamber, I_{sp} and minimum impulse bit variation (a major contributor to the guidance accuracies) are also functions of the operating thrust level and both increase as thrust level increases. Thus, the choice is influenced by the increase in performance versus the reduction in guidance accuracy due to an increase of the tailoff uncertainty.

Figure 3-19 shows the change in specific impulse as a function of the operating thrust level. It indicates that by changing from the 1,050 minimum available thrust level to 1,700 pounds of thrust, an increase of 8 seconds of specific impulse can be achieved. Figure 3-20 shows the effect of total propellant weight change as a function of a change in the available midcourse and orbit trim specific impulse. For the conditions stated, approximately 125 pounds of propellant can be saved by this increase in minimum thrust level.

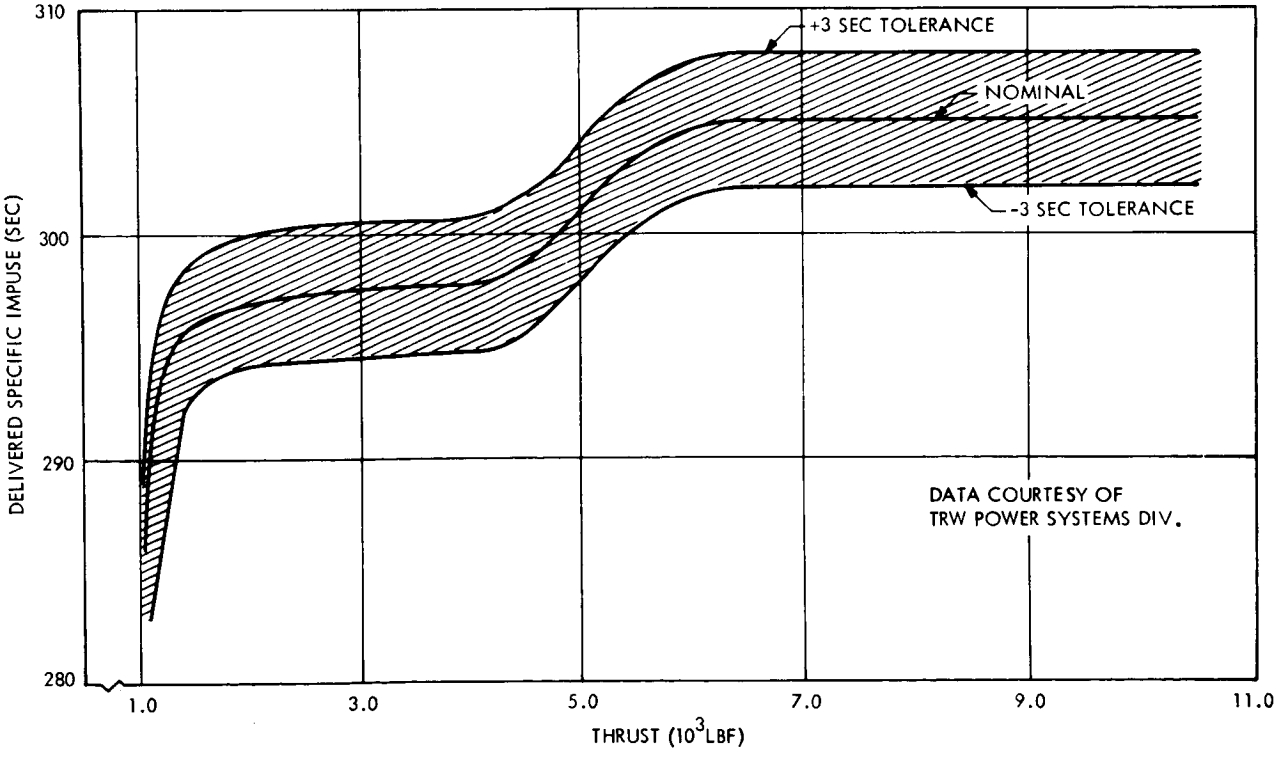

Figure 3-19. Effect of Thrust Level on I_{sp} for the LEMDE Thrust Chamber Assembly

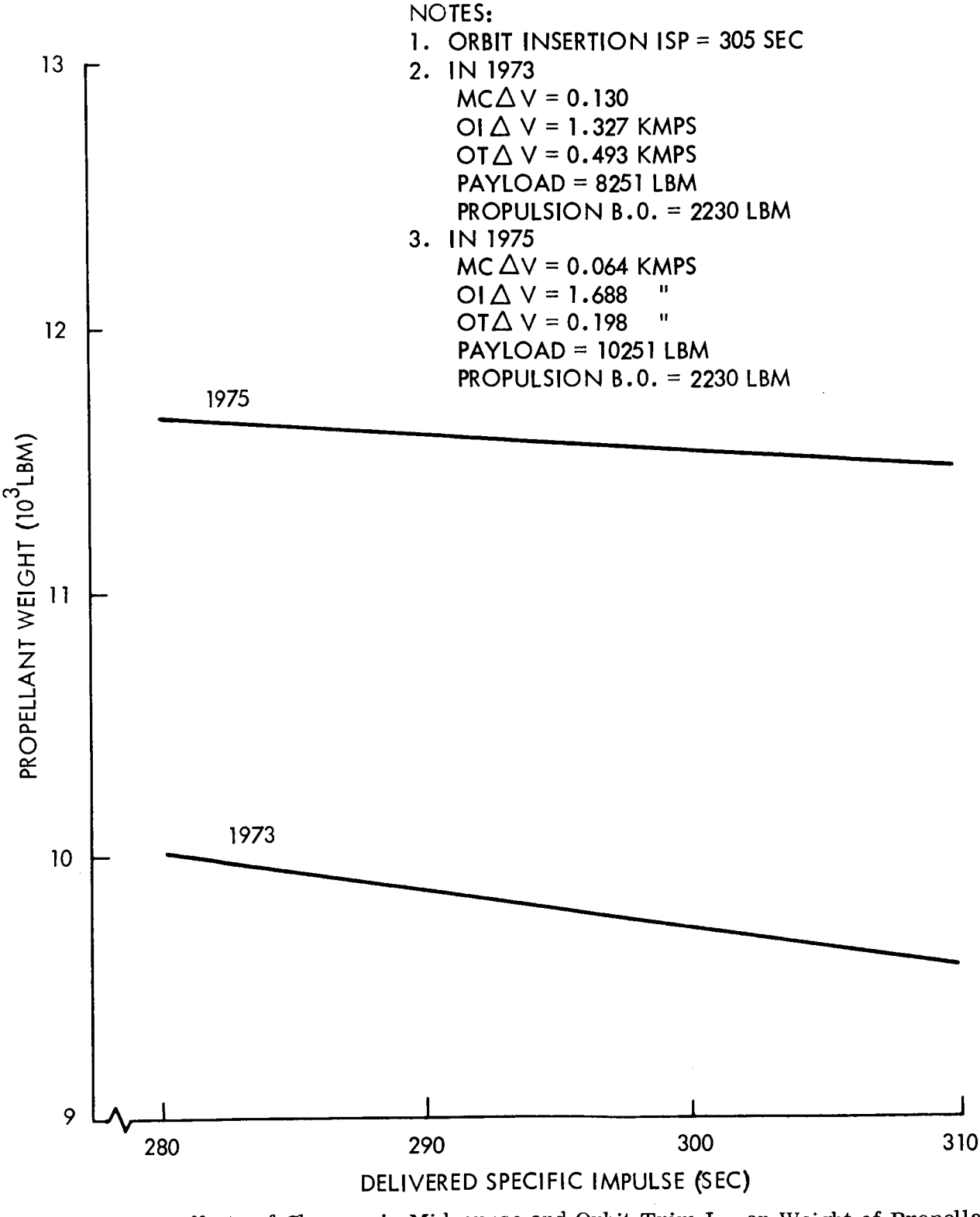

Figure 3-20. Effects of Changes in Midcourse and Orbit Trim I_{sp} on Weight of Propellant

Mitigating the immediate selection of the higher thrust are the curves shown in Figure 3-21 and Figure 3-22. The more important of the two is the plot of impulse variability versus thrust level since if the accuracy of a given maneuver is known, operating procedures can easily be generated to accommodate comparatively large magnitudes of tailoff impulse or minimum impulse bits.

These data, recently received, differ from previously published tailoff and variance data such that complete analysis has not been made at this time. Therefore, a firm recommendation, based on a quantitative system study cannot be submitted. Thus, as a conservative approach, the minimum thrust level of 1,050 pounds is used in the baseline design.

3.3.2. Propellant Selection

As noted earlier, the propellants used by LEMDE are A-50 fuel and nitrogen tetroxide (NTO) for the oxidizer. A review of available state-of-the-art propellants reveals that NTO is the most suitable oxidizer. However, monomethyl hydrazine (MMH) could be used as a substitute fuel. Thus, in the fuel selection the choice is between the A-50 and MMH.

Table 3-8, Fuel Properties, lists a few of the salient physical and performance properties of the two candidate fuels in combination with NTO. The significant points from this table are: (1) MMH has a lower freezing point. (2) While there is an approximate 3 percent difference in specific gravity, the change in reactant ratio to have equal volume flow rates (and therefore equal size tanks) results in only slightly more than 1 percent increase in required propellant volume. (3) There is only a 2 second increase in theoretical performance in favor of the A-50/NTO combination, and data from Reaction Motors Division, Thiokol Chemical Corporation, the Marquardt Corporation and TRW, Power Systems Division, indicate that actual delivered specific impulse of the A-50/NTO combination is only 0 to 3 seconds greater than the MMH/NTO combination. Thus, in conclusion, neither propellant offers a distinct advantage. The lower freezing point of MMH cannot be fully exploited because the nitrogen tetroxide freezes at 11.8 degrees Fahrenheit. The 1 percent increase in propellant volume is directly proportional to propellant tank weight, which for Voyager is only five pounds. Neither is distinctly better in delivered performance.

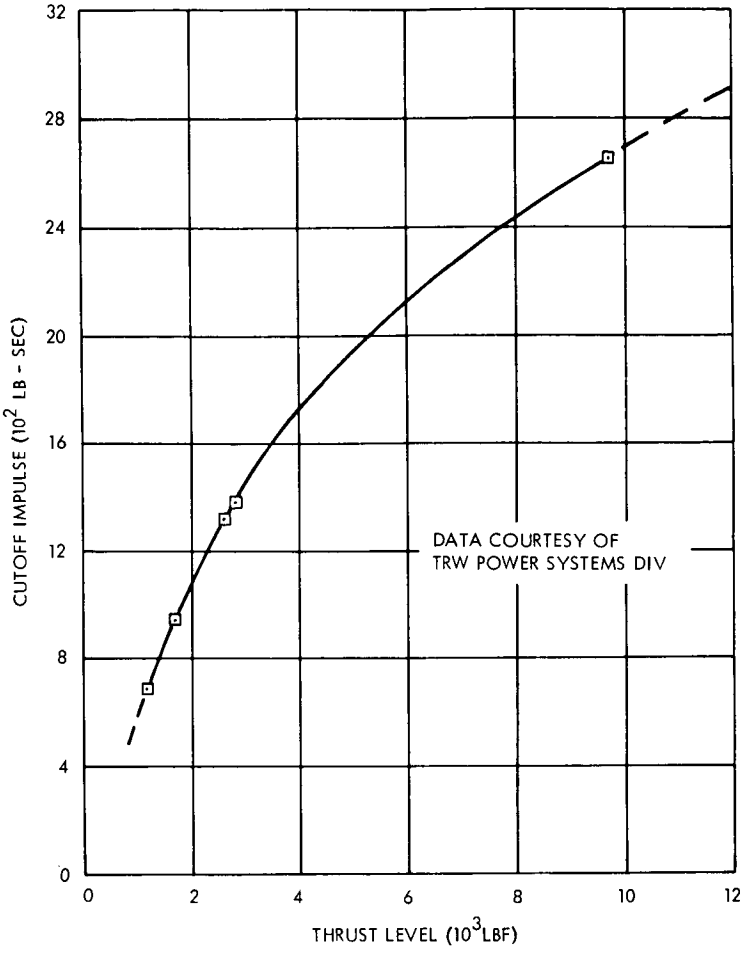

Figure 3-21. LEMDE Cutoff Impulse as a Function of Operating Thrust Level

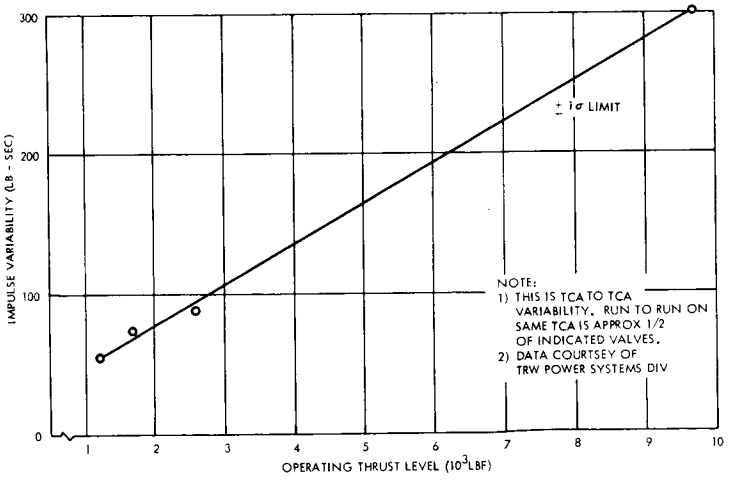

Figure 3-22. Impulse Variability as a Function of Thrust Level

Table 3-8. Fuel Properties

	A-50	MMH
Molecular Weight	41.8	46.1
Freezing Temperature (°F)	18	-63
Normal Boiling Point (°F)	170	189
Specific Gravity @ 70°F	0.90	0.87
Theoretical Vacuum Specific Impulse* (Bray analysis, NTO Oxidizer) (sec)	330@ MR=1.6	328@ MR=1.65
Delivered Specific Impulse (sec)	305	302-305
* Bell Aerosystems Data		

From Table 3-9 it may be observed that a great deal more test data is available for A-50. This data was furnished by TRW.

Table 3-9. Test Comparison N_2O_4/MMH versus N_2O_4/A-50

LMDE Engine Injector (Qual B Configuration)

Propellant	C* (Ft/Sec)	Number of Tests	Total Duration
N_2O_4/A-50	5460 - 5500	~ 200	~ 60,000
N_2O_4/MMH	5460 - 5470	3	35

The final area in which the MMH and A-50 were compared is that of contributions to severe pressure spikes at propellant ignition. This phenomenon has been investigated and reported[1] by the Marquardt Corporation, supported by North American Aviation and Grumman Aircraft

(1) Juran, Warren & Stechman, R. Carl, Ignition Transients in Small Hypergolic Rockets, AIAA Paper No. 67-515 dated July 1967.

Corporation, under contract to the NASA Manned Spacecraft Center. In brief, it was the findings of the program that under certain conditions of ambient pressure, hardware temperature, and operating duty cycle, severe pressure spikes could be encountered upon ignition. The energy source for the overpressure condition was derived from fuel, and water and nitrates derived from the fuel. These deposits resulted from operation of the engine in a temperature-duty cycle regime that prevented evaporation of residual fuel between operating pulses. Among other conclusions and recommendations from the test phase of this study it was noted that monomethylhydrazine produces lower ignition pressures than A-50 at the same hardware temperatures. This conclusion was also predicted by analysis discussed earlier in the reference since MMH is more volatile than the hydrazine that remains after evaporation of the UDMH in the A-50 mixture.

It is acknowledged that under certain conditions of temperature, pressure and duty cycle MMH offers an advantage over A-50 in suppressing ignition pressure spikes. However, the hardware, duty cycle and general requirements of the Voyager mission profile are substantially different from the above test conditions, so no firm conclusions can be drawn.

In conclusion, the basic factors for selection of MMH or A-50 are the availability of a wealth of test data and experience with A-50 in the LEMDE TCA versus some possibility of suppression of an ignition spike with MMH. Because of this preponderance of test data and the better known performance using A-50, it is selected for the baseline design. This comparison can be more meaningfully reevaluated at the conclusion of the current LEMDE demonstration program being conducted for MSFC.

3.3.3. Head End Designs

The basic tradeoff for the head end or fuel control elements is whether to use the existing control components, as shown in Figure 3-18 LEMDE Propellant Flow Control Schematic, or a dual valve system as shown in Figure 3-23. The basic difference between the two systems is that in the modified version the variable area cavitating venturi control valves and the associated linkage and actuators have been removed. All other elements remain essentially the same.

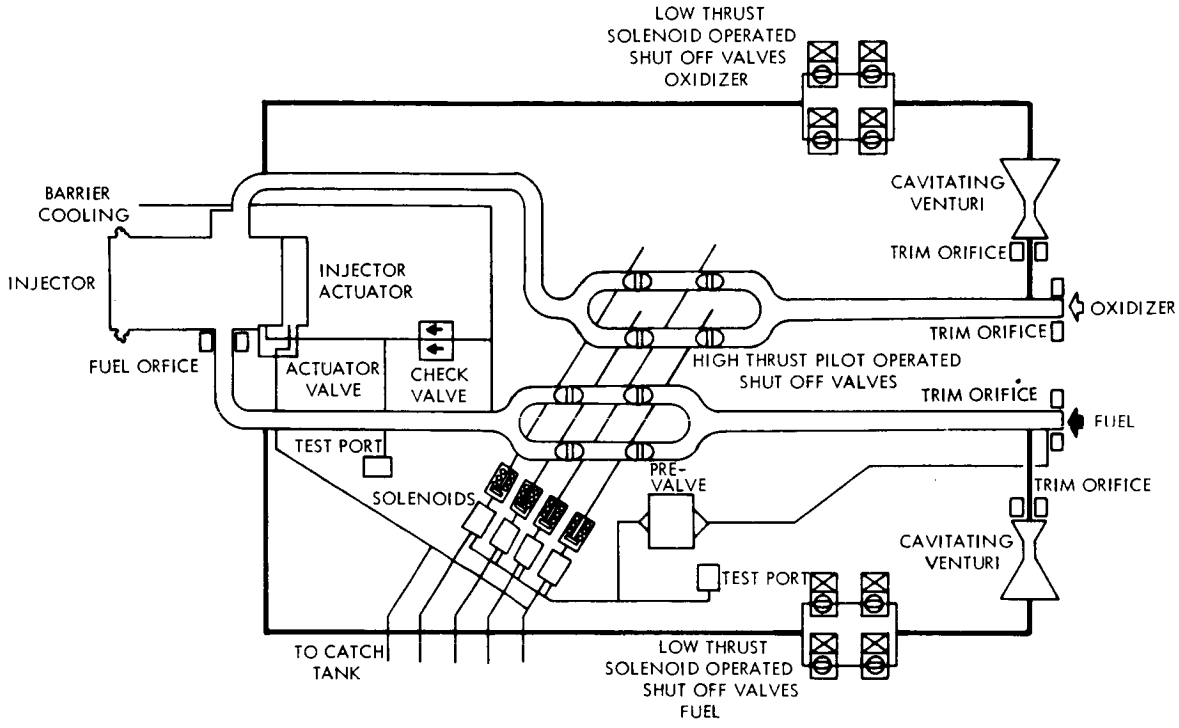

Figure 3-23. Voyager Spacecraft Engine Flow and Control Schematic

The potential advantages for the modified version are in the areas of component weight reduction and simplification of the throttling actuator mechanism. The flow control valves, throttle actuator and throttle linkage, which weigh approximately 40 pounds, would be replaced by a single quad-redundant solenoid valve and a simplified new design injector actuator, whose combined weight is on the order of 18 pounds. Thus, the net weight saving to the thrust chamber is approximately 22 pounds.

The principal disadvantages to the modified approach are:

a. A new injector actuator will have to be designed, developed and qualified. While this can be a basically simple design offering two positions of operation, it will mean new hardware and require the aforementioned testing.

b. The result of the modifications noted above plus the fact that existing components will be removed from the flow path, implies a considerable change in the hydraulic

characteristics and dynamics of the system. It therefore means that considerable testing will have to be accomplished to establish the characteristics as well as bit, tailoff variability and other basic performance parameters. This will be demonstrated to some extent in the current MSFC-sponsored LEMDE demonstration program.

The existence of the LEMDE thrust chamber of equipment that is capable of providing the control and switching to the high and low thrust modes of operation lead to the logical conclusion that this assembly should be used "as is" for the Voyager mission. Further, it would appear to be equally logical that modifications could be made to simplify the throttle and actuator, without effecting hydraulic flow characteristics which would effect a weight saving and accomplish a considerable simplification of the control assembly.

The baseline system reflects the use of the existing hardware.

3.3.4. Nozzle Expansion Section Design

As shown in Figure 3-24, the expansion section of the nozzle is constructed with an ablative material to an expansion ratio of 16:1. From that point to the exit, at expansion ratio of 47.5:1, it is a radiative cooled columbium alloy design.

During operation the metallic expansion section has a temperature profile as shown in Figure 3-25. The high temperature of 2200 degrees Fahrenheit presents an intolerable heat source for the spacecraft configuration and must be reduced to acceptable levels. Two immediate solutions are evident:

a. An all-ablative nozzle can be used, or

b. Insulation can be applied externally to the nozzle extension.

The use of an ablative skirt will apparently solve the problem but with a significant weight penalty. External application of insulation needs further effort to achieve a lasting bond between the columbium skirt and the insulating material. Finally, some changes in the

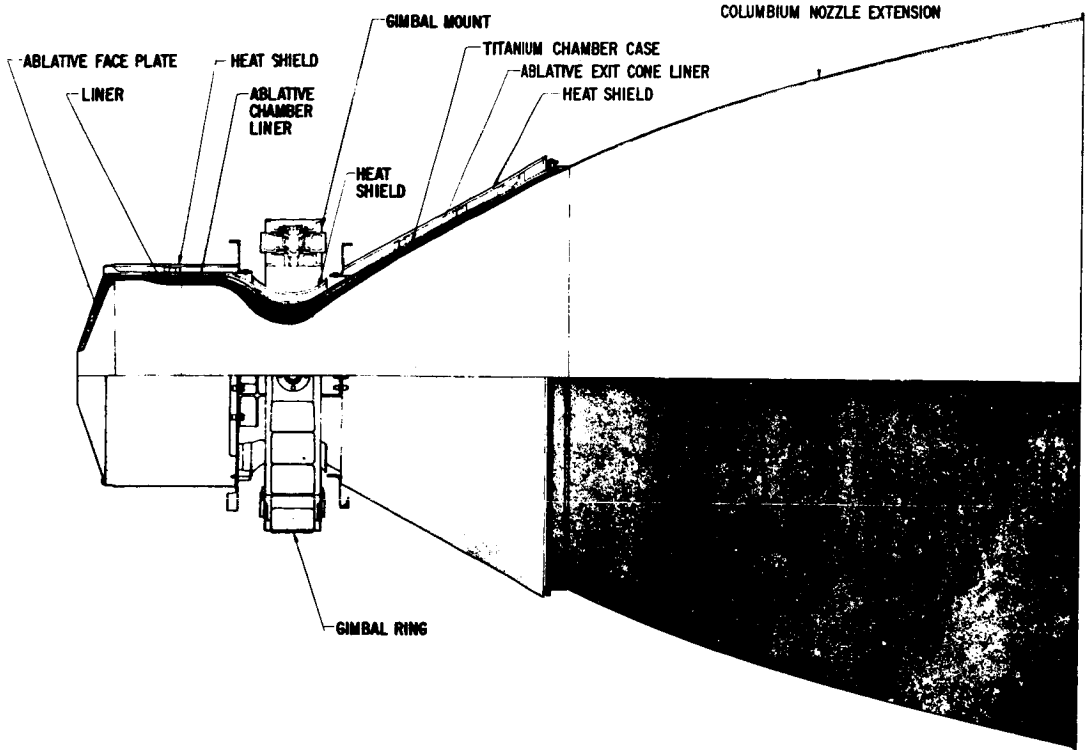

Figure 3-24. Thrust Chamber Profile

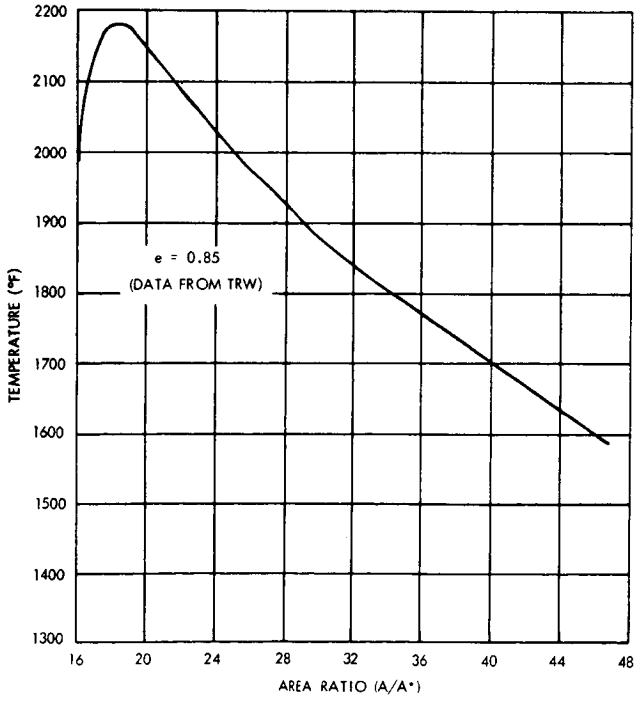

Figure 3-25. Radiation-Cooled Nozzle Extension Temperature

spacecraft design may permit the use of a radiation skirt. The present recommendation is external insulation, pending solution of the bonding problem.

3.4. PARAMETRIC WEIGHT STUDY

A correlation of mission velocity requirements, payload weight (all burn-out weight other than propulsion subsystem hardware), propulsion system burnout weight (including unusable propellants) and propellant loading requirements for the LEMDE baseline Propulsion Subystem is shown in Figures 3-26 and 3-27. Velocity requirements assumed were shown in Table 2-1.

For this analysis a specific impulse of 305 lbf-sec/lbm for LEMDE high thrust mode and 289 lbf-sec/lbm for LEMDE low thrust mode was used.

It is noted that for a given propulsion subsystem burnout weight and payload weight, the 1973 mission requires approximately 1 percent more propellant than the other three missions considered. This is due to the extremely long propulsion subsystem operation (due to high ΔV requirements) in the low thrust level mode when the engine I_{sp} is 289 lbf-sec/lbm. Requirements between the 1975 through 1977 missions are significantly less than 1 percent.

Figure 3-28 and 3-29 show the effects of variations in orbit insertion and midcourse maneuver specific impulse, respectively, on propellant requirement.

3.5. TANK DESIGN

3.5.1. Requirements

As pointed out in Milestone Report VOY-P-TM-13, Propulsion Requirements, the major considerations in the sizing of the propulsion system are:

a. The tank should be sufficiently large so that growth in the planetary vehicle weight can be accommodated; and

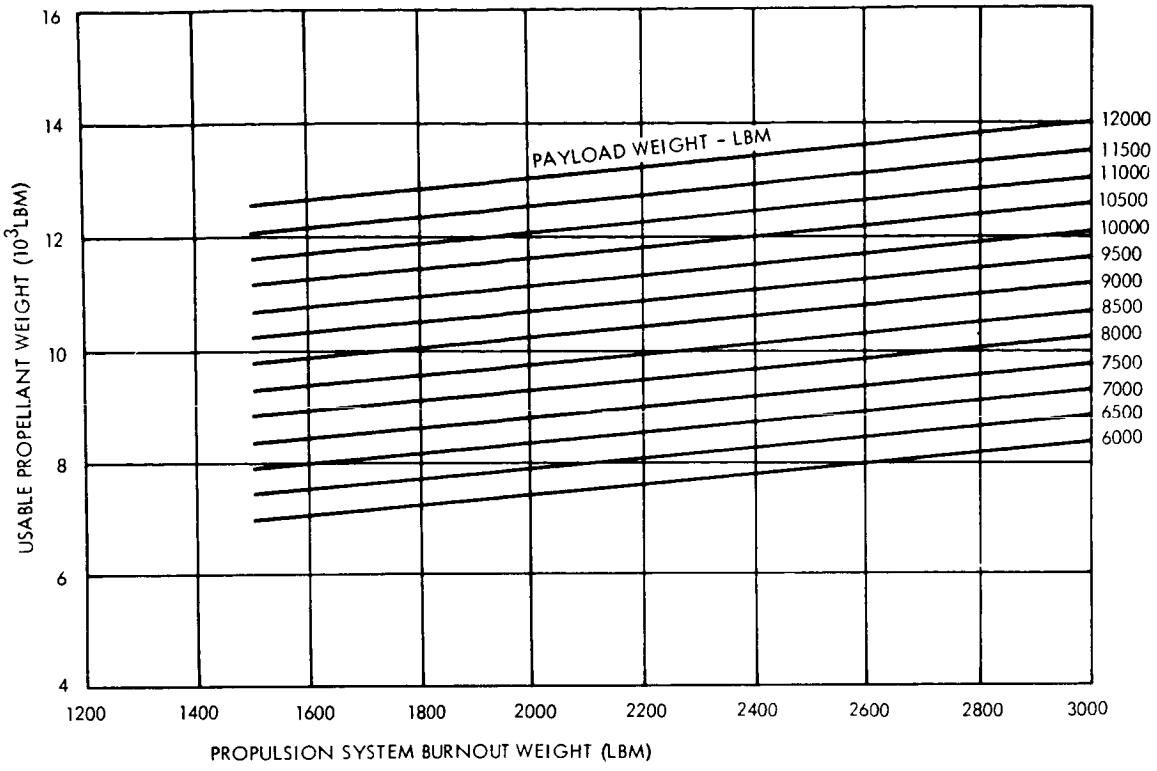

Figure 3-26. Propellant Requirements (1973, LEMDE)

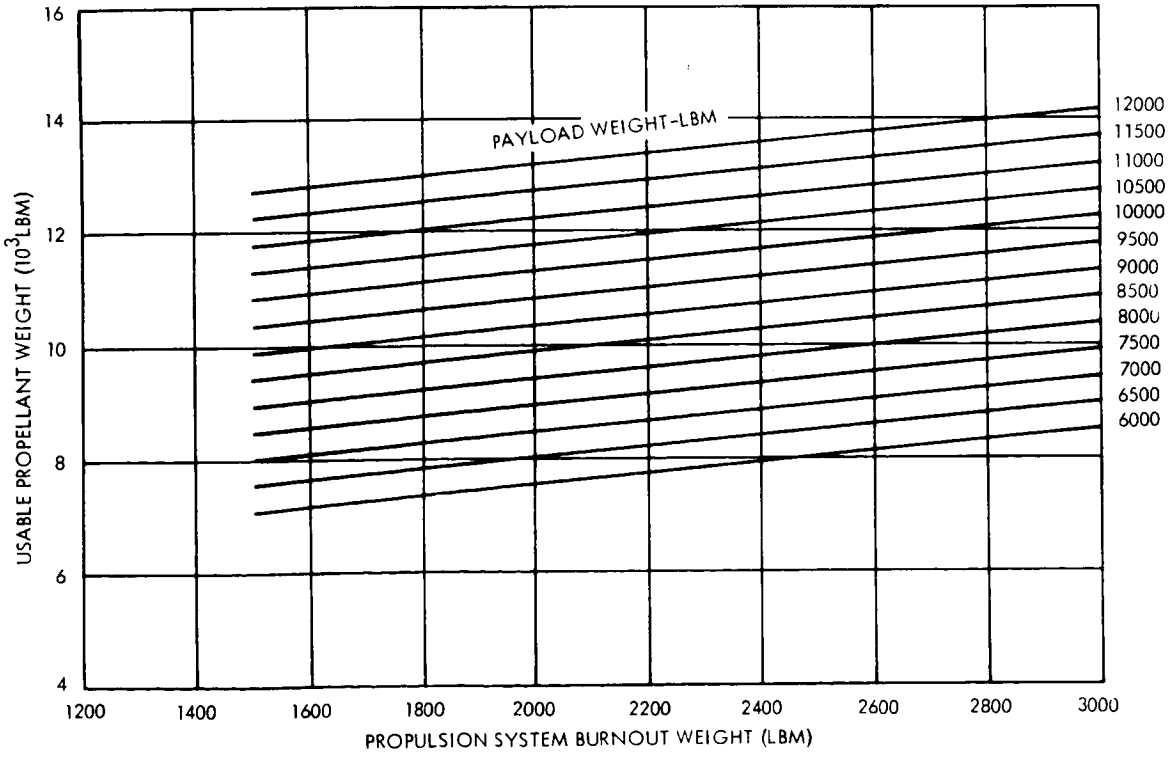

Figure 3-27. Propellant Requirements (1975, 1977, 1979 LEMDE)

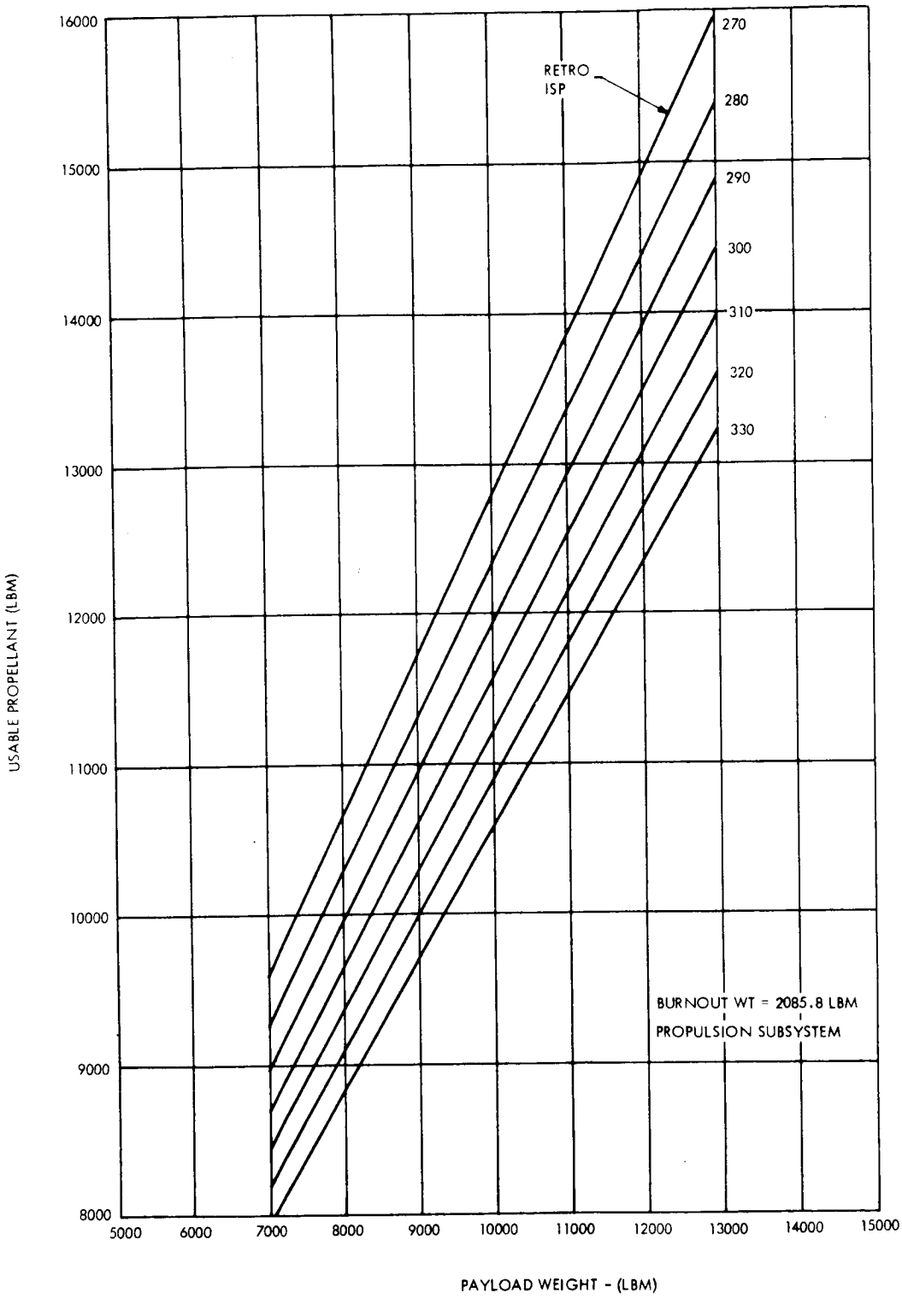

Figure 3-28. Propellant Requirements 1973

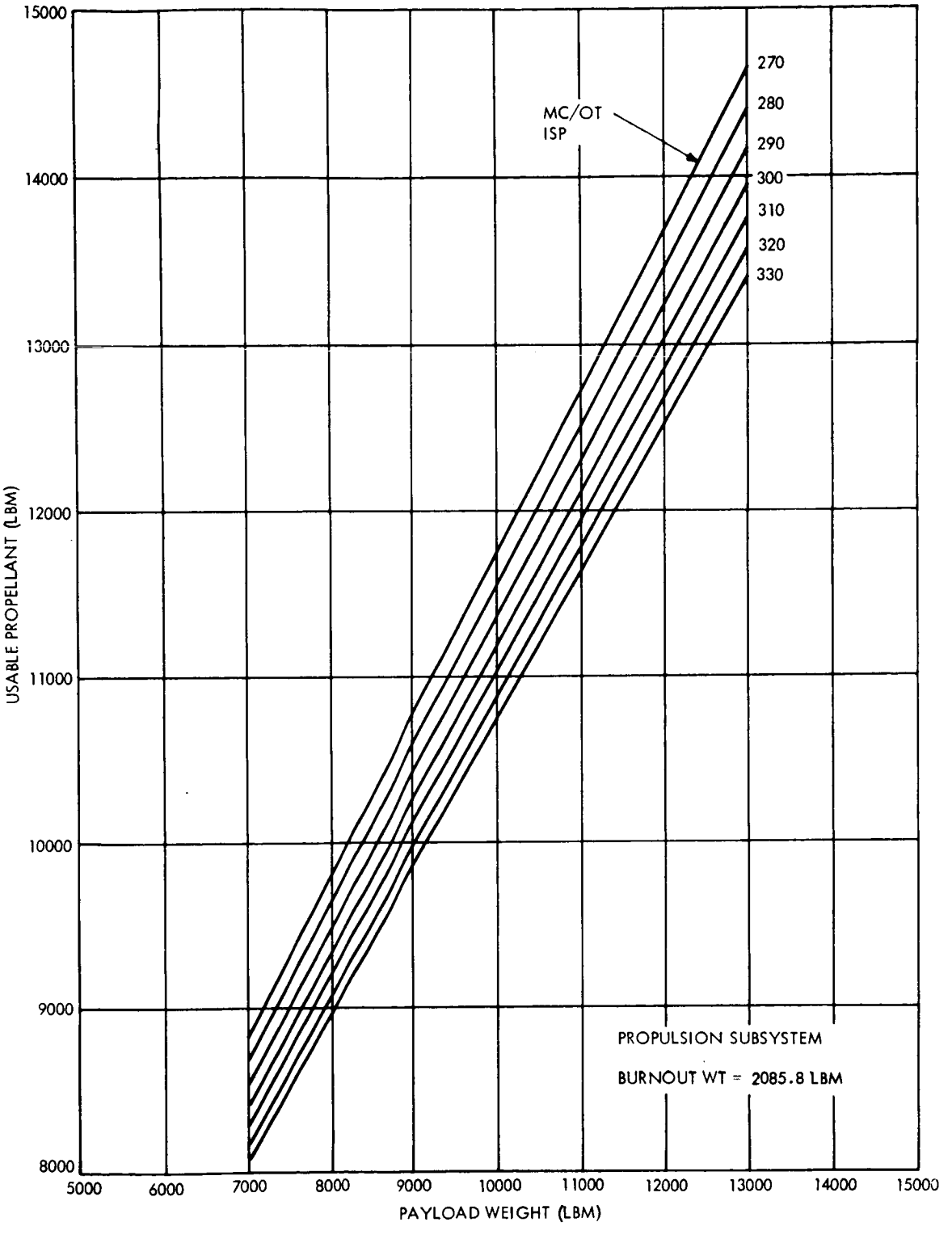

Figure 3-29. Propellant Requirements 1973

b. Mission flexibility should be provided for other Mars missions and missions to other planets.

Considering the many factors that are included within these two broad constraints, such as the number of planetary vehicles per launch vehicle, a minimum launch period, a program contingency, a variable weight of capsule, the ΔV requirements and the propulsion system, the propellant tanks should be sized for a 26,000 pound vehicle. This in turn results in the need for approximately 12,600 pounds of usable propellants. To determine the required propellant tank volume, 400 pounds were added to the usable propellant as a residual in the tanks, and then a 5 percent ullage factor was used to allow for propellant acquisition and motion control devices and an ullage volume over the propellants. Totaling these quantitites at 100 degrees Fahrenheit, maximum allowable temperature resulted in a propellant tank volume requirement of approximately 196 cubic feet. Since the propellant volume flow rate is equal, all tanks will be of equal size. To meet the volume requirements four spherical tanks 54.5 inches inside diameter will be required.

Safety factor was also a design requirement that had to be specified before preliminary designs could be completed. Consistent with current spacecraft practices, a factor of safety of 2.0 as the ratio of burst strength to operating strength was selected. This is to be applied at the maximum anticipated operating temperature of the component, specified at 100 degrees Fahrenheit.

The above requirements define the design criteria for the propellant tankage. When the propellant volume has been established, the present tankage requirements can be generated.

The pressurant tanks must hold sufficient gas to fill the 196 cubic foot propellant tanks at 235 psia. The 2:1 safety factor at 100 degrees Fahrenheit, with fully charged tanks applies. A 15 percent allowance for leakage was provided.

With the requirements established, major tradeoffs in the design of the tank were conducted and are discussed in the following paragraphs.

3.5.2. Material Selection Tradeoffs

For the propellants being considered, the choice of applicable materials quickly converges on the use of 6Al-4V titanium alloy or a special 301 stainless steel, subjected to a new cyroform process. Table 3-10 lists a few applicable areas of comparison for each of the materials with a general summary of the comparative results. Each area will now be discussed in detail.

Table 3-10. Material Tradeoffs

Item	6Al-4V Titanium	301 Stainless Cryoformed
Strength/Density	Excellent	Good
Brittle Fracture Resistance	Good	Might be better
Manufacturing Experience	Extensive	Limited
Compatibility	Demonstrated	Under test

The strength-to-density ratio of titanium (160,000 psi/0.160 pounds per cubic inch) is a significant 18 percent over that of cryoformed stainless steel (240,000 psi/0.29 pounds per cubic inch). Thus, for all pressure vessels designed under the same criteria, titanium tanks will always be lighter than tanks using cryoformed stainless steel. For the baseline system the weight advantage is approximately 250 pounds, dry weight, considering both propellant and pressurant tanks.

In the area of brittle fracture, it is generally agreed that materials with face-centered cubic crystalline structures, typical of the austinetic stainless steel family, of which 301 is a member, is more resistant to brittle fracture than those materials with hexagonal, typical of titanium alloys, or body-centered cubic structures. It is also felt, however, that the amount of brittle fracture toughness decreases as the amount of cold work increases. This is

illustrated by the curves taken from Reference (1) (Figure 3-30) which plot the fracture toughness parameter, K1C, versus the tensile strength of the material. While these curves are not conclusive, they are indicative of the trend of data. It should be also noted that the general categories of aluminum, titanium and steel are specified and not a specific alloy. The conclusion drawn from these data is that the 301 stainless steel might be better than the titanium alloy in resistance to brittle fracture.

Viewing these two materials from the manufacturing point of view, the following comments can be made. In the manufacture of cryoform tanks a preform is required. This can be done by conventional methods of either deep drawing or machining. In either event manufacturing tooling is required. Normally, this will be hard tooling and therefore will limit the flexibility in design changes. To perform the stretch forming operation, the total tank must be assembled. It is filled with a cryogenic liquid, normally nitrogen, and pressurized such that a 6 to 8 percent increase in diameter is experienced. This method of fabrication has an obvious advantage in that the welds used for attaching bosses, trunnions, inlet or outlet ports are subjected to the same work hardening process. Welds which have been subjected to the cryoform process have demonstrated strength equal to the parent material. Thus, local thickening for weld preparation is not required in the cryoform materials. A potential problem with this method of fabrication is that the accessibility to the internal surface is limited. Consequently, measurement and inspection techniques are similarly limited. This would include such operations as direct measurements of thickness or perhaps X-raying of critical areas.

Titanium tanks are usually manufactured from machined thick forgings, thus, there is a degree of flexibility allowable in the diameter of the tanks without major modifications to the basic tooling. Relocation of bosses and trunnions is no more difficult with titanium than the stainless steel except that titanium requires local thickening if welding if to be accomplished.

(1) Campbell, J.E., "Current Methods of Fracture Toughness Testing of High Strength Alloys with Emphasis on Plane Strain", DMIC (Defense Metals Information Center) Report 207, August 31, 1964, Battelle Memorial Institute, Columbus, Ohio.

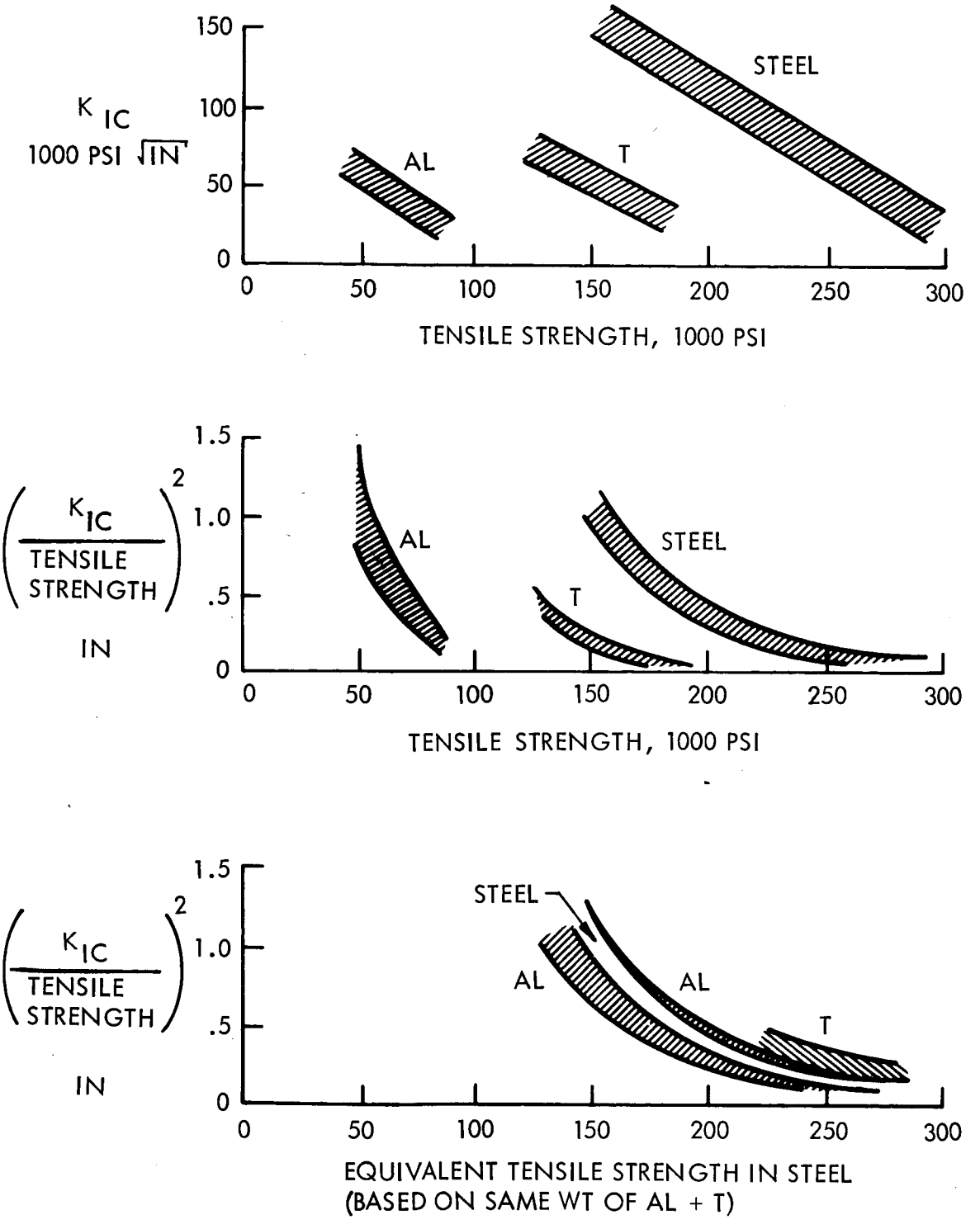

Figure 3-30. Tensile Strength Curves

Titanium, because it is machined to final dimensions on wall thickness and weld areas prior to weld assembly, is capable of being accurately and totally inspected for dimensional compliance to the specifications. Further, welds in critical areas can be X-rayed prior to the final assembly process.

Many examples of titanium are available. A few noteworthy ones are: the LEM descent stage propellant tankage, the LEM ascent propellant tankage, and the Titan Transtage propellant tankage. During the development and qualification cycles of those programs, all aspects of the manufacture and test cycle have been thoroughly investigated and documented. The cyroformed stainless steel, on the other hand, has not had the benefit of such intensive usage or investigation.

No discussion of materials for propellant tankage would be complete without consideration of the compatibility with the propellant. The development and qualification testing on the Apollo LEM vehicle tankage uncovered a problem of stress corrosion with NTO in contact with the titanium alloy. This problem was of such magnitude that it received intensive industry and governmental investigation. The results of this intensive effort are far-reaching and manifest themselves in every area of the tank and propellant manufacture and use cycle. The list of "Do's and Do Not's" includes such items as: "Do not" clean with methyl alcohol or certain grades of grades of freon; "do" use green (inhibited) NTO, and "do" glass shot peen the interior surface of the propellant tanks. The conclusion drawn is that once the problem was uncovered, means were available to eliminate it. Thus, the basic requirements for manufacture of a propellant compatible titanium tank is to use the developed manufacture and test procedures and insure their adherence by strict quality control.

Considering the 301 S.S., in data received from ARDE, Inc., which reported tests conducted at other industrial sites for any of the propellants under consideration for Voyager, stress corrosion in 301 cryoformed stainless steel has not been discovered. In some cases there has been evidence to show that there is better corrosion resistance with the cryoformed material than there was in the annealed state.

In summary of the discussion of tankage materials, the General Electric baseline design shows titanium used throughout. The basis for this selection is the increased strength-to-weight ratio, which results in an approximate 250 pound tank weight saving compared to the 301 stainless. Also, the abundance of titanium manufacturing and test experience characterizes it as a state-of-the-art material.

3.5.3. Mounting Techniques

Figure 3-31 presents several possible methods of mounting the tanks in the vehicle structure. These methods are to be considered applicable to either pressurant or propellant tank installation. Each of these configurations is briefly described and the salient advantages and disadvantages of each configuration are noted in Table 3-11.

A review of the six configurations with their attendant advantages and disadvantages eliminated configurations 1 and 4 immediately because of heavy weight and the possibility of tank damage, respectively. Of the remaining configurations, numbers 2 and 5 suffer from a slight weight penalty. However, they do have the possibility of convenient growth. Designs 3 and 6 are the lightest weight configurations but are the most complex to machine. Thus, from the tank design viewpoint there is no clear advantage to any single design, and it is on the basis of flexibility and ease of installation into the vehicle plus the slight weight advantage offered by the trunnion-mounted design that this type was selected for the baseline configuration.

3.5.4. Design Limits

As previously mentioned in paragraph 3.5.1 nominal operating propellant tank pressure is 235 psia. Due to the isolation check valves in the pressurization lines, variations in ullage temperature will produce ullage pressure variations. It should also be noted that variations in propellant temperatures will cause significant variations in ullage pressure due to changes in vapor pressure. In considering the duty cycle involved in the Voyager mission, it was

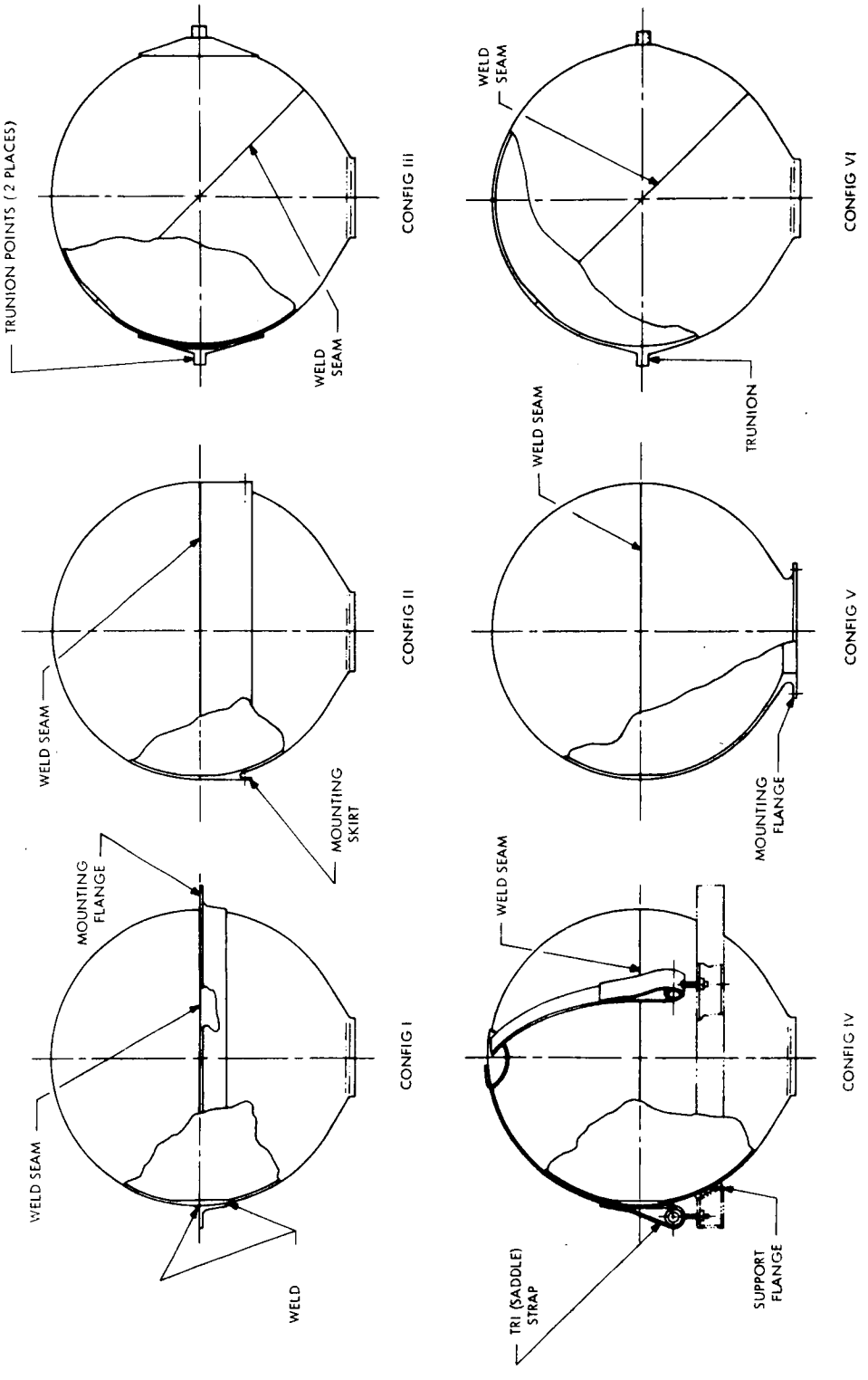

Figure 3-31. Propellant Tank Support Configurations

Table 3-11. Tank Configuration Comparative Chart

Configuration	Approximate Weight (lb)	Vol. Increase Capability	Remarks:
I Flange Mount	170.0	Yes	Poor Mounting Method. Excessive weight due to major discontinuity. High bending loads in shell require greater thicknesses and larger transitions
II Skirt Mount	154.5	Yes	Most commonly used on cylindrical tank. Gives flexibility at moderate weight.
III Trunion Mount	152.1	No	Difficult machining operations. Cannot be modified to increase volume by adding cylindrical section. Requires third attach point to prevent rotation. Weight advantage over other concepts.
IV Strap Mount	Includes Strap Assy. 157.5	Yes	Straps may buckle tank when preloaded. Okay for small dia. thick walled spheres, questionable for large thin walled spheres and cylinders
V Cover Flange	161.5	Yes	Discontinuity at cover requires additional study and testing. High weight compared to other designs.
VI Integral Stud Mount	148.2	No	Difficult machining operations. Cannot be modified to increase volume by adding cylindrical section. Requires third attach point to prevent rotation. Weight advantage over other concepts.

determined that the worst condition (system operating within specification limits) which could be encountered is as follows:

a. Environmental control system functioning with specification limits but conditioning to +40°F prior to orbital insertion maneuver. Pressurant stabilized at +40°F.

b. Following completion of orbital insertion maneuver the environmental control system commences to operate at +100°F (upper limit for system).

The conditions specified above will (1) produce approximately 0°F ullage temperature with +40°F propellant temperature. In the ensuing coast phase, the ullage temperature will rise to 100°F and the propellant temperature will increase from 40°F to 100°F. The subsequent propellant tank pressure increase will be as follows:

a. Oxidizer Tank - The oxidizer tank pressure will increase approximately 50 psi due to volumetric expansion of the helium pressurant and an additional 24 psi due to the increase in vapor pressure of the NTO. The total increase in tank pressure is approximately 74 psi with a resulting tank pressure of 309 psia.

b. Fuel Tank - The fuel tank pressure will also increase 50 psi due to volumetric expansion of the pressurant. However, due to lower vapor pressure characteristics of A-50 fuel, the resulting vapor pressure increase is only 3.0 psi. Thus, the resulting fuel tank pressure is 288 psia.

Using the above criteria as a guideline, it was decided to size the baseline configuration for 300 psig maximum operating pressure at 100°F. For these conditions propellant tank characteristics are shown parametrically in Figure 3-32. Tankage weights as a function of volume are shown in Figure 3-33, and the selected propellant tank design with associated hardware is shown in Figure 3-34.

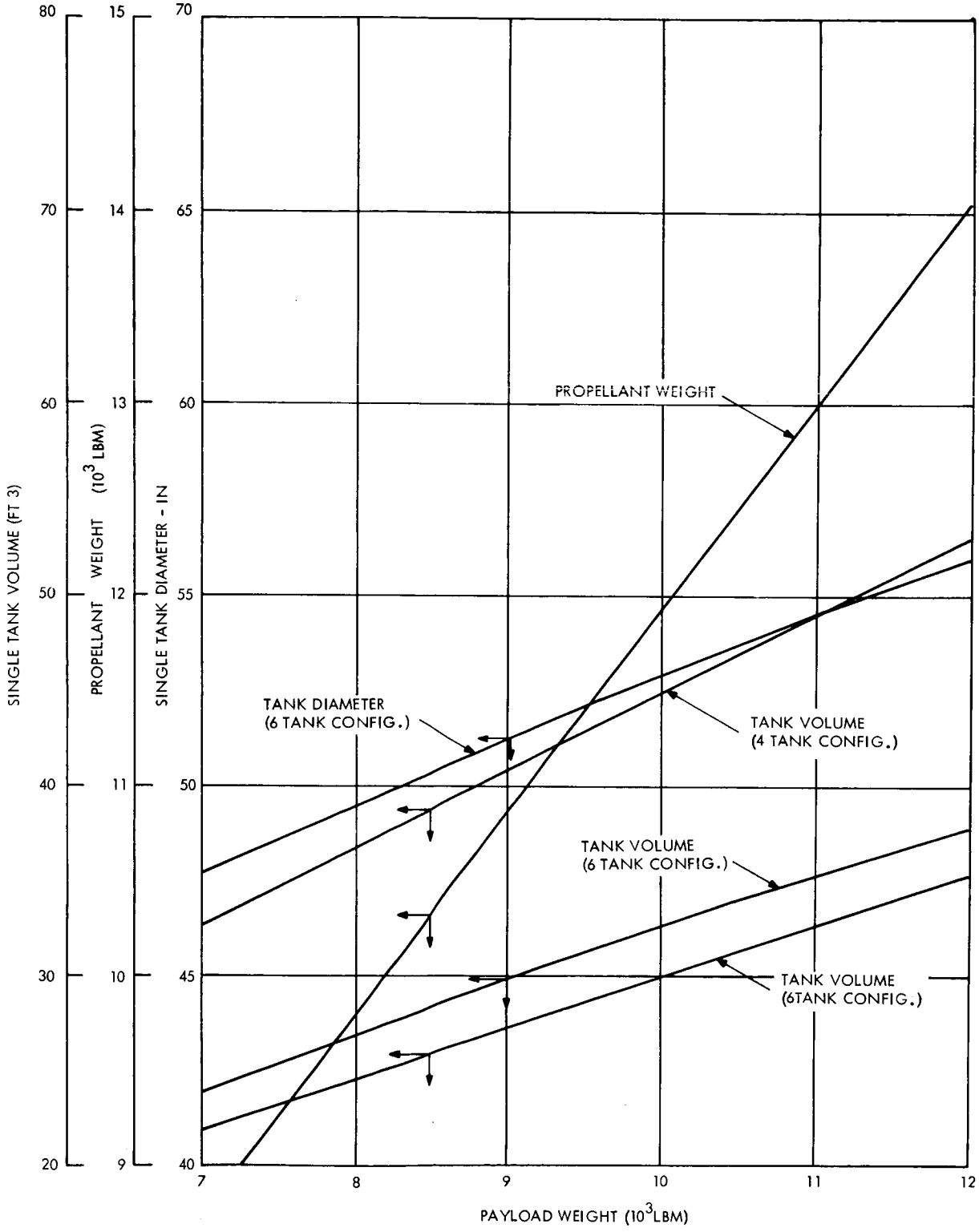

Figure 3-32. Propellant Tank Parameters as a Function of Payload

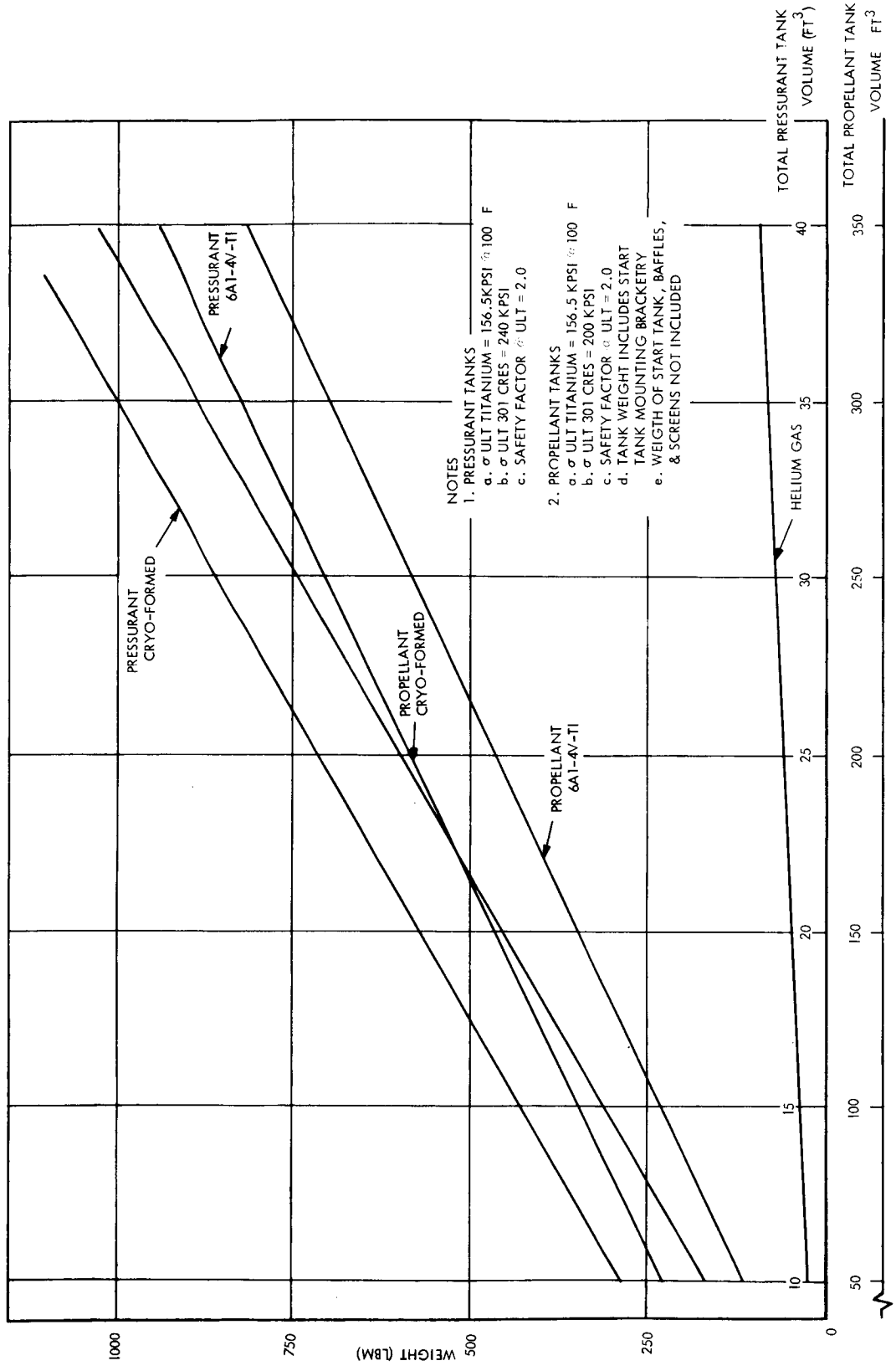

Figure 3-33. Tank Weight as a Function of Volume

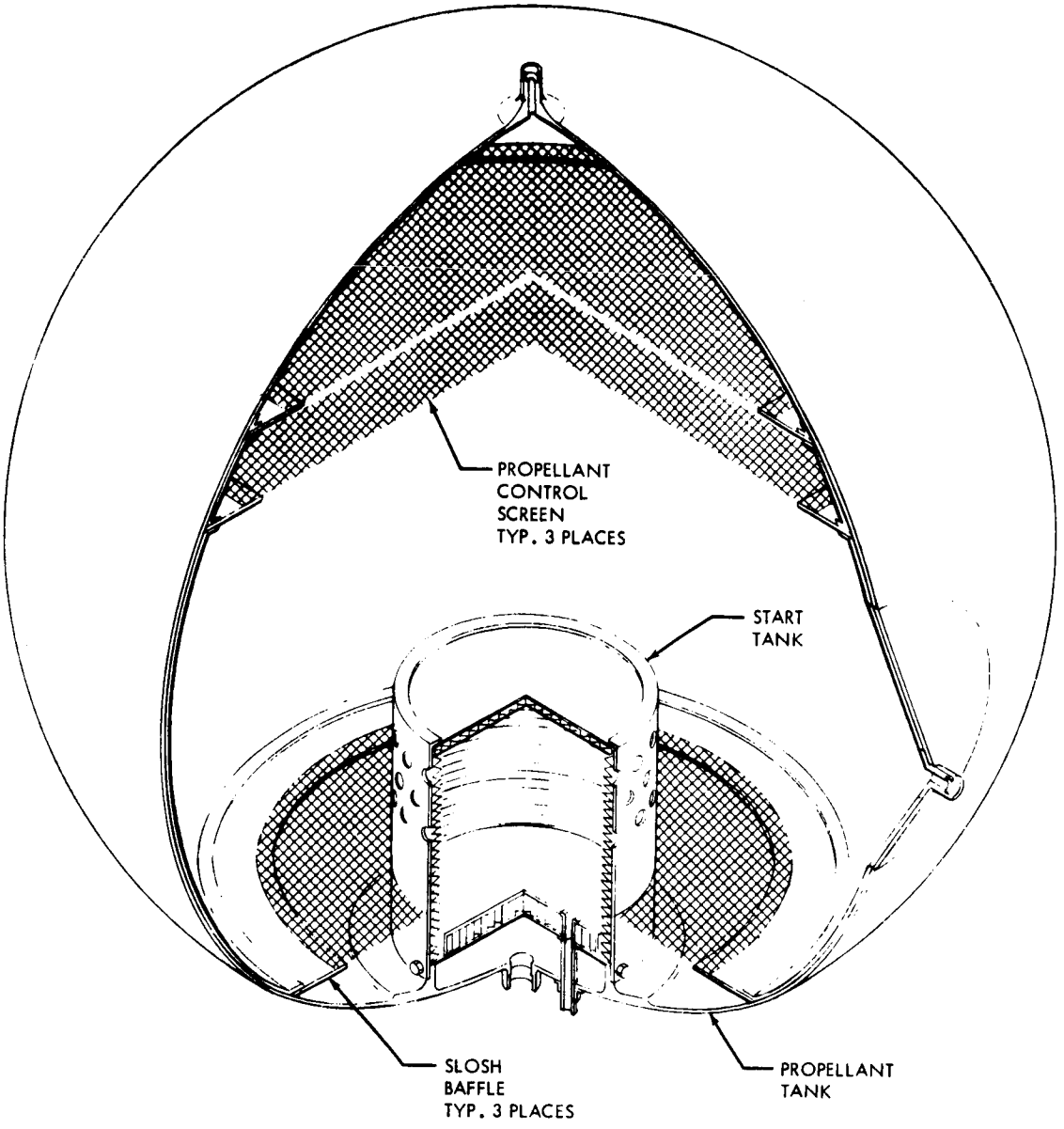

Figure 3-34. Propellant Tank Design

Pressurant storage bottles were sized to contain the required quantity of helium at 70°F and 3600 psig. The worst case condition (system operating within specification limits) which could be encountered is as follows:

a. Pressurant bottles loaded to 3600 psig at 70 degrees Fahrenheit and system locked-up.

   Note: It was considered that the temperature of the pressurant during the loading cycle would approach 200 degrees Fahrenheit and that pressurant loading would be accomplished in 2 stages with a cooling period between stages. First stage loading pressure could be slightly in excess of 3000 psig without exceeding the design limits of a Factor of Safety of 2.0 based on the UTS of 6Al-4V-Ti at a given temperature.

b. After the system is locked-up at 3600 psig and 70 degrees Fahrenheit it was assumed that the environmental control unit could allow an ambient temperature of 100 degrees Fahrenheit, thus producing an internal bottle pressure of 3800 psig due to thermal expansion of the pressurant.

Using the specified criteria as a design guideline the baseline configuration was sized for 3600 psig at 70°F but stressed for 3800 psig at 100°F. A Factor of Safety of 2.0 on burst pressure with a reduction of 6Al-4V-Ti UTS to 156,500 psi was used in the stress computations.

Table 3-12 summarizes the salient pressurant and propellant tank design features.

Table 3-12. Tank Design Data Summary

Propellant Tanks			Pressurant Tanks	
Criteria	Design Data	Remarks	Design Data	Remarks
Regulated Pressure	235 psia	Nominal Regulator Setting ±5 psi	235 psia	Required to satisfy TCA specified inlet conditions
Nominal Operating Pressure	235 psia		3600/400 psig	
Maximum Operating Pressure	300 psig	Considers temperature changes on locked-up system	3800 psig	Pressure includes 200 psi rise due to temp. variation on locked-up system.
Maximum Operating Temperature	100°F		100°F	
Ultimate Strength 6Al-4V-Ti	156,500 psi		156,500 psi	Reduction in allowable strength due to temperature
Leakage Allowance	1×10^{-6} scc/sec	Included to account for diffusion thru tank membrane	15 percent	Included to account for random system leakage
Unknown Process Allowance	N/A		25%	
Req'd Volume (4 sphere total)	187 ft^3 + 5% ullage = 196 ft^3		21.5 ft^3	Reduction due 15% leakage requirement and lower regulated pressure.
Weight of Pressurant/ Propellant	Design 13K lbm '73 9965 lbm		53.9 lbs	$W_G = \frac{N P_t V_t}{R T_i} \left[\frac{1}{1 - P_f/P_i} \right]$
Design Factor of Safety	2.0 at 100°F	Based on 300 psig at 100°F and 156,500 UTS for 6Al-4V-Ti	2.0	Based on 3800 psi max. operating pressure and 100°F, 156,500 psi max. allowable UTS for 6Al-4V-Ti
Weight (Total 4 Spheres each)	453.1 lbs	Includes 30% weight of membrane for Flanges, Fittings, & Trunions	500.5 lbs.	Includes 15% weight of membrane allowance for trunion and fitting.

4. SUBSYSTEM DESIGN

Up to this point the major tradeoffs that effect the design of the propulsion system have been presented. The baseline design consists of an LEMDE thrust chamber without auxiliary thrusters; a helium regulated gas pressurization system; screens, baffles and a start tank as a method of propellant acquisition and propellant motion control; the A-50 and NTO propellants; trunnion mounted titanium propellant and pressurant tanks. In this section the rationale used in selecting a particular generic type of hardware or a particular approach will be presented. To provide continuity to the discussion it will be referenced against the baseline configuration.

Figure 4-1 shows a simplified schematic drawing of the baseline propulsion subsystem. The several call-outs on the figure are generally used to denote operating functions rather than the name of a particular piece of hardware. In the succeeding paragraphs each of these functional areas will be discussed in detail.

In designing the subsystem, major attention has been given to mission success, i. e., high reliability. Other criteria in decreasing order of importance were: flexibility of performance during the mission; growth to other missions; weight; and finally, cost considerations.

4.1. PRESSURIZATION SYSTEM

The selection of the number of tanks to be used to store the pressurant is mainly a function of the ease with which they can be packaged into the vehicle since it can be shown that until minimum gage is encountered, total propellant tankage weight is independent of the number of tanks used.

Because of the packaging considerations, four spherical pressurant tanks were selected. With this decision, the advisability of a common manifold, as shown in Figure 4-2A, versus isolating tanks separately or in combination as shown in Figure 4-2B and C was investigated. The points favoring manifolding all storage tanks together are:

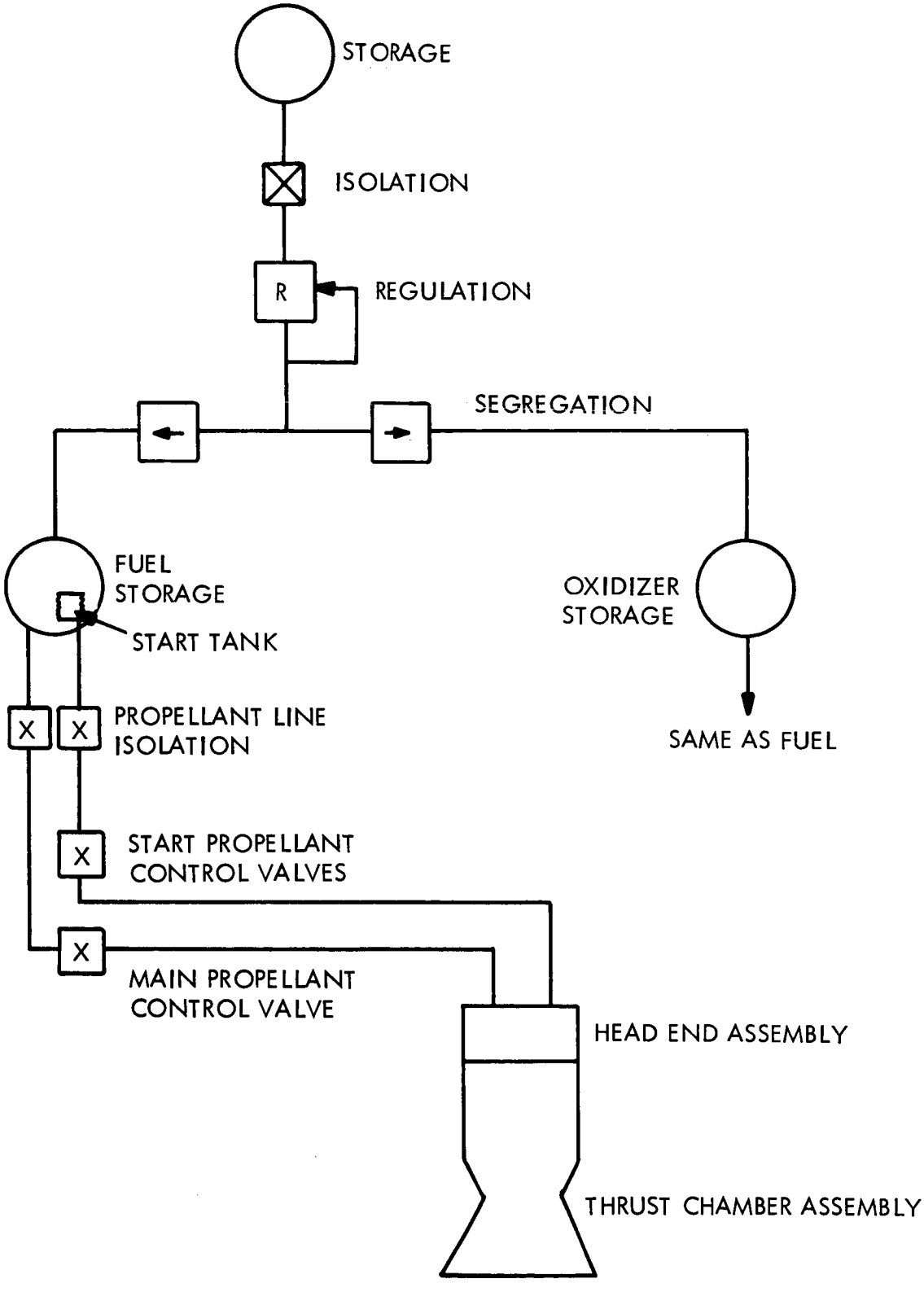

Figure 4-1. Simplified Propulsion Subsystem Schematic

A. COMMON MANIFOLDING

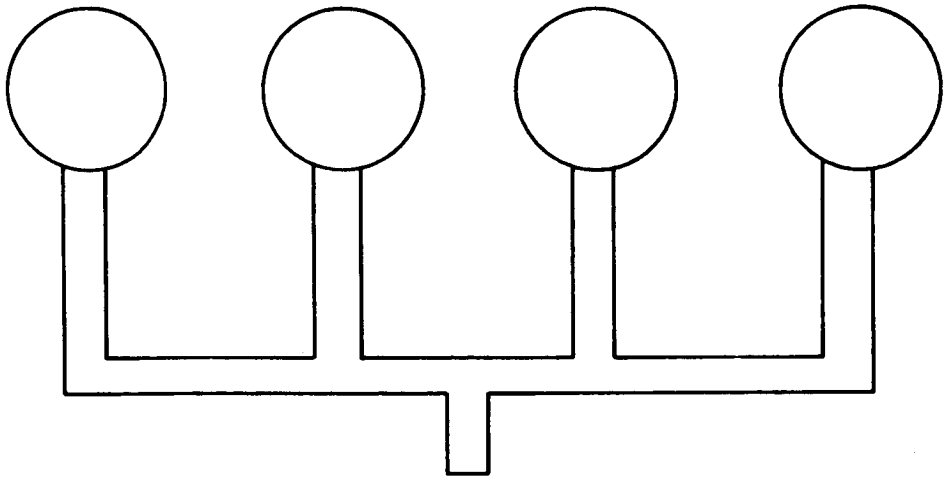

B. SEPARATE ISOLATION

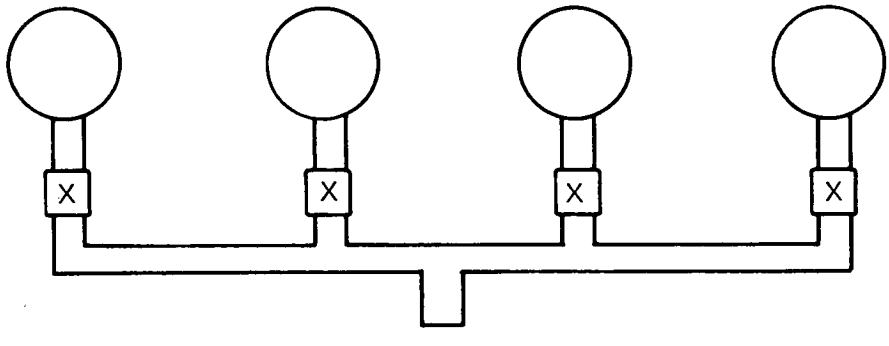

C. COMBINATION ISOLATION

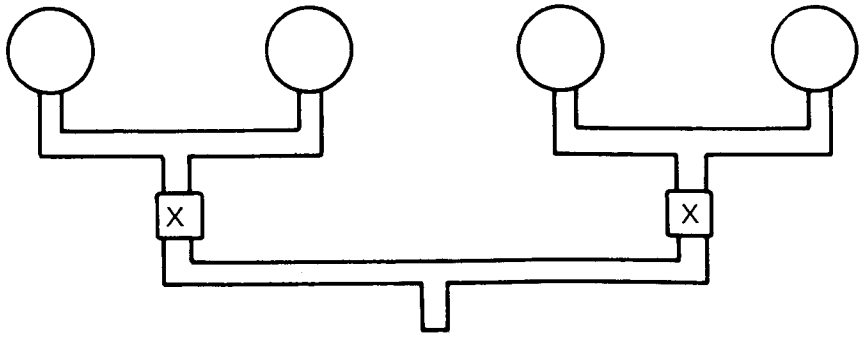

Figure 4-2. Methods of Pressurant Tank Manifolding

a. The total number of components is reduced; thus there is a saving in weight and an implication of increased reliability.

b. There are no pressure surges to be encountered on the downstream components when switching from an empty to a full tank.

c. There will be uniform weight distribution of pressurant gas about the vehicle centerline.

d. The total volume is available for use at any time; and thus an implication of the flexibility of the system.

e. A common manifold system is easy to manufacture, test and pad load.

f. The requirements for telemetry are less with a common system.

The principal argument in favor of separate tanks is that leakage is controlled and cannot deplete the entire supply. This argument usually considers the catastrophic loss of pressurant due to micrometeoroid penetration, which is discussed in section VOY-D-361.

The baseline system uses a common manifold for all tanks. It is felt that the probability of a catastrophic leak can be maintained sufficiently low with this approach which avoids the penalties of added hardware and required switching associated with separate tanks.

The next major area to discuss is whether or not an isolation network is required between the common tank manifold and all downstream components. If such an isolation network is provided, it would be used to:

a. Prevent internal leakage - i. e., through in-line solenoid valves, regulators, check valves, etc.

b. It would limit external leakage from downstream components and lines and fittings.

c. It would relieve the operating pressure on downstream components during the launch acceleration and vibration environments.

d. It would provide a measure of assurance that all operations could be completed within the budgeted supply of pressurant.

Since the use of an isolation device is highly dependent upon the amount of leakage, a limited study was conducted into what constitutes an acceptable leakage rate. To determine what would be achievable, an estimate was made of the potential number of leakage points in the pressurant side of the propulsion module. (Pressurant required to replace any propellant loss due to leakage was not considered, since that quantity of pressurant would be required during normal mission operations.) For the baseline system, approximately 130 possible leakage paths were counted. Using that number, it is possible to calculate a curve of pressurant volume lost versus a leakage rate per joint for a given time period. The time limit assumed for the operation of the propulsion portion of the Voyager vehicle was one year. This plot is shown in Figure 4-3. For an assumed total pressurant loss of two cubic feet (approximately 15% of total load). The allowable leakage rate is then on the order of 3.5×10^{-3} SCC/sec. This number represents a reasonable compromise between what could be allowed and what is easily achieved and documented when testing.

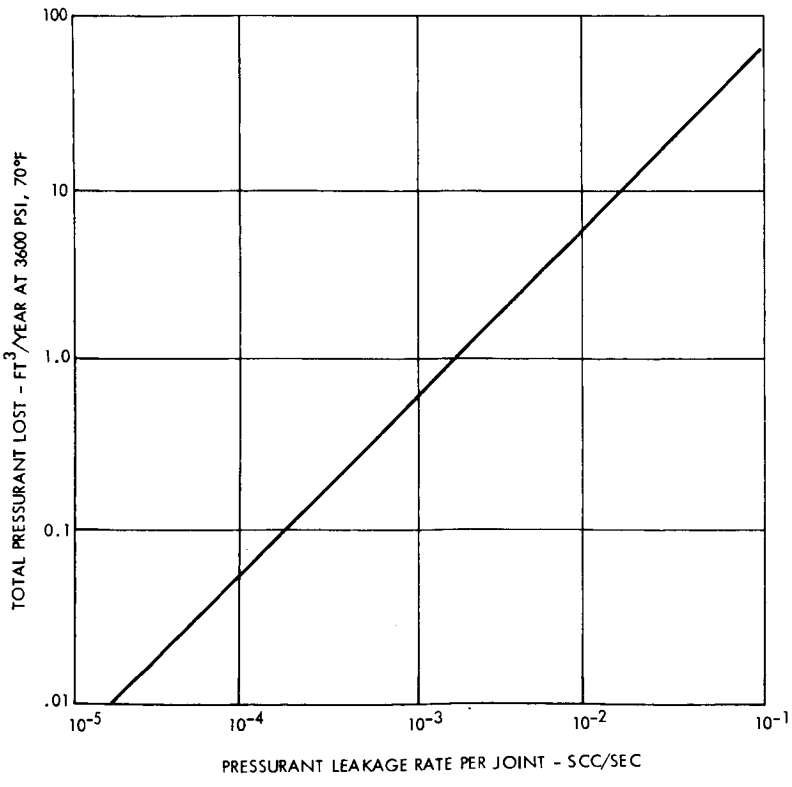

Figure 4-3. Total Pressurant Loss from 130 Joints vs. Leakage Rate Per Joint

Because of the above reasons it would appear that isolation would be desirable. However, there are penalties involved. These include:

a. An increase in the system weight.

b. An increase in the number of components with the attendant implication on reliability.

c. An increase in the manufacturing and assembly cycle.

d. An increase in the command sequence to operate the system.

In spite of these penalties, it appears that isolation is still a desirable feature to incorporate in the subsystem design. Methods for implementing isolation are:

a. A motor driven valve - heavy, requires high electrical power, does not guarantee a positive seal - cyclicable.

b. Solenoid valves, either powered or latching - have disadvantages similar to motor driven valve - principally, does not guarantee a leak-free seal.

c. Squib actuated valves - these are comparatively lightweight, require little power, are highly reliable and usually provide an extremely low leakage seal. The disadvantage is that a network would be required to provide for the various phases of the mission profile.

d. Lockup of the downstream regulators - does not meet any of the criteria for isolation.

Based on a conservative design approach, the baseline design reflects the use of a network of squib actuated valves. A tradeoff then develops into the method in which the network will be constructed. Figure 4-4 reflects three possible methods of accomplishing this.

Method "A" reflects a series parallel arrangement where redundancy is provided for each function. Any number of four-valve segments can be placed in parallel to accommodate as many starts or principal operating periods as are felt necessary.

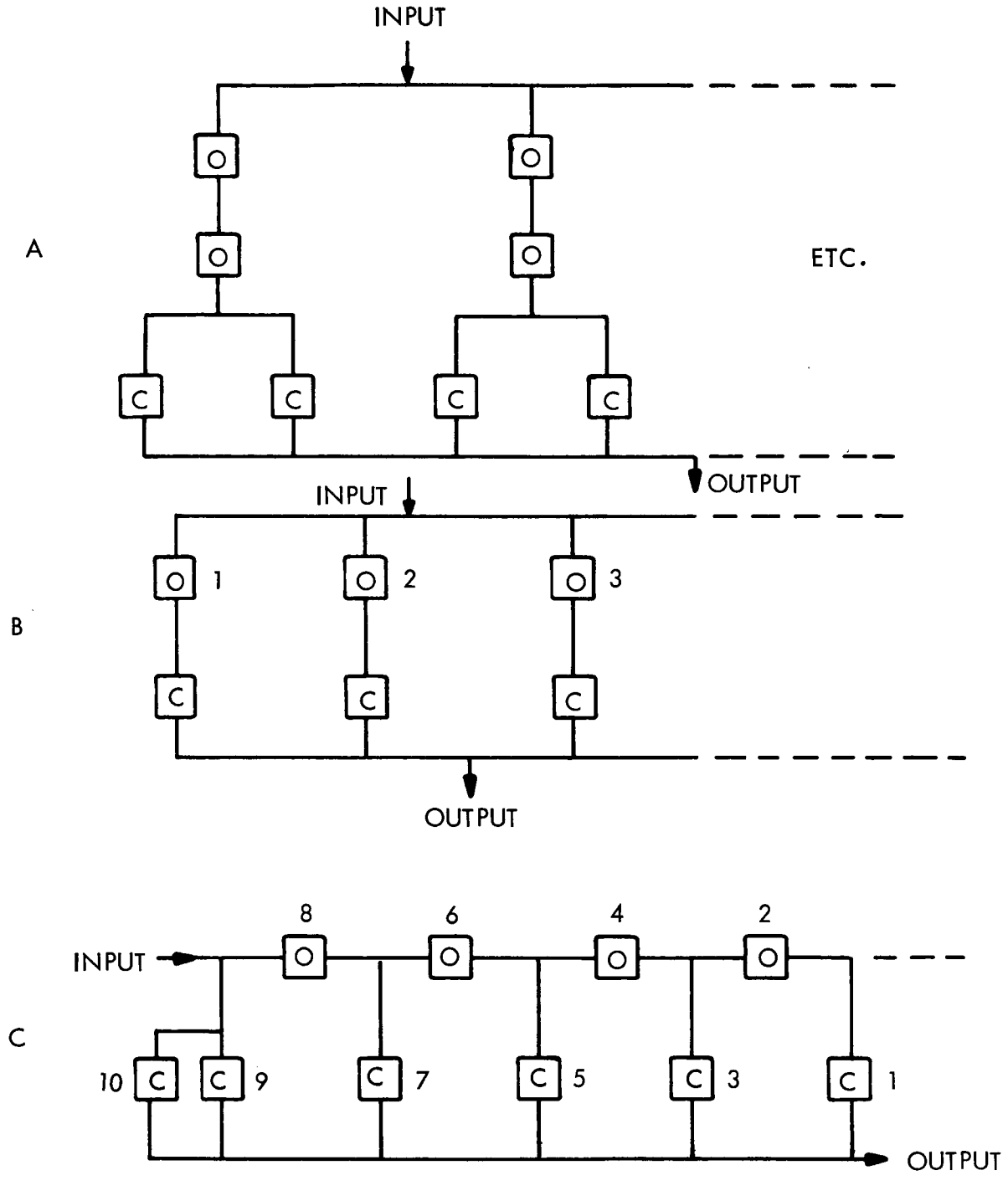

Figure 4-4. Methods of Squib Valve Isolation

Method "B" is similar to "A" except that no redundancy is provided. If valve 1 was called upon to open and it did not, it would be necessary to use pair 2. If that didn't work, pair 3, etc. If the open valve in pair 1 failed to close, there is no method to provide system isolation.

Method "C" provides redundancy of function without a doubling up of components. For system operation, normally closed valve 1 is opened. At the termination of the maneuver, normally open valve 2 is closed. It is should fail to close, valve 4 would be fired, etc. Similarly, if valve 1 failed to open, valve 3 would bc fired. If that failed, valve 5, etc. Under normal operating conditions, however, valve 4 does provide redundancy in closing to valve 2, and similarly, 6 to 4, and 8 to 6. It should be noted that valves 9 and 10 are parallel redundant to provide assurance of opening of the system. As with the other schemes, there is no limit to the number of pairs that can be used.

Because Method "C" uses half the number of components of Method "A" for the same number of operating periods and does provide redundancy lacking in Method "B", it was chosen as the method of isolation for the baseline design. The number of banks of valves was chosen to provide isolation after near earth maneuvers, near Mars maneuvers and after-orbit trim maneuvers. One additional set was provided for overall system redundancy.

As noted in paragraph 3-1, Pressurization Studies, a regulated system was chosen as the preferred method of pressurizing the propellant. In providing a regulation function, two basic methods are available. The first is a standard regulator which senses downstream pressure and, depending on that pressure, adjusts an internal orifice for more or less gas. This method is widely used and typical examples are the descent and ascent stages of the Apollo LEM vehicle.

The second method of regulation shown in Figure 4-5 is solenoid valve, that controls the flow of gas between the pressurant and the propellant tanks and a pressure switch that senses pressure in an accumulator to open or close the solenoid valve. This is typical of the Titan Transtage system.

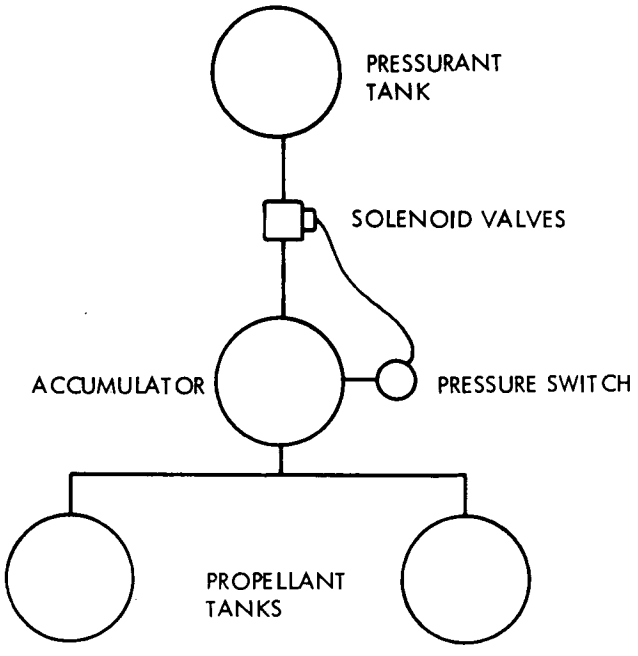

Figure 4-5. Solenoid Valve Pressure Regulation

Regulators have the desirable properties of:

a. Constant pressure output within a very close tolerance band.

b. A minimum number of series functions are required to achieve regulation.

c. The device is self-contained.

d. They are state-of-the-art components used throughout industry.

e. No electrical power is required for their operation.

The principal disadvantage of the regulator is that it is subject to contamination, causing internal leakage and allowing pressure to build up on the downstream components.

The advantages and disadvantages of the solenoid system are opposite to those listed for the regulators. Because of the apparent simplicity in a regulator system, coupled with the addition of upstream isolation, the regulators appear to be the better selection and are thus shown in the baseline design.

Since a failure of a regulator in the open or leaking position can cause downstream pressures to increase above design limits, a sensing and switching network has been incorporated as a flexible safety feature within the regulator function. This is a pressure switch and solenoid valve arrangement. The pressure switch will sense either over pressure or under pressure downstream of the regulators and through an electronic switching network, signal the solenoid valves upstream of the regulators to open or close. This will take the suspect component out of the circuit and place the standby regulator on line. Ground command override of the switching network is included to be used in "health checks" and in the event abnormal operations are required. Solenoid valves are used for this function since the leakage requirements do not have to be strict due to upstream isolation. It is also a convenient method of changing operating components, that allows the flexibility of later changes if desired.

The next area of system tradeoff is in the pressurant lines that feed each of the propellant tanks. Since the lines feed the propellant tanks, there is a possibility of vapors or liquid migrating up the pressurant lines to a common point. Under these conditions the pressure rise in the line could be sudden and appreciable. The tradeoff to be made is in determining methods to maintain segregation of the two propellants.

Figure 4-6 shows 3 methods of providing segregation of fuel and oxidizer in the pressurant lines. In case A, two completely separate pressurization systems are used for the propellant tanks; one for each propellant. There is a possibility of a tie-in between storage tanks if isolation valves are used and opened and closed immediately before and after each maneuver. The obvious advantage for this configuration is that the propellants are totally segregated until they are mixed for the combustion process. The disadvantages are that there is a complete duplication of upstream hardware and each side must work for system operation. Thus, there is an increase in system weight and a decrease in system reliability.

Case B shows a network of squib actuated valves similar to the network described for isolation of the pressurant storage vessels. The advantage to this system is that positive isolation is assured if the valves operate. The disadvantages are that a valve must operate

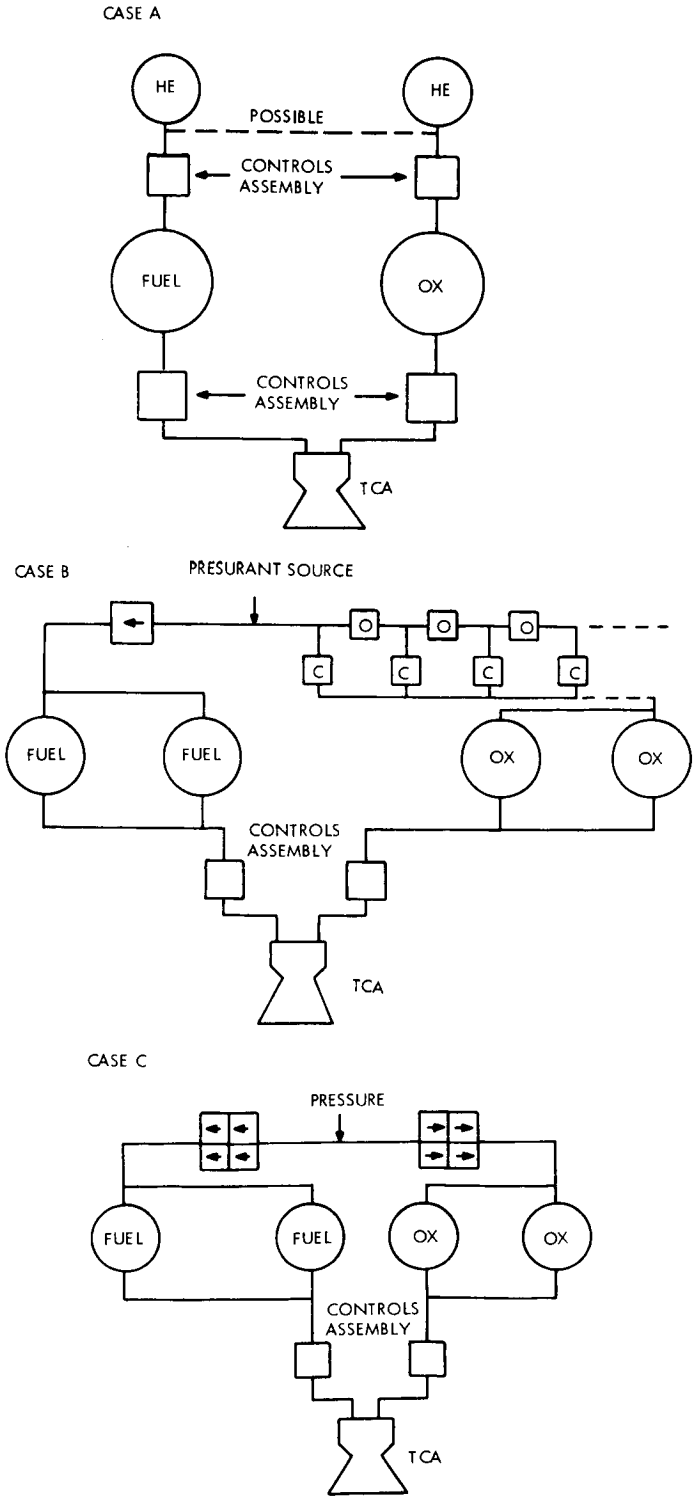

Figure 4-6. Methods of Providing Propellant Segregation in the Pressurant Lines

to provide isolation, the number of operations or periods of burn are limited, and the valves must be opened and closed immediately before and after each maneuver. Strict programming of the start and shut down sequence is required.

Case C shows quad-redundant check valves in each propellant pressurant feedline. This is the same system as is being used on the Apollo LEM descent stage for a like function. The advantages of this system are that it is simple, passive and flexible.

However, there exists the potential of propellant vapor leakage past the poppets in the reverse direction. A brief investigation was conducted to determine the potential extent of pressure rises due to this leakage and the subsequent reactions.

In the first instance it was assumed that both propellants are leaking past the check valves at the following leak rates, which were determined to be the maximum permissible for typical valves under consideration:

a. $N_2O_4 = 1.26 \times 10^{-7}$ lb/sec

b. $NO_2 = 1.78 \times 10^{-7}$ lb/sec

c. A - 50 = 1.97×10^{-7} lb sec

The presence of NO_2 is considered because at 70°F, N_2O_4 is 15 percent dissociated into NO_2. If one assumes an instantaneous combustion type reaction between N_2O_4 and N_2H_4 or UDMH, 0.13 to 0.18 calories per second will be generated plus N_2, CO, and H_2O. There is some evidence that the combustion reaction does not occur but that either NH_4NO_3 or $N_2H_5NO_3$ and water are formed. This neutralization reaction will produce even less heat but does produce a solid product. Since the N_2O_4 is very dry, both types of reaction probably occur, so that the amount of nitrate formed will be much less than a complete reaction of this type would indicate. The nitrate salt would deposit on the tubing wall and possibly in the check valves. Any salt that deposits in the check valves might eventually interfere with the sealing of the poppets.

The second instance assumes that only N_2O_4 or A-50 is leaking at maximum rate, in which case it would take a day to fill the volume bounded by the check valves and the regulator with N_2O_4 and about 1/2 to 1 minute to fill the volume with fuel, to the same pressure of the N_2O_4 (14.7 psi at 70°F) or the A-50 (2.1 psi at 80°F). Operation of the system might then release all of this vapor into the other tank, but this small quantity of propellant would produce so little heat that no effect would be noticed. In an experiment at JPL using much higher concentrations than would be present in this case, N_2O_4 was vaporized into a chamber containing N_2H_4 in the bottom. The only effect observed was a white smoke.

4.2. PROPELLANT STORAGE SYSTEM

The next major items in the schematic are the propellant tanks and start tanks. Detailed discussion of the design tradeoffs for these items were covered in Section 3.0. Therefore, assuming a fixed design, the remaining tradeoff is in the method in which the tanks are aligned to the vehicle axis and interconnected to each other. The basic tradeoff is the effect on the CG travel for all possible alignments and interconnections. The basic methods of aligning and interconnecting the tanks are as shown in Figure 4-7. Cases "A" and "B" are interconnected to show parallel feed from the tanks, while "C", "D" and "E" show series flow. Also note that Cases "A" and "C" are aligned with the fuel (and oxidizer) tanks each on the same principal vehicle axis.

Shown in the figure is the movement of the C.G. of the vehicle as propellant is consumed. Point 1 represents the C.G. location at liftoff (for this discussion the tanks are assumed full); point 2 represents the location at the instant when one tank of each propellant is full and the opposite is empty (propellant half used); and point 3 represents the location of the C.G. at the completion of mission (all propellant has been used). For simplicity in this discussion it is assumed that the tanks are equally spaced from the center line of the vehicle and also the amount of residual propellant does not affect the terminal location of the C.G.

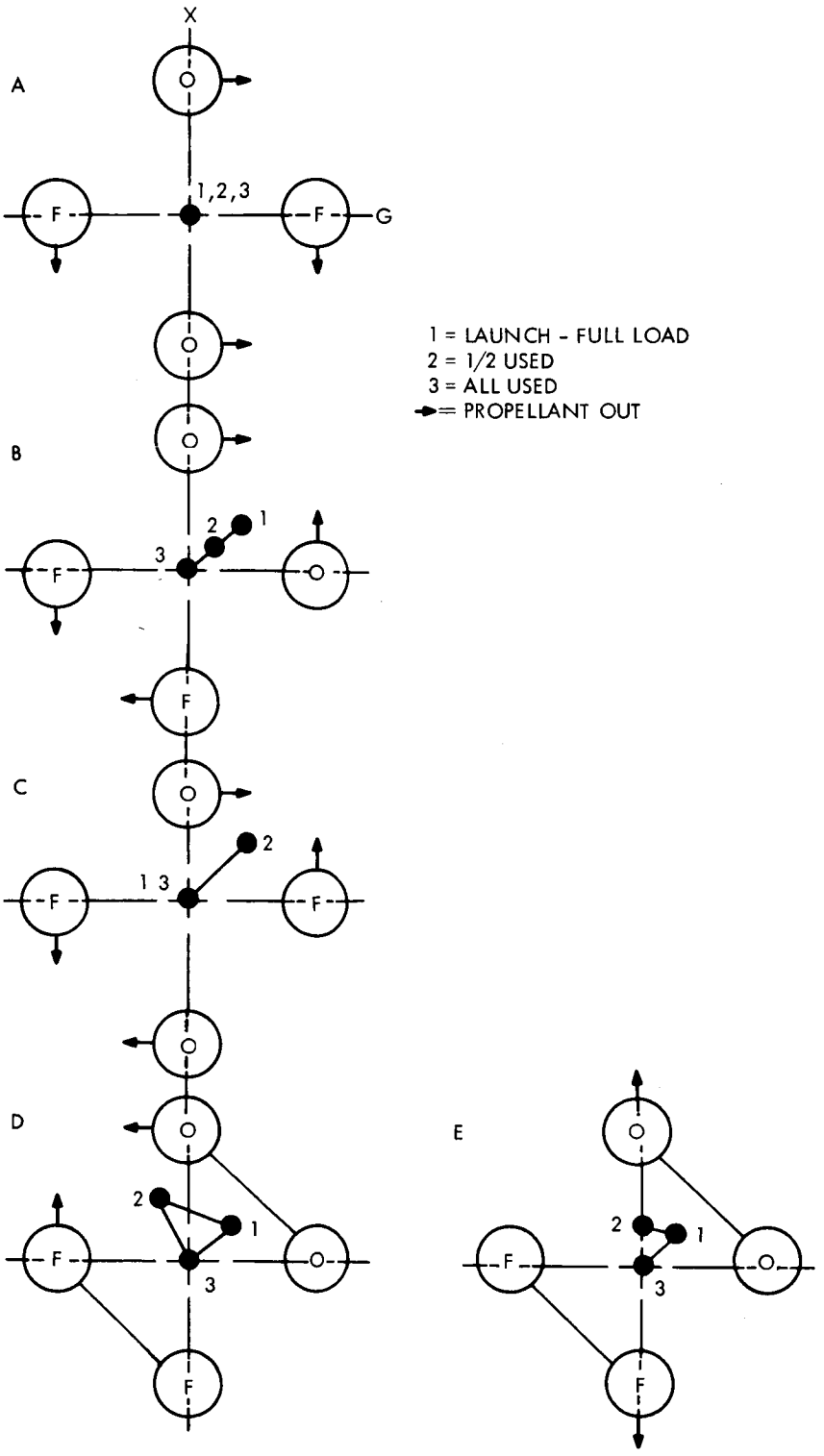

Figure 4-7. Possible Tank Alignments and Interconnections

It will be noted in Case "A" that the C. G. remains at the center of the system at all times during the mission profile. In Case "B", where the tanks are not symmetrically aligned, the C. G. has an initial displacement along a line that is at 45° to the principal axis. As propellant is consumed, the C. G. will travel along this line until at end of mission it is on the center line. In Case "C", where the flow is in series and the tanks are symmetrically aligned, the C. G. will start at the center of the system and move away from the center at an angle to the principal axis. This movement will continue until condition 3 is reached, at which time the C. G. will move back to the center of the system. Case "D" shows unsymmetrical alignment of the tankage and series flow from adjacent tanks. Of all configurations, the C. G. travel in this is the most severe. It initially starts along the 45° incline to the principal axis in the first quadrant. As fuel is used it moves further from the center of the system and into the second quadrant. When condition 2 is reached, the mass center is furthest from the center line of the vehicle and as in Case "C", it is also the maximum travel. As additional propellant is used, the C. G. moves directly toward the center of the system, arriving there at end of mission. In the last configuration, the tanks are nonsymmetrically aligned, they are connected in series and flow is from opposite tanks. As with Case "D", the initial location of the C. G. is offset on a 45° angle. It then moves in an arc until condition B is reached, at which time it travels along the principal axis towards the fuel tank, terminating at the center of the system at end of mission.

Table 4-A lists the coordinates of the C. G. for each of the cases and for each condition within the cases. Also shown in the gimbal offset angle for each case. From these data it will be noted that Cases "C" and "D" have totally unacceptable displacement of the center of gravity. Cases "B" and "E" show an equal initial displacement of the C. G. In Case "B" this offset is decreasing immediately from start of propellant usage. Case "E", on the other hand, remains nearly constant until one of the fuel and oxidizer tanks is empty. Of the two, "B" would be preferred on the basis of C. G. movement. In Case "A" the C. G. always remains on the center of the system. Thus, from the C. G. travel point of view, Case "A" would be selected for the baseline configuration.

Table 4-A. Propulsion Tank Configurations

	$\overline{Z}$	$\overline{X}$	$\overline{Y}$	Gimbal
Case "A" - Launch	136.99	.17	.48	.4°
- 1/2 Used	142.73	.23	.66	.5°
- Empty	155.56	.37	1.07	.7°
Case "B" - Launch	136.99	2.77	3.08	3.2°
- 1/2 Used	142.73	2.06	2.50	2.3°
- Empty	155.56	.48	1.18	.8°
Case "C" - Launch	136.99	.17	.48	.4°
- 1/2 Used	142.73	10.02	6.78	9.2°
- Empty	155.56	.37	1.07	.7°
Case "D" - Launch	136.99	2.77	3.08	3.2°
- 1/2 Used	142.73	10.02	5.46	8.1°
- Empty	155.56	.48	1.18	.8°
Case "E" - Launch	136.99	2.77	3.08	3.2°
- 1/2 Used	142.73	3.20	.66	2.8°
- Empty	155.56	.48	1.18	.8°

Note:

Total Usable Propellant
5000 lb Fuel
8000 lb Oxidizer

PSP Stowed in Launch Position
Hi-Gain Antenna Deployed
5000 lb Lander

Arguments against parallel flow are:

a. There is a potential for more severe propellant shoshing or fluid motion under low gravities, and

b. Because of possible propellant migration between tanks, the autopilot and thrust vector control system would have to be designed for a "worst case" C. G. offset, namely the condition where one fuel tank is full and one oxidizer tank is full.

There are several points which tend to mitigate the above disadvantages. At this time the magnitude of a possible propellant motion and slosh control problem with one or two tanks full is not defined. It is felt, however, that the motion control screens and baffles installed in each tank are sufficiently well understood that problems in either the motion or the migration area will be minimized.

In summary, the baseline configuration shows the propellants tanks symmetrically mounted and emptying in parallel from a common pressurant source. It is probable that the attempt to minimize C. G. travel during any phase of the mission profile outweighs possible problems associated with propellant motion or migration. It is also likely that the motion and migration problems will be adequately handled by the screens, baffles and the response of the thrust vector control system.

Isolation of the propellant from the main and start valves is the next major area of tradeoff in the propellant storage portion of the subsystem. As with isolation of the pressurant system discussed earlier, isolation here is centered about allowable leakage rates through the propellant valves. It is realized that because of the separate main and start lines, two leakage criteria have to be established. However, it is logical to assume that because of the larger size and the basic type of valve, it will be easier to prevent leakage with the solenoid type start valve. Thus, the discussion will center about leakage through the main engine valve.

The first effect of leakage through the valve is the obvious loss of propellant. For an assumed useful propulsion system life of one year, the amount of propellant lost as a function of the leakage rate is plotted in Figure 4-8. Establishing 20 pounds as an allowable total for each propellant the curve leakage shows that a leakage rate of 3×10^{-4} SCC/second of fuel and 3×10^{-4} scc/second of oxidizer can be tolerated. On the assumption of a direct viscosity ratio correlation (Figure 4-9), the corresponding helium leakage rates were calculated as 1.5×10^{-2} scc/second and 4×10^{-3} scc/second which are well within the state-of-the-art for helium leak detection test methods. Thus, from the weight lost and testability aspects, there is no major drawback to an allowable propellant leakage of $2\text{-}3 \times 10^{-4}$ SCC/second propellant.

Assuming the leakage rate of $2\text{-}3 \times 10^{-4}$ scc/second (which incidentally is 6 times larger than the current LEM specification,) there are at least two other areas that must be considered. First is the question of the thrust produced and hence spacecraft velocity change due to the leakage of either propellant, and second that of the thrust effect of leakage of both propellants

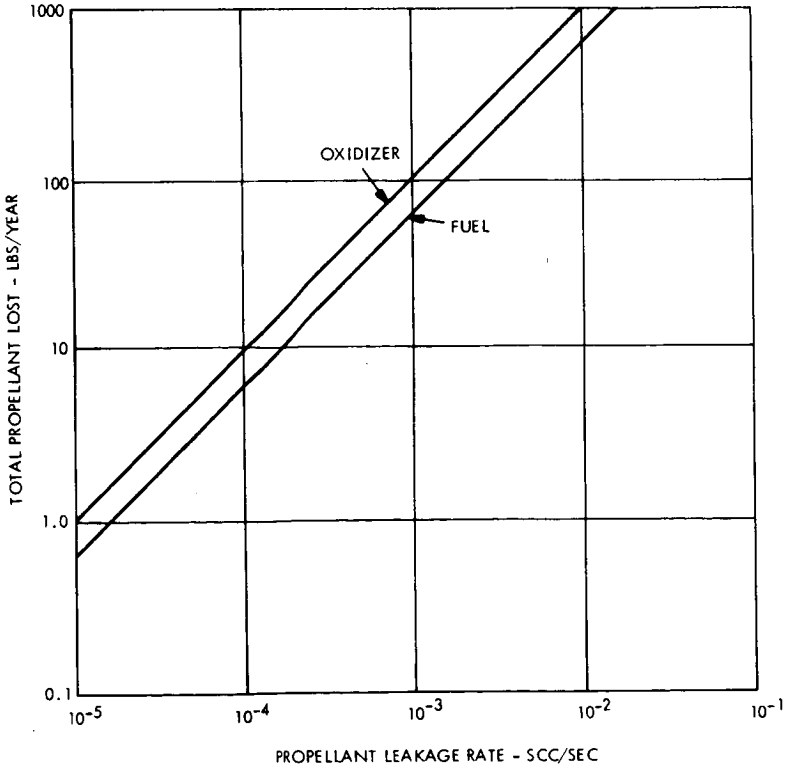

Figure 4-8. Total Propellant Lost vs. Propellant Leakage Rate

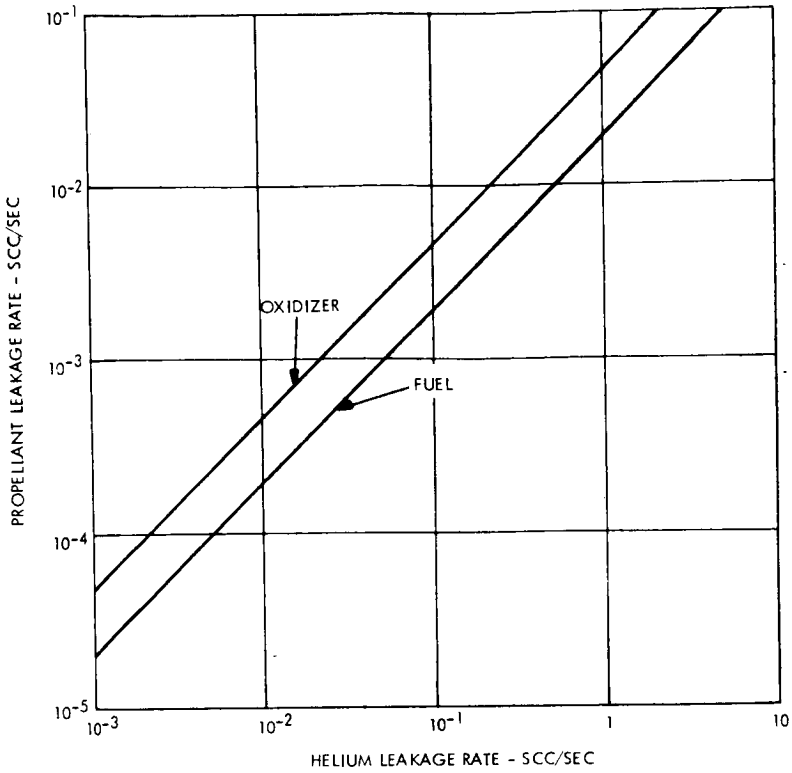

Figure 4-9. Propellant Leakage Rate vs. Helium Leakage Rate

in an optimum fashion (for combustion). In the case of single propellant leakage, it is assumed the thrust is provided by the molecular velocity of the leaking propellants according to the expression:

$$F = \frac{\dot{W}\ V}{g}$$

where

F = Thrust in pounds

$\dot{W}$ = Flow rate in pounds per seconds

g = Acceleration of gravity

V = Average molecular velocity of the fluid in feet per second

and further, the average velocity of the fluid molecules is given by the expression:

$$V = 3.28\sqrt{\frac{8k\ T}{\pi\ M}}$$

where:

V = Average molecular velocity in feet per second

k = Boltzmann's constant - 1.38×10^{-6} dyne-centimeter per degrees Kelvin

T = Absolute temperature of the fluid in degrees Kelvin

M = Mass of one molecule of the fluid

From these expressions the fluid velocities can be determined and result in a thrust of 2.3×10^{-5} lbf for fuel and 1.7×10^{-5} lbf for oxidizer. The maximum thrust level acting over the one-year life of the vehicle imparts a total impulse of 740 lbf-sec. Further, assuming that the vehicle is in the transit state results in a change of velocity of .345 meters per second due to fuel leakage and .25 meters per second for the oxidizer.

On the assumption that both fuel and oxidizer are leaking in such a fashion as to produce an I_{sp} of 280 Sec, the equation for thrust under the stated conditions gives a thrust level of 1.8×10^{-4} lbf., a total impulse of 5600 lb-second and a resultant velocity change of 2.6 meters per second. This is obviously a worst case condition, but even it can be tolerated. The more likely conditions resulting from leakage of both propellants is as described in paragraph 4.1.

The last effect of possible leakage is the compatibility of the propellants with the materials in the chamber. According to the manufacturer, although substantiating test data is limited, there is no physical change in the ablative materials due to prolonged exposure to either propellant or representative derivatives of each. Thus, this area does not appear to be a problem.

To be most effective, an isolation network in the propellant lines should be similar in design and configuration to that shown for the pressurant system. However, a definite limitation exists in that developed and qualified, normally open, squib actuated 1-1/2" valves required by the propellant line do not exist at this time. There is sufficient time within the present schedule to implement a complete program for this piece of hardware, should the need be

proven. While a redundant isolation network, as discussed, solves the problem, it should also be possible to take advantage of the considerable development and qualification effort that has been expended on the main valves for the LEMDE thrust chamber, and develop those to meet realistic and reasonable leakage requirements. Thus, the tradeoff in controlling leakage is whether to include an existing and qualified ball valve as opposed to a development and qualification program for a large (1-1/2" line diameter) explosive actuated valve to operate in a liquid line. Because of the existence of the basic hardware plus the flexibility that is available with solenoid operated valves, it is currently recommended that any development effort be expended in improving the leakage characteristics of the LEMDE main propellant valve, if required. However, to preclude catastrophic loss of hardware during pad test, pad servicing, or booster powered flight, parallel normally closed squib actuated valves (2 inch, available from Titan program) are shown in the main line.

A tradeoff study also develops in the area of whether or not a means should be provided to depressurize the propellant tanks after the orbit insertion maneuver. The disadvantage of retaining pressurized propellant tanks arises from the small probability that an initial failure, from the effects of stress corrosion or micrometeoroid impact, will lead to an explosive structural disintegration. This could result in directing of unsterile structural fragments onto paths which will impact the planet, violating the quarantine requirement.

A violent disintegration of the tank structure due to initial failure of a pressurized tank requires that the tank static stress level be high and that the stress concentration associated with local penetrations or material failures exceeds the material strength. For titanium vessels of the sort employed in the Voyager spacecraft, estimates of the critical static stress level are of the order of 60 percent of the yield strength. The significance of this critical level is that with higher static stresses, a penetration or local failure will be propagated violently, whereas if the stress is below this level, the contents of the tank will be expelled through the hole in a slow stream, without propagating or expanding the failure.

The maximum propellant tank operating conditions for the Voyager spacecraft are 300 psi tank pressure and 100°F tank temperature at a factor of safety of 2:1. This results in a hoop stress of approximately 77,000 psi. At 100°F the yield strength of 6AL4V titanium is 146,500 psi. Therefore, the maximum operating stress is 52.5% of yield which is considerably below the 60% critical level.

From the above results, it has been concluded that it should not be necessary to depressurize the Voyager propellant tanks after orbit insertion.

4.3. DESIGN SUMMARY

The result of all the tradeoff studies previously noted are shown in Figure 4-10. A summary of the propulsion subsystem characteristics is shown in Table 4-1 and a synthesized operational duty cycle is shown in Figure 4-11.

To provide additional safety in the design of the system, a burst disk and a relief valve in series are included in each pressurant line for the fuel and the oxidizer tanks.

It will also be noted on the schematic that test and service ports are provided to all sections of the propulsion module. While end-to-end testing cannot be accomplished because of the inclusion of squib actuated valves, each section can be tested for its leak tightness and functional characteristics.

Immediately upstream of each set of quad-redundant check valves in the propellant pressurant lines is a normally opened explosive valve. The function of this component is to provide positive isolation of the propellant lines after the completion of all propulsion activities. This is in conformance with the requirements for maintaining planetary quarantine. It will be noted that if either of the valves operate successfully, the isolation will be complete. Thus, there is also redundancy in the isolation function.

A preliminary failure mode and effects analysis chart is presented in Table 4-2.

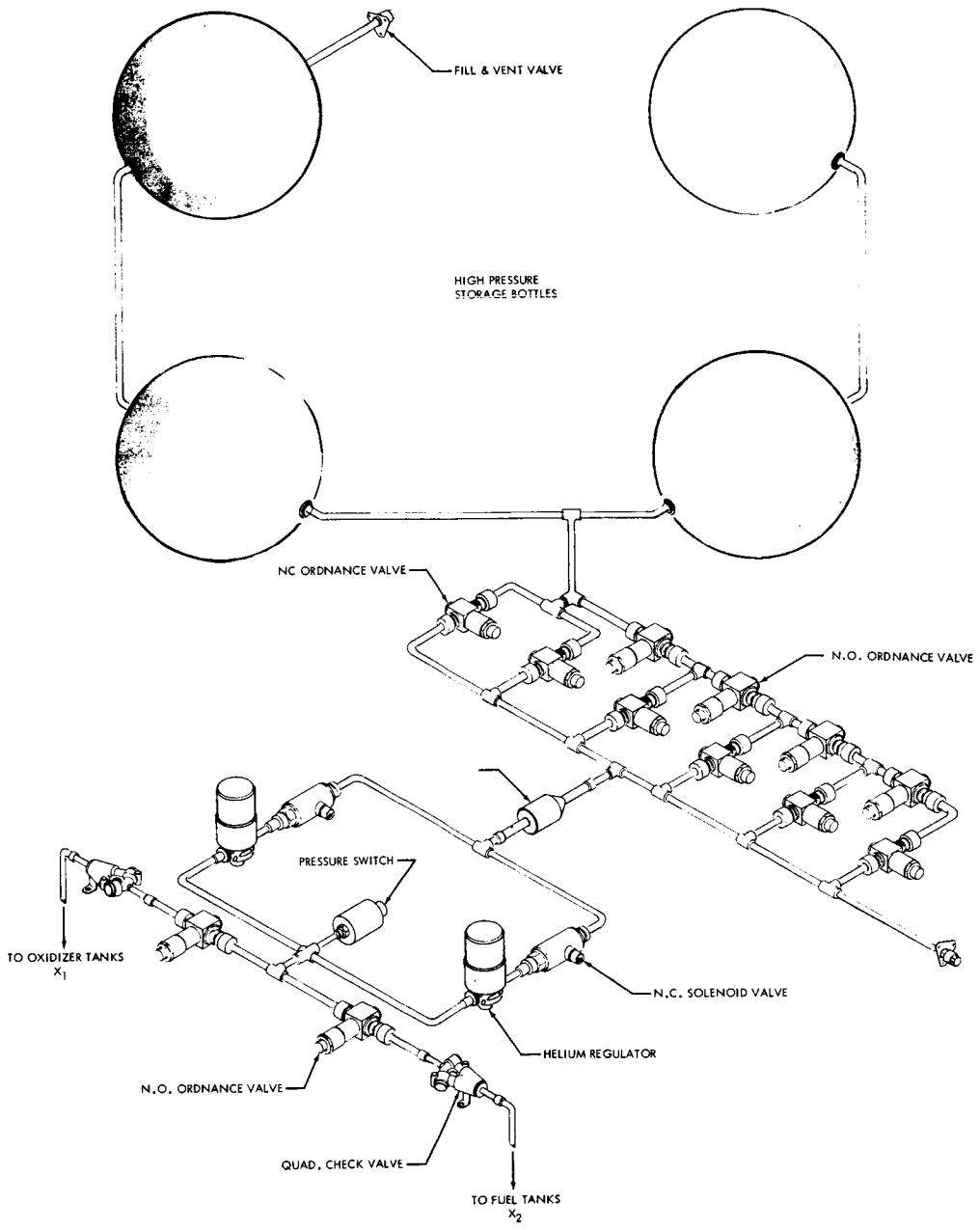

PRESSURIZATION SYSTEM

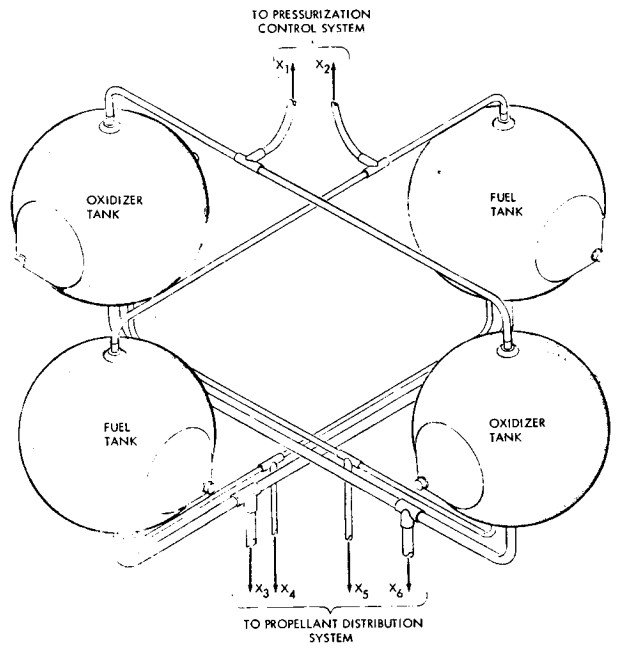

PROPELLANT TANKS & INTERCONNECTS

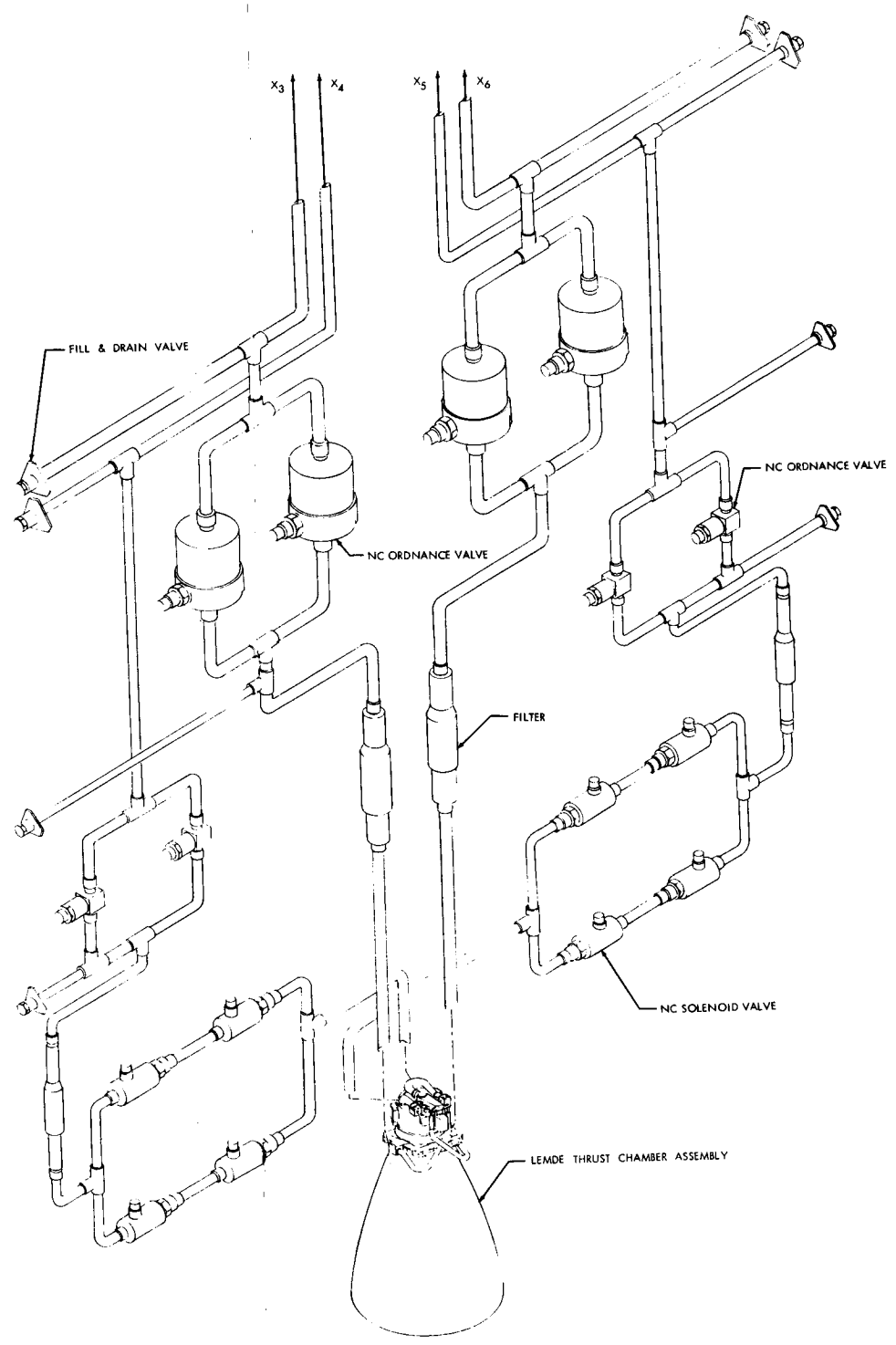

PROPELLANT DISTRIBUTION SYSTEM

Figure 4-10. Propulsion Subsystem Characteristics

Table 4-1. Propulsion Subsystem Characteristics*

General	
Propellants	
Oxidizer	N_2O_4
Fuel	A-50
Pressurant	Helium
Gross Weight, LBM (Less Structure)	12079.2
Burnout Weight, LBM	2085.3
Dry Weight, LBM	1769.7
Thrust Chamber	
Type	Ablative Chamber with radiatively cooled skirt
Expansion Area Ratio	47.5:1 W/Skirt
Throat Area, IN^2	57.01
Throat Diameter, IN	8.52
Exit Diameter, IN	58.72
Propellant System	
Total Loaded Propellant Weight, LBM	10255.7
Usable Propellant Weight, LBM	**9994.0
Propellant (Midcourse), LBM	930.0
Propellant (Retro), LBM	7050.0
Propellant (Orbit Trim), LBM	2014.0
Propellant Tank Pressure, PSIA	235
Pressurant System	
Pressurant Weight, LBM	53.9
Initial Storage Pressure, PSIA	3600

Inert Weight Breakdown - LEMDE	No.	Unit Weight (LBM)	Total Weight (LBM)
Thrust Chamber	1	409.0	409.0
Propellant Feed System			
Propellant Tank System	4	157.28	629.1
Plumbing			72.0
Unusable Propellant			261.7
Pressurization System			
Pressurant Tank	4	125.12	500.5
Plumbing			39.5
Helium			53.9
Miscellaneous Hardware			82.9
Telemetry System			36.7
Total			2085.3

*Based on Payload Weight of 8450 LBM **Includes 45.3 LBM Lost Propellant

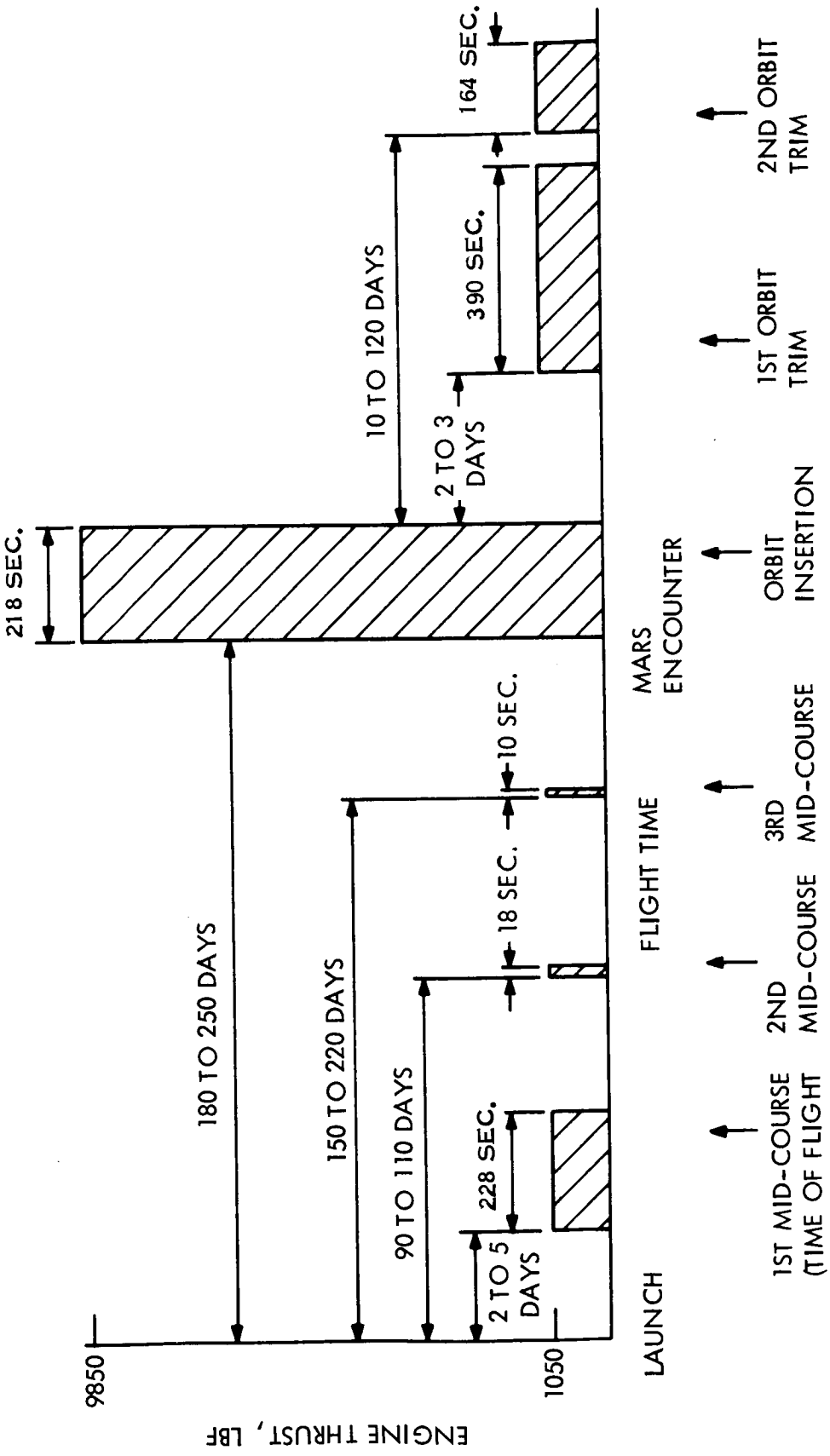

Figure 4-11. Flight Duty Cycle-1973 Voyager Mission

Table 4-2. Failure Mode and Effects - Propulsion Subsystem

COMPONENT	FUNCTION	DUTY CYCLE	FAILURE MODE	FAILURE CAUSE	FAILURE EFFECT	COMPENSATING PROVISIONS OR BACKUP
1. He Tank	Store pressurant	Continuous	a. Leakage b. Rupture	a. Diffusion through walls and imperfections b. Excessive stress	a. Ranges from none to mission failure b. Mission failure	a. 15% excess gas carried, leakage beyond this degrades or aborts mission. b. Conservative design and test
2. Transducers Temp. & Press.	Diagnostic Information	Continuous	No signal or signal in error	Several	Loss of failure analysis data	Failure has no effect on prime mission
3. High Pressure Lines & Fittings	Transmit pressurant	Continuous	a. Leakage b. Rupture	a. Diffusion through walls, joints and imperfections b. Excessive stress	a. Ranges from none to mission failure b. Mission failure	a. 15% excess gas carried; leakage beyond this degrades or aborts mission. b. Conservative design and checkout
4. Propellant & Pressurant Fill valves	Loading system on ground	At least one cycle in prelaunch	Leakage	Opening at valve seat	Ranges from none to mission failure.	Valves capped off after filling.
5. Explosive Squib Valves,NO and NC	Seal off and pressurize	All are one-shot devices	Failure to explode or operate	Squib failure or valve jam	Loss of redundancy to loss of mission	Dual bridge wires, dual squib, stand-by bank of valves
6. Filters	Remove foreign matter to protect parts	During engine operation	Blockage by foreign matter	Foreign matter in system & valve chip generation	Ranges from none to mission failure	Control of system, pressurant and propellant cleanliness
7. Solenoid valve	Control flow of pressurant to regulators	During engine operation	Failure to open or close,leakage	Stuck or frozen shaft,bad seat, failed coil	Negligible; valve out capability	Two valves in parallel
8. Pneumatic Regulator	Reduce He pressure to propellant tanks	During engine operation	Open and over-pressurization	Poppet sticking in open position	Mission degraded to mission failure.	Standby regulator provision plus sensing & switching to cut out bad regulator & cut in good regulator
9. Pressure Switch	Sense malfunction of regulator & switch to backup regulator	Only in event of regulator failure	No signal or signal in error	Broken elements distortion of elements	Mission degraded or failed but only when combined with regulator failure	Not required unless regulator fails
10. Explosive Squib Valve, NO	Isolate propellants after final maneuver	All one shot devices	Failure to explode or operate, leakage	Squib failure or valve jams	Possible contamination of planet by loss of Spacecraft	Dual bridge wires, two valves in series
11. Pressure check valve	Separate propellant vapors	Continuous	a. Leakage b. Failure to open	a.Bad seat b.Stuck or frozen shaft	a. Ranges from none to loss of mission b. Loss of mission	Quad-redundant valves for both propellant
12. Burst Diaphragms	Isolates relief valves during normal operation	One-shot device used in event of regulator failure	Premature burst	Fatigue of poor quality disk	Pressure applied to relief valves,no degradation	This feature provided to minimize leakage failure,degrades mission only when relief valves are bad
13. Relief Valve	Relieves propellant tank over pressure after rupture of Burst Diaphragms	Only in event of over pressurization of propellant tanks.	a. Leakage b. Failure to open	a. Bad seat b. Stuck or frozen shaft	a. Ranges from none to loss of mission b. Mission failure	a. Backed up by Burst Diaphragms b. Not required unless both Regulators fail.
14. Low Pressure Lines and Fittings	Transmit pressurant	Continuous	Leakage	Diffusion thru walls, joints & fittings	Ranges from none to mission failure	Excess gas carried
15. Propellant Tanks	Propellant storage	Continuous	Leak or rupture	Overpressure or overstress	Ranges from none to mission failure	Conservative design and test
16. Low pressure lines and fittings	Transmit propellants	Continuous	Leakage	Leakage through joints	Ranges from none to loss of mission	Conservative design and test
17. Explosive Squib Valve, N.C.	Isolates propellant tanks & maintain propellant off of main propellant valves during boost.	One shot devices	a.Failure to open b.Leakage	a.Squib failure or valve jams b.Bad seal	a. Loss of mission b. Negligible	Parallel redundant valve, dual bridge wires
18. Solenoid Valve	Controls flow of propellant from start tanks to thrust chamber	During engine operation	Failure to open or close,leakage	Stuck or frozen shaft, bad seat, failed coil	Negligible;pair out capability	Quad-redundancy protects from all 3 modes
19. Test Port Valve	Pressure check system on ground	At least once in pre launch checkout	Leakage	Opening at valve seat	Ranges from none to loss of mission	Valves will be capped off after final system check out
20. Variable Venturi	Regulate propellant flow to the thrust chamber	During engine operation	Actuator failure	Coil failure, stuck or frozen shaft	Ranges from degraded mission to loss of mission	Engine will start and operate at all Venturi settings
21. Fuel prevalve	Controls fuel flow to operate main propellant valves	During engine operation	Failure to open or close;leakage	Stuck or frozen shaft,failed coil, bad seat	Ranges from none to loss of mission	Redundant valve
22. Main propellant valves	Control propellant flow to the thrust chamber	During engine operation	Failure to open or close;leakage	Stuck or frozen shaft,failed coil, bad seat	Ranges from none to loss of mission	Quad-redundancy in all 3 modes
23. Thrust chamber	Mixes propellants, contains & directs hot gas	During engine operation	Rupture of chamber	Burnout of ablative material,over temperature	Loss of mission	Controlled burn times

4.4. OPERATING SEQUENCE

This section describes a step by step sequence of operation for the propulsion subsystem beginning with the pre-maneuver activities and continuing until completion of the propulsion maneuver. The normal sequence of operation will be described first, followed by a degraded, abnormal or emergency operation and concluded by proposed inflight "health checks" of the subsystem. All the component find numbers referenced in this operating sequence are listed on the propulsion Subsystem Schematic Figure 4-12.

4.4.1. Normal Operating Sequence

4.4.1.1. Pre-Maneuver Activities

The timing of these activities is not critical. The optimum time would be sufficiently in advance to allow telemetry readout of pressures, temperatures and valve positions which could allow changes to alternate modes of operation if required.

a. Open pressure isolation squib valve K2 to provide pressurant to solenoid valves K11 and K12.

b. Open propellant isolation squib valves K15, K16, K17, K18, K19, K20, K25, and K26 to allow propellant flow to the quad redundant start valves and main propellant valves. These squib valves do not have to be activated simultaneously but may be sequenced in any manner; however, it would be best to activate them in pairs, as K15 and K16, K17 and K18, etc. The activation of these valves is required only for the first maneuver.

c. Solenoid valve K11 is open allowing pressurant to flow through regulator R1 to pressurize propellant tanks to the desired level.

d. Select high or low thrust level mode. For orbit insertion, select the high thrust level mode sifficiently in advance to allow for the possibility of orbit insertion at the low thrust mode if it is apparent that the high thrust mode can not be obtained.

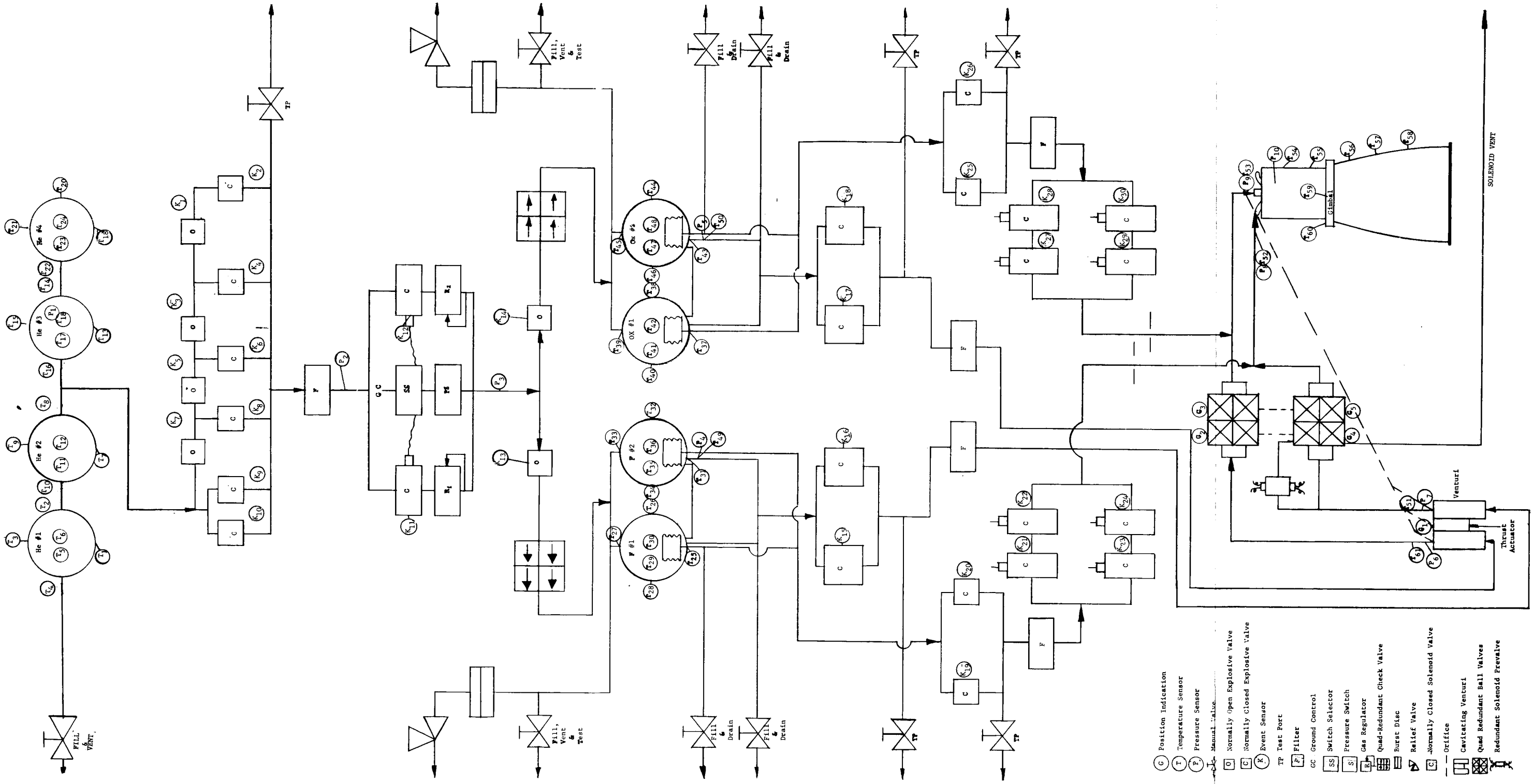

PROPULSION SUBSYSTEM SCHEMATIC

Figure 4-12. Propulsion Subsystem Schematic

FOLDOUT FRAME

95

FOLDOUT FRAME

95/86

4.4.1.2. Start Sequence

a. At T=O, open solenoid valves K21, K22, K23, K24, K27, K28, K29, and K30 (Quad redundant start line valves) simultaneously to allow propellant flow from the start tanks into the engine. The engine fires by hypergolic ignition.

b. After propellants have been settled, (T+12) open the main propellant valves G2, G3, G4, and G5.

c. Approximately 3 seconds after step 2, at T+15 sec., close start tank solenoid valves K21, K22, K23, K24, K27, K28, K29, and K30, terminating propellant flow from the start tanks.

4.4.1.3. Shut Down Sequence

After desired correction or insertion has been accomplished, the autopilot, with a timer as backup, will provide a signal to close the main propellant valves G2, G3, G4, and G5, which will shut down the engine.

4.4.2. Alternate Modes of Operation

a. If pressure isolation squib valve K2 fails to open during the initial pre maneuver activity, squib valve K4 will be opened to provide pressurant to the solenoid valves K11 and K12. If squib valve K4 fails to open, squib valve K6 will be opened and so forth.

b. In the event propellant tank pressure exceeds specifications (either high or low) during a maneuver operation, the sequencer will automatically open solenoid valve K12 and close solenoid valve K11. This will put regulator R2 into use and take regulator R1 out. Command override for either valve is provided.

4.4.3. Long Term Shut Down Sequence

a. To reduce pressurant leakage from the system during long coast periods, the pressurant spheres may be isolated by closing the normally open squib valve which is located just up-stream of the valve which is allowing flow. For example, if valve K2 is open, close valve K1, or if valve K4 is open, close valve K3, etc.

b. If isolation of the pressurant spheres is used, the normally closed squib valve just up-stream of the valve used to isolate the system must be opened during the next pre-maneuver activities. For example, if valve K1 was used to isolate the system, squib valve K4 must be opened. If valve K3 was used to isolate the system, valve K6 must be opened. Five parallel paths for the pressurant flow are provided. Four flow paths are for normal usage with one path being provided for backup. Pressurant isolation steps must be coordinated with the planned mission profile to provide for the required number of maneuvers.

4.4.4. In-Flight Health Checks

Health checks on the propulsion subsystem will be performed during flight. These checks will consist of: 1) providing gimbal signals to the engine actuators and evaluating the actuator position feedback signals, 2) providing high/low thrust selection signals to the venturi actuator and evaluating the venturi position signals, 3) providing open/close signal to pressurant solenoid valves and evaluating position indication and pressure changes, and 4) evaluating all pressurant system and propellant tank pressure and temperature telemetry readouts during flight.

4.5. TELEMETRY REQUIREMENTS

The telemetry requirements presented in Table 4-3 were selected primarily to verify propulsion system performance and to diagnose malfunctions and/or failures should they occur.

A history of events, pressures, temperatures, and valve positions is necessary for in cruise and post maneuver evaluation of system status or operations. These analyses will provide a basis for improving spacecraft performance on subsequent maneuvers and/or launch operations. Maneuvers may be aborted if necessary and attempted later if proper techniques are employed in telemetry sampling.

Examples of telemetered data utilization which justify the selection of the listed instrumentation are:

Table 4-3. Telemetry List (Sheet 1 of 3)

	SYMBOL	VARIABLE MEASURED		SAMPLE RATE OPERATING MODE (sec)	SAMPLE RATE COAST MODE (sec)	RANGE	(2) CATEGORY
(1)	T1	He Bottle #1 Temp	Pos 1	14.92	2984	-100 to 200°F	IC
	T2	" " " "	Pos 2	"	"	"	"
	T3	" " " "	Pos 3	"	"	"	"
	T4	" " " "	Pos 4	"	"	"	"
	T5	" " " "	Pos 5	"	"	"	"
	T6	" " " "	Pos 6	"	"	"	"
	T7	" " #2 "	Pos 1	"	"	"	"
	T8	" " " "	Pos 2	"	"	"	"
	T9	" " " "	Pos 3	"	"	"	"
	T10	" " " "	Pos 4	"	"	"	"
	T11	" " " "	Pos 5	"	"	"	"
	T12	" " " "	Pos 6	"	"	"	"
	T13	" " #3 "	Pos 1	"	"	"	"
	T14	" " " "	Pos 2	"	"	"	"
	T15	" " " "	Pos 3	"	"	"	"
	T16	" " " "	Pos 4	"	"	"	"
	T17	" " " "	Pos 5	"	"	"	"
	T18	" " " "	Pos 6	"	"	"	"
	T19	" " #4 "	Pos 1	"	"	"	"
	T20	" " " "	Pos 2	"	"	"	"
	T21	" " " "	Pos 3	"	"	"	"
	T22	" " " "	Pos 4	"	"	"	"
	T23	" " " "	Pos 5	"	"	"	"
	T24	" " " "	Pos 6	"	"	"	"
	T25	Fuel Tank #1 Temp	Pos 1	"	"	0 to 200°F	"
	T26	" " " "	Pos 2	"	"	"	"
	T27	" " " "	Pos 3	14.92	2984	"	IC
	T28	" " " "	Pos 4	"	"	"	"
	T29	" " " "	Pos 5	"	"	"	"
	T30	" " " "	Pos 6	"	"	"	"
	T31	" " #2 "	Pos 1	"	"	"	"
	T32	" " " "	Pos 2	"	"	"	"
	T33	" " " "	Pos 3	"	"	"	"
	T34	" " " "	Pos 4	"	"	"	"
	T35	" " " "	Pos 5	"	"	"	"
	T36	" " " "	Pos 6	"	"	"	"
	T37	Oxid. Tank #1 Temp	Pos 1	"	"	"	"
	T38	" " " "	Pos 2	"	"	"	"
	T39	" " " "	Pos 3	"	"	"	"
	T40	" " " "	Pos 4	"	"	"	"
	T41	" " " "	Pos 5	"	"	"	"
	T42	" " " "	Pos 6	"	"	"	"
	T43	" " #2 "	Pos 1	"	"	"	"
	T44	" " " "	Pos 2	"	"	"	"

Table 4-3. Telemetry List (Sheet 2 of 3)

	SYMBOL	VARIABLE MEASURED		SAMPLE RATE OPERATING MODE (sec)	SAMPLE RATE COAST MODE (sec)	RANGE	CATEGORY
	T45	Oxid. Tank #2 Temp	Pos 3	14.92	2984	0 to 200°F	IC
	T46	" " " "	Pos 4	"	"	"	"
	T47	" " " "	Pos 5	"	"	"	"
	T48	" " " "	Pos 6	"	"	"	"
	T49	Fuel Tank Outlet Temp		"	-	"	IIA, B, C
	T50	Oxid. " " "		"	-	"	"
	T51	Fuel Venturi Outlet		"	-	"	"
	T52	Engine Inlet Fuel Temp		"	-	"	"
	T53	Engine Inlet Oxid. Temp		"	-	"	"
	T54	T/C Ext. Wall Temp. #1		"	-	0 to 1000°F	"
	T55	" " " " #2		"	-	"	"
	T56	" " " " #3		"	-	"	"
	T57	" " " " #4		"	-	"	"
	T58	" " " " #5		"	-	"	"
	T59	Gimbal Surface Temp #1		"	-	"	"
	T60	" " " #2		"	-	"	"
	T61	Oxid. Venturi Outlet Temp		"	-	0 to 200°F	"
	P1	He Bottle Press		"	2984	0 to 4000 psi	IC
	P2	He Regulator Inlet Press		"	-	0 to 4000 psi	"
	P3	He " Outlet "		"	-	0 to 400 psi	"
	P4	Fuel Tank Outlet Press		"	2984	"	"
	P5	Oxid. " " "		"	2984	"	"
	P6	Oxid. Venturi Outlet Press		"	-	"	IIA, B, C
	P7	Fuel " " "		"	-	"	"
	P8	Engine Inlet Fuel Press		"	-	"	"
	P9	" " Oxid. "		"	-	"	"
	P10	T/C Injector Press		1.492	-	0 to 200 psi	"
(3)	K1	Event He Cont Expl V1v Bank #1		14.92	-	0 to 28 VDC	IIA
	K2	" " " " " " "		"	-	"	"
	K3	" " " " " " #2		"	-	"	"
	K4	" " " " " " "		"	-	"	"
	K5	" " " " " " #3		"	-	"	"
	K6	" " " " " " "		"	-	"	"
	K7	" " " " " " #4		"	-	"	"
	K8	" " " " " " "		"	-	"	"
	K9	Event He Sol v1v. Abv. Reg. Bank #1		"	-	"	"
	K10	" " " " " " #2		"	-	"	"
	K11	" Fuel Pressurant Isolation Valve		"	-	"	"
	K12	" Oxid. " " "		"	-	"	"
	K13	" Fuel Prevalve #1		"	-	"	"
	K14	" " " #2		"	-	"	"
	K15	" Oxid. " #1		"	-	"	"
	K16	" " " #2		"	-	"	"

Table 4-3. Telemetry List (Sheet 3 of 3)

SYMBOL	VARIABLE MEASURED	SAMPLE RATE OPERATING MODE (sec)	SAMPLE RATE COAST MODE (sec)	RANGE	CATEGORY
K17	Event Expl. Valve #1 in Low Thrust Fuel Line	14.92	-	0 to 28 VDC	IIA
K18	" " " #2 " " " " "	"	-	"	"
K19	" Sol Valve #1 " " " " "	"	-	"	"
K20	" " " #2 " " " " "	"	-	"	"
K21	" " " #3 " " " " "	"	-	"	"
K22	" " " #4 " " " " "	"	-	"	"
K23	" Expl. Valve #1 " " " Oxid. "	"	-	"	"
K24	" " " #2 " " " " "	"	-	"	"
K25	" Sol " #1 " " " " "	"	-	"	"
K26	" " " #2 " " " " "	"	-	"	"
K27	" " " #3 " " " " "	"	-	"	"
K28	" " " #4 " " " " "	"	-	"	"
G1	Venturi Actuator Position	"	-	0 to 100%	"
G2	Main Propellant Valve Position #1	"	-	"	"
G3	" " " " #2	"	-	"	"
G4	" " " " #3	"	-	"	"
G5	" " " " #4	"	-	"	"

(1) One temperature readout for each pressurization bottle and propellant tank which is an average of the six measurements on each component.

(2) CATEGORY I (Required)

A. Measurements needed to perform certain command and control flight operations.

B. Measurements needed to ascertain the command and control status of the spacecraft.

C. Measurements needed to detect malfunctions which can be alleviated by a command control action.

CATEGORY II (Desired)

A. Measurements which can support diagnostic failure analyses.

B. Measurements which can support corroboration of the system design.

C. Measurements which can indicate future system design needs.

(3) Event and position requirements will be shown as "on or off" state in the telemetry readout.

a. Pre and post firing helium bottle temperatures and pressure allow calculation of gas usage during maneuvers.

b. Helium bottle temperature and pressures histories enable the detection and calculation of gas leakage.

c. Engine propellant inlet pressures and temperatures can be used to calculate propellant flow rates. Line and component resistances must also be known.

d. For fixed geometry systems, chamber pressure can be used to calculate engine thrust.

e. Helium bottle, thrust chamber, and propellant tank temperature measurements allow the confirmation of thermal design.

f. Thrust actuator position indicator will allow checkout of the actuator prior to actual use.

g. In case of system malfunction, the event signals may be utilized to pinpoint specific failures.

h. Pressurization system pressures and temperatures may indicate regulator malfunction and provide the signal through the switch selector to change to the other regulator.

i. Thrust chamber assembly temperatures allow the confirmation of thermal analysis and determination of heat inputs to the vehicle.

4.6. POWER REQUIREMENTS

The electrical power requirements for the propulsion subsystem are shown in Table 4-4.

4.7. SYSTEM WEIGHT

A weight summary based on the system schematic is shown in Table 4-5.

Table 4-4. Propulsion Subsystem Power Requirements (Sheet 1 of 2)

Nomenclature	Qty	Voltage (DC)	Unit Power (Watts)	Total Power (Watts)	Remarks
Explosive Valve	8	28	168*	1344*	Actuated individually as required by system (normally 2 per maneuver)
Solenoid Valve	2	28	56	122*	
Pressure Switch	1	28	7	7	Required continuously through each maneuver
Switch Selector	1	28	7	7	Required continuously through each maneuver
Explosive Squib Valve	2	28	168*	366*	Required after last maneuver only
Explosive Squib Valve	8	28	168*	1344*	Required prior to first maneuver only
Solenoid Valve	8	28	56	488	Required for first 20 seconds of each maneuver
Pressure Transducer	3	3.2	.010	.030	Required continuously through mission
Pressure Transducer	7	3.2	.010	.07	Required continuously through each maneuver
Temperature Transducer	48		.0165	.78	Required continuously through mission
Temperature Transducer	13		.0165	.22	Required continuously through each maneuver

Table 4-4. Propulsion Subsystem Power Requirements (Sheet 2 of 2)

Nomenclature	Qty	Voltage (DC)	Unit Power (Watts)	Total Power (Watts)	Remarks
Engine Venture Actuator	1				
Steady State Holding		28	90**		Required continuously through engine burn
Steady State Holding (One channel failed)		28	180**		
Standby Holding - no load		28	15**		Required from just after thrust level selection until engine start
Actuation Motion (stall)		28	280**		Required for thrust level selection
Actuation Motion (initial peak transient of .005 sec. max. duration)		28	336**		
Actuation Motion (One channel failed)		28	270*		
Prevalve	1	28	100	100	Required continuously through each maneuver
Ball Shutoff Valve	1	28	265	265	Required continuously through each maneuver

*Pulses of 50 Milliseconds Maximum
**Additional .80 watts required at 15VDC as reference and command voltage

Table 4-5. Propulsion Subsystem Weight Summary

Component	Qty Per System	Unit Weight lb.	Total Weight lb.	Line Size in.
I. Pressurization System				
A. Tank Assembly				
1. Tanks	4	125.12	500.5	
Total				
B. Control Assembly				
1. Ordnance Valve (N. O.)	6	1.75	10.5	0.5
2. Ordnance Valve (N. C.)	4	1.75	7.0	0.5
3. Filter	1	2.5	2.5	0.5
4. Solenoid Valve (N. C.)	2	1.25	2.5	0.5
5. Regulator	2	5.0	10.0	0.5
6. Switch selector	1	0.25	0.25	-
7. Pressure switch	1	0.7	0.7	0.5
8. Check valve (quad.)	2	1.0	2.0	0.5
Total			35.5	
C. Fill, Vent, & Test Ass'y.				
1. Fill Valve (Manual)	3	1.0	3.0	0.5
2. Test Valve (Manual)	1	1.0	1.0	0.5
Total			4.0	

Table 4-5. Propulsion Subsystem Weight Summary (Sheet 2 of 4)

Component	Qty Per System	Unit Weight lb.	Total Weight lb.	Line Size in.
D. Misc. Hardware				
1. Relief Valve/Burst Disc	2	2.0	4.0	0.5
2. Distribution Manifold	2	1.5	3.0	0.5
3. Tubing & Fittings			13.7	0.5
4. Misc. bracketry			9.5	
Total			30.2	
TOTAL PRESSURIZATION SYS.			570.2	
II. Propellant System				
A. Tank Assembly				
1. Tank	4	113.28	453.1	
2. Baffles & screens	4	24.0	96.0	
3. Positive Expulsion Bellows Assembly	4	20.0	80.0	
Total			629.1	
B. Control Assembly				
1. Ordnance Valve (N. C.)	4	8.0	32.0	1.5
2. Filter	2	3.0	6.0	1.5
3. Ordnance Valve (N. C.)	4	1.75	7.0	0.5
4. Filter	2	1.5	3.0	0.5
5. Solenoid Valve (N. C.)	8	1.25	10.0	0.5
Total			58.0	

Table 4-5. Propulsion Subsystem Weight Summary (Sheet 3 of 4)

Component	Qty Per System	Unit Weight lb.	Total Weight lb.	Line Size in.
C. Fill, Vent, & Test A'ssy				
1. Fill Valve (Manual)	2	1.0	2.0	0.5
2. Fill Valve (Manual)	2	4.0	8.0	1.5
3. Test Valve (Manual)	4	1.0	4.0	0.5
Total			14.0	
D. Misc. Hardware				
1. Tubing & Fittings			32.1	
2. Misc. Bracketry			20.6	
Total			52.7	
TOTAL PROPELLANT SYSTEM WEIGHT			753.8	
III. Telemetry System				
1. Pressure Transducers	10	0.25	2.5	
2. Temperature Sensors	61	0.15	9.2	
3. Cable & Misc. Bracketry			25.0	
Total			36.7	
IV. Engine System				
1. Engine	1	409.0	409.0	
Total			409.0	
TOTAL PROPULSION SYSTEM DRY WEIGHT			1769.7	

Table 4-5. Propulsion Subsystem Weight Summary (Sheet 4 of 4)

Component	Qty Per System	Unit Weight lb.	Total Weight lb.	Line Size in.
V. Residuals				
A. Pressurant				
1. Storage bottles	4	2.55	10.2	
2. Propellant tanks	4	10.92	43.7	
B. Propellant				
1. Unusual propellant			105.3	
2. Random outage			124.6	
3. Fuel bias			31.8	
Total			315.6	
TOTAL PROPULSION SYSTEM WEIGHT AT BURN-OUT			2085.3	
VI. LOST PROPELLANT (Start/ stop transient)			45.3	
TOTAL PROPULSION SYSTEM WET LAUNCH WEIGHT (Less Usable Propellant)			2130.6	

Table 4-6 covers random outage quantities for a 9994 lb. propellant load (nominal 1973). Table 4-7 covers quantities of trapped, residual, and lost propellant inventory for a 9994 lb. usable propellant load. A summary of the total propellant inventory is shown in Table 4-8. Figure 4-13 defines fuel bias, random outage, unusable propellants as a function of usable propellant load.

Table 4-6. Random Outage Quantities
for
9994 lb Usable Propellant Load
(Nominal 1973)

	Fuel	Oxidizer
* Check valve variation (± 0.5 psi)	15.1	22.3
* Isolation squib variation (± 0.5 psi)	7.8	11.2
* Engine repeatability (O/F = 1.6 ± 0.014)	34.2	51.4
* Thrust vector - C.G. alignment (± 1.26°)	8.0	12.9
* Loading accuracy (± 0.5%)	19.5	31.0
* Propellant filter clogging (F, +0.5 psi 0, + 0.7 psi)	5.6	13.5
* Check valve malfunction (+1.5 psi)	23.5	33.5
Root sum square ($\sigma_{rss} = \sqrt{\Sigma \sigma_i^2}$)	49.6	75.0

* Criteria obtained from (Reference 1) & corrected for propellant loading & configuration variations.

Reference (1) TWR Report on Lem Descent Stage Application; Final Report, Volume I - Propulsion

Table 4-7. Quantities of Trapped, Residual, & Lost Propellants

	Fuel	Oxidizer
Trapped Propellant		
Propellant Lines	12.7	20.3
Engine	9.2	14.8
Total Trapped	21.9	35.1
Residuals in Tanks		
* Tank Wetting	3.7	5.9
* Propellant Vapor	2.1	31.4
Start Tanks	2.0	3.2
Total Residuals	7.8	40.5
Lost Propellant		
Start transient (6 cycles)	6.0	7.8
Shutdown transient (5 cycles)	14.5	17.0
Total Lost	20.5	24.8
TOTAL TRAPPED, RESIDUALS & LOST	50.2	100.4

* Values obtained from Reference (1)

Table 4-8. Propellant Inventory Summary

for

Nominal 1973

	QUANTITY (LB)		
	Fuel	Oxidizer	Total
Usable Propellants (1973)	3826.4	6122.3	9948.7
Unusable Propellants - Trapped, Residuals & Lost	50.2	100.4	150.6
Random Outage - Root sum square	49.6	75.0	124.6
Bias	31.8	-	31.8
Total Unusable, Outage, & Bias	131.6	175.4	307.0
TOTAL LOADED PROPELLANT	3958.0	6297.7	10255.7

4.8. INTERFACE DEFINITION

The electrical and mechanical interfaces between the propulsion subsystem and the indicated subsystems are described in the following paragraphs.

4.8.1. Electrical Interfaces

The electrical interfaces are shown schematically in Figure 4-14 which lists the telemetry outputs below each propulsion element. A functional interface block diagram is shown in Figure 4-15. This diagram depicts schematically the component location, the electrical signal required to operate the component, and the source of that signal.

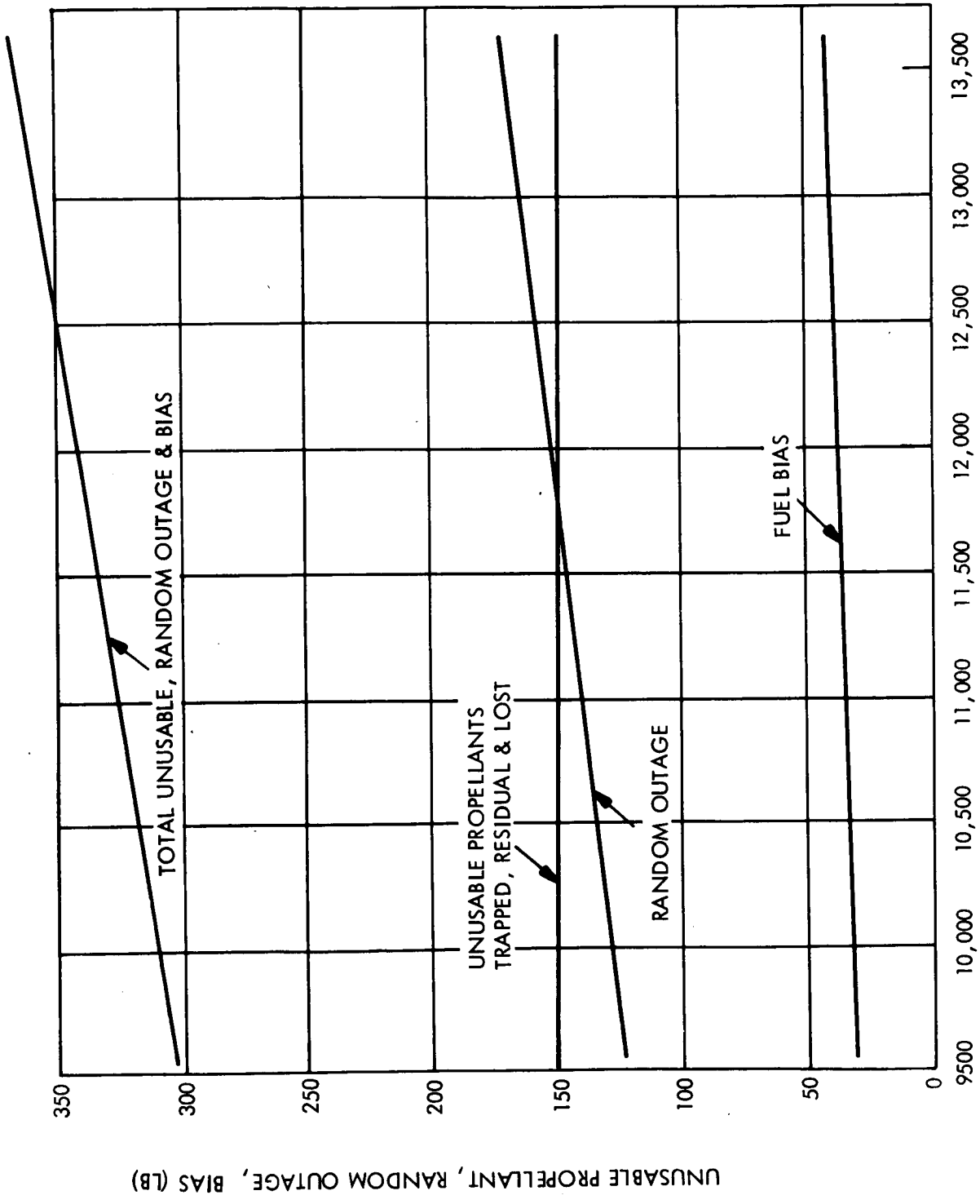

Figure 4-13. Propellant Required to Accomp. Mission

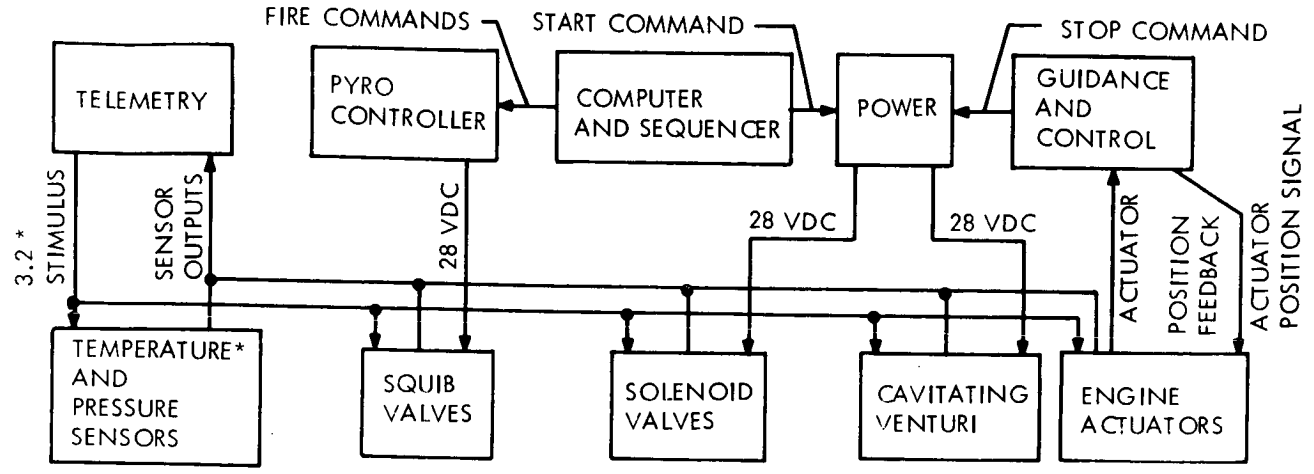

HE TANK PRESS (1)
HE TANK SKIN TEMP. (24)
HE REGULATOR INLET PRESS (1)
HE REGULATOR EXIT PRESS (1)
PROPELLANT TANK PRESS (2)
PROPELLANT TANK TEMP (26)
VENTURI EXIT PRESS (2)
VENTURI EXIT TEMP (2)
ENGINE INLET PRESS (2)
ENGINE INLET TEMP. (2)
THRUST CHAMBER EXTERNAL SURFACE TEMP (5)
COMBUSTION CHAMBER PRESSURE (1)
GIMBAL TEMP. (2)

PRESSURANT N.O. (6)
PRESSURANT NC (4)
PROPELLANT NC (4 SETS OF 2)

PRESSURANT N.C. (2)
PROPELLANT N.C. (4 SETS OF 2)
MAIN PROPELLANT BALL VALVES (1 SET OF 4)

THRUST ACTUATOR (1)

GIMBAL ACTUATOR (2)

*NO VOLTAGE STIMULUS REQUIRED FOR TEMPERATURE SENSORS

Figure 4-14. Electrical Interfaces for Propulsion Subsystem

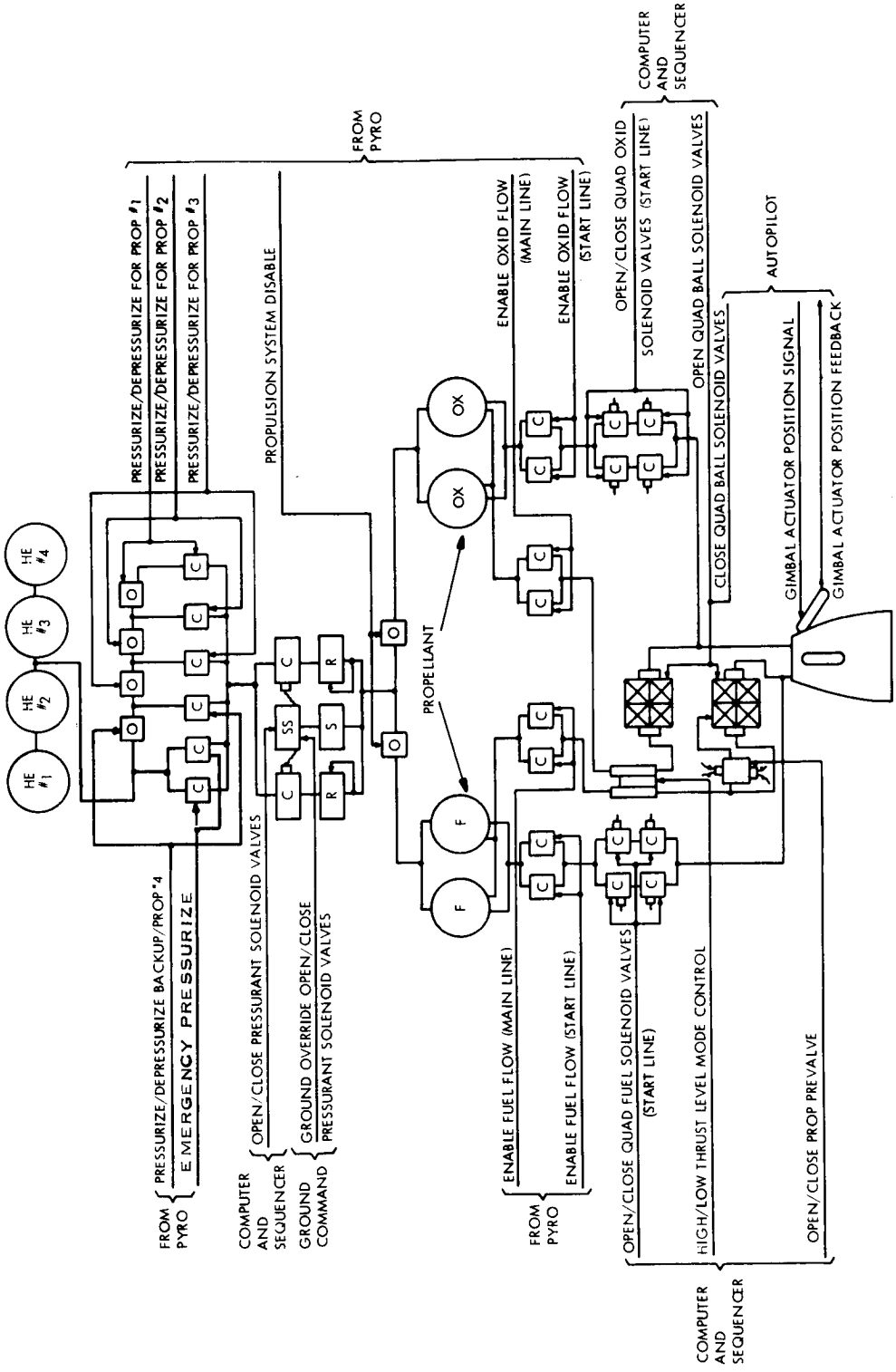

Figure 4-15. Propulsion Functional Interface Block Diagram

4.8.2. Mechanical Interfaces

The mechanical interfaces consists of the physical, environmental, and operational controls required to ensure proper mating of the indicated subsystems to the propulsion subsystem. These interfaces are described in Table 4-9.

Table 4-9. Mechanical Interfaces For Propulsion Subsystem

Subsystem	Interface
Spacecraft Bus	a. Attachment points between propulsion subsystem and bus structure.
	b. Electrical harness connectors to bus connectors.
Environmental Control	a. Propellant tank heaters and thermostatic controls.
	b. Insulation and radiation shielding for maintaining propulsion subsystem temperature between +40°F and +100°F.
Operational Service Equipment	a. Provide hardpoints for support and handling fixture.
	b. Provide adjustment for aligning thrust vectors relative to planetary vehicle CG.
	c. Provide fill, drain, and test ports.

4.9. TEST & SERVICING

Testing of the propulsion module will be accomplished at two servicing panels. Access to these panels will be provided in the structure above the electronics bay.

One service panel will provide services for propellant loading, pressurization and pneumatic testing. This panel will provide for the isolation of oxidizer and fuel access points and will contain all pneumatic pressurization and test points. Manual valves will be provided for isolation during test and final loading procedures prior to sealing the system. All access points will be double sealed prior to launch. Manual valves will be designed such that all valve stems are capable of being capped prior to launch. Trays will be provided in the basic spacecraft structure to prevent any possible propellant spillage from contacting other parts of the vehicle equipment.

The other service panel will provide electrical service to the spacecraft. The design will be such that the connection points are held to a minimum (preferably one). This panel will provide the capability of checking out the propulsion electrical network with tests such as continuity, current and voltage monitoring, squib valve "no fire" tests and simulated flight profile. It will also contain a limited number of hardwire instrumentation channels

The basic layout of the propellant service panel is shown in Figure 4-16 and Figure 4-17.

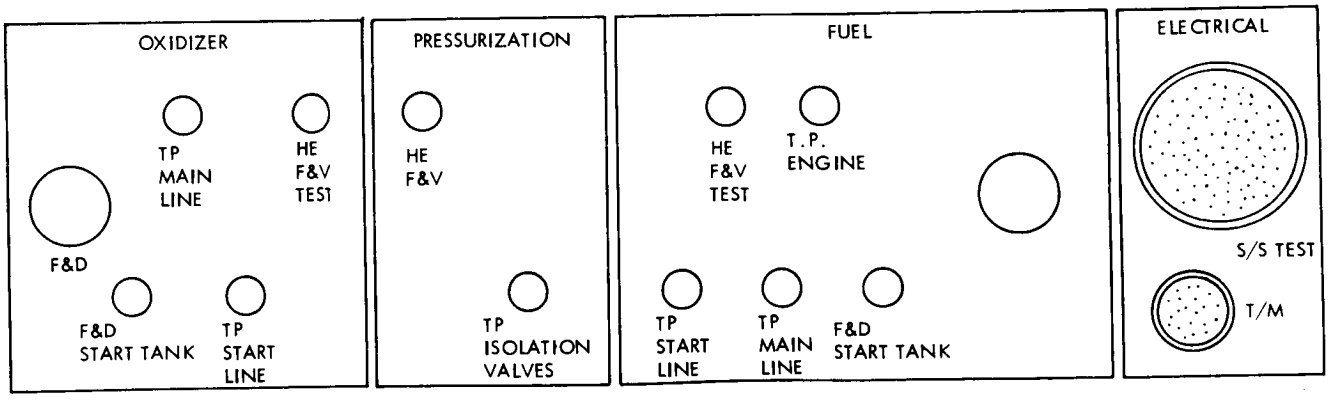

Figure 4-16. Propulsion Subsystem Servicing and Test Panel Schematic

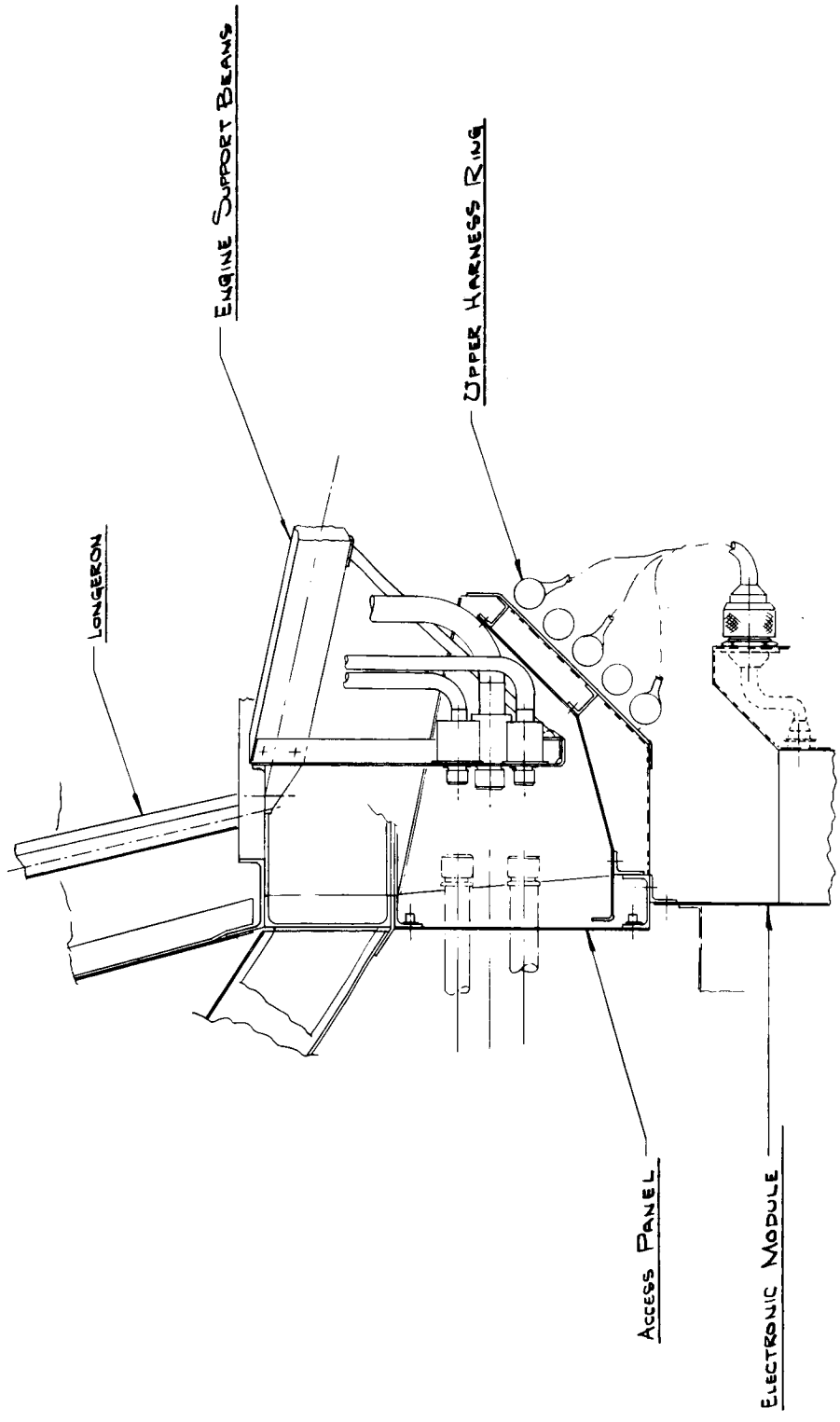

Figure 4-17. Propulsion Servicing Panel Location

5. ALTERNATE DESIGN APPROACHES

In preparing the system update reflected in this report, the major effort was spent in designing a system around the LEMDE thrust chamber assembly. However, to investigate more fully the total liquid propulsion picture, several alternate designs were investigated in varying degrees of depth. The principal efforts in this area were spent on a LEMDE system, using auxiliary thrusters for midcourse and orbit trim maneuvers, with the main chamber in standby for these functions. Under normal operations, the main chamber would only be used for the orbit insertion maneuver. The second major effort was spent in an investigation of the Agena engine as a modular replacement for the LEMDE thrust chamber assembly. This represented a radical departure from the LEMDE system in that it is a turbo-pumped system. Additional effort was expended in adapting the thrust chamber assembly used on Titan transtage for application to Voyager. Lastly, limited data is presented based on an approach using four Apollo subscale thrust chambers for all propulsive efforts.

Acknowledgement is hereby made to the Bell Aerosystems of Buffalo, N.Y., for their contribution and assistance in supplying data on the Agena engine and to the Aerojet General Corporation, Sacramento, California, for their contributions of the transtage and Apollo subscale system data.

5.1. LEMDE/AUXILIARY THRUSTERS

An alternate LEMDE configuration incorporating four auxiliary thrusters to be used for midcourse corrections, orbit trim, and propellant settling is shown in Figure 5-1. A trade study was conducted to examine the implications of employing this auxiliary thruster system on the Voyager spacecraft to augment the capabilities of the LEMDE engine for performing propulsive maneuvers.

The auxiliary thrusters are considered to be of benefit to the Voyager spacecraft in that they can be used to (1) allow the LEMDE system to be sealed off until orbit insertion, (2) ease the requirement imposed on the autopilot and gimbal actuator for LEMDE, and (3) reduce leakage during period of long coast. Details of these aspects are discussed in VOY-D-274.

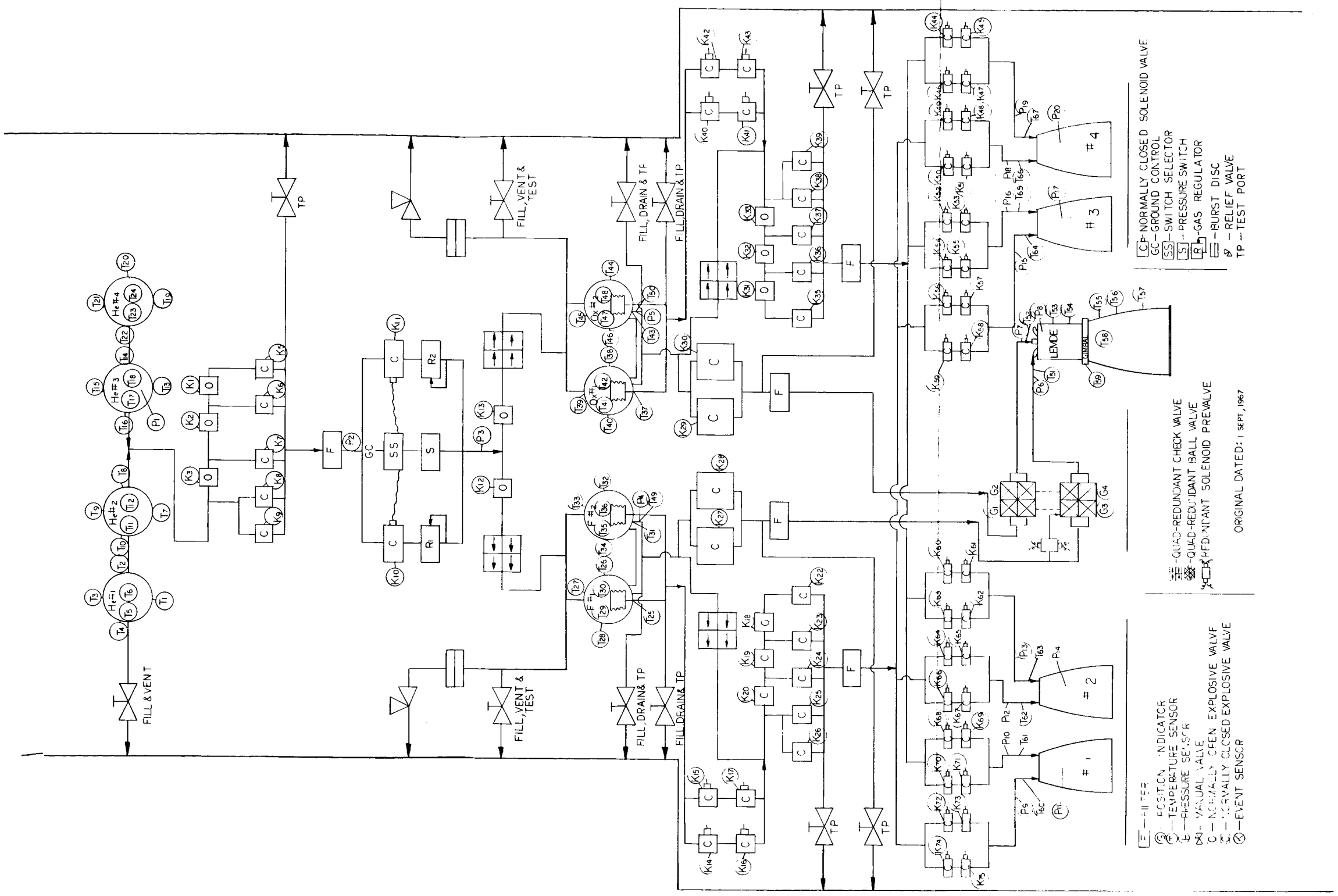

Figure 5-1. Propulsion Subsystem Schematic/Auxiliary Thrusters

FOLDOUT FRAME

FOLDOUT FRAME

The system design consists of four 100-lbf thrust bipropellant engines symmetrically located about the roll axis and properly oriented to the pitch and yaw axes. A positive expulsion system (start tanks) is utilized for propellant acquisition under zero-g conditions. The start tanks are an integral part of the main propellant tanks and are of the same configuration as those used in the baseline propulsion subsystem.

Squib valves isolate the LEMDE until the main engine is required for orbit insertion. If long duration engine operation is required for mid-course maneuver or orbit trim, propellants are acquired from the main tanks after propellant settling by the auxiliary thrusters. Series-parallel squib valves may be used to isolate the auxiliary thrusters if excess leakage is detected.

The addition of auxiliary thrusters complicates the schematic of the system because of the addition of many components. Each of these components is a potential source of failure and therefore probably has a degrading effect on reliability. Also the propulsion system weight is increased by approximately 117 pounds. The increase in engine specific impulse (295 lbf-sec/lbm for auxiliary thrusters as compared to 289 lbf-sec/lbm for LEMDE, low thrust) does not overcome the increase in dry weight within the payload range of interest.

The addition of the thrusters also complicates the spacecraft design and degrades to some extent the modularity of the propulsion subsystem.

5.1.1. Performance Data

Based on data for thrust chambers of the type envisioned for this application (Marquardt R4D or RMD C-1), a delivered specific impulse of 295 seconds can be expected. The requirement to provide an impulse bit of any magnitude with a tailoff impulse uncertainty of less than 107 lb-sec is well within the capabilities of the thrusters. Figure 5-2 shows that complete maneuvers can be made within the allowable tailoff impulse bit variations.

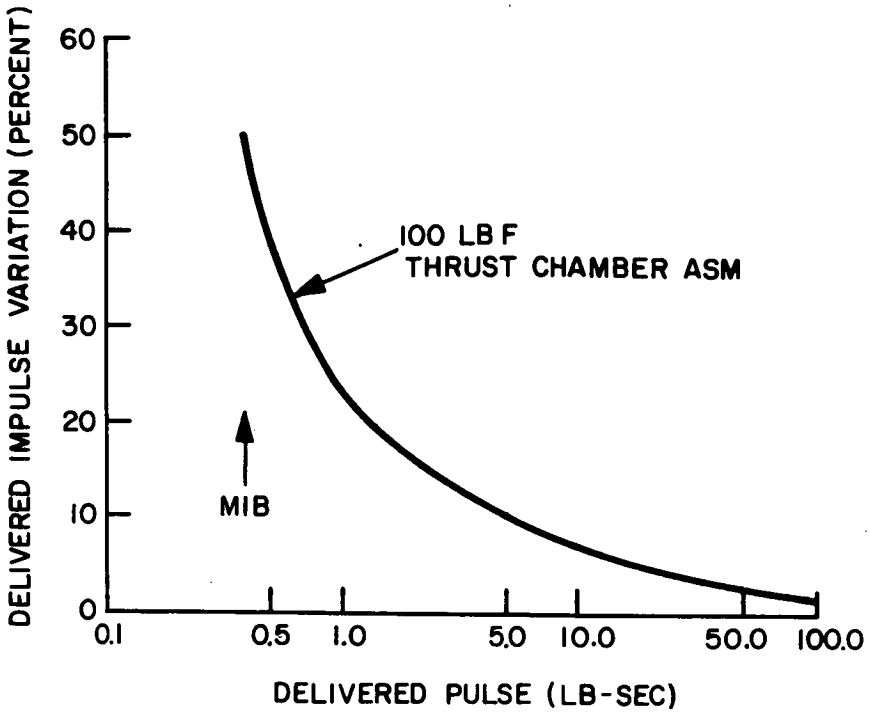

Figure 5-2. Impulse Variability for Auxiliary Thrusters

5.1.2. Auxiliary Thrusters System Weights

Table 5-1 is a detailed weight summary of the auxiliary thrusters hardware used on the system shown in Figure 5-2. The additional weight of 117.6 pounds for the auxiliary thruster system is added to the main propulsion system burnout weight of 2085.3 pounds, resulting in a total auxiliary thruster system burnout weight of 2202.9 pounds. The weights shown were derived as follows: Engine weight is based on the weight of representative available hardware (i.e., RMD C-1 version); weights of valves and check valves are representative of available hardware; weight of tubing and fittings is based on normal tube routing and normal tube connecting points, with stainless steel tubing used in all cases; bracketry and shielding include support structure for the engines and micrometeoroid protection shielding.

Table 5-1. Auxiliary Thruster Configuration Weight Summary

Additional Components Required for Auxiliary Thruster Configuration	Qty per System	Unit Wt (lb)	Total Wt (lb)
1. Engine	4	16.1	64.4
2. Ordnance Valve (N.O.)	8	1.1	8.8
3. Ordnance Valve (N.C.)	6	0.9	5.4
4. Check Valve (Quad.)	2	0.9	1.8
5. Tubing & Fittings	-	-	4.4
6. Bracketry & Shielding	4	8.2	32.8
			117.6

5.1.3. Parametric Weight Study

A correlation of mission velocity requirements, payload weight, propulsion subsystem burnout weight (including unusable propellants), and propellant loading requirements for the LEMDE/auxiliary thruster subsystem is shown in Figures 5.3 and 5.4. Velocity requirements assumed for this correlation are listed in Table 2.1.

Other assumptions made were specific impulses of 305 lbf-sec/lbm for LEMDE high thrust mode and 295 lbf-sec/lbm for the auxiliary thrusters. (For comparison purposes, the LEMDE low thrust specific impulse is 289 lbf-sec/lbm.)

The propellant required by the auxiliary thruster subsystem is slightly less than that required for the baseline propulsion subsystem, assuming constant payload and propellant subsystem burnout weight. This is due to the higher ISP for the auxiliary system. However,

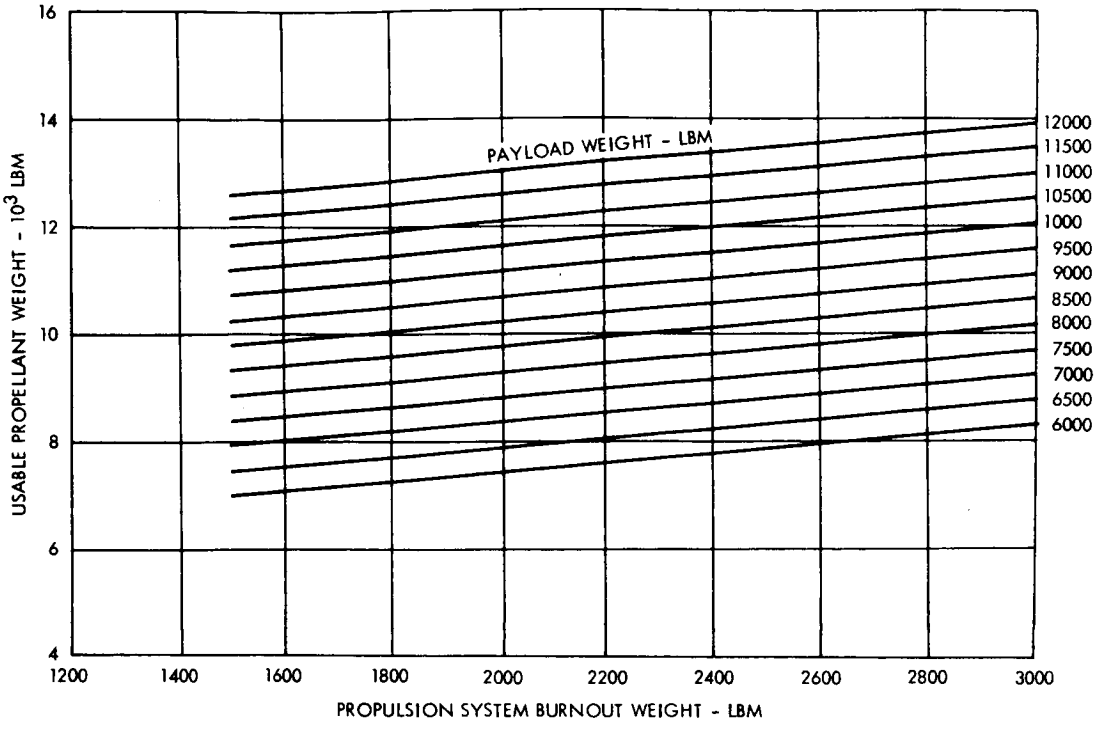

Figure 5-3. Propellant Requirements, Auxiliary Thrusters and LEMDE, 1973

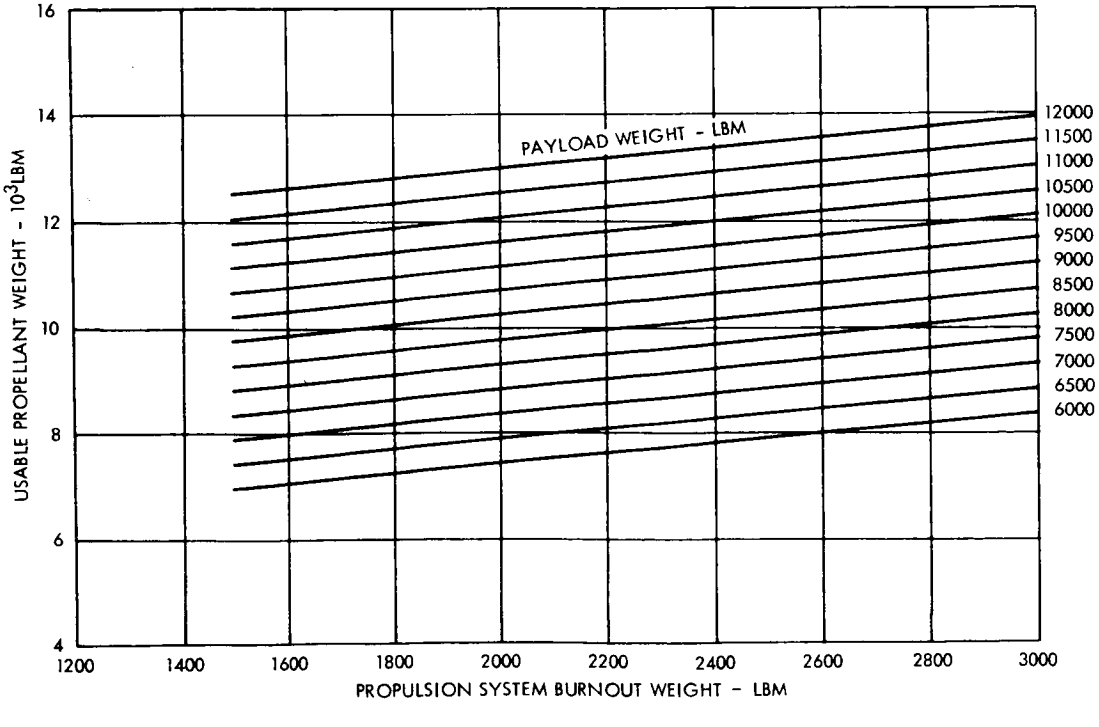

Figure 5-4. Propellent Requirements, Auxiliary Thrusters and LEMDE, 1975, 1977, 1979

the weight saved by utilizing less propellant is more than offset by the added weight of the auxiliary system hardware (approximately 117 lbm).

A specific comparison of propellant requirements is shown in Table 5-1. Since they are linear functions, any payload or burnout weight will result in the same differential propellant weight. The 1973 mission shows the greatest difference due to the long low thrust mode operation to achieve the 493 mps orbit trim velocity requirement (see Table 5-2).

Table 5-2. Propellant Requirements

Mission	Payload (lbm)	Burnout Weight (lbm)	Propellant LEMDE (lbm)	Required LEMDE/Aux. Thrusters (lbm)
1973	10000	1500	10828	10729
1975	10000	1500	10679	10638
1977	10000	1500	10671	10632
1979	10000	1500	10669	10632

5.1.4. Installation in Spacecraft

The use of auxiliary thrusters presents a mounting and packaging problem for some vehicle configurations. Consider the configuration shown in Figure 5-5. as typical. The indicated installation appears to be the most logical selection, since the auxiliary thrusters are at the aft end of the vehicle, the thrust axis is aligned parallel with the main engine, they are the maximum distance away from the solar array, and the maximum distance away from the deployed appendages. However, there are several problems associated with this installation.

a. Their location is several feet away from the propellant supply. Further, the electronic equipment module is between the supply and the thrusters. This could mean that the propellant lines would have to run near the electronic equipment bays, which restricts access and will add problems at vehicle assembly.

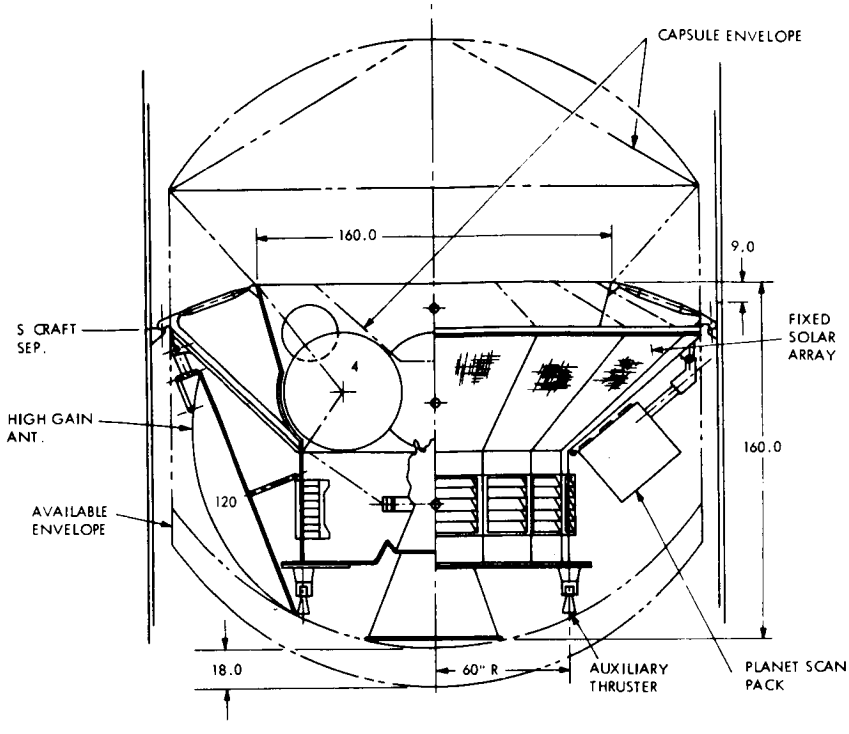

Figure 5-5. Auxiliary Thruster Configuration

b. The remote location with respect to the rest of the propulsion components tends to make more difficult a totally modularized propulsion system.

c. The thrusters are located as far aft as possible. However, there is still the problem of jet impingement on the exit cone of the main engine. This would be particularly true if a 30-degree gimbal angle was employed.

d. The remote and exposed location requires micrometeoroid protection for the valving and active components of the thrust chamber assembly. It also means that whenever the thrusters are in the shadow, active environmental control may be required to maintain the thrust chamber within specified operating limits prior to ignition.

5.2. AGENA ENGINE STUDY

The basic pump fed, regeneratively cooled Agena engine, Bell Aerosystems Models 8096 and 8247, has the longest, most extensive development and flight proven experience of any engine considered for the Voyager spacecraft. Bell's Model 8517B, which has been proposed for the Voyager bus in four possible modifications, is a conceptual modification to

Model 8533. The Agena 8533 engine is a pump fed, regeneratively cooled engine which operates on N_2O_4/50% UDMH + 50% N_2H_4 propellants to produce 18,000 pounds of thrust. Presently the 8533 engine is in the contract definition phase of development and is expected to be operational by 1970. A configuration layout of the 8533 engine is shown in Figure 5-6.

5.2.1. Model 8533 Description

The updated Model 8533 in the Agena engine family, insofar as possible, uses unchanged components from the Model 8096 engine and the Gemini target vehicle engine, Model 8247. Bell's approach to the 8533 engine design has been to minimize changes so that reliability and performance capability would be preserved. Figure 5-7 shows a flow schematic of this multistart engine.

The thrust chamber is of welded forged aluminum with drilled passages for regenerative cooling. The 50-50 fuel blend acts as the coolant. The chamber operates at a nominal chamber pressure of 500 psia. The aluminum injector utilizes a triplet injection pattern.

Propellants are supplied to the engine by fuel and oxidizer pumps which are gear driven from a common, gas generator powered turbine. To allow multiple restarts, metallic bellows start tanks are used.

The bellows start tanks provide fuel and oxidizer for initial gas generator start. The gas generator then continues to drive the turbine pump. The pumped propellants are diverted to the gas generator and, after initial start, the turbine pump gas generator system runs bootstrap. The turbine pump recharges the start tanks during the start transients of each run.

Engine operation is terminated normally by removing power from the gas generator and fuel valve solenoids or, if turbine speed exceeds 29,500 rpm, by the electronic gate sensing the overspeed condition.

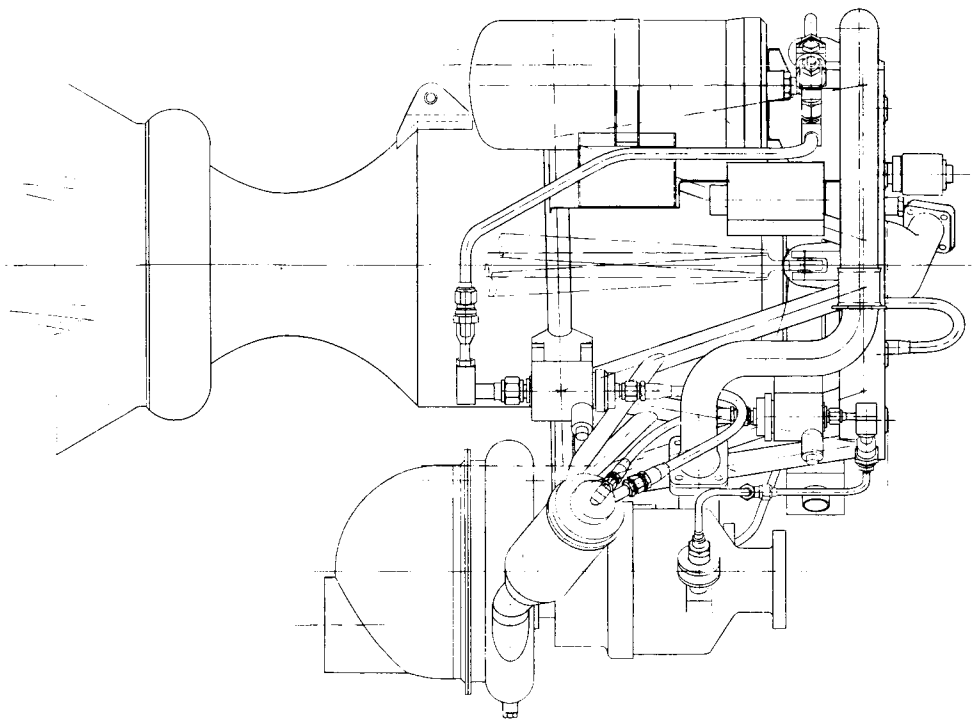

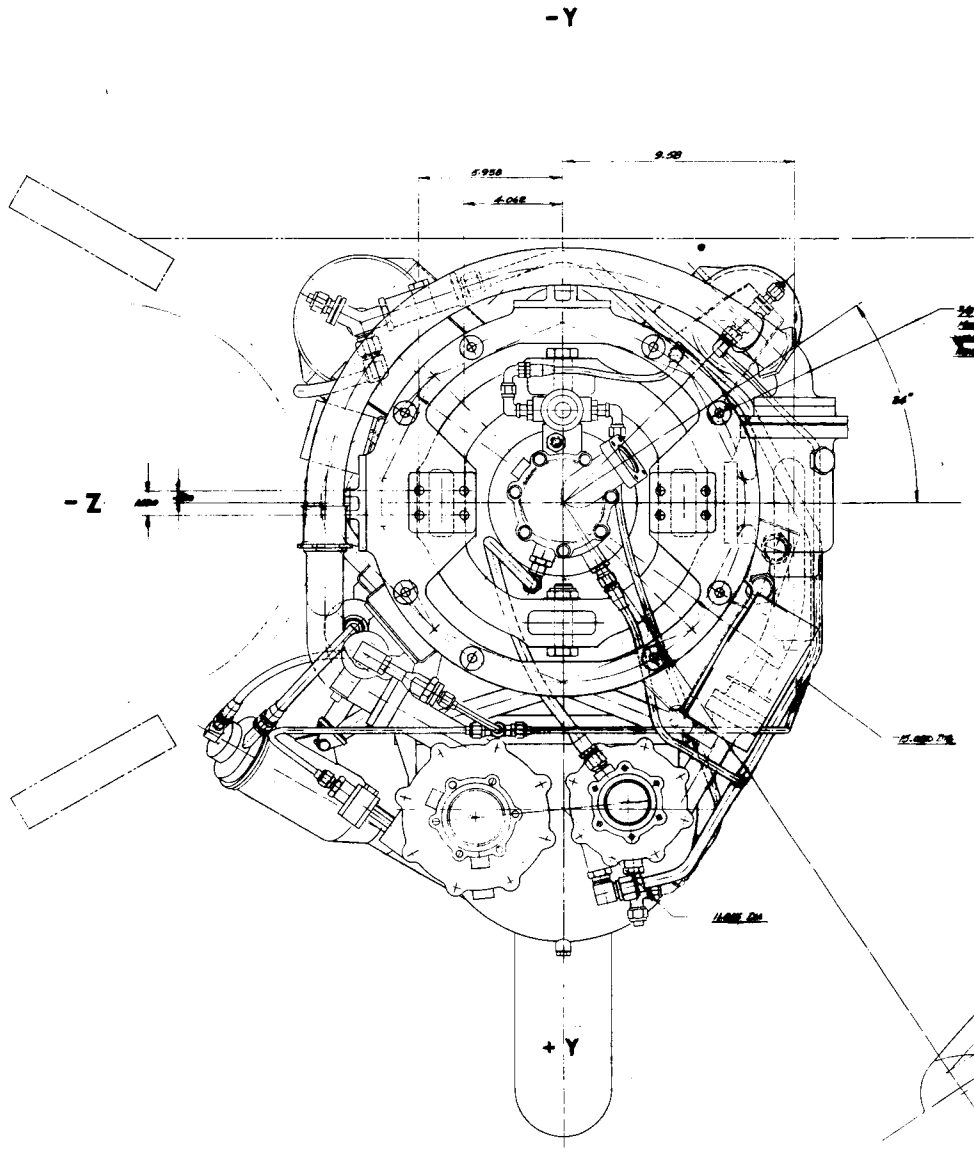

FOLDOUT FRAME 1

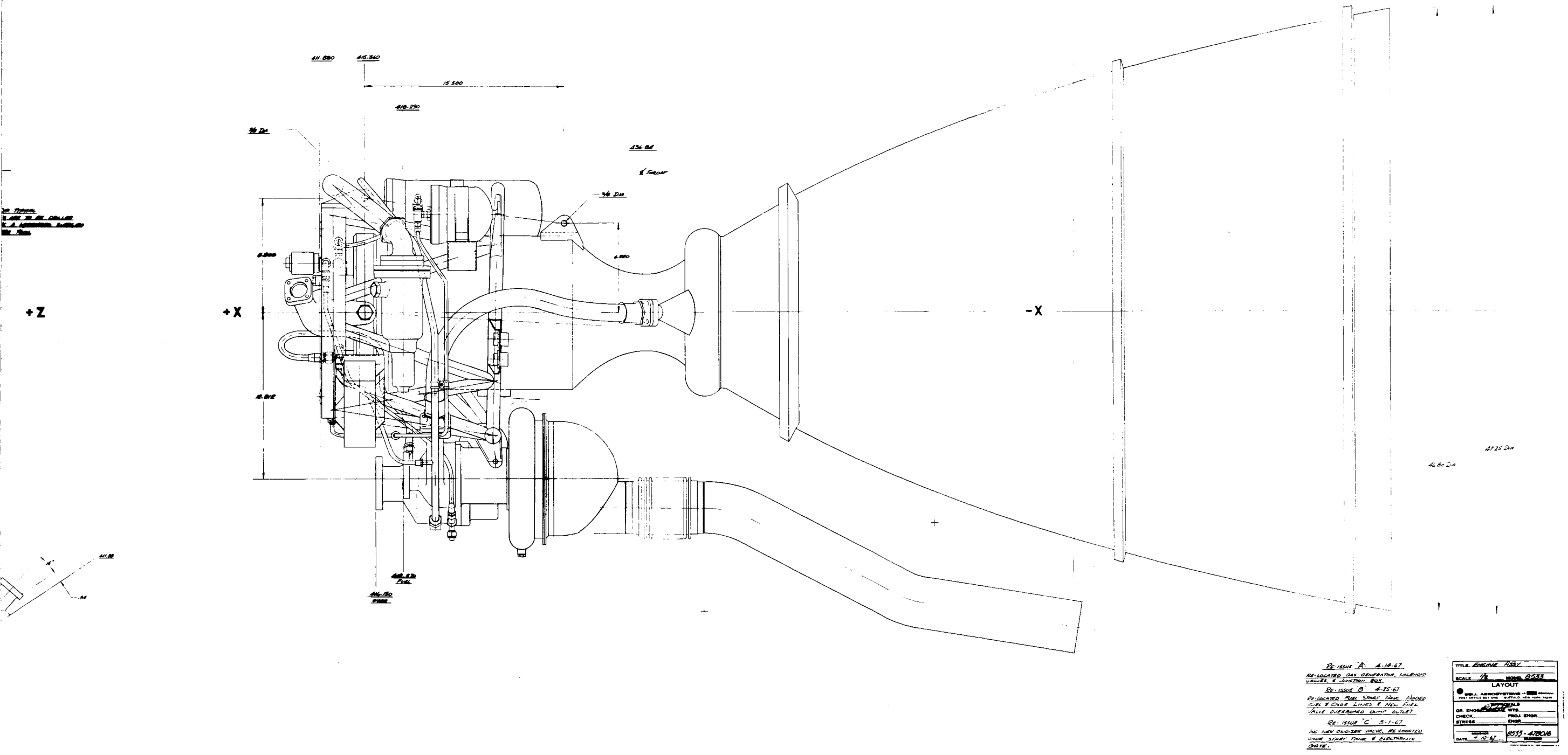

Figure 5-6. Agena Model 8533 Engine Assembly

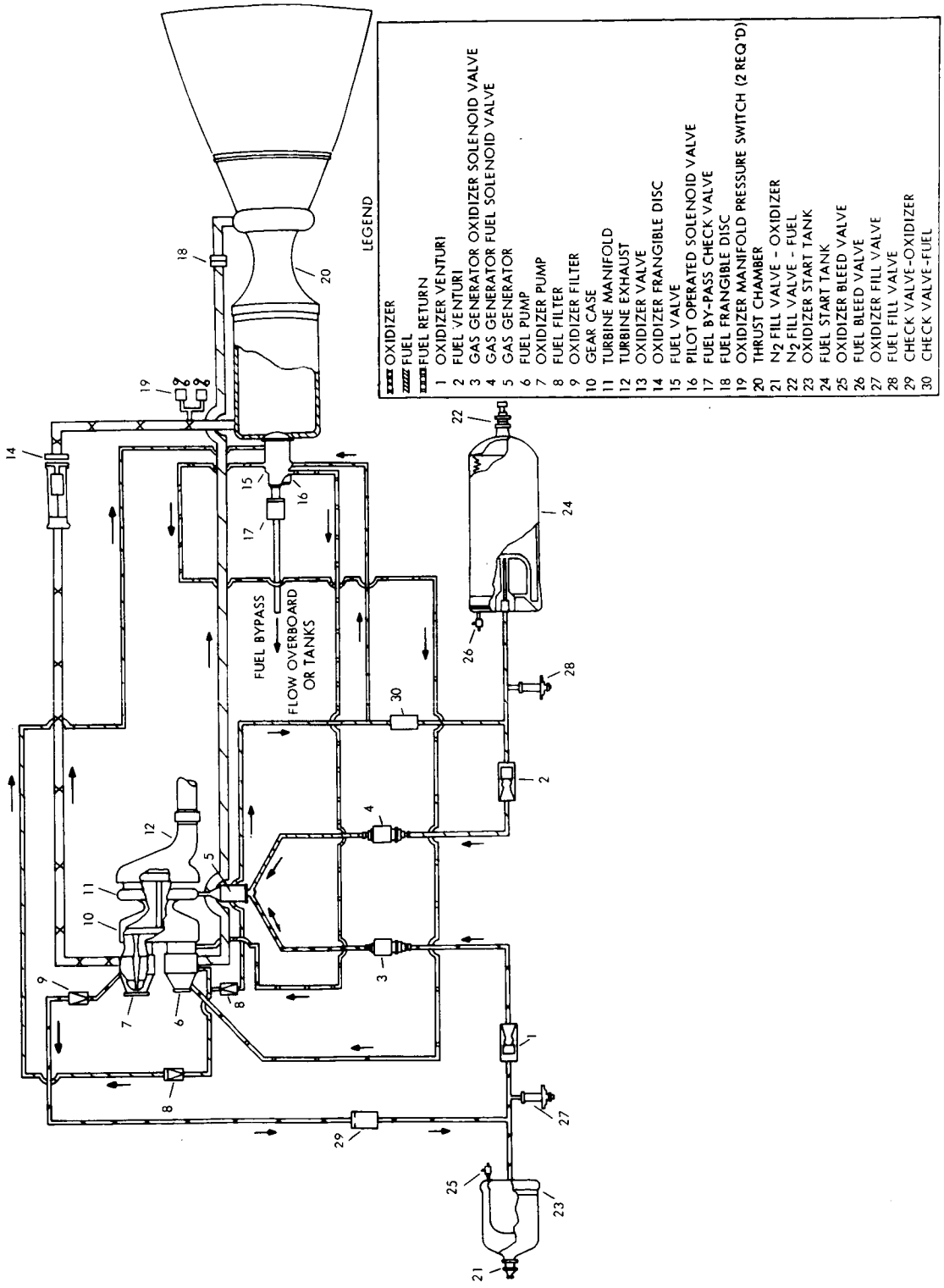

Figure 5-7. Flow Schematic Agena Model 8533 Multistart Engine

Removal of power from the main fuel valve pilot operated solenoid allows it to open and release hydraulic pressure from the main fuel valve poppet, which shuttles under spring load to terminate thrust chamber fuel flow and initiate fuel flow overboard through the spring loaded bypass valve.

Simultaneous removal of power from the gas generator solenoid valves terminates propellant flow to the gas generator, allowing the turbine pump assembly to decelerate. As the gas generator port pressures decay below start tank pressures, the dual check valves close, trapping propellants at high pressures in the start tanks for subsequent firings. Further deceleration of the turbine pump assembly reduces the pump discharge pressures, allowing the fuel bypass and main oxidizer valves to close under spring pressures, terminating overboard fuel and oxidizer flow. The setting of the fuel bypass valve closing pressure assures adequate cooling of the thrust chamber after termination of firing.

In addition to the thrust chamber assembly, turbine pump assembly, and start tanks, other major engine components include a turbine exhaust duct, propellant valves and gimbal ring.

The design data for the 8533 engine is summarized in Table 5-3.

5.2.2. Voyager Model 8517B Description

Bell Aerosystems Model 8517B engine has been proposed for the Voyager bus in four possible modifications. This proposed Voyager engine is a conceptual design modification to the Agena Model 8533. The Model 8517B engine modifications are applicable to both the N_2O_4 - MMH and N_2O_4 - .5 UDMH + .5 N_2H_4 propellant combinations. The Agena engine 8533 is currently under development with the N_2O_4-50/50 propellant combination. The only mandatory change for operation on N_2O_4 - MMH is a fuel pump discharge port area increase of approximately 1 percent to accomodate the lower density of the MMH fuel.

Table 5-3. Model 8533 Engine Characteristics

Characteristic	Nominal Value
Propellant Combination	N_2O_4/50-50
Thrust Level lb	18,000
Mixture Ratio: Engine	1.8
Thrust Chamber	1.9
Chamber Pressure, psia	500
Characteristic Length, L*, in	68.0
Area Ratio	90
Min. Engine Life (After Acceptance Test), sec	750
Restart Capability	Multiple
Weight Statement	
Total Engine Dry Weight, lb	345
Total Engine Wet Weight, lb	359
Total Engine Operating Weight, lb	368
Oxidizer Pump Feed Pressure at 60 °F, psia	38
Fuel Pump Feed Pressure at 60 °F, psia	19
Max. Fuel (Coolant) Feed Temperature, °F	90
Gimbal Capability, degrees	±3.5
Envelope	
Overall Length, in.	82.7
Maximum Diameter, (excluding exhaust duct), in.	47.3

The governing ground rules for the Bell Voyager studies were an engine propellant supply pressure of 210 psia (required for pressure fed engine operation) and the limitation of Agena engine design changes to the modification category to capitalize on the development investment in the existing basic engine. The four conceptual designs were generated to meet the mid-course correction, orbit insertion, and orbit trim requirements of the Voyager Bus with propulsion redundancy for orbit insertion.

In order of increasing design change, the four Model 8517B modifications are:

a. Modification 1 - Fixed 18K pump fed engine for use with 6 vernier engines of 100-lb thrust: Remove start tanks and insulate nozzle extension.

b. Modification 2 - Dual mode 17K/5K engine capable of pump and pressure fed operation for use with 4 vernier engines of 100-lb thrust: Remove start tanks, insulate nozzle extension, modify fuel and ox pump housings (change discharge port area, incorporate high static pressure seals and pump bypass circuits with check valves), modify propellant valves for low ΔP, and modify injector to high ΔP wide flow range design.

c. Modification 3 - Trimode 17K/5K/1K engine capable of pump fed operation and pressure fed operation at two additional thrust levels: Remove start tanks, insulate nozzle extension, modify fuel and ox pump housings (change discharge port area, incorporate high static pressure seals and pump bypass circuits with check valves), modify propellant valves for low ΔP, modify injector to high ΔP wide flow range design with gas assist injection manifold, and add gas assist controls (i.e., regulator) and idle mode propellant valves incorporating cavitating venturis.

d. Modification 4 - Dual-mode 10K/1K engine capable of pump and pressure fed operation: Remove start tanks, insulate nozzle extension, modify fuel and ox pump housings (change discharge port area and incorporate high static pressure seals), modify injector to very high ΔP wide flow range design, modify gas generator for reduced power level and add idle mode propellant valves incorporating cavitating venturis.

At the 210 psia propellant supply pressures of the Voyager Bus the start tanks of the current Agena engine are unnecessary and may be eliminated. The basic turbomachinery (e.g., pump impellers, seals, bearings, gear box, turbine and gas generator) and pump fed engine cycle of the current Agena engine are retained intact in all four modifications for Voyager. The basic thrust chamber of the current Agena engine is also retained without change. This includes the regeneratively cooled combustion chamber and convergent/divergent nozzle, refractory metal nozzle extension, and the thrust chamber contour to the current expansion ratio of 90:1. The changes in the thrust chamber assembly are limited to the addition of insulation to the refractory metal nozzle extension for all four modifications and injector design changes for the dual and trimode modifications.

The engine system weight and nominal performance obtainable with these modifications are given in Table 5-4 for the N_2O_4-50/50 and N_2O_4-MMH propellant combinations. The engines are designed for 2000-second operating time at full thrust without refurbishment. With an operational life margin of 2 to 1 and an acceptance test allowance of 250 seconds, the minimum life (after acceptance test) will be 750 seconds at full thrust.

Of the four proposed engine modifications, the 8517B Mod. 2 is recommended as the most promising. This preference is based on (1) lighter weight, (2) precision small impulse bits with auxiliary motors, (3) higher performance than Mod. 3, (4) less extensive modification of present hardware than either Mod. 3 or Mod. 4, and (5) with minimum design compromise, the pressure fed mode of operation provides redundant capability for midcourse correction, orbit insertion and orbit trim maneuvers without the turbine pump.

5.2.3. Model 8517B Mod. 2 Engine Operation

The basic flow schematic of the dual-mode Agena engine modification is given in Figure 5-8. Propellants are supplied to the engine at the main oxidizer and fuel valves located at the pump inlets (13) and (14). These fuel operated, solenoid piloted ball valves admit propellants to the engine for both the pump and pressure fed modes of operation and are the master propellant shutoff for extended periods of space coasting. The engine is wet with propellants downstream of the main valves up to the fuel bypass check valve (17) and the oxidizer pump discharge and bypass check valves (20) and (22) from the previous run. However, the main valves limit the quantity of propellant that can be lost through pump seal leakage (or expansion leakage through check valves) during extended coast periods to the volume trapped between the main valves and these check valves.

The propellant supply pressure of 210 psia (required for pressure fed operation) permits rapid turbopump acceleration by gas generator bootstrap operation without the use of high pressure start tanks.

Table 5-4. Agena Model 8517B Engine Modification for Voyager Bus

	Pump Fed - Orbit Insertion				Pressure Fed - Abort Orbit Insertion				Idle Mode - M.C. Corr. and Orb. Trim				Agena Eng. Wt.	Total
	F (lb)	P_c (psia)	R	I_{sp} (sec)	F (lb)	P_c (psia)	R	I_{sp} (sec)	F (lb)	P_c (psia)	R	I_{sp} (sec)	(w/o Prop.) (lb)	Eng. Wt. (lb)
N_2O_4-50/50														
Mod. 1. Agena + 6 x 100 lb Engines	18,000	500	1.81	319.9	600	80	1.60	290.0	400	80	1.60	290.0	340	379
Mod. 2. Agena + 4 x 100 lb Engines	17,920	502	1.60	318.3	4910	140	1.60	312.8	400	80	1.60	290.0	342	368
Mod. 3. Agena Engine - Const. R	17,920	502	1.60	318.3	4910	140	1.60	312.8	980	28	1.60	292.9	358	481
Variable R	18,000	500	1.81	319.9	4910	140	1.60	312.8	980	28	1.60	292.9	358	481
N_2O_4/MMH														
Mod. 1. Agena + 6 x 100 lb Engines	17,790	497	1.86	318.8	600	80	1.65	290.0	400	80	1.65	290.0	340	379
Mod. 2. Agena + 4 x 100 lb Engines	17,210	483	1.80	318.0	4710	135	1.80	313.6	400	80	1.65	290.0	342	368
Mod. 3. Agena Engine - Const. R	17,600	499	1.65	316.1	4820	139	1.65	311.0	960	28	1.65	290.8	358	481
Variable R	17,090	477	1.86	318.8	4710	135	1.80	313.6	960	28	1.65	290.8	358	481
Mod. 4. Low Thrust Agena Engine	10,610	300	1.65	313.5	960	28	1.65	290.8	960	28	1.65	290.8	358	358

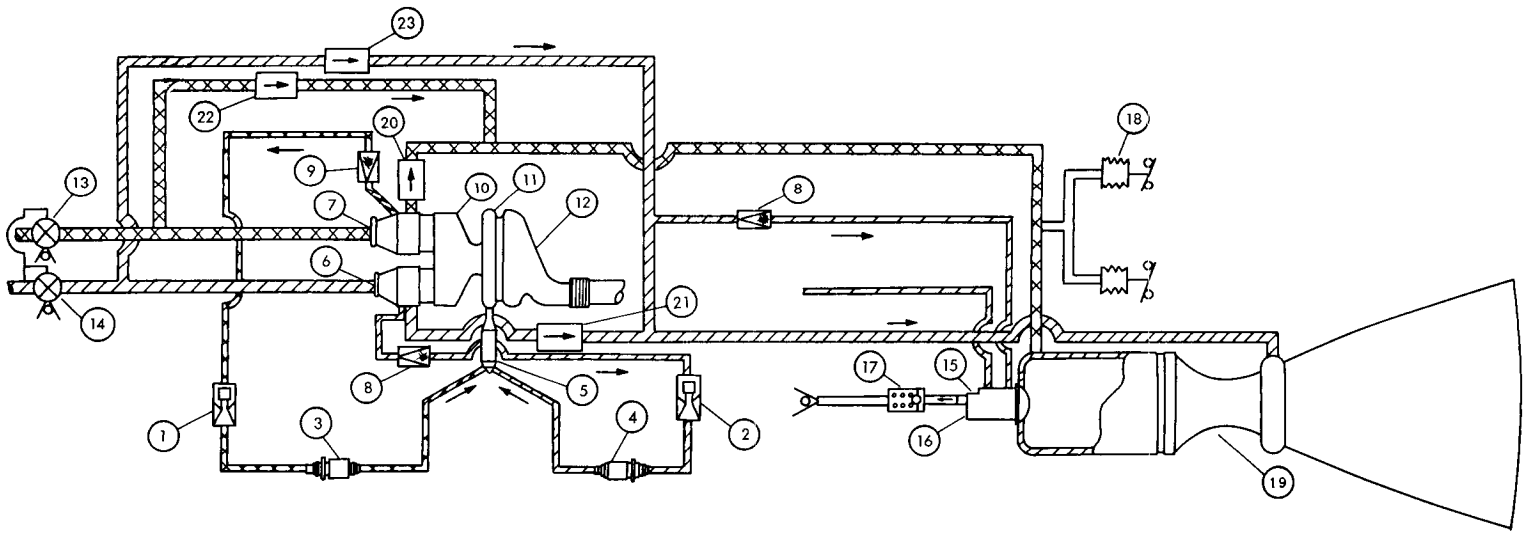

LEGEND

OXIDIZER
FUEL

1 OXIDIZER VENTURI
2 FUEL VENTURI
3 GAS GENERATOR OXIDIZER SOLENOID VALVE
4 GAS GENERATOR FUEL SOLENOID VALVE
5 GAS GENERATOR
6 FUEL PUMP
7 OXIDIZER PUMP
8 FUEL FILTER
9 OXIDIZER FILTER
10 GEAR CASE
11 TURBINE MANIFOLD
12 TURBINE EXHAUST
13 OXIDIZER VALVE (FUEL OR GAS OPERATED - SOLENOID PILOTED)
14 FUEL VALVE (FUEL OPERATED)
15 FUEL VALVE IN HEAD
16 PILOT OPERATED SOLENOID VALVE
17 FUEL BYPASS CHECK VALVE
18 OXIDIZER MANIFOLD PRESSURE SWITCH (2)
19 THRUST CHAMBER
20 OXIDIZER PUMP CHECK VALVE
21 FUEL PUMP CHECK VALVE
22 OXIDIZER PUMP BYPASS CHECK VALVE
23 FUEL PUMP BYPASS CHECK VALVE

Figure 5-8. A Flow Schematic Agena Dual Mode 8517B Mod. 2 Engine

5.2.3.1. Pump Fed Mode Operation

The engine may be fired in the pump fed mode by supplying 28 volt power to the main oxidizer and fuel valve pilot solenoids and the gas generator solenoid valves (3) and (4). The propellants will then flow, under supply pressure, to the gas generator, where they ignite hypergolically and initiate turbine pump acceleration. At a predetermined pressure level the oxidizer pump discharge check valve is forced open, allowing propellant to flow to the thrust chamber. At a predetermined pressure level the fuel pump discharge check valve is forced open, allowing fuel to flow through the coolant jacket, fuel valve-in-head (15), and overboard. When oxidizer fills the thrust chamber feed line, manifold and injector, the oxidizer manifold pressure switches activate, providing power to the fuel valve-in-head pilot solenoid which actuates providing hydraulic pressure to shuttle the spring loaded poppet of the fuel valve terminating bypass flow and allowing fuel to enter the thrust chamber, where it combusts hypergolically with the oxidizer. The pressure switch control assures an oxidizer lead to the chamber for smooth ignition.

Pump fed engine operation is terminated normally by removing power from the gas generator and fuel valve-in-head solenoids to obtain fast shutdown of gas generator and thrust chamber combustion, followed by the relatively slow shutdown of the main oxidizer and fuel valves to permit override flow to cool down the thrust chamber during turbine pump deceleration.

Removal of power from the fuel valve-in-head pilot operated solenoid (16) allows it to open and release hydraulic pressure from the fuel valve poppet (15) which shuttles under spring load to terminate thrust chamber fuel flow and initiate fuel flow overboard through the spring loaded bypass valve (17).

Simultaneous removal of power from the gas generator solenoid valves (3) and (4) terminates propellant flow to the gas generator, allowing the turbine pump assembly to decelerate. Deceleration of the turbine pump assembly reduces the pump discharge pressures (to engine supply level), allowing the fuel bypass (17) and oxidizer check valves (20) and (22) to close under

spring pressures, terminating overboard fuel and oxidizer flow after the main oxidizer and fuel valves (13) and (14) close. The setting of the fuel bypass valve closing pressure assures adequate fuel cooldown of the thrust chamber after termination of combustion.

If turbine speed exceeds the safe value of 29,500 rpm at any time during pump fed operation, an electronic gate sensor will remove voltage from the gas generator solenoid valves (3) and (4) to shut down the turbopump. Engine operation will then continue in the pressure fed mode with propellants supplied to the thrust chamber through the oxidizer and fuel pump bypass check valves (22) and (23).

If the turbopump fails to turn due to malfunctions such as binding rotating parts (e.g., bearing failure), gas generator failure (e.g., plugging) or gas generator solenoid valve failure, the engine will automatically go into the pressure fed mode of operation without the aid of malfunction sensors.

5.2.3.2. Pressure Fed Mode Operation

The engine may be fired in the pressure fed mode by supplying 28 volts to the pilot solenoids of the main oxidizer and fuel valves (13) and (14). The gas generator solenoid valves are not energized. The propellants will then flow, under supply pressure (210 psia), through the low cracking pressure-low ΔP oxidizer and fuel pump bypass check valves (22) and (23) to the thrust chamber, where fuel flows through the cooling jacket and out the fuel bypass check valve (17) while the oxidizer injection manifold is bleeding in. When the oxidizer fills the thrust chamber feed line and injector manifold, the back pressure developed by stabilized oxidizer injection actuates the oxidizer manifold pressure switches (18) which supply voltage to the fuel valve-in-head solenoid (16). The fuel valve-in-head (15) then shuttles to terminate fuel bypass flow and initiate fuel injection into the combustion chamber. This sequence arrangement insures an oxidizer lead for smooth hypergolic ignition in the thrust chamber.

The engine is shut down from the pressure fed mode of operation by removing voltage from the fuel valve-in-head solenoid (16) and the main oxidizer and fuel valve pilot solenoids (13)

and (14). The fast closing fuel valve-in-head (15) terminates combustion and initiates fuel cooldown bypass flow during the relatively long main fuel and oxidizer valve (14) and (13) closing interval. The fuel bypass cooling and the quenching oxidizer override in the combustion chamber reduces the aluminum thrust chamber temperature to safe levels for stagnant residual cooling fuel. After the main propellant valves seat, the bypass fuel flow ceases when the pressure in the regenerative cooling jacket drops to the reseating pressure of the bypass check valve (17). Oxidizer override ceases when the pressure drops to the reseating pressure of the oxidizer pump bypass check valve (22).

5.2.4. Model 8517B Mod. 2 Performance

5.2.4.1. Minimum Impulse Bit

The minimum impulse bit capability of Agena engine modification No. 2 was estimated by extrapolation of test data for the currently operational 16,000-pound Agena engine and the 3,500-pound pressure fed LEM ascent engine. The resulting nominal shutdown impulse, minimum impulse bit, and 3σ variations are given as follows:

Engine Operating Mode	Pump Fed	Pressure Fed
Shutdown Impulse, lb-sec.	2000 ±600	714 ±125
Min. Programmed Impulse, lb-sec.	11,000 ±6000	825 ±173

The minimum-time programmed impulses given above include the respective shutdown impulses (i.e. residual impulse generated after shutdown signal). Conservatism was applied to these estimates in proportion to the extent of the extrapolation. It can be expected that detailed design study (including computer simulation and engine design optimization for minimum impulse bit) will indicate the feasibility of low minimum impulse bit and variance for the Voyager mission requirements in the pressure fed mode. However, since the four vernier engines that would be used with Model 8517B, Mod. 2 can readily supply this minimum impulse bit without compromise, the main engine capability is close enough to the requirement to serve as operational backup. Main engine design compromise for minimum impulse bit capability is not recommended at this time.

5.2.4.2. Weight Breakdown

The engine weight breakdown for the Model 8517B Mod. 2 is shown in Table 5-5. The nozzle extension is 90:1 area ratio and the nozzle is fully insulated. The total engine dry weight is 368 pounds, including the four 100-pound thrust auxiliary thrusters.

Table 5-5. Agena Model 8517B Mod. 2 Weight Summary

Element	Weight (lb.)
Thrust Chamber with Injector	83.1
Divergent Nozzle Extension	55.3
Nozzle Insulation	27.0
Propellant Valves	23.7
Turbine Pump Assembly	62.2
Mount Assembly	47.7
Gimbal Ring	14.1
Exhaust Duct	10.1
Lines, Electrical	18.8
Agena Engine Assembly - Dry	342.0
4 Auxiliary Thrusters	26.0
Total Engine Dry Weight	368.0

5.2.4.3 Engine Performance

The delivered specific impulse for the 8517B Mod. 2 is based on Model 8533 data. The delivered Isp performance is predicted as 318.3 seconds at a mixture ratio of 1.60 (N_2O_4 + 50/50) in the pump fed mode of operation. Performance in this mode allows for the loss in Isp due to turbine pump operation. In the pressure fed mode a performance penalty is paid due to the reduced chamber pressure, however, no loss is incurred for pump operation. The resultant Isp performance in the pressure fed mode is then 312.8 seconds.

The Model 8533 will have a multiple restart capability. This capability will be maintained in the 8517B engine, and the engine may be fired in any duty cycle without restriction, up to a total time of 750 seconds.

As an advantage for Voyager application, the space coast data on the basic Agena engine is extensive in quantity and duration but is highly classified.

5.2.5. Model 8517B Mod. 2 Reliability

The reliability assessment of the Model 8517B Mod. 2 engine is based on the experience and demonstrated performance of the Model 8096, Model 8247, and the development testing of the Model 8533 engine. The excellent reliability records of these engines support the theoretical reliability prediction.

Based upon the use, wherever possible, of components that have successful records of reliability, the employment of proven manufacturing processes and techniques that have been subjected to extensive testing, and seven years of flight experience with Model 8096 and 8247 engines, the reliability of the Model 8533 engine has been assessed at 0.999 for a successful first start and 0.9934 for 16 starts. The reliability of the Model 8517B Mod. 2 engine is assumed by Bell to be the same as Model 8533, since the hardware changes would not affect the pump fed cycle significantly. This reliability assessment is only for the pump fed mode of operation.

A failure rate analysis conducted for the Model 8533 engine reveals the following tabulation which shows the proportionate first start failure rate (λ) for the major subassemblies or parts of the engine:

Thrust Chamber Assembly	19.67% of (λ)
Nozzle Extension	0.5
Turbine Pump Assembly	72.03
Exhaust Duct	0.27
Electronic Gate	5.36
Cable Assembly	2.17
	100.0 %

5.2.6. Installation in Spacecraft

This is discussed in Section VOY-D-220 and shown in Figure 5-9.

5.2.7. Engine Interface Requirements

The information presented below is in accordance with the Model 8533 engine specification and remains essentially correct for the conceptual 8517B Mod. 2 engine.

5.2.7.1. Gimbal Rates

The Model 8533 gimballing system draws fuel from the turbine pump to power a motor-pump which supplies 3000 psi hydraulic aid to the gimbal actuators. The gimballing actuating system shall have a maximum steady state fuel flow of 9.0 gallons per minute (or about 1.1 lb/sec).

The Model 8517B Mod. 2 engine is capable of gimballing ±6.0 degrees in a square pattern. The gimballed mass acceleration is 30 rad/sec^2 and the velocity is 0.628 rad/sec in a square pattern. These are maximum gimbal rates to which the engine is designed. The gimballed mass moment of inertia is 50 slug-ft^2.

5.2.7.2. Heat Outputs

Complete temperature time histories of the Model 8533 are not presently available; however, the equilibrium temperatures and emissivities of the major heating surfaces are available. Table 5-6 presents the equilibrium surface temperature and Table 5-7 presents emissivities.

5.2.7.3. Mechanical Interface

The engine is mounted and attached to the vehicle structure with a mounting ring and gimbal ring. The mounting ring outer diameter is 16.25 ±0.030 inches, with a mounting bolt circle diameter of 15.00 ±.030 inches.

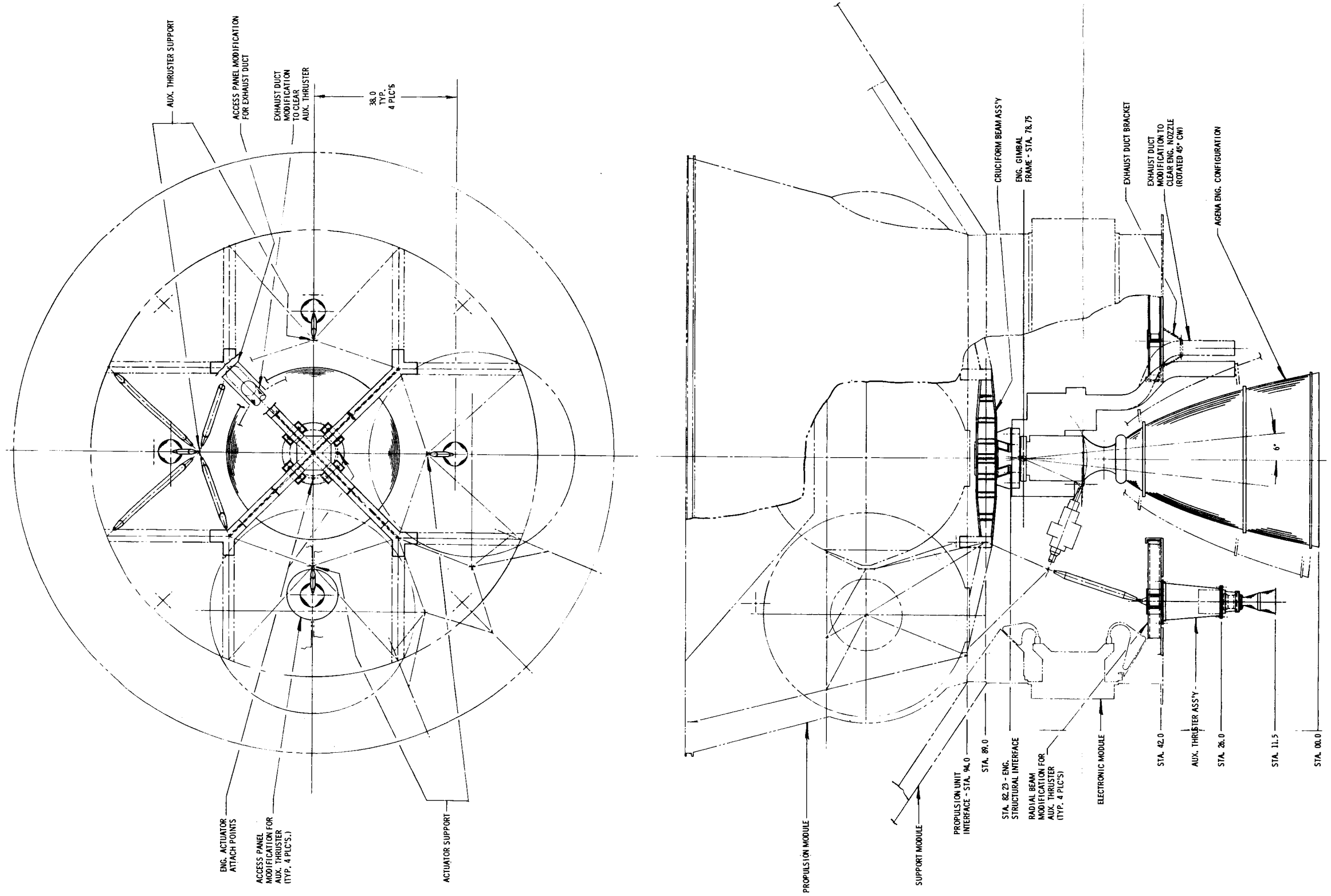

NOTES:
1. EXCEPT AS NOTED FOR MODIFICATIONS, ACCESS PANELS & RADIAL BEAMS OMITTED IN TOP VIEW FOR CLARITY.
2. EXCEPT AS NOTED, HELIUM & PROPELLANT TANKS & SUPPORT STRUCTURE OMITTED FOR CLARITY.
3. SOLID LINES INDICATE CHANGE FROM LEMDE CONFIGURATION EXCEPT AS NOTED FOR EXHAUST DUCT.

Figure 5-9. Agena Thrust Chamber Adaptation

Table 5-6. Agena Equilibrium Temperatures for Major Heating Surfaces

Surface	Temp.
Thrust Chamber, Injector	400 °F
Thrust Chamber, Entrance to Convergent Section	300 °F
Chamber Throat	290 °F
End of Regeneratively Cooled Section (ϵ = 12)	140 °F
Nozzle Extension (Insulated)	2725 °F
Turbine Manifold and Gas Generator	1450 °F
Turbine Exhaust Duct	1200 °F

Table 5-7. Agena Emissivities for Major Heating Surfaces

Surface	Emissivity
Thrust Chamber (6061 Al)	0.09 (min) 0.20 (max)
Turbine Exhaust Duct (304 S/S)	0.40
Nozzle Extension (Discilicide Coating)	0.65 (max)
Turbopump Case	0.60

5.2.7.4. Electrical Requirements

The electrical interface power requirements as supplied to the engine are:

a. Voltage - 19.5 to 30.5 vdc.
b. Source Impedance - 0.05 ohm, dc to 250 cps.
c. Transient - ±50 volts for 10 microseconds with a 2-per-second repetition rate.
d. Ripple - 1.2 volts rms, 30 to 150,000 cps.

The maximum electrical loads do not exceed 8.2 amperes in the Agena application.

5.2.7.5. Pneumatic Requirements

During all engine operations, or while the engine is loaded with propellants, helium gas is used to pressurize the oxidizer pump secondary seal cavity.

5.2.8. Summary

Of the four proposed modifications to the Agena Model 8533 engine for possible Voyager spacecraft application, the Bell conceptual Model 8517B Mod. 2 is recommended as the most promising. This preference stems primarily from a lighter weight, higher performance, minimum design change, and a capability for redundant operation in all Voyager spacecraft duty cycle modes. This proposed engine, which offers increased performance and operational capabilities for the Voyager spacecraft, is worthy of continued detailed design analysis beyond the Task D effort.

Bell's estimate of a three sigma tailoff impulse bit of 714 ±125 lb-sec. for the Model 8517B Mod. 2 in the pressure fed mode is very promising. Future mission analysis for Voyager might indicate that minimum impulse bit error requirements can be relaxed or development experience with the Agena engine may result in better impulse bit precision. If either of these two possibilities should develop, this engine could perform the Voyager duty cycle entirely in the pressure fed mode without the auxiliary thrusters as presently comtemplated. As a result, both the Agena engine and the spacecraft would benefit through enhanced mission capability. Operation of the Agena engine in a single pressure fed mode would reduce the basic engine weight by at least 73 pounds by eliminating the turbopump assembly, would produce a higher system reliability as a result of reduced design complexity, and would increase the probability for Voyager mission success.

The need for further design and development definition of the Agena engine for possible application to the Voyager spacecraft is indicated.

5.3. TRANSTAGE ENGINE STUDY

The transtage engine (AJ 10-138) program was initiated in December 1963 with the present flight schedule continuing into the latter part of 1971. A total of 55 engines was delivered by Aerojet during the basic transtage program.

The current transtage engine is well developed, as evidenced by over 2100 static tests for a cumulative duration of 102,903 seconds and a flight program during which the engines fired for 8,248 seconds. A rigorous sea level and altitude simulation pre-flight rating test program was completed in January 1965.

Based on design and test data analyses, the transtage engine has good potential for performing the midcourse maneuvers, orbit insertion, and orbit adjustments required for the Voyager mission. The application of the AJ 10-138 engine to the spacecraft would require a fully ablative or insulated nozzle extension to provide a lower heat flux than the current radiation cooled nozzle.

5.3.1. Engine Description

The pressure fed transtage engine has multiple restart capability, produces 8000 pounds of thrust, and operates on the N_2O_4 + Aerozine 50 storable propellant combination. The engine assembly consists of an ablative thrust chamber, radiation cooled nozzle extension, bipropellant valve assembly, injector, thrust mount assembly, and propellant feed lines.

At present, the transtage engine system application consists of two paired engines as the third stage propulsion system for the Titan III standard space launch vehicle (SSLV). Each engine is a separate entity, being unified only through a common propellant feed system and electrical system provided by the vehicle integrating contractor.

Nominal engine performance ratings are based on fuel and oxidizer being supplied to the engine at the standard interface inlet conditions of 155 psia and 75°F. The engine is designed

for a normal service life of 500 seconds, including a minimum of three starts and three shutdowns after engine acceptance tests.

Transtage is comparatively free of complexity in design and mode of operation. Present design changes contemplated for the Voyager spacecraft entail a change in mixture ratio from 2.0:1 to 1.6:1, use of an insulated nozzle extension with an expansion ratio of 60:1, and demonstration of the required impulse bit capability for the Voyager mission. Table 5-8 gives the general characteristics of the existing Transtage and the proposed modification for Voyager.

Table 5-8. Transtage Design and Operational Characteristics

Characteristic	Existing	Voyager Mod.
Performance		
1. Isp, sec.	302	314
2. Thrust, lb	8000	8000
3. Mixture ratio	2:1	1.6:1
4. Chamber pressure, psia	105	105
Envelope and Interfaces		
1. Supply pressure, psia	155	155
2. Overall length, in. max	81.6	90.5
3. Nozzle extension dia. in. max	47.1 (Rad.)	57.7 (Insul.)
4. Expansion ratio	40:1	60:1
5. Gimbal capability	±6 1/2°	±6 1/2°
Mass Properties		
1. Weight, dry, lb	211	237
2. Weight, wet, lb	227	253

5.3.2. Performance

The transtage engine can be adapted to varying levels of operation using essentially the same hardware for the the types of operating change shown in Figure 5-10. Performance changes of the magnitude shown in this figure would require minor redesign to the current transtage

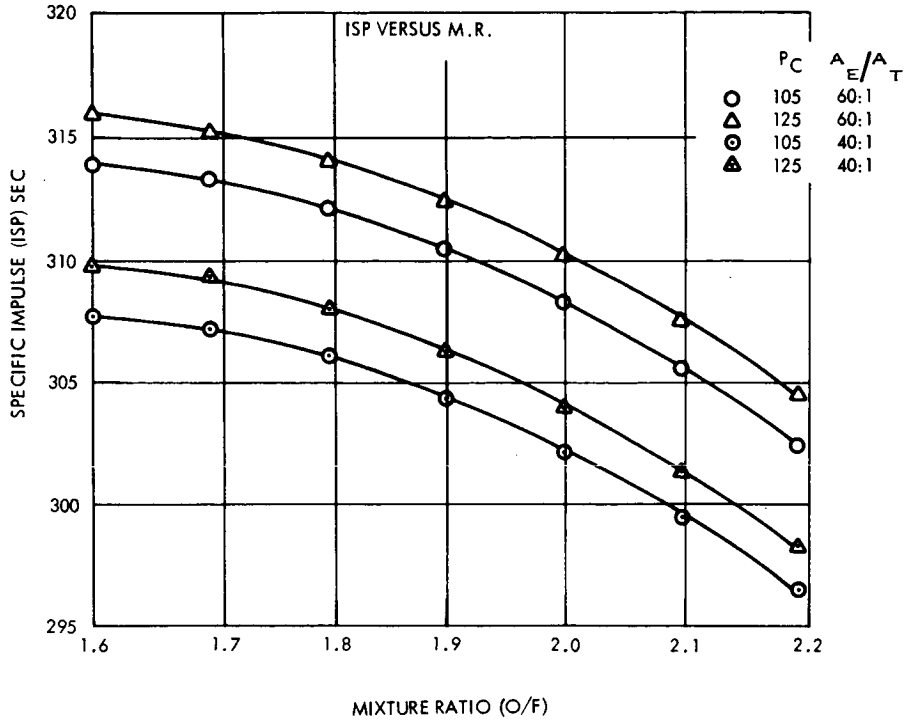

Figure 5-10. Transtage Performance Data

and nominal verification test programs. During the peripheral testing the transtage has given satisfactory performance from mixture ratios of 2.0 down to 1.45.

5.3.2.1. Minimum Impulse Bit

Although transtage has no requirement for minimum impulse capability or demonstration, Aerojet has determined a minimum impulse bit capability through use of a transient Performance Engine Computer Program. The estimated transtage minimum impulse bit capability is shown in Figure 5-11. The data to develop the curve in this figure is based on actual flight data and use of the computer program to extrapolate the impulse bits that could be obtained by pulsing the engine at various thrust levels. As can be seen from the curve, the three sigma variation expands as the thrust level is increased. The incorporation of a more rapid decay suppression circuit could concievably reduce the three sigma to less than 150 lb-sec for the higher thrust levels.

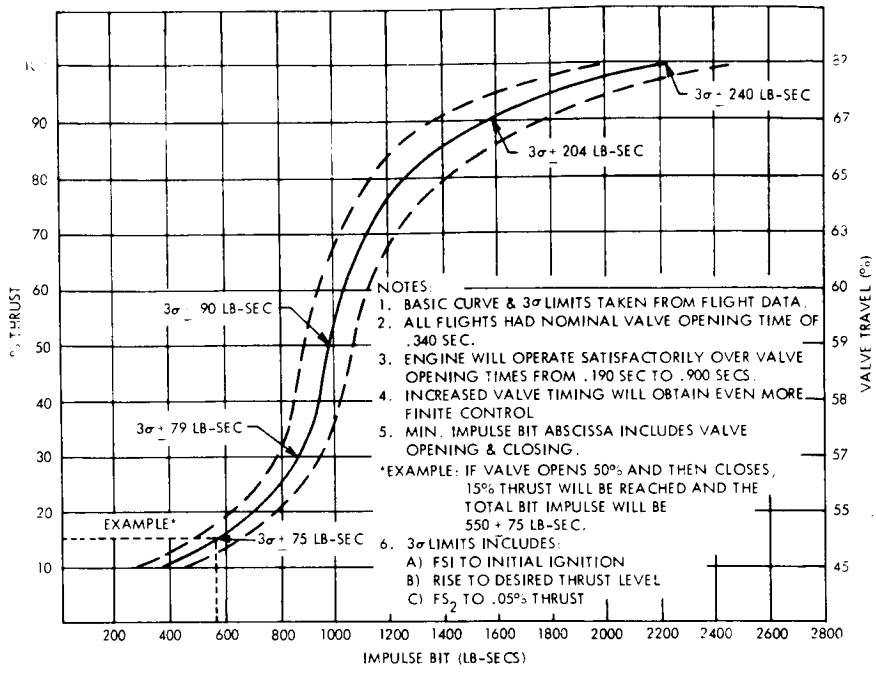

Figure 5-11. Transtage Minimum Impulse Bits

5.3.2.2 Reliability

The transtage contractual reliability demonstration requirement was established at 0.87 with a 90 percent confidence level. To date, based on the formal reliability demonstration sample which included PRFT, full duration acceptance tests and flight tests, the reliability of a single transtage is 0.964 at 90 percent confidence. Projecting to the end of the existing flight schedule, a demonstrated reliability of 0.974 is possible.

During the transtage program, a complete modes of failure analysis was conducted and reliability predictions were made based on development and production hot firing test data and failure report information. The predicted reliability for a 3-burn 500-second mission is 0.998 at this time.

5.3.3. Summary

Of the three alternate engines studied for adaptability to the updated Voyager 1973 spacecraft, transtage is a close second to the LEMDE in design and development maturity. Although similar to the LEMDE in many design aspects, transtage has a decided weight advantage and a higher performance in the Voyager modification. Estimated MIB variance for this engine look promising but needs test verification. Reliability of the transtage engine is good and is anticipated to improve through the present flight program.

Since transtage is close to meeting the Voyager spacecraft propulsion requirements in its current design, a thorough design optimumization study of this engine for the spacecraft propulsion system is recommended.

Installation in the spacecraft is discussed in Section VOY-D-220 and shown in Figure 5-12.

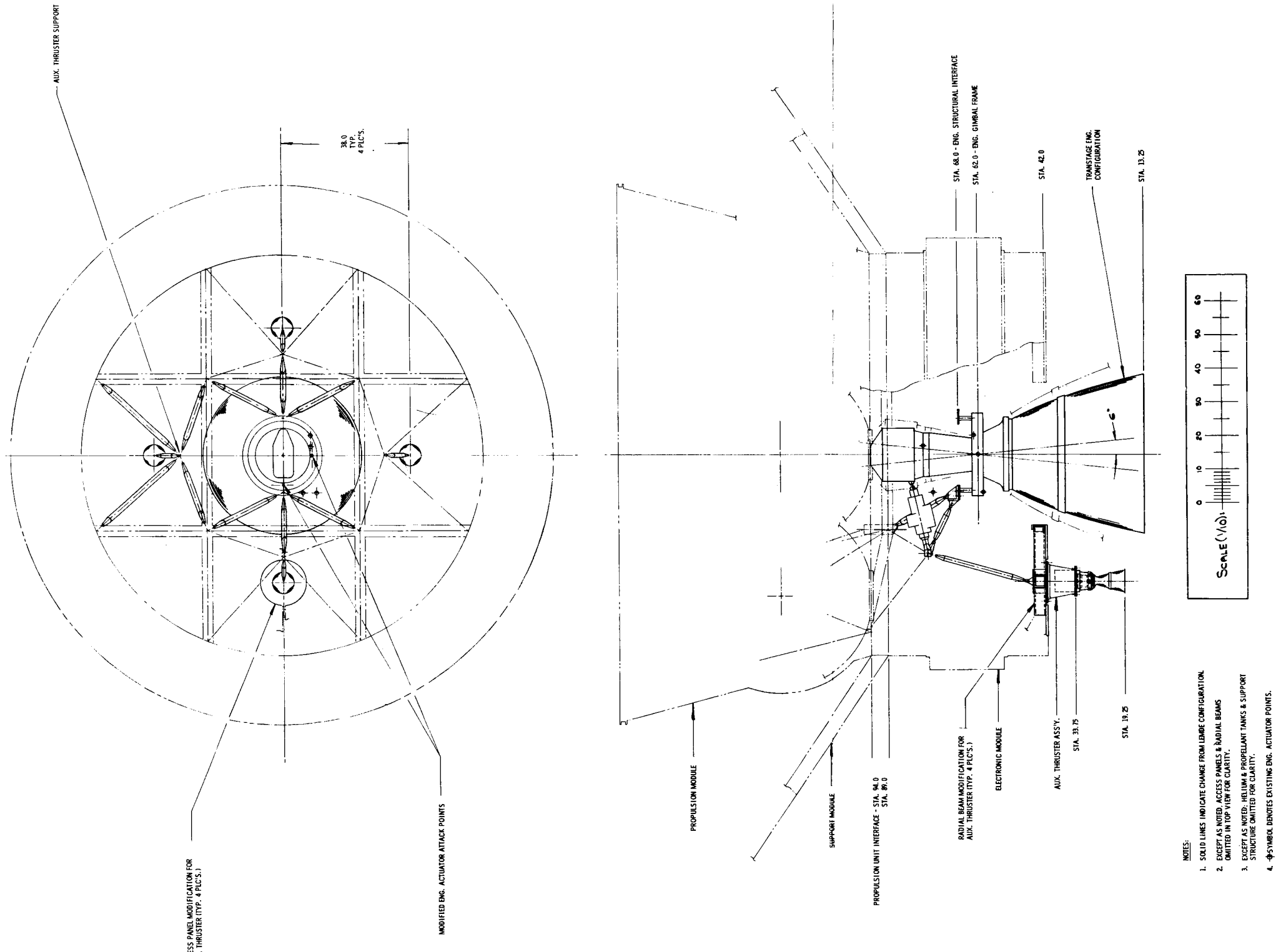

Figure 5-12. Transtage Thrust Chamber Adaptation

FOLDOUT FRAME

FOLDOUT FRAME

5.4. APOLLO SUBSCALE ENGINE

5.4.1. Description and Performance

The Apollo subscale engine (AJ 10-131) was initially developed by Aerojet in 1962 under the Air Force Program 706 (Saint), in which testing was completed through PFRT at simulated altitude conditions. In the nominal configuration, this engine is pressure fed and delivers 2200 pounds of thrust at altitude with a 60:1 area ratio nozzle. Nominal engine performance is given in Table 5-9.

Table 5-9. Apollo Subscale Engine Performance

Characteristic	As Exists	Voyager
Thrust, lb	2200	2200
I_{sp} - Vacuum	309	312.5
Expansion Ratio	60:1	60:1
M.R.	2.0	1.6
Duration, sec	1024	1000
Chamber Pressure, psia	100	100
Propellants	N_2O_4/A50	N_2O_4/A50
Restarts	Unlimited	Unlimited
Weight, lb	98 (rad.)	103 (Insul)

To date, this engine in its various configurations has accumulated over 25,000 seconds of firing time during 555 tests. A summary of this test experience is shown in Table 5-10. Modifications to the engine were made during the Apollo subscale test program and Aerojet's Voyager inhouse test program. The Voyager test program was initiated to evaluate the ablative chamber/injector design over a typical Voyager spacecraft duty cycle and to determine pulse mode performance.

Table 5-10. Apollo Subscale Engine Test Summary

Performance	Saint	Apollo Subscale	Voyager Research	All
Ablative Thrust Chambers Fired at:				
Sea Level	30	21	6	57
Altitude	6	6	0	12
Longest Total Duration for Single Chamber, sec	364	1024	440	1024
Maximum Number of Restarts, Single Chamber	54	37	51	54
Total Tests	278	193	104	555
Cumulative Duration, sec	10,189	13,450	1936	25,575

The four Apollo subscale engine configuration provides an engine out capability which increases reliability and the probability for mission success. From design and operational standpoints, the four Apollo subscale engine arrangement is capable of performing the midcourse corrections, orbit insertion, and orbit adjustments required for the Voyager mission. The application of the AJ10-131 engine to the Voyager spacecraft requires a fully ablative or insulated nozzle extension to provide a lower heat flux than the radiation cooled nozzle.

Currently no development work is in progress on the Apollo subscale engine.

5.4.2. Minimum Impulse Bit

A major advantage of the Apollo subscale engine for Voyager is its demonstrated ability to produce low minimum impulse bits with attendant low three sigma impulse bit variations. Currently, MIB performance has been estimated for the other three engine candidates but not demonstrated to Voyager requirements. Test data on impulse bit performance for this engine is shown in Figure 5-13. The specific data points on this figure represent the average of 10

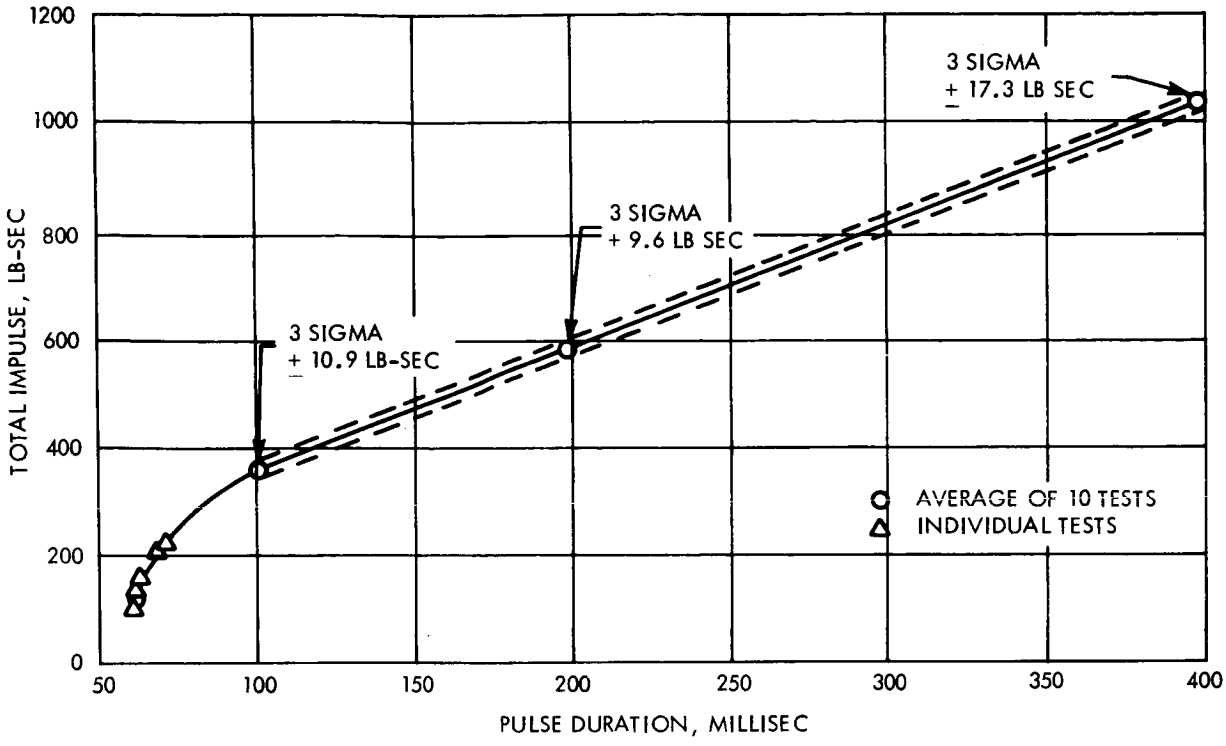

Figure 5-13. Apollo Subscale Impulse Bit Demonstration

tests and range in pulse width from 0.064 to 0.400 second. Of particular significance in this figure is the low calculated three sigma impulse bit variation.

5.4.3. Summary

The Apollo Subscale engine is a moderately mature design, and with minor changes to its current design is a good candidate for use on the Voyager spacecraft. This engine in the four engine configuration has redundant operational capability, due to the possibility of engine out, and can complete all phases of the Voyager spacecraft mission in the two engine mode.

Modifications required for Voyager application include a change in mixture ratio from 2.0:1 to 1.6:1 and the use of insulation on the 60:1 area ratio nozzle extension. Engine MIB and low three sigma impulse variance have been demonstrated and the design operating life of 1000 seconds is adequate for the Voyager mission.

Due to the minor redesign predicted on this engine for application to the Voyager spacecraft, a detailed systems design analysis of this engine in the two and four engine operating modes is recommended. This is required to establish the operational capability, from all system aspects, of the Apollo subscale engine to perform the Voyager spacecraft mission.

5.5. SUMMARY OF CANDIDATE PROPULSION SYSTEMS

5.5.1. Introduction

In accordance with the Task D guidelines, the Voyager spacecraft system has been updated, using the LEMDE engine as the primary candidate for the propulsion system. Adaptation of the Agena and transtage engines were then considered as secondary candidates for packaging into the propulsion system in place of the LEMDE engine. In addition, due to its potential attractiveness for Voyager, the subscale Apollo engine in the four-engine configuration was also considered.

All four of the candidate engines considered during Task D have the potential performance capability to meet the Voyager Spacecraft mission requirements. Usable propellant required versus payload weight to meet the 1973 Voyager mission requirements for the candidate systems is shown in Figure 5-14.

5.5.2. Discussion of Candidate Engines

5.5.2.1. General

From an overall Voyager mission capability standpoint, Figure 5-14 indicates that the transtage engine has a definite weight advantage over the other three candidates. However, many other characteristics enter into the determination of the probability of mission success and must be assessed prior to a selection of the best system. Proper weighting of development status and competing system characteristics are major considerations in the selection process. The development status and competing characteristics for the four candidate

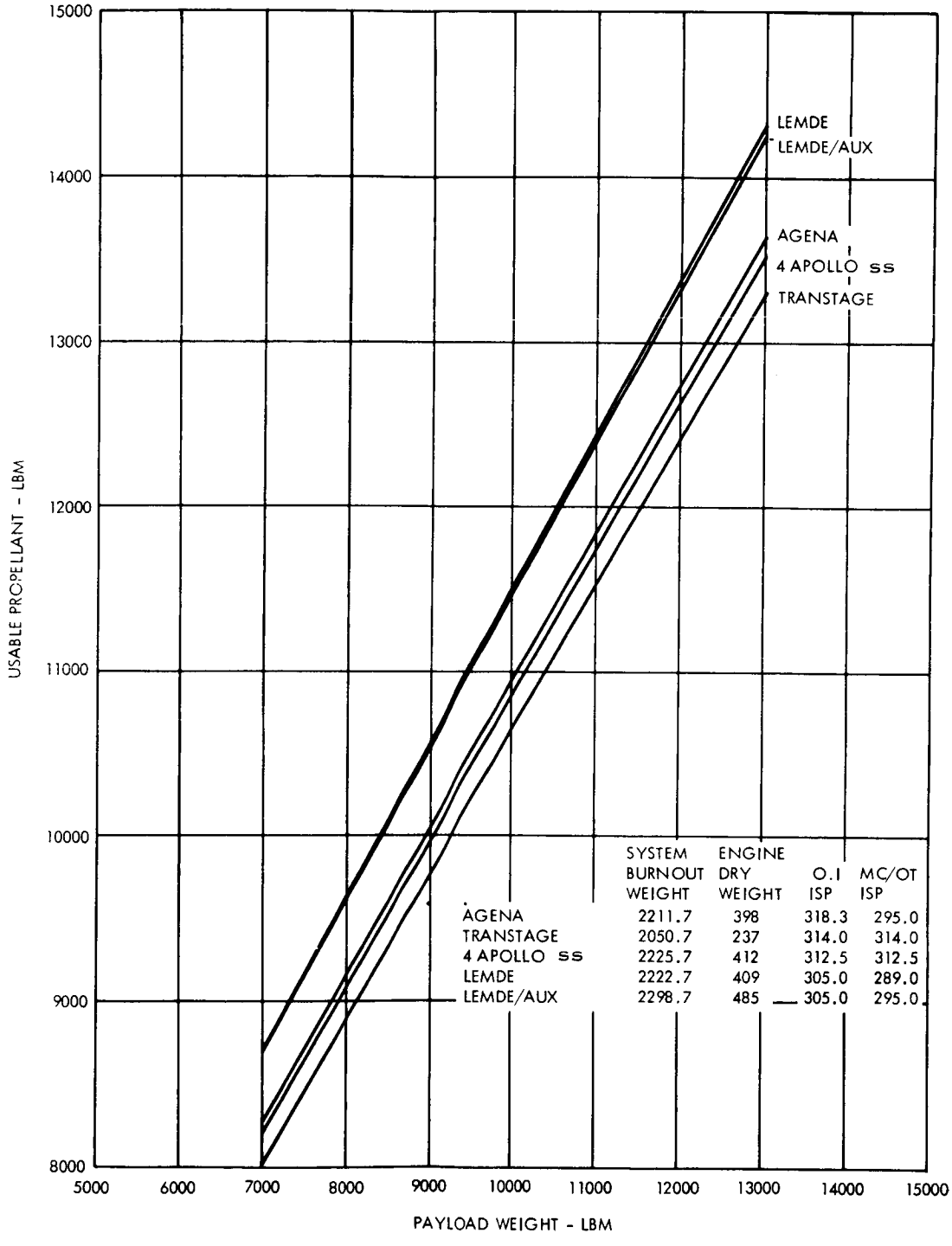

Figure 5-14. System Propellant Requirements Summary, 1973

propulsion systems are listed in Tables 5-11 and 5-12, respectively. Due to the varying degrees of development on these engines for application to the Voyager spacecraft, the characteristics in these tables are mostly of a qualitative nature.

5.5.2.2. LEMDE Engine

For high probability of mission success, which has top priority in the selection of spacecraft elements, the maturity of the LEMDE man-rated engine design and the current TRW LEMDE Voyager demonstration test program would bear heavily toward its selection for the Voyager spacecraft. In addition, the LEMDE engine has good growth potential for meeting all Voyager requirements at a single thrust level, due to possible MIB three sigma error improvement. The resultant benefits of this less complex design would be an improvement in system capability, enhanced reliability, and an increase in the probability for mission success.

5.5.2.3. Agena Engine

Although the basic Agena engine (Bell Models 8096 and 8247) has the most extensive developmental and flight proven experience, the conceptual Model 8517B Mod. 2 engine for Voyager application has a lower anticipated system reliability than the other candidate systems. This is due to its design and operational complexity and its present conceptual state of development. The Agena 8517B Mod. 2 is a modification of the Bell 8533 engine, which is currently in the definition phase of development and expected to be operational by 1970.

Given time for design definition followed by a design verification test program, the Agena 8517B Mod. 2 offers an attractive capability for Voyager application. From Bell's estimated performance for this engine in the pressure fed thrust mode, the expected minimum impulse bit and three sigma variation of 825 ± 173 lb sec make this engine very promising for operation at one thrust level in meeting the requirements of Voyager duty cycle. Operation of the 8517B engine at a single pressure fed thrust level would significantly reduce its weight, markedly simplify the engine design, and enhance its reliability.

Table 5-11. Voyager Candidate Propulsion Systems Development Status Matrix (Sheet 1 of 2)

System	System Characteristics	Development Status
1. LEMDE W & W/O Aux. Th.	Model - LEMDE (TRW) Sys. Operation LEMDE - dual mode - 9850 & 1050 lb. f. LEMDE & Aux. Th. -Tri mode 9850, 1050 & 400 lb. f. Sys. Wgt. LEMDE LEMDE & Aux. Th. Fixed wgt. 1813.7 1813.7 Lemde 409.0 409.0 4 Aux. Th. ------ 76.0 B/O Wgt. 2222.7 2298.7 lb.m	1. Prop. Sys. configuration optimized for LEMDE operation. 2. Only system TCA designed for man rating. 3. Voyager engine demonstration program underway for operational, duration and MIB characterization. 4. Performance capability essentially constant w or w/o Aux. Thrusters. 5. Design verification testing of propellant subsystem for adequacy is the pacing system development area. 6. LEMDE TCA mature design - moderate modification. 7. Flight experience - None.
2. AGENA W. Aux. Th.	Model - 8517B Mod. 2 (Bell) Sys. Operation Agena-Dual Mode - 17920 & 4910 lb.f. Agena & Aux. Th. - Tri Mode - 17920, 4910 & 400 lb.f. Sys. Wgt. Fixed Wgt. 1813.7 Agena 322.0 4 Aux. Th. 76.0 B/O Wgt. 2211.7 lb.m.	1. Basic Agena Engines (8096 & 8247) - Very mature designs Model 8533-Under develop, operational 1970 Voyager Model 8517B - Conceptual state 2. Model 8517B engine requires major design changes from Model 8533 and complete engine design verification testing for the Voyager duty cycle. 3. Estimated MIB characterization based on tests data from 8096 & 8247 engines & LEM Ascent engine: 8517B (Pump Fed) High MIB & poor repeatab. 8517B (Pres. Fed) Low MIB & good repeatab. 4. Model 8517B requires design optimization studies.

Table 5-11. Voyager Candidate Propulsion Systems Development Status Matrix (Sheet 2 of 2)

System	System Characteristics	Development Status
2. AGENA (Continued) W. Aux Th.		5. Engine and propellant subsystems design verification testing for adequacy are both pacing system develop. areas. 6. Refine prop. sys. design for Agena operational optimization. 7. Flight experience - Extensive - over 200 flights on 8096 and 8247
3. TRANSTAGE	Model - AJ10-138 (AEROJET) Sys. Operation Transtage - Single Mode - 8000 lb.f. Sys. Wgt. Fixed Wgt. 1813.7 Transtage 237.0 B/O Wgt. 2050.7 lb.m	1. Transtage TCA mature design - 2160. static tests of 102, 903 sec. firing time. Moderate modification. 2. Flight experience - 12 Titan III A & C launches as of July, 67. 3. Fair predicted MIB capability but requires engine demonstration program primarily for MIB characterization. 4. Prop. Sys. design configuration needs refinement for Transtage operational optimumization. 5. Same as LEMDE Item 5.
4. Apollo Subscale	Model - AJ10-131 (AEROJET) Sys. Operation Apollo 4SS - Single Mode - 4x2200 - 8800 lb.f. Engine out mode - 2x2200 - 4400 lb.f. Sys. Wgt. Fixed Wgt. 1813.7 Apollo 4SS 412.0 B/O Wgt. 2225.7 lb.m	1. Apollo subscale moderately mature design-555 static tests of 25000 sec. firing time. 2. Good MIB performance obtained on a typical Voyager Bus test program. 3. Same as LEMDE Item 5. 4. Same as Agena Item 6. 5. Flight experience - none 6. No development work in progress.

Table 5-12. Voyager Candidate Propulsion Systems Competing Characteristics Matrix

Competing Characteristic	LEMDE	Agena	Transtage	Apollo Subscale
1. Complexity	Moderate no. of Components	Most no. of engine components	Least no. of Components	Moderate no. of Components
2. Voyager Modification	Moderate	Major	Minor	Minor - Moderate
Design changes	State of the art	State of the art	State of the art	State of the art
Development	Minimal risk	Extensive tests	Verificat. tests	TCA & System Tests
3. Engine Characteristics				
Weight	409 lb.m + 76 lb.m (Aux. Th.)	322 lb.m + 76 lb.m (Aux. Th.)	237 lb.m	412 lb.m (Tot. of 4)
Length	90.5 in.	82.7 in.	90.5 in.	64.0 in.
Diameter, nozzle exit	59.0 in. (ϵ =47.5)	47.3 in. (ϵ =90)	57.7 in. (ϵ =60)	30.6 in. (ϵ =60)
Spec. Impulse	305 sec.	318.3 sec.	314 sec.	312.5 sec.
4. Mission Capability				
Orbit Insert Cap.	Single Mode	Dual Mode	Single Mode	Dual Mode
MC&OT Cap.	Dual Mode w. A. Th.	Dual Mode	Single Mode	Dual Mode
MIB and Variance	Est. Good & Demo. Prog. Underway	Est. Good, no Demo. Prog.	Est. Good	Excellent, Demo.
Operating Life	Good & Demo. Prog. Underway	Excellent, 2000 sec des. life	Good, 500 sec. Op. life	Good in 4 Eng. Mode, 1000 sec. Op. life. Accept. in 2 Eng. Mode
Attitude Control	Roll ACS req'd	Roll ACS req'd for 0.1.	Roll ACS req'd	Good all Oper. Modes
Exh. Plume Therm. Effect	Acceptable	Acceptable	Acceptable	Fair
5. Growth Capability				
Reliability	Excellent-Man Rated Design	Fair basic design proven	Good-Ext. Devel. tests & flight exper.	Good
Design & Develop.	Simplify design, reduce weight, improve Isp and MIB char.	Modify design specifically for Voyager, reduce wgt. & improve MIB char.	Optimized design for Voyager & Verify by Demostrat. test prog.	Opt. design for Voyager & verify by Demostrat. Test Program

5.5.2.4. Transtage Engine

The low weight transtage engine candidate is basically similar to the LEMDE engine in design and mode of operation. This Aerojet engine looks promising for development at a single thrust level (8000 lbf) to satisfy the Voyager spacecraft duty cycle. Currently, the transtage engine has no requirement for minimum impulse capability, but Aerojet has estimated from flight test data an attractive MIB capability for this engine. High system reliability can be expected for transtage if it were developed for application to the Voyager spacecraft.

5.5.2.5. Apollo Subscale Engine

The Apollo subscale engine in the four engine configuration offers the advantage of engine out capability and the ability to continue the Voyager mission in a two engine mode of operation. This engine, as the LEMDE and transtage engines, operates with an ablatively cooled thrust chamber but has the lowest design maturity and development testing experience.

An Aeroject inhouse Voyager test program evaluated the Apollo subscale engine's ablative chamber/injector design and demonstrated its pulse mode impulse bit performance. Currently, this engine offers the best demonstrated impulse bit and variance capability of the four candidates considered for the Voyager spacecraft. At present, no development work is underway on the Apollo subscale engine.

5.5.3. Conclusion

All four of the candidate engines considered for the Voyager spacecraft during Task D have the potential capability to satisfy the Voyager mission requirements.

As discussed above, the Agena, transtage and the Apollo subscale engines have varying predicted design and performance advantages over the LEMDE engine for the Voyager mission. However, the real merit of these potential advantages can only be obtained from system design definition analyses followed by demonstration test programs for design verification and system adequacy.

During the system update, the spacecraft propulsion system was updated with the LEMDE engine as the primary candidate and the alternate engines were considered for packaging into this system. Based on the attractiveness of the three alternate engines for the Voyager spacecraft, as shown in Figure 5-14, there is justification for conducting propulsion system design optimization studies on each engine. In this manner, more definitive comparisons and conclusions can be made as to their full potential.

Each of the alternate engines studied during Task D require system design definition and verification test programs, to varying degrees, to validate their predicted capability for the Voyager mission. Assuming the availability of program time and funding, it is recommended that consideration be given to conducting concurrent detailed design definition studies for each alternate system. Through the results of these studies, justification for possible design verification test programs on one or more of the candidates would be established.

VOY-D-370
APPENDIX A

DETAILED ANALYSIS OF THE SELECTED PROPELLANT MOTION CONTROL DEVICES

A.1 ANALYSIS OF SELECTED DESIGN

The function of the bellows is to provide sufficient impulse to settle the propellants to the outlet of the main tank, firing the engine at low thrust. An expression for the time required to settle propellants is presented in Reference 1, based on empirical equations for the rate of penetration of the vapor phase into the liquid phase for low viscosity fluids derived by Masica and Salzman (Reference 2). This expression is

$$t = \frac{H_L}{0.48\sqrt{aR}\left[1 - \left(\frac{0.84}{B}\right)^{B/4.7}\right]} \qquad \text{(A-1)}$$

where:

a = acceleration (ft/sec^2)

B = Bond number

H_L = Height of liquid above outlet (ft)

R = Tank radius (ft)

t = time (sec)

Reference 1, Chrysler Corp. Memorandum dated 7 Aug. 1967, from M. C. Ziemke to Claud Gage, subject "Voyager Propellant Control Studies - Preliminary Results."

Reference 2, W. J. Masica and J. A. Salzman, "An Experiment Investigation of the Dynamic Behavior of the Liquid-Vapor Interface Under Adverse Low-Gravitational Conditions," Paper presented at Symposium on Fluid Mechanics and Heat Transfer Under Low Gravitational Conditions, Palo Alto, California, June 1965.

The acceleration will be dependent on the amount of propellants to be settled, and will influence the Bond number (along with fluid properties).

From the firing times, the amount of propellants consumed during the start phase of each maneuver can be calculated. These requirements are listed below.

Propellant Settling Requirements

Maneuver	Duration (sec)	Propellant (lb)
Mid-Course 1	12	43.5
Mid-Course 2	11	39.8
Mid-Course 3	10	36.4
Orbit Insertion	10	36.4
Orbit Trim 1	10	36.4
Orbit Trim 2	8.5	30.8

A common duration of 12 sec per maneuver was selected to simplify valve sequencing command requirements. This yields a total propellant weight of 260 pounds.

The screens provide a dual function: (1) they enhance propellant acquisition by providing gas-liquid separation and (2) they limit fluid motion under zero-gravity for improved slosh damping effectiveness. A discussion of the detailed analysis of these effects follows:

The first discussion deals with screens located within the propellant tanks that utilize the surface tension forces (capillary pressure) developed at the screen by the liquid-vapor interface to confine the liquid within the tank to one side of the screen. By proper location and sizing of the screens, the liquid position in the tank can be controlled. The capillary pressures developed across the meniscus of a liquid-gas interface are directly proportional to the liquid surface tension, and inversely proportional to the radius of curvature of the meniscus in accord with Laplaces law:

$$\Delta P_{cap} = \frac{\sigma}{6R} \qquad \text{(A-2)}$$

where

ΔP_{cap} = capillary pressure drop ($lb_f/in.^2$)

σ = liquid surface tension (lb_f/ft)

R = radii of curvature of the liquid vapor interface (in.)

Capillary forces are always present, although under relatively high gravitational conditions they are insignificant compared to the other forces present. In a reduced gravity environment, however, the capillary forces become a signficant factor in the motion and position of the fluid. Under very low gravity the equilibrium position of the propellant within the tank will be determined by the surface tension forces between the liquid and its container.

For propellant tanks with simple internal geometry (cylinder, sphere, etc.), the equilibrium position of the liquid can be altered by extremely small disturbing forces. This is because of the large radius of curvature of the liquid-gas interface in the propellant tanks. If screens are placed across the liquid-gas interface, the meniscus of large radius is broken up into many menisci of smaller radius at each opening in the screen. The smaller radii greatly increase the capillary pressure across the liquid vapor interface (Equation A-2). With the increased capillary pressure, a much larger disturbing force is required to reorient the liquid. For example, if the liquid is under adverse acceleration, the hydrostatic pressure of the liquid at the screen must overcome the capillary pressure developed at the liquid-vapor interface before the liquid will flow through the screen. The hydrostatic pressure in a liquid is defined as

$$\Delta P_{hydro} = \frac{\rho ah}{(12)^3 g_c} \qquad \text{(A-3)}$$

where

ρ = liquid density (lb_m/ft^3)

a = acceleration (ft/sec^2)

h = liquid height (in.)

g_c = conversion factor ($lb_m\ ft/lb_f\ sec^2$)

The maximum height of liquid that a screen can support against an adverse acceleration is then determined by equating the hydrostatic and capillary pressures developed in the system.

$$\Delta P_{cap} = \Delta P_{hydro} \tag{A-4}$$

$$\frac{\sigma}{6R} = \frac{\rho a h_{max}}{(12)^3 g_c} \tag{A-5}$$

$$h_{max} = \frac{288 \sigma g_c}{Ra\rho} \tag{A-6}$$

From Figure A-1 the radius of curvature of the meniscus between a pair of wires is

$$R = \frac{x + d\,(1-\cos \alpha)}{2 \cos\,(\theta - \alpha)} \tag{A-7}$$

where

θ = contact angle between the liquid and the screen.

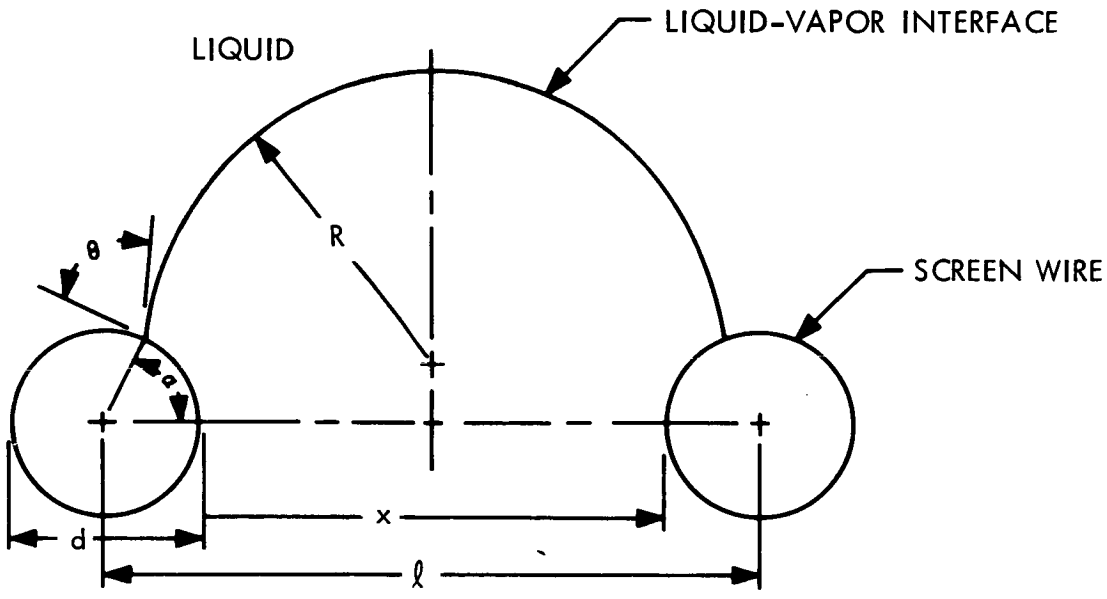

Figure A-1. Screen Geometry

For maximum capillary pressure (with $\theta = 0^\circ$), the angle α is 0° (Reference 3). Therefore

$$R = \frac{x}{2}$$

$$h_{max} = \frac{576\sigma g_c}{\rho a x} \qquad \text{(A-8)}$$

The maximum heights of N_2O_4 and A-50 that can be supported by screens of various mesh size under adverse accelerations are shown in Figures A-2 and A-3, respectively.

Reference 3, M. P. Hollister, "Propellant Containment Utilizing Screen Mesh and Perforated Plate Surfaces," LMSC Report A665481, December 1964.

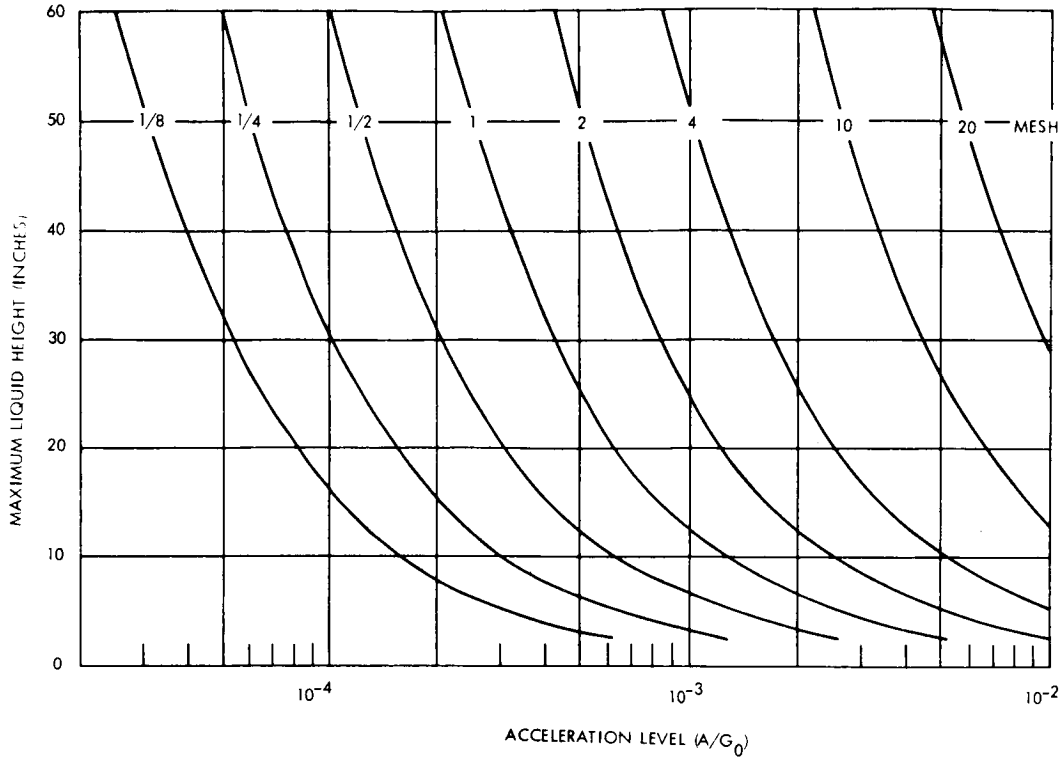

Figure A-2. Maximum Height of N_2O_4 Which Can Be Supported by Screens as a Function of Adverse Acceleration and Screen Mesh

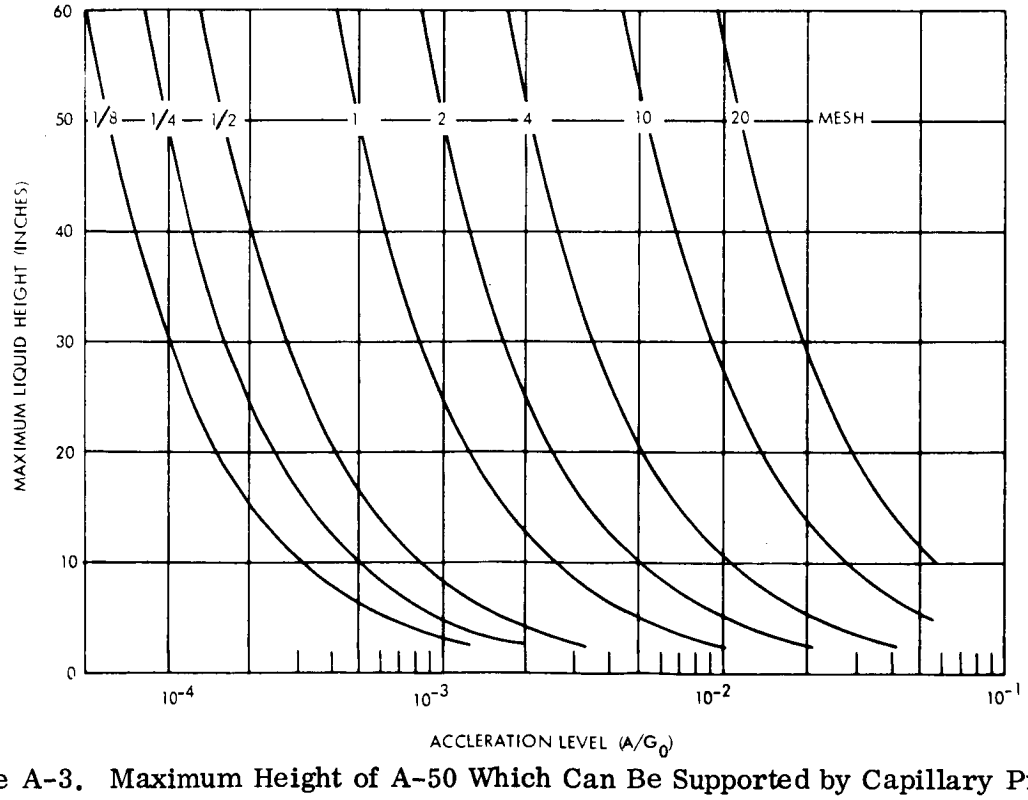

Figure A-3. Maximum Height of A-50 Which Can Be Supported by Capillary Pressure as a Function of Screen Mesh Size and Adverse Acceleration Level

From Equation A-8 and Figures A-2 and A-3, it is seen that, if properly sized, screens can be effectively utilized to maintain the liquid position against relatively large adverse accelerations. A screen placed above the liquid surface will damp large amplitude slosh waves and prevent significant quantities of the liquid propellant from shifting forward and impacting upon the forward surface of the tanks. In a low gravity environment, a wetting liquid ($\theta < 90^{\circ}$) will climb the tank walls to the screen, and then move out across the screen until it is completely wetted on the liquid side (Reference 4). The ullage gas initially below the screen then becomes a gas bubble trapped within the liquid. The ullage gas trapped below the screen must, however, be prevented from reaching the propellant feed lines. This can be achieved by locating a second screen well below the liquid surface. If the trapped gas bubble reaches the lower screen the surface tension forces created at the screen will maintain a wetted screen on the lower side, thereby preventing any gas from flowing through the screen. The ullage gas bubble will then be trapped between the lower and upper screens, away from the propellant feed lines.

A single screen located below the liquid surface will also control the position of the liquid below it. However, the liquid above it will be free. If the liquid levels are predictable, screens can be located just under the liquid surface, and relatively small amounts of liquid will be free. Large amounts of liquid remaining above the screen could have adverse effects upon the attitude control system. To preclude this situation, screens should, for maximum reliability, be located both above and below the expected nominal liquid level.

Next to be discussed is slosh damping. There has been little investigation of the slosh damping effectiveness of screens and literature on this subject is naturally quite limited. However, there have been numerous studies on the use of perforated metal baffles for the same purpose. Data on perforated baffles have been utilized to obtain some indication of the probable damping characteristics of screens.

Reference 4, R. G. Clodfelter and R. C. Lewis, "Fluid Studies in a Zero Gravity Environment," ASD Technical Note 61-84, June 1961.

It was found in various experiments that ring baffles can be perforated to a large degree and still maintain their slosh damping effectiveness. By using small perforations (about 0.02 in.), the baffles remained reasonably effective up to a perforation area (or porosity) of 30 percent.

A 100 mesh screen with a wire size of 0.004 in. diameter was investigated. Although this geometry provides a slightly higher porosity (36 percent), the screen hole sizes are less than half the diameter of the openings in the perforated baffle. In addition, the screen extends over the entire liquid surface, whereas the ring baffle only partially covers the surface. Considering the increased liquid surface area over which the screen acts, and the smaller openings, the screen should be at least as effective as the perforated baffle of the same porosity.

Considering the baffles, the damping effectiveness of these devices is dependent on their configuration and location with respect to the fluid surface. In general, for slosh damping in spherical containers, the optimum baffle width has been found to be $d/R = 0.125$. For rigid baffles, the optimum baffle thickness to width ratio is $t/w = 0.01$ to 0.04. Within this range, variations in the thickness ratio do not appreciably degrade the damping effectiveness. Figure A-4 shows the effectiveness in terms of damping ratio for a solid ring baffle over a range of depths below the liquid surface.

There is also a structural requirement that the baffle must withstand the forces imposed upon it by the sloshing liquid. These forces will be dependent on the magnitude of the exciting forces and coupling effects between the liquid and spacecraft guidance system. Weights were calculated for the baffle location shown in Figure A-5 which is for a propellant tank loaded to its maximum capacity and t/w ratios of 0.01 and 0.04. These weights are listed below:

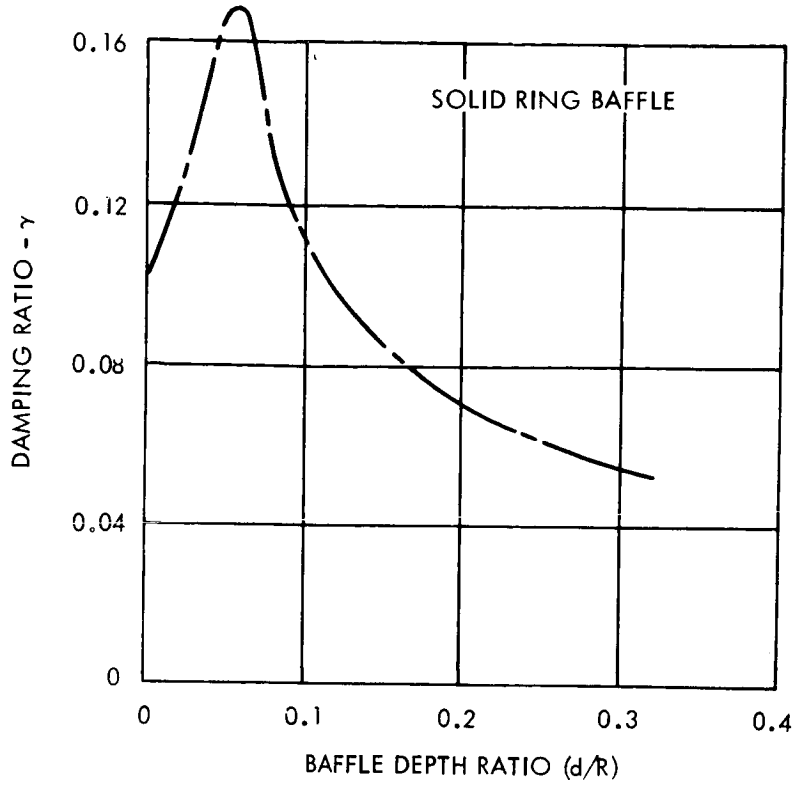

Figure A-4. Damping Ratio for Baffles and Screens

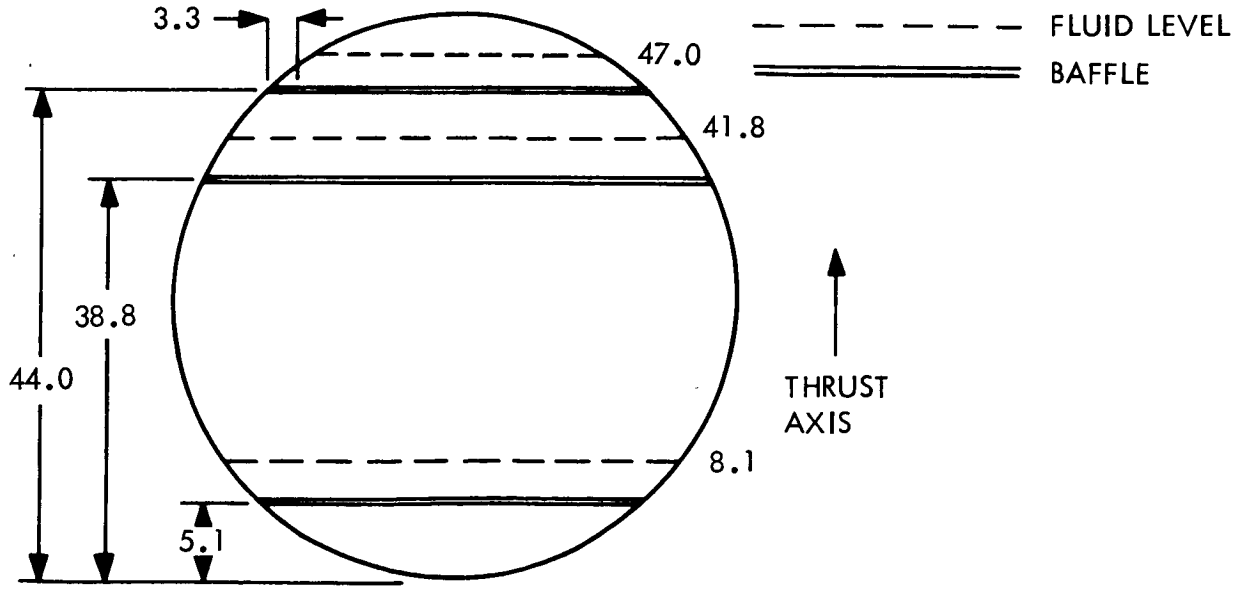

Figure A-5. Ring Baffle Dimensions for Optimum Damping

Characteristics of Optimum Ring Baffle Arrangement

Width (in.)	Thickness (in.)	Total Weight Per Tank (lb)		
		Al	SS	Ti
3.3	0.033	3.08	9.24	5.24
3.3	0.132	12.32	37.0	20.9

Flexible baffles were also investigated briefly. The optimum thickness ratio for a flexible baffle is only $t/w = 0.001$. Therefore, a flexible baffle is considerably lighter than a rigid metal one of the same width and provides increased damping effectiveness on the basis of weight. Potential flexible baffle materials include nylon, mylar and teflon. Of these only the latter is compatible with the propellants, and problems in joining the baffle to the tank and screen would have to be solved. Therefore, flexible baffles are not recommended for this application.

A three baffle arrangement was evolved to provide optimum damping for the fluid levels corresponding to the mission profile for a tank filled to its maximum propellant capacity. Figure A-5 shows these fluid levels and the location of the baffles. Width and thickness of all baffles is identical. The baffles are placed so that they are initially 3 in. below the liquid level for each maneuver. Theoretically, maximum damping effectiveness is achieved when the baffle is at the liquid level. In reality, maximum damping effectiveness is achieved when the baffle is slightly below the liquid surface so that the baffle does not break the surface during the liquid oscillation. Slight variations of the liquid level with respect to the baffle position, as is associated with usage during small mid-course and orbit trim corrections, do not appreciably affect the damping effectiveness.

It should be noted that fixed ring baffles are most effective for suppressing slosh under thrusting acceleration, and an auxilliary system (such as screens) are needed to control fluid motion under 0g and to provide gas-propellant separation.

VOY-D-380
PLANET SCAN PLATFORM SUBSYSTEM

1. FUNCTION AND REQUIREMENTS

1.1. MISSION

The mission of the Planet Scan Platform (PSP) Subsystem is to protect, environmentally control, and physically and operationally support the Mars-oriented science sensors.

1.2. BASELINE PLANET ORIENTED SCIENCE INSTRUMENTS

Preliminary design of the Planet Scan Platform Subsystem is based on these planet oriented instruments:

a. High resolution television

b. Medium resolution television (two cameras)

c. Ultraviolet spectrometer

d. High resolution infrared spectrometer

e. Broad-band infrared spectrometer

f. Infrared radiometer.

The specific requirements of these instruments are discussed in VOY-D-240.

1.3. ATTITUDE CONTROL

The Voyager Spacecraft will be stabilized with two axes to the sun and the third axis to Canopus. Attitude control of the Planet Scan Platform, relative to the spacecraft, will be three-axis, with two axes used to erect a perpendicular to the orbit plane and a third axis used to track Mars in the orbit plane. This concept emerged from PSP configuration studies

that were performed during Task A and is adopted as a requirement since it is ideal* for the science instruments and has the potential for simple and reliable implementation.

Design of the attitude control system will produce the steadiness requirements of the photo-imaging equipment as well as pointing accuracy consistent with a useful science mission. Attitude control will be implemented to provide for automatic operation as required by paragraph 3.3.3.2 of the 1 January 1967 draft of the General Specification for the 1973 Voyager Mission. A design goal is the ability to point along the Mars local vertical at any time during the 1973 design orbital mission; a design requirement shall be the ability to point along the Mars local vertical during the prime data acquisition period of the 1973 design orbital mission.** Also, as required by paragraph 3.3.3.3.2 of the 1973 Voyager General Specification, this pointing capability will be maintained even if capsule separation is not effected.

1.4. THERMAL CONTROL

The Planet Scan Platform will provide for temperature control of the science instruments. Detector cooling is not a function of the PSP, but the packaging design will consider the required cold space viewing for the instruments requiring detector cooling.

1.5. STRUCTURAL REQUIREMENTS

The Planet Scan Platform structure will provide integrity during handling in a gravitational field, launch or orbit injection thrusting in the stowed position, and orbit trim thrusting after deployment. Micrometeorite protection consistent with the required high probability of mission success will be provided.

---

* Image motion compensation, if required, need only be performed in one axis. Constant orientation about the local vertical is ideal for mapping, stereo, and line scanning experiments.

** The prime data acquisition periods occur when the spacecraft is below 3000 kilometers altitude and the sub-spacecraft point is illuminated by the sun.

1.6. INTERFACE REQUIREMENTS

The Planet Scan Platform Subsystem will provide for the science instruments as well as itself, the necessary hardline links to the spacecraft to transmit electrical power, engineering telemetry and command information, as well as science data. The design will endeavor to provide telemetry information, such as data concerning pointing direction, which is useful in analyzing science data.

1.7. RELIABILITY

Proper operation of the Planet Scan Platform Subsystem is absolutely essential to a successful Voyager mission; furthermore, the mission duration is long compared to that of most spacecraft currently flying. A design policy shall be to utilize conservative, simple, and proven implementations to the greatest degree consistent with mission requirements. The design shall consider use of redundancy, as well as capacity for operation in alternate modes, should component failures degrade the primary mode of operation. Where feasible, failure isolation will be implemented to reduce the impact of component failures on the entire system.

1.8. FLEXIBILITY

The Planet Scan Platform design will recognize that the characteristics of the baseline instruments are poorly known and will change; a design policy will be to avoid solutions that are limiting as far as changes which may logically be expected in the process of spacecraft development. An example is that a thermal control concept which cannot tolerate reasonable increases in dissipated power should be avoided. The design must have the capability to tolerate possible non-nominal situations as well as the variations of viewing conditions with arrival date.

One of the goals for the 1973 Voyager mission is to develop techniques and hardware for later Voyager missions. However, this goal is of lower priority (See Voyager 1973 Mission Specifications, paragraph 3.1.3) than accomplishment of a high quality 1973 mission. Therefore, the Planet Scan Platform Design shall place strong emphasis on the 1973 mission with design concessions to later missions when the penalties are minimal.

2. TRADE ANALYSES

2.1. VIEWING ANALYSIS

2.1.1. Mission Associated Viewing Requirements and Considerations

A worthwhile goal for the Voyager preliminary design is to configure a flexible spacecraft - one that will provide a proven vehicle for future interplanetary missions and not force unwanted constraints on these later flights. Existence of a costly, proven, but inflexible, design may preclude a desirable mission; indeed, the objectives of later Voyager missions will likely be strongly influenced by the findings of early missions. On the other hand, highly adaptable spacecraft design usually results in added complexity - usually the hardware which flies is somewhat less adaptable than initial estimates. The Voyager PSP has a rather complicated function that is absolutely essential to a successful mission. The very nature of its function makes it difficult to effectively apply redundancy; the length of a Voyager mission imposes severe reliability requirements. Flexibility at a cost of reliability is a poor bargain for Voyager.

Fundamental to the determination of an acceptable PSP design is an understanding of the viewing capabilities of a particular configuration as well as viewing requirements of candidate missions. In order to assess quantitatively the viewing capability of a given configuration, the following, reasonable, assumptions are invoked:

a. The Voyager science mission requires that the PSP be stabilized about three axes. Two degress of freedom are used to erect a perpendicular to the orbit plane; the third degree of freedom is used to track the Mars local vertical.

b. With a nominal mission, a very large proportion of the science data will be collected while the PSP is tracking the Mars local vertical.

c. Special provisions for line-of-sight clearance for off-nadir viewing are not required. Off-nadir pointing will be scheduled for times when the necessary line-of-sight is available.

d. The nadir tracking loop will employ Mars horizon sensors for control. These sensors must have a relatively wide field of view in the plane of the orbit due to the large change of Mars' subtended angle from periapsis to apoapsis.

e. In the interest of reliability and simplicity, the nadir tracking loop will not be designed to distinguish between Mars and the spacecraft.

These assumptions imply that, for a particular configuration, orbits can be classified according to impact on the PSP attitude control system:

a. Attitude control sensor interference will not occur for certain orbits.

b. Sensor interference occurs at points in some orbits where data acquisition is not desired. With these orbits, the PSP can be programmed to avoid interference. However, if the potential for interference exists, sooner or later it will occur due to a non-nominal operational situation.

c. For certain orbits, sensor interference will occur in the prime viewing region.

Orbits of the third class should be avoided. These same classifications apply to the narrow field of view science sensors, but the consequences of interference are different. The implication on a science sensor is only that the sensor line of sight temporarily intersects the spacecraft, precluding viewing. If the horizon sensors acquire the spacecraft, diagnosis of the problem and a command from Earth will likely be required to resolve the difficulty - a minimum of a full orbit's science data would probably be lost. A PSP design is desired that does not have a potential for attitude control sensor interference; interference with the science sensor line-of-sight is to be avoided during the prime data acquisition region of the orbits.

2.1.2. Techniques for Viewing Analysis

In-orbit operations with a Voyager spacecraft will be simplified if the fields of view of all instruments and sensors never have the possibility of spacecraft blockage. A computerized analysis tool has been developed to evaluate, for a particular PSP implementation, which orbits of all possible orbits have the property that field of view interference will not occur. A particular orbit is identified by the clock and cone angles of the line perpendicular to the orbit plane (the orbit normal-Figure 1). A region in clock and cone angle space then represents the orbit planes that are acceptable (based on the no interference criteria) to a

particular implementation; an example of such a region is given in Figure 2. These acceptable viewing regions can be shifted in clock angle by moving the mounting point around the spacecraft and, to a lesser degree, in cone angle by moving the mounting point axially along the spacecraft.

A second analysis tool is used to supplement this program. Given that line-of-sight interference will occur for a given orbit, it is important to identify the consequences of the viewing restriction - does the blockage occur during prime data acquisition time? An illustration of the kinds of information available from this second analysis tool is given in Figure 3. A blockage of the medium resolution TV line-of-sight by the engine nozzle is the subject of the illustrative investigation.

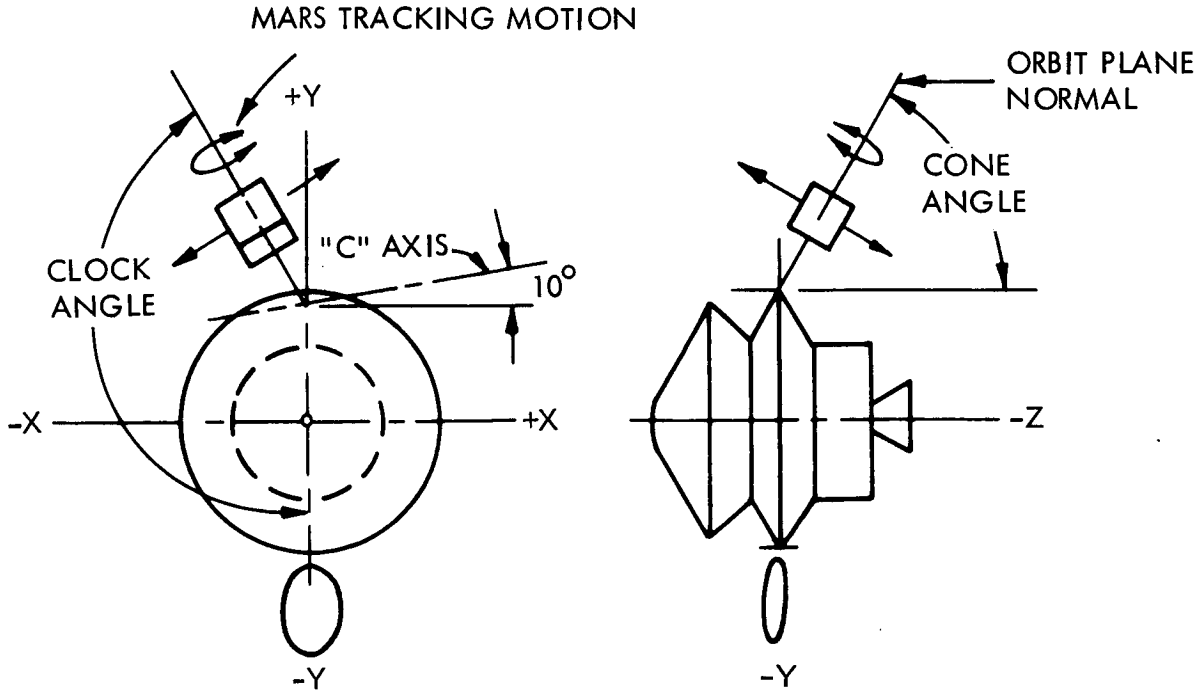

Figure 1. Planet Scan Platform Geometry

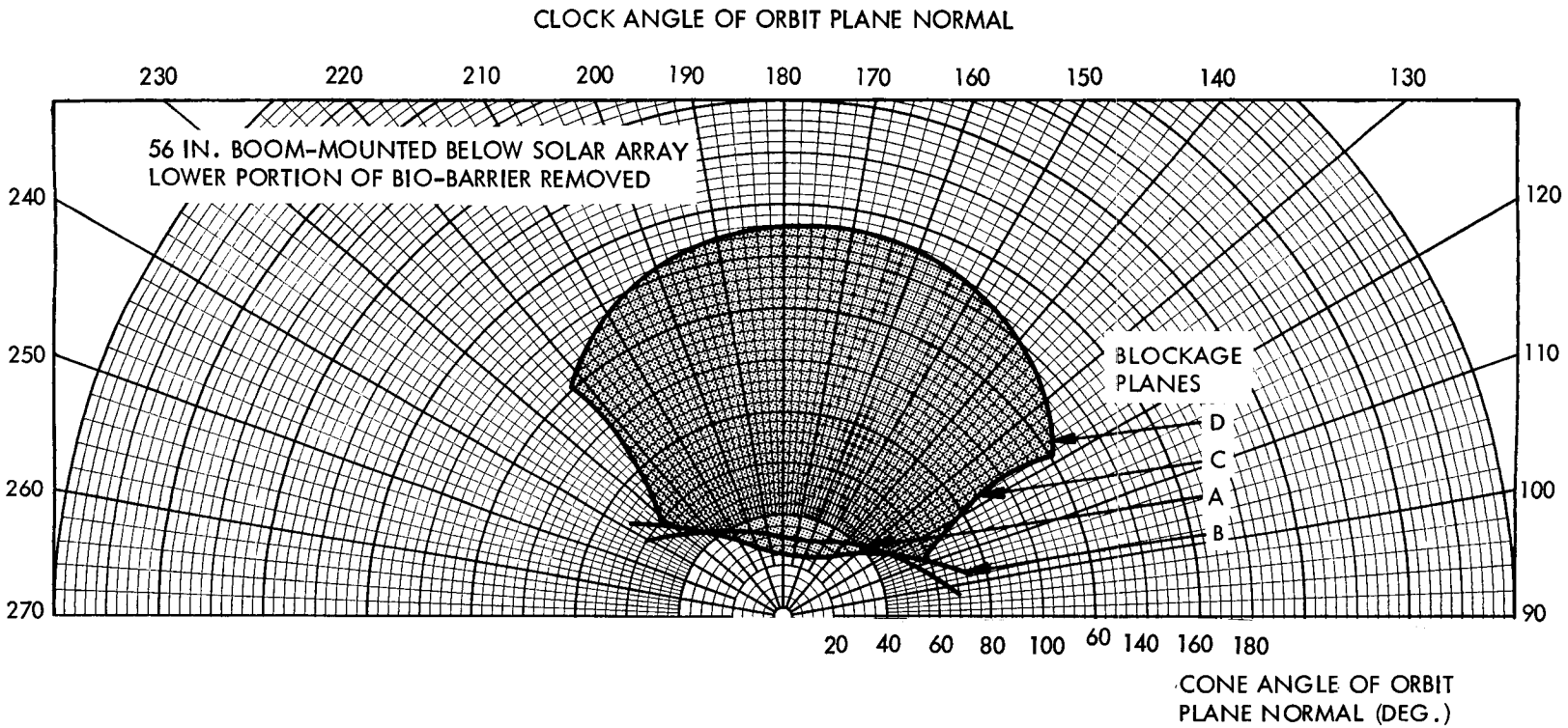

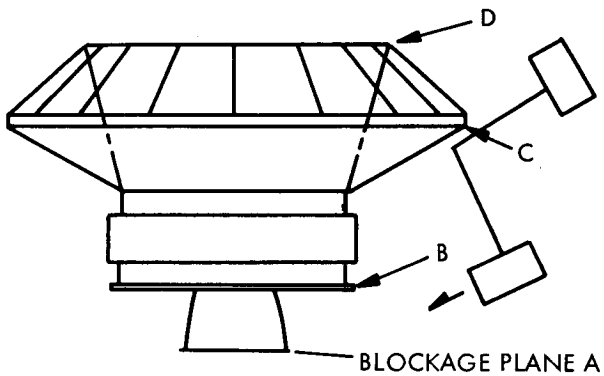

ACCEPTABLE ORBITS

Figure 2. PSP Orbit Coverage Example

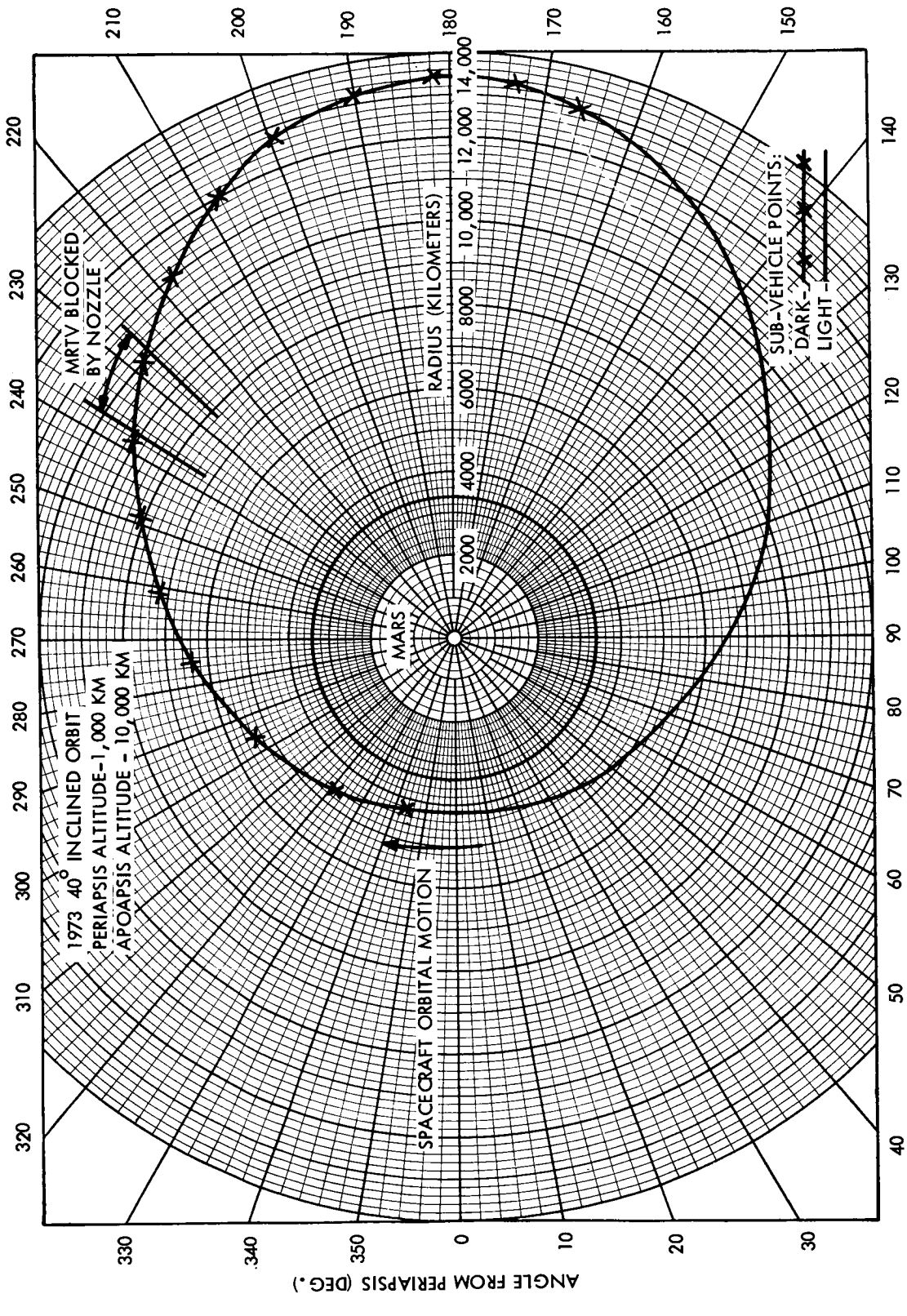

Figure 3. Orbit Conditions for 15 Days After Arrival Date of March 7, 1974

2.1.3. Viewing Requirements for Various Missions

An understanding of the viewing requirements of the PSP is essential for proper consideration of flexibility and intelligent selection of configuration. This section examines the progression of the orbit normal for missions that are (more or less) candidates for Voyager. All orbits are elliptical with periapsis altitude of 1000 kilometers and apoapsis altitude of 10,000 kilometers. These specific questions are considered:

a. If a PSP design is implemented for a particular orbit inclination and arrival date, what is the impact on viewing if the arrival date is changed within the same mission opportunity?

b. What are the viewing problems in creating a design which is adaptable to orbits of various inclinations?

c. Assuming that a PSP design is created for specific orbit inclination for the 1973 opportunity, is it likely this design can handle similar orbit inclinations in later opportunities?

These questions have not really been exhaustively examined; the results presented here are a combination of selective analytical investigation and intuition.

One would expect that for a given opportunity and fixed orbit inclination, the viewing requirements will not vary too greatly with arrival date. Figure 4 verifies this hypothesis for 40-degree inclination orbits for two 1973 arrival dates.

Figure 5 represents the progression of the orbit normal for four different orbit inclinations for the same arrival date. It is notable that a given orbit plane is equally well described by each of two normals; hence, two trajectories are shown for each mission. If either trajectory lies within the region of "no interference" orbits for a given PSP configuration, then the design will handle that orbit without spacecraft interference.

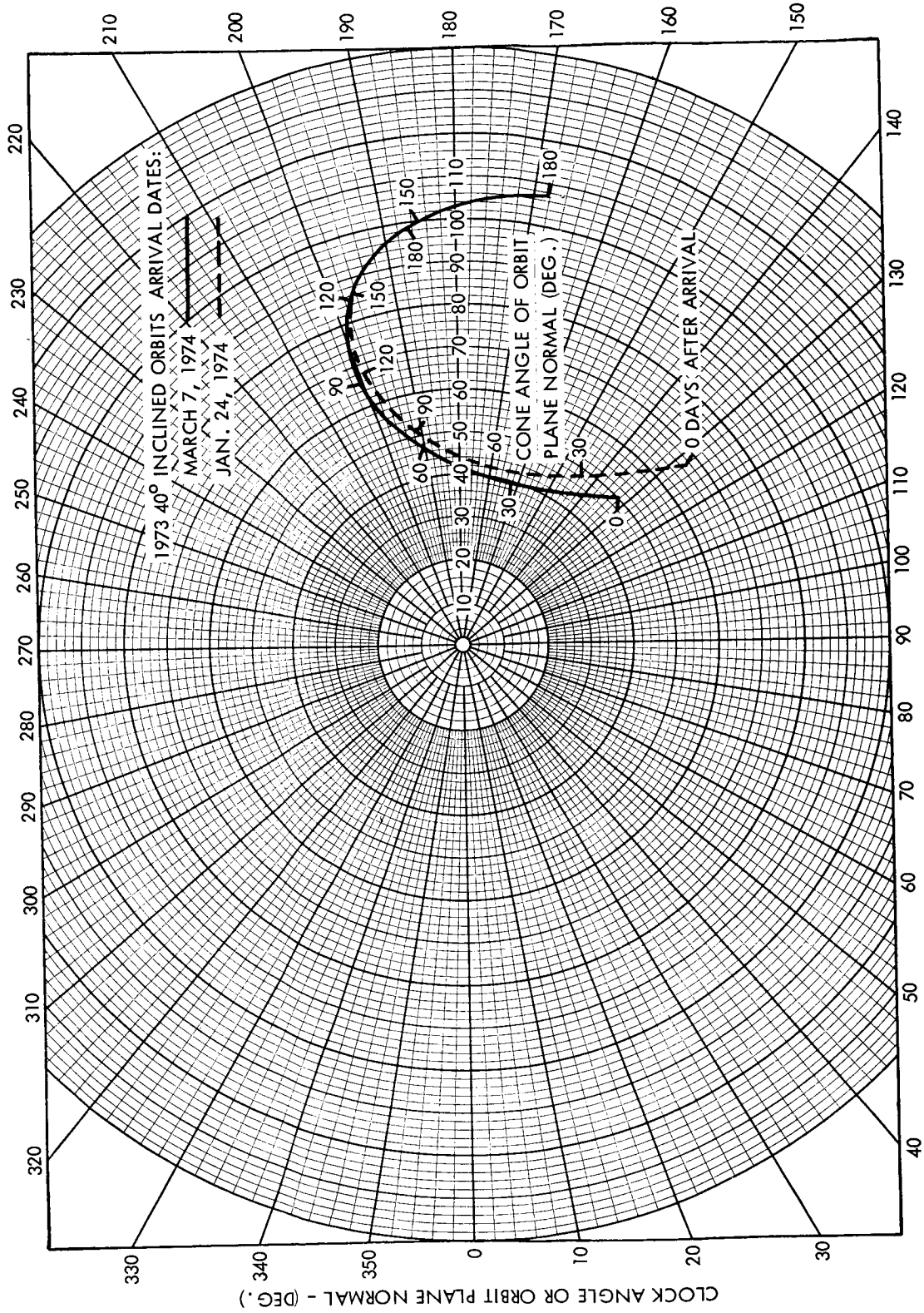

Figure 4. Effect of Arrival Date on Progression of Orbit Normal

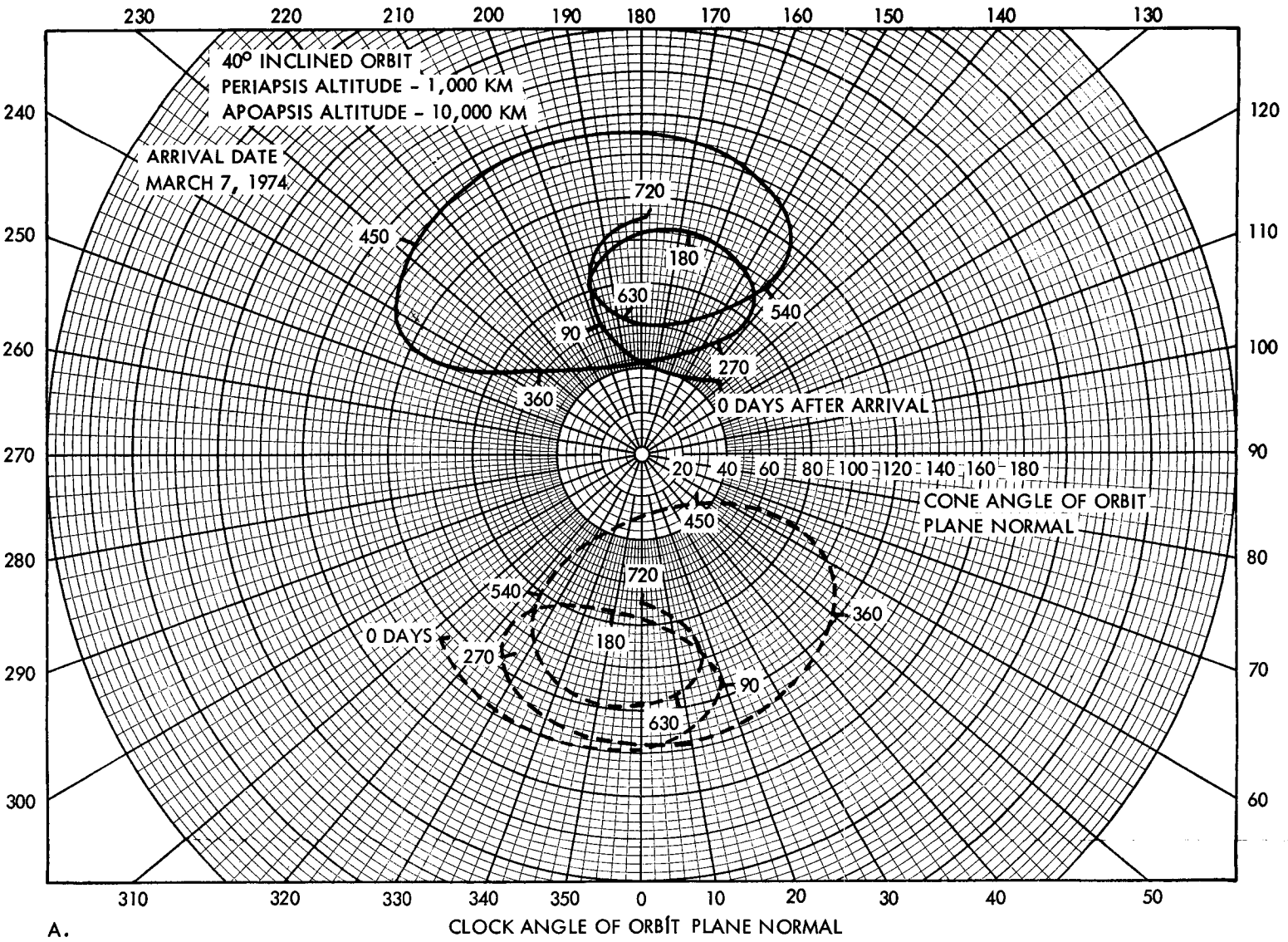

A.

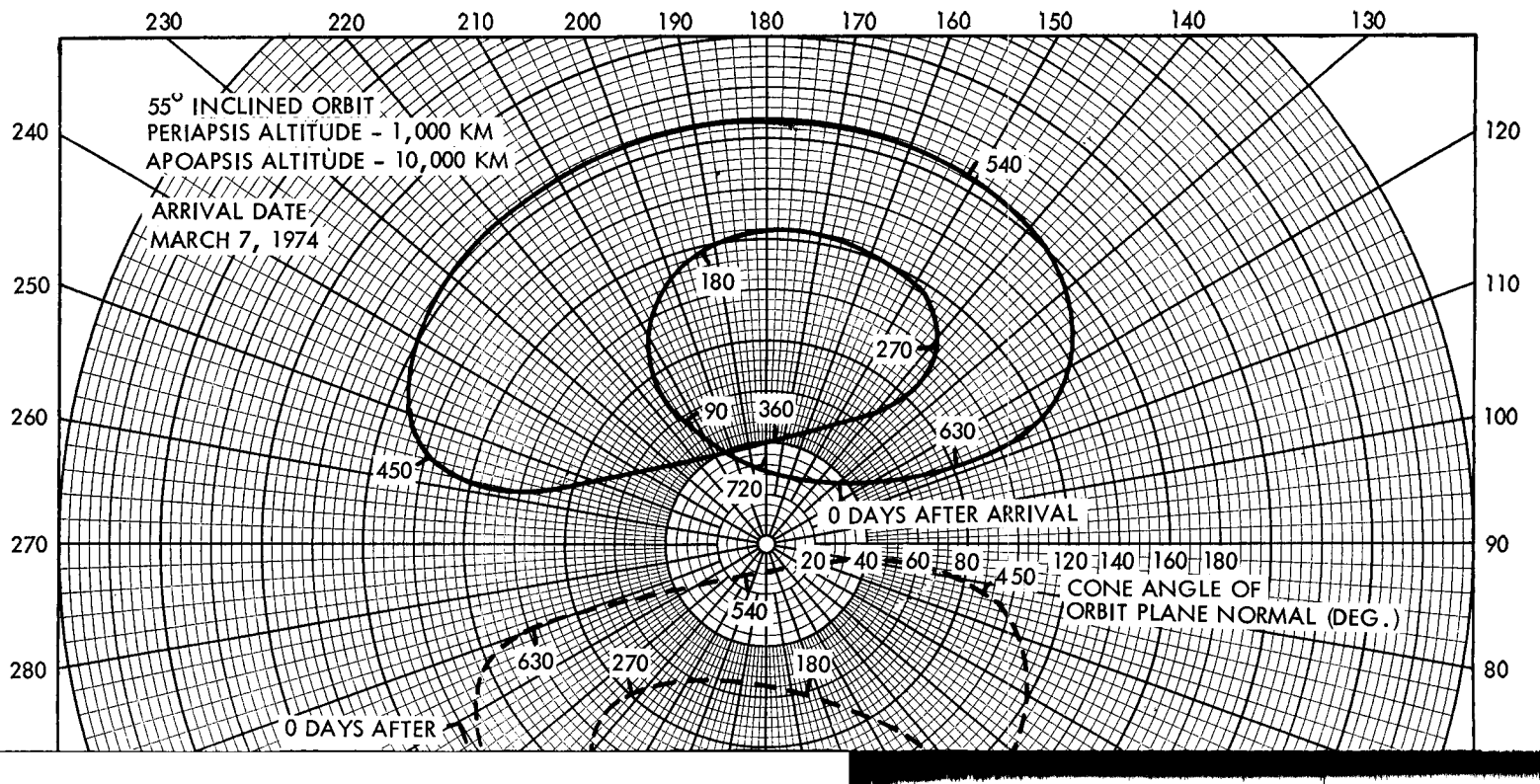

FOLDOUT FRAME

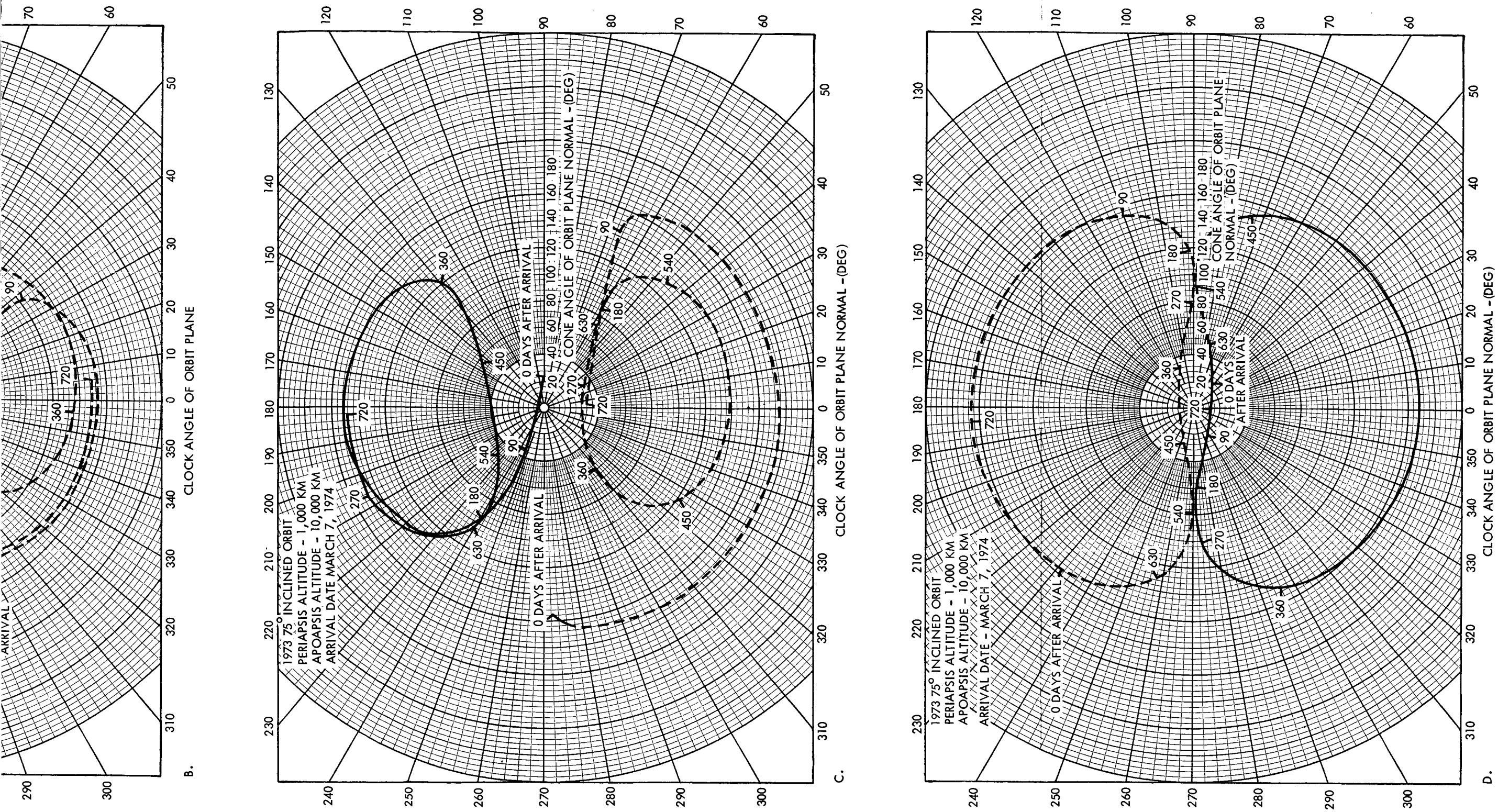

Figure 5. Effect of Inclination on Orbit Normal Progression

FOLDOUT FRAME 2

FOLDOUT FRAME 3

FOLDOUT FRAME 4

All missions will experience sun interference when the trajectory passes through a cone angle of 90 degrees. With this situation, the sun lies in the orbit plane and it is possible that the PSP will be controlled by ground command to minimize the possibility of pointing the instruments toward the sun.

Figure 6 shows the progression of the orbit normal for the design orbits (selection of the design orbits is discussed in VOY-D-260) for the 1973-79 opportunities.

Study of these plots reveals that a one-year mission in 1973 with a 40-degree orbit inclination, as compared to other opportunities and inclinations, is very favorable from a PSP viewing standpoint. This fact led to selection of a baseline PSP configuration for a 1973 orbit of 40-degree inclination as discussed in the next section, along with consideration of approaches for increasing viewing capability without unreasonable boom lengths.

2.1.4. Viewing Aspects of Baseline Configuration Selection

The content of this section represents a summary of the viewing analysis work which lead to selection of the 1973 baseline configuration. Preliminary work such as viewing versus boom length trades is not discussed, but the way in which these analyses were performed is well illustrated in Section 2.1.5. The gimbal articulation approach of using two degrees of freedom to erect a normal to the orbit plane and a third to track Mars in the orbit plane permits several gimbal alternatives; the two important ones are illustrated in Figure 7. On the left, a single non-retractable deployment axis is used in conjunction with a three-axis gimbal located near the center of gravity of the PSP. The concept on the right combines the deployment function with the two axes which erect the normal to the orbit plane. A significant difference in the two approaches, which was an important consideration in establishing the concept on the right as the baseline configuration, is that this gimbal configuration provides significantly better viewing for a given boom length. This difference is illustrated quantitatively in Figure 7.

FOLDOUT FRAME 1

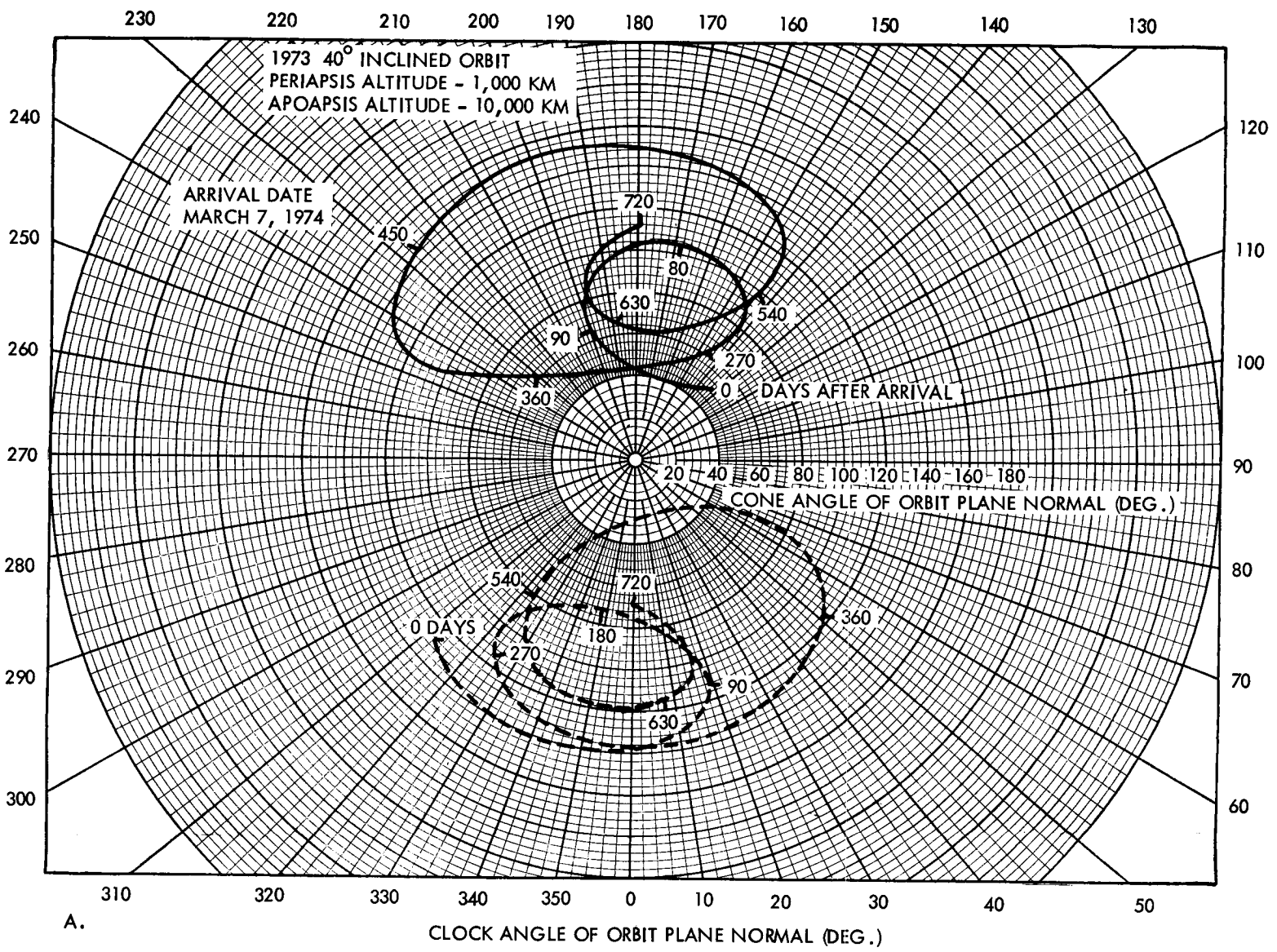

A.

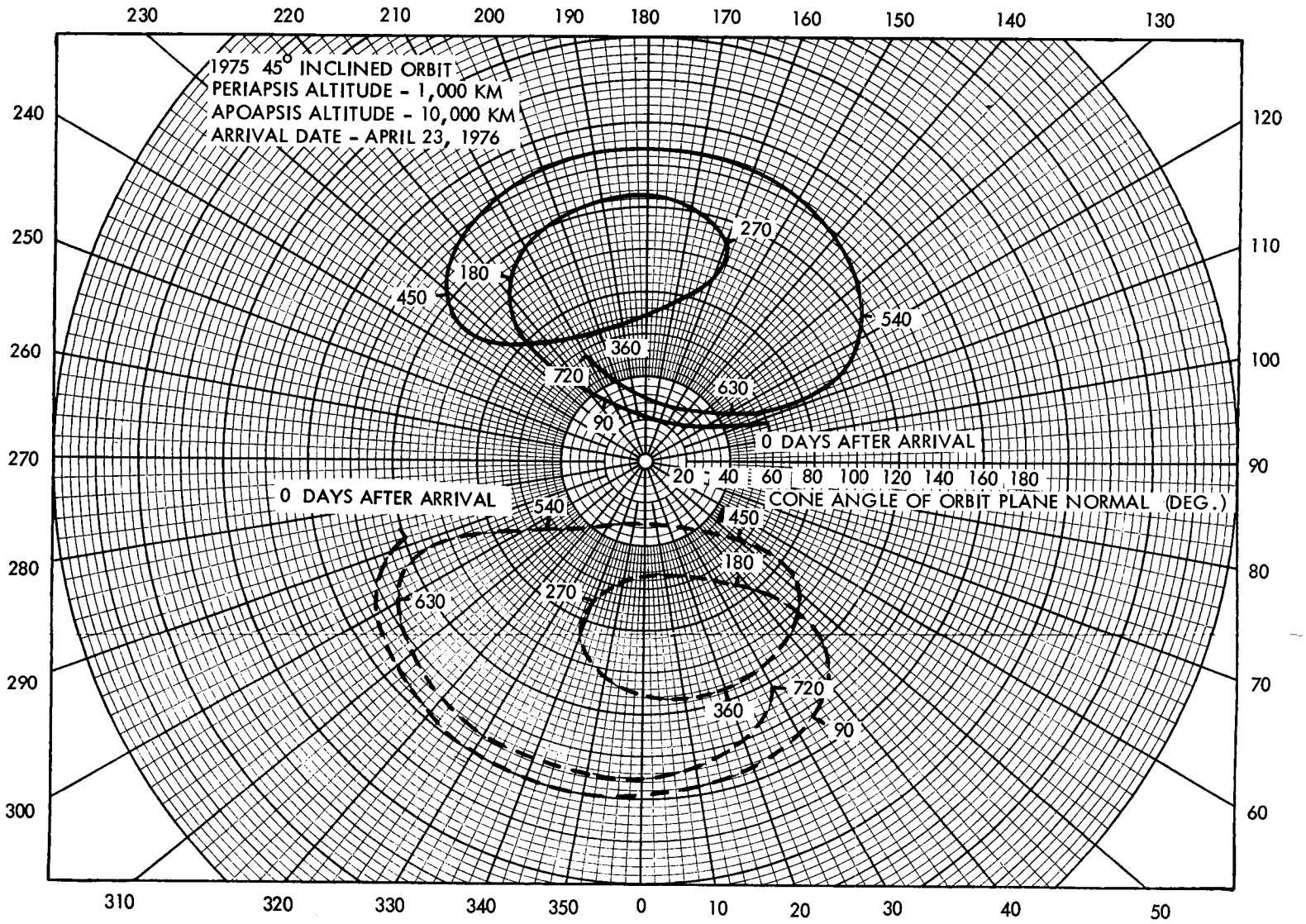

B.

FOLDOUT FRAME 2

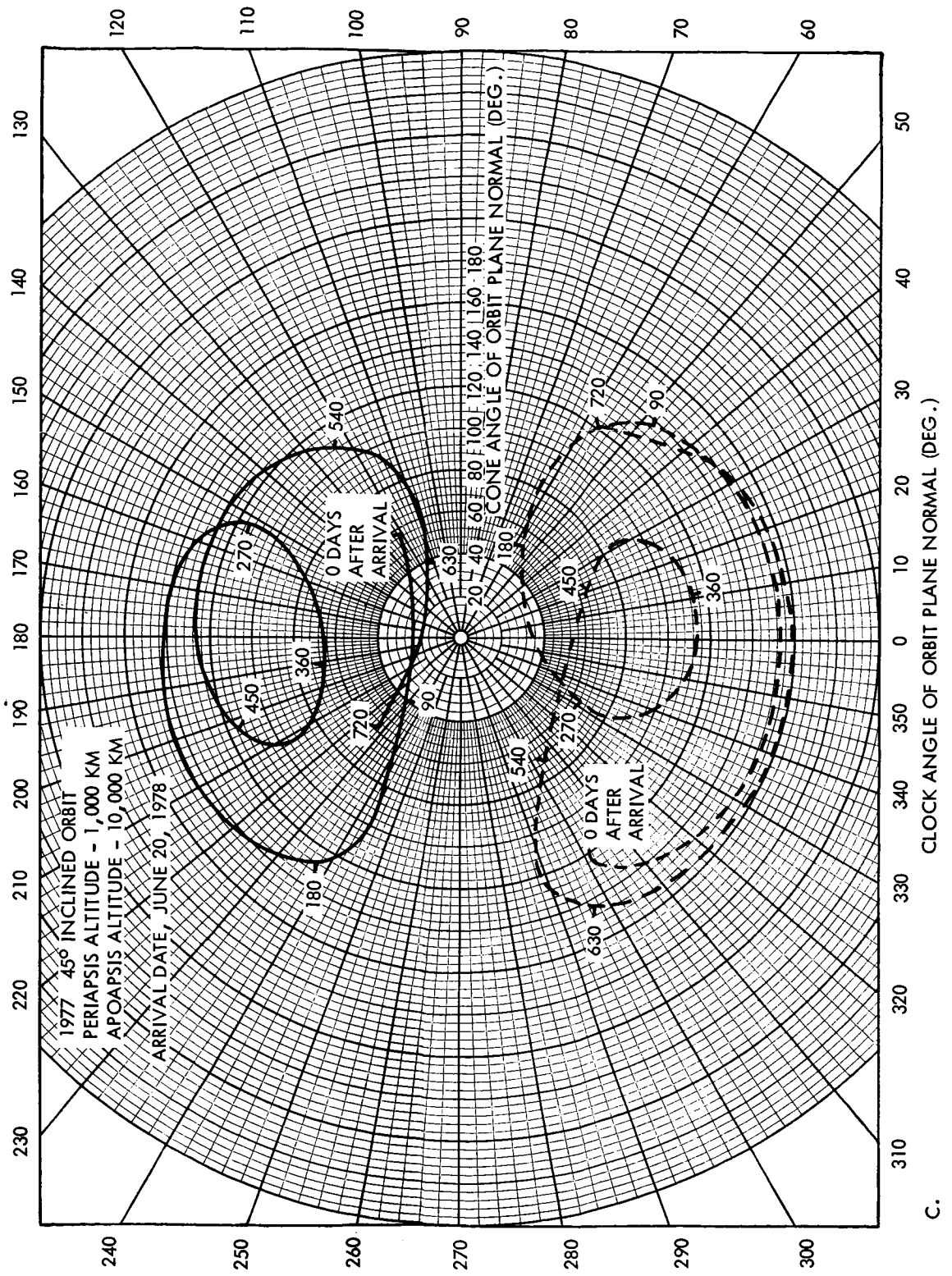

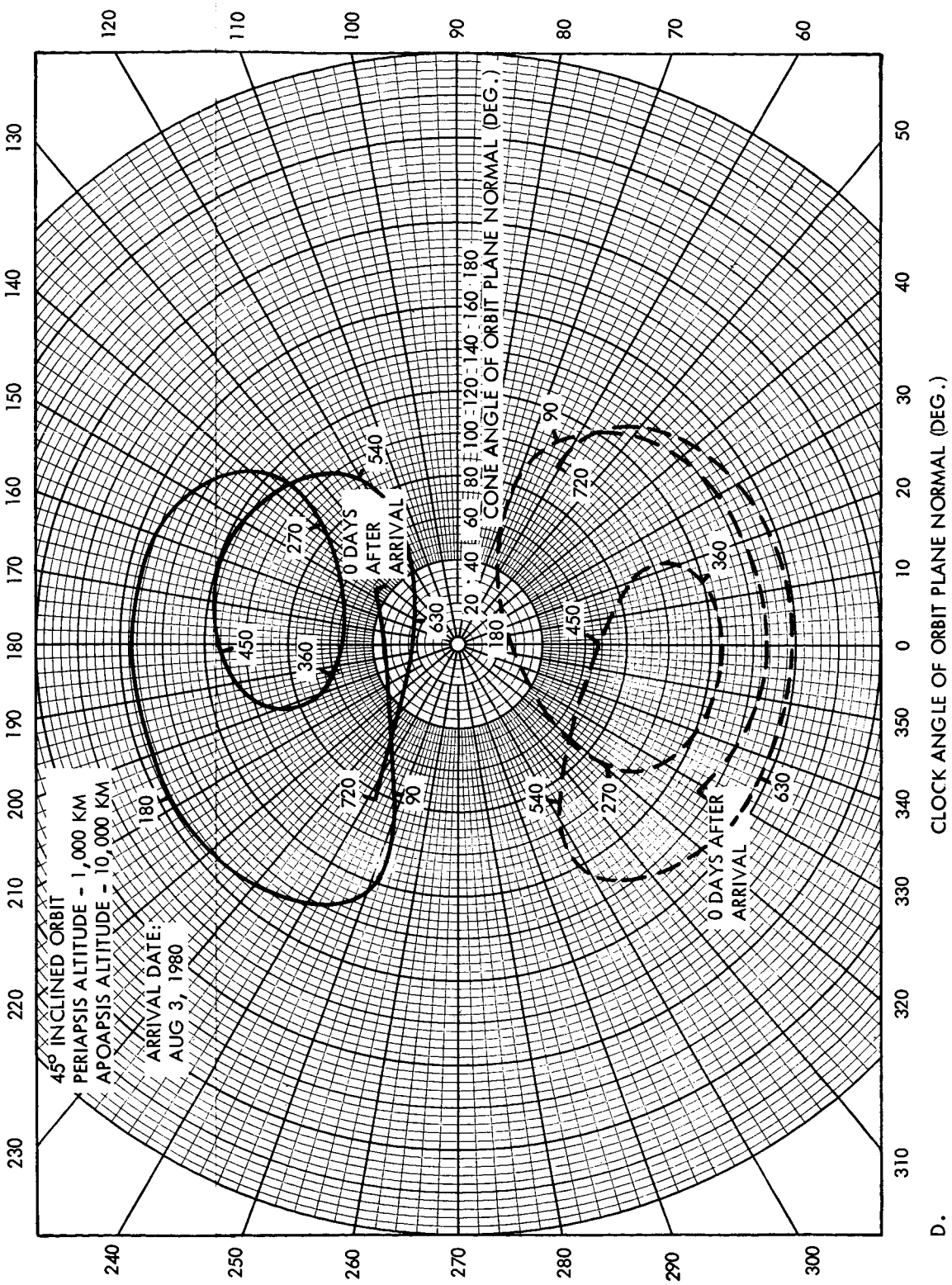

Figure 6. Effect of Launch Opportunity on Orbit Normal Progression

FOLDOUT FRAME 4

FOLDOUT FRAME 3

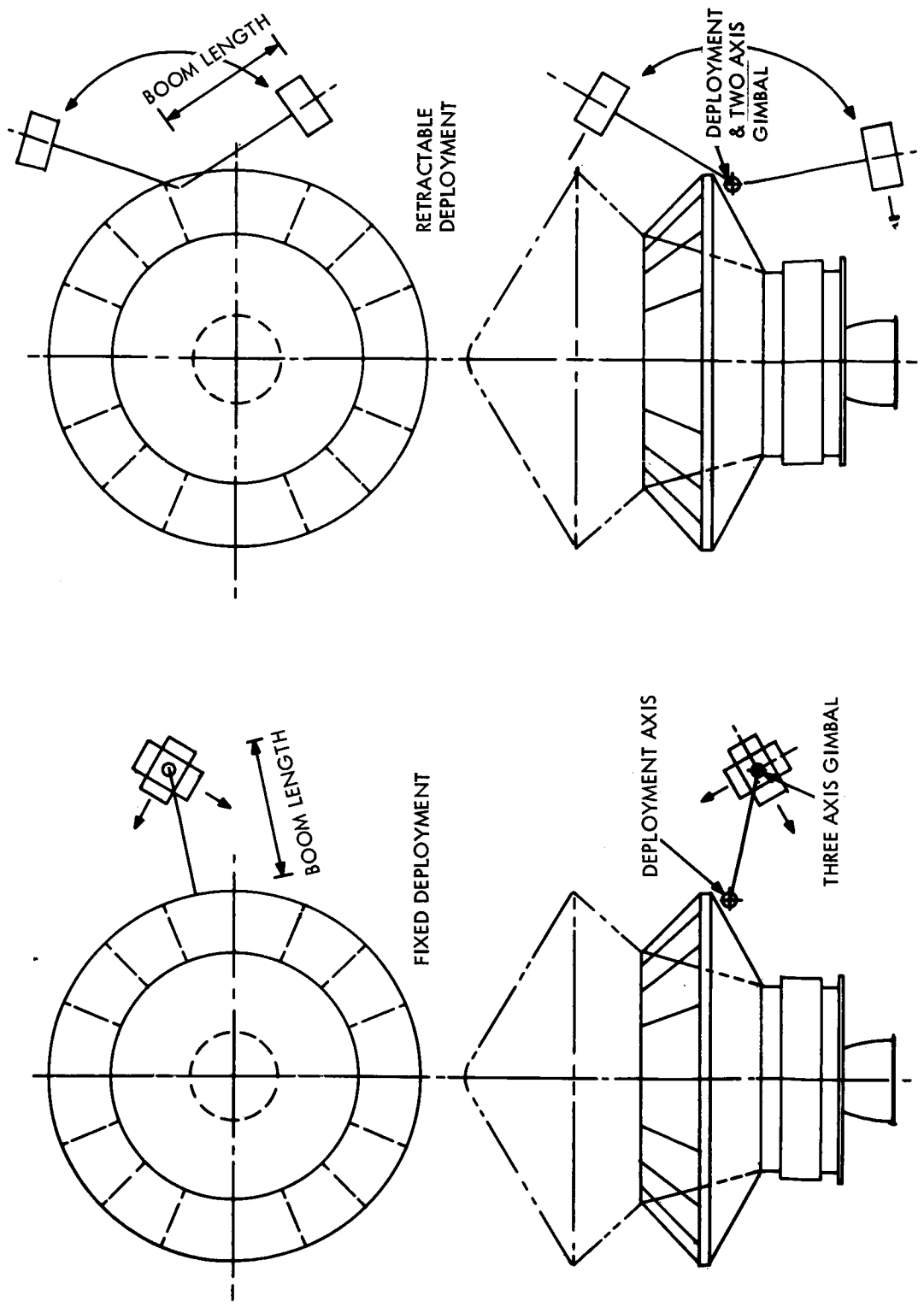

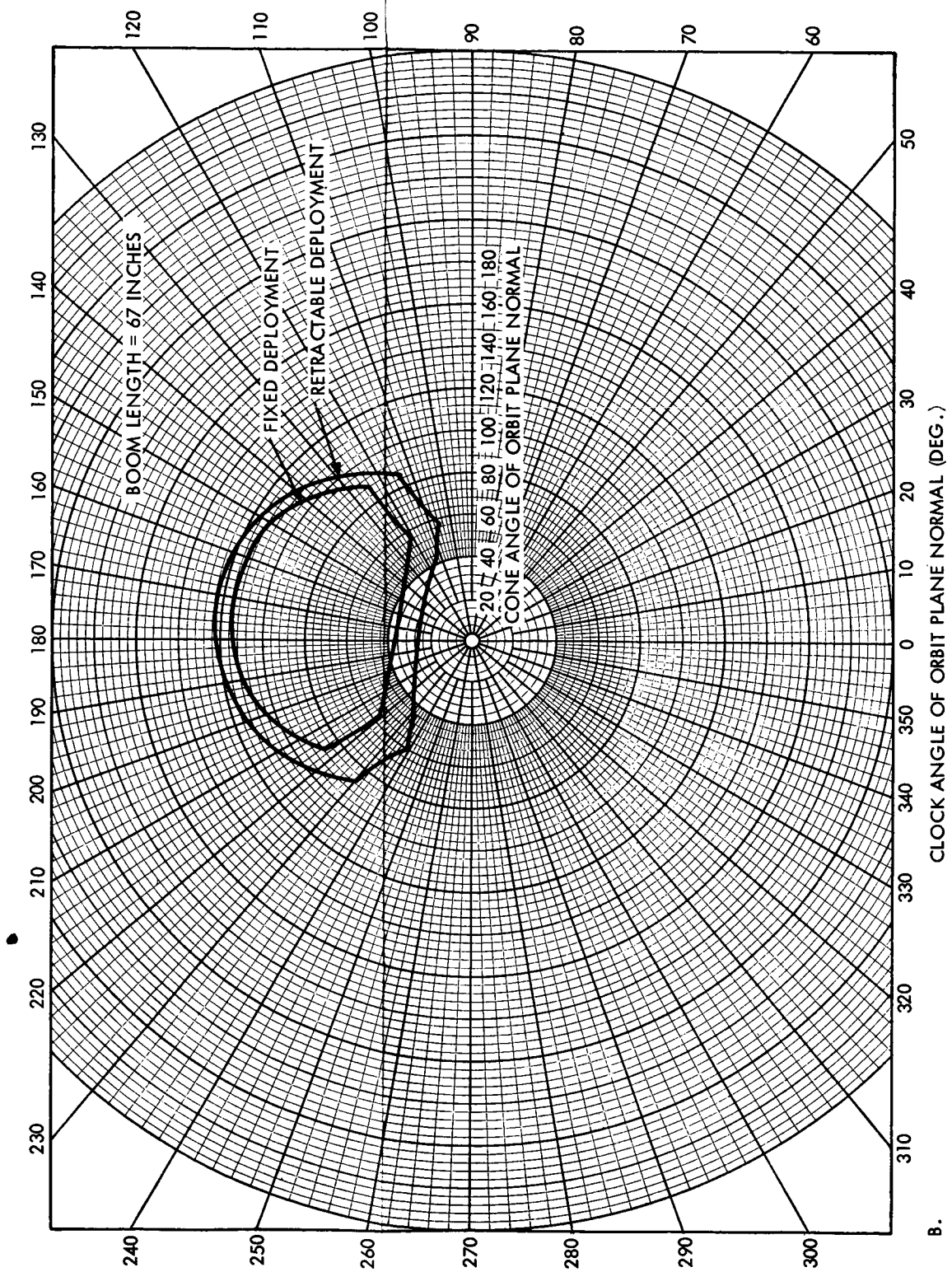

Figure 7. PSP Orbit Coverage with Alternate Gimbal Configurations

As indicated in Section 2.1.3, the viewing requirements for the first 360 days of the 1973 design orbit are much easier to fulfill than 1973 orbits of higher inclination or orbits of similar inclination for later opportunities; design penalties are apparent in establishing a PSP configuration to provide the wider coverage requirements of later missions. In this report, the design of a PSP for the 1973 opportunity is pursued and the viewing problems and alternatives involved in obtaining the more general coverage required by other missions are discussed in the next section. Important influences on the 1973 baseline configuration selection are:

a. Vehicle blockage* of the attitude control sensors is to be avoided for the nominal mission.

b. Vehicle blockage** of the science instruments is permitted, but should not occur during times when the sub-vehicle point is illuminated by the sun and the orbiter altitude below 3000 kilometers.

c. Capsule separation shall not be required to obtain the necessary PSP field of view. This consideration is obtained from the 1 January 1967 draft of the 1973 Voyager Specification (paragraph 3.3.3.3.2).

As determined from Figure 5, the orbit normal for the first 360 days of the design 1973 trajectory moves so as to be reasonably well covered by a PSP mounting point near the +Y axis of the spacecraft at a clock angle of 170 degrees. In general, coverage is improved by locating the vehicle pivot point at a large radius, so it is natural to consider the two mounting locations illustrated in Figure 8. The terms "above solar array mounting" and "below solar array mounting" are used in a generic sense and the actual mounting points analyzed are representative. Vehicle blockage maps (with the capsule in place) are also shown for these two mounting locations in Figure 8. For a given boom length, mounting below the solar

* Attitude control sensor blockage is defined to occur if the spacecraft intrudes into a region five degrees on either side of the plane swept by the attitude control sensors.

** Science instrument blockage is defined to occur if the spacecraft intrudes into a five-degree half-angle cone centered on the sensor boresight.

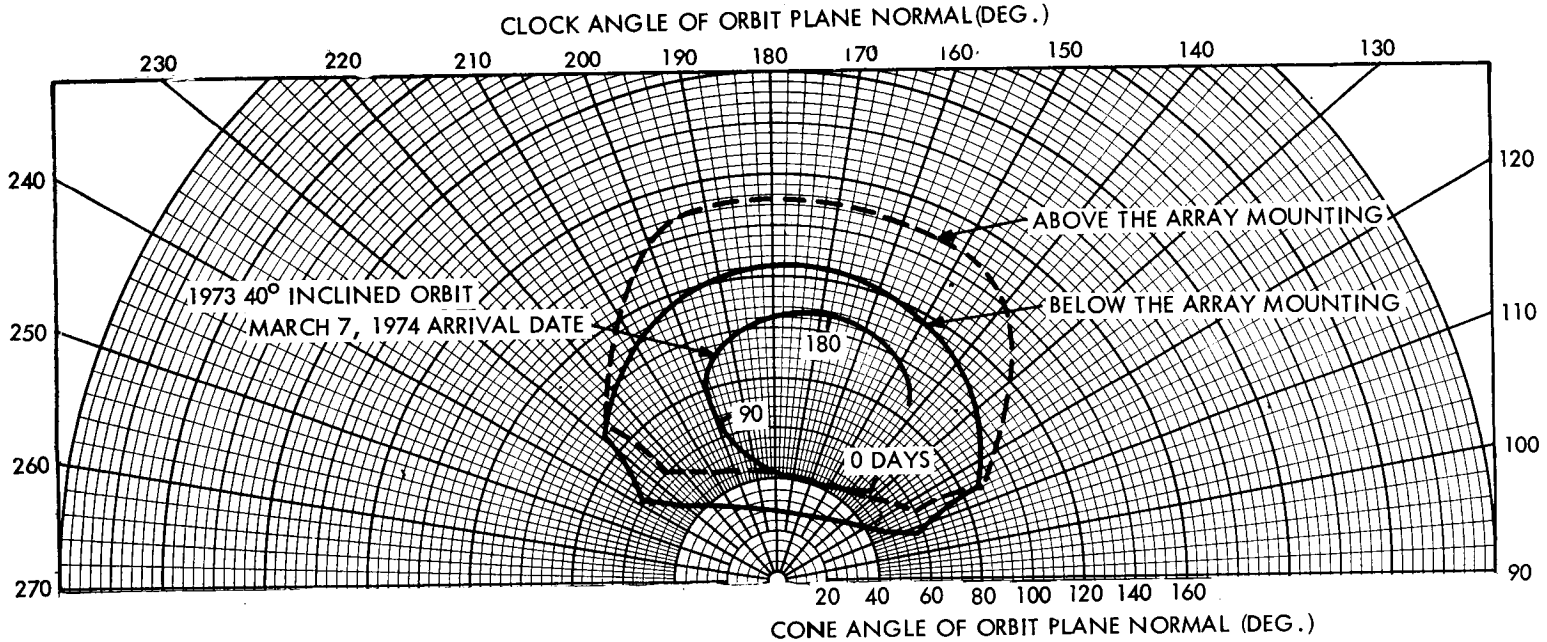

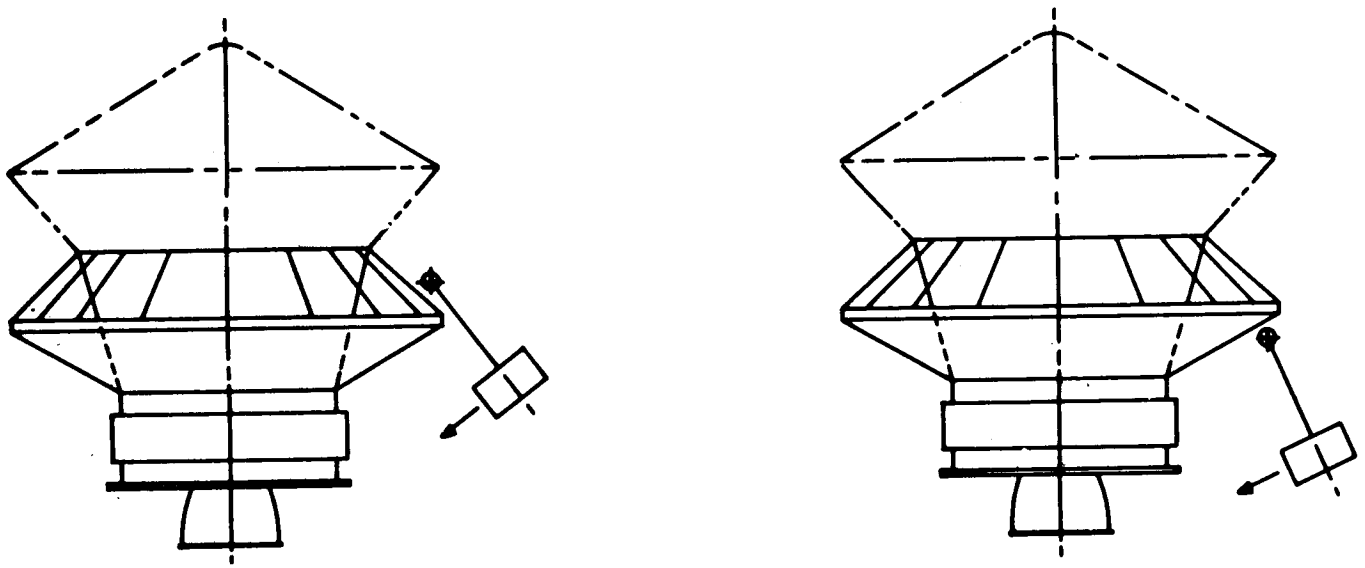

Figure 8. Comparison of Above and Below Array Mountings for Equal Boom Lengths

array results in considerably less engine nozzle interference than "above the array mounting." Figure 9 presumes that the "above the array" pivot point is mounted near the vehicle -Y axis or that a second Canopus sensor has been used to orient the spacecraft +Y axis to Canopus. For this case, the two mounting locations are quite competitive from a sensor interference standpoint. It should be noted that the source of blockage for the early 1973 orbits is not the same; mounting above the solar array results in biobarrier interference. Unfortunately, all viewing instruments cannot be mounted in the same viewing plane as the attitude control sensors. For both mounting points, certain of the science instruments will be blocked during parts of the early orbits. Figure 10 indicates the extent of the blockage in a typical early orbit for a medium resolution television camera (which has the poorest location from a blockage standpoint in the baseline science package). The "below solar array mounting" results in minimal blockage at times when the instruments will not be in use. The "above array mounting" experiences blockage during the prime data acquisition regions of the early orbits of the mission. This viewing advantage was probably the strongest factor leading to the selection of "below the array mounting" for the baseline configuration.

An important viewing consideration is the black space view requirement for radiative cooling of instrument detectors. Using "above the array mounting" in conjunction with 180 degree roll capability permits identification of a surface of the PSP (the surface opposite the mounting boom) which will never be illuminated by the sun. With the 1973 design orbit and "below the array mounting", the angle between the sun line and the perpendicular to this surface gets as small as 40 degrees and a large sun shade is required for detector shielding.

The infrared radiometer has a large field of view (± 60 degrees) perpendicular to the orbit plane that will rarely be completely free of spacecraft blockage. Except for the data loss, this does not arouse serious concern.

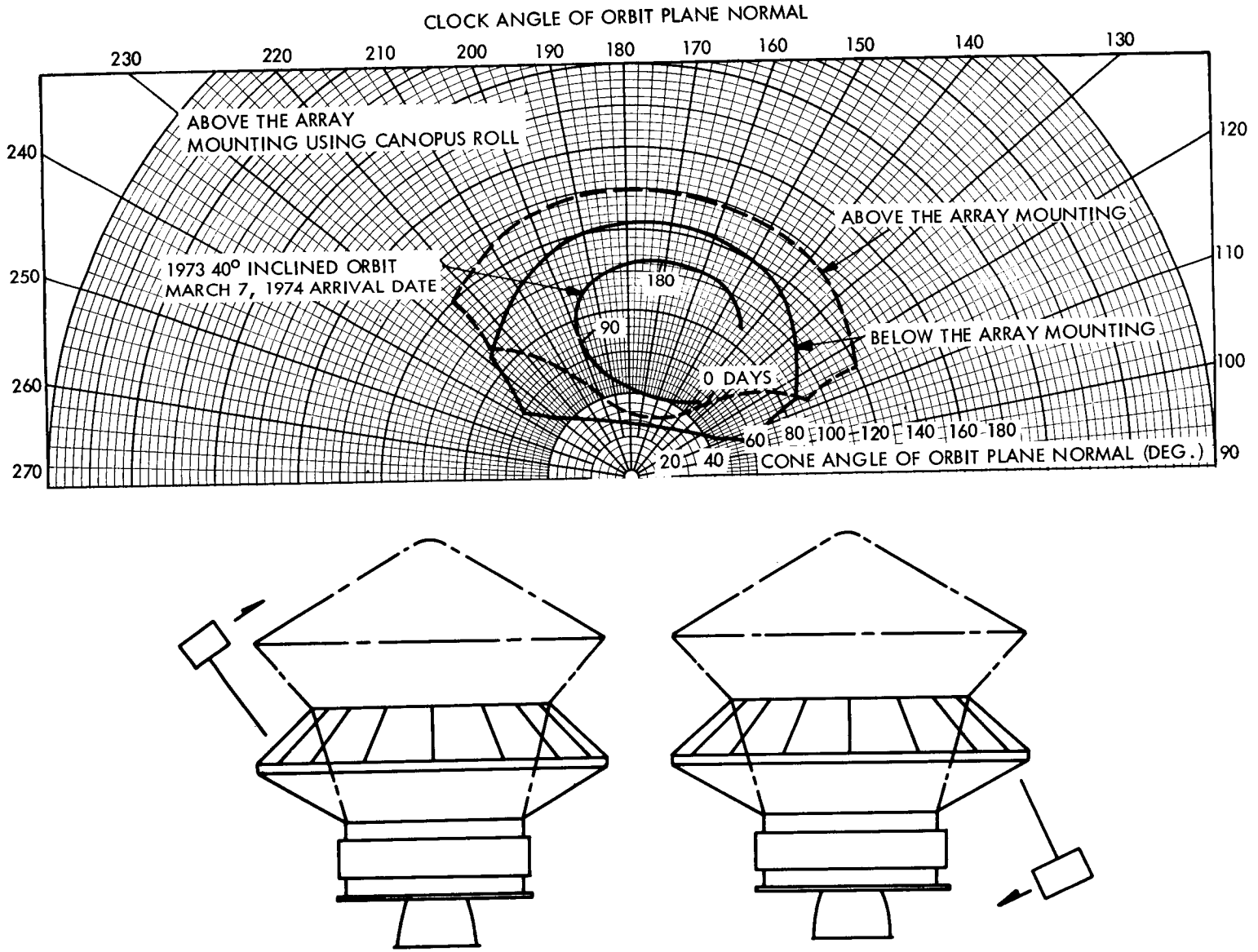

Figure 9. Comparison of Above and Below Array Mountings for Equal Boom Lengths

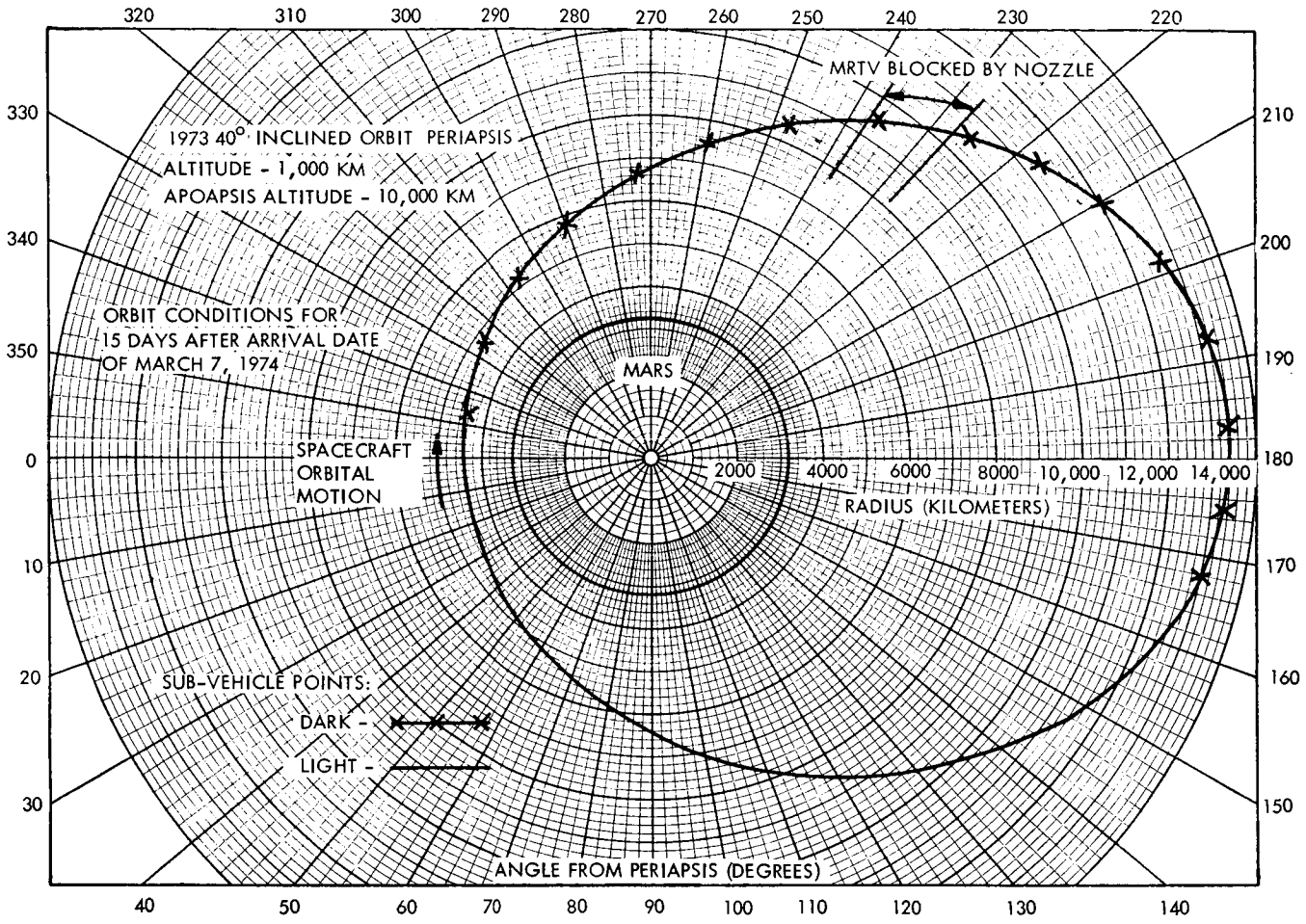

10a

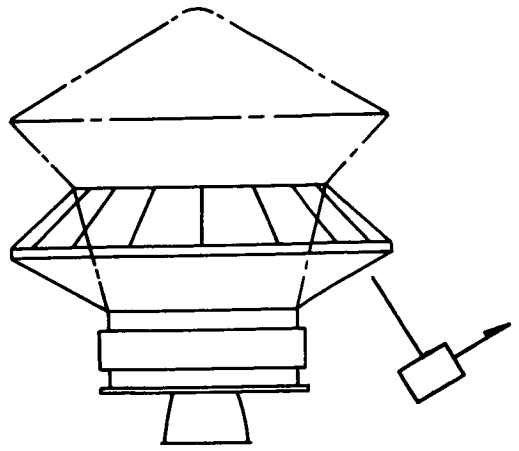

A.

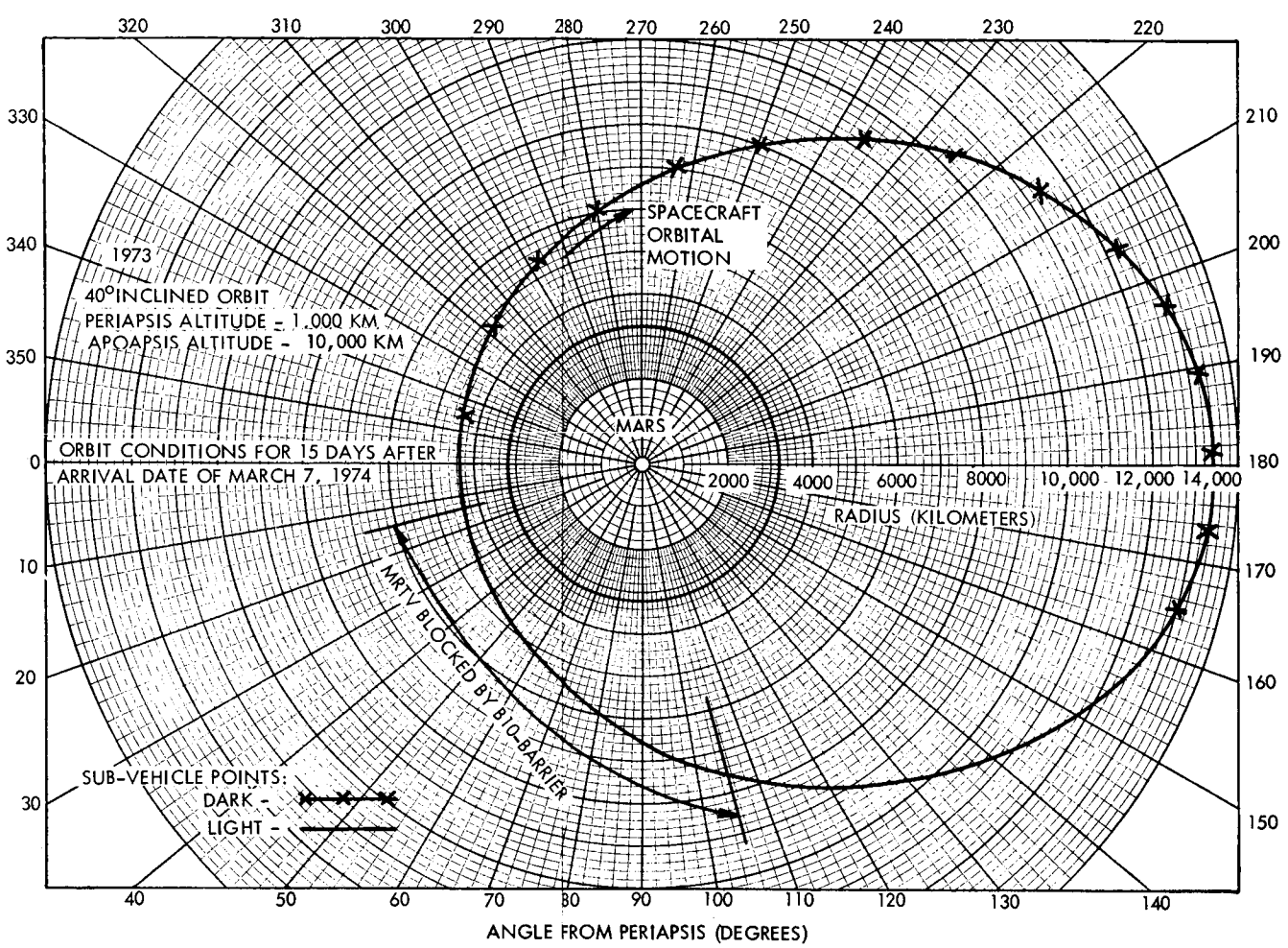

10b

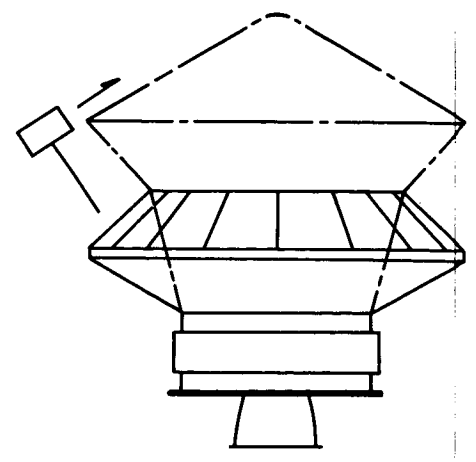

B.

Figure 10. Comparison of "Above the Array Mounting" (with 180° Canopus Roll) and "Below the Array Mounting"

FOLDOUT FRAME 23

FOLDOUT FRAME 24

2.1.5. Techniques for Wider Viewing

Techniques for improving PSP coverage have been examined and will be covered briefly in this section. The system implications of certain of these approaches have not been carefully studied, but some of the more obvious implications will be mentioned. For lengthened, high-quality Voyager science missions in the later opportunities, viewing improvements will be necessary.

To obtain viewing coverage for all orbits, a design must be created that will handle all orbits with normals in a hemisphere. This objective can be approached with the techniques illustrated in Figure 11. The scan platform pivot point is located at a large radius and either very high or very low so it can "look around the corner" of the spacecraft and obtain coverage of approximately one quarter of the sphere. A 180-degree Canopus roll then permits coverage of a second quarter of the sphere. With the capsule in place, the above

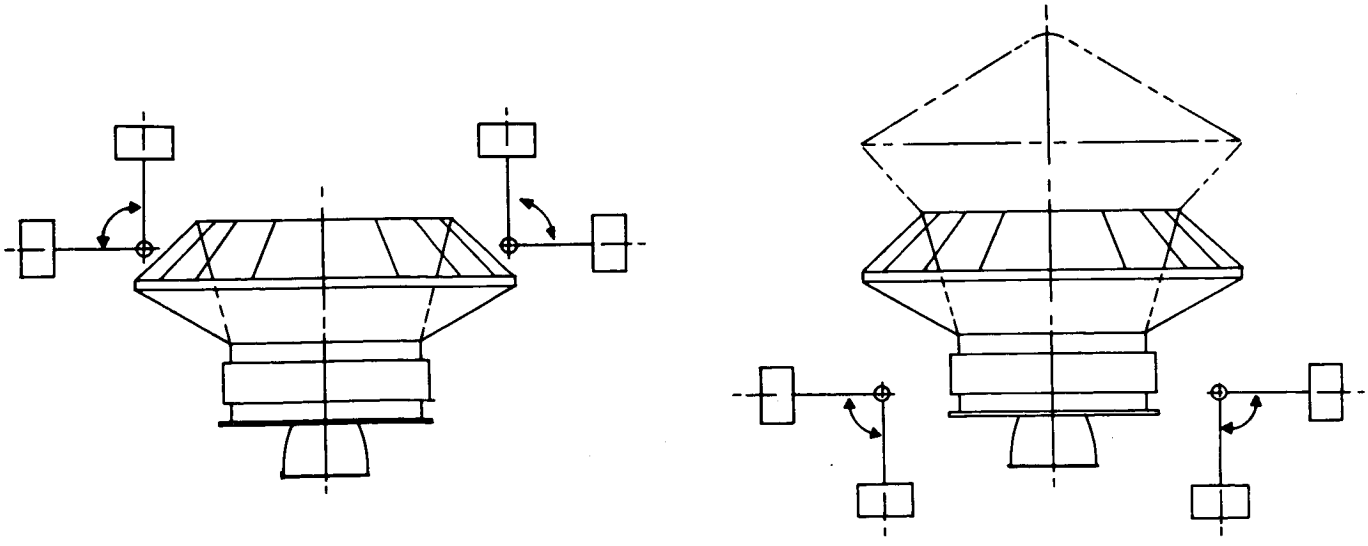

Figure 11. Techniques for Improving Viewing Coverage

the array mounting location is plagued with the severe viewing difficulties discussed in the previous section. In fact, the studies conducted support the generality that, presuming reasonable boom lengths, any above the array PSP mounting will encounter capsule blockage difficulties if the early orbit normals have either very high or very low cone angles. Voyager candidate orbits seem to have this common characteristic (see Figures 5 and 6). However, removal of the capsule and lower portion of the biobarrier, would provide viewing that is very satisfactory as indicated in Figure 12. Also, as discussed in the previous section, this mounting produces a PSP surface that is never illuminated by the sun.

Figure 13 illustrates the coverage obtained using a very low deployment point. Such a mounting point, although excellent from a viewing standpoint, imposes several vehicle systems problems. Mounting structure is not available in this region and if it is implemented, there will result a vehicle cost in weight and reliability. Also, components in this region are vulnerable to the engine plume and damage during shroud separation.

For polar orbits similar to Figure 5d, a scan platform located near the spacecraft $\pm X$ axis will require a very small range of clock angle motion, but the necessary range of cone angle will be troublesome.

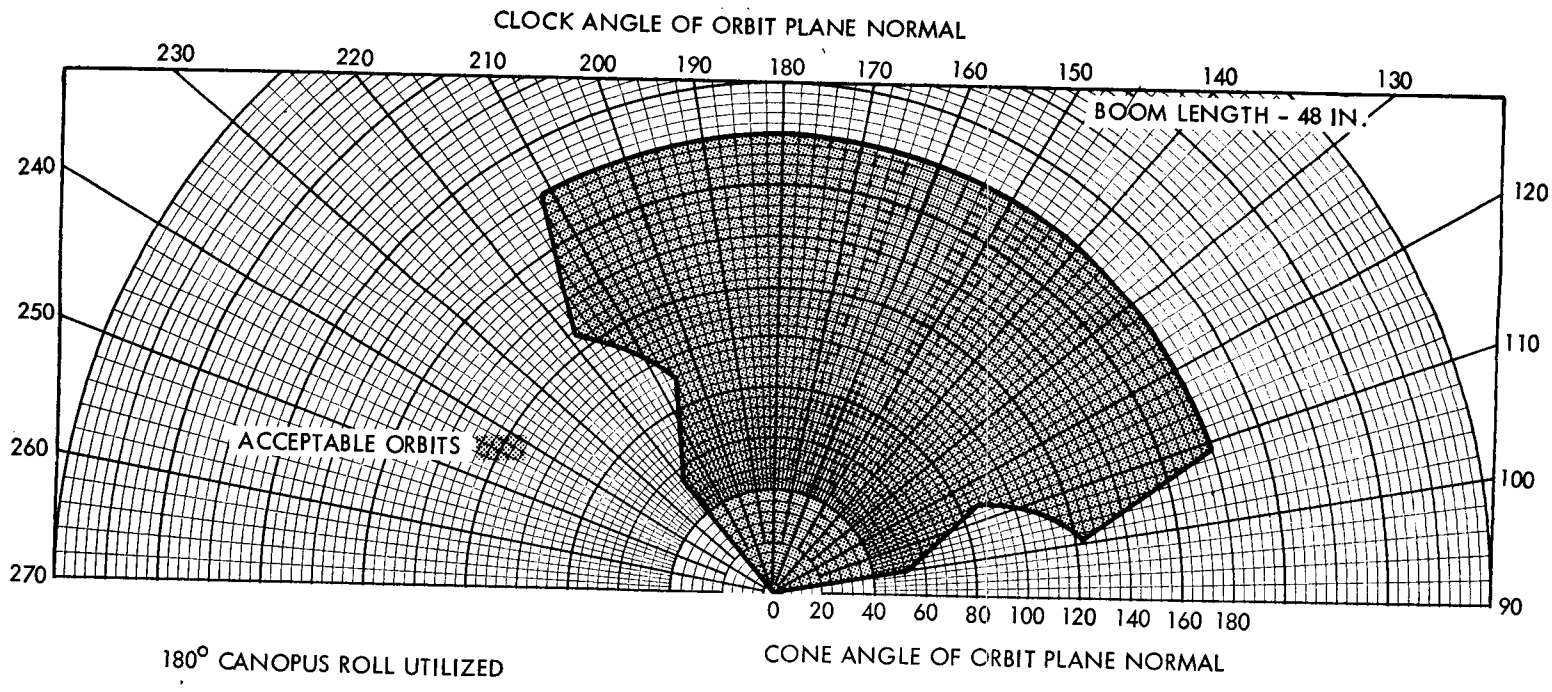

180° CANOPUS ROLL UTILIZED

MOUNTING ABOVE SOLAR ARRAY - LOWER SECTION OF BIO-BARRIER REMOVED

A.

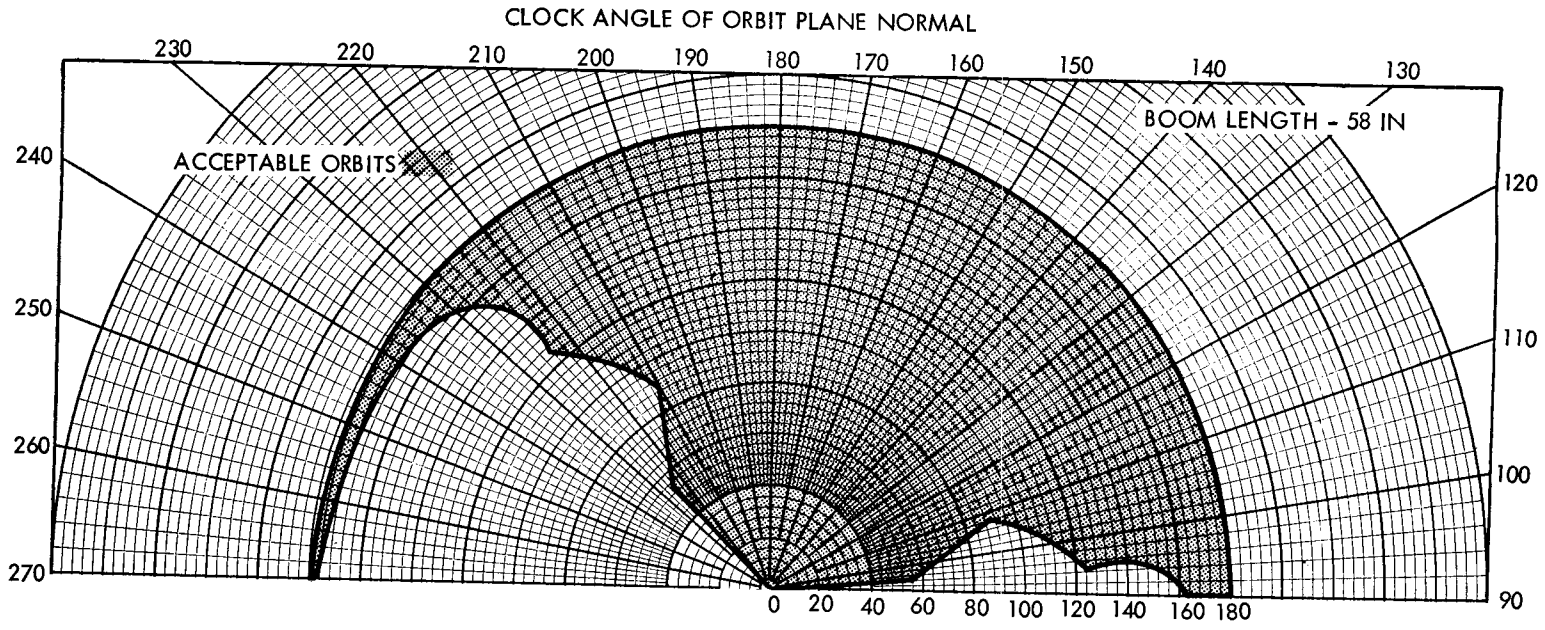

180° CANOPUS ROLL UTILIZED

MOUNTING ABOVE SOLAR ARRAY - LOWER SECTION OF BIO-BARRIER REMOVED

B.

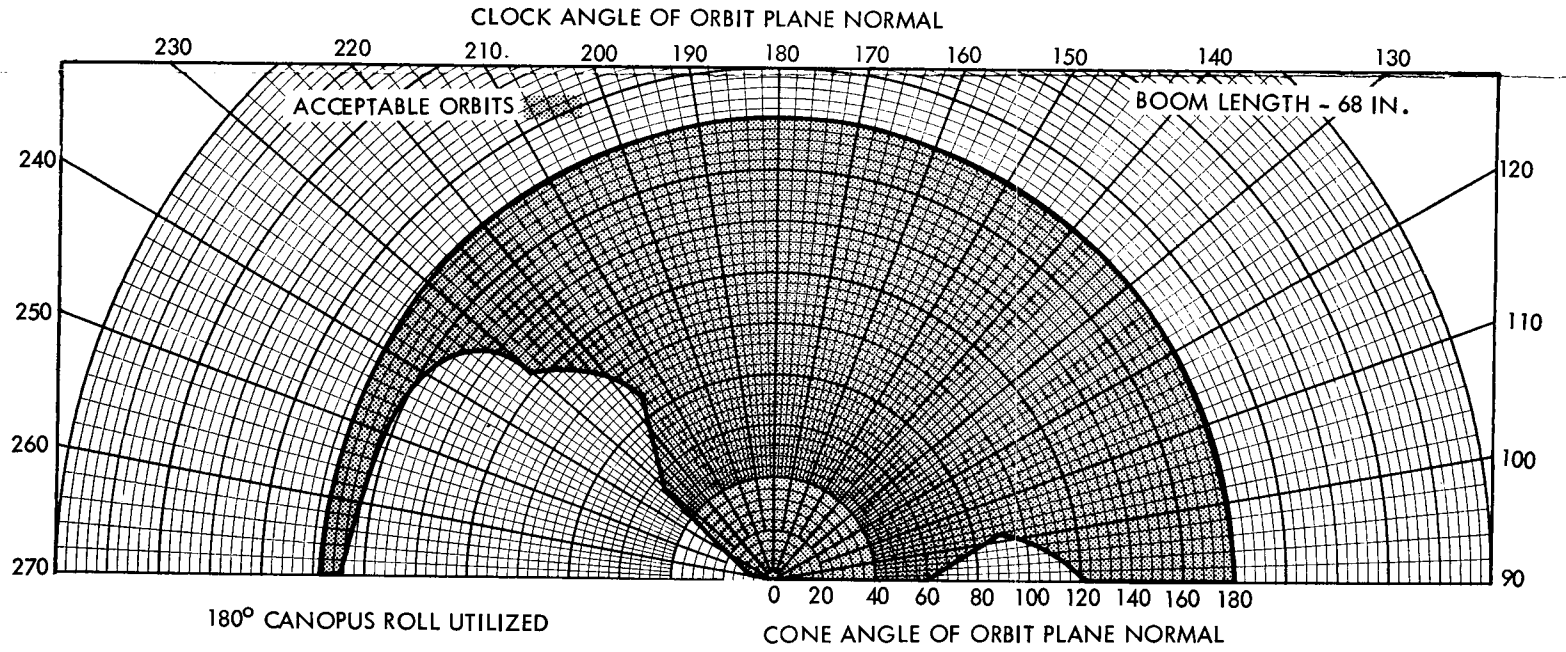

180° CANOPUS ROLL UTILIZED

MOUNTING ABOVE SOLAR ARRAY - LOWER SECTION OF BIO-BARRIER REMOVED

C.

Figure 12. Study to Examine Techniques for Obtaining Improved Coverage (High Vehicle Mounting)

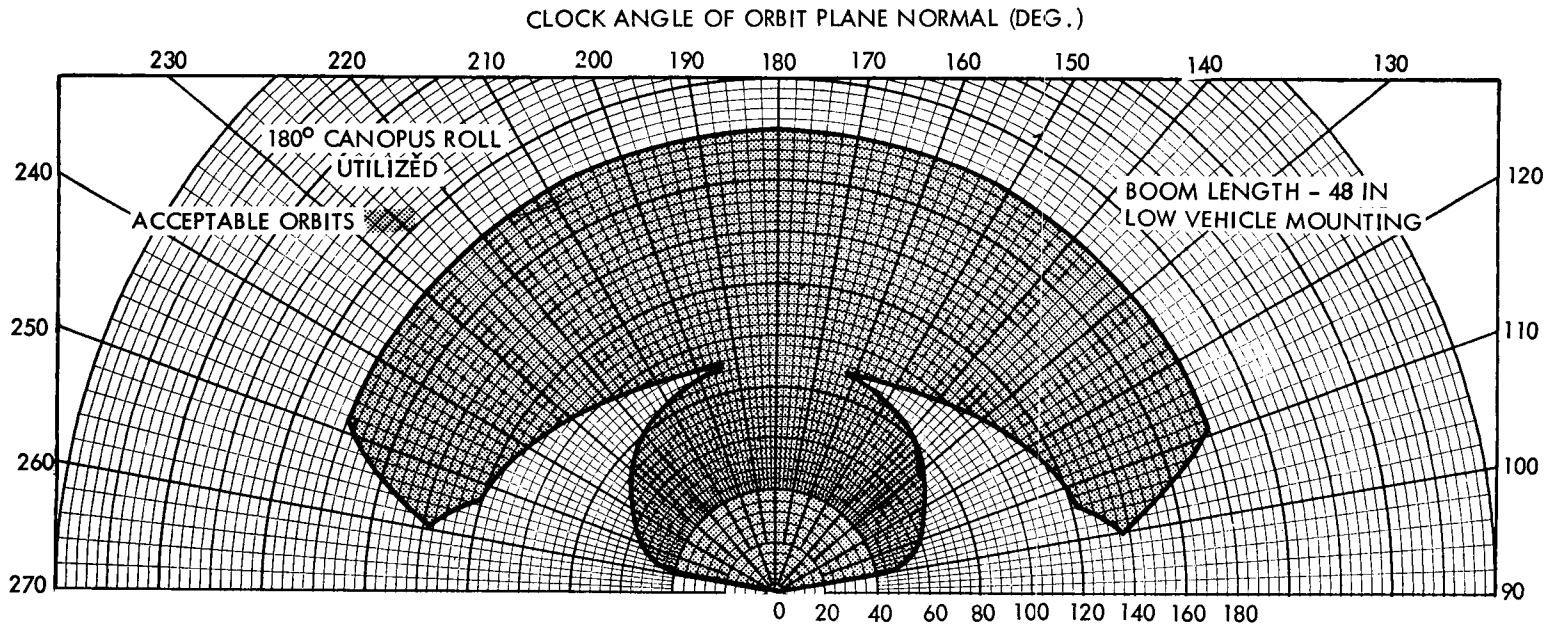

A.

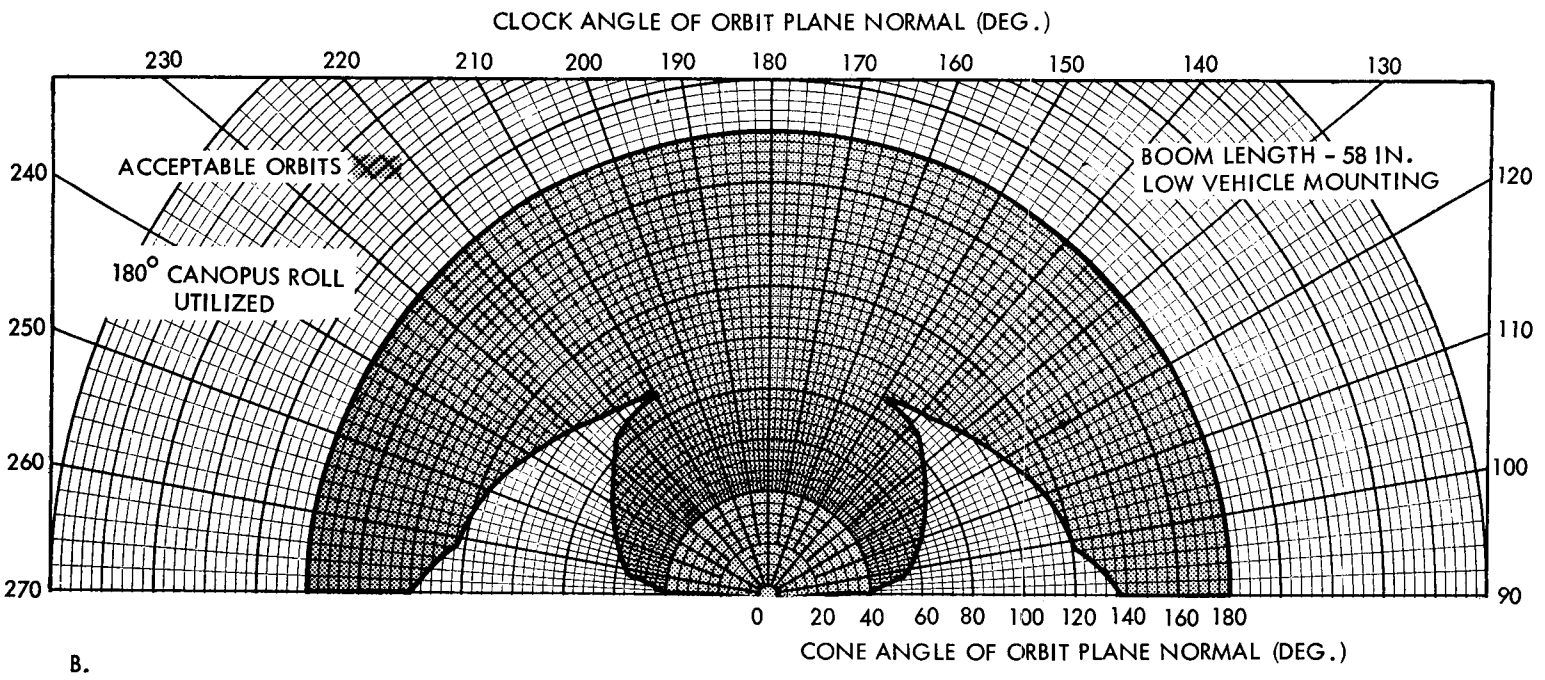

B.

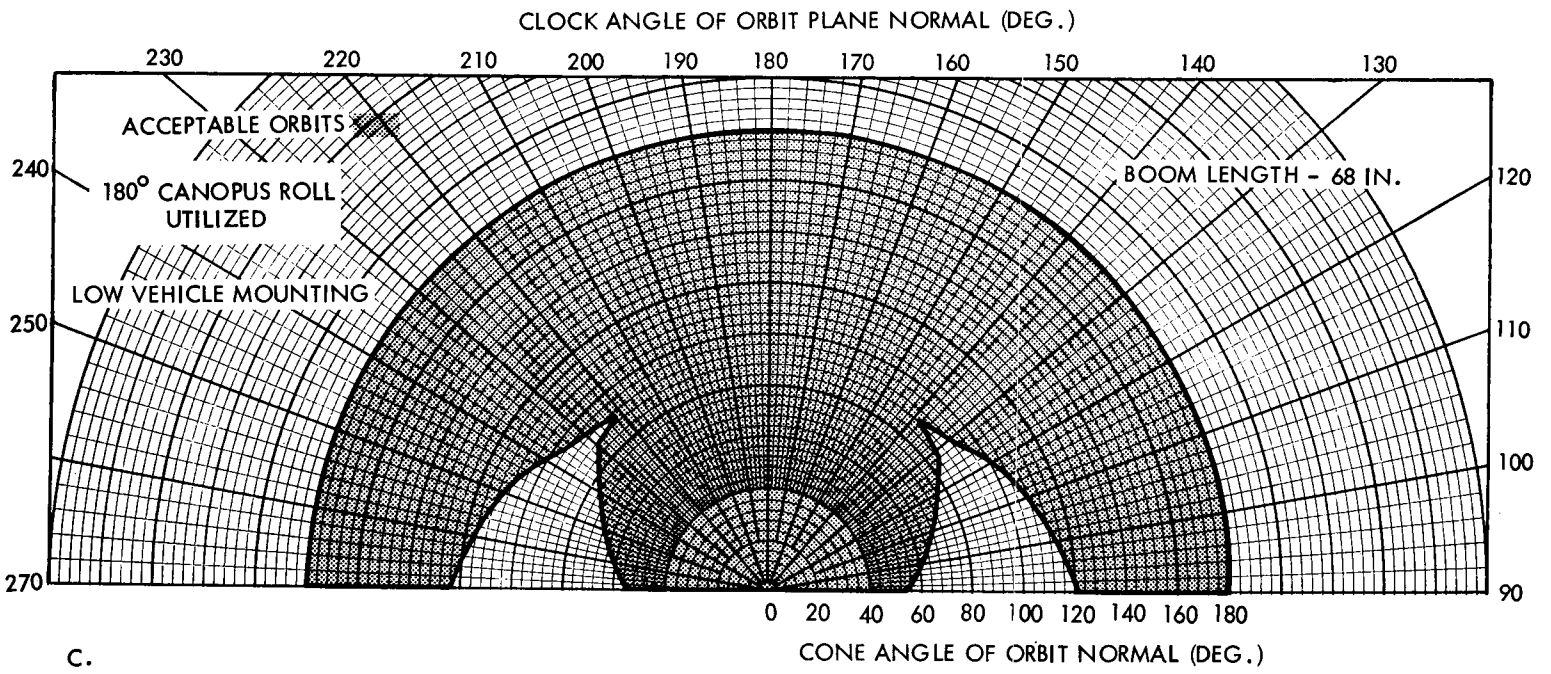

C.

Figure 13. Study to Examine Techniques for Obtaining Improved Coverage (Low Vehicle Mounting)

FOLDOUT FRAME 2

FOLDOUT FRAME 2/30

2.2. GIMBALLING AND DEPLOYMENT

Any implementation of a PSP will require a degree of compromise between science data quality and engineering design practicality. One might body-fix science instruments so as to dispense with the problem of articulation completely and accept the degradation in quality of science data. Articulation schemes of increasing complexity can be devised for various degrees of improvement in quality of the science mission. A study of this nature was conducted during Task A which yielded the result that a three-axis scan platform similar to the indicated Task D configuration could be implemented that would produce excellent science data performance and an appropriately high probability of success. However, this study, as well as the work done during this update, does not prove, beyond doubt, that this is the best of all possible approaches. A revised form of the techniques developed during the Task C Optimum Application of Redundancy Study could be used to quantitatively identify the configuration that will result in the greatest "Science Expected Worth" for a given weight. Such a study would produce a rational comparison of articulation techniques such as body fixing certain instruments, use of multiple platforms, or use of a single platform. To date, however, the recommendations of Task A are valid and, after brief re-examination, were accepted as a "ground rule" for Task D (paragraph 1.3).

2.2.1. Fixed Versus Retractable Deployment

The general gimbal articulation approach of Tasks A and B permits gimbal alternatives, the important ones were illustrated in Figure 7. A major advantage of the preferred retractable system is that the center of gravity of the spacecraft is located at nearly the same position for the orbit adjust maneuver as at termination of orbit injection. With the fixed deployment system, the nominal engine gimbal angle will be changed approximately six degrees by deployment of the PSP. This has implications on the autopilot design that would result in a more complex control or larger orbit trim errors or both.

Another major advantage of the retractable system is that the PSP moves at the end of a long lever arm, which provides better viewing angles by seeing around obstructions such as the rim of the bio-barrier and engine nozzle. This means a shorter boom for a given viewing capability, a point developed in Section 2.1.

To avoid autopilot resonance during orbit trim, the critical frequencies of the scan platform should be above four cycles per second. The fixed deployment approach would use a one-shot, locking mechanism for deployment, which would likely permit the necessary stiffness, and the proximity of the articulation gimbals to the center of gravity of the PSP will significantly reduce gimbal loads during orbit trim. With the preferred approach, the gimbals, which erect the orbit plane normal, are subjected to much higher moments during orbit trim thrusting, and with actuators of reasonable weight, it seems unlikely that the necessary gimbal spring rates can be developed to give a sufficiently high natural frequency. The retractable system must either re-latch, with a reliability penalty, or incorporate enough weight to provide sufficient actuator torque to pre-load the PSP in a snug down position without actually latching. Also, the additional gimbal load capability will be welcome during ground handling and testing.

2.2.2. Mounting Point Location

The location of the point where the PSP is mounted to the spacecraft is of fundamental importance in determining viewing capability and fixing the stowage and deployment clearance envelope. Pivot point locations considered were just forward of the separation plane, with clock angle deployment, and just aft of the separation plane with either cone or clock deployment. The trade between these locations, resulting in placement below the separation plane, is made primarily on the basis that full view capability is required when the capsule is in place. Table 1 summarizes gimbal location considerations and Figure 14 illustrates the baseline gimbal configuration.

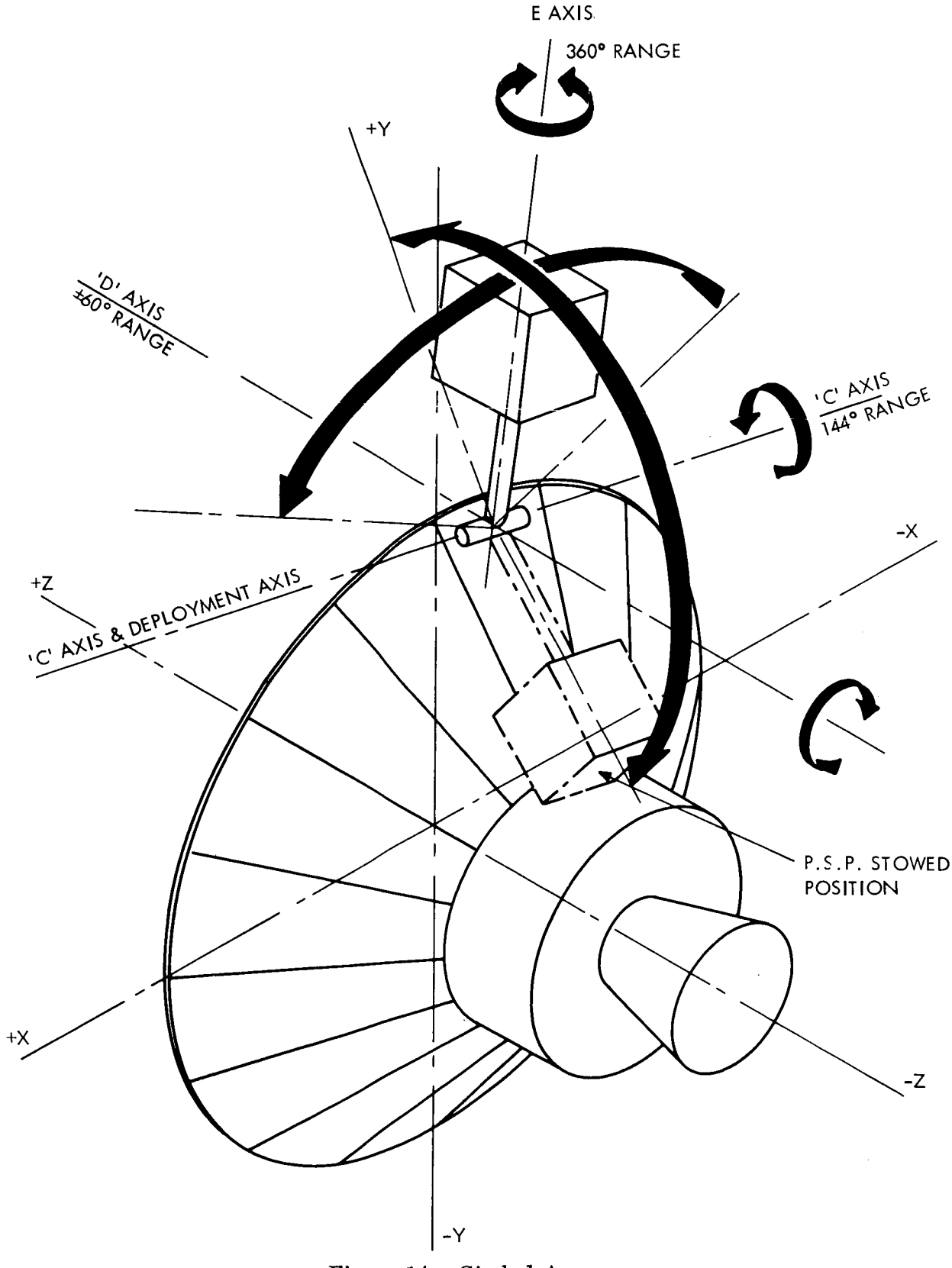

Figure 14. Gimbal Axes

Table 1. Gimbal Location Considerations

ABOVE SEPARATION PLANE	BELOW SEPARATION PLANE
With use of 180° Canopus roll, one surface of PSP never views sun or spacecraft.	Improved viewing with capsule in place. Less susceptible to change of capsule dimensions.
Maximum free micrometeorite shielding during transit.	Less constriction on growth of PSP envelope. Does not require removal of a prime structural strut.
Solar array is not blocked during transit	Deployment gimbal usable for articulation without operation near gimbal lock position.
PSP location farther from rocket plume.	180° Canopus roll not required for 1973 design orbit.

2.3. ATTITUDE CONTROL

The platform is carried to the vicinity of Mars in a stowed condition. Subsequent to the orbit insertion function, it is deployed and oriented. During orbit trim maneuvers, the platform is retracted during engine firing.

The platform is mounted on a boom attached to the periphery of the spacecraft near the Y axis. Mounting is accomplished through a three-axis gimbal, each axis of which is driven by a separate control loop. The function of attitude control is to articulate the platform in a manner required by the science instruments. Two loops (gimbals C and D) operate in an "open" loop fashion to erect a perpendicular to the orbit plane under predetermined control of the C&S subsystem. The third loop (gimbal E) tracks the Mars local vertical.

Figure 14 shows the relation of the spacecraft and PSP gimbal axes. In the figure, the PSP has been deployed and the E axis has been erected perpendicular to the orbit plane by rotations about the C and D axes. Therefore, Mars local vertical will be tracked by rotation

about the E axis. The expected gimbal movements in each axis are C = 144 degrees, D = ± 60 degrees and E = 360 degrees.

2.3.1. Control of Gimbals C and D

The control loops for the gimbals C and D are very similar to those proposed during Task A. Two degrees of freedom are required to erect a normal to the orbit plane. Because the angles change at less than 0.6 degrees per day over the mission orbital life, a stepper motor that is operated periodically to change gimbal angle in 3/16 degree increments is the selected actuator. Signals to change angle are received from the C&S Subsystem. Between steps, the controls loops are dormant and require no power except for the logic electronics. Figure 15 is the block diagram of the baseline configuration.

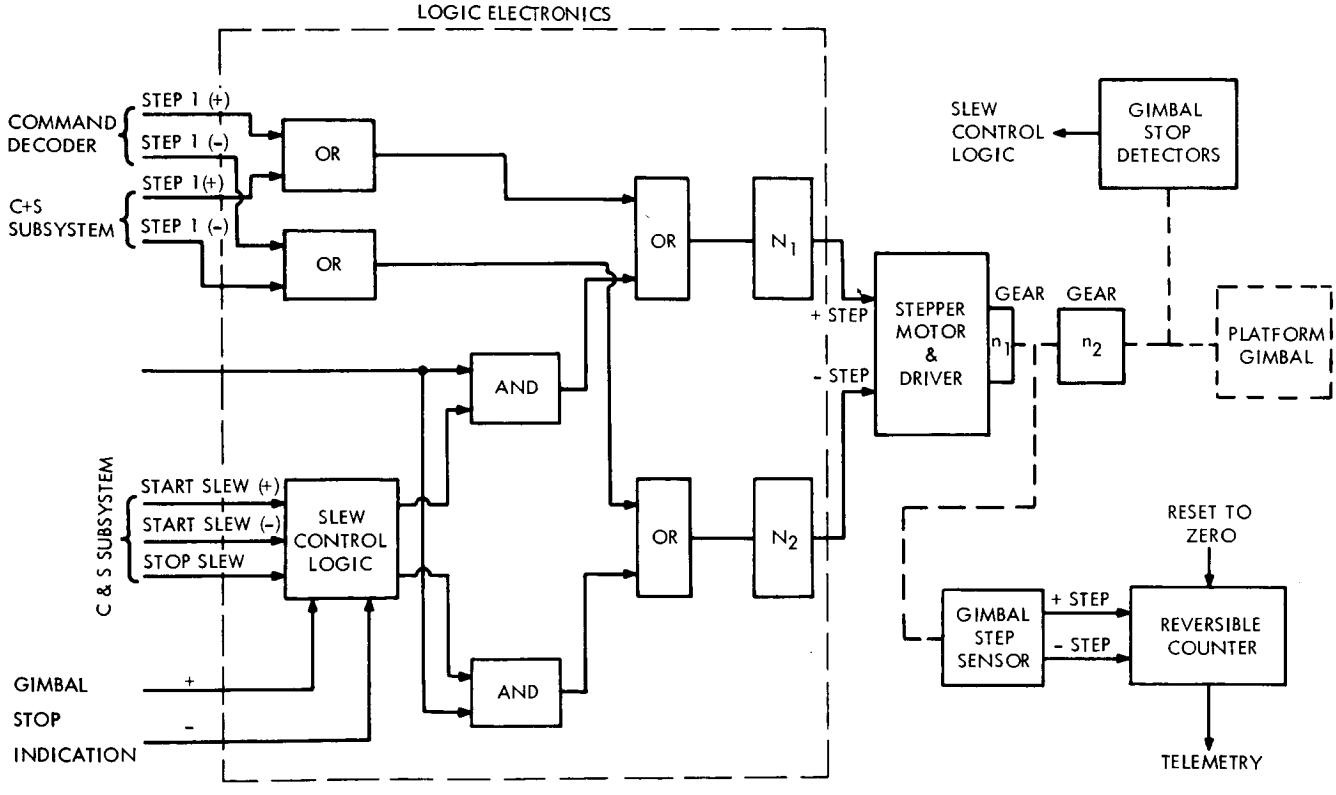

Figure 15. Open Loop Axis Block Diagram

Continuous drive control loops were considered and quickly eliminated because of control loop complexity and the continuous power drain of the motor and driving electronics. There did not appear to be any major advantages to continuous control of these axes.

2.3.2. Control of Mars Tracking Gimbal (Gimbal E)

After two gimbals have been used to erect a perpendicular to the orbit plane, it remains for the third gimbal to provide tracking of the planet around this perpendicular. During this time, the spacecraft is stabilized to the Sun/Canopus reference in a limit cycle mode of operation with deadband of ± 0.5 degrees and a rate of about 1 degree per hour. These movements are small enough and slow enough that the spacecraft attitude can be assumed to be fixed inertially.

Tracking rates in a 1000 x 10000 kilometer orbit vary from 10^{-4} to 10^{-3} radians/second in a fashion shown in Figure 16. The major design goal is to obtain very smooth tracking at these low orbital rates, so that the random movement of the platform may be kept small during the exposure time of the photoimaging instruments.

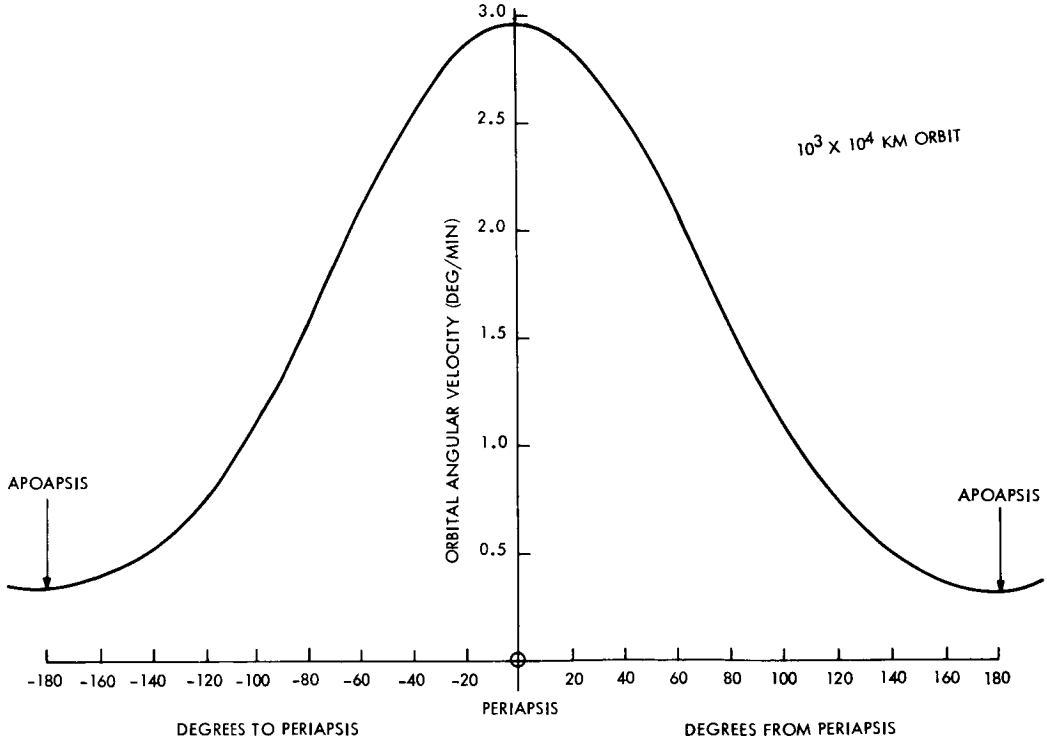

Figure 16. Orbit Rate versus Position in Orbit

The exact magnitude of the requirement varies with the science exposure times, but it appears that the random movement must be less than 1.5×10^{-5} radians/second.

It is currently planned to compensate for orbital rate by image motion compensation in the science instruments, where required. The resolution of the baseline instruments are 10 meters and 100 meters, and it is the former which establishes the control loop requirements. The design goal is to limit the random platform movement such that the ground trace movement shall be less than 3 meters, or about 1/3 of a resolution element. At a periapsis altitude of 1000 kilometers,

$$\Delta\theta_R \leq \frac{3m}{1000\ Km} = 3 \times 10^{-6} \text{ radians}$$

The expected exposure time is about 0.2 second. Consequently,

$$\Delta\dot{\theta}_R \leq \frac{3 \times 10^{-6} \text{ radians}}{0.2 \text{ sec}} = 15 \times 10^{-6} \text{ radians/sec}$$

Normal orbital tracking rate ($\dot{\theta}_o$) is a maximum of 1×10^{-3} radians/sec at periapsis so that the requirement during an exposure time is

$$\frac{\dot{\theta}_R}{\dot{\theta}_o} \leq \frac{15 \times 10^{-6}}{1 \times 10^{-3}}$$

$$\Delta\dot{\theta}_R \leq 1.5\% \text{ of orbital rate}$$

Tracking requirements vary with exposure time. For example,

t_{exp} = 10 msec

$$\Delta\dot{\theta}_R \leq \frac{3 \times 10^{-6}}{10^{-2}} = 3 \times 10^{-4}$$

$$\frac{\dot{\theta}_R}{\dot{\theta}_o} \leq \frac{3 \times 10^{-4}}{1 \times 10^{-3}} = 30\% \text{ of orbital rate}$$

t_{exp} = 1 sec

$$\Delta\dot{\theta}_R \leq \frac{3 \times 10^{-6}}{1} = 3 \times 10^{-6} \text{ rad/sec}$$

$$\frac{\dot{\theta}_R}{\dot{\theta}_o} \leq \frac{3 \times 10^{-6}}{1 \times 10^{-3}} = 0.3\% \text{ of orbital rate}$$

At short exposure times, where larger values of rate change can be tolerated, the emphasis should be on reducing fast platform movements or jitter, rather than slow drifts. As exposure time increases, the slower movements of the platform become increasingly important.

The probability of the science image motion compensation (IMC) removing these random motions should also be considered. At periapsis, the ground trace rate due to orbital rate is about 3000 meters/second. In order to remain fixed on a point during picture taking, for a 0.2 second exposure, the IMC angular movement and rate are

$$\dot{\theta} = \frac{3 \times 10^{3}}{1 \times 10^{6}} = 3 \times 10^{-3} \text{ rad/sec}$$

$$\dot{\theta} = 3 \times 10^{-3} \times 0.2 = 6 \times 10^{-4} \text{ radians}$$

These movements are much larger and faster than the expected rates due to platform control loop variations, so that if the IMC can track a point on the surface at that rate, then it can also remove random platform movements.

If an open loop type of IMC is employed, that is, one in which a predetermined rate of image motion is compensated, then the control loop random motions will not be reduced.

Platform movements are in general due to two sources. Gimbal drive non-linearities can produce random platform motions. In addition, motors, shutters, etc., on the platform can cause mechanical disturbance independent of the driving mechanism. Both of these are aggravated by the cantilever boom arrangement of the platform with its expected low damping factor. Preliminary analysis shows that for torsional "shocks" which cause an initial disturbance of one milliradian, it takes 18 seconds before amplitude drops below 3×10^{-6} radians if $\omega_n = 10$ cps and damping factor is 0.5 percent of critical.

2.3.3. Gimbal E Control Trade Studies

Three approaches to meeting the requirement for smooth tracking were considered. The control loops evaluated can be classed as low, medium or high performance designs with corresponding increases in complexity.

The low performance design, which uses a stepping motor to position the platform, is the simplest. When the pointing error detected by a platform mounted horizon sensor exceeds an allowable value, a platform step occurs. Between steps, the platform is ideally at rest. However, the stepping action plus resulting torsional vibrations cause objectionable smearing of data from the continuous scan science as well as the photoimaging instruments.

The medium performance design provides a continuous platform drive to eliminate the stepping motion. The control loop is designed to minimize the random motions of the platform due to sensor noise, gimbal friction variations, etc. Its sensitivity to disturbances caused by science instruments, platform resonances, etc. is limited by the noise and resolution of the horizon sensor.

The high performance design utilizes a gyro as a high gain, low noise sensor to detect platform motions with respect to an inertial reference. The horizon sensor is used to update the inertial reference, which is constantly changing as the spacecraft orbits the planet.

In consideration of each design, the probability of image motion compensation within the science instruments reducing the effects of random platform motions was discounted. Multi-axis image motion compensation capability in Voyager photoimaging instruments is rather unlikely as is the possibility that dynamic coupling can be reduced to the point where permitted random motions in one axis would not couple into the other axes. The goal is to design a platform capable of meeting jitter requirements on its own.

2.3.3.1. Low Performance Control Loops

The simplest positioning control loop is obtained with a stepping motor actuator. A platform mounted horizon sensor detects errors to the local vertical. When the error exceeds a predetermined value, the platform is stepped to reduce the error. After stepping, the platform structural resonances are allowed to decay and the platform position remains fixed during science data gathering. A simplified block diagram is shown in Figure 17.

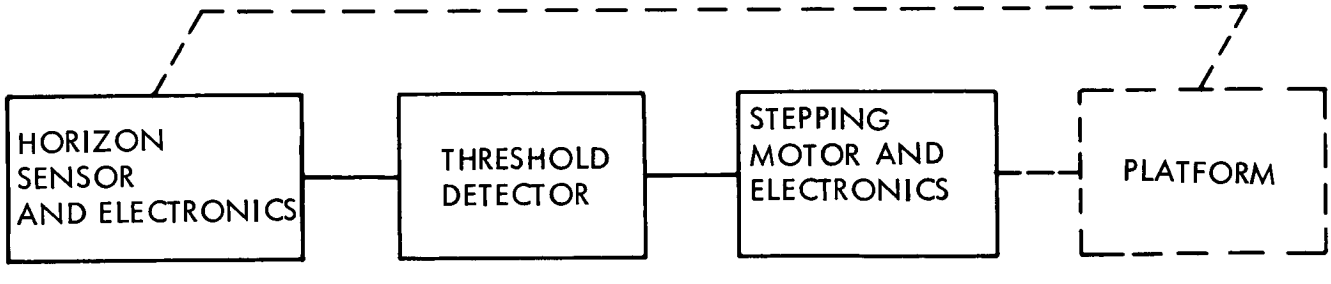

Figure 17. Stepping Motor Actuator Block Diagram

This design is not recommended because the steps and resulting platform transients appear unacceptable to the science instruments. The probable low structural damping of the cantilevered platform permits the platform transients to continue above acceptable levels for long periods of time. Assuming a stepping threshold of 1 degree, steps would occur every 20 seconds at periapsis. Unacceptable transients would persist for longer than the 20 seconds between steps.

Improvements in the structural damping characteristics, or easing of the desire for uninterrupted strip mapping and willingness to accept severely degraded data from the continuous sampling instruments would make this alternative most attractive because of its simplicity and minimum power requirements.

2.3.3.2. Medium Performance Control Loops

2.3.3.2.1. Recommended Design. A block diagram of the recommended Mars tracking loop is shown in Figure 18. A DC-torquer motor with tachometer feedback is illustrated. These drives have been used successfully on gyro rate tables and stable platform drives when steady rates are required. The position input is furnished from the horizon sensor. The outer position loop can be a very low gain and low bandwidth system. At the maximum tracking rate of 0.05 degrees per second, a loop velocity constant of 0.05 will produce a tracking error of 1 degree. This corresponds to a bandwidth of about 0.05 rad/second. Electronics gain K_p can provide the desired loop gain after a final configuration is chosen.

Since tracking rates are unidirectional, even lower bandwidths (and larger tracking errors) are tolerable if the horizon sensor alignment is biased to remove the error.

The mathematical block diagram of Figure 19 shows a direct drive torquer. Estimate of gimbal friction torque is 1 ft-lb maximum. Required accelerations of the platform are very small so that the torquer size is primarily determined by the gimbal friction. For the present, a 7 lb-ft unit was chosen. Its characteristics are shown in Table 2. A desirable drive amplifier would be a pulse-width modulator type in order to reduce the power

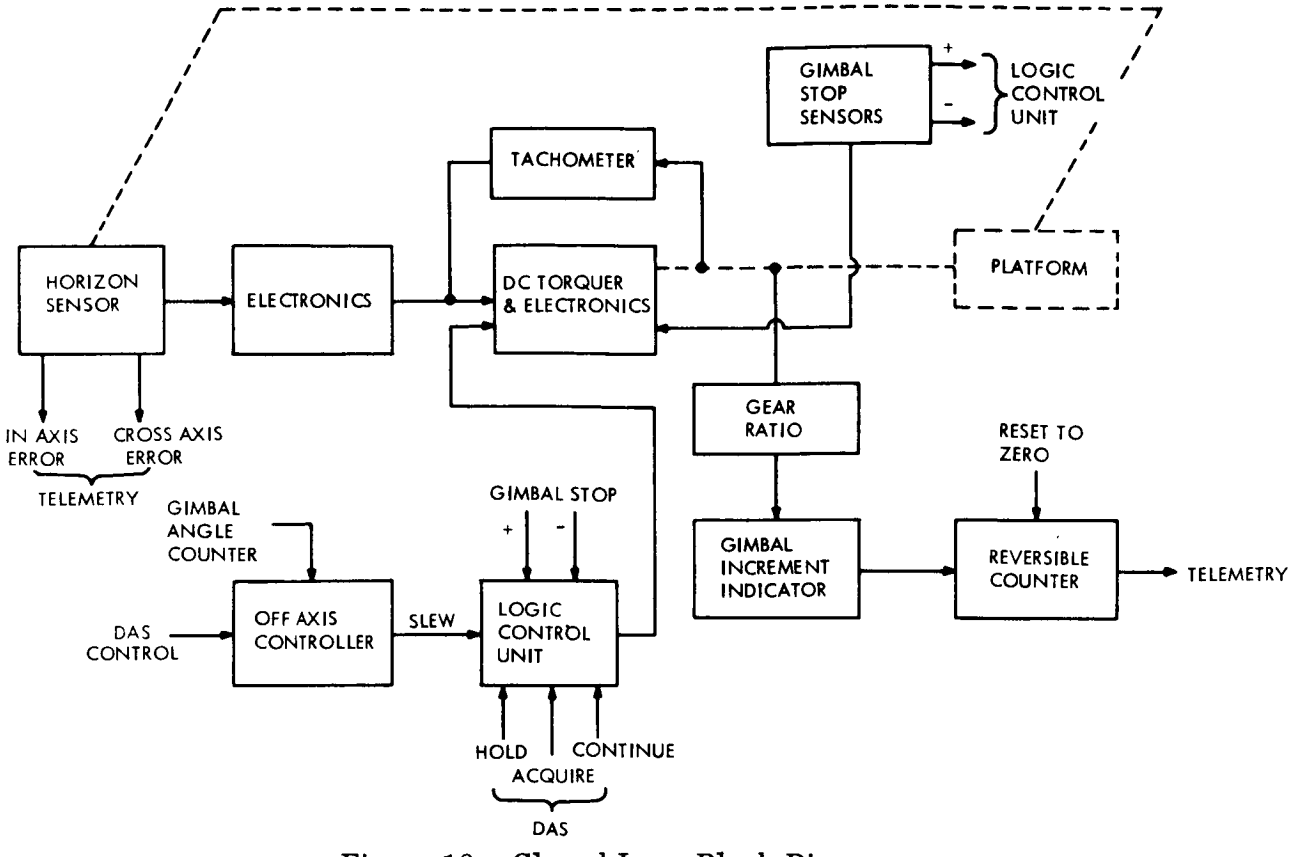

Figure 18. Closed Loop Block Diagram

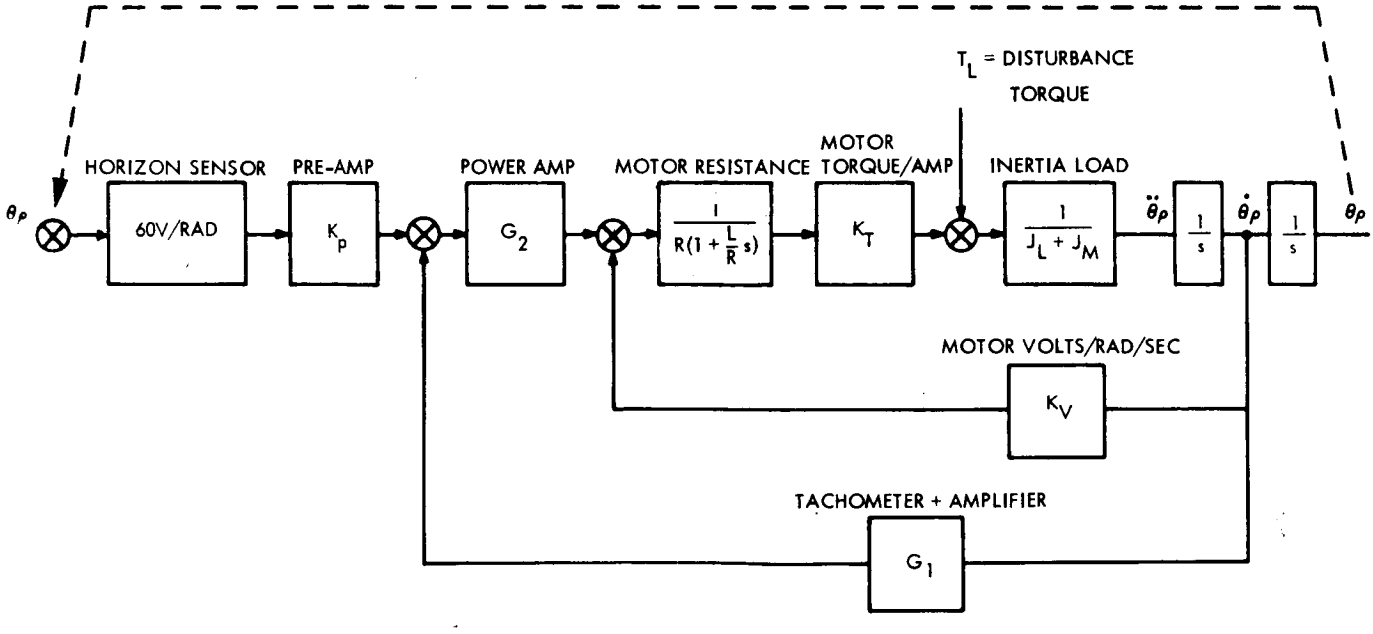

Figure 19. Platform Control Loop

Table 2. DC Torquer Characteristics

Type:	Inland Motor Corp. T-5730 (B)
Peak Torque:	7 lb-ft
Resistance (R):	3.5 ohms
Inductance (L):	0.01 henrys
Torque Constant (K_T):	0.8 lb-ft/amp
Back EMF (K_V):	1.09 V/rad/sec
Load Inertia (J_L):	15 slug-ft^2
Motor Inertia (J_m):	5×10^{-3} slug-ft^2
Ave. Power @ 1 lb-ft:	4 watts
Motor Friction:	0.1 lb-ft
Peak Power:	200 watts
Motor Time Constant:	0.02 seconds

dissipation. This PWM will introduce some random motions to the gimbal that may not be tolerable; in that case, a continuous drive amplifier may be required. The average power dissipation is 4 watts for continuous drive.

The inner motor/tachometer loop is a relatively fast servo. The tachometer feedback is applied to reduce random variations of the output gimbal resulting from gimbal friction variations as well as ripple torques and brush frictions within the torquer.

To determine the disturbance torque rejection capability of the tachometer loop, consider the block diagram, which has been redrawn in a more convenient form in Figure 20. An output gimbal disturbance torque (T_L) enters the loop as shown in Figure 20. The ratio of θ_p/T_L, which is the disturbance torque rejection ratio, can be derived

$$\frac{\dot{\theta}_p}{T_L} = \frac{\text{Forward gain}}{1 + (\text{Forward gain})\ (\text{Feedback gain})}$$

$$= \frac{\dfrac{1}{s\ (J_L + J_M)}}{1 + \left(K_v + G_1\ G_2\right)\left(\dfrac{K_T}{R\ (1 + \frac{L}{R}\ S)}\right)\left(\dfrac{1}{(J_L + J_M)\ s}\right)}$$

Recognizing that $J_L >> J_M$, $\frac{L}{R} << 1$, and assuming $G_2 = 1$, and $G_2 = 400$ volt/radian/second

$$\frac{\dot{\theta}_p}{T_L} = \frac{1}{91.6\ (0.164s + 1)}$$

A plot of this is shown in Figure 21.

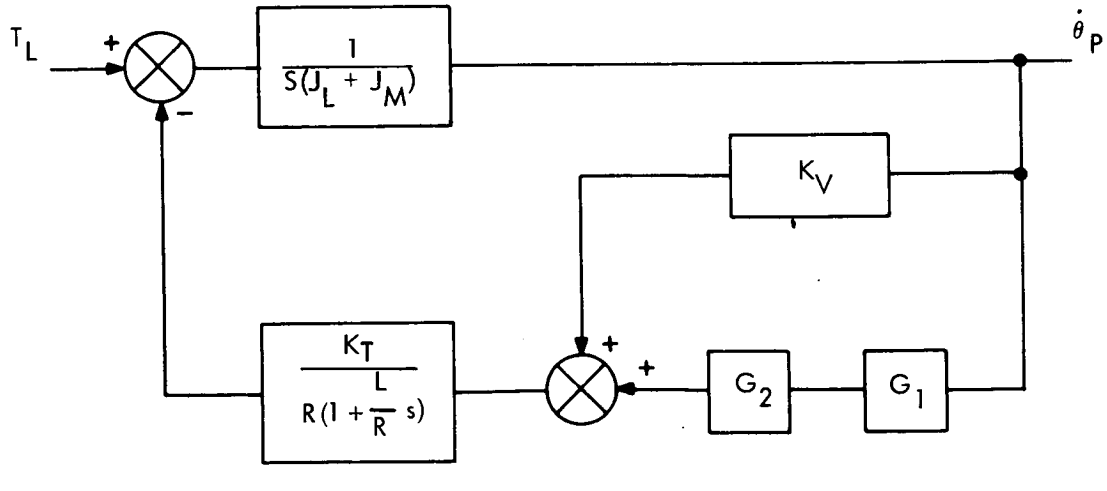

Figure 20. Tachometer Loop Response to Disturbances

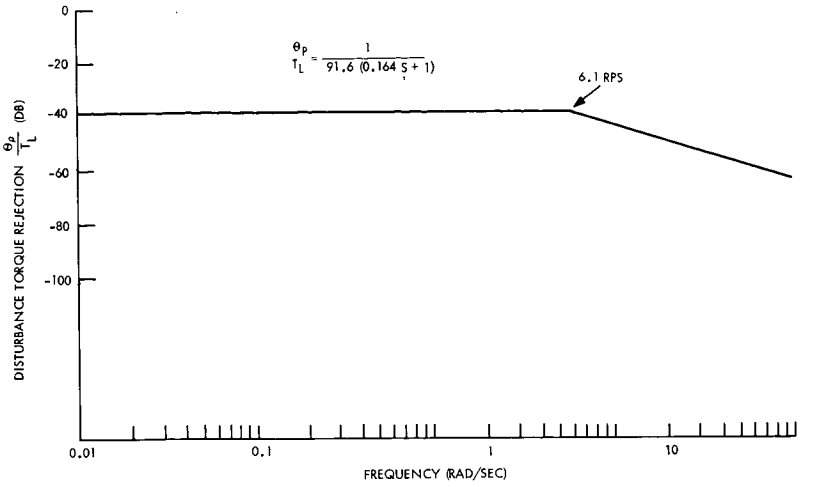

Figure 21. Disturbance Torque Rejection

The figure shows that for torque disturbances up to about 1 cps, the resulting platform rate change is reduced to about 1 percent of its value without feedback. Assuming a maximum velocity of 10^{-3} rad/second, 50 db of tachometer feedback will reduce short term variations of two-to-one in gimbal friction to about 1 percent variation in gimbal rate; this is within the tracking requirements on rate (less than 1.5 percent of orbital rate).

The tachometer gain G_1 is a combination of the gain of the tachometer and succeeding amplifier. Tachometers with gains of 10V/rad/sec are available; these would require an amplifier gain of about 40.

Although tachometer ripple, which is less than 1 percent at a low frequency of about 0.075 radians/second, is not expected to be a problem, a rate gyro mounted on the platform could serve as a very sensitive tachometer with low noise. This is not felt to be necessary at this time.

It should be noted that the disturbance torque rejection characteristic may be changed somewhat when inner loop stability is considered. Gain G_2, which is shown as a constant will in fact include compensation networks for loop stability purposes. As a result, the

rejection at frequencies between 1/2 and 1 cps may be reduced. Further analysis is required. At frequencies above 1 cps, the main rejection mechanism is the platform inertia itself. This preferred design allows an alternate mode of operations to meet the steadiness requirement. The mode would disable the drive during picture-taking. This would require some synchronization of platform drive and science, which should not be a problem since signals to take pictures are already on the platform. If the platform were stopped just before picture taking around periapsis, where orbit rate is 0.05°/second, it would be 20 seconds before the pointing error built up to one degree. Satisfactory reacquisition could probably be done in less than 10 seconds, at which time the platform drive could be disabled for the next sequence of data. This neglects any platform vibrations resulting from the driving torque being alternately applied and removed. Adjusting the selected system for this mode of operation is made available by means of the HOLD mode of operation described in paragraph 3.3.6.

The error buildups due to coasting of platform and orbital advancement during picture-taking could be monitored by the horizon sensor and telemetered to the ground with the science data to allow gridding of pictures.

A disadvantage of the DC torquer drive is use of brushes and permanent magnets. However, the expected life for brushes in 10^8 revolutions, well above the expected 10^4 revolutions.

2.3.3.2.2. Medium Performance Alternates Considered. Use of the DC torquer without tachometer feedback was also considered. The torquer ripple, which is about 4 percent for the selected motor, would produce comparable speed variations. Gimbal friction variations would also cause changes in gimbal rate, which might go undetected by the horizon sensor. For both of these reasons, the tachometer was felt necessary to provide rejection of low frequency rate variations.

An AC servo motor and gear train was also considered with tachometer feedback. Because of the low gimbal rates, a large gear ratio of about 100,000:1 would be required to assure smooth running of the motor. Although an AC tachometer could provide feedback analogous to the DC torquer case, its lower sensitivity and residual noise at low speeds would require a larger gear ratio between it and the output gimbal, lowering its sensitivity to torque variations. The requirement for two-phase power at 90-degree phase angle (currently not available on the spacecraft), the addition of AC voltage with attendant phase shift problems, and the modulation electronics for motor drive are also distinct disadvantages. The large gear ratio would also require a clutch between motor and output shaft to prevent damaging the gear train when the motor stalls or the output shaft is turned by hand.

Another alternative considered was the use of a synchronous motor as an actuator because of its constant speed characteristics under varying loads. Because of its relatively high speed, a large gear train (on the order of 100,000:1) would be required to drive the gimbal. This would allow use of a low torque motor, such as size 11. Synchronous motors are designed to operate over a limited frequency range when the voltage is constant; in this case it would be required to operate over a speed range of about 10 to 1. Synchronous motors have been used in this type of variable speed application. It requires that the voltage and frequency be adjusted simultaneously in response to an error signal. The motor will then adjust its synchronous speed. A two-phase motor is required which would normally require two-phase power. However, a single-phase with capacitor phase-shifting for starting is probably satisfactory. A clutch would be required. Torque characteristics and transients in speed as frequency and voltage vary continuously over this range were not fully evaluated during this study.

2.3.3.3. High Performance Control Loop

The sensitivity of the medium performance loops are limited by the resolution of the horizon sensor, which has a position error resolution of 10^{-3} radians. It would take about 70 seconds to detect a constant 15×10^{-6} radians/second rate error. The unidirectional travel of the platform and careful design of the actuator can probably keep control loop-

induced movement within requirements. If platform movements are introduced by science instrument disturbances, platform resonances, or spacecraft jet firings, they may exceed requirements and may go undetected by the control loop because of their small amplitude.

An alternate approach requires mounting a gyro on the platform as the prime position sensor and using the horizon sensor to update the gyro. Because of its greater sensitivity ($\sim 10^{6}$ radian), it can detect very small random platform movements in addition to providing a smooth driving signal. A block diagram is shown in Figure 22.

This is analogous to a stable platform control, except that unlike a stable platform where the objective is to hold an inertial reference fixed, the reference here would be constantly changing.

At the starting gimbal stop, the gyro is in the rate mode. When Mars comes into the horizon sensor field of view, the gyro will be uncaged to hold its inertial references. The gyro output will be used to drive the platform actuator, which will position the platform on which the gyro and horizon sensor are mounted. The horizon sensor continuously tracks Mars, developing error information. When a predetermined deadband is exceeded, an increment of current will be applied to the gyro torquer. This increment would be continuously applied causing the gyro reference to change at a constant rate, slightly greater or less than the orbital rate so that the horizon sensor error drifts through the deadband. When the deadband is again exceeded, the torquing current would be changed by additional increment.

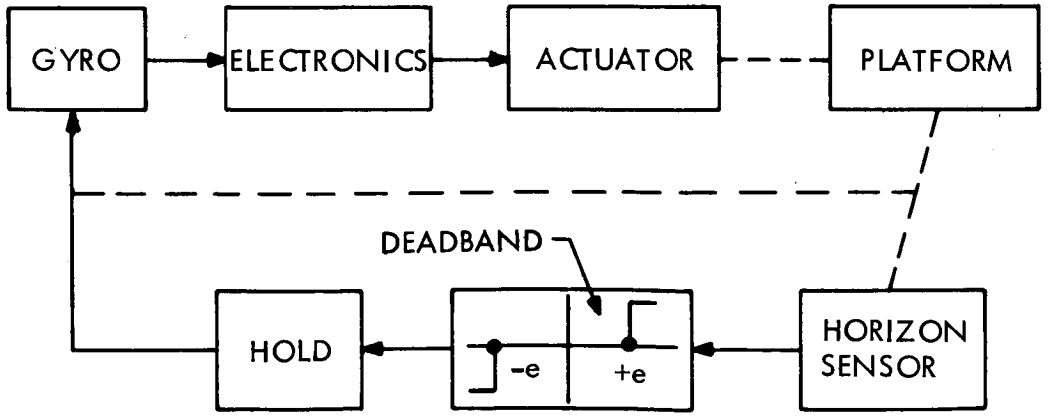

Figure 22. Position Gyro Sensor with Update

The maximum rate of change of orbital rate does not exceed 0.1 milliradian/sec^2 so that the gyro reference rate matches orbital rate to within 3 percent around periapsis without continuous updating. At this maximum change of orbital rate and a horizon sensor deadband of 16 milliradians, the maximum rate at which increments will be applied is about once every ten minutes since the rate error is about 3 percent of 1 milliradian/second.

The above discussion neglected gyro drift. Typically, this is about 10^{-6} radians/second which is negligible compared to the minimum orbital rate of 10^{-4} radians/second. Gyro noise power spectrum is about 7×10^{-9} deg^2/Hz. If a simple lag network filter with a time constant of one second is used at the gyro output, the rms noise N_s is

$$N_s^2 = N_G \frac{1}{2\tau}$$

$$= \left(7 \times 10^{-9} \frac{\text{deg}^2}{\text{Hz}}\right)\left(\frac{1}{2\tau} \frac{1\text{ Hz}}{2\pi\text{ rad}}\right)$$

$$= 0.55 \times 10^{-9} \text{ deg.}^2$$

$$N_s = 2.24 \times 10^{-5} \text{ deg.}$$

$$N_s = 4.1 \times 10^{-7} \text{ rad (rms)}$$

This is about an order of magnitude less than allowed movement of 3×10^{-6} radians.

In the above alternative, the gyro was operating in its uncaged or position mode. A comparable control loop using the rate gyro mode of operation would operate similarly (Figure 23). The gyro would detect platform rate and would operate in the absence of a bias signal to keep the platform fixed. When tracking commences, a bias voltage will be summed with the gyro signal to drive the platform actuator. The platform will rotate at a rate such that the gyro output will cancel the bias signal. The horizon sensor will develop error information as before, and when the deadband is exceeded, it will change the bias so that the gyro output

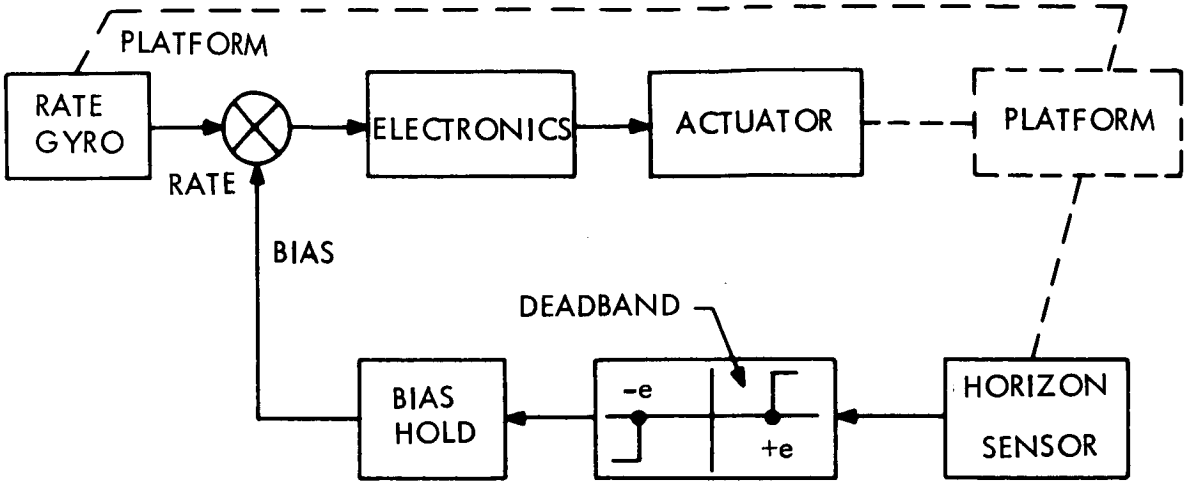

Figure 23. Rate Gyro Sensor with Update

(and consequently, platform rate) will increase. The increment rate, drift and noise considerations are similar to operation in the uncaged mode since the objective is still to match platform rate to orbital rate with horizon sensor updating.

The gyro can also be used in a rate mode as a sensitive tachometer. The most critical tracking requirements occur around periapsis where tracking rates are maximum (about 10^{-3} radians/sec), and should be changing slowly. Any sudden changes in platform rate can be detected by the gyro, and can be fed back to the gimbal drive to reduce the effects of the disturbance. In this case, it acts very similar to the tachometer of the DC torquer system, except that it is sensitive to changes in inertial rate rather than platform/spacecraft relative rates.

This high performance system was not recommended for several reasons. Although the platform movements due to science induced disturbances, spacecraft limit cycle, platform resonances, etc., are not well defined, they are not expected to be large. No gyros are planned in the other control loops which would be subject to a similar kind of platform movement.

2.3.4. Horizon Sensors

Horizon sensors were reviewed to determine those suitable for use in the Mars tracking loop. The sensor detects the horizon attitude about the gimbal axis in order to establish a local

vertical. Only one axis sensing is required for gimbal control, but it is desirable for picture gridding to sense cross-axis error also. Requirements are a resolution and accuracy of about 0.1 degree, with low noise (less than 0.025 degrees peak-to-peak) so as to allow smooth tracking of the local vertical. Because of the uncertainty of the Mars atmosphere and its colder temperature, a long wavelength (10-40 microns) is desirable to reduce thermal contrast and to increase signal level. The sensor must accommodate a Mars disc whose subtended angle varies from 25 to 105 degrees. Mission life is six months stowage to Mars and six months minimum in orbit.

2.3.4.1. Radiation Balance Sensors

Radiometric type sensors using thermopile detectors appear to be the most promising. Two types, one with no moving parts, and a second using thermally actuated gimbals for planet tracking, have been proposed by Barnes and Quantic Industries, respectively.

Proposed Lunar Planetary Horizon Sensor (LPHS). In this Barnes sensor, the detector elements are arranged in a narrow strip so that the field of view in one axis is approximately 1 x 90 degrees, with each detector 1 x 1 degree. When the planet is centered with no error, the number of non-irradiated detector elements on opposite sides of the planetary disc are equal. Resolution at this point is 0.5 degree. An analog interpolation is made to determine how much of the outermost detectors are irradiated in order to improve the overall resolution of the sensor to about 0.1 degree.

To understand its operation, consider Figure 24, which shows a string of individual thermopile detectors contained in one sensor head. (Because of the large Mars subtended angle and limited field of view of the sensor optics, two heads will be required although only one is shown here). The planetary disc is superimposed on the detector as shown.

By means of a field effect transistor sampler, each thermopile of the head is scanned starting from No. 1 inward until the first irradiated one is detected. The detectors starting from No. 13 are scanned in like manner. In addition, an analog interpolation is made of the degree

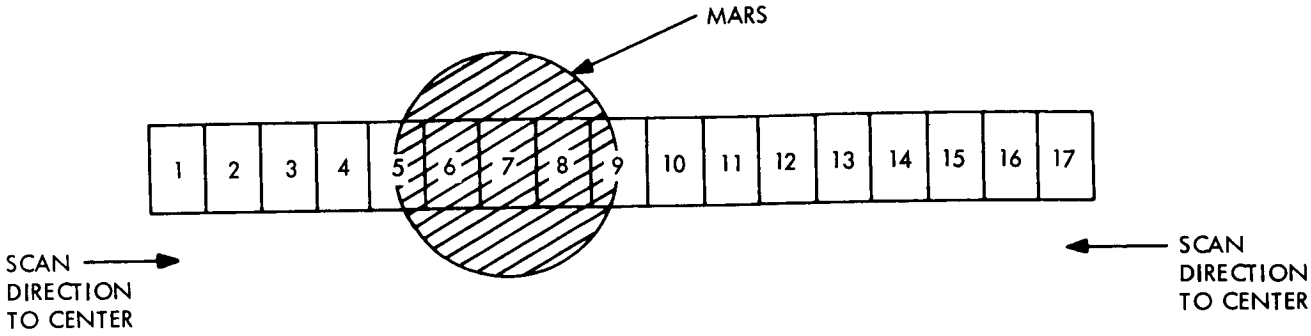

Figure 24. Single Axis Horizon Sensor

of radiation of the first thermopile to be irradiated on each side to allow resolution of error to better than the 1 degree width of the thermopile. An error is generated if the planet disc is not centered.

The expected characteristics of this type sensor are as follows for the single-axis version with two heads and electronics:

a. ±0.1 degree accuracy, with noise output of ±0.02 degree

b. Scale factor 1 volt/degree, with time constant of about 0.5 second.

c. Power 4.9 watts

   Weight 5.5 pounds

   Volume 150 cu in.

d. 5 year life expected - no moving parts

e. Sample rate 6 times/second

An engineering model of the detector portion has been built and tested in environment with satisfactory results. Although this model provided a digital output only, the analog interpolation appears feasible.

A degree of discrimination against the sun is achieved by counting past the first irradiated element (detector 5 of Figure 24) and detecting whether the next innermost one (No. 6) is also fully irradiated. In Figure 24 it is, and nulling of the error proceeds. If not, then it is assumed that the sun is irradiating the detector, and counting continues to the next irradiated element. If the sun irradiated element is next to the one irradiated by Mars, the sensor will null out to an error of 0.5 degree. If this error is unacceptable, logic can be incorporated that compares the diameter of Mars determined by the cross-axis sensor against the in-axis value, and uses this information to discriminate against the sun.

The sensor will not be damaged by viewing the sun, since individual thermocouples of the thermopile detect differences in temperature across the junction, and the differences will be small.

2.3.4.2. Gimballed Radiometric Type

This type has been proposed by both Barnes and Quantic Industries, differing primarily in the gimbal mechanism. The Quantic Industries device looks most promising and will be described.

Two sensor heads point at diametrically opposite points on the planetary horizon. A gimballed mirror in each head operates to direct the Mars radiation on a 1 by 4 degree mosaic of detectors.

Consider Figure 25, which shows two heads positioned so that they see opposite edges of the horizon. Each head has four detectors that operate to position the head so that the horizon edge lies between detectors 2 and 3. The actuator is a thermally-actuated gimbal (See Figure 25b.) Current and therefore heating of the thermal gimbals is proportional to the error, and causes the mirror to deflect until null is reached. Readout of gimballed mirror position is done by optical pickoff using a digital code on back of the mirror. The outputs of the two heads are combined to drive the platform.

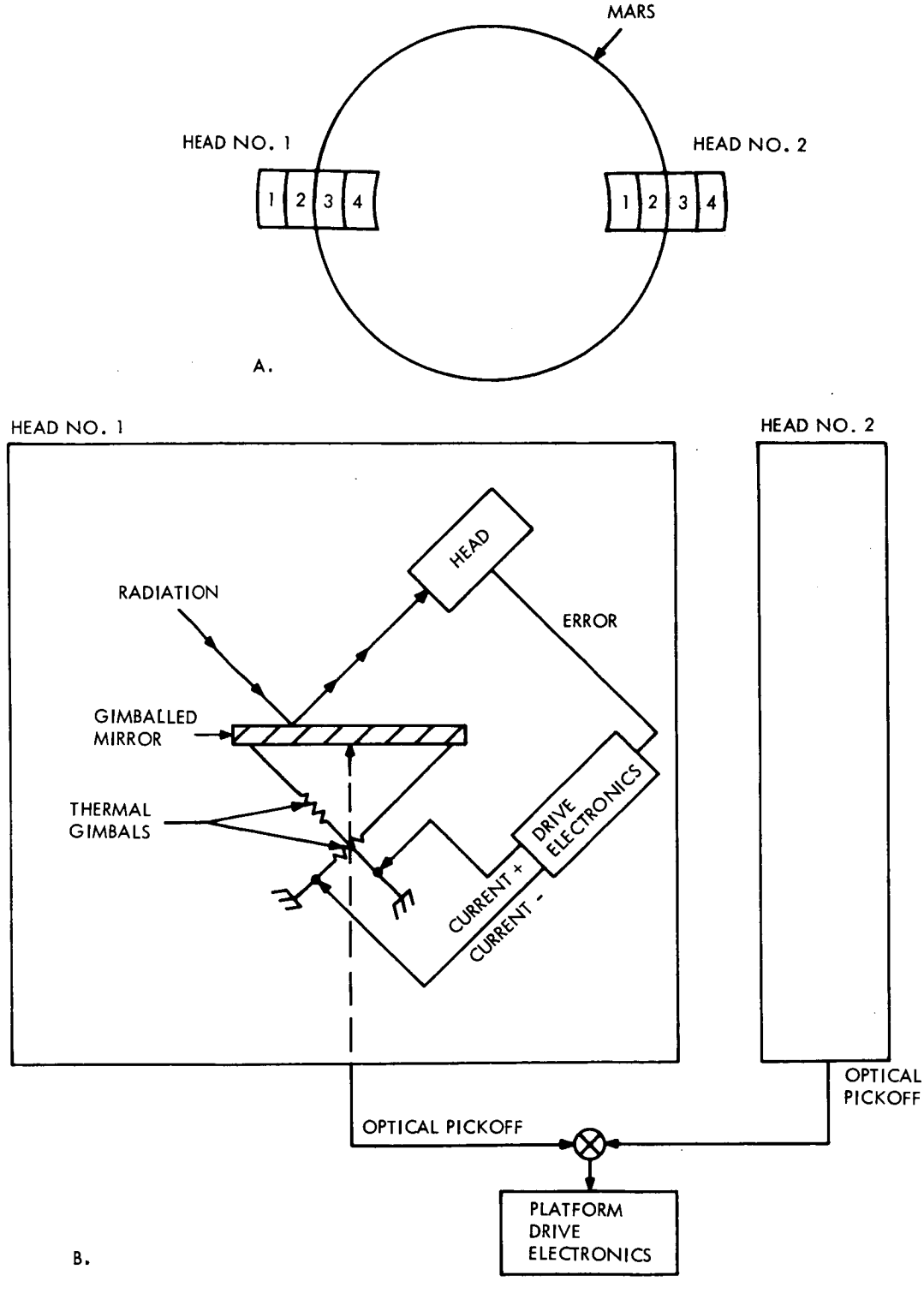

Figure 25. Gimballed Sensor

It should be noted that the gimballing is slow and involves no sliding friction. Once null is obtained, it is primarily used to accommodate small, slow vehicle movements such as limit cycle, and changing disc size.

Sun discrimination is again possible by comparing the levels of radiation in detectors 3 and 4 when irradiated. If number 3 is looking at the sun, its output will be much higher than that of number 4. Logic can be employed to cause the mirror to move until number 3 is within the Mars disc.

Some of the expected characteristics of this sensor are as follows for the single axis version that requires two heads:

a. ±0.05 degree accuracy, noise output of ±0.03 degrees.

b. Scale factor of 1 volt/degree, time constant of one second.

c. Power 4 watts (tracking), (peak 10 watts during acquisition).

Weight 5 pounds

Volume 100 in^3.

d. Expected life exceeds one year.

2.3.4.3. Other Scanners

Both dithered and conical scanners were briefly considered. There are flight-proven models of each available from the OGO and Nimbus programs, respectively. Although both can possibly be used to track Mars, they are designs peculiar to Earth rather than Mars tracking (e.g., surface temperature, orbit ellipticity, atmospheric constituents) and would require significant design changes. The use of moving parts is also undesirable.

2.3.5. Off-Nadir Pointing

Several alternatives were considered for effecting off-nadir pointing of the closed loop. Alternatives that depend on the use of the horizon sensor were discarded so that the commanded mode will be available in event of sensor failure. Gimbal position is monitored for telemetry by a non-volatile counter that counts pulses produced by a geared-up increment indicator. For off-nadir pointing with the preferred design, the desired position is placed in a second counter and the drive activated until the counters compare.

2.4. THERMAL CONTROL TRADE ANALYSES

For preliminary design purposes, the PSP is divided into four thermal regions. Thermal coupling will be maximized within each region to provide uniform temperatures, whereas thermal isolation will be required between regions because of different temperature requirements. The four thermal regions are:

1. All of the science payload aboard the PSP except:
   a. High-resolution IR spectrometer detector
   b. Entire broad-band IR spectrometer
2. Optics and electronics of the broad-band IR spectrometer and the high-resolution IR spectrometer detector
3. Broad-band IR spectrometer detector which operates at moderately low temperatures.
4. Broad-band IR spectrometer detector which operates at very low temperatures.

The temperature requirements for each region are as follows:

1. Operating Temperature Ranges

   Thermal Region No. 1 +15 to +35 °C (59 to 95 °F)

Thermal Region No. 2 -43 to -33°C (-45 to -27°F)

Thermal Region No. 3 -148 to -138°C (-235 to -215°F)

Thermal Region No. 4 27 to 45°K (-411 to -379°F)

2. Storage (non-operating) Temperature Ranges

All Regions +5 to +45°C (41 to 113°F).

The weight and power dissipated during operation of the science instruments in the baseline configuration are given in Table 3; a typical duty cycle is given in Figure 26. Note that much of the supporting electronics is located in the spacecraft bus. During transit when the PSP is stowed, the instruments do not operate and consequently draw no power.

Table 3. Baseline Science Payload Weight and Power Division Between PSP And Bus

Science Instrument	Total Wt. (lb)	PSP Wt. (lb)	Bus Wt. (lb)	Total Power* (Watts)	PSP* (Watts)	Bus Power* (Watts)
MRTV No. 1	38	26	12	35	15	20
MRTV No. 2	38	26	12	35	15	20
HRTV	59	47	12	20	10	10
HRIRS	30	18	12	14	5	9
BBIRS	16	9	7	5	2	3
IRR	20	13	7	6	2	4
UVS	32	23	9	16	4	12
TOTALS	233	162	71	131	53	78

*Peak power

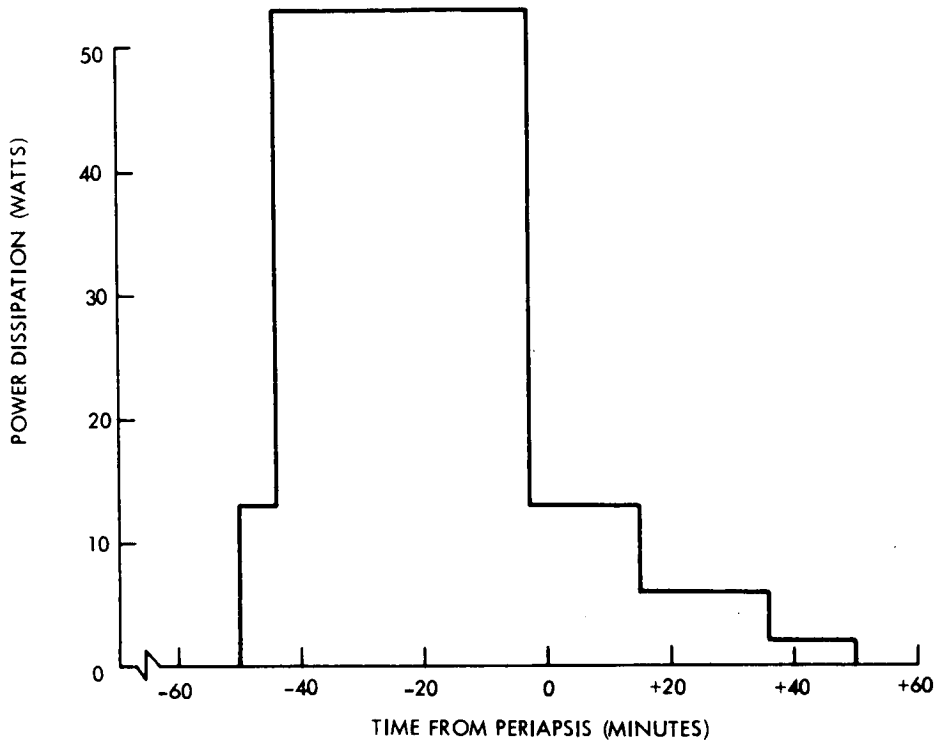

Figure 26. Typical PSP Mounted Science Instrument Power Profile

Considerations that govern the thermal control of the PSP are:

a. Changes in the thermal environment during transit

b. Variations in power consumption of the science instruments

c. Variations in the orientation of the PSP during operation in the vicinity of Mars

d. Sun occultation

e. Mars albedo and planetary radiation

2.4.1. Thermal Control During Transit

During transit, temperatures must be maintained between 41 and 113°F. An assessment of the thermal coupling of the PSP with the spacecraft indicates that maintenance of these temperatures by slaving the PSP to the spacecraft is not feasible.

The simplest technique for controlling temperatures is to utilize heaters within the PSP package. Power can be minimized by surrounding the external surfaces of the PSP with superinsulation blankets.

The following conditions were incorporated into the design analysis:

a. The effective emissivity of the insulation is 0.008.

b. The projected surface area normal to the solar vector is approximately 10 square feet, which results in approximately 2 watts of heat leaked into the PSP through the insulation.

c. Conductive coupling with the spacecraft results in a heat leak into the PSP of zero to three watts corresponding to temperature differences between the spacecraft and PSP of 0 and 70°F, respectively.

d. Radiation interchange with the spacecraft is negligible.

The results of this analysis are shown in Figure 27a which depicts the spectrum of heater power required to maintain PSP temperatures in the range 41 to 113°F. For a minimum temperature of 41°F the heater power required is approximately 6 to 11 watts. In order to maintain the upper limit of 113°F, approximately 13 to 19 watts are required.

The maximum heater power curve represents the absence of any solar load or spacecraft coupling, while the minimum heater power curve includes absorbed solar energy and spacecraft coupling. As a point of interest, Figure 27b shows the heater power that would be required if one surface of the PSP had thermal louvers in a closed position ($\epsilon = 0.1$) instead of being covered with a super-insulation blanket.

2.4.2. Thermal Control During Orbital Operations

Thermal control of the deployed PSP during Mars operations is predicated on thermal isolation between region two, containing the BBIR and the HRIR, and region one containing the remainder of the scientific instruments. At Mars encounter, some insulation will be ejected

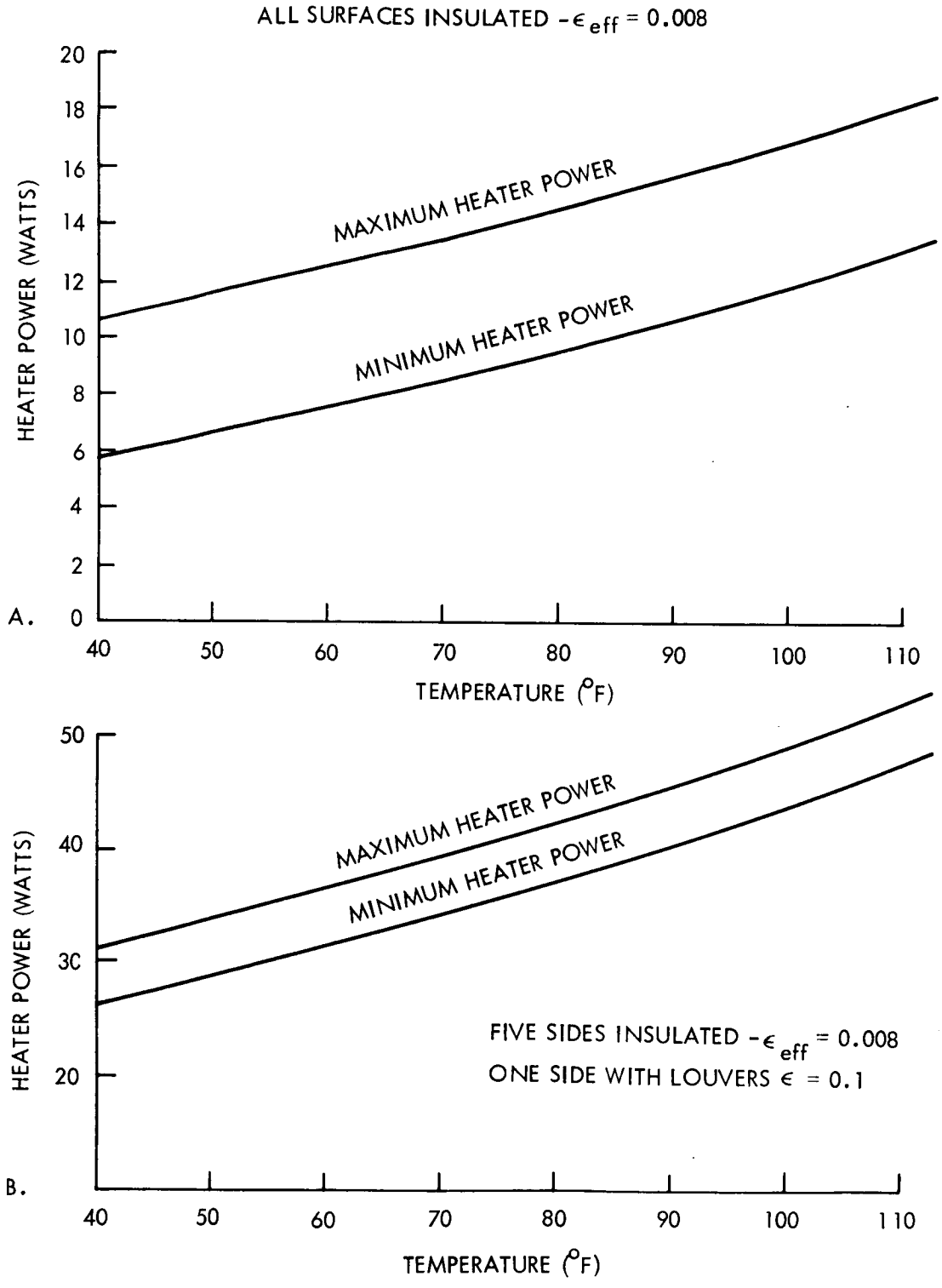

Figure 27. PSP Heater Power During Stowage

with lens covers. Thermal control within each region relies on sufficient heater power to account for heat leakage through the insulation blankets and thermal shorts. The thermal inertia of the equipment damps out temperature excursions due to power pulses and solar flux impingement. This rather simple thermal control approach is possible because of the very low nominal instrument power level, the relatively short peak power duration and the high thermal inertia of the instruments.

2.4.2.1. Thermal Control of Region One

This region contains all of the science instruments except the BBIR and the HRIR. The instruments, which must be maintained between 59 and 95^{o}F during operation, weigh 135 pounds. The orbit average power is 4.4 watts with a peak of 46 watts occurring for 47 minutes near peripasis. Except for the aperture areas, the complete surfaces of the region are covered with insulation blankets.

The heat loss from region one occurs by:

a. Heat leak through insulation

b. Heat leak through apertures

c. Heat leak to region two, which is at a considerably lower temperature

The requisite operating temperature is attained by effecting the appropriate thermal balance between the above heat losses and the instrument and heater power. This thermal balance is summarized in Table 4.

During the period of peak power load, 46 watts are dissipated by the science packages. If it is assumed that all of this power is absorbed by the instruments, the thermal inertia will limit the rate of temperature rise to 5^{o}F/hr. During the 47-minute power pulse, a temperature rise of less than 5^{o}F will be experienced.

Table 4. Thermal Balance for Region One

	HEAT LOSS - WATTS			HEAT GAIN - WATTS	
	Thermal Region 1 = 59°F	Thermal Region 1 = 95°F		Thermal Region 1 = 59°F	Thermal Region 1 = 95°F
Through Insulation	7	9	Instrument Dissipation	4.4	4.4
Through Apertures*	2.5	3.5	Heater Power Demand Region 2 = -45°F	6.8	10.7
To Region 2**					
T Region 2 = -45°F	1.7	2.6	Region 2 = -27°F	6.6	10.4
T Region 2 = -27°F	1.5	2.3			
Total Heat Loss			Total Heat Gain		
T Region 2 = -45°F	11.2	15.1	Region 2 = -45°F	11.2	15.1
T Region 2 = -27°F	11.0	14.8	Region 2 = -27°F	11.0	14.8

* The heat leak through the apertures was conservatively based on a total aperture area of 0.68 square feet with an effective emissivity of 0.1. The best source of present information indicates that the apertures will probably consist of quartz or beryllium lenses with an outer coating of vacuum deposited aluminum. Typically these result in emissivities considerably lower than 0.1.

**The heat leak to region 2 was based on an insulation blanket between the regions having an effective emissivity of 0.008, and on a conductive resistance of 200°F/watt between the two regions.

One final consideration is the effect of a solar load on the external surfaces. If it conservatively assumed that direct solar incidence occurs on as much as 5 square feet of the insulated surface area of region one. The solar energy absorbed will be approximately 1.0 watts. In this event, the heater power required to maintain requisite temperatures will be reduced by approximately 10 to 15 per cent. Since the sum of absorbed solar and internal energy is less than the required heater energy to maintain specified temperatures, there can be no overheating problem due to possible solar flux impingement.

2.4.2.2. Thermal Control of Region Two

Region two contains the BBIR and HRIR, which weigh 27 pounds and must be maintained in the range -45^{o}F to -27^{o}F. The orbit average power dissipation is 0.92 watts with a peak of 7 watts occurring for 65 minutes near periapsis. Once again all surfaces of the region will be completely insulated except for apertures.

Heat loss occurs through the insulation blankets and apertures while heat gain occurs by heat leak from region one and by instrument and heater dissipation. Table 5 summarizes the thermal balance for region two.

During the 65-minute peak power load of 7 watts, the instrument mass will rise at a rate of less than 4.5^{o}F/hr. Over the 65-minute period, the total rise will be less than 5^{o}F, which is considered quite insignificant. The effect of direct solar impingement is similar to that described previously in region one. A very conservative estimate of the maximum absorbed solar load is 1.0 watts, which when added to the dissipated power is still less than the rate of heat leak, so that an over-temperature condition cannot occur.

2.4.2.3. Total Operating Power Requirements

Considering the PSP as an entity, it is clear that the maximum operation heater demand will occur when the temperatures of each region are a maximum, that is with thermal region one = 95^{o}F and thermal region two = -27^{o}F. For this condition the total PSP power

Table 5. Thermal Balance for Region Two

	HEAT LOSS (Watts)			HEAT GAIN (Watts)	
	Thermal Region 2 = -45°F	Thermal Region 2 = -27°F		Thermal Region 2 = -45°F	Thermal Region 2 = -27°F
Through Insulation	2	3	Instrument Dissipation	0.92	0.92
Through Apertures*	2.7	3.3	From Region 1**		
			Region 1 = 59°F	1.7	1.5
			Region 1 = 95°F	2.6	2.3
			Heater Power Demand		
			Region 1 = 59°F	2.08	3.88
			Region 1 = 95°F	1.18	3.08
Total Heat Loss	4.7	6.3	Total Heat Gain		
			Region 1 = 59°F	4.70	6.30
			Region 1 = 95°F	4.70	6.30

*Aperture area = 1.83 ft^2 with effective emissivity of 0.1. This is considered to be conservatively high since the aperture of the BBIR with area of 1.8 square feet will be gold-coated ($\epsilon \approx 0.04$).

**Same assumption as given in Table 4 for Region 1.

demand will be 13.78 watts (without solar effects which could reduce this by 1 watt). The heat leak between regions one and two does not affect the total PSP power demands, since this heat flow merely increases the power demands of region one, but decreases that of region two by the same amount.

The minimum power demand for the PSP occurs when the temperatures of each region are at their lower limits, that is with thermal region one = 59°F and thermal region two = -45°F. For this condition the power demand is 8.9 watts. Solar loads could reduce this by ~1 watt.

2.4.3. Failure Mode Considerations

Failure of a science instrument will reduce the nominal power levels of a region; very simple considerations yield the maximum additional heater power that would be required to maintain the requisite temperatures. The worst case for region one would require an additional 4.4 watts, while in region two, less than one additional watt of heater power would be necessary. Heaters are well proven and have outstanding performance records in space applications.

2.4.4. Design Considerations

The thermal control analysis was predicated on effective isolation of the regions. Since the operating temperature ranges can differ by as much as 140°F, a high thermal resistance interface must be designed. This can be accomplished by separating the two regions by a superinsulation blanket. Physical structural attachments between the two regions will be designed to give a high resistance. It is considered that an overall resistance of 200°F/watt for the attachments is feasible.

The small heat flows and power requirements associated with the PSP require that very careful detailed design and testing be accomplished to assure that the proper thermal balance is effected. By biasing the design toward the low ends of the temperature ranges, the appropriate thermal margins will result.

Thermal coupling within regions is enhanced by the basic design approach os isolating regions from each other and from the external space environment. Radiation coupling will be accomplished by utilizing highly emissive black paints within the compartments. Thermal conductive coupling will be accomplished by mounting instruments on common structures where possible.

2.4.5. Superinsulation Blankets

Since the thermal design is based on heat leakage through the insulation blankets, and heaters to effect the proper balance, it is evident that if the insulation is too efficient in impeding heat leak, temperatures exceeding the prescribed upper limit may be experienced. It is highly desirable to design an insulation system for the PSP that exhibits highly predictable and repeatable thermal performance. A program to develop such a system has been under development at GE for military spacecraft. The system, which will be referred to as Rigid Superinsulation, consists of layers of either aluminized or gold-coated 1/4-mil mylar sheets separated by low-density mylar honeycomb. The honeycomb separators are 0.050-inch thick with 3/4-inch cell size and 0.005-inch walls. The metalized sheets are either bonded or ultrasonically welded (the latter being preferable) to the honeycomb separators. Both the honeycomb separators and the metalized mylar sheets are perforated with small holes to provide adequate venting.

Preliminary laboratory tests indicate effective emissivities on the order of 0.01 for 15 layers of the metalized mylar. It is felt that better performance that is competitive with flexible superinsulation can be obtained. The rigid superinsulation has the advantage of resisting crushing during assembly, handling and shipping of the PSP and does not require through penetrations for attachments. Attachment hardware can be bonded to the insulation assembly. Mechanical tests have indicated the feasibility of this approach. It is precisely the crushing effect and the penetrations which contribute to the predictability and repeatability problems with flexible superinsulation. Once models of the rigid blankets are fabricated and tested for thermal performance, a high degree of confidence exists for repeating that performance on the flight article and the possibility of attaining effective emissivities that are too low are minimized.

2.4.6. Effect of Changing PSP Power Dissipation

The option exists for locating all of the electronics associated with the science instruments in the PSP package or, as in the baseline design, mounting as much of this equipment as possible in the spacecraft bus. From thermal considerations, it is desirable to reduce power dissipation levels in the PSP package to relatively low values. This approach results in minimum heater requirements and minimum excursions in temperature due to varying absorbed loads and power duty cycles during Mars orbits. Low operating power also infers that less heater power is required to maintain instrument temperatures at requisite levels if instruments are turned off for considerable lengths of time in Mars orbit.

For example, if all supporting electronics were located in the PSP, the power profiles during operation would be as follows:

	Average Power (Watts)	Peak Power (Watts)
Region 1	11.5	112
Region 2	2.5	19

During periods of peak power the rate of temperature rise for regions one and two would be approximately 10^{o}F/hr and 7^{o}F/hr. These are of the order of twice the rates for the proposed design. Furthermore, during orbital periods when instrument power is off for considerable lengths of time, the heater requirements would be 11.5 watts and 2.5 watts greater than normal operational requirements. In the baseline design only an additional 4.4 and 0.92 watts are required. As a rule, heater requirements to maintain minimum temperatures when instruments are off for extended periods in orbit are proportional to operating power levels.

A further consideration is that if the power level is increased to much higher levels than presently considered for the system, large variations in average dissipated power are more probable and would likely require an active louver system to accommodate the variation in loads.

2.4.7. Optimization of Design

It is evident that at least in principle, an optimum design exists where the internal power instrument dissipation just balances the total heat leak in each region so that during normal operation no heater power is required. If, for example, some of the electronics for region one, totaling 2.4 watts of average orbital power, is returned from the bus to the PSP so that the dissipated power equals 6.8 watts, no heater power would be required for region 1 during operation. Similarly, if additional region two electronics totalling 1.18 watts presently located in the bus were packaged within region two of the PSP, the total average instrument power would be 2.1 watts which would just balance the heat leak. The total power savings compared to the present design would be 8.9 watts. (However, there would be, as indicated previously, wider temperature excursions during peak power loads.) The situation would require very precise control on the insulation performance, which may not be entirely feasible. Good design practice dictates that in a thermal control system such as that proposed temperatures be intentionally biased low with a small amount of heater power required to trim up to minimum temperature levels. At the expense of being slightly off a design point theoretically optimized with respect to minimum power, adequate design margin for contingencies is attained.

The present design concept of reducing PSP operating power levels by locating electronics in the spacecraft meets the goal of requiring minimum heater power while at the same time providing adequate design margin.

2.4.8. Detector Cooling Considerations

Detector cooling is considered to be a function of the individual science instruments, but the PSP must be configured with appropriate consideration for the cooling requirements of the instruments. Accordingly, the implications of the detector cooling requirements have been investigated.

2.4.8.1. High Resolution Infrared Spectrometer

The high resolution infrared spectrometer incorporates a detector that requires cooling to -60°C (213°K) for proper function. Reliability, weight and power penalties, and overall complexity clearly indicate selection of passive radiation cooling from among other candidates of mechanical refrigeration, stored open-cycle refrigerants, and thermo electrics. The detector of the HRIR instrument on the Nimbus Spacecraft is cooled to about 200°K with a similar arrangement. To use this simple, reliable method of cooling, the instrument window through which the back of the detector mounting plate looks to space must be designed and oriented so that direct or reflected sunlight does not illuminate the aperture; spacecraft and planetary radiative heat fluxes must also be restricted. At -60°C, the detector plate has a radiating capability of over 10 milliwatts per square centimeter before reduction for view factor to the window. This is sufficient to reject the detector heat load at the desired operating temperature, providing reasonable care is taken with the instrument thermal design.

2.4.8.2. Broad Band Infrared Spectrometer

The broad-band infrared spectrometer has cooling requirements at several temperature levels. If a mercury-doped germanium detector is used in channel one to sense radiation to 15 microns wavelength, it must operate in the 27 to 45°K temperature range. The PbSe detector of the second channel as well as the chopper for channel one, require temperatures of 130°K, and the optics and chopper for channel two require 235°K. Detector cooling to 45°K for long periods of operation at Mars will require weight and power penalties that are beyond consideration for early Voyager missions. Compromise in operating time or detector temperature is required if currently allocated instrument package weight and power are not to be greatly exceeded.

2.4.8.2.1. Passive Cooling. Passive radiation cooling of the detector must be eliminated as a possibility at 45°K. At 45°K, a surface radiating directly to space has a potential heat rejection capability of about 0.02 milliwatts per square centimeter. This is in contrast to

the average solar flux at Mars of 62 mw/cm^2, 3100 times larger. The average thermal flux from albedo and planetary emission for a Mars oriented surface in a 1,000-10,000 kilometer orbit is 2.6 mw/cm^2, or 130 times the emissive power at 45^{o}K. If the instrument body is internally gold-coated, as well as the detector plate face, internal radiation alone would prevent the detector plate from cooling to 45^{o}K if the instrument walls are above 92^{o}K.

Heat flow from the instrument body to the detector mount through the mechanical supports will also add to the cooling load. Because of the requirement of preventing any of the sun or planetary flux from impinging on the detector radiator, an elaborate array of radiation shields will be required. These shields will of necessity restrict the view to space of the detector radiator, further reducing its radiating potential. If shields are gold coated on the inside, and they occupy 50 percent of the radiators view factor, the shield temperature must be restricted to 66^{o}K, which is difficult to achieve.

Considering that all the factors of the previous paragraphs will act simultaneously to prevent achievement of 45^{o}K by direct radiation to space, it seems highly unlikely that even extensive development will achieve this goal. Detector cooling to this temperature by radiation in a vacuum chamber has recently been reported. However, achievement of that temperature in an instrument mounted in the PSP by radiation cooling alone seems very remote.

Cooling of the PbSe detector of Channel 2 and the chopper of Channel 1 to 130^{o}K is accomplished in the Mariner Mars 1969 installation of the BBIR instrument, by an 85 square inch radiator that is located in the shadow of the spacecraft. As of the date of this report, there is cautious optimism at JPL that this temperature can be achieved, although it has not yet been demonstrated. There is some concern that the 85 square inch radiator may not be quite large enough to reach 130^{o}K temperature.

Applying this instrument to the Voyager PSP does not improve its cooling capability relative to the Mariner installation. There is no surface that is completely shaded as there is with Mariner. Shades will have to be erected to shield the radiator from the sun and from the

spacecraft. At 130°K it is expected that successful radiator design will require rather extensive development.

The remaining thermal requirements of the BBIR, such as holding the telescope, monochromator, and Channel 2 chopper at 235°K, will be relatively simple to accomplish by radiation to space.

Because of the exceedingly difficult if not completely impossible task of cooling the BBIR Channel 1 detector to 45°K for six months, possibilities of satisfactory utilization of an alternate detector which would require cooling to 80°K have been identified. At 80°K, a radiating plate can radiate 10 times the heat flux that it could at 45°K, although it is still restricted to 0.2 mw/cm^2. This factor of ten increase in radiating capability may be sufficient to make radiation cooling possible for the BBIR low temperature detector. A staged radiator may be capable of cooling the entire instrument.

In a staged radiator design, heat is rejected at several temperature levels. With a five-stage radiator design, the instrument body, well insulated from all external heat sources, could be cooled to 235°K by the first stage plate. Lower temperature stages are successively supported from the next warmer plate to reduce support conduction and interstage radiation, so then, perhaps, the third stage could be used for the 130°K cooling load. The low temperature detector could be coupled to the fifth stage for the lowest temperature heat rejection. A five-stage radiator proposed for detector cooling of an earth satellite instrument had calculated stage temperatures of 198, 158, 113, 87, and 75°K, respectively, and a fifth stage heat rejection capability of 60 mw. The first stage plate is 21.4-inch diameter, and the shield 28-inch diameter by 19-inches high. A possible arrangement of such a device is shown in Figure 28. Identifying a satisfactory design for the shades to prevent incident radiation on the detector radiator and still permit a relatively free view to space is probably the most critical design requirement.

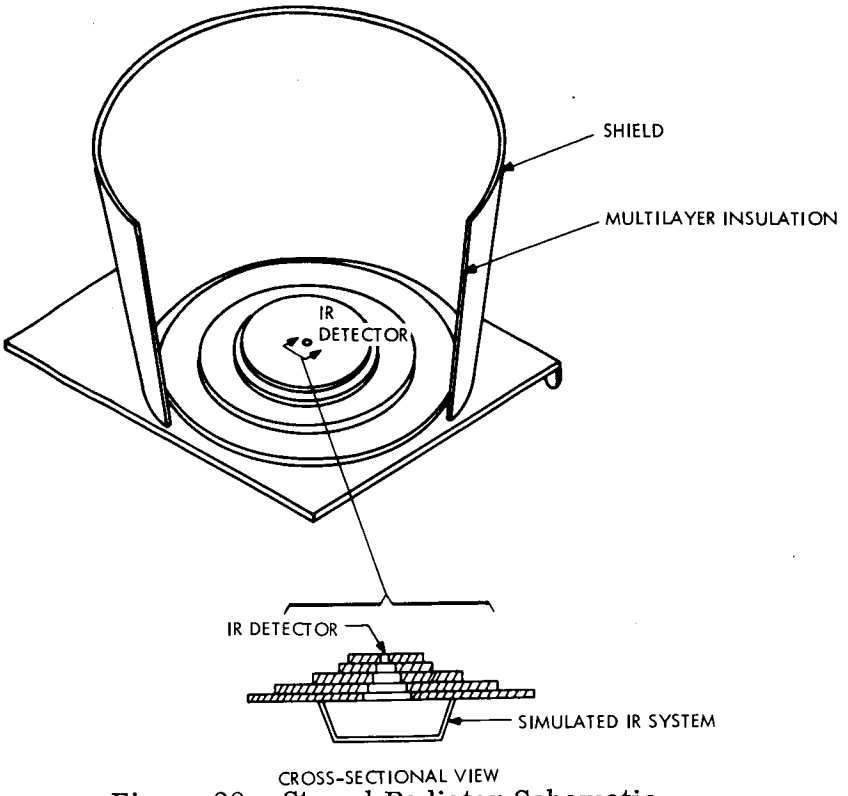

Figure 28. Staged Radiator Schematic

2.4.8.2.2. Gas Expansion Cooling. The BBIR instrument with its channel one detector cooled to 27°K is included in the Mariner Mars 1969 Spacecraft. The low temperature cooling operation is performed by a two-stage nitrogen-hydrogen Joule-Thomson cryostat. Eleven pounds of tanks and fluid are needed to provide 24 minutes of useful instrument operation. Possibly, gas remaining after orbit injection and orbit trim maneuvers could be used for gas expansion cooling but operating life would still be limited to a few hours, at most. The Joule-Thomson inversion curves show that helium must be cooled below 50°K, and preferably below 30°K, before it can be used for this type of refrigeration.

This helium gas could provide short term cooling after passing through a miniature turbo-electric expander. It is estimated that it could provide 10 watts of cooling at 45°K for 15 hours, or one watt at the same temperature for 30 hours.

2.4.8.2.3. Open Cycle Cryogenic Storage. A stored-cryogenic, open-cycle refrigerator is a possible means of cooling an instrument detector. Previous study has shown that stored parahydrogen, in either solid or liquid form, has the greatest cooling potential per pound of weight. Unfortunately, hydrogen is a very low density material and the insulated container volume becomes large.

For six-months operation at Mars, less than 1 watt useful cooling at $80^{o}K$ would require at least 150 pounds and nearly a four-foot diameter tank. This would be a very large addition to the PSP and the tank probably could not be located within the spacecraft because of excessive heat flow to the cold gas through the connecting pipe.

2.4.8.2.4. Thermoelectric Cooling (Peltier Effect). A thermoelectric device can be used to extract heat at one temperature and reject it at a higher temperature. Thus for instrument cooling, the thermoelectric element transfers heat from the detector to a higher temperature space radiator. The radiator dissipates the detector cooling load plus the electrical power input to the cooler. The efficiency of a Peltier cooler drops off with decreasing temperature and reaches a point where only negligible cooling is available. A temperature of about $150^{o}K$ represents the lower temperature limit for any significant heat load for a staged device. The effects are illustrated in the following example.

A commercially available, four-stage cooler can pump 10 mw cooling load from $181^{o}K$ to $300^{o}K$ with an expenditure of 5.6 watts electrical power. Thus the overall cooling efficiency is 0.18 percent. This same device will pumpt 50 mw cooling load from 198 to $300^{o}K$ with the same electrical power consumption, increasing its efficiency to nearly 1 percent.

A Peltier cooler by itself does not now appear to be useful for the cryogenic temperatures required for the BBIR instrument. Continued development of these devices to optimize their efficiency at lower temperature may improve performance for future consideration. In addition, a space qualification program would need to be initiated.

2.4.8.2.5. Thermoelectric Cooling (Ettinghausen Effect). If a magnetic field is imposed perpendicular to an electric current, a temperature gradient is established that is perpendicular to both the electric and magnetic fields. This phenomenon is referred to as the Ettinghausen effect. An Ettinghausen device coupled to a multi-stage Peltier cooler is practical down to temperatures of 100^{o}K. A large amount of development work is required in this area in materials research as well as performance characteristics. Efficiency is expected to be very low.

2.4.8.2.6. Electro-Mechanical Refrigeration. A number of small, closed-cycle refrigerators are now available and are under extensive development for detector cooling. Sterling cycle machines have the highest efficiency, providing several watts cooling at 77^{o}K or lower for as low as 100 watts electrical input and 15 pounds weight. All the Sterling cycle machines operable to date are relatively short-lived, requiring maintenance after approximately 250 hours operation. All of the low power consumption machines have a reciprocating compressor and consequently are a source of vibration. A turbine type machine is under development that has low vibration and long operating lifetime, but its efficiency is low and the power requirement approaches 300 watts for a miniature 77^{o}K unit. A potentially longlife combination rotary reciprocating unit has been under development to provide 2 watts cooling at 77^{o}K for about 100 watts input, but flight suitable equipment is estimated at least 3 to 5 years away. None of these machines seem particularly attractive to include in the PSP.

2.4.8.2.7. Conclusion. The cooling requirements of the broad-band infrared spectrometer exceed the current state of technology. Unless a successful development effort can achieve the required cooling, some compromises in temperature or operating life will be necessary.

2.5. STRUCTURAL DESIGN AND PACKAGING ALTERNATIVES

The PSP exists to service the science instruments and therefore the basic configuration is strongly influenced by the requirements of the science instruments. Many of these will change as instrument design progresses, but certain general requirements are recognized:

a. The PSP must be designed to accommodate launch and orbit injection loads in the stowed position and orbit trim loads after deployment.

b. Micrometeorite protection of instruments consistent with the required probability of mission success is necessary.

c. The design must consider the low vibration requirement during photo-imaging.

d. The variation in operating temperature requirements of instruments will require two thermal regions.

e. Minimum structure weight is desired.

2.5.1. Instrument Support

These considerations lead directly to a center boom support, which uses the extended deployment boom for mounting of the instruments. This approach produces excellent mounting rigidity for accurate instrument bore-sighting. Thermal compartmentation requires that the infrared spectrometers be thermally isolated from the support boom which will result in a small alignment degradation. The baseline design (Figure 29) has an envelope that is nearly a cube and favors central support of the instruments.

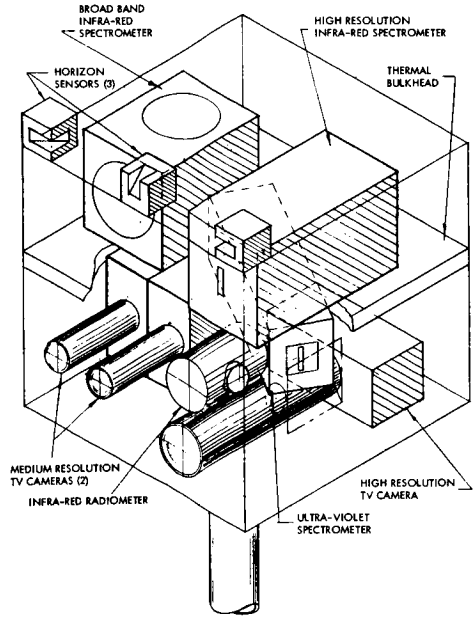

Figure 29. PSP Internal Arrangement

2.5.2. Outer Wall Construction

Very little structure is required to support the insulation. The lightest weight system would be a fabric netting reinforcement of the insulation blanket such that the blanket would be self supporting from a few hard points, or from a light-weight frame at the corners of the PSP envelope. Such a system would be adequate to support the insulation, but would not provide other functions, such as micrometeorite protection, thermal gradient dissipation, handling protection, or hard point attachment provisions.

A stronger envelope can be obtained with reinforced fiberglass which has a certain degree of resilience and can absorb minor handling loads without damage. However, for maximum strength and rigidity a sandwich structure is preferred such as aluminum honeycomb.

Micrometeorite protection favors the use of two walls; however the usual honeycomb structure does not give optimum protection, due to channeling of the debris resulting from the first impact, which concentrates the load on the inner skin. In addition the inner skin is not free to flex in order to absorb the energy and this increases the chance of rupture. Optimum design for micrometeorite protection would have internal shear webs spaced at wider intervals.

Thus, to provide a balanced multifunctional design, a two-wall internally stiffened panel appears to be the most useful approach. This arrangement accomplishes all of the functions postulated; insulation support, protection against dust, dirt, handling and micrometeorites, and also provides heat paths for equalization of internal temperature gradients.

2.5.3. Hard Point Provisions

The stowed support arrangements require some lateral attachment to prevent resonance during launch and orbit insertion. Three general approaches have been considered including direct support of the boom by an external bracket truss, an internal truss arrangement that feeds the load directly from the hard points to the central boom, and brackets that

distribute the load from the hard points to a honeycomb panel which then transmits the load to the central boom, or to the instruments directly, in the case of shelf-mounted arrangements.

The internal truss or panel arrangements can provide dual functions in transmitting the loads from the hard points, and also in compartmentalizing the PSP, providing stiffening for the external envelope, and if necessary providing support surfaces for the electronics and cabling inside the PSP.

The choice between the internal truss or the bracket-honeycomb panel alternatives is not conclusive and will depend on the results of a more detailed design study. For purposes of the baseline design, the internal truss, integrated with a central thermal control isolation barrier is the preferred arrangement.

2.5.4. Orbit Trim Support

Two methods appear feasible for holding the PSP in the stowed position and preventing vibration during the low thrust orbit adjust maneuvers. The PSP can be held against its lateral attachment supports by preloading with the cone drive gimbal, or a latch can be used to re-establish the stowed condition.

The orbit adjust loads are quite low compared to the boost loads. Thus the preloading moment required from the deployment gimbals is within a reasonable range (200 to 400 lb-ft). This use of the gimbals gives highest reliability since there is no possibility of a latch failure when there is no latch. The weight penalty of the reuseable latch is also avoided. Thus, the use of the gimbal motor for the snug down force and the use of separation nuts for a one-shot release, appear optimum as long as the orbit adjust loads are low. With high loads, the gimbal weight could become excessive, and then the reusable latch would be favored.

2.5.5. Thermal Compartmentation

The infrared spectrometers require a very low temperature, -30 to -60°C; the other instrumentation operates best at higher temperatures.

The use of thermal compartmentation provides a satisfactory thermal environment for the instruments, and in addition facilitates the rejection of heat from the higher power dissipators, since these happen to be the instruments that also require higher operating temperature.

The baseline design provides for a two-zone compartmentation, with the upper zone at a temperature of -43° to -33°C and the lower zone held at 15° -35°C. This should be sufficient, but if not, the upper zone could be divided into individual compartments, one for the high resolution spectrometer and one for the broad-band spectrometer.

2.5.6. Structural Damping

The configuration of the scan platform results in a low natural frequency and low inherent structural damping; structural damping is desirable so that disturbances disappear rapidly and are less likely to affect photoimaging. To increase structural damping, some mode such as surface friction or flexural hysterisis must be used to convert kinetic energy into heat. Design effort is required to obtain structural damping in the support tube. Design techniques are available for increasing structural damping; effort toward this goal is desirable to improve jitter performance.

3. DESCRIPTION OF REFERENCE DESIGN

3.1. VIEWING CAPABILITY

Viewing capability of the science sensors is controlled by three influences. The first influence is the desire for no vehicle blockage of the science sensor line-of-sight. The second influence is the requirement that attitude control sensor interference not preclude proper orientation of the PSP. The third influence is that the gimbals must have the necessary mechanical freedom to accomplish the pointing.

Figure 30 indicates the range of orbits for which a medium resolution television camera has unimpeded viewing. The medium resolution cameras are located at the surface of the PSP closest to the spacecraft and are the most critical instruments from a blockage standpoint. The design orbit is also plotted for reference; in the early part of the mission, it is evident that the camera is blocked at some point in the orbit. Figure 31 is an examination of three of the early orbits that shows that the blockage occurs well away from the prime data acquisition regions.

Figure 32 indicates the range of orbits for which the horizon sensors have a clear field of view. Figure 33 shows the mechanical range of the PSP translated into clock and cone angle space. The baseline scan platform can function throughout the 1973 design orbit with no attitude control interference by the spacecraft and inconsequential science sensor blockage.

3.2. GIMBALLING AND DEPLOYMENT

Figure 14 represents the preferred PSP gimbal arrangement. The "C" or cone angle axis is used for deployment as well as tracking the orbit normal vector. The second degree of freedom necessary for orbit normal tracking is provided by the "D" or cross-cone axis. The "C" and "D" axes are located in front of the solar array at a clock angle of 170 degrees. Mechanical limits of motion of these axes in clock and cone angle space is illustrated in Figure 33. The "E" or Mars tracking gimbal provides 360^{o} capability for following the apparent motion of Mars in the orbit plane; location of the limit point of the "E" gimbal travel has not been investigated. However, the prime data collection region of the orbit is so small that selection of a suitable rewind point should be straightforward.

The boom length is the minimum consistent with acceptable fields of view of the instruments and horizon sensors. With the boom length selected, the plane swept by the horizon scanners is sixty-six inches from the "C" axis.

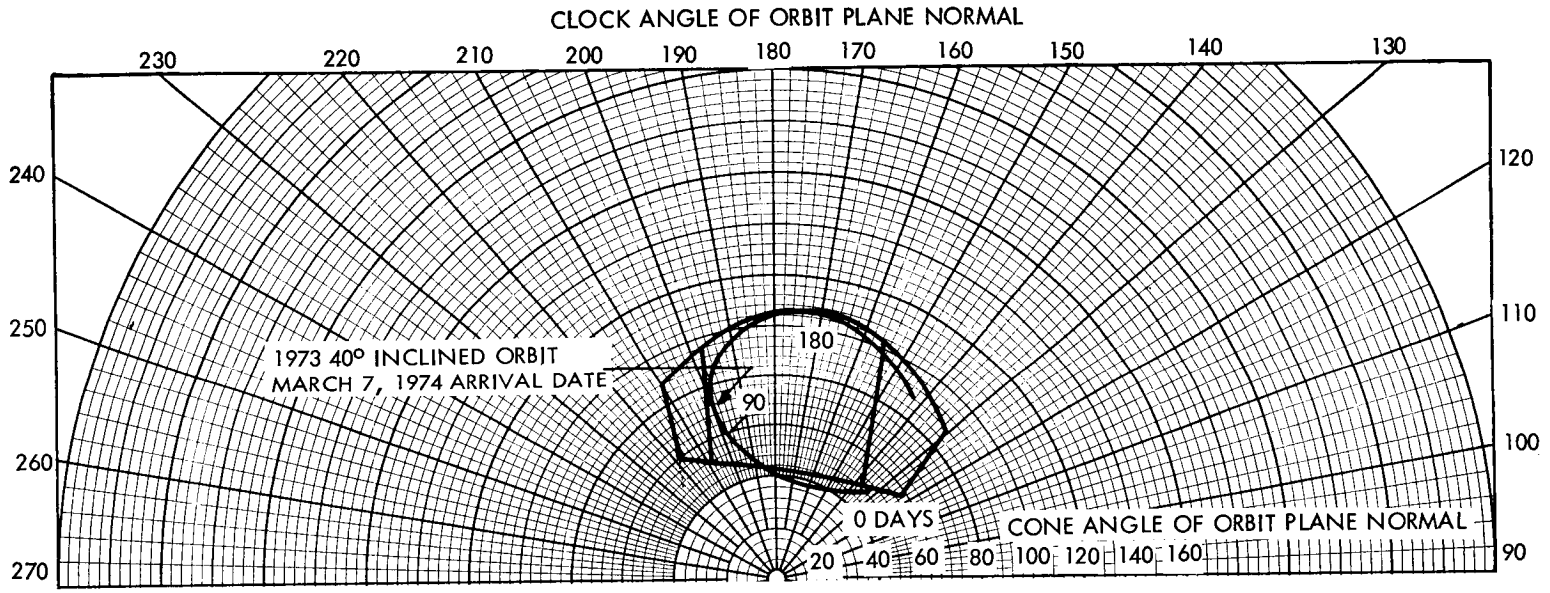

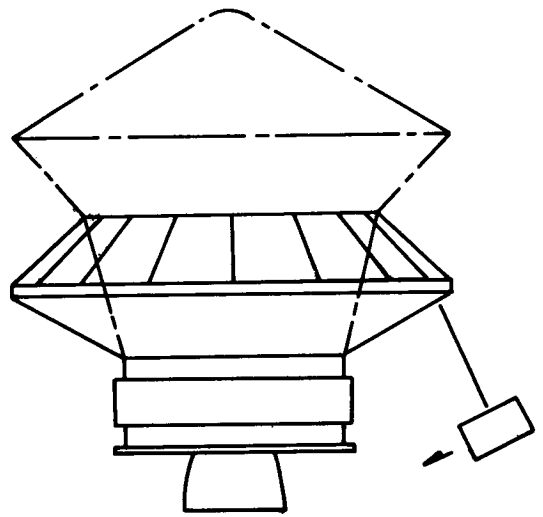

Figure 30. MRTV Coverage Reference Design

FOLDOUT FRAME 1

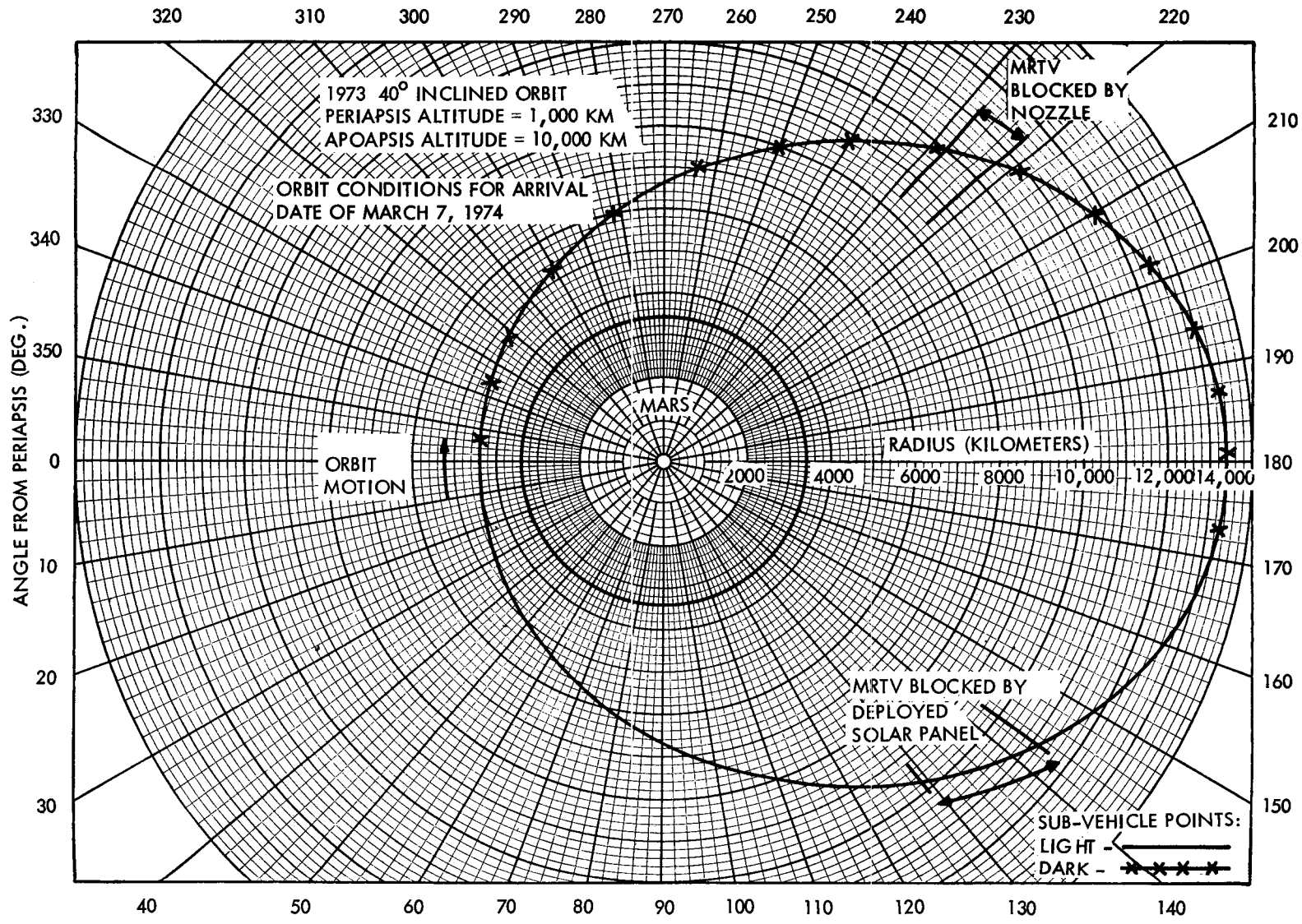

FOLDOUT FRAME 2

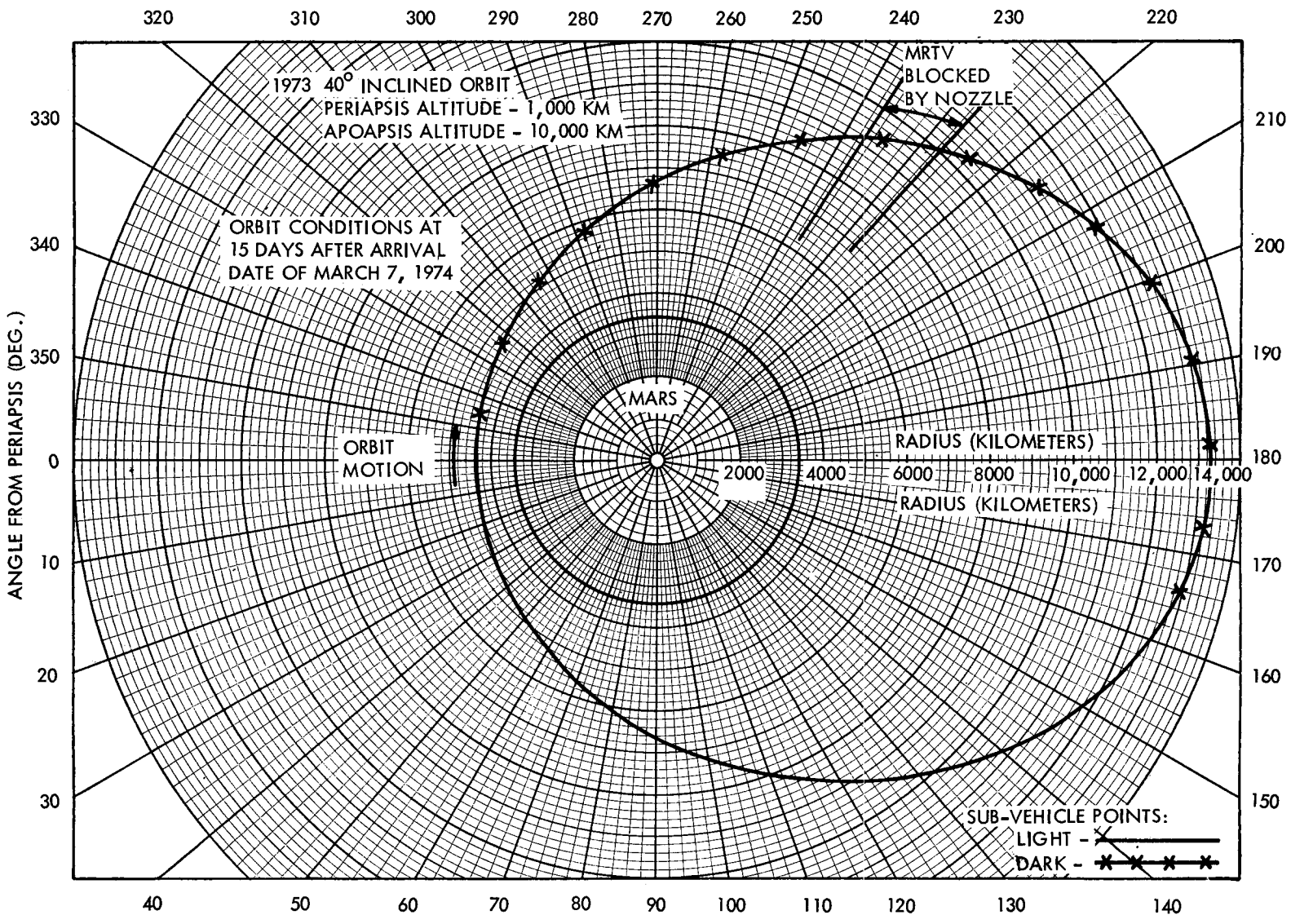

FOLDOUT FRAME 3

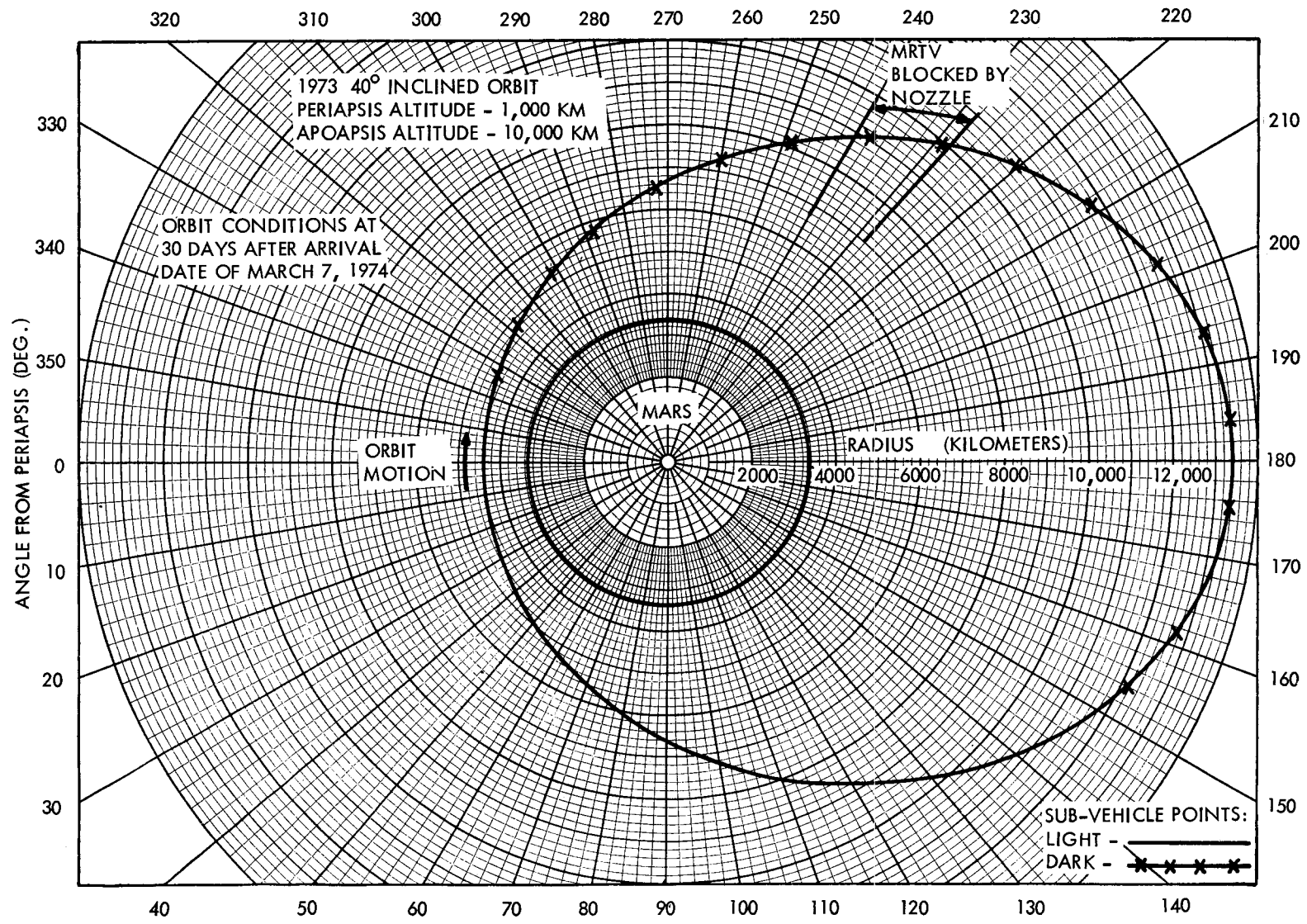

Figure 31. MRTV Blockage for Three Early Orbits, Reference Design

FOLDOUT FRAME 4

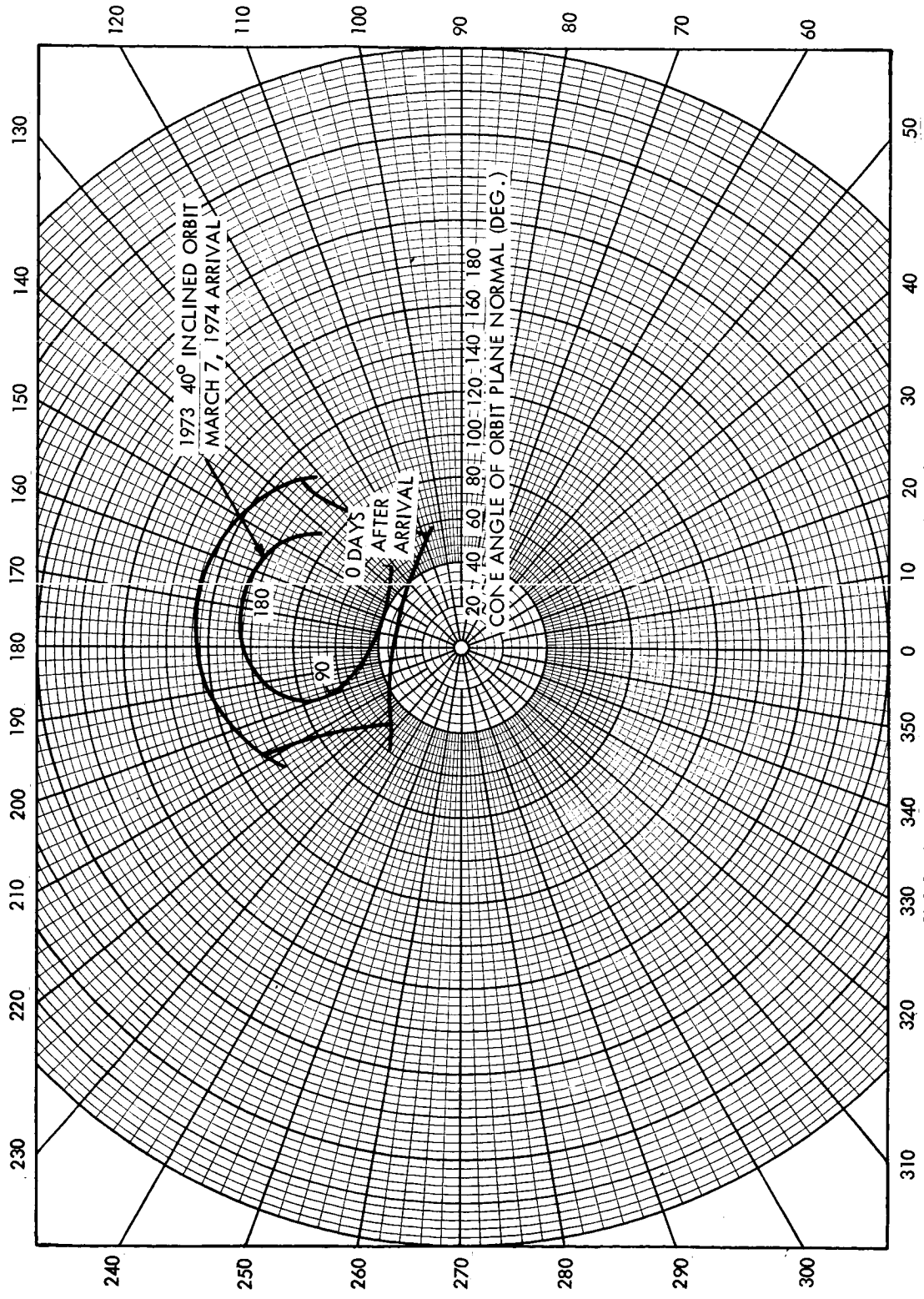

Figure 32. Attitude Control Sensor Coverage, Reference Design

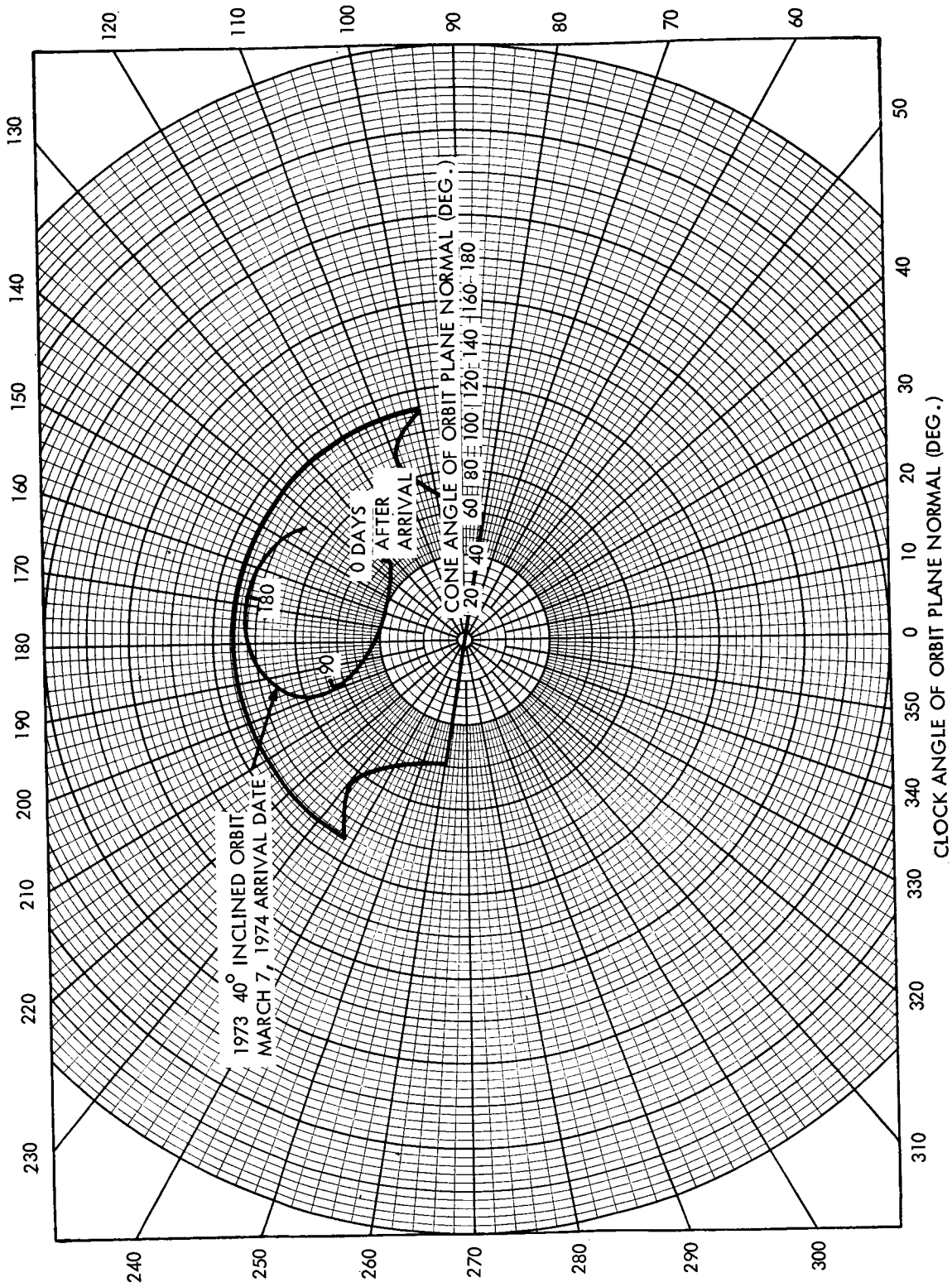

Figure 33. Gimbal Mechanical Limits, Reference Design

The PSP is supported during launch, boost, transit, and orbit insertion by the deployment boom and two attachment points. This arrangement is shown in Figure 34. Both axial and lateral loads are shared by the three-point support system. The two attachment points are stiff in every direction except in a direction along the boom axis where the support attachments have a small amount of flexibility. This assures low loads on the boom from misalignment or thermal expansion, and forces the boom to take all components of load parallel to the boom axis.

In the direction perpendicular to the boom axis, the two support attachments take all load, either as compression, tension or shear. The two attachments are not required to resist bending loads.

Since the PSP supports act in a direction close to the center of gravity, the bending moments applied are primarily due to the inertia of the PSP as it resists rotational accelerations experienced by the entire spacecraft. The boom itself will resist the moments that try to bend the boom at the PSP, while the torsion around the boom axis is taken by compression in one attachment and tension in the other.

Release is accomplished by firing the two 3/8-inch diameter separation nuts, each of which have redundant cartridges. The bolts are ejected into bolt catchers and held in a retracted position by springs. This frees the two attachment points and permits deployment.

It should be noted that the side view stowage arrangement, and the capability for removing the covers prior to release and deployment of the PSP provide a degraded mode of value in case the PSP release or deployment fails. The covers would still be open and the PSP instruments could be turned on to view in the direction of 260^{o} clock, 90^{o} cone, which is the direction provided when the PSP is in the center of its normal operating range with the Mars tracking axis turned in the general direction of the evening terminator. Although this direction would not generally point directly at nadir, it would provide an interesting traverse of some portions of the planet for most orbits under consideration.

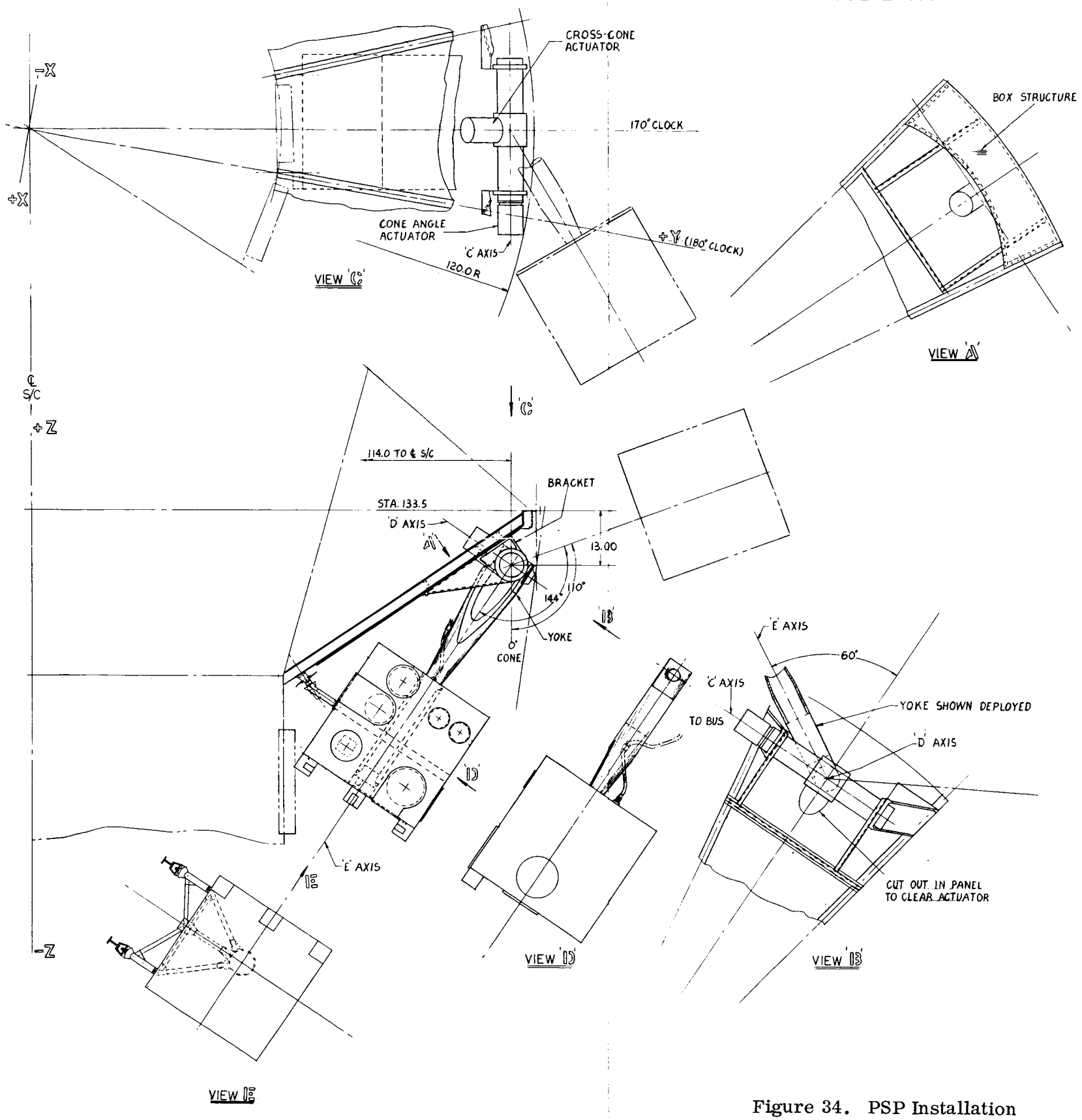

Figure 34. PSP Installation

FOLDOUT FRAME

FOLDOUT FRAME

After release of the PSP, the cone motion gimbal is driven for a 14^{o} travel, which clears the PSP from the attachments and permits full operation of the cross cone and Mars tracking axis drives. This motion also actuates a lanyard backup device for a functionally redundant actuation of the science covers.

During orbit trim thrusting, the cone drive actuator is used to preload the PSP in the stowed position.

3.3. ATTITUDE CONTROL

The PSP Subsystem provides orientation for the science instruments. The platform is mounted on a boom attached to the periphery of the spacecraft in the vicinity of the +Y axis; mounting is effected through a three-axis gimbal, each axis of which is driven by a separate control loop. The gimbal arrangement is shown in Figure 14. Two loops operate in an "open" loop fashion (under predetermined control of the C&S subsystem) to erect a perpendicular to the orbit plane. The third loop tracks the center of Mars under control of a Mars horizon sensor. In a secondary mode, this loop can be commanded to point in any direction permitted by the gimbal mechanical design.

Attitude control is probably the most complicated and critical function of the PSP. The design philosophy is to provide an extremely stable local vertical tracking platform. Difficult requirements like image motion compensation are relegated to the instrument with those requirements. The reliability of the PSP is not to be burdened by the exotic pointing requirements of one instrument.

3.3.1. Requirements for Gimbals C and D Control

a. The torque/speed characteristic of the stepper motors is such that they can drive the gimbal load in a zero G field at a slew speed of 3/16 degree per second. Moment of inertia is about 200 slug ft^2 maximum. The detent torque must be sufficient to prevent gimbal motion during firing of the attitude control jets.

b. The control loop electronics shall respond to pulses from the C&S (or command decoder in back up) and for each pulse the gimbal movement shall be 3/16 degree. A step sensor shall detect each step change of the gimbal.

c. Stops shall be provided to limit gimbal travel in both plus and minus direction. A stop detector shall indicate occurrence of gimbal stop with an accuracy of 3/16 degree.

d. Discrete step and slew modes of operation shall be provided.

e. Gimbal backlash shall be less than 0.05 degrees per axis. Gimbal step error shall be less than 0.125 degrees per axis.

3.3.2. Description of C and D Loops

A "step 1 +" or "step 1 - " command from either the C&S (or command decoder as backup) is applied at the input to stepper motor via the OR gate and N_1 (see Figure 15) which converts the single pulse from the C&S into several pulses. The succeeding gear ratio must be adjusted to match the stepper motor to the gimbal load. The value of N_1 is selected so that one pulse from the C&S subsystem provides multiple pulses to compensate for the gear ratio so as to drive the gimbal through 3/16 degrees. The value of the gear ratio and consequently N_1, are determined by the size of the motor step and the motor load requirements.

Slew operation at a rate of 3/16 degree per second can be commanded by the C&S subsystem. A start slew (+) or start slew (-) sets a flip-flop in the slew control electronics which controls a succeeding AND gate. The gate permits application of a train of clock pulses to be applied to the stepper motor via the OR gate and N_1. The clock pulses occur at the rate of 1 pulse/second. Slewing is stopped by a "stop slew" command from the C&S. If gimbal stop is encountered, slewing stops automatically. Each step of the output gimbal is detected by two magnetically operated reed switches located on a shaft geared up from the gimbal by n_2. They are operated by a bar magnet attached to the shaft. The step sensor output pulses are accumulated in a reversible counter and stored in a core memory to guard against power failure transients. Each time negative gimbal stop is encountered, the counter is set to

zero. Thereafter, the counter counts up the positive steps and counts down the negative steps. The output of the counter provides a direct indication of gimbal angle which can be telemetered to ground.

Limit sensors detect full positive or full negative angular displacement of each gimbal.

In the event of C&S failure, pulses can be sent via the Command Decoder to cause the PSP to perform in its discrete mode of operation. No back up for slew mode is provided.

3.3.3. Requirements for Gimbal E Control

After two gimbals have been used to erect a perpendicular-to-the-orbit plane, it remains for the third gimbal to allow tracking of the planet around this perpendicular. Tracking rates in a 1000 km by 10,000 km orbit vary from 10^{-4} to 10^{-3} radians per second. A major design goal is to obtain very smooth tracking at these low rates, so that random movement of the platform may be kept small during the exposure times of the photo-imaging equipment. The magnitude of the requirement varies with the exposure time, but it appears that the random rates must be below approximately 10^{-5} radians/second. Considerable design care will be required to meet this stability requirement. The Voyager Spacecraft will be stable in Mars orbit and the stability approach adopted is to control excitations which will disturb the normally stable spacecraft. Stepping drives have been virtually eliminated as reasonable structural damping does not allow dynamic effects to settle rapidly enough. This passive approach to stability permits a relatively simple, low bandwidth servomechanism, but requires careful design of equipment within the PSP to surpress dynamic excitation.

Specific requirements are as follows:

a. The control loop shall track Mars local vertical to within ± 8 milliradians with random rates not to exceed ± 1.5 percent of orbital rates. The subtended angle of Mars may vary from 25 to 105 degrees.

b. Tracking rates shall be orbital which may vary from 10^{-4} to 10^{-3} radians/second.

c. Gimbal stops shall be provided to limit gimbal travel. Slew rate is not critical but it shall be maximized so as to enable rewind from one gimbal stop to the other in minimum time.

d. The ability to point off-axis and to hold the desired position shall be provided.

e. Horizon sensor outputs and gimbal angle position shall be telemetered.

3.3.4. Description of Gimbal E Loop

A block diagram of the closed loop control is shown in Figure 18. Errors to the local vertical are detected by the horizon sensor which is mounted on the platform, and after amplification are applied to the dc torquer to reposition the platform. Tachometer feedback is employed to reduce the effects on tracking smoothness of gimbal friction and motor non-linearities. Limits of travel are detected by the gimbal stops whose outputs are applied to the Logic Unit.

The gimbal angle is monitored by means of a geared up shaft on which is mounted a sensor similar to that used in the Gimbal C and D loops. Essentially, it counts the shaft revolutions. Each revolution generates a pulse which is counted in a reversible counter.

Off-axis pointing is effected by loading the desired position into an off-axis counter and then activating the drive; slewing continues until the gimbal position counter compares with the off-axis counter.

3.3.5. Error Analysis

A detailed error analysis has not been performed for scan platform pointing, but detailed analysis of similar open loop controls for the high gain antenna has indicated errors of one degree (3σ). Limited analysis has also shown that errors in the Mars tracking loop will be of this order. A more detailed error analysis should be performed to determine what degree of problem exists in pointing the very narrow field of view high resolution camera at a previously observed object on the surface of Mars.

3.3.6. Commands

Table 6 indicates the commands which are used to manipulate the two axes which erect the orbit plane normal (C and D axes); this command list is identical to Task B. Table 7 summarizes the commands used to control the Mars tracking loop.

Table 6. C and D Gimbal Commands

(C and D Axes)	Primary Source	Backup Source
Move C Gimbal $+3/16^{o}$	C&S	C.D.
Move C Gimbal $-3/16^{o}$	C&S	C.D.
Move D Gimbal $+3/16^{o}$	C&S	C.D.
Move D Gimbal $-3/16^{o}$	C&S	C.D.
Slew C Gimbal (+)	C&S (Deployment)	C.D.
Slew C Gimbal (-)	C.D.	--
Slew D Gimbal (+)	C.D.	--
Slew D Gimbal (-)	C&S (Deployment)	C.D.
Stop Slew	C&S (Deployment)	C.D.
Lock Gimbals (for Orbit Trim)	C&S	C.D.
Release Gimbal Lock	C&S	C.D.

Table 7. E Gimbal Commands

Command	Primary Source	Backup Source	Action
Hold	D.A.S.	C.D.	Drive is disabled and "E" axis holds a constant pointing direction until next command is received.
Acquire/ Track	D.A.S.	C.D.	If Mars is within the field of view of the horizon sensor, tracking commences. Otherwise acquisition commences by driving in the negative direction*.

*The positive direction is the direction of gimbal motion during nadir tracking.

Table 7. "E" Gimbal Commands (Continued)

Command	Primary Source	Backup Source	Action
Continue/ Track	D.A.S.	C.D.	Same as ACQUIRE/TRACK except acquisition commences by driving in the positive direction*.
Slew (+) to x Position	D.A.S.	C.D.	Gimbal is driven in the positive direction* to x position.
Slew (-) to x Position	D.A.S.	C.D.	Gimbal is driven in the negative direction* to x position.

*The positive direction is the direction of gimbal motion during nadir tracking.

For the Mars tracking axis, the slew commands are used only for off-nadir pointing. For typical automatic nadir tracking, the following commands might be issued by the Data Automation Subsystem at times referenced to periapsis. Presume that the platform is tracking the Mars local vertical near the end of the prime data acquisition region of the orbit. Following completion of photoimaging, it may be desirable to temporarily stop the platform to use the ultraviolet spectrometer; this is accomplished by a HOLD command. After a suitable time interval to take UV spectrometer data, a CONTINUE/TRACK command would be issued; the platform will then reacquire and again track the Mars local vertical. At the conclusion of the portion of the orbit useful for science data, a second HOLD is commanded. After a time interval sufficient for the apparent motion of Mars to take it past the gimbal stop, an ACQUIRE/TRACK command is issued, the platform will rewind, acquire Mars, and repeat the cycle. Combinations of these three commands permit very versatile automatic operation. The sequence of commands can be altered by ground command.

3.4. THERMAL CONTROL

Temperature control of the PSP is achieved by passive means. The preferred design has relatively low average power dissipation per unit mass, which allows the use of inherent thermal inertia to damp temperature variations during periods of high instrument activity. Super-insulation is used with controlled emissivity surfaces so that, when the platform is within operating temperature limits, there will be a net loss of heat. Thermostatically controlled heaters are used to replace the energy loss.

An insulating bulkhead is used to separate the PSP into two thermal regions. The first is maintained in the temperature range of 15 to 35^{o}C and houses all instruments except the two infrared spectrometers. The second region is maintained at -43 to -33^{o}C; this second region is located at the top of the package which is a surface of known sun orientation and available for radiative detector cooling.

Table 8 summarizes the heater power requirements for design of the PSP thermal control system. These are based on minimum temperature levels which must be maintained. It should be noted that the sizing of the heaters provides sufficient contingency to maintain temperatures at the upper bound of the respective temperature range during both Transit and Mars orbital conditions when all instrument power is off.

Table 8. Heater Power Requirements

	Transit	Normal Operation	Mars Orbits with All Instrument Power Off	Heater Size
Region 1 (Warm Zone)	6	6.8	11.2	15
Region 2 (Cold Zone)	5	2.1	3.0	5
Total Power (Watts)	11	8.9	14.2	20

Detector cooling is considered to be a function of the individual science instruments, but the PSP must be configured with appropriate consideration for the cooling requirements of the instruments. Accordingly, the implications of detector cooling were investigated during the study. The detector of the high resolution infrared spectrometer can be cooled to -60°C by passive thermal radiation to space provided a location for the space viewing window that does not have any incident sunlight is found on the PSP. If solar incidence negates radiation cooling, this detector could be cooled by a multi-stage thermoelectric device operating at about 6 watts power load. Commercially-available thermoelectric cooling units require space use qualification.

The low temperature detector of the broad band infrared spectrometer as currently defined requires cooling to 45°K or lower. This is an unrealistic, if not impossible requirement for 6-months continuous operation within reasonable PSP weight and size restraints and spacecraft power availability. It could be cooled by a 200-pound solid hydrogen refrigerator or by a 500-watt closed cycle cryostat. It could be cooled by gas expansion as is being done for Mariner Mars 1969, but only for a day or two at most.

If the BBIR temperature requirement is changed to 80°K, passive detector cooling may become possible. This depends on whether a system of shades can be designed to block the solar, planetary, and spacecraft heat fluxes from a space-viewing detector radiator. Because of PSP motion, a satisfactory shade design may be impossible to devise. In the event that passive cooling to 80°K cannot be arranged, the only practical alternative for long-term operation will be higher detector temperature at the sacrifice of radiation measurements to 15 microns wavelength.

3.5. BASELINE DESIGN, STRUCTURE AND PACKAGING

Figure 35 gives the size, shape, weight, volume, power, and temperature requirements for the seven instruments that comprise the instrument package assumed for the baseline design. The total weight of this package amounts to 233 pounds. This PSP weight is reduced significantly by locating much of the supporting electronics on the bus. Studies

A. HIGH RESOLUTION TELEVISION

GROUND RESOLUTION		- 10 meter (at 1000 KM RANGE)
WEIGHT:	OPTICS	- 24 lb
	SENSOR	- 25 lb
	ELECTRONICS	- 10 lb
	TOTAL	- 59 lb
VOLUME:	OPTICS	- 393 in^3
	SENSOR	- 735 in^3
	ELECTRONICS	- 360 in^3
	TOTAL	- 1,488 in^3
POWER:	TOTAL	- 20 watts
TEMP.:	OPERATING	- 15° to 35°C
	STORAGE	- 5° to 45°C

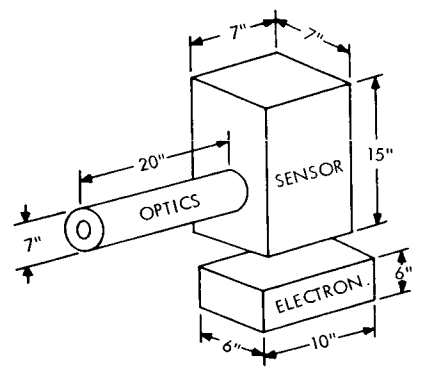

B. MEDIUM RESOLUTION TELEVISION

GROUND RESOLUTION		- 100 m (at 1000 km range)
WEIGHT:	OPTICS	- 2 x 10 lb
	SENSOR	- 2 x 18 lb
	ELECTRONICS	- 2 x 10 lb
	TOTAL	- 2 x 38 = 76 lbs.
VOLUME:	OPTICS	-2 x 126 in^3
	SENSOR	- 2 x 432 in^3
	ELECTRONICS	- 2 x 360 in^3
	TOTAL	- 2 x 918 = 1,836 in^3
POWER:	TOTAL	- 2 x 35 = 70 watts
TEMP.:	OPERATING	- 15° to 35°C
	STORAGE	- 5° to 45°C

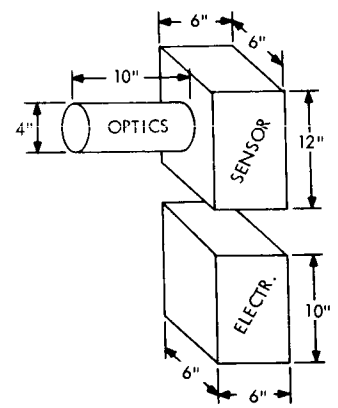

C. ULTRAVIOLET SPECTROMETER

VIEW APERTURE		- 4 x 4 in.
FIELD OF VIEW		- 2° x 6°
WEIGHT:	TOTAL	- 32 lb
VOLUME:	SENSOR	- 1,540 in^3
	ELECTRONICS	- 3 x 54 = 166 in^3
	TOTAL	- 1,706 in^3
POWER:	TOTAL	- 16 watts
TEMP.:	OPERATING	- 0° to 40°C
	STORAGE	- 10° to 55°C

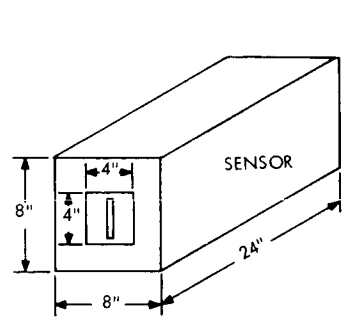

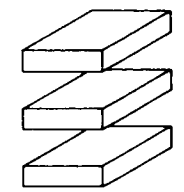

3 EACH ELECTRONICS
6" x 6" x 1 1/2"

D. HIGH RESOLUTION INFRARED SPECTROMETER

FIELD OF VIEW		- 1° x 4°
WEIGHT:	SENSOR	- 16 lb
	ELECTRONICS	- 14 lb
	TOTAL	- 30 lb
VOLUME:	SENSOR	- 2,400 in^3
	ELECTRONICS	- ≈ 500 in^3
	TOTAL	- ≈ 2,900 in^3
POWER:	TOTAL	- 14 watts
TEMP.:	OPERATING	- -60°C to 10°C
	STORAGE	- 30°C to 50°C

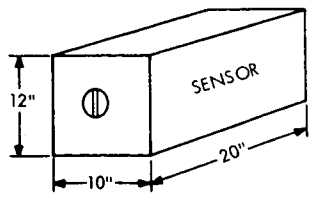

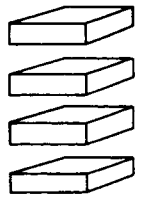

4 EACH ELECTRONICS
6" x 6" x 3 1/2"

E. BROAD-BAND INFRARED SPECTROMETER

APERTURE		- three 10 in. dia.
FIELD OF VIEW		- 5° toward planet
WEIGHT:	TOTAL	- 16 lb
VOLUME:	TOTAL	- 1,850 in^3
POWER:	TOTAL	- 5 watts
TEMP.:	DETECTOR (OPERATING):	45° K
	SENSOR (OPERATING):	-30°C to -40°C
	ELECTRONICS (OPER):	- 40°C to +40°C
	SENSOR (STORAGE):	-30° C to -40°C
	ELECTRONICS (STORAGE):	-50° C to + 55°C

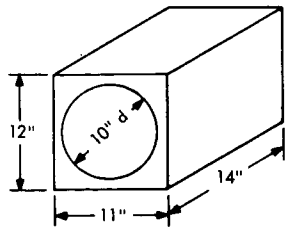

F. INFRARED RADIOMETER

APERTURE		- 5 in. diameter
FIELD OF VIEW		- 10 mr (scanned over 120°)
WEIGHT:	TOTAL	- 20 lb
VOLUME:	SENSOR	- 123 in^3
	ELECTRONICS	- 490 in^3
	TOTAL	- 613 in^3
POWER:	TOTAL	- 6 watts
TEMP.	OPERATING	- -20° to +50°C
	STORAGE	- -50° to +55°C

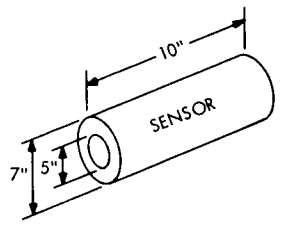

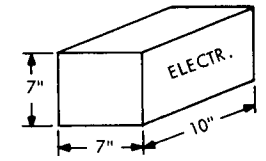

Figure 35. Packaging Requirements of Baseline Instruments

indicate that approximately 70 pounds can be relocated, reducing the deployed payload to 162 pounds. Table 9 gives a summary of the estimated weight of the baseline design.

Table 9. PSP Weight Estimates

INSTRUMENT	WEIGHT (LB)
Photoimaging	99
High Resolution Infrared Spectrometer	18
Broad-Band Infrared Spectrometer	9
Infrared Radiometer	13
Ultraviolet Spectrometer	23
Structure and Thermal Control	35
Gimbals and Control Drives	52
Stowage, Release, Deployment and Support Provisions	17
Cabling	17
	283

Figure 29 shows the baseline arrangement of instruments in the PSP envelope. This arrangement anticipates that the operational philosophy on the 1973 Voyager mission will strongly favor the mapping experiment, postponing use of stereo capability and the commanded pointing mode until late in the mission. Accordingly, all instruments except the ultraviolet spectrometer are pointed along the local vertical; the ultraviolet spectrometer is mounted at an angle of approximately 60 degrees from the TV line-of-sight so that it normally points at black space above the planet horizon. In order to obtain a traverse of the limb, the tracking drive is disabled and the orbital movement brings the ultraviolet spectrometer across the

limb with the slit parallel to the horizon. This procedure will improve the quality of the ultraviolet spectrometer data as the error in knowledge of the angular rate of the scan platform with respect to the spacecraft will be zero.

The two medium resolution cameras are boresighted as vidicon readout rate is not great enough to obtain strip mapping with a single camera. The cameras are presumed to incorporate optical deflection for use in the stereo mode. Optical deflection may also be incorporated in the ultraviolet spectrometer for nadir viewing without using the off-nadir pointing mode of the platform. The fact that all instruments are not boresighted is intended to be illustrative of the possibility that operational advantages may accrue from alternate arrangements. Today, no one really knows the Voyager operational requirements; the baseline package permits reasonable flexibility.

Two infrared spectrometers are isolated by a thermal bulkhead that divides the PSP into two thermal zones and are located near the top of the package where black space viewing is available. The broad-band infrared spectrometer has one aperture viewing black space; the slit aperture of the high resolution infrared spectrometer is aligned parallel to the Mars tracking axis so that in normal viewing, the slit is perpendicular to the ground track and parallel to the planetary limb.

The horizon sensors that control the nadir tracking drive are mounted at upper corners of the package in order to improve the unobstructed view. Three horizon sensor heads are used; the middle sensor is used to measure cross-axis error for use in interpretation of data.

The outer walls are 32 inches on a side and are supported from the top and bottom by the central support cylinder that transmits all loads to the bearings supported by an extension of the deployment boom. Thus the center cylinder supports the envelope entirely independent of the instruments themselves, and any slight impact, or deflection of the outer envelope does not directly affect the instruments or their alignment. This arrangement gives maximum protection against operational loads such as acoustic vibration and ground handling "accidents".